# Nonspectator Reactivity of Nontrigonal Tricoordinate Phosphorus Ligands

by

Akira Tanushi

B.S. Chemistry
The University of Tokyo, 2014
M.S. Chemistry
The University of Tokyo, 2016

Submitted to the Department of Chemistry
as Partial Fulfillment of the Requirements for the Degree of

DOCTOR OF PHILOSOPHY IN CHEMISTRY

at the

MASSACHUSETTS INSTITUTE OF TECHNOLOGY

September 2021



Signature of Author: _____
Department of Chemistry
June 11, 2021

Certified by: _____
Alexander Thomas Radosevich
Associate Professor of Chemistry
Thesis supervisor

Accepted by: _____
Adam P. Willard
Associate Professor of Chemistry
Graduate Officer

This doctoral thesis has been examined by a Committee of the Department of Chemistry as follows:

Professor Mircea Dincă: _____
Chairman

Professor Alexander T. Radosevich: _____
Thesis Advisor

Professor Christopher C. Cummins: _____
Department of Chemistry

# Nonspectator Reactivity of Nontrigonal Tricoordinate Phosphorus Ligands

by

Akira Tanushi

Submitted to the Department of Chemistry on June 11, 2021 in partial fulfillment of the requirements for the Degree of Doctor of Philosophy in Inorganic Chemistry

## ABSTRACT

This thesis describes novel 'nonspectator' reactivity of geometrically deformed tricoordinate phosphorus ligands that diverge from traditional supporting roles of phosphines in transition metal catalysis. Chapter 1 presents an overview of the chemistry of higher coordinate phosphorus ligands in transition metal complexes. Chapter 2 describes experiments validating the enhanced electrophilicity of nontrigonal $C_s$-symmetric P(III) compounds as compared to typical trigonal P(III) ligands with quasi-$C_{3v}$ local symmetry. Specifically, phosphorus K-edge XANES spectroscopy combined with time-dependent DFT calculation reveal ca. 1.5 eV bathochromic shift in the position of P K-edge onset. In Chapter 3, the development of nonspectator reactivities of a novel chelating ligand containing a nontrigonal P(III) center with Group 8 Ru complexes is presented. In a first finding, a unique net insertion of nontrigonal P(III) ligand into a Ru–H bond, yielding a five-coordinate phosphorus center in which of the substituents is a transition metal (i.e. metallohydrophosphoranes). The mechanistic investigation of the net insertion shows an α-H-migration between Ru–P bond in a reversible and controllable fashion. Chapter 4 extends the nonspectator reactivity to metal–ligand cooperative bond activation to Group 9 metal systems. Various transformations, such as heterolytic splitting of carbon dioxide and cooperative O–H addition of phenol, are achieved by a designed Ir–P bond with a bifunctional reactivity. Finally, Chapter 5 presents results on the net insertion of nontrigonal P(III) ligands into Group 10 metal–carbon bonds, and the factors governing the insertion reactivity is discussed. Taken together, the versatile nonspectator reactivities provide a conceptually new role of higher coordinate phosphorus ligands as a viable platform for novel bond activation and group transfer processes.

Thesis Supervisor: Alexander T. Radosevich

Title: Associate Professor of Chemistry

# Acknowledgement

First, I would like to express my sincere gratitude to Professor Alexander Radosevich for his continuous support and guidance throughout my entire Ph.D. course. I laugh at it now, but I did not even know his name when I first met him on the visiting weekend at MIT. Since we started together at MIT, however, not only was Alex a knowledgeable and creative chemist, but he has also been truly educational in every aspect of my interaction with him. Alex let me pursue every project I was interested in and guided me in the right direction when I was in trouble. Without him, I could not have grown up as a confident scientist in the way I envisioned. Alex, I am so proud of being a member of your group and becoming one of your first Ph.D. graduates at MIT. I cannot simply imagine any better advisor than you.

I was blessed to have wonderful lab mates in the Radosevich group. I want to offer special thanks to Gregory Cleveland, Seung Jun Hwang, Aya Eizawa, and Myles Drance, with whom I have worked on the research projects metallophosphoranes. They were great sources for motivation, helpful advice, and all the fun we have had for the last five years. Connor Gilhula, Hanna Moon, Gen Li, Soohyun Lim, Gisselle Pombar, Jeff Lipshultz, Yuzuru Kanda, Seung Youn Hong, Trevor Nykaza, Jared Mattos, Julian Cooper, Krysta Dummit, Tyler Harrison, Yi-Chun Lin, Colet te Grontenhuis, Morgan Lecomte, Ayan Maity, Avispa Ghosh, Shuhei Kusumoto, Shin-ho Kim-Lee, Julien Légaré Lavergne, Nick Qin, Nolwenn Mahieu, thank you for making our lab a fantastic place to be. I am sure I will miss these years surrounded by such talented people with great personalities.

Throughout my doctoral work, I was fortunate to work with many amazing chemists outside the Radosevich group. Thank you to my committee members, Professor Mircea Dincă and Professor Christopher Cummins, for the valuable suggestion and support for my dissertation. I am also sincerely grateful to Dr. Peter Müller for the X-ray data collection of so many crystals I brought to you. I have also had wonderful collaborators outside MIT. My sincere gratitude goes to Professor Scott Daly and Professor Jason Keith for the Phosphorus K-edge XANES spectroscopy and Professor Stefan Grimme and Hagen Neugebauer for the computational mechanistic studies.

Outside the lab, good friends have always surrounded my life in Cambridge. Since it was the first time for me to live outside Japan, the tremendous support from my friends helped me a lot. I especially thank the members of Ames, a band I formed with friends in Boston. Playing music with you was always fun, even when I was depressed.

Finally, I would like to express my greatest appreciation to my family for their unconditional love and support. My mother and brother encouraged and helped me throughout my life, even when we are physically not close. My father, who ceaselessly supported me physically, mentally, and financially to the last breath, is always watching over me. Without them, I could not have completed the doctoral course research.

June 11, 2021

Akira Tanushi

# Table of Contents

Abstract ..... - 3 -

Acknowledgement ..... - 4 -

List of Figures ..... - 9 -

List of Tables ..... - 12 -

**CHAPTER 1 INSIGHT INTO HIDDEN CHEMISTRY OF HIGHER COORDINATE PHOSPHORUS LIGANDS: CHALLENGES AND OPPORTUNITIES - 13 -**

1-1. Tricoordinate Phosphorus Ligands – Tunable 'Spectator' Ligands in Transition Metal Catalysis.... ..... - 14 -

1-2. Growing Chemistry of Lower Coordinate Phosphorus Ligands ..... - 17 -

1-3. Hidden Chemistry of Higher Coordinate Phosphorus Ligands ..... - 19 -

1-4. Synthesis and Reactivity of Metallophosphoranes ..... - 22 -

1-5. Proposed 'Nonspectator' Reactivities of $PR_3$ Ligands through Higher Coordinate Phosphorus Ligands ..... - 37 -

1-6. Enhanced Accessibility to Higher–Coordinate Phosphorus Species by Geometrically Constrained Nontrigonal Tricoordinate Phosphorus Compounds ..... - 49 -

1-7. Conclusion and Outlook ..... - 57 -

1-8. References ..... - 58 -

**CHAPTER 2 VALIDATION OF BIPHILICITY OF NONTRIGONAL PHOSPHORUS COMPOUNDS BY P K-EDGE XANES AND TDDFT CALCULATION ..... ..... - 67 -**

2-1. Introductory Remarks: Validation of Biphilic Hypothesis ..... - 68 -

2-2. P K-edge XANES for Electronic Structure Determination ..... - 69 -

2-3. Synthesis and Structures of Molecular Phosphorus Compounds ..... - 70 -

2-4. Electronic Structure Analysis of Molecular Phosphorus Compounds ..... - 74 -

2-5. Discussion on Biphilic Hypothesis ..... - 80 -

2-6. Conclusion and Outlook ..... - 85 -

2-7. Experimental Section ..... - 86 -

2-8. References ..... - 90 -

**CHAPTER 3 SYNTHESIS OF RUTHENAHYDROPHOSPHORANES VIA NONSPECTATOR REACTIVITY OF NONTRIGONAL P(III) LIGANDS: NET INSERTION, INTRAMOLECULAR A-H-MIGRATION AND HYDRIDE ADDITION ..... - 93 -**

3-1. Introductory Remarks: Access to Group 8 Metallohydrophosphoranes ..... - 94 -

3-2. Synthesis of Tridentate Ligand L1 ..... - 96 -

3-3. Insertion of Nontrigonal P(III) Ligand into Ru–H ..... - 98 -

3-4. Direct Observation of Intramolecular H-migration from Ru to P and Mechanistic Investigation ..... - 110 -

3-5. Effect of Perturbation of the Ru Coordination Environment on Reversible Intramolecular α-H-migration ..... - 118 -

3-6. Synthesis of Metallohydrophosphorane from Metal–phosphine by Reactions with Exogenous Hydride Sources ..... - 123 -

3-7. Nonspectator L/X Switching of Cationic Cyclopentadienylruthenium(II) Complexes with Nontrigonal Phosphorus(III) Ligands ..... - 131 -

3-8. Conclusion and Outlook ..... - 136 -

3-9. Experimental Section ..... - 137 -

3-10. References ..... - 150 -

**CHAPTER 4 METAL–LIGAND COOPERATIVE REACTIVITY OF GROUP 9 COMPLEXES OF NONSPECTATOR PHOSPHOSRUS(III) LIGANDS ..... - 153 -**

4-1. Introductory remark: Metal–Ligand Cooperation with Electrophilic Ligands ..... - 154 -

4-2. Synthesis of Low-valent Rh(I)/Ir(I) $PR_3$ Complexes ..... - 157 -

4-3. Cooperative Activation of C=E Bonds by $IrCl(PPh_3)(L1)$ ..... - 162 -

4-4. Cooperative Activation of E–H Bonds by $IrCl(PPh_3)(L1)$ ..... - 173 -

4-5. Sequential Cooperative Reactivity of $RhCl(PPh_3)(L1)$ ..... - 179 -

4-6. Conclusion and Outlook ..... - 183 -

4-7. Experimental Section ..... - 184 -

4-8. References ..... - 194 -

**CHAPTER 5 INSERTION OF NONSPECTATOR PHOSPHORUS LIGANDS INTO GROUP 10 TRANSITION METAL–CARBON BONDS ..... - 199 -**

5-1. Introductory Remarks: Spectator and Nonspectator Roles of Tricoordinate Phosphorus Ligands in Chemistry of Group 10 Metal–Carbon Bonds ..... - 200 -

5-2. Synthesis of Bidentate P^P–Chelate Ligand L2 and L3 ..... - 202 -

5-3. Metalation of L2 with Group 10 M–Me Precursors ..... - 204 -

5-4. DFT Calculation to Understand the Different Reactivity within Group 10 Triad ..... - 210 -

5-5. Metalation of Tridentate Ligand L1 with Group 10 Metal–Alkyl Precursors ..... - 214 -

5-6. Reactivity of Dialkyl Group 10 Metal–phosphine Complexes ..... - 221 -

5-7. Conclusion and Outlook ..... - 229 -

5-8. Experimental Section ..... - 230 -

5-9. References ..... - 245 -

**APPENDIX A . SUPPLEMENTARY DATA FOR CHAPTER 2 ..... - 249 -**

A.1. X-ray Diffraction Data ..... - 249 -

A.2. DFT Calculation ..... - 253 -

A.3. Multinuclear NMR spectra ..... - 255 -

**APPENDIX B . SUPPLEMENTARY DATA FOR CHAPTER 3 ..... - 259 -**

B.1. X-ray diffraction ..... - 259 -

B.2. DFT Calculation ..... - 309 -

B.3. Multinuclear NMR spectra ..... - 311 -

**APPENDIX C . SUPPLEMENTARY DATA FOR CHAPTER 4 ..... - 358 -**

C.1. X-ray Diffraction ..... - 358 -

C.2. DFT Calculation ..... - 439 -

C.3. Multinuclear NMR spectra ..... - 440 -

**APPENDIX D . SUPPLEMENTARY DATA FOR CHAPTER 5 ..... - 466 -**

D.1. X-ray Diffraction ..... - 466 -

D.2. DFT calculation ..... - 492 -

D.3. Multinuclear NMR spectra ..... - 496 -

# List of Figures

**Figure 1-1.** Frontier electronic structures of a $C_{3v}$ symmetric $PR_3$ and their major bonding interactions with metal *d* orbitals. ..... - 15 -
**Figure 1-2.** Classification of the diverse family of phosphorus ligands according to P-coordination number. ..... - 17 -
**Figure 1-3**. Difference between 2c-2e and 3c-4e bonding models. ..... - 19 -
**Figure 1-4.** Frontier electronic structures of $C_{2v}$-symmetric $PR_4^-$ and their major bonding interactions with metal *d* orbitals. ..... - 20 -
**Figure 1-5.** (a) CO insertion into the Pt–OMe bond of **1.72** and (b) computed reaction free energies by MacGregor (units: kcal·mol$^{-1}$)..... - 39 -
**Figure 1-6.** Qualitative depiction of the modulation of frontier orbital energies of $PR_3$ when its geometry changes from $C_{3v}$, $C_s$ to $C_{2v}$. ..... - 49 -
**Figure 2-1**. Solid state structure of **2.2**. Thermal ellipsoid plots rendered at the 50% probability level. ..... - 72 -
**Figure 2-2.** Comparison of P K-edge XANES spectra for $P(NMePh)_3$, **2-1** and **2-2**. ..... - 74 -
**Figure 2-3.** Comparison of experimental (solid line) and simulated (dashed line) P K-edge XANES spectra for $P(NMePh)_3$, **2.1** and **2.2**. Individual transitions are represented by red bars and indicate relative differences in calculated oscillator strength. The transitions are labeled according to the predominant calculated MOs mixing in the excited states. The labels correspond to those provided in Figure 2-4. ..... - 75 -
**Figure 2-4.** Truncated MO correlation diagram of molecular P(NNN) complexes. Frontier orbitals relevant to the XAS results and reactivity at phosphorus are highlighted in red and connected by dashed lines to show how they transform across the series. ..... - 75 -
**Figure 2-5.** Selected donor-acceptor Kohn-Sham orbitals from DFT calculations of $P(NMePh)_3$ and **2.1**. ..... - 76 -
**Figure 2-6.** Qualitative frontier molecular orbital diagrams depicting the electronic structure arising from nontrigonal perturbation of a model $\sigma^3$-P compound. ..... - 80 -
**Figure 2-7.** Definition of geometrical parameters used to index the computational structures of $P(NH_2)_3$ within local $C_s$ symmetry. Hydrogens are omitted for clarity. ..... - 81 -
**Figure 2-8**. Contour maps depicting the orbital of (a) Total electronic energy, (b) LUMO energies, (c) ΔHOMO–LUMO for all $P(NH_2)_3$ structures with $C_s$-symmetry. Energies are shown in a units of Hartrees. Points corresponding to the structures of $P(NMePh)_3$, **2.1** and $C_{2v}$-**2.1** are superimposed as black points. ..... - 82 -
**Figure 3-1.** Divergent metalation of trigonal and nontrigonal 8-P-3 compounds. ..... - 94 -
**Figure 3-2.** $^{31}$P NMR spectra of (a) **L1** (b) **3.3** (c) **3.4** in $CDCl_3$. Units are ppm relative to 85% $H_3PO_4$..... - 97 -
**Figure 3-3.** Thermal ellipsoid plots rendered at the 50% probability level for **L1**. Hydrogens are omitted for clarity. ..... - 97 -
**Figure 3-4.** Thermal ellipsoid plots rendered at the 50% probability level for **3.3**. Hydrogens, solvent molecules of crystallization and phenyl rings of $PPh_3$ ligands are omitted for clarity. ..... - 99 -

**Figure 3-5.** Thermal ellipsoid plots rendered at the 50% probability level for **3.4**. Hydrogens except H(1) and phenyl rings of $PPh_3$ ligands are omitted for clarity. Only one of the three independent molecules in the unit cell is shown. - 100 -
**Figure 3-6.** Canonical structures corresponding to hydride transfer from M→P. - 102 -
**Figure 3-7.** Calculated electron density for **3.3** in the plane defined by Ru–P–H coordinates. Electron density contours (—), gradient vector field (—), bond paths (—), bond critical points (•), and atomic basins (▬) are depicted. Units are Å. - 104 -
**Figure 3-8.** Comparison of P K-edge XANES spectra for **3.3** (blue) and **3.4** (red). - 106 -
**Figure 3-9.** Comparison of experimental (solid line) and simulated (dashed line) P K-edge XANES spectra for **3.3** and **3.4**. Individual transitions are represented by red bars and indicate relative differences in calculated oscillator strength. The transitions are labeled with calculated MOs mixing in the excited states. - 107 -
**Figure 3-10.** Truncated MO correlation diagram of **2.1**, **3.3**, **3.4**. Frontier orbitals relevant to the XAS results and reactivity at phosphorus are highlighted in red and connected by dashed lines to show how they transform across the series. - 107 -
**Figure 3-11.** Selected donor-acceptor Kohn-Sham orbitals from DFT calculations of **3.3**, and **3.4**. - 108 -
**Figure 3-12.** $^{31}P\{^{1}H\}$ NMR spectra of (a) **3.6**, (b) **3.7** and (c) **3.4** in $C_6D_6$. Units are in ppm. Inset figures show $^{1}H$ -coupled $^{31}P$ NMR spectra. - 111 -
**Figure 3-13**. Thermal ellipsoid plots rendered at the 50% probability level for **3.7**. Hydrogen atoms except H(1), carbon atoms in phenyl groups of $PPh_3$ and solvent molecules of crystallization are also omitted for clarity. Only one of the two independent molecules contained in the unit cell is shown. - 113 -
**Figure 3-14.** (a) Kinetic experiments of intramolecular H-transfer. Plot of ln[**3.7**] vs time monitored ($[\mathbf{3.7}]_0$ = 2.6 mM, $C_6D_6$) at 313 K – 333 K. (b) Eyring plot of ln($k$/T) versus 1/T ($k$ = first-order rate constant, T = temperature in Kelvin) for the reaction of **3.7** to give **3.4**. - 115 -
**Figure 3-15.** Computed reaction and activation free energies at the ZORA-PBE0-D4/ZORA-def2-QZVPP/PBEh-3c level of theory for the hydride transfer from **3.7** to **3.4** for two mechanisms. All values are given in $kcal \cdot mol^{-1}$. - 116 -
**Figure 3-16**. Couputed structures for Transition states **TS1**-**TS4**. Hydrogen atoms except H(1) and phenyl rings of $PPh_3$ ligand are omitted for clarity. - 117 -
**Figure 3-17**. $^{31}P$ NMR spectra of (a) **3.3**, (b) **3.16** (c) **3.17** (d) **3.18**. Units are in ppm relative to 85% $H_3PO_4$. - 124 -
**Figure 3-18.** Thermal ellipsoid plots rendered at the 50% probability level for **3.16**. Hydrogen atoms except H(1) and ones in $BH_4$ ligand, carbon atoms in phenyl groups of $PPh_3$ are omitted for clarity. - 125 -
**Figure 3-19**. Variable-temperature (193 K – room temperature) $^{1}H$ NMR spectra of complex **3.16** in the region of $BH_4$ ligand. (solvent: $CD_2Cl_2$) - 126 -
**Figure 3-20**. Important $^{1}H$ NMR and $^{31}P$ NMR signals and couplings in **3.17**. - 127 -
**Figure 3-21.** Thermal ellipsoid plots rendered at the 50% probability level for (a) **3.23** (b) **3.24**. Recrystallization solvents and Hydrogen atoms are omitted for clarity. - 132 -
**Figure 3-22.** $^{31}P\{^{1}H\}$ spectra of (a) **3.23** (b) **3.25** (c) **3.26**. Units are in ppm relative to 85% $H_3PO_4$. Inset spectra are (b) $^{1}H$-coupled $^{31}P$ NMR spectra of **3.25**, (c) $^{19}F$ NMR spectra of **3.26**. - 135 -

**Figure 4-1**. Simplified frontier MO diagrams for MLC system with poralized $M^{\delta-}$–$L^{\delta+}$ bond..... - 154 -
**Figure 4-2**. (left) classic metal–centered activation (right) proposed metal–ligand cooperative activation... ..... - 156 -
**Figure 4-3**. Thermal ellipsoid plots rendered at the 50% probability level for **4.1**. Hydrogens, solvent molecules of crystallization and phenyl rings of $PPh_3$ ligands are omitted for clarity..... - 158 -
**Figure 4-4**. Thermal ellipsoid plots rendered at the 50% probability level for **4.3**. Hydrogens and phenyl rings of $PPh_3$ ligands are omitted for clarity..... - 159 -
**Figure 4-5.** Structure of **4.3**, with hydrogen atoms omitted for clarity. Two phosphorus atoms and their substituent atoms are depicted with thermal ellipsoids at 50% probability (inset: selected structural parameters). ..... - 160 -
**Figure 4-6.** $^{31}P\{^{1}H\}$ NMR spectra of (a) **4.2** (b) **4.6** (c) **4.7** (d) **4.8**. Units are ppm relative to 85% $H_3PO_4$. . ..... - 163 -
**Figure 4-7.** Thermal ellipsoid plots rendered at the 50% probability level for **4.7**. Hydrogens and phenyl rings of $PPh_3$ ligands are omitted for clarity..... - 164 -
**Figure 4-8.** Calculated energy differences of C=N and C=O cycloaddition to **4.2** for EtNCO and DippNCO. ..... - 167 -
**Figure 4-9.** Thermal ellipsoid plots rendered at the 50% probability level for **4.8**. Hydrogens and phenyl rings of $PPh_3$ ligands are omitted for clarity..... - 169 -
**Figure 4-10.** Thermal ellipsoid plots rendered at the 50% probability level for **4.11**. Hydrogens and phenyl rings of $PPh_3$ ligands are omitted for clarity..... - 172 -
**Figure 4-11.** $^{31}P\{^{1}H\}$ NMR spectra and $^{1}H$ NMR (only low-field region) of (a) **4.2** (b) **4.14** (c) **4.15** (d) **4.16**. Units are ppm relative to 85% $H_3PO_4$. Insets show $^{1}H$-coupled $^{31}P$ NMR spectra.... - 173 -
**Figure 4-12.** Driving force of cooperative addition compared to metal–centered addition products calculated at B3LYP.def2-TZVP level of theory. ..... - 176 -
**Figure 4-13**. Thermal ellipsoid plots rendered at the 50% probability level for **4.20**. Hydrogens atoms except *P*–H, phenyl rings of $PPh_3$ ligands and recrystallization solvents are omitted for clarity. Only one of the four molecules in the unit cell is displayed, ..... - 180 -
**Figure 5-1.** Structure for **L3**, with hydrogen atoms and solvent molecules omitted for clarity. Two phosphorus atoms and their substituent atoms are depicted with thermal ellipsoids at 50% probability..... - 203 -
**Figure 5-2.** Metalation of **L2** with group 10 complexes of the formula $L_2M(Cl)(Me)$. Reaction conditions: (*i*) (cod)Pt(Cl)(Me), benzene, RT, 90% (*ii*) (cod)Pd(Cl)(Me), benzene, RT, 99%. (*iii*) $(Me_3P)_2Ni(Cl)(Me)$, benzene, RT, 37%. ..... - 204 -
**Figure 5-3.** $^{31}P$ NMR spectra of (a) **L2**, (b) **5.6**, (c) **5.7**, (d) **5.8** in $CD_2Cl_2$. Units are ppm relative to 85% $H_3PO_4$..... - 205 -
**Figure 5-4.** Thermal ellipsoids rendered at the 50% level for (a) **5.6**-*cis*, (b) **5.7′** and (c) **5.8′**. Hydrogen atoms and solvent molecules are omitted for clarity..... - 206 -
**Figure 5-5.** Calculated Gibbs free energy of methyl α-migration for Ni, Pd and Pt complexes at the B3LYP/def2-TZVP level of theory. ..... - 210 -
**Figure 5-6.** IBO depictions of M–P bonds and LOBA oxidation states. Numbers in parentheses correspond to the partial charge distributions of IBO. Orbital isosurface contains 80% of the integrated electron density of the orbital. ..... - 212 -

**Figure 5-7.** Thermal ellipsoids rendered at the 50% level for **5.10´**. Hydrogen atoms are omitted for clarity. ..... - 215 -
**Figure 5-8** Thermal ellipsoids rendered at the 50% level for **5.12**. Hydrogen atoms are omitted for clarity. ..... - 217 -
**Figure 5-9.** $^{31}P$ NMR spectra of (a) **5.13** in $C_6D_6$ and (b) **5.5**, (c) **5.16** in $CDCl_3$. Units are ppm relative to 85% $H_3PO_4$. (Inset) $^{19}F$ NMR spectrum of **5.16** in $CDCl_3$. ..... - 224 -
**Figure 5-10.** $^{31}P$ NMR spectra of (a) **5.13** (b) **5.17**, (c) **5.18** + **5.19** (d) **5.20** in $C_6D_6$. Units are ppm relative to 85% $H_3PO_4$. ..... - 227 -

## List of Tables

**Table 2-1.** Selected Bond Distances (Å) and Angles (°) for $P(NMePh)_3$, **2-1**, **2-2**..... - 71 -
**Table 3-1.** Selected bond distances (Å) and Angles (º) for **L1**, **3.7** and **3.3**. ..... - 114 -
**Table 3-2.** Selected NMR spectroscopic data for $RuX(CO)(PPh_3)$(**L1**) (**3.4, 3.12, 3.13**). ..... - 120 -
**Table 3-3.** Selected bond distances (Å) and Angles (º) for **3.16** and **3.4**. ..... - 125 -
**Table 5-1**. Relationships between $J_{Pt-P}$ values and Pt–P bond lengths in **5.6**-*cis* and **5.6**-*trans*..... - 206 -
**Table 5-2.** Driving force of metallophosphorane formation from **5.11** and **5.12** calculated at B3LYP/def2-TZVP level..... - 218 -

# Chapter 1 Insight into Hidden Chemistry of Higher Coordinate Phosphorus Ligands: Challenges and Opportunities

## 1-1. Tricoordinate Phosphorus Ligands – Tunable 'Spectator' Ligands in Transition Metal Catalysis

Phosphorus-based ligands display a rich and varied coordination chemistry with transition metals.[1] The most dominant member of the family is tricoordinate phosphorus ($\sigma^3$-P) ligands. The ubiquity and importance of $\sigma^3$-P ligands in transition metal chemistry would be difficult to overstate. $\sigma^3$-P Ligand complexes are legion, and the chemistry of this exceptionally broad area is the subject of voluminous literature.[2-4] With applications in catalysis, inorganic synthesis, and macromolecular chemistry, $\sigma^3$-P ligands are quite arguably the most versatile transition metal ligands. While prototypical $\sigma^3$-P compounds—which are classified as L-type donors to metals within the Covalent Bond Classification—are overwhelmingly regarded as inert spectators in coordination chemistry, the development of designer phosphorus ligands to elicit specific chemistry has become in itself a major research thrust.

Within an idealized $C_{3v}$ point group, a phosphine displays a relatively high energy HOMO derived from a mixture of phosphorus 3s and $3p_z$ orbitals, producing an occupied MO with electron density oriented away from the phosphorus substituents (Figure 1-1).[5] The result is an orbital with appropriate symmetry and energy to engage as a two-electron donor ligand. A degenerate set of P–X $\sigma^*$ antibonding orbitals deriving from phosphorus $3p_x$ and $3p_y$ atomic orbitals lies high in energy and the potential electrophilic reactivity of phosphine ligands is often disregarded, though they are energetically accessible for $\pi$-backbonding from the metal in an analogous fashion to carbonyl ligands. The strength of this donation is generally tied to the energy level of the antibonding orbital set, with more electronegative substituents on phosphorus leading to stronger backbonding.

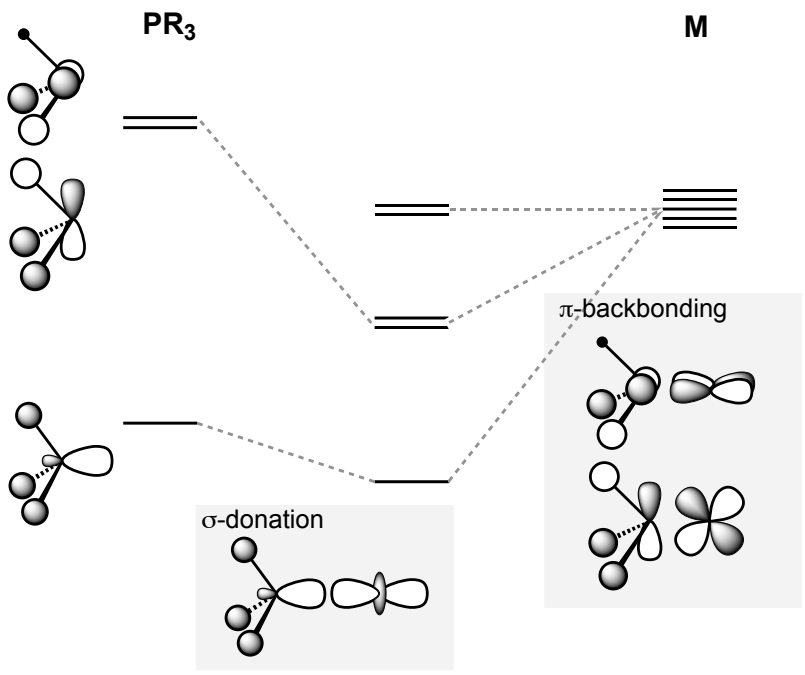


**Figure 1-1.** Frontier electronic structures of a $C_{3v}$ symmetric $PR_3$ and their major bonding interactions with metal *d* orbitals.

The practicality of $\sigma^3$-P ligands arises from their ability to modify the electronic and steric environment of their complexed metal center in a predictable manner based on P-substituents. To that end, quantitative parameters have been established in order to gauge such structural effects. Historically, the Tolman electronic parameter and cone angles have received the most attention.[6] Electronic parameters have primarily been quantified by the vibrational stretching frequencies of CO ligands in metal carbonyl complexes featuring $\sigma^3$-P ligands, with higher stretching frequencies being caused by decreased π-donation from the metal to the carbonyl.[7, 8] The balance of σ-donation and π-acceptance directly influences the metal center's capacity to donate to the carbonyl, with lower σ-donation and higher π-acceptance leading to CO stretching frequencies. Steric parameters take multiple forms, but in general, they are geometric quantities extracted from space-filling

models.[9-11] A specific $\sigma^3$-P ligand with an appropriate electronic and steric contribution for targeted catalytic reactivity can be selected with these parameters.

## 1-2. Growing Chemistry of Lower Coordinate Phosphorus Ligands

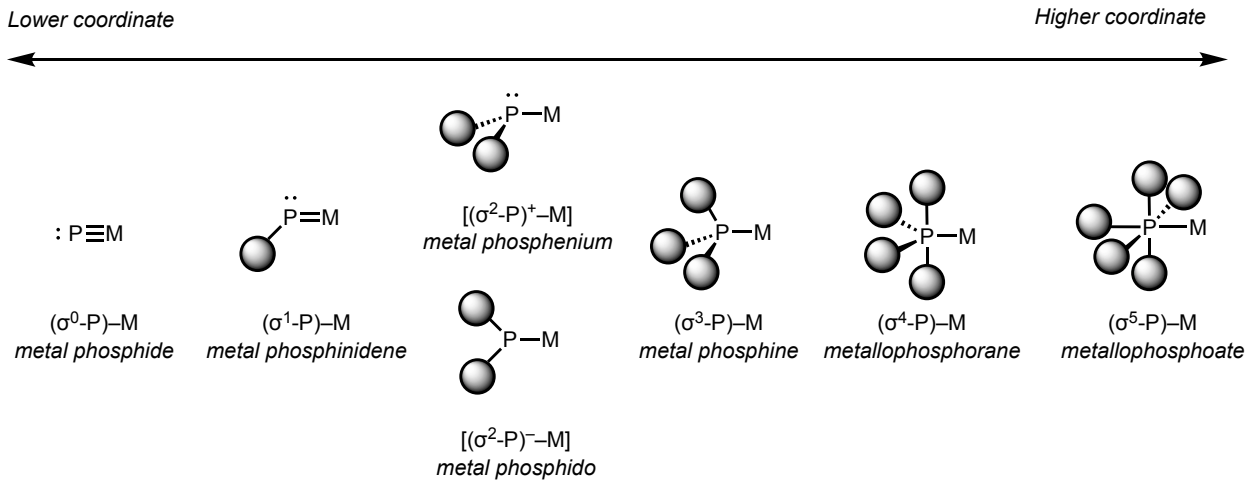


**Figure 1-2.** Classification of the diverse family of phosphorus ligands according to P-coordination number.

Lower-coordinate P ligands are also well-known and increasingly common (Figure 1-2, *left*). Divalent phosphorus ($\sigma^2$-P) ligands for metals are classified into two categories; phosphenium ligands ($\sigma^2$-$P^+$) and phosphido ligands ($\sigma^2$-$P^-$).[12] Phosphenium ligands are analogous to Fischer carbenes and have electron-withdrawing substituents (e.g. halides, amides, alkoxides), which stabilize σ-orbital and destabilize π-orbital.[13-15] The P center is susceptible to nucleophilic attack to afford ($\sigma^3$-P)–M complexes. The properties of phosphido ligands are opposite to phosphenium; they have electron-donating substituents (e.g. alkyls, aryls, hydrides) and susceptible to electrophilic attack. Phosphinidene ($\sigma^1$-P) ligand complexes have also been intensely studied as the phosphorus analogues of carbenes.[16-20] Electrophilic (Fisher-type) phosphinidene complexes are particularly versatile and are reversibly interconverted with ($\sigma^3$-P)–M complexes via cycloaddition to π-bonds (C=C, C≡C, C=X, C≡X). Terminal phosphide complexes (M≡P), formally '$\sigma^0$-P' ligand complexes without any P substituents other than the metal, were first

synthesized by Cummins[21] and Schrock[22] and are also subject to addition reactions resulting in $\sigma^1$-P or $\sigma^2$-P complexes.[23-26]

## 1-3. Hidden Chemistry of Higher Coordinate Phosphorus Ligands

By contrast, higher coordinate P ligands ($\sigma^4$-P and $\sigma^5$-P) are substantially less prevalent (Figure 1-2, *right*). As compared to their lower-coordinate phosphorus congeners, complexes with higher-coordinate phosphorus ligands and their interconversion with ($\sigma^3$-P)–M complexes have not attracted as much attention.[27-30] Whereas literature about higher-coordinate P ligands has been gradually accumulated over the last four decades, most of these works remain as the reports of novel compounds or reactions, and there has not been much discussion about general trends of their electronic structures and reactivities as a group of compounds.

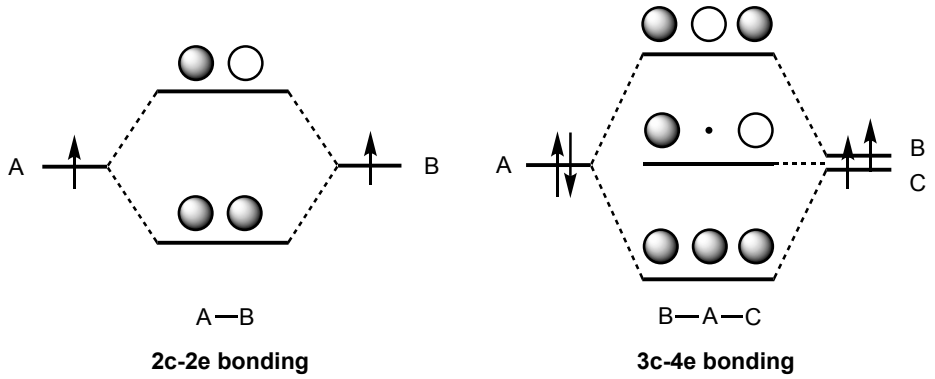


**Figure 1-3**. Difference between 2c-2e and 3c-4e bonding models.

Here we discuss the electronic structures of metallophosphoranes briefly. Metallophosphoranes are considered as '*electron-rich*' hypervalent molecules, in which 10 electrons are formally associated with the pentacoordinate phosphorus center (10–P–5).[31] Different from tricoordinate or lower-coordinate phosphorus ligands, the classic 2-centre 2-electron (2c-2e) bonding model (Figure 1-3, *left*) does not fully describe the hypervalent bonding of higher-coordinate phosphorus ligands. The 3c-4e bonding model has been widely accepted to explain such atoms having an expanded octet (Figure 1-3, *right*). The bonding situation is described in the simple frontier orbital diagrams, in which a pair of electrons occupies the nonbonding orbitals

based on the two outer atoms.[32] The formal bond order of these two bonds is calculated to be 0.5. The three atoms are in a linear arrangement since the p-orbital of the central atoms is involved in 3c-4e bonding. In pentacoordinate phosphorus systems, 3c-4e bonding is found in the apical bond consisting of the $3p_z$ orbital of central P atom and two orbitals of outer atoms. Due to the localization of nonbonding orbital on the terminal atoms, outer atoms are commonly electronegative elements with low energy orbitals (e.g. F, O, N).

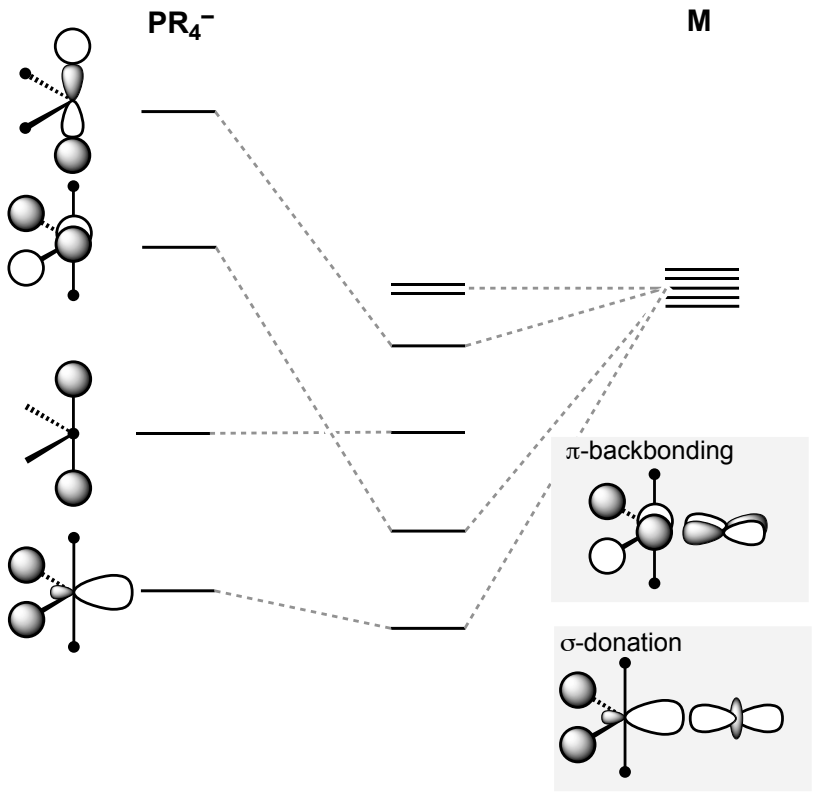


**Figure 1-4.** Frontier electronic structures of $C_{2v}$-symmetric $PR_4^-$ and their major bonding interactions with metal *d* orbitals.

The metal substituents occupy the equatorial position in all metallophosphoranes reported to date. Based on the 3c-4e bonding model, the qualitative frontier orbitals of $C_{2v}$-symmetric phosphoranide anion ($PR_4^-$) can be derived (Figure 1-4). As with the case of $PR_3$ ligands, the

interactions of $PR_4^-$ with a metal fragment described as the combination of σ-donation from P to M and π-backdonation from M to P. Nakazawa argued that the backdonation is more important factor in the M–P bonding of metallophosphoranes based on crystallographic and IR spectroscopic data.[33]

## 1-4. Synthesis and Reactivity of Metallophosphoranes

### *1-4-1. Synthetic routes to metallophosphoranes*

Here we briefly outline the reported syntheses of metallophosphoranes to date. In most cases, metallophosphoranes are synthesized by (I) ligand addition at P to ($\sigma^3$-P)–M complexes, or (II) metalation of $\sigma^5$-P compounds (phosphoranes) (Scheme 1-1). From ($\sigma^3$-P)–M complexes, the P atm increases its coordination number by accepting an attack from (a) internal nucleophiles (e.g. deprotonated amine of the ligand) or (b) external nucleophiles. From $\sigma^5$-P compounds, substitution of a P-substituent with metal fragment(s) occurs via (c) $S_N2$ halide substitution or (d) nucleophilic attack of deprotonated phosphoranes. Minor pathways not shown in Scheme 1-1 will be briefly covered too.

**Scheme 1-1**. General synthetic routes of metallophosphoranes.

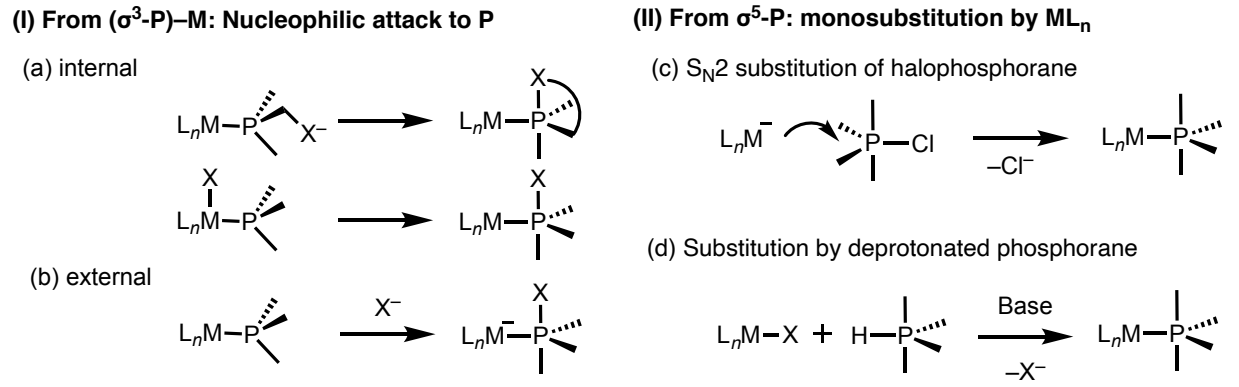


### *1-4-2. First metallophosphorane and intramolecular α-migration (Riess)*

Riess and co-workers reported the first isolation and structural characterization of a metallophosphorane in 1981 (Scheme 1-2).[34] They investigated the behavior of a series of bicyclic phosphoranes HPR(ONO) (R = Ph, benzyl, allyl, vinyl; ONO = $(OCH_2CH_2)_2N^{3-}$) as ligands for

group 6 transition metals.[35-37] The bicyclic phosphoranes HPPh(ONO) (**1.1**) coordinated to $Cp(CO)_3MCl$ (Cp = $\eta^5$-$C_5H_5$, M = Mo, W) in the $\sigma^3$-P form (**1.2**),[38] and successive abstraction of the chloride ligand led to the coordination of the nitrogen (**1.3**). Deprotonation of the amine of **1.3** led an internal nucleophilic attack to afford $\eta^2$-P,N–metallophosphoranes **1.4 (**Scheme 1-1(a)), which can be further converted to $\eta^2$-P,O–metallophosphorane **1.5** at higher temperatures.

**Scheme 1-2**. Synthesis of $\eta^2$-P,N– and $\eta^2$-P,O–bicyclic metallophosphoranes reported by Riess.

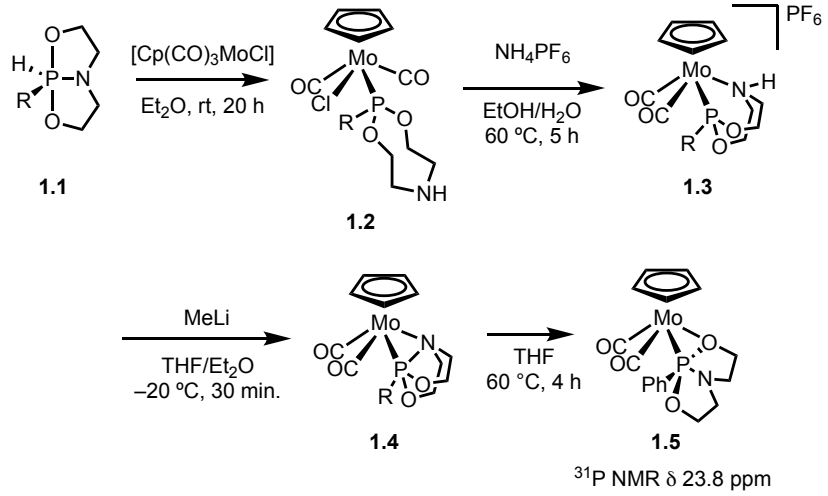


Riess and co-workers also metalated **1.1** and derivatives with group 8 precursors.[39-41] Similar metalation of **1.1** with $CpFe(CO)_2Cl$ followed by anion exchange gives complex **1.6**, which was deprotonated to afford metallophosphorane **1.7** with an $\eta^2$-P,N chelation mode (Scheme 1-3a). Upon heating metallophosphoranes **1.3** in THF, the phenyl group on the phosphoranide ligand migrated to the iron center to form complex **1.8**, This reaction is one of the very few examples of α-migration processes between M–P bonds. Treatment of the iron–phosphine–aryl complexes **1.8** with gaseous hydrogen chloride regenerated the cationic monocarbonyl complexes **1.6**. On the other hand, in an analogous transformation of allyl congener **1.9**, the allyl congener of $\eta^2$-P,N metallophosphorane **1.7** (**1.10**) afforded an iron vinyl complex **1.11** instead of the expected allyl

complex (Scheme 1-3b). The reverse reaction from **1.11** to **1.9** did not proceed upon treatment with gaseous hydrogen chloride. The authors proposed a reaction mechanism from the observe stereochemistry when substituted allyl group was used instead; iron inserts into an allylic C–H bond followed by a 1,3-proton shift to the terminal vinyl or allyl carbon atom, and finally the P–C bond cleaves to give the final iron vinyl complex (Scheme 1-3c).

**Scheme 1-3.** Iron(II) metallophosphoranes and group transfer processes between Fe–P bonds reported by Riess.

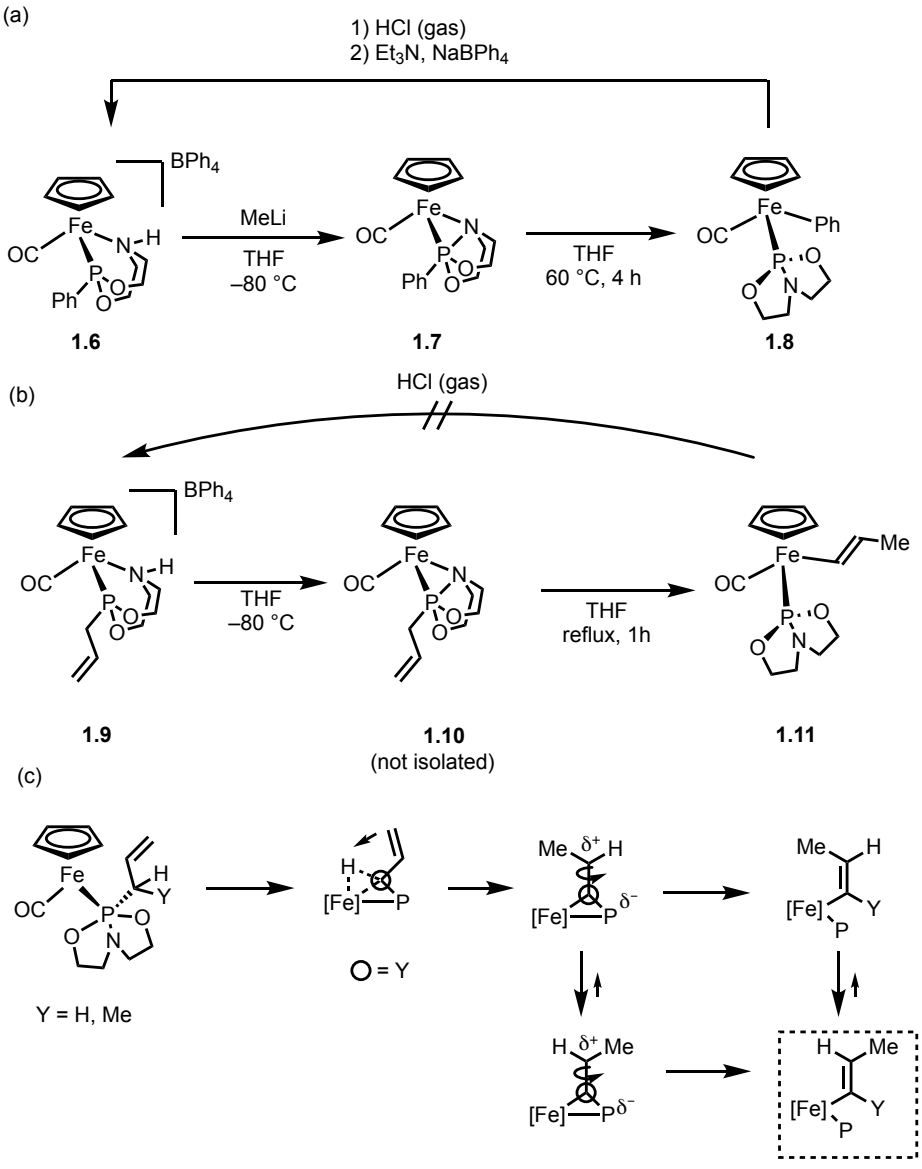

*1-4-3. Development of tetracyclic metallophosphoranes (Riess and Lattman)*

As another example of the internal nucleophilic route (Scheme 1-1a), Riess and co-workers synthesized and characterized metallophosphoranes with cyclamphosphoranide ligands.[42,43] In solution, a polycylic form of cyclamphosphorane (**1.12a**) is in equilibrium with an open tautometric form (**1.12b**) (**1.11a**:**1.12b** = 4:1). Treatment of cyclamphosphorane with $MClCp(CO)_3$ (M = Mo, W) followed by chloride abstractions by $NaBPh_4$ yielded cationic complexes **1.13** (M = Mo) and **1.14** (M = W), respectively. Deprotonation of the amines in **1.13** and **1.14** by methyllithium results in intramolecular nucleophilic attack to phosphorus, forming metallophosphoranes **1.15** (M = Mo) and **1.16** (M = W), respectively. The crystal structure of **1.15** shows a distorted trigonal bipyramidal structure around the phosphorus center with a $\eta^2$-P,N coordination mode of the ligand ($d_{Mo-P}$ = 2.444 Å).

**Scheme 1-4.** Synthesis of cyclammetallophosphoranes by Riess.

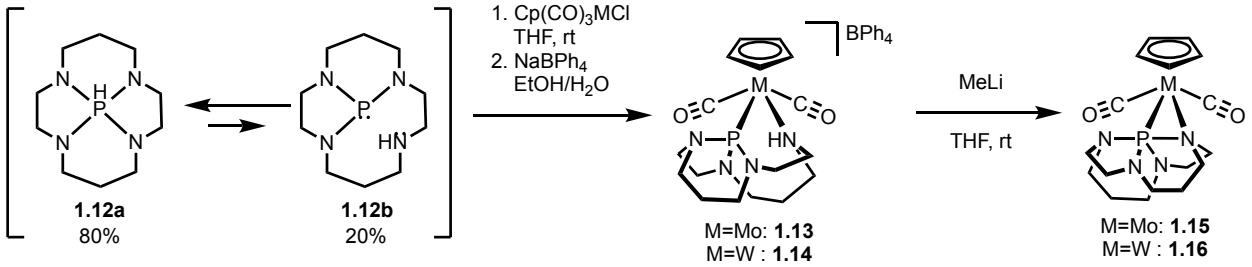


Lattman and co-workers prepared a series of metallophosphoranes derived from cyclenphosphorane (**1.17a**). Despite the structural similarity, the synthesis of metallophosphoranes with **1.17a** was performed with a different approach from the cyclamphosphorane systems of Riess. Due to its smaller ring size compared to cyclamphosphorane, the polycyclic closed form of

cyclenphosphorane (**1.17a**) is so stable that the corresponding open tautomer form (**1.17b**) is not observed.

**Scheme 1-5**. Synthesis of cyclenmetallophosphoranes by Lattman.

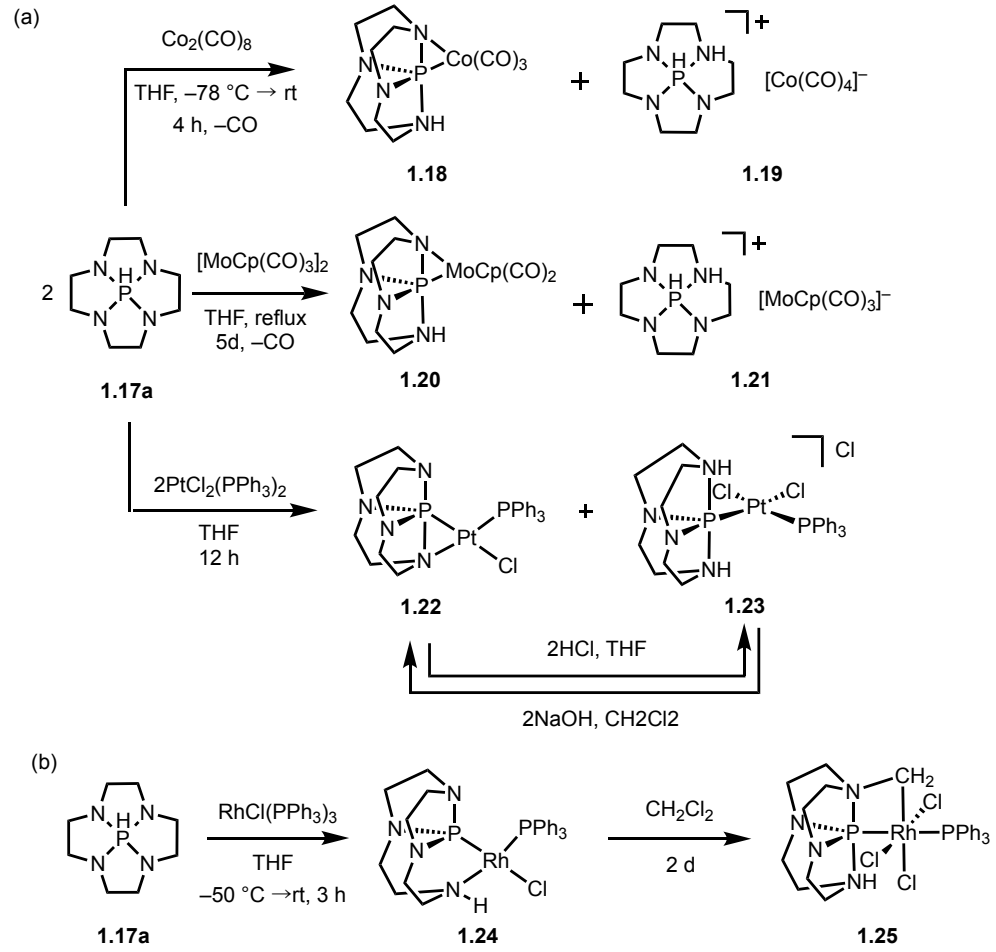


Upon metalation of **1.17a** with metal fragments, a P–N bond cleavage occurs much less frequently and the reactions directly yields $\eta^2$-(P,N)-metallophosphoranes, in which an amine without deprotonation coordinates to the P center (Scheme 1-5a). Treatment of **1.17a** with in THF at –78 °C yields a 1:1 mixture of metallophosphorane **1.18** and an ionic product **1.19**.[44-46] Similar reactivity was observed in the reaction of **1.17a** with $[MoCp(CO)_3]_2$ in THF under reflux to afford a mixture of metallophosphorane **1.20** and ionic product **1.21**. A reaction of **6a** with a similar

platinum precursor $PtCl_2(PPh_3)_2$ yields totally different products from the previous Rh case.[47,48] Complexes **1.23** and **1.24** can be reversibly interconverted by acid/base reactions using HCl and NaOH. Gavrilov and Bondarev reported similar syntheses of Group 9 and Group 10 metallophosphoranes with three metallacycles.[49-54]

One particularly notable reactivity of cyclenphosphorane-based metallophosphoranes reported by Lattman is treatment of **1.17a** with Wilkinson's catalyst, which yields Rh(I) complex **1.24** via a P–N bond cleavage.[55] Complex **1.24** undergoes an unusual oxidative addition of dichloromethane to form a Rh(III) complex **1.25** (Scheme 1-5b). For a reaction mechanism, the authors suggested an initial oxidative addition of dichloromethane forms a $CH_2Cl$–Rh–Cl moiety and the nucleophilic axial nitrogen atom of cyclenphosphorane attacks the carbon to initiate migration of $Cl^-$ to Rh.

*1-4-4. Spirocyclic metallophosphoranes synthesized by external nucleophilic attack (Nakazawa and Miyoshi)*

**Scheme 1-6.** (a) Syntheses of metallophosphoranes by nucleophilic attack to $CpFe(CO)_2(PR_3)PF_6$ complexes and (b) proposed reaction mechanism by Nakazawa and Miyoshi.

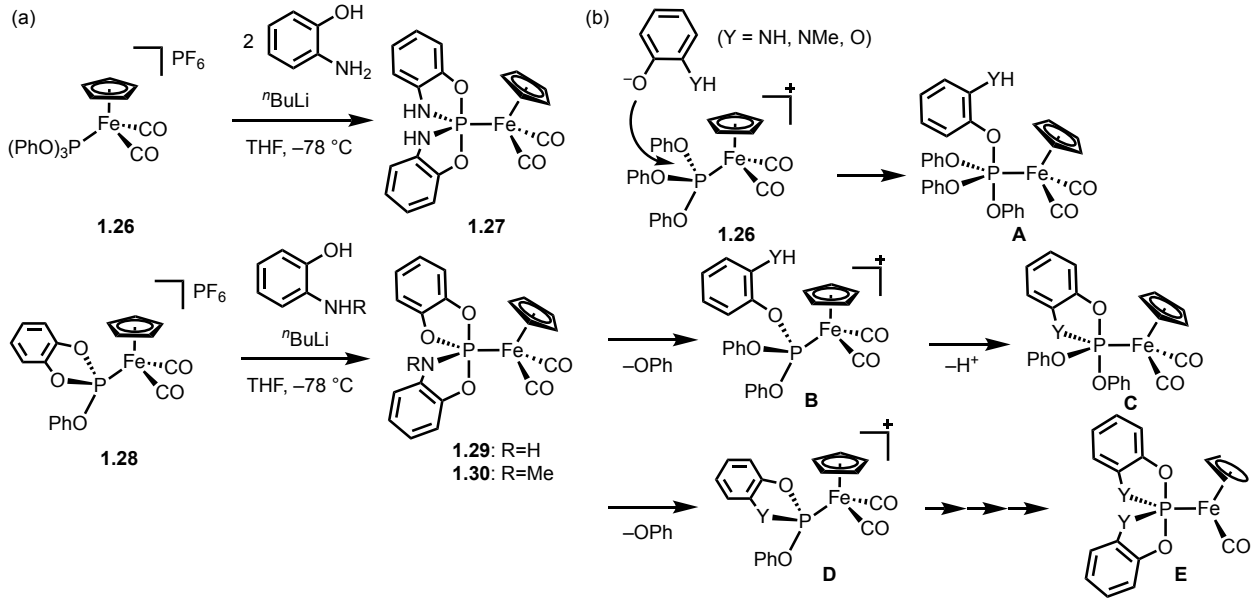


Nakazawa, Miyoshi and co-workers established a novel synthetic method of generating metallophosphoranes via nucleophilic attack to ($\sigma^3$-P)–M complexes (Scheme 1-1(b)). Treatment of $[Cp(CO)_2FeP(OPh)_3]PF_6$ (**1.26**) with 2-aminophenol (2 equiv.) and butyllithium (1 equiv.) afforded metallophosphorane **1.27**. (Scheme 1-6a).[56] Although phosphorane ligands containing nitrogen substituents often exhibit $\eta^2$-P,N–coordination to the metal, the $\kappa^1$-*P*-metallophosphorane is exclusively formed in this reaction. The authors explained this by the high rotational barrier around phosphorus; the $Cp(CO)_2Fe$ moiety, whose electron-donor ability stabilizes 3c-4e bonding by donating electrons to vacant antibonding orbital, is equatophilic while the electronegative oxygen atoms are apicophilic, leaving the nitrogen substituents too distal to engage in an $\eta^2$ coordination mode. Treatment of $[CpFe(CO)_2\{P(OC_6H_4O)(OPh)\}]PF_6$ (**1.28**) with *o*-

$HOC_6H_4NHR$ (1 equiv.) in the presence of butyllithium yielded metallophosphoranes $CpFe(CO)_2\{P(OC_6H_4O)(OC_6H_4NR)\}$ (**1.29**: R = H, **1.30**: R = Me).

Interestingly, the desired iron phosphorane complexes were not obtained when one of the CO ligands of **1.26** was substituted with phosphines or phosphites. The authors explained that the replacement of CO (π-acceptor) makes the P atom of $P(OPh)_3$ too electron-rich to be susceptible to nucleophilic attack. It is notable that the nucleophilic attack is always observed at phosphorus and never at the CO ligands. Based on the results the authors proposed a mechanism for the metallophosphorane formation. The reaction is initiated by a nucleophilic attack of phenoxide moiety to the tricoordinate phosphorus ligand of **1.26**. The resulting metallophosphorane **A** undergoes the dissociation of to recover metal–phosphine type complex **B**. Then a deprotonation of the YH moiety is followed by its nucleophilic attack to the P center, resulting metallophosphorane **C**. Another dissociation of phenoxide leads to metal–phosphine complex **D**. The second substrate reacts with the P center similarly to the process from **1.26** to **D** to form the final metallophosphorane product (Scheme 1-6b).

*1-4-5. Metalophosphorane syntheses by external nucleophilic attack (Lattman and Anand)*

Similar spirocyclic metallophosphorane with a bis(catechol)phosphoranide ligand was synthesized by Lattman and co-workers.[57, 58] Treatment of chlorophosphorane (**1.31**) with $Na[Mn(CO)_5]$ yielded metallophosphorane $(cat_2P)Mn(CO)_5$ (**1.32**, cat = *o*-$C_6H_4O_2$) (Scheme 1-7a). Complex **1.32** represents the first example of a metal undergoing nucleophilic substitution of a chlorophosphorane to give an $\eta^1$-metallophosphorane (Scheme 1-1(c)). Exposure of metallophosphorane **1.32** to air results in hydrolysis of two P–O bonds of different catechol

equivalents, yielding metal–phosphoryl complex **1.33**.[59, 60] Treatment of chlorophosphorane **1.31** with Na[Co(CO)$_3$(PPh$_3$)] in THF at –78 °C affords metallophosphorane **1.32**. Further dissociation of catechol occurs in THF solution to yield complex **1.34**. Cobalt-based metallophosphorane **1.35** was also synthesized by nucleophilic substitution reaction of **1.31**.[61]

**Scheme 1-7**. Synthesis of metallophosphoranes by nucleophilic substitution of phosphorane reported by (a) Lattman and (b) Anand.

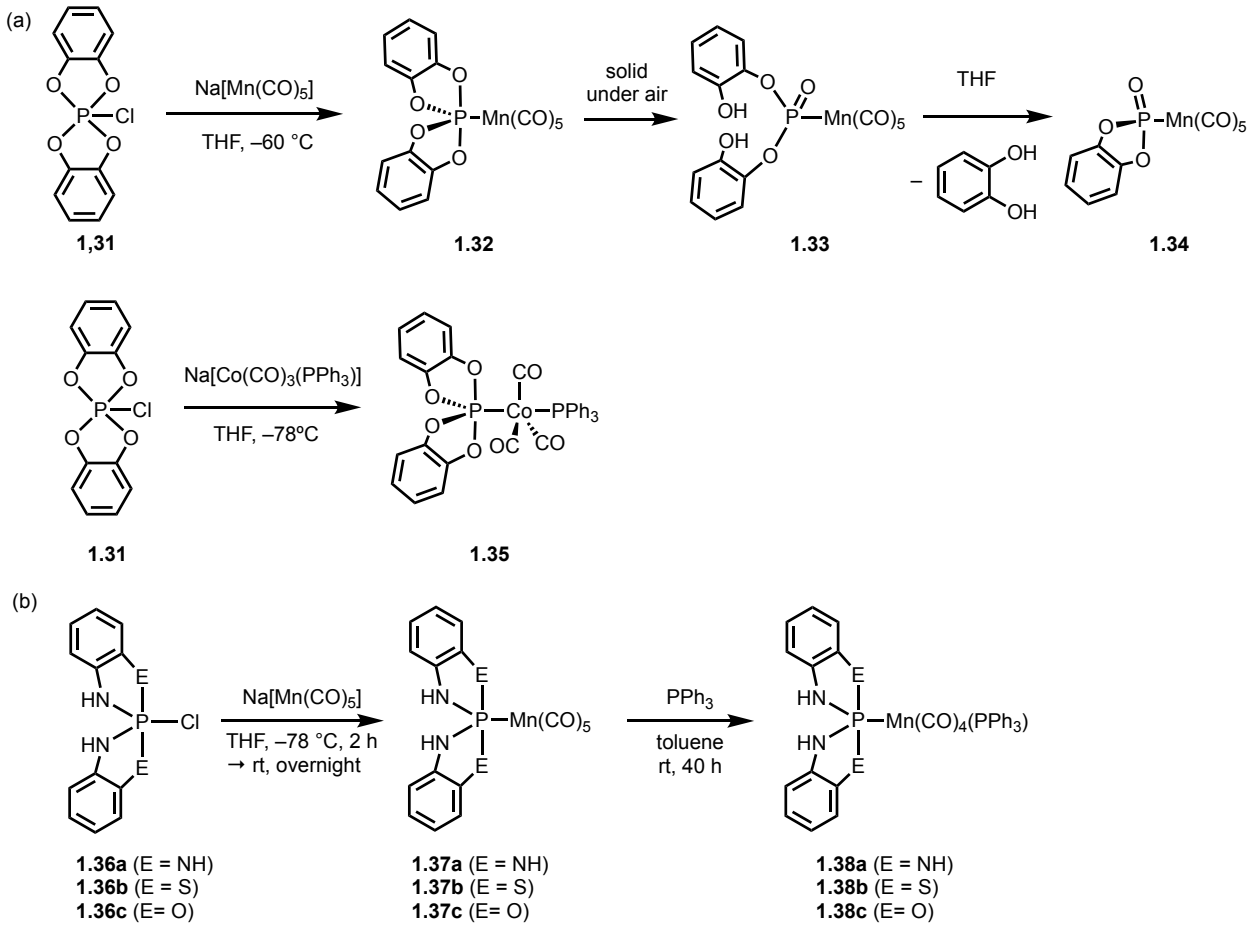


Anand and co-workers used this strategy to access metallophosphoranes **1.37a–1.37c** starting from spirocyclic chlorophosphoranes **1.36a-c** and Na[Mn(CO)$_5$] (Scheme 1-7b).[62] Reactions of

the metallophosphoranes **1.37a**-**1.37c** with $PPh_3$ gave $Mn(CO)_4(PPh_3)$ complexes **1.38a**-**1.38c** with loss of a carbonyl ligand, showing the robustness of M–P bonds in the metallophosphoranes. The authors also reported synthesis of spirocyclic metallophosphoranes with different P-substituents[63, 64]

*1-4-6. Migration of naphthyl group from P to M (Miyamoto)*

**Scheme 1-8**. Synthesis of iridium spirophosphorane and migration of naphthyl group from P to Ir

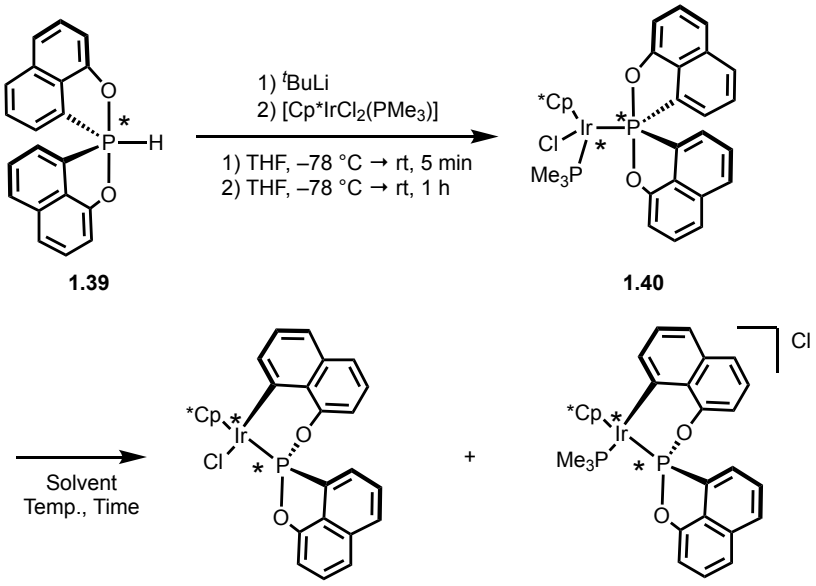


| Solvent | Temp./°C | Time/h | Yield (*RR* or *SS* : *RS* or *SR*) **1.41a** | **1.41b** |
|---|---|---|---|---|
| xylene | 150 | 8 | 97% (<1:>99) | 0% |
| EtOH | 80 | 3 | 0% | 60% (84:16) |
| PhCN | 190 | 3 | 41% (<1:>99) | 36% (50:50) |

Miyamoto and co-workers investigated the use of a napthol-based spirophosphoranide as a ligand for late transition metals. Spirophosphorane **1.39**, which was synthesized from 8-lithio-1-naphthoxy lithium and phosphorus trichloride followed by protonation, was deprotonated with *tert*-butyllithium and treated with metal fragments to afford various metallophosphoranes by

substitution of halide ligands (Scheme 1-1(d)). [65-68] Particulary interesting example is Ir(III) metallophosphorane **1.40**, synthesized from a reaction of spirophosphorane **1.39** and [Cp*$IrCl_2(PMe_3)$] (Scheme 1-8). Although complex **1.40** is stable in chloroform, THF or acetonitrile under reflux condition, the decomposition proceeds upon heating in xylene, ethanol, and benzonitrile, giving rise to P–C bond cleavage of the naphthyl group. Riess reported a similar migration of phenyl and allyl groups from Fe to P (Scheme 1-3). Upon migration, $PMe_3$ or a chloride ligand dissociated to afford either a neutral or cationic product (**1.41a, 1.41b**), whose ratio depends on the solvent and temperature. Proposed key intermediates in this process are oxygen/carbon apical phosphoranides generated through the dissociation of $PMe_3$ or $Cl^-$ ligand and Berry pseudorotation (Chart 1-1). Cleavage of the apical P–C bond and a 1,2-sigmatropic shift gives the migration products.

**Chart 1-1.** Proposed intermediates for migration of naphthyl group from P to Ir.

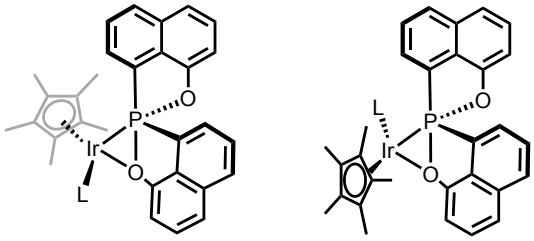


*1-4-7. Other spirophosphorane syntheses by nucleophilic substitution by deprotonated phosphoranes*

Nucleophilic substitution by deprotonated phosphoranes (Scheme 1-1(d)) has been the most used method to synthesize spirophosphoranes recently. Montgomery and co-workers reported group 9 and 10 transition metal complexes with various types of $\sigma^4$-P ligands[69-73]. Martin [74, 75] and

Akiba [76, 77] independently reported syntheses and reactivity of metallophosphoranes derive from $Rf_2PH$ (Rf = *o*-$C_6H_4C(CF_3)_2O$).

*1-4-8. Recent unexpected formation of macrocyclic metallophosphoranes (Jones and Chirik)*

**Scheme 1-9.** Formation of macrocyclic metallophosphoranes from pincer complexes

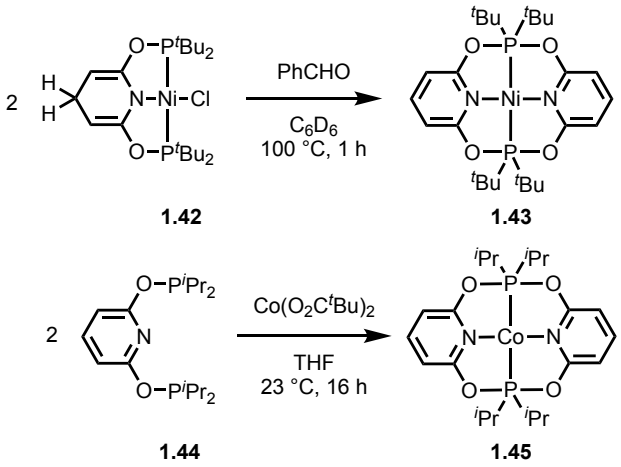


Jones and co-workers treated Ni(II)–PNP pincer complex **1.42** with benzaldehyde at 100 °C to obtain an unusual PNPN macrocycle complex **1.43** with formation of some uncharacterized paramagnetic byproducts (Scheme 1-9).[78] Independently, Chirik and co-workers treated tridentate ligand $^{iPr}$PONOP (**1.44**) with anhydrous cobalt pivalate at room temperature yielded a paramagnetic complex **1.34** with two pentacoordinate P centers, instead of the anticipated product of ($^{iPr}$PONOP)Co(O$_2$C$^t$Bu)$_2$. [79] The authors could not isolate or characterize the product containing the remainder of one $^{iPr}$PONOP ligand. Obtained crystal structures of **1.43** and **1.45** both showed planar PNPN macrocycle structures and the electronegative oxygen atoms taking apical positions of the trigonal bipyramid phosphorus. The geometry around the pentacoordinate phosphorus centers of **1.43** are close to trigonal bipyramid. The mechanisms of these reactions and the roles of PhCHO and carboxylate ligands remain unknown.

*1-4-9. Six-coordinate phosphorus ligand (Wagler)*

Wagler has reported an interesting stepwise increase in the coordination number of a phosphorus ligand (Scheme 1-10).[80] A reaction of bis(pyridonate) complex $Ru(OPy)_2(nbd)$ (**1.46**) (OPy = 2-pyridonate) with tricoordinate phosphorus ligand $PPh(OPy)_2$ led to substitution of nbd accompanied by insertion of the P(III) center into the Ru–O bond to give metallophosphorane **1.47**. Treatment of **1.47** with carbon monoxide induced an rearrangement of the $\kappa^2$-pyridonate to form another P–O bond and affords complex **1.48** with a hexacoordinate phosphorus center.

**Scheme 1-10.** Stepwise increase of P-coordination number to hexacoordinate P ligand.

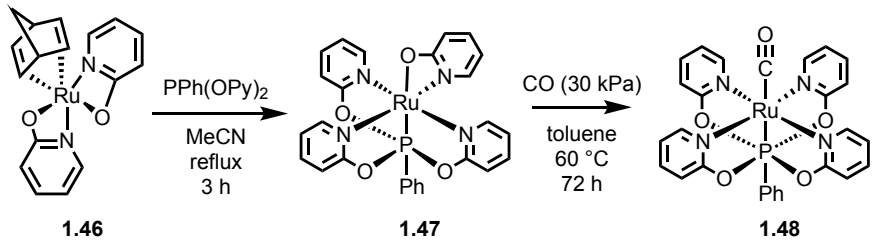


**1.46** **1.47** **1.48**

*1-4-10. P-centered oxidative addition to ($\sigma^2$-P)-M complexes (Ebsworth)*

Different from all of the examples above, Ebsworth reported syntheses of metallophosphoranes from lower-coordinate phosphorus complexes by oxidative addition of fluorine or chlorine. A reaction of $Ir(CO)Cl_2(PEt_3)_2PCl_2$ (**1.49**) with $Cl_2$ yielded tetrachlorophosphorane complex $Ir(CO)Cl_2(PEt_3)_2(PCl_4)$ (**1.50**) (Scheme 1-11).[81] The identity of **1.50** was further supported by reactivity studies; a reaction of **1.50** with $PEt_3$ in dichloromethane recovers complex **1.49** with formation of $Et_3PCl_2$ and reaction with $Ir(CO)Cl(PEt_3)_2$ gives **1.49** and $Ir(CO)Cl_3(PEt_3)_2$.

**Scheme 1-11.** Synthesis of iridium metallophosphoranes with halide substituents.

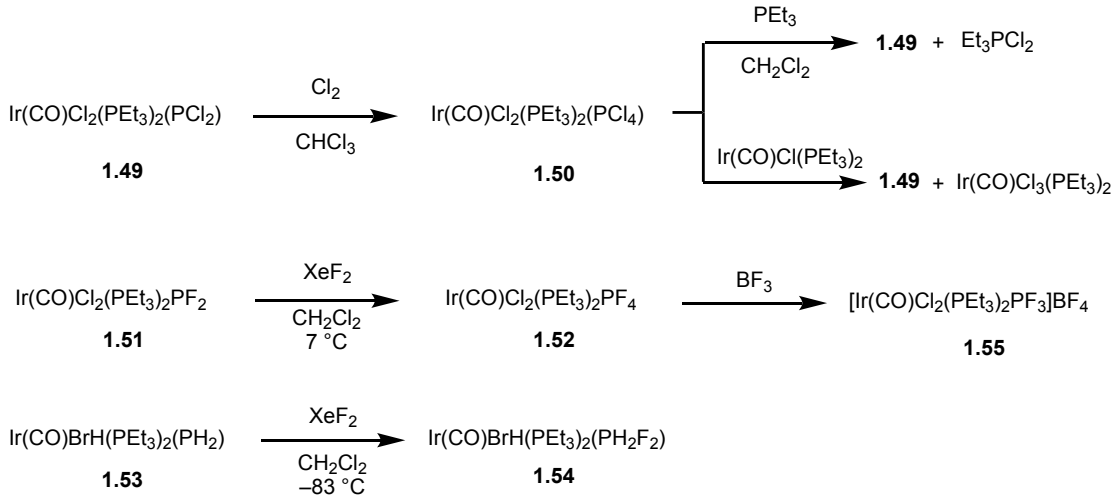


A fluorine analogue of compound **1.50** was similarly prepared. A reaction of $Ir(CO)Cl_2(PEt_3)_2(PF_2)$ (**1.51**) with $XeF_2$ yields metallofluorophosphorane $Ir(CO)Cl_2(PEt_3)_2(PF_4)$ (**1.52**). [82] Complex **1.52** is the sole example of structurally characterized acyclic metallophosphorane. [83] A reaction of $PH_2$ complex **1.53** with $XeF_2$ at –83°C yielded metallophosphorane **1.54** with $PH_2F_2$ ligand, which is not stable above –63°C. Treatment of **1.52** with $BF_3$ led to fluoride abstraction from the $PF_4$ ligand to give salt **1.55**.

The authors also reported preparations of Pt metallophosphoranes with halogen substituents (Scheme 1-12). Treatment of $PtCl(PEt_3)_2(PCl_2)$ (**1.56**) with $XeF_2$ yielded metallofluorophosphorane **1.57**. A reaction of *trans*-$PtHCl(PEt_3)_2$ (**1.58**) and equimolar amount of $PCl_3$ in $CH_2Cl_2$ yields metallophosphorane *trans*-$PtCl(PEt_3)_2(PH_2Cl_2)$ (**1.59)** alongside metal-phosphine complexes *cis*-$PtCl_2(PEt_3)_2$ (**1.60**) and *trans*-$PtCl_2(PEt_3)_2$ (**1.61**). Treatment of *trans*-$PtHBr(PEt_3)_2$ (**1.62**) with $PBr_3$ in $CH_2Cl_2$ yields a mixture of complexes: metallophosphorane *trans*-$PtBr(PEt_3)_2(PH_2Br_2)$ (**1.63)**, *cis*-$PtBr_2(PEt_3)_2$ (**1.64**) and *trans*-$PtBr_2(PEt_3)_2$ (**1.65**). Complexes **1.59** and **1.63** are rare examples of metallophosphoranes containing P–H bonds. Due

to the lack of isolated products, however, the authors noted that they could not completely exclude the possibilities that the products are anionic six-coordinate phosphorus species $[PtX(PEt_3)_2(PH_2X_3)]^-$.

**Scheme 1-12.** Synthesis of platinum metallophosphoranes with halide substituents

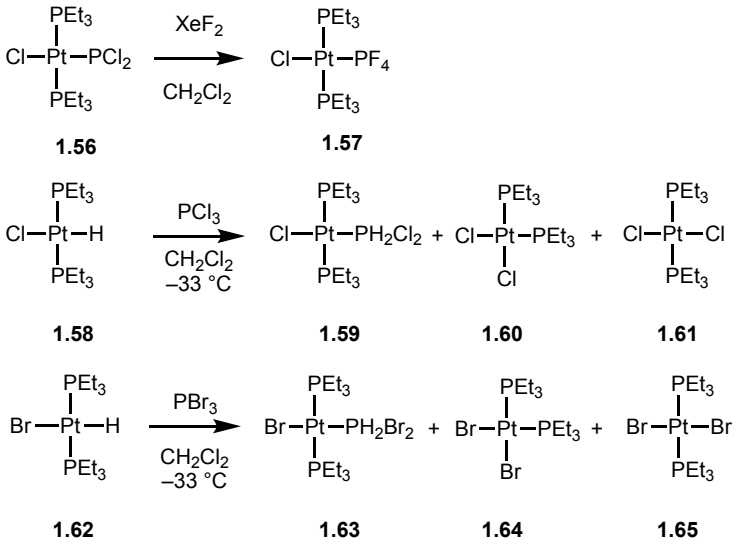

## 1-5. Proposed 'Nonspectator' Reactivities of $PR_3$ Ligands through Higher Coordinate Phosphorus Ligands

### *1-5-1. Electrophilic reactivity of $PR_3$ ligand in transition metal complexes*

Most of the tricoordinate phosphorus ligands do not exhibit electrophilic properties, making them 'spectator' ligands in transition metal complexes. In contrast, there have been quite a few reports of 'nonspectator' reactivities of $\sigma^3$-P ligands, in which addition of internal or external groups to the P center yields higher-coordinate phosphorus intermediates. We will review such metallophosphorane intermediates in various proposed reactions mechanisms.

### *1-5-2. Phosphine-assisted reduction of Pd(II) complexes*

**Scheme 1-13.** (a) Fluoride-induced reduction of $PdCl_2$ reported by Verkade and Mason and (b) proposed mechanism through metallophosphorane intermediate.

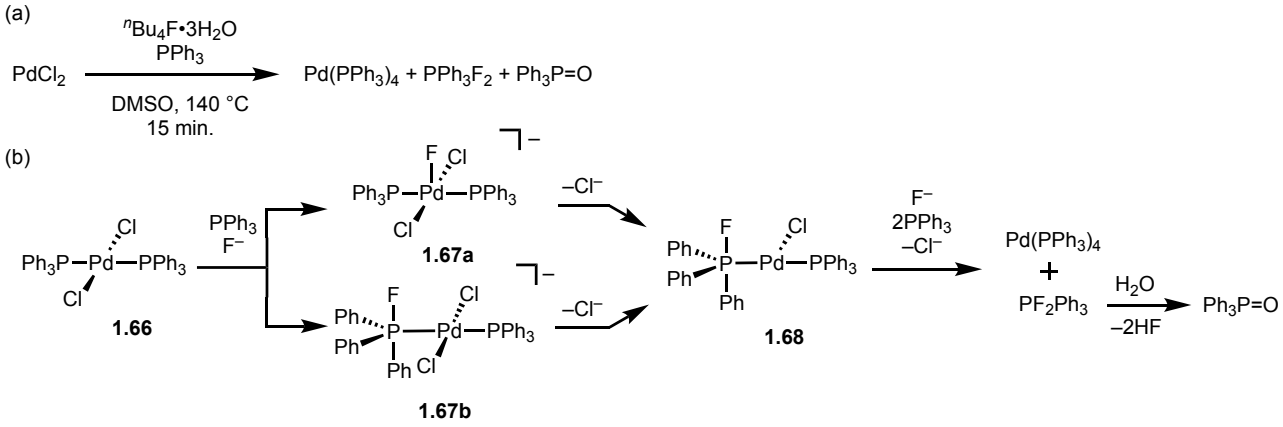


Verkade and Mason proposed metallofluorophosphorane intermediates in fluoride-induced reduction of Pd(II) phosphine complexes to Pd(0) species. (Scheme 1-13).[84-86] Addition of $^n$Bu$_4$F·3H$_2$O (2.5 eq.) and excess triphenylphosphine to a solution of $PdCl_2$ led to the formation of $Pd(PPh_3)_4$ with byproducts of $R_3PF_2$ and $R_3P$=O. The proposed mechanism is shown; nucleophilic attack of $F^-$ to *in-situ* generated Pd(II) complex $PdCl_2(PPh_3)_2$ (**1.66**) yields anionic complexes

$PdCl_2F(PPh_3)_2$ (**1.67a**) or $PdCl_2(PFPh_3)(PPh_3)$ (**1.67b**), followed by $Cl^-$ dissociation to give metallophosphorane $PdCl(PFPh_3)(PPh_3)$ (**1.68**). Another P–F bond formation is accompanied by the transfer of two electrons from Pd to P to give $Pd(PPh_3)_4$ and difluorophosphorane $PF_2Ph_3$, which is transformed into $Ph_3P{=}O$ by hydrolysis. Similar reactivity is observed when other monodentate or bidentate phosphines ($PPh_2Me$, dppm, dppe, dppp, dppb) are used instead of triphenylphosphine.

**Scheme 1-14**. (a) Pd dimer formation reported by Grushin and Alper and (b) reaction mechanism proposed by MacGregor.

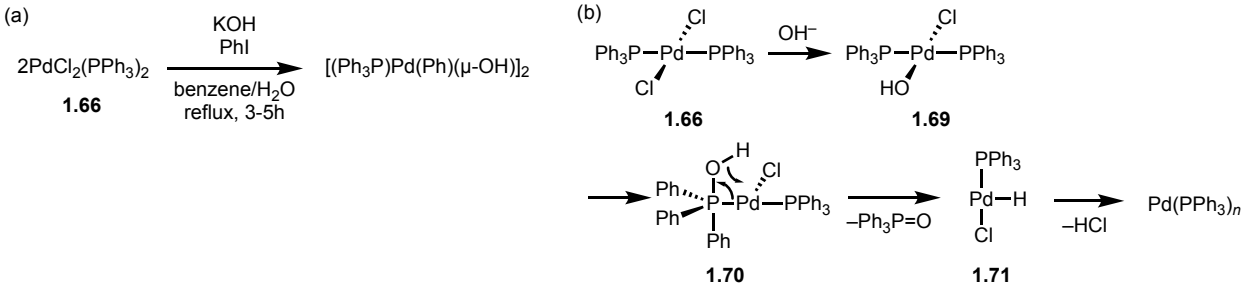


Grushin and Alper reported similar hydroxide-induced reduction of $PdCl_2(PPh_3)_2$ (**1.66**) to Pd(0) species. (Scheme 1-14a).[87] Treatment of **1.66** with $OH^-$ in the presence of iodobenzene gives triphenylphosphine oxide and Pd(II) dimer $[(Ph_3P)_2PdPh(\mu\text{-}OH)]_2$. Although they suggested a mechanism without a metallophosphorane intermediate in the initial report, MacGregor later proposed another mechanism with metallophosphorane formation. (Scheme 1-14b).[88] In the mechanism, **1.69** undergoes M–OH formation followed by the intramolecular migration of $OH^-$ from Pd to P to form metallophosphorane $PdCl\{P(OH)Ph_3\}(PPh_3)$ (**1.70**). Dissociation of $Ph_3P{=}O$ yields complex $PdHCl(PPh_3)$ (**1.71**) with a Pd–H bond and reductive elimination of HCl affords the Pd(0) species, which undergoes oxidative addition of PhI to give the final palladium dimer.

*1-5-3. Migratory insertion of CO into Pt–OMe bond*

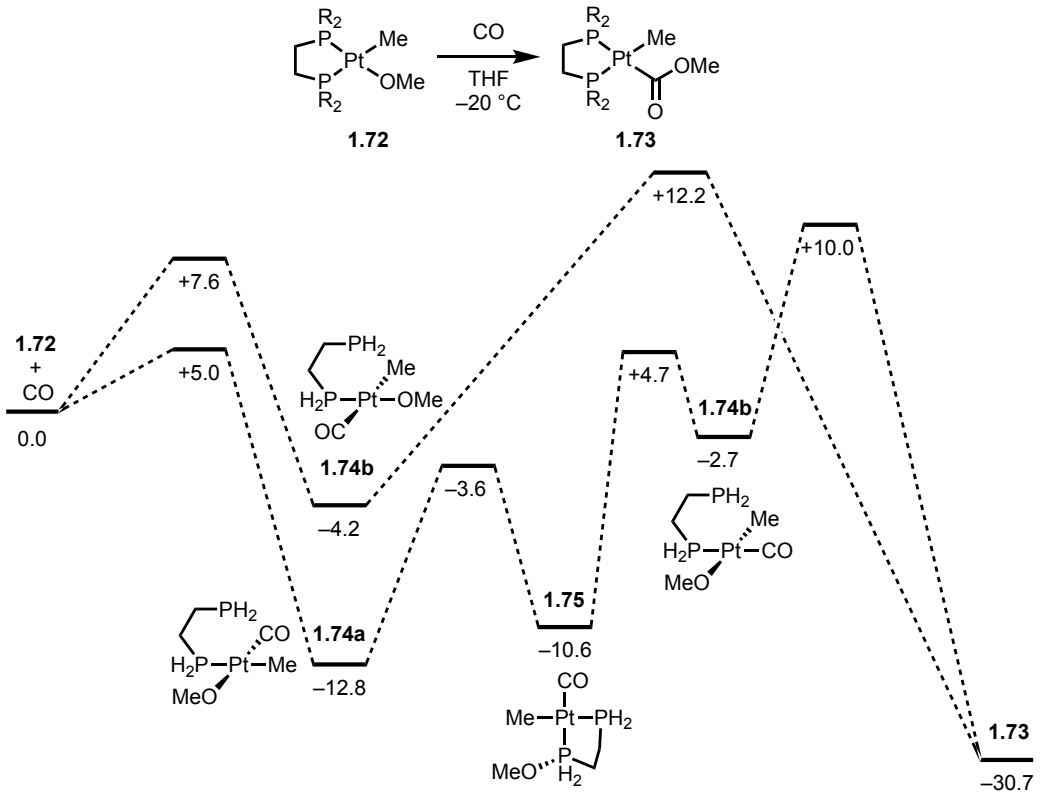


**Figure 1-5.** (a) CO insertion into the Pt–OMe bond of **1.72** and (b) computed reaction free energies by MacGregor (units: kcal·mol$^{-1}$).

Whilst computationally modelling the migratory insertion of CO into Pt–OMe bonds, MacGregor and co-workers found a pathway involving metallophosphorane formation (Figure 1-5). [89] Initial reaction of CO with modeled starting complex PtMe(OMe)($PR_2CH_2CH_2PR_2$) (**1.72)** can give two isomers of PtMe(OMe)($\kappa^1$-$PH_2CH_2CH_2PH_2$) (**1.74a** and **1.74b**). Although the more stable isomer **1.74a** does not undergo CO insertion into the Pt–OMe bond to give final product PtMe(COOMe)($PR_2CH_2CH_2PR_2$) (**1.73**), the calculation revealed a pathway of isomerization from **1.74a** to a third isomer **1.74c** through metallophosphorane intermediate **1.75**. This pathway with metallophosphorane formation was assumed to be likely since a lower energy pathway was

suggested for insertion into the Pt–OMe bond of **1.74c** ($E$(TS) = +10.0 kcal·mol$^{-1}$) than into that of **1.74b** ($E$(TS) = +12.2 kcal·mol$^{-1}$).

### *1-5-4. M–C/X exchange reactions*

**Scheme 1-15**. (a) Me/Ph exchange and (b) proposed metallophosphorane intermediate reported by Swierczewski.

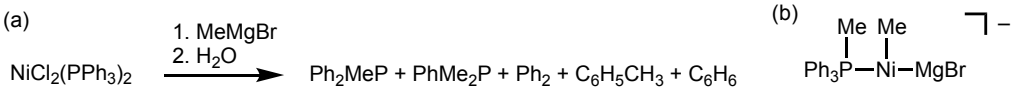


The first proposal of metallophosphorane was long before the first characterization of metallophosphorane. In 1971, Swierczewski and co-workers proposed the formation of metallophosphorane $Ph_3MeP$–Ni(Me)–MgBr as an intermediate in the reaction of $NiCl_2(PPh_3)_2$ and MeMgBr to form $PMePh_2$ and $PMe_2Ph$ via Me/Ph exchange. (Scheme 1-15).[90]

**Scheme 1-16**. (a) Ph/OR exchange reaction reported by Pregosin and (b) proposed reaction mechanism through metallophosphorane **1.79**.

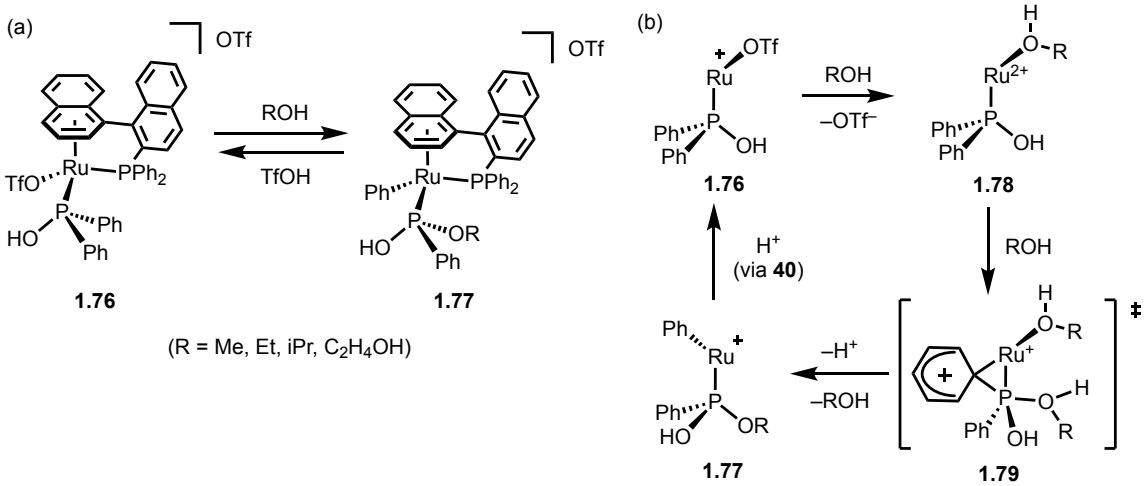

Pregosin and co-workers studied reversible Ph/OR exchange reactions between Ru–P bonds and proposed a metallophosphorane intermediate in the process. (Scheme 1-16).[91-93] Treatment of Ru complex **1.76** with several alcohols results in stereospecific formation of Ru–Ph complex **1.78**. The reaction of **1.77** with triflic acid to recover **1.76** also proceeds stereospecifically. They proposed a mechanism including a transition state involving a metallophosphorane to explain the observed stereospecific feature. Solvent substitution of **1.76** to form **1.78** and the following Ph migration is suggested to undergo through metallophosphorane transition state **1.79**; the pentacoordinate phosphorus center of **1.79** was formed by bridging a Ph group over the Ru–P bond with another alcohol attached to P, resulting in stereoinversion.

**Scheme 1-17.** (a) Rh–Ph/F exchange reaction and (b) proposed reaction mechanism reported by Grushin and Marshall. (c) Model reaction of Rh–Ph/F exchange computed by MacGregor.

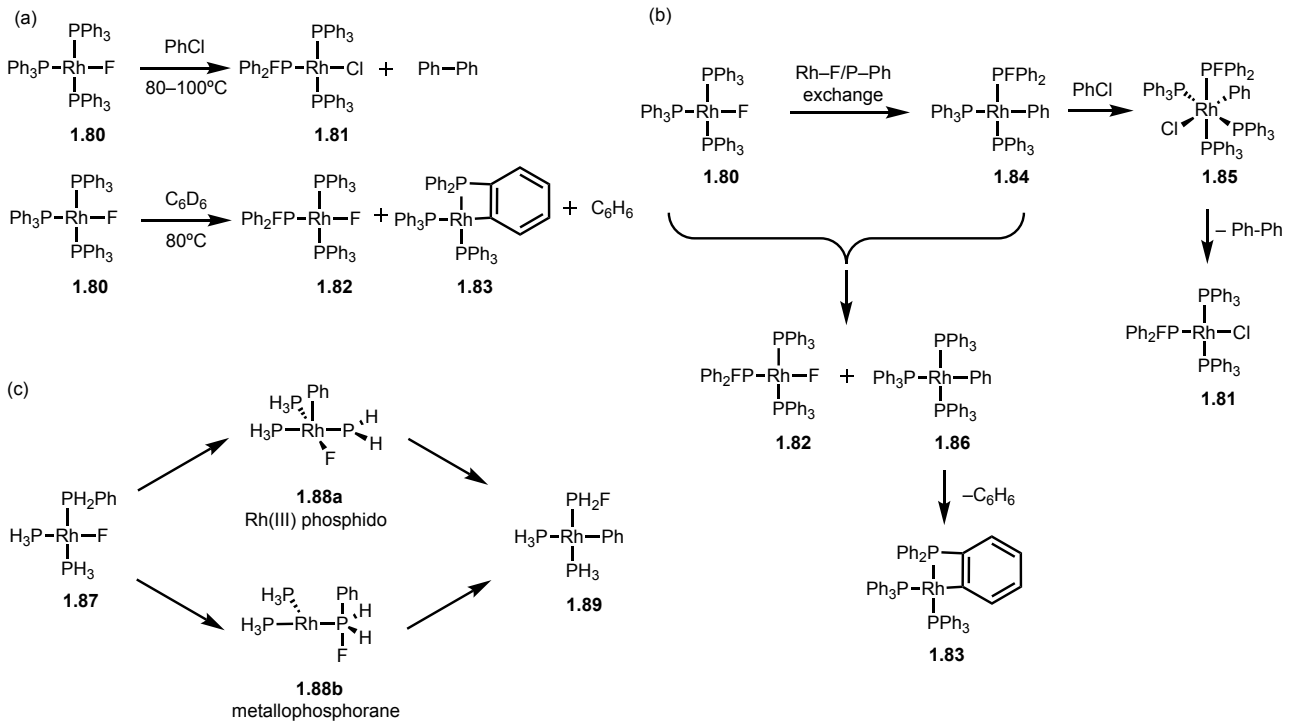


MacGregor and co-authors computationally suggested the formation of a metallophosphorane in the Rh–Ph/F exchange reaction reported by Grushin and Marshall. (Scheme 1-17). [94 - 96]

Treatment of $RhF(PPh_3)_3$ (**1.80**), the fluoride analogue of Wilkinson's catalyst, with chlorobenzene led to an unusual cleavage of the C–Cl bond accompanied by P–F bond formation to yield fluorophosphine complex *trans*-$RhCl(PFPh_2)(PPh_3)_2$ (**1.81**) and biphenyl. It was also found that the thermal decomposition of **1.80** in $C_6D_6$ at 80 °C affords a mixture of Rh complexes *trans*-$RhF(PFPh_2)(PPh_3)_2$ (**1.82**) and $Rh(PPh_3)_2\{PPh_2(C_6H_4)$-κ*C*,κ*P*$\}$ (**1.83**) in a 1:1 ratio. As shown in the proposed mechanism by Grushin, both reactions were suggested to involve a Rh–F/P–Ph exchange process to form $RhPh(PFPh_2)(PPh_3)_2$ (**1.84**). In the first reaction, oxidative addition of PhCl to **1.84** forms a hexacoordinate Rh(III) complex $RhClPh(PPh_3)_3(PFPh_2)$ (**1.85**), followed by a reductive elimination of biphenyl to yield **1.81** In the second reaction, intermolecular F/Ph exchange between **1.80** and **1.84** results in **1.82** and $RhPh(PPh_3)_3$ (**1.86**), the latter of which is converted to **1.83** via dissociation of benzene. To understand the mechanism of Rh–F/P–Ph exchange from **1.80** to **1.84**, MacGregor used model complex $RhF(PH_3)_2(PH_2Ph)$ (**1.87**) and characterized two reaction pathways through Rh(III) phosphido $RhPhF(PH_2)(PH_3)_2$ (**1.88a**) or metallophosphorane $Rh(PH_3)_2(PPhFH_2)$ (**1.88b**), respectively. The activation barrier of the metallophosphorane pathway (31.0 kcal·mol$^{-1}$) was ~5 kcal·mol$^{-1}$ lower than the Rh(III)-phosphide pathway (35.9 kcal·mol$^{-1}$), suggesting that the formation of metallophosphorane is more plausible in the process.

### *1-5-5. M–N/Cl exchange reactions*

Donahue and co-workers reported reactions of hexamethylphosphorus triamide with tungsten complexes and proposed the W–Cl/$NMe_2$ exchange process through metallophosphorane

intermediates.[97] Treatment of *trans*-$WCl_4(PMePh_2)_2$ with two equivalents of $P(NMe_2)_3$ produced ~15 % $WCl_3(NMe_2)(PMe_2Ph)_2$ (**1.87**) (Scheme 1-18).

**Scheme 1-18**. Proposed reaction mechanism for M–N/Cl exchange by Donahue.

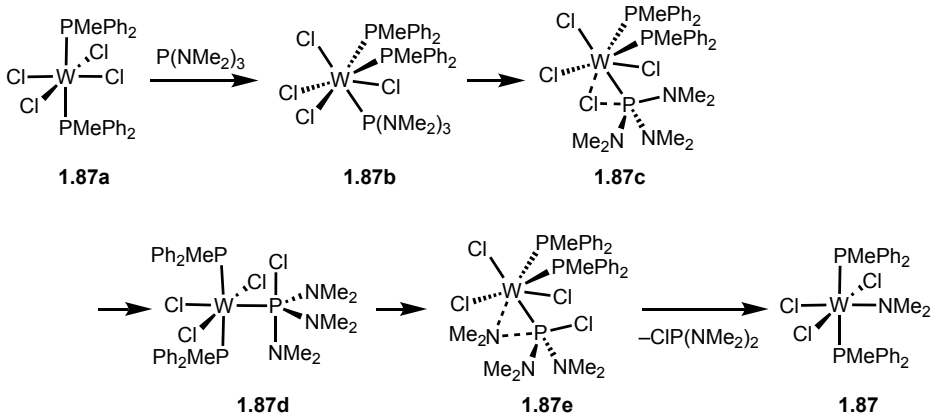


The authors proposed that the first step is the formation of a 7-coordinate complex (**1.87b**) from *trans*-$WCl_4(PMePh_2)_2$ (**1.87a**), followed by the migration of chloride from W to P through the transition state (**1.87c**) to form the metallophosphorane (**1.87d**). Then a migration of $NMe_2$ group from P to W through the transition state (**1.87e**) is accompanied by the dissociation of $ClP(NMe_2)_2$ to result the final product **1.87**.

### *1-5-6. Phosphine-assisted CF bond activation*

Metallofluorophosphorane intermediates have also been proposed as intermediates in C–F bond activation. Milstein and coworkers reported a reaction between $IrMe(PEt_3)_3$ (**1.88**) and $C_6F_6$ to yield *trans*-$Ir(PEt_3)_2(PFEt_2)(C_6F_5)$ (**1.89**) alongside methane and ethane. (Scheme 1-19a).[98] Using *trans*-$Ir(Me)(PH_3)_2(PH_2Et)$ (**1.90**) as a model complex, MacGregor computationally studied the mechanism of the C–F activation accompanied by M–F/P–R exchange (Scheme 1-19b).[99] In the suggested mechanism, a reaction between **1.90** and $C_6F_6$ initially forms encounter complex

**1.91**, which undergoes C–F bond cleavage via four-membered transition state **1.92** to yield metallophosphorane $IrMe(C_6F_5)(PH_2FEt)(PH_3)_2$ (**1.93**). Intramolecular Et migration from P to Ir affords $IrMeEt(C_6F_5)(PH_3)_2(PH_2F)$ (**1.94**) and following $\beta$-H elimination and reductive elimination, results in product *trans*-$Ir(C_6F_5)(PH_3)_2(PH_2F)$ (**1.95**) alongside $C_2H_4$ and $CH_4$.

**Scheme 1-19.** (a) Activation of hexafluorobenzene reported by Milstein and (b) Proposed reaction mechanism through metallophosphorane by MacGregor.

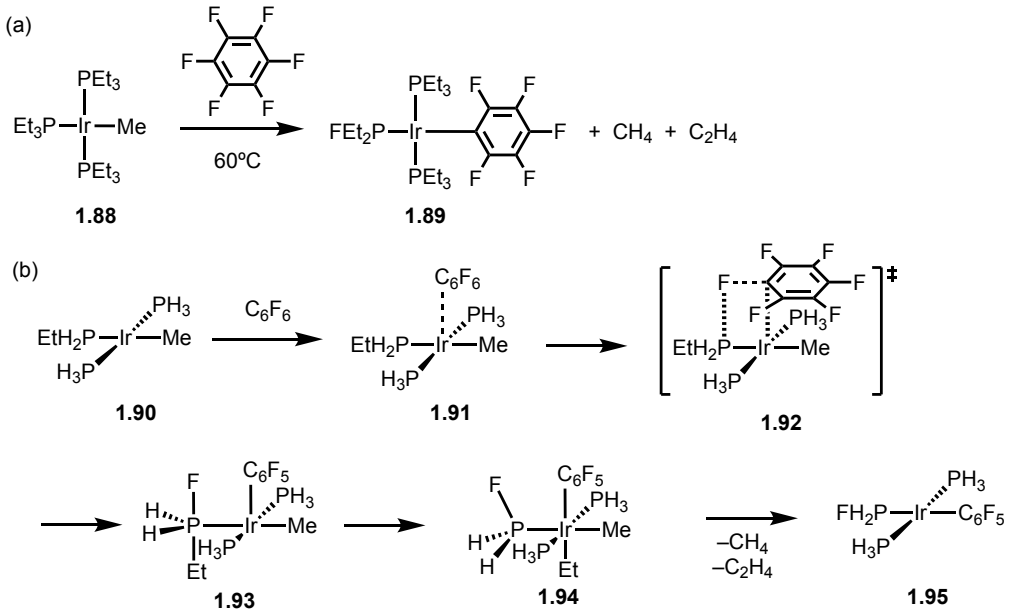


Perutz and coworkers reported similar activation of pentafluoropyridine by $Pt(PR_3)_2$ (**1.96**: R = Cy, **1.97**: R= $^i$Pr) to give $PtR(PR_3)(PFR_2)(C_5F_4N)$ (**1.98**: R = Cy, **1.99**: R= $^i$Pr),[100] and Grushin reported analogous $C_6F_6$ activation by **1.96** to yield $PtR(PCy_3)(PFCy_2)(C_6F_5)$ (**1.100**). Although these reactions can also be understood by a phosphine-assisted cooperative mechanism, computational studies of the first reaction with the model system of $Pt(PH_3)(PH_2Me)$ (**1.101**) showed more complicated features; whereas the lowest energy pathway to form $PtMe(PH_3)(PH_2F)(C_5F_4N)$ (**1.102**) involved cooperative 4-membered transition state **1.103**, the calculation suggested that metal-centered oxidative addition to give $PtF(PH_3)(PH_2Et)(C_5F_4N)$

(**1.104**) is also available.[101] In the latter case, encounter complex $Pt(PH_3)(PH_2Me)(\eta^2\text{-}C_5F_5N)$ (**1.105**) undergoes direct oxidative addition to yield *cis*-**1.104** or phosphine-assisted C–F activation to yield metallophosphorane $Pt(PH_3)(4\text{-}C_5F_4N)(PH_2FMe)$ (**1.106**), which is converted to *trans*-**1.104** via intramolecular $F^-$ transfer. Although the metal-centered oxidative addition was not experimentally observed for the reaction of **1.98** and **1.99** with pentafluoropyridine, reactions of **1.96** and **1.97** with 2,3,5-trifluoro-4-(trifluoromethyl)pyridine yield an oxidative addition product, suggesting there is a delicate balance between the phosphine-assisted C–F activation and metal-centered oxidative addition.

**Scheme 1-20.** (a) Activation of pentafluoropyridine reported by Perutz and (b) activation of hexafluorobenzene by Grushin. (c) Proposed reaction mechanism by MacGregor.

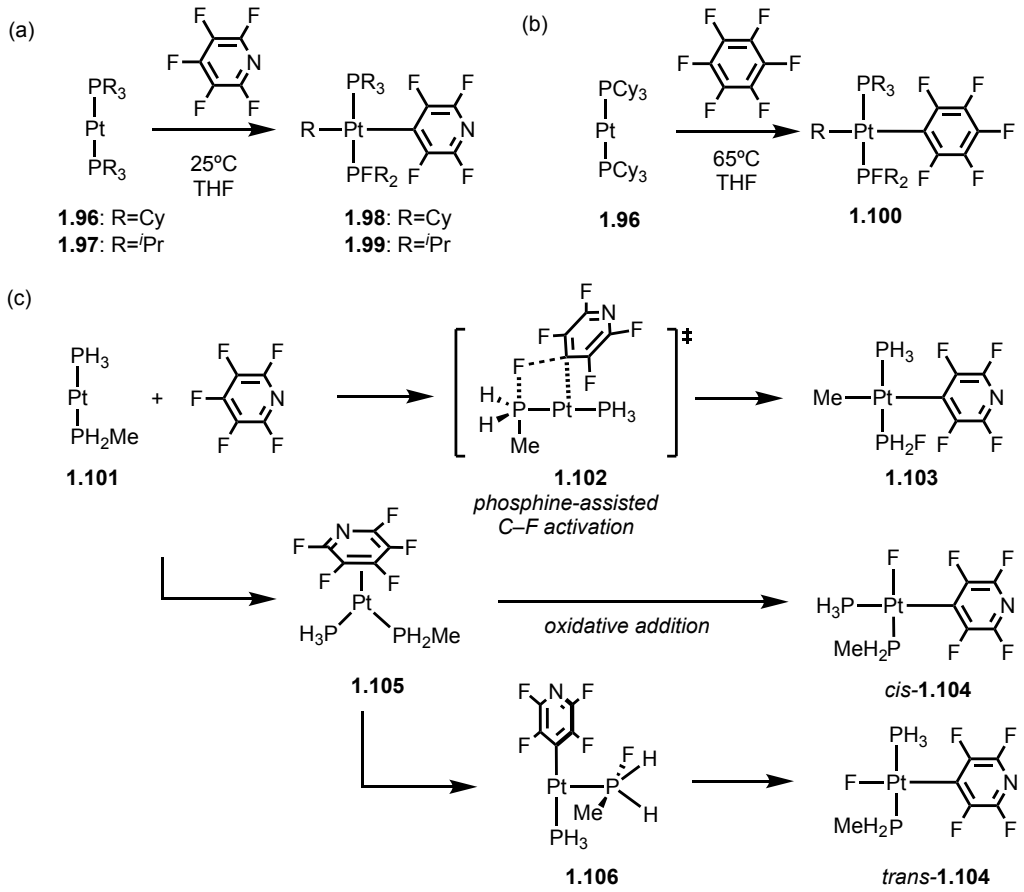

Perutz and coworkers also reported that the reaction of $Ni(cod)_2$ and pentafluoropyridine in the presence of $PEt_3$ yields *trans*-[$NiF(2\text{-}C_5F_4N)(PEt_3)_2$] as a major product. (Scheme 1-21).[102] Computational studies by McGrady and MacGregor explained the regioselectivity by the formation of a metallophosphorane.[103] In the suggested mechanism, initial reaction of model complex $Ni(PMe_3)_2$ (**1.107**) and pentafluoropyridine forms encounter complex **1.108** followed by phosphine-assisted C–F activation to give transient metallofluorophosphorane **1.109**. The stabilization of **1.109** by neighboring group assistance from the pyridyl nitrogen is the reason of the selective C–F activation at the 2-position. Fluoride migration to Ni affords the final product *trans*-$NiF(2\text{-}C_5F_4N)(PMe_3)_2$ (**1.110**).

**Scheme 1-21.** (a) Activation of pentafluoropyridine by $Ni(cod)_2$ in the presence of triethylphosphine and (b) proposed reaction mechanism.

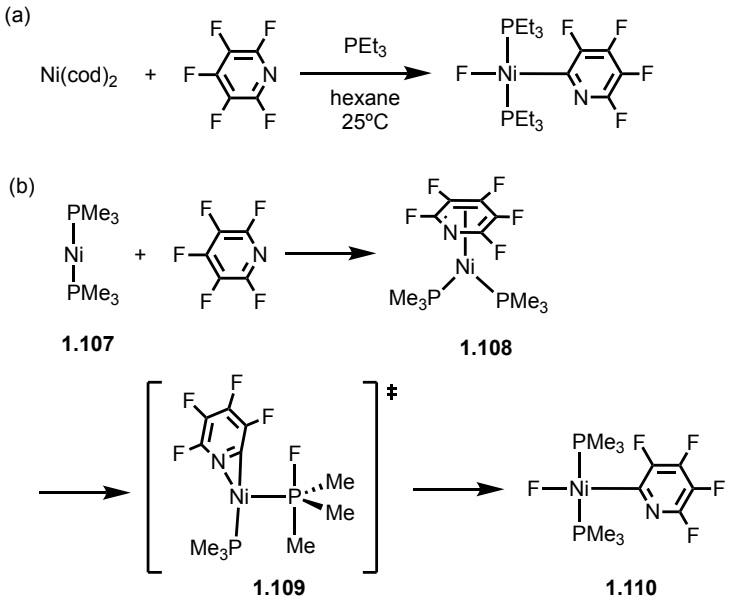

*1-5-7. P–C reductive elimination*

Metallophosphoranes have also been proposed as intermediates in P–C reductive elimination to give phosphonium species. In computationally studying the Ph–F reductive elimination from three-coordinate PdF(Ph)($PMe_3$) (Scheme 1-22), Yandulov found that migration of Ph from Pd to $PMe_3$ proceeds with a lower kinetic barrier than the reductive elimination.[104]

**Scheme 1-22.** Computed reaction energies of P–C reductive elimination from PdF(Ph)($PMe_3$) by Yandulov.

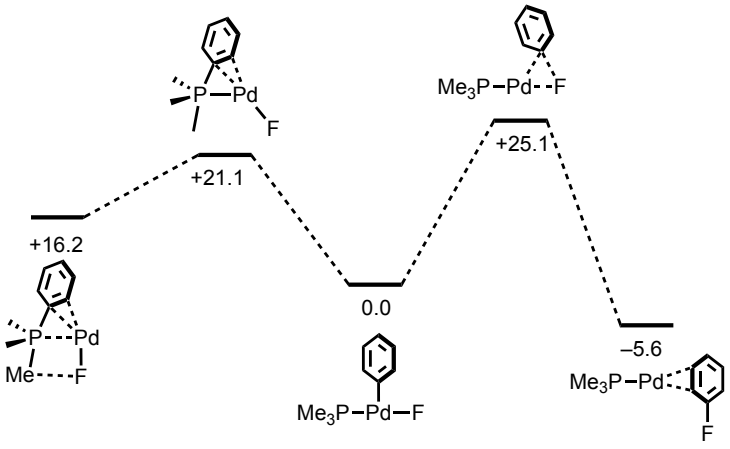


**Scheme 1-23**. (a) P–C reductive elimination of Pd allyl complex and (b) proposed reaction mechanism through metallophosphorane intermediate **1.114** reported by Ozawa.

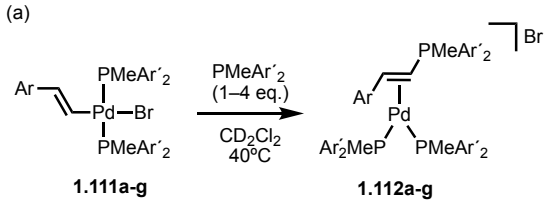


| | Ar | Ar´ |
|---|---|---|
| **1.111a** | Ph | Ph |
| **1.111b** | 4-$MeOC_6H_4$ | Ph |
| **1.111c** | 4-$MeC_6H_4$ | Ph |
| **1.111d** | 4-$F_3CC_6H_4$ | Ph |
| **1.111e** | 4-$O_2NC_6H_4$ | Ph |
| **1.111f** | 4-$O_2NC_6H_4$ | 4-$MeC_6H_4$ |
| **1.111g** | 4-$O_2NC_6H_4$ | 4-$FC_6H_4$ |

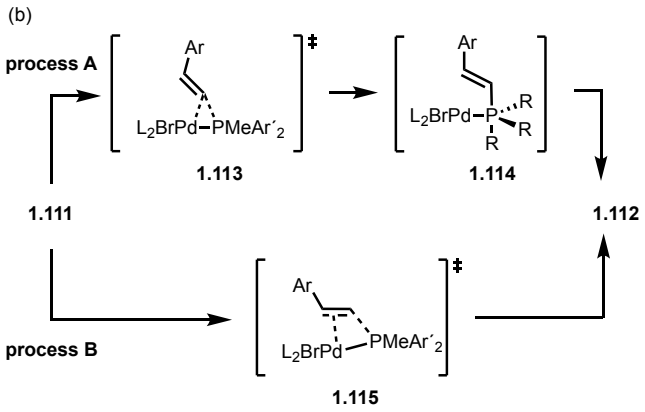


Ozawa reported P–C reductive elimination from styrylpalladium phosphine complexes *trans*-PdBr(CH=CHAr)(PMeAr´$_2$) (**1.111a-g**) in the presence of additional PMeAr´$_2$ to give [Pd($\eta^2$-

ArCH=CHPMeAr′$_2$)(PMeAr′$_2$)$_2$]Br (**1.112a-g**) (Scheme 1-23).[105] The authors proposed a mechanism with the metallophosphorane intermediate **1.114** (process A), which is more favorable than a direct reductive elimination of phosphonium from Pd(II) complex (process B) based on their kinetic studies (Scheme 1-23). The reductive elimination process is accelerated by electron-donating Ar′ and they attributed this to the stabilization of metallophosphorane intermediate **1.114**.

## 1-6. Enhanced Accessibility to Higher–Coordinate Phosphorus Species by Geometrically Constrained Nontrigonal Tricoordinate Phosphorus Compounds

*1-6-1. Electronic background of geometrical distortion on $\sigma^3$-P compounds*

Although the nonspectator reactivities we reviewed in the previous section all suggested the involvement of higher coordinate phosphorus ligands, these reaction intermediates are not stable enough to isolate or directly characterize.

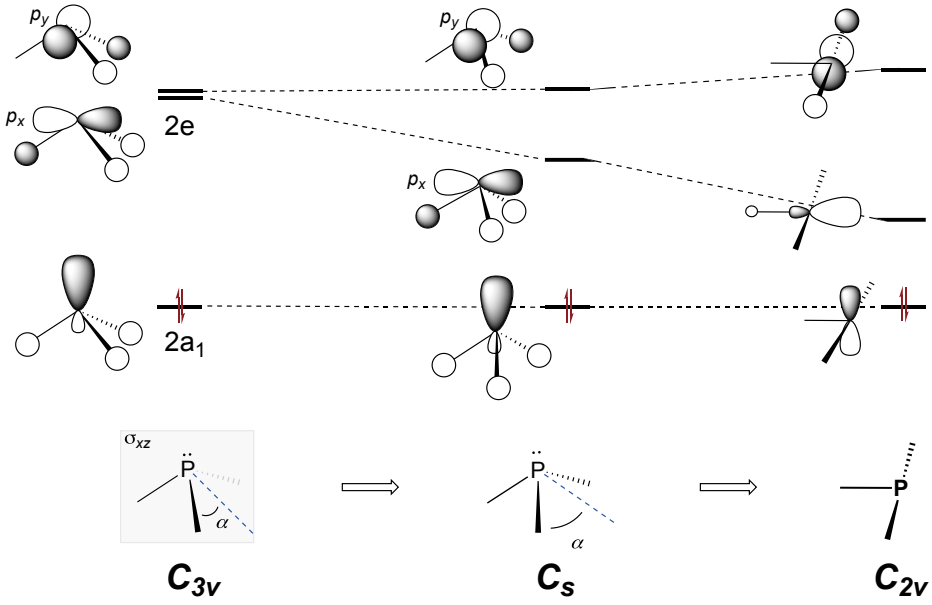


**Figure 1-6.** Qualitative depiction of the modulation of frontier orbital energies of $PR_3$ when its geometry changes from $C_{3v}$, $C_s$ to $C_{2v}$.

For improving an access to higher coordinate P compounds from $\sigma^3$–P compounds, quite a few research groups including us have utilized the application of nontrigonal geometrical deformation to the tricoordinate phosphorus ligands.[106-109] For instance, upon a distortion from its original trigonal pyramidal ($C_{3v}$) to T-shape ($C_{2v}$) by expanding an R–P–R bond angle, the energetic modulation of frontier orbital energies is qualitatively described in Figure 1-6. The $2a_1$ HOMO in

$C_{3v}$ symmetry gradually loses bonding interaction and becomes slightly higher in energy upon desymmetrization. On the other hand, one of the degenerated 2e LUMOs will be largely stabilized due to the decreasing antibonding interactions. As a result, the HOMO–LUMO energy gap significantly decreases in the $\sigma^3$-P compounds with lower symmetry, leading to higher reactivity. In particular, the enhanced electrophilicity enables the P atom to function as an accepter, thus increasing the P-coordination number. More quantitative discussion will be provided in Chapter 2, where we demonstrate the biphilicity of nontrigonal phosphorus triamides experimentally and computationally.

### *1-6-2. Oxidative addition at $\sigma^3$-phosphorus species*

**Scheme 1-24.** P(III)–P(V) equilibrium between macrocyclic tetra-aza-phosphorus compounds

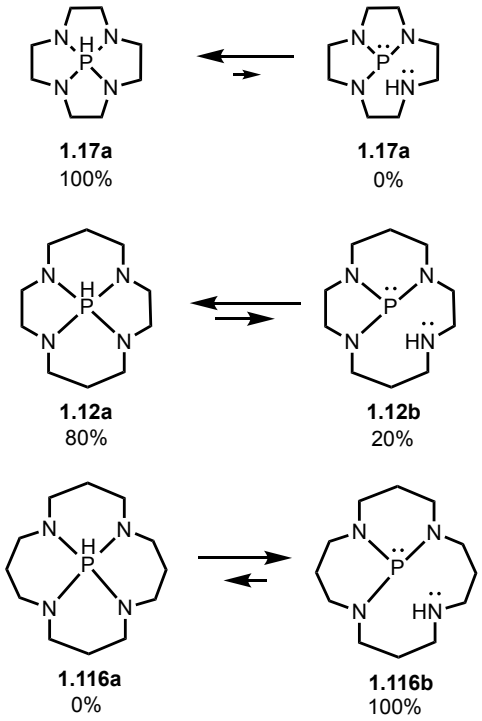

As early examples, cyclamphosphorane **1.12a** cyclenphosphorane **1.17a**, which were also used or synthesis of metallophosphoranes by Riess and Lattman (see section *1-4-3*), are considered as products of N–H oxidative addition of pendant amines to corresponding $\sigma^3$-P open tautomers. Importance of geometrical distortion for $\sigma^5$-P formation is suggested by different equilibriums in these systems; early works by Atkins and Richman showed that the smaller the ring sizes, the more phosphoranes are formed (Scheme 1-24).[110, 111]

**Scheme 1-25**. E–H oxidative addition to P(ONO) compound **1.117**.

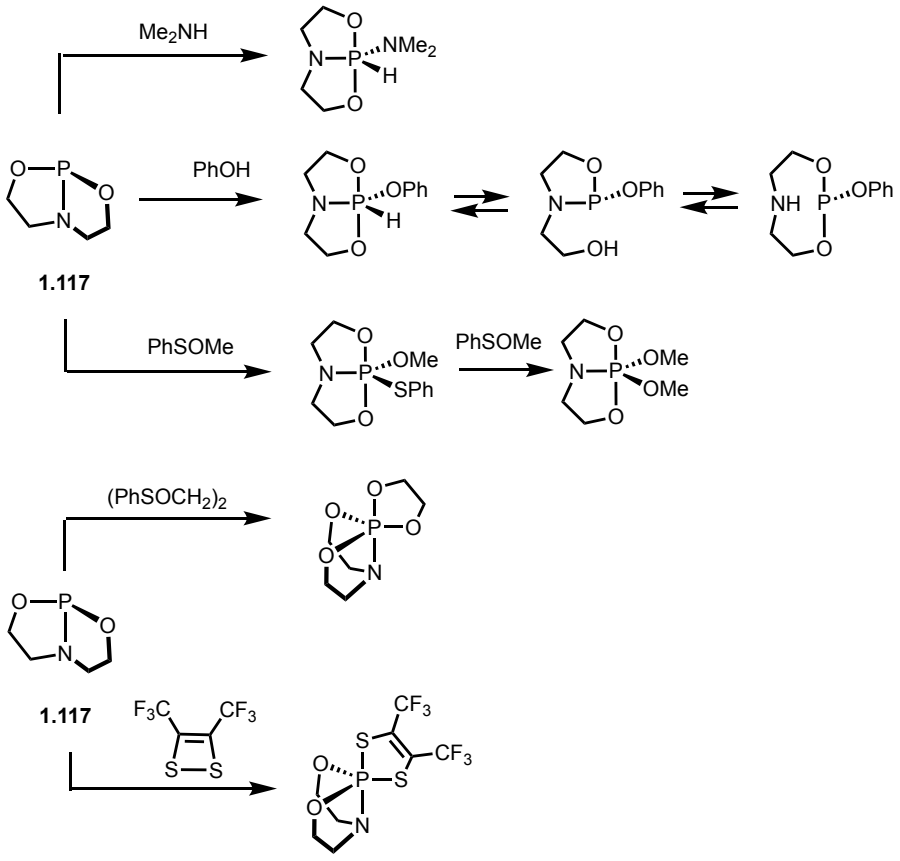


Bicyclic P(ONO) compounds have been intensely studied in this area. Wolf[112 - 115] and Denney[116] discovered E–H oxidative addition of exogenous molecules to O,N,O-bicyclic P(III) compound **1.117** (Scheme 1-25). Arduengo designed a further geometrically distorted P(ONO)

compound **1.118**, whose X-ray solid-state structure shows an approximate $C_{2v}$-symmetric T-shape geometry with a large O–P–O angle (168.8º) and acute N–P–O angles (84.0º and 84.9º) (Scheme 1-26a).[117-120] The authors proposed three resonance structures of compound **1.118** (Scheme 1-26b). The introduced vinylic moieties donate electrons and make phosphorus atoms electron-rich (formal 10-P-3 compound). The nitrogen and oxygen substitutes of the P donate electron density to the out-of-plane phosphorus 3p orbital to stabilize the planer structure. As a result, the linear O–P–O bond and the leave little p-character for the phosphorus lone pair orbital (Bent's rule), making the P lone pair have high s-character and low nucleophilicity.

**Scheme 1-26**. (a) Synthesis, (b) resonance structures and (c) N–H and O–H oxidative addition of T-shaped O,N,O-phosphacycle compound **1.118** developed by Arduengo.

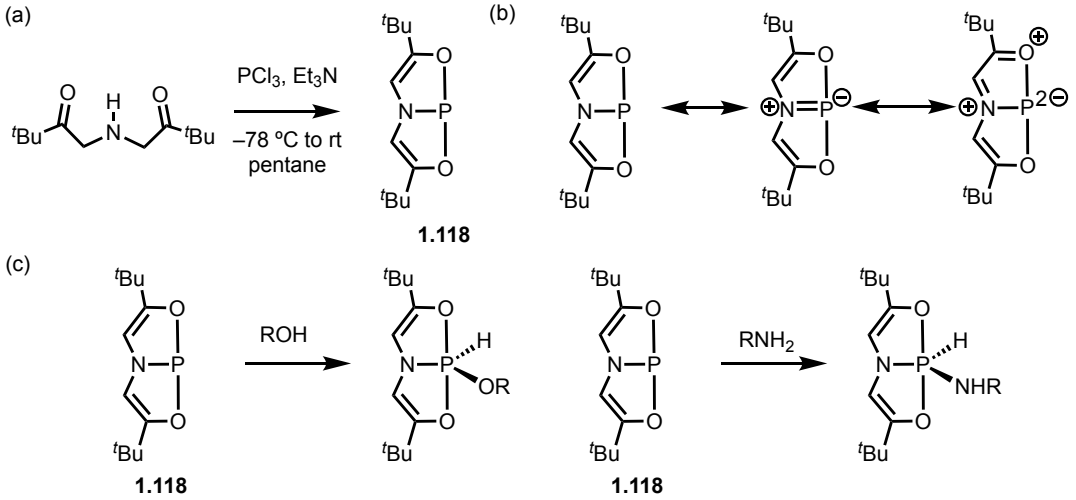


Formation of isolable N–H and O–H oxidative addition products was shown and Radosevich proposed a mechanism for an oxidative addition of butylamine, based on a third-order dependence of the rate constant on butylamine and computational results (Scheme 1-26a).[121] The reaction is initiated by a coordination of the lone pair of butylamine to the P atom of **1.118**, followed by a deprotonation of the adduct and formation of final phosphorane **1.119** via proton transfer to the phosphoranide. This mechanism suggests the tricoordinate phosphorus atom acts as an electrophile

in an initial step, supporting the hypothesis of enhanced electrophilicity by the geometrical distortion. Radosevich also showed a novel reactivity of **1.118** with ammonia borane to give dihydride product **1.120** (Scheme 1-27b).[122] The $H_2$ addition process is reversible via transfer hydrogenation with N=N double bonds and they applied the P(III)/P(V) redox cycle to the transfer hydrogenation of azobenene.

**Scheme 1-27.** (a) N–H oxidative addition of butylamine to **1.118** and proposed reaction mechanism (b) catalytic transfer hydrogenation of azobenzene using P(III)/P(V) redox cycle by Radosevich.

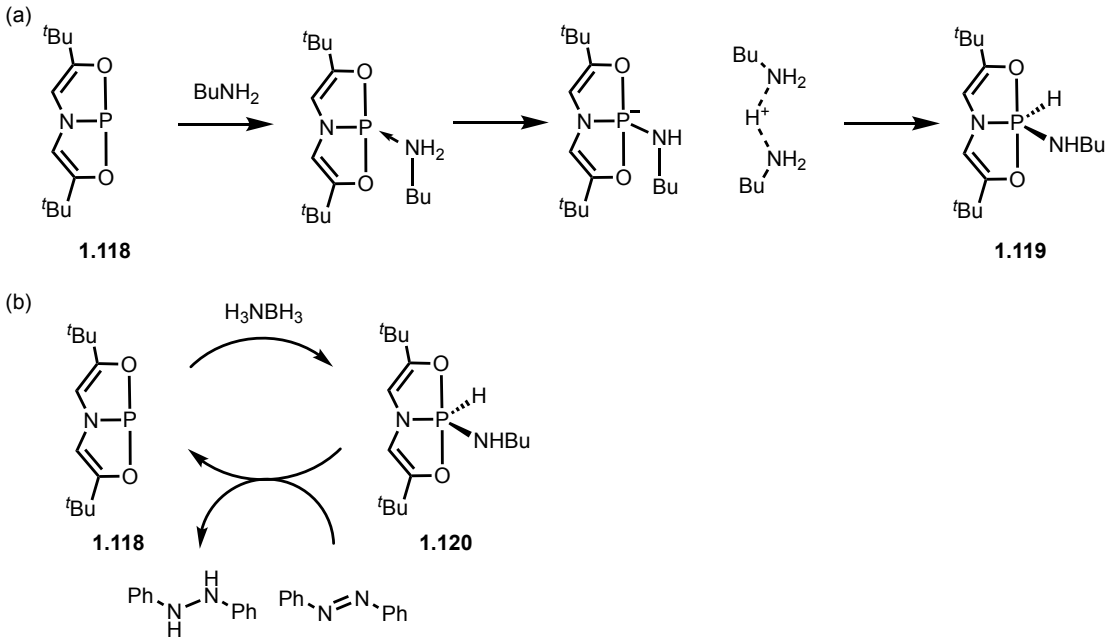


Radosevich also designed a novel butterfly-shaped phosphorus triamide **1.121** with approximate $C_s$ symmetry (Scheme 1-28).[123-126] The compound functions as a new platform to activate various O–H and N–H, bonds give corresponding stable phosphorane species (Scheme 1-28a). Bonds as strong as C–F bond can be activated on the P center and additional ligand metathesis and reductive elimination provide a synthetic cycle based on the P(III)/P(V) transformation (Scheme 1-28b). [127] Oxidative addition of benzylthiol was also enabled by a synthesis of novel phosphorus triamide **1.122**, in which an ethylene bridge further constrains the

geometry and prevents the formation of $\sigma^3$-P open tautomerization via P–N bond cleavage (Scheme 1-28c).[128]

**Scheme 1-28.** (a) Oxidative addition of primary alcohol and amines to **1.121**. (b) Oxidative addition of C–F bond to **1.121** and P(III)/P(V) synthetic cycle. (c) Different reactivities of **1.121** and **1.122** to addition of benzylthiol.

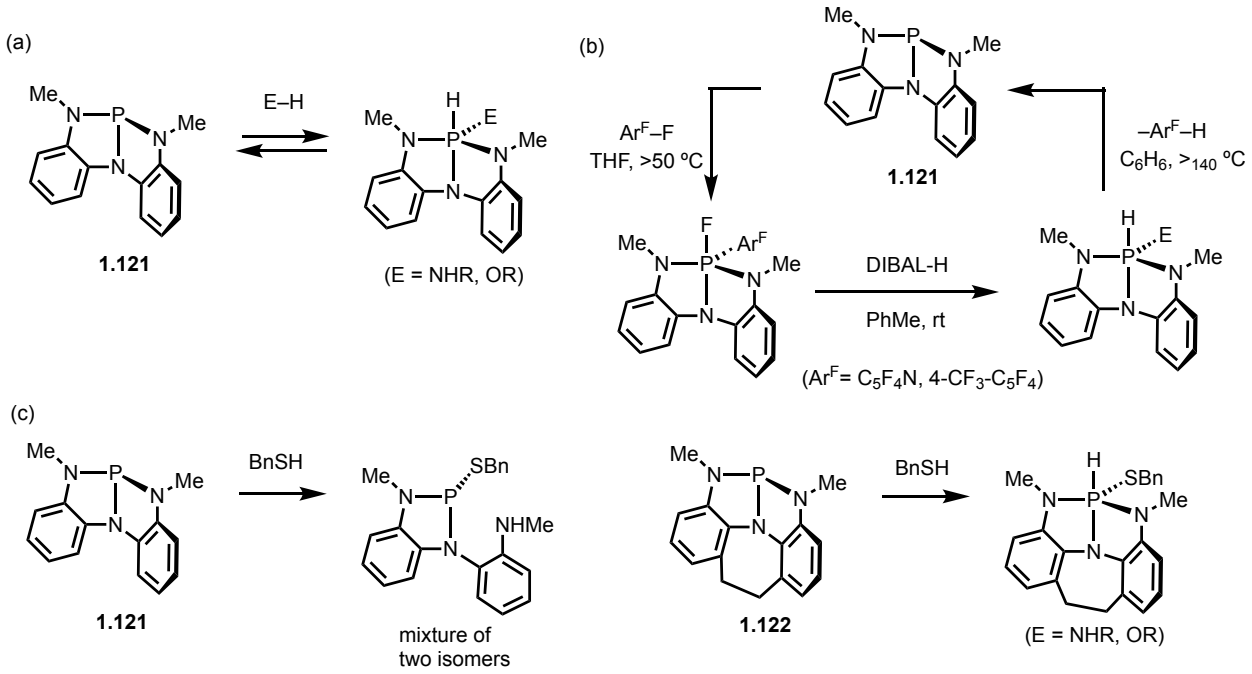

**Scheme 1-29.** Reactions of P(ONO) compound **1.123** with ammonia and water.

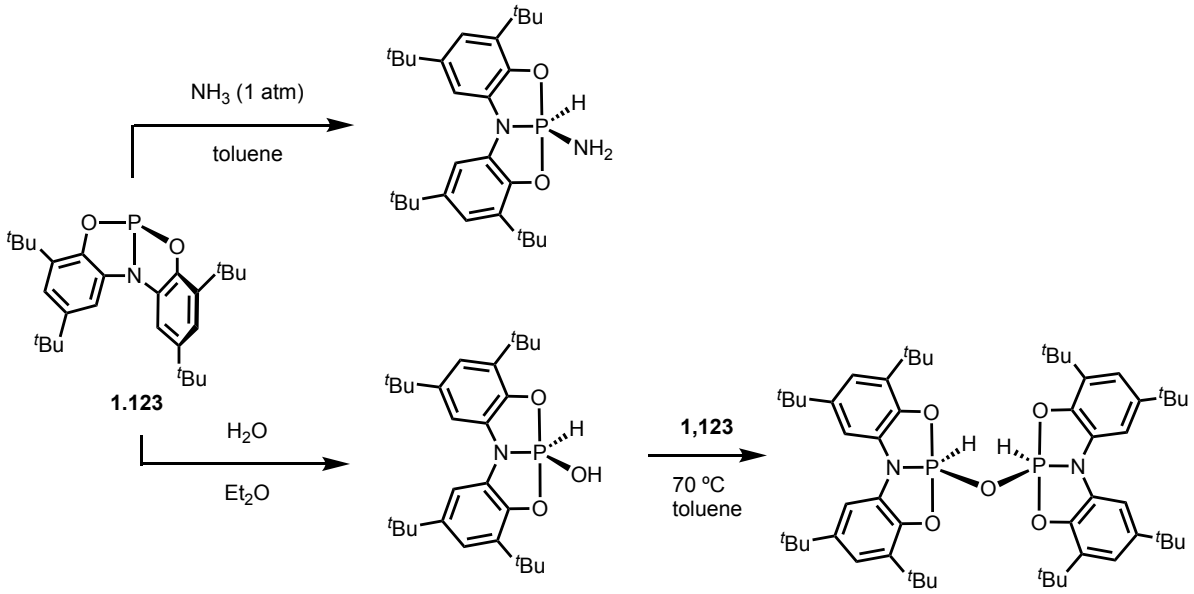


Recently, Aldridge and Goicoechea also reported novel $C_s$-symmetric P(ONO) compound **1.123** and its oxidative addition of N–H and O–H bonds with particular focuses on small molecules such as $H_2O$ and $NH_3$ (Scheme 1-29). [129] They also studied the oxidative transformation of **1.123** with alkoxides, which form 10–P–4 phosphoranides instead of 10-P–5 phosphoranes. [130, 131] Recently, Zeng and Zhu reported activation of carbon–halogen bonds by **1.123** to yield corresponding phosphoranes.[132]

Novel design of geometrically constrained phosphorus(III) compounds has been studied more and more intensely these days. For instance, Wang reported the first N,N,N-bicyclic P(III) compound **1.124** with a $C_{2v}$ symmetry in the solid-state structure [133]. Uhl reported C,C,C-bicyclic phosphine **1.125** with $C_s$ symmetry and its reactivity.[134, 135] Although oxidative addition on the P center has not reported for these systems so far, the significant differences in the geometry and electronic structures suggest a high potential of new reactivities.

**Chart 1-2.** Examples of recently synthesized geometrically constrained tricoordinate phosphorus

compounds by (a) Wang and (b) Uhl.

(a)

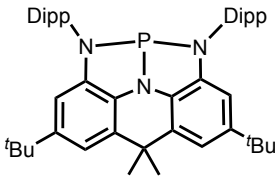


(b)

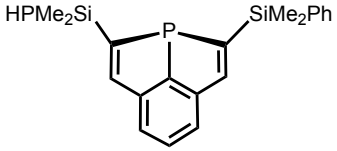

## 1-7. Conclusion and Outlook

In Chapter 1, we provided an overview of the background and previous studies of higher coordinate phosphorus ligands. In contrast to the well-known 'spectator' behavior of phosphine ligands, recent computational work suggested several 'nonspectator' electrophilic reactivities of tricoordinate phosphorus ligands to yield species with higher coordinate phosphorus ligands such as metallophosphoranes. Despite their potential involvement in many interesting reactions, however, higher coordinate phosphorus ligands have not gathered much attention compared to tricoordinate and lower-coordinate congeners, mainly due to their low stability and accessibility. Although geometrical distortion of tricoordinate P(III) compounds has been intensely studied as a method to facilitate the formation of P(V) species, most work along this line have been conducted with nonmetal phosphorane species.

As a central hypothesis of this thesis, we projected that the improved access to pentacoordinate P compounds by geometrical deformation would be applicable when there is a metal substituent. We herein describe our development of unique 'nonspectator' reactivities with the use of 'biphilic' nontrigonal phosphorus triamides as ligands in transition metal complexes in the following chapters.

## 1-8. References


1. Significant portion of Chapter 1 was prepared in collaboration with Dr. Gregory Cleveland and Dr. Aya Eizawa in preparation for publication as a review on hypervalent phosphorus ligands.
2. Kamer, P. C. J.; van Leeuwen, P. W. N. M. *Phosphorus(III) Ligands in Homogeneous Catalysis: Design and Synthesis;* John Wiley & Sons, Ltd, **2012**.
3. Laroshenko, V. *Organophosphorus Chemistry: From Molecules to Applications*; John Wiley & Sons, Ltd, **2019**.
4. Pignolet, L. M. *Homogeneous Catalysis with Metal Phosphine Complexes*; Springer, **1983**.
5. Cotton, F. A.; Wilkinson, G.; Murillo, C. A.; Bochmann, M. The Group 15 Elements: P, As, Sb, Bi. In *Advanced Inorganic Chemistry,* 6th ed. John Wiley & Sons, Ltd, **1999**; pp 380-443.
6. Tolman, C. A. Steric Effects of Phosphorus Ligands in Organometallic Chemistry and Homogeneous Catalysis. *Chem. Rev.* **1977**, *77*, 313–348.
7. Tolman, C. A. Electron Donor-Acceptor Properties of Phosphorus Ligands. Substituent Additivity. *J. Am. Chem. Soc.* **1970**, *92*, 2953–2956.
8. Serron, S.; Huang, J.; Nolan, S. P. Solution Thermochemical Study of Tertiary Phosphine Ligand Substitution Reactions in the Rh(Acac)(CO)($PR_3$) System. *Organometallics* **1998**, *17*, 534–539.
9. Bilbrey, J. A.; Kazez, A. H.; Locklin, J.; Allen, W. D. Exact Ligand Cone Angles. *J. Comp. Chem.* **2013**, *34*, 1189–1197.
10. Immirzi, A.; Musco, A. A Method to Measure the Size of Phosphorus Ligands in Coordination Complexes. *Inorg. Chim. Acta.* **1977**, *25*, L41–L42.
11. Clavier, H.; Nolan, S. P. Percent Buried Volume for Phosphine and N-Heterocyclic Carbene Ligands: Steric Properties in Organometallic Chemistry. *Chem. Comm.* **2010**, *46*, 841–861.
12. Rosenberg, L. Metal Complexes of Planar $PR_2$ Ligands: Examining the Carbene Analogy. *Coord. Chem. Rev.* **2012**, *256*, 606–626.
13. Gudat, D. Cationic Low Coordinated Phosphorus Compounds as Ligands: Recent Developments. *Coord. Chem. Rev.* **1997**, *163*, 71–106.
14. Nakazawa, H. The Chemistry of Transition Metal Complexes Containing a Phosphenium Ligand. *J. Organomet. Chem.* **2000**, *611*, 349–363.
15. Waterman, R. Metal-Phosphido and -Phosphinidene Complexes in P–E Bond-Forming Reactions. *Dalton Trans.* **2009**, *1*, 18–26.
16. Cowley, A. H.; Barron, A. R. The Quest for Terminal Phosphinidene Complexes. *Acc. Chem. Res.* **1988**, *21*, 81–87.
17. Cowley, A. H. Terminal Phosphinidene and Heavier Congeneric Complexes. The Quest Is Over. *Acc. Chem. Res.* **1997**, *30*, 445–451.
18. Lammertsma, K.; Vlaar, M. J. M. Carbene-Like Chemistry of Phosphinidene Complexes − Reactions, Applications, and Mechanistic Insights. *Eur. J. Org. Chem.* **2002**, 1127-1138.
19. Lammertsma, K. Phosphinidenes. *Top. Curr. Chem.* **2003**, *229*, 95–119.

20. Aktaş, H.; Slootweg, J. C.; Lammertsma, K. Nucleophilic Phosphinidene Complexes: Access and Applicability. *Angew. Chem. Int. Ed.* **2010**, *49*, 2102–2113.

21. Laplaza, C. E.; Davis, W. M.; Cummins, C. C. A Molybdenum–Phosphorus Triple Bond: Synthesis, Structure, and Reactivity of the Terminal Phosphido Complex[Mo(P)$(NRAr)_3$]. *Angew. Chem. Int. Ed.* **1995**, *34*, 2042–2044.

22. Zanetti, N. C.; Schrock, R. R.; Davis, W. M. Monomeric Molybdenum and Tungsten Complexes That Contain a Metal–Phosphorus Triple Bond. *Angew. Chem. Int. Ed.* **1995**, *34*, 2044–2046.

23. Johnson, B. P.; Balazs, G.; Scheer, M. Complexes with a Metal-Phosphorus Triple Bond. *Top. Curr. Chem.* **2004**, *232*, 1–23.

24. Cummins, C. C. Terminal, Anionic Carbide, Nitride, and Phosphide Transition-Metal Complexes as Synthetic Entries to Low-Coordinate Phosphorus Derivatives. *Angew. Chem. Int. Ed.* **2006**, *45*, 862–870.

25. Johnson, B. P.; Balázs, G.; Scheer, M. Low-Coordinate E1 Ligand Complexes of Group 15 Elements—A Developing Area. *Coord. Chem. Rev.* **2006**, *250*, 1178–1195.

26. Balázs, G.; Gregoriades, L. J.; Scheer, M. Triple Bonds between Transition Metals and the Heavier Elements of Groups 14 and 15. *Organometallics* **2007**, *26*, 3058–3075.

27. Montgomery, C. D. Structures and Structural Distortions of Metalated Phosphoranes. *Phosphorus, Sulfur, Silicon Related Elem.* **1993**, *84*, 23–34.

28. Dillon, K. B. Phosphoranides. *Chem. Rev.* **1994**, *94*, 1441–1456.

29. Nakazawa, H.; Kubo, K.; Miyoshi, K. Metallaphosphorane Chemistry: Preparations, Structures, and Reactivities. *Bull. Chem. Soc. J.* **2001**, *74*, 2255–2267.

30. Goodman, J.; Macgregor, S. A. Metallophosphoranes: The Hidden Face of Transition Metal–Phosphine Complexes. *Coord. Chem. Rev.* **2010**, *254*, 1295–1306

31. For N–X–L nomenclature (N: the number of valence electrons formally present, X: the central element, L: the number of ligand atoms bonded to the central atoms), see: Perkins, C. W.; Martin, J. C.; Arduengo, A. J.; Lau, W.; Alegria, A.; Kochi, J. K. *J. Am. Chem. Soc.* **1980**, *102*, 7753−7759.

32. Green, M. L. H.; Parkin, G. The Classification and Representation of Main Group Element Compounds That Feature Three-Center Four-Electron Interactions. *Dalton Trans.* **2016**, *45*, 18784–18795.

33. Nakazawa, H.; Kubo, K.; Miyoshi, K. Metallaphosphorane Chemistry: Preparations, Structures, and Reactivities. *Bull. Chem. Soc. J.* **2001**, *74*, 2255–2267.

34. Wachter, J.; Mentzen, B. F.; Riess, J. G. Synthesis and Crystal Structure of a $(\eta^5\text{-}C_5H_5)(CO)_2$-Molybdenum Bicyclophosphoranide: The First Transition Metal Complex with a“R4P$^-$”-Ligand. *Angew. Chem. Int. Ed.* **1981**, *20*, 284–285.

35. Vierling, P.; Riess, J. G. New Molybdenum and Iron Phosphoranides. Mechanism and Stereochemistry of the Rearrangement and Migration of a Phosphorus-Bound Allylic Group into an Iron-Bound Vinylic Group. *Organometallics* **1986**, *5*, 2543–2550.

36. Jeanneaux, F.; Grand, A.; Riess, J. G. Synthesis and Molecular Structure of an Aminophosphoranide Transition-Metal Adduct. First Transition-Metal Derivative Having a Cyclic N-P(V)-M Arrangement. *J. Am. Chem. Soc.* **1981**, *103*, 4272–4273.

37. Vierling, P.; Riess, J. G. Synthesis and Reactivity of Transition Metal Phosphoranides Having Three-Membered Phosphorus-Metal Nitrogen (or Oxygen) Rings. *Phosphorus Sulfur Relat. Elem.* **1987**, *30*, 261–264.

38. Wachter, J.; Jeanneaux, F.; Riess, J. G. Derivatives of [$\eta^5$-Cyclopentadienyl]Molybdenum Tricarbonyl Hydride and Chloride, $\eta^5$-$C_5H^5Mo[CO]^3X$ [X = Hydrogen, Chlorine], Containing a Bicyclic Phosphorus-Nitrogen Ligand. *Inorg. Chem.* **1980**, *19*, 2169–2172.

39. Vierling, P.; Riess, J. G.; Grand, A. Reversible, Nitrogen-Assisted Migration of a Phenyl Group from Phosphorus to Iron in $CpFe(CO)[PhP(OCH_2CH_2)_2NH]^+PF_6^-$. *J. Am. Chem. Soc.* **1981**, *103*, 2466–2467.

40. Vierling, P.; Riess, J. G. Activation of a Carbon-Hydrogen Bond in an Iron Phosphoranide Adduct. Unprecedented Rearrangement and Migration of a Phosphorus-Bound Allyl Group into an Iron-Bound Vinyl Group. *J. Am. Chem. Soc.* **1984**, *106*, 2432–2434.

41. Vierling, P.; Riess, J. G.; Grand, A. Coordination Chemistry of the Bicycloaminophosphorane Ph(H)P[(OCH2CH2)2N], a Potential P/N Ligand. Access to Iron and Ruthenium Phosphoranides. Reversible Migration of a Phenyl Group between Iron and Phosphorus: Crystal and Molecular Structure of $\eta^5$-$CpFe(CO)[P(OCH_2CH_2)_2N](\eta^1$-$C_6H_5)$. *Inorg. Chem.* **1986**, *25*, 4144–4152.

42. Dupart, J. M.; Grand, A.; Pace, S.; Riess, J. G. Synthesis and Molecular Structure of a Transition-Metal Cyclamphosphoranide. A Pentacyclic Structure with the Metal Bridging a Phosphorus-Nitrogen Bond. *J. Am. Chem. Soc.* **1982**, *104*, 2316–2318.

43. Dupart, J. M.; Grand, A.; Riess, J. G. Coordination Chemistry of Cyclamphosphorane. Access to Transition-Metal Cyclamphosphoranides. Crystal and Molecular Structure of Dicarbonylcyclopentadienylmolybdenum Cyclamphosphoranide Complex. *J. Am. Chem. Soc.* **1986**, *108*, 1167–1173.

44. Lattman, M.; Chopra, S. K.; Cowley, A. H.; Arif, A. M. Reactions of Cyclenphosphorane with Transition-Metal Carbonyl Dimers and Hydrides: Synthesis of Phosphoranide Adducts and Metal Carbonyl Anions and the x-Ray Crystal Structure of $(CyclenP)MoCp(CO)_2$. *Organometallics* **1986**, *5*, 677–683.

45. Lattman, M.; Chopra, S. K.; Burns, E. G. Pentacoordinate Phosphorus in Transition-Metal Chemistry. *Phosphorus Sulfur Relat. Elem.* **1987**, *30*, 185–188.

46. De Meester, P.; Lattman, M.; Chu, S. S. C. Tricarbonyl($\eta^2$-cyclenphosphoranido)cobalt(I) *Acta Cryst.* **1987**, *C43*, 162–164.

47. Lattman, M.; Burns, E. G.; Chopra, S. K.; Cowley, A. H.; Arif, A. M. Reaction of "Cyclenphosphorane" with Cis-Dichlorobis(Triphenylphosphine)Platinum(II). Formation of Bidentate and Monodentate Phosphoranide Adducts and x-Ray Crystal Structure of (η2-CyclenP)$PtClPPh_3$. *Inorg. Chem.* **1987**, *26* , 1926–1929.

48. Lattman, M.; Anand, B. N.; Chu, S. S. C.; Rosenstein, R. R.; Synthesis and Reactivity of Transition Metal-Substituted Phosphoranes, *Phosphorus Sulfur Relat. Elem.,* **1983**, *18*. 303-306,

49. Gavrilov, K. N. First Example of Tricyclic Hydrophosphorane Coordination with Palladium(II). *Russian J. Coord. Chem.* **1995**, *21*, 414.

50. Mikhel', I. S.; Gavrilov, K. N.; Lechkin, D. V.; Rebrov, A. I. The First Example of Coordination of a Tricyclic Hydrophosphorane with Platinum(II). *Russ. Chem. Bull.* **1997**, *46*, 1359–1360.

51. Gavrilov, K. N.; Polosukhin, A. I.; Bondarev, O. G.; Lyubimov, S. E.; Lyssenko, K. A.; Petrovskii, P. V.; Davankov, V. A. Synthesis and Properties of Pentacoordinated Phospha Derivatives of Iso-Leucinol A Rare Example of Using of Hydrophosphoranes as Ligands in Asymmetric Catalysis. *J. Mol. Catal. A* **2003**, *196*, 39.

52. Bondarev, O. G.; Mikhel, I. S.; Tsarev, V. N.; Petrovskii, P. V.; Davankov, V. A.; Gavrilov, K. N. Platinum and Rhodium Complexes with Isoleucinol-Based Bi- and Tricyclic Hydrophosphoranes. *Russ. Chem. Bull.* **2003**, *52*, 116.

53. Gavrilov, K. N. First Palladated Phosphorane: Complexation of a Tricyclic Hydrophosphorane with $Pd(COD)Cl_2$. *Russian J. Inorg. Chem.* **1997**, *42*, 1676-1683.

54. Gavrilov, K. N.; Korostylev, A. V.; Polosukhin, A. I.; Bondarev, O. G.; Kovalevsky, A. Yu.; Davankov, V. A. Complexation of Hydrophosphoranes: Possible Mechanism and Coordination Activity. *J. Organomet. Chem.* **2000**, *613*, 148–158.

55. Burns, E. G.; Chu, S. S. C.; De Meester, P.; Lattman, M. Three-Fragment Oxidative Addition of Dichloromethane to a Mononuclear Rhodium(I) Complex with Concomitant Formation of a Metal-Phosphoranide Bond. *Organometallics* **1986**, *5*, 2383–2384.

56. Nakazawa, H.; Kubo, K.; Miyoshi, K. An Unprecedented Synthetic Route for a Metallaphosphorane Complex. Nucleophilic Attack of Lewis Base on a Trivalent Phosphorus Atom Coordinating to a Transition Metal. *J. Am. Chem. Soc.* **1993**, *115*, 5863–5864.

57. Lattman, M.; Anand, B. N.; Chu, S. S. C.; Rosenstein, R. R. Synthesis and Reactivity of Transition Metal-Substituted Phosphoranes. *Phosphorus Sulfur Relat. Elem.* **1983**, *18*, 303–306.

58. Lattman, M.; Anand, B. N.; Garrett, D. R.; Whitener, M. A. Synthesis and Spectroscopic Study of a Transition Metal-Substituted Phosphorate: 2-Pentacarbonylmanganese-2,2′-Spirobi(1,3,2-Benzodioxaphosphole). *Inorg. Chim. Acta* **1983**, *76*, L139–L140.

59. Lattman, M.; Anand, B. N.; Chu, S. S. C.; Rosenstein, R. D. Reactivity of Transition-Metal-Substituted Phosphoranes: Spectroscopic and x-Ray Crystal Structural Study of the Hydrolysis of Pentacarbonyl(2,2'-Spirobi[1,3,2-Benzodioxaphosphol-2-Yl])Manganese. *Organometallics* **1984**, *3* (5), 670–674.

60. Chu, S. S. C.; Rosenstein, R. D.; Lattman, M.; Anand, B. N. Reactivity of Transition Metal-Substituted Phosphoranes: Crystal and Molecular Structure of 2-Pentacarbonylmanganese-1,3,2-benzodioxaphosphole-2-oxide. *J. Organomet. Chem.* **1984**, *265*, 45–52.

61. Lattman, M.; Morse, S. A.; Cowley, A. H.; Lasch, J. G.; Norman, N. C. Synthesis, Spectral Properties, and Geometry of a Metallophosphorane. *Inorg. Chem.* **1985**, *24* (9), 1364–1366.

62. Anand, B. N.; Bains, R. Reactivity of Transition Metal Substituted Phosphoranes: Carbonyl Substitution Reactions at Transition Metal Centre. *Indian J. Chem.* **1997**, *36A*, 77–79.

63. Anand, B. N.; Bains, R.; Usha, K. Synthesis and Characterization of Four-Membered, Spirobicyclic, Transition-Metal-Substituted Phosphoranes. *J. Chem. Soc., Dalton Trans.* **1990**, No. 7, 2315.

64. Anand, B. N.; Bains, R.; Aggarwal, K.; Usha, K. Symbiotic Reactions between Five- and Six-Membered Hypervalent Spirobicyclic Phosphoranes and Transition Metal Carbonylates. *Indian J. Chem.* **1995**, *34A*, 27–30.

65. Kajiyama, K.; Hirai, Y.; Otsuka, T.; Yuge, H.; Miyamoto, T. K. First Isolations and Structures of the *Cis* -Bis(Phosphoranido) Palladium(II) and Platinum(II) Complexes. *Chem. Lett.* **2000**, *7*, 784–785.

66. Kajiyama, K.; Yuge, H.; Miyamoto, T. K. First Isolations and Structures of Cis -Bis(Phosphoranido) Complexes. *Phosphorus, Sulfur, Silicon Relat. Elem.* **2002**, *177*, 1433–1436.

67. Kajiyama, K.; Sato, I.; Yamashita, S.; Miyamoto, T. K. Syntheses and Characterization of Novel *Trans* -Bis(Phosphoranido)Platinum(II) Complexes: Reactions of Lithium Bis(Naphth-1,8-Diyl-8-Oxy)Phosphoranide with *Cis* -$PtCl_2(PR_3)_2$ (R = OPh, OMe, Me). *Eur. J. Inorg. Chem.* **2009**, 5516–5521.

68. Kajiyama, K.; Nakamoto, A.; Miyazawa, S.; Miyamoto, T. K. Diastereoselective Formation of Metallaphosphacyclo Iridium(III) Complexes from Phosphoranido Iridium(III) Complex. *Chem. Lett.* **2003**, *32*, 332–333.

69. Jelier, B. J.; Montgomery, C. D.; Parlane, F. G. L. Deprotonation of a Hydrophosphorane and Synthesis of the Ni(II) Metallophosphorane $[NiCl\{P(OC_6H_4N(CH_3))_2\}(P(CH_3)_3)_2]$. *Inorg. Chim. Acta* **2014**, *413*, 121–127.

70 Burgada, R.; Laurenço, Mécanisme de formation et de transformation des spirophosphoranes : V. Synthése et tautomérie PIII PV spirophosphoranes liaison P–H dérivant des aminoalcools substitués au carbone et à l'azote. *J. Organomet. Chem.* **1974**, *66*, 255–270.

71. Faw, R.; Montgomery, C. D.; Rettig, S. J.; Shurmer, B. Synthesis and Crystal Structure of the Nickel(II) Phosphoranide Complex *Trans* -$(PMe_3)_2[(C_4H_6O_3)_2P$-*P*]NiCl. *Inorg. Chem.* **1998**, *37*, 4136–4138.

72. Carroll, H. K.; Parlane, F. G. L.; Reich, N.; Jelier, B. J.; Montgomery, C. D. Phosphoramidite Complexes of Pd(II), Pt(II) and Rh(I): An Effective Hydrosilylation Catalyst of 1-Hexyne and 1-Octene. *Inorg. Chim. Acta* **2017**, *465*, 78–83.

73. Carroll, H. K.; Brown, M. L.; Yap, V. C.; Magnuson, J. R.; Reich, N. A. J.; Macdonald, A. G. P.; Montgomery, C. D. Rapid Interconversion of Diastereomers of $[PdCl\{P(OC_6H_4NMe)_2\}\{P(OC_6H_4NMe)OC_6H_4NHMe\}]$. *Inorg. Chim. Acta* **2020**, *501*, 119239.

74. Chopra, S. K.; Martin, J. C. A Phosphoranide (10-P-4) Anion Coordinating to Transition Metals, as a Lewis Base and a n-Acceptor. *Heteroat. Chem.* **1991**, *2*, 71–79.

75. Martin, J. C.; Chopra, S. K.; Moon, C. D.; Forbus, T. R. Hypervalent Phosphorus Species as Aromatic and Metallic Species. *Phosphorus, Sulfur, Silicon Relat. Elem.* **1993**, *76*, 87–90.

76. Toyota, K.; Yamamoto, Y.; Akiba, K. A Hypervalent Phosphorane^Palladium Cation Complex Bearing Benzaldehydey. *J. Chem. Res.* **1999**, 386–387.

77. Toyota, K.; Yamamoto, Y.; Akiba, K. Synthesis and Crystal Structure of a Rhodium(III) Complex Bearing a Hypervalent Phosphorus(V) Ligand as a Bidentate Ligand and Equilibrium between Bidentate and Monodentate Structures in Solution. *J. Organomet. Chem.* **1999**, *586*, 171–175.

78. Kundu, S.; Brennessel, W. W.; Jones, W. D. Synthesis and Reactivity of New Ni, Pd, and Pt 2,6-Bis(Di-*Tert*-Butylphosphinito)Pyridine Pincer Complexes. *Inorg. Chem.* **2011**, *50*, 9443–9453.

79. Obligacion, J. V.; Zhong, H.; Chirik, P. J. Insights into Activation of Cobalt Pre-Catalysts for $C(sp^2)$−H Functionalization. *Isr. J. Chem.* **2017**, *57*, 1032–1036.

80. Gericke, R.; Wagler, J. Phosphorus as Lone Pair Donor and Ligand Acceptor: A Paddlewheel with Ru←P Axis: Phosphorus as Lone Pair Donor and Ligand Acceptor: A Paddlewheel with Ru←P Axis. *Eur. J. Inorg. Chem.* **2018**, 86–90.

81. Ebsworth, E. A. V.; McManus, N. T.; Pilkington, N. J.; Rankin, D. W. H. An Iridium Complex of 5-Co-Ordinated Phosphorus. *J. Chem. Soc., Chem. Commun.* **1983**, *9*, 484.

82. Ebsworth, E. A. V.; Holloway, J. H.; Pilkington, N. J.; Rankin, D. W. H. An Iridium(III) Complex Containing a PF4-Group Bound to the Metal. *Angew. Chem. Int. Ed.* **1984**, *23*, 630–631.

83. Blake, A. J.; Cockman, R. W.; Ebsworth, E. A. V.; Henderson, S. G. D.; Holloway, J. H.; Pilkington, N. J.; Rankin, D. W. H. Complexes of Iridium and Platinum Containing 5-Coordinated Phosphorus. *Phosphorus Sulfur Relat. Elem.* **1987**, *30*, 143–146.

84. Mason, M. R.; Verkade, J. G. Fluoride-Assisted Reduction of Palladium(II) Phosphine Complexes. *Organometallics* **1990**, *9*, 864–865.

85. Mason, M. R.; Verkade, J. G. Fluoride-Induced Reduction of Palladium(II) and Platinum(II) Phosphine Complexes. *Organometallics* **1992**, *11*, 2212–2220.

86. McLaughlin, P. A.; Verkade, J. G. Fluoride-Catalyzed Reduction of Palladium(II) to Palladium(0)−Phosphine Complexes. *Organometallics* **1998**, *17*, 5937–5940.

87. Grushin, V. V.; Alper, H. Alkali-Induced Disproportionation of Palladium(II) Tertiary Phosphine Complexes, $[L_2PdCl_2]$, to LO and Palladium(0). Key Intermediates in the Biphasic Carbonylation of ArX Catalyzed by $[L_2PdCl_2]$. *Organometallics* **1993**, *12*, 1890–1901.

88. Macgregor, S. A.; Neave, G. W. Theoretical Study of the CO Migratory Insertion Reactions of Pt(Me)(OMe)(Dppe) and Ni(Me)(OR)(Bpy) (R = Me, O-*p*-$C_6H_4CN$): Comparison of Group 10 Metal−Alkyl, −Alkoxide, and −Aryloxide Bonds. *Organometallics* **2004**, *23*, 891–899.

89. Bryndza, H. E. Mechanism of Carbon Monoxide Insertion into Metal-Oxygen Bonds. Reaction of $(DPPE)Pt(OCH_3)R$ (R = $CH_3$ or $OCH_3$) with CO. *Organometallics* **1985**, *4*, 1686–1687.

90. Green, M. L. H.; Smith, M. J.; Felkin, H.; Swierczewski, G. Substitution at Phosphorus in the Reaction between Dichlorobis(Triphenylphosphine)Nickel and Methylmagnesium Bromide. *J. Chem. Soc. D,* **1971**, *3*, 158b.

91. Geldbach, T. J.; Drago, D.; Pregosin, P. S. Alcohol Induced Stereospecific P–C Bond Cleavage to Afford Ru–Phenyl Derivatives Containing Three Different Types of Stereogenicity: Novel and Unprecedented Complexes of P(OH)(OR)Ph. *Chem. Commun.* **2000**, *17*, 1629–1630.

92. Geldbach, T. J.; Pregosin, P. S.; Bassetti, M. Synthesis, Kinetics, and Stereochemistry of P−C Bond Breaking and P−C Bond Making Reactions: Ruthenium−Arene Binap Chemistry. *Organometallics* **2001**, *20*, 2990–2997.

93. Geldbach, T. J.; Pregosin, P. S. $\eta^1$ to $\eta^6$ Ru−Arene π Complexation: New Bonding Modes and P−C Bond Cleavage Chemistry. *Eur. J. Inorg. Chem.* **2002**, 1907-1918.

94. Grushin, V. V.; Marshall, W. J. The Fluoro Analogue of Wilkinson's Catalyst and Unexpected Ph−Cl Activation. *J. Am. Chem. Soc.* **2004**, *126*, 3068–3069.

95. Macgregor, S. A.; Roe, D. C.; Marshall, W. J.; Bloch, K. M.; Bakhmutov, V. I.; Grushin, V. V. The F/Ph Rearrangement Reaction of $[(Ph_3P)_3RhF]$, the Fluoride Congener of Wilkinson's Catalyst. *J. Am. Chem. Soc.* **2005**, *127*, 15304–15321.

96. Macgregor, S. A.; Wondimagegn, T. Mechanism of the $[RhF(PPh_3)_3]$ to *Cis*-$[RhPh(PPh_3)_2(PFPh_2)]$ Interconversion: P−C Activation and F/Ph Exchange via a Metallophosphorane Pathway. *Organometallics* **2007**, *26*, 1143–1149.

97. Jayarathne, U.; Mague, J. T.; Donahue, J. P. Hexamethylphosphorus Triamide: A Chloride-for-Dimethylamido, $Me_2N^-$, Exchange Reagent. *Polyhedron* **2013**, *58*, 13–17.

98. Blum, O.; Frolow, F.; Milstein, D. C–F Bond Activation by Iridium(I). A Unique Process Involving P–C Bond Cleavage, P–F Bond Formation and Net Retention of Oxidation State. *J. Chem. Soc., Chem. Commun.* **1991**, 258–259.

99. Erhardt, S.; Macgregor, S. A. Computational Study of the Reaction of $C_6F_6$ with $[IrMe(PEt_3)_3]$: Identification of a Phosphine-Assisted C−F Activation Pathway via a Metallophosphorane Intermediate. *J. Am. Chem. Soc.* **2008**, *130*, 15490–15498.

100. Jasim, N. A.; Perutz, R. N.; Whitwood, A. C.; Braun, T.; Izundu, J.; Neumann, B.; Rothfeld, S.; Stammler, H.-G. Contrasting Reactivity of Fluoropyridines at Palladium and Platinum: C−F Oxidative Addition at Palladium, P−C and C−F Activation at Platinum. *Organometallics* **2004**, *23*, 6140–6149.

101. Nova, A.; Erhardt, S.; Jasim, N. A.; Perutz, R. N.; Macgregor, S. A.; McGrady, J. E.; Whitwood, A. C. Competing C−F Activation Pathways in the Reaction of Pt(0) with Fluoropyridines: Phosphine-Assistance versus Oxidative Addition. *J. Am. Chem. Soc.* **2008**, *130*, 15499–15511.

102. Cronin, L.; Higgitt, C. L.; Karch, R.; Perutz, R. N. Rapid Intermolecular Carbon−Fluorine Bond Activation of Pentafluoropyridine at Nickel(0): Comparative Reactivity of Fluorinated Arene and Fluorinated Pyridine Derivatives. *Organometallics* **1997**, *16*, 4920–4928.

103. Nova, A.; Reinhold, M.; Perutz, R. N.; Macgregor, S. A.; McGrady, J. E. Selective Activation of the *Ortho* C−F Bond in Pentafluoropyridine by Zerovalent Nickel: Reaction via a Metallophosphorane Intermediate Stabilized by Neighboring Group Assistance from the Pyridyl Nitrogen. *Organometallics* **2010**, *29*, 1824–1831.

104. Yandulov, D. V.; Tran, N. T. Aryl-Fluoride Reductive Elimination from Pd(II): Feasibility Assessment from Theory and Experiment. *J. Am. Chem. Soc.* **2007**, *129*, 1342–1358.

105. Wakioka, M.; Ozawa, F. Substituent Effects on P−C Reductive Elimination from Styrylpalladium(II) Phosphine Complexes. *Organometallics* **2010**, *29*, 5570–5578.

106. Chu, T.; Nikonov, G. I. Oxidative Addition and Reductive Elimination at Main-Group Element Centers. *Chem. Rev.* **2018**, *118*, 3608–3680.

107. Brand, A.; Uhl, W. Sterically Constrained Bicyclic Phosphines: A Class of Fascinating Compounds Suitable for Application in Small Molecule Activation and Coordination Chemistry. *Chem. Eur. J.* **2019**, *25*, 1391–1404.

108. Abbenseth, J.; Goicoechea, J. M. Recent Developments in the Chemistry of Non-Trigonal Pnictogen Pincer Compounds: From Bonding to Catalysis. *Chem. Sci.* **2020**, *11*, 9728–9740.

109. Mondal, M. K.; Zhang, L.; Feng, Z.; Tang, S.; Feng, R.; Zhao, Y.; Tan, G.; Ruan, H.; Wang, X. Tricoordinate Nontrigonal Pnictogen-Centered Radical Anions: Isolation, Characterization, and Reactivity. *Angew. Chem. Int. Ed.* **2019**, *58*, 15829–15833.

110. Richman, J. E.; Atkins, T. J. Polyaminophosphoranes II. Cyclen Phosphorane - a Novel P(V) Tautomer. *Tetrahedron Lett.* **1978**, *19*, 4333–4336.

111. Richman, J. E.; Atkins, T. J. Polyaminophosphoranes III. P(III)-P(V) Tautomerism in Four Nitrogen Cage Phosphorane. *Tetrahedron Lett.* **1978**, *19*, 5149–5152.

112. Houalla, D.; Sanchez, M.; Wolf, R.; Osman, F. H. Mise En Evidence d'un Hydroxyphosphorane a Liaison P-H. *Tetrahedron Lett.* **1978**, *19*, 4675–4678.

113. Wolf, R. Organo Phosphorus Tautomers Involving Change of Co-Ordination Number on Phosphorus. *Pure Appl. Chem.* **1980**, *52*, 1141–1150.

114. Bonningue, C.; Houalla, D.; Sanchez, M.; Wolf, R.; Osman, F. H. Bicyclic Phosphanes: Synthesis, Stereochemistry, and Conformation. *J. Chem. Soc. Perkin Trans. 2* **1981**, *1*, 19.

115. Bonningue, C.; Houalla, D.; Wolf, R.; Jaud, J. Bicyclic Phosphanes. Part 2. Spontaneous Dimerization of a Constrained Bicyclic Phosphane. The Crystal and Molecular Structure of a Tricyclic Compound Containing the Dioxadiazadiphosphecine Ring. *J. Chem. Soc. Perkin Trans. 2* **1983**, 6, 773–776.

116. Denney, D. B.; Denney, D. Z.; Hammond, P. J.; Huang, C.; Tseng, K.-S. Structures of Some Bicyclic and Tricyclic Phosphoranes in Solution. *J. Am. Chem. Soc.* **1980**, *102*, 5073–5077.

117. Culley, S. A.; Arduengo, A. J. Synthesis and Structure of the First 10-P-3 Species. *J. Am. Chem. Soc.* **1984**, *106*, 1164–1165.

118. Arduengo, A. J.; Stewart, C. A.; Davidson, F.; Dixon, D. A.; Becker, J. Y.; Culley, S. A.; Mizen, M. B. The Synthesis, Structure, and Chemistry of 10-Pn-3 Systems: Tricoordinate Hypervalent Pnicogen Compounds. *J. Am. Chem. Soc.* **1987**, *109*, 627–647.

119. Arduengo, A. J.; Stewart, C. A. Low-Coordinate Hypervalent Phosphorus. *Chem. Rev.* **1994**, *94*, 1215–1237.

120. Driess, M.; Muresan, N.; Merz, K.; Päch, M. Formation of a Bowl-Shaped, Pentacyclic Phosphonium Cage by Methylation of a Nucleophilic Phosphinidene. *Angew. Chem. Int. Ed.* **2005**, *44*, 6734–6737.

121. Zhao, W.; McCarthy, S. M.; Lai, T. Y.; Yennawar, H. P.; Radosevich, A. T. Reversible Intermolecular E-H Oxidative Addition to a Geometrically Deformed and Structurally Dynamic Phosphorous Triamide. *J. Am. Chem. Soc.* **2014**, *136*, 17634–17644.

122 Dunn, N. L.; Ha, M.; Radosevich, A. T. Main Group Redox Catalysis: Reversible P III/P V Redox Cycling at a Phosphorus Platform. *J. Am. Chem. Soc.* **2012**, *134*, 11330–11333.

123. Lin, Y. C.; Hatzakis, E.; McCarthy, S. M.; Reichl, K. D.; Lai, T. Y.; Yennawar, H. P.; Radosevich, A. T. P-N Cooperative Borane Activation and Catalytic Hydroboration by a Distorted Phosphorous Triamide Platform. *J. Am. Chem. Soc.* **2017**, *139*, 6008–6016.

124. Lin, Y. C.; Gilhula, J. C.; Radosevich, A. T. Nontrigonal Constraint Enhances 1,2-Addition Reactivity of Phosphazenes. *Chem. Sci.* **2018**, *9*, 4338–4347.

125. te Grotenhuis, C.; Mattos, J. T.; Radosevich, A. T. Addition Reactions of a Phosphorus Triamide to Nitrosoarenes and Acylpyridines. *Phosphorus, Sulfur Silicon Relat. Elem.* **2020**, *195*, 940–946.

126. Lipshultz, J. M.; Fu, Y.; Liu, P.; Radosevich, A. T. Organophosphorus-Catalyzed Relay Oxidation of H-Bpin: Electrophilic C-H Borylation of Heteroarenes. *Chem. Sci.* **2021**, *12*, 1031–1037.

127. Lim, S.; Radosevich, A. T. Round-Trip Oxidative Addition, Ligand Metathesis, and Reductive Elimination in a PIII/PVSynthetic Cycle. *J. Am. Chem. Soc.* **2020**, *142*, 16188–16193.

128. Radosevich, A. T.; Moon, H. W.; Maity, A. Ancillary Tethering Influences $\sigma^3$-P vs $\sigma^5$-P Speciation and Enables Intermolecular S−H Oxidative Addition to Nontrigonal Phosphorus Compounds. *Organometallics* **2021**, *ASAP*. https://doi.org/10.1021/acs.organomet.0c00750

129. Robinson, T. P.; De Rosa, D.; Aldridge, S.; Goicoechea, J. M. On the Redox Reactivity of a Geometrically Constrained Phosphorus(III) Compound. *Chem. Eur. J.* **2017**, *23*, 15455–15465.

130. Robinson, T. P.; Lo, S. K.; De Rosa, D.; Aldridge, S.; Goicoechea, J. M. On the Ambiphilic Reactivity of Geometrically Constrained Phosphorus(III) and Arsenic(III) Compounds: Insights into Their Interaction with Ionic Substrates. *Chem. Eur. J.* **2016**, *22* (44), 15712–15724.

131. Robinson, T. P.; De Rosa, D. M.; Aldridge, S.; Goicoechea, J. M. E-H Bond Activation of Ammonia and Water by a Geometrically Constrained Phosphorus(III) Compound. *Angew. Chem. Int. Ed.* **2015**, *54* (46), 13758–13763.

132. Wang, P.; Zhu, Q.; Wang, Y.; Zeng, G.; Zhu, J.; Zhu, C. Carbon-Halogen Bond Activation by a Structurally Constrained Phosphorus(III) Platform. *Chinese Chem. Lett.* **2021**, *32*, 1432–1436.

133. Mondal, M. K.; Zhang, L.; Feng, Z.; Tang, S.; Feng, R.; Zhao, Y.; Tan, G.; Ruan, H.; Wang, X. Tricoordinate Nontrigonal Pnictogen-Centered Radical Anions: Isolation, Characterization, and Reactivity. *Angew. Chem. Int. Ed.* **2019**, *58*, 15829–15833.

134. Hentschel, A.; Brand, A.; Wegener, P.; Uhl, W. A Sterically Constrained Tricyclic PC3 Phosphine: Coordination Behavior and Insertion of Chalcogen Atoms into P−C Bonds. *Angew. Chem. Int. Ed.* **2018**, *57*, 832–835.

135. Brand, A.; Hentschel, A.; Hepp, A.; Uhl, W. Dihalides of Sterically Constrained Tricyclic Phosphines, Lewis Acidity and Fluoride Affinity, Chloride Abstraction, and a Phosphonium Cation, Dimethylphosphorane. *Eur. J. Inorg. Chem.* **2020**, *2020*, 361–369.

# Chapter 2 Validation of Biphilicity of Nontrigonal Phosphorus Compounds by P K-edge XANES and TDDFT Calculation

A significant portion of the work described in this chapter has been published in:

Lee, K.; Blake, A.; Tanushi, A.; McCarthy, S.; Kim, D.; Loria, S.; Donahue, C.; Spielvogel, K.; Keith, J.; Daly, S.; et al. Validating the Biphilic Hypothesis of Nontrigonal P(III) Compounds. *Angew. Chem. Int. Ed.* **2019**, *58*, 6993–6998.

## 2-1. Introductory Remarks: Validation of Biphilic Hypothesis

As introduced in Chapter 1, nontrigonal deformation of tricoordinate phosphorus compounds colocalize both donor and acceptor reactivity at a single phosphorus site, resulting unusual reactivities such as oxidative addition of E–H bonds (E = OR, NHR). Although the 'biphilic' character of nontrigonal $\sigma^3$-P compounds is evident on an empirical basis, to date the observed reactivity has not been quantitatively correlated with an underlying electronic feature.

In Chapter 2, we quantify the impact of nontrigonal distortion on the electronic structure of $\sigma^3$-P. Phosphorus K-edge XANES combined with TDDFT calculation was applied for a series of related phosphorus triamide compounds. We show that the descent from trigonal to nontrigonal symmetry decreases the energy of the pre-edge X-ray absorption transition in otherwise compositionally analogous compounds, indicating the presence of an energetically low-lying unfilled orbital for nontrigonal $\sigma^3$-P consonant with an increased electrophilicity. These data along with electronic structure calculations suggest the structures of $\sigma^3$-P compounds with further enhanced biphilic reactivity and catalysts. The work in Chapter 2 connects the prior observations of biphilic reactivity for nontrigonal $\sigma^3$-P with insight into the electronic influence exerted by symmetry-lowering molecular distortion, providing an experimental and theoretical framework for the development of 'nonspectator' reactivity in later chapters.

## 2-2. P K-edge XANES for Electronic Structure Determination

While the connection between molecular and orbital electronic structure is well-described for $\sigma^3$-P compounds within local threefold symmetry (i.e. the pyramidal inversion coordinate),[1,2] the electronic effect of deviation from a typical $C_{3v}$ trigonal pyramid toward lower symmetry ($C_{2v}$ or $C_s$) structures is less commonly considered.[3] More specifically, an experimental demonstration of how the $C_{3v} \rightarrow C_s$ structural deformation controls $\sigma^3$-P frontier orbital energies has not been explicitly presented. A comprehensive experimental study quantifying the effect of nontrigonal distortion on phosphorus-based frontier orbital energies and elucidating how these orbitals correlate with bonding orbitals in $\sigma^5$-P compounds would be instrumental in establishing a rational framework for design of next-generation compositions of nontrigonal $\sigma^3$-P that exhibit improved biphilic reactivity and performance.

In principle, phosphorus K-edge X-ray absorption spectroscopy (XAS), an element-specific technique that allows for direct measurement of unoccupied frontier orbital composition and energy, represents a powerful tool for probing orbital structure of phosphorus-based comounds.[4-7] Indeed, phosphorus K-edge X-ray absorption near-edge structure (XANES) spectroscopy, which probes dipole-allowed transitions from the core P 1s → empty orbitals containing phosphorus p character,[8,9] can be used to extract valuable information concerning electronic structure and chemical bonding in phosphorus compounds of diverse structure and composition.[10] For instance, Daly and co-workers recently demonstrated that the combination of phosphorus K-edge XANES and TDDFT calculation is useful in predicting ligand-induced electronic structures, metal−ligand bonding properties and reactivity for transition metal-phosphine complexes.[11-14]

## 2-3. Synthesis and Structures of Molecular Phosphorus Compounds

**Chart 2-1**. Molecular P(NNN) compounds investigated in this study.

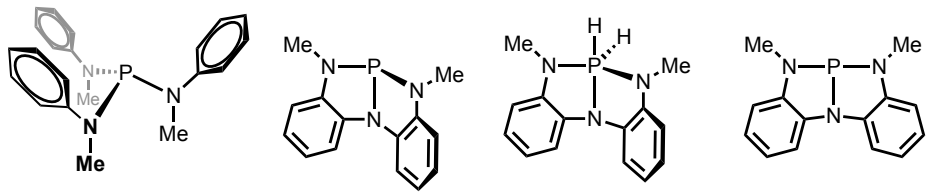


Molecular P(NNN) compounds investigated in this work are shown in Chart 2-1 and relevant structural metrics for all the compounds are collected in Table 2-1. To assess the impact of nontrigonal distortion within phosphorous triamide compounds, a high-symmetry trigonal phosphorus compound was required as a benchmark for comparison. The homoleptic tris(methylanilide) of phosphorus(III) (i.e. $P(NMePh)_3$) was therefore prepared by threefold ligand substitution of phosphorus trichloride by *N*-methylaniline according to the procedure of Rydon and Tonge.[22] The X-ray structure of $P(NMePh)_3$ confirmed the $C_3$ symmetric structure, where the angles ($\angle$N–P–N = 101.3°) and distances ($d$(P–N)=1.719 Å) are all equivalent in the primary bonding environment of phosphorus. The *N*-aryl moieties are displayed in all-*syn* helical fashion proximal to the phosphorus lone pair, with the less sterically demanding methyl substituents on the concave face of the trigonal pyramid. It is worth noting the contrast between the $C_3$ molecular symmetry of $P(NMePh)_3$ and the $C_s$ molecular symmetry of the related homoleptic triamide $P(NMe_2)_3$ reported by Mitzel;[15] evidently, the aryl substituents play a controlling role in favoring the high-symmetry trigonal structure.

**Table 2-1.** Selected Bond Distances (Å) and Angles (°) for $P(NMePh)_3$, **2-1**, **2-2**.

| metric | $P(NMePh)_3$ | **2.1** | **2.2** |
|---|---|---|---|
| $d(P_1–N_1)$ | 1.7193(19) | 1.7610(12) | 1.7879(9) |
| $d(P_1–N_2)$ | 1.7193(19) | 1.7190(13) | 1.7098 (10) |
| $d(P_1–N_3)$ | 1.7193(19) | 1.7014(14) | 1.7088(9) |
| $\angle N_2–P_1–N_3$ | 101.33(9) | 115.21(7) | 146.00 |
| $\angle N_1–P_1–N_2$ | 101.33(9) | 90.08(6) | 86.14 |
| $\angle N_1–P_1–N_3$ | 101.33(9) | 90.51(6) | 86.32 |

**Scheme 2-1.** Synthesis of **2.2.**

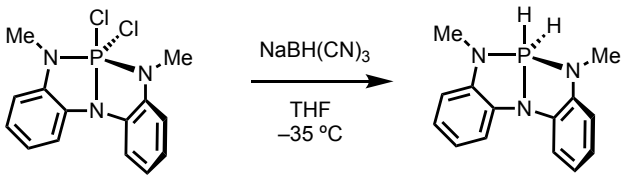


**2.3** **2.2**

The synthesis of all the nontrigonal compounds investigated in this study have been reported previously, aside from **2.2**.[16] Compound **2.2** was prepared by halide ligand substitution of **2.3** **(**dichloride adduct of **2.1**) with excess sodium cyanoborohydride as the hydride donor (Scheme 2-1). The $^{31}P\{^1H\}$ NMR spectrum of **2.2** in $C_6D_6$ showed a singlet at δ −67.7 ppm, which is split into a triplet of septets ($J$ = 523 Hz, 17 Hz) in the fully-coupled $^{31}P$ NMR spectrum. The magnitudes of these coupling constants are consistent with the dihydridophosphorane formulation of **2.2**, with large $^1J_{P–H}$ coupling to two hydrogen nuclei and smaller $^3J_{P–H}$ coupling to the six equivalent hydrogen nuclei of the two methyl groups. The corresponding $^1H$ NMR spectrum resolves the

complementary coupling partners, with a doublet at 7.07 ppm (2H, $J$ = 523 Hz) assigned to the apparently equivalent P–H hydrides and a doublet at 2.44 ppm (6H, $J$ = 17 Hz) assigned to the *N*–methyl groups.

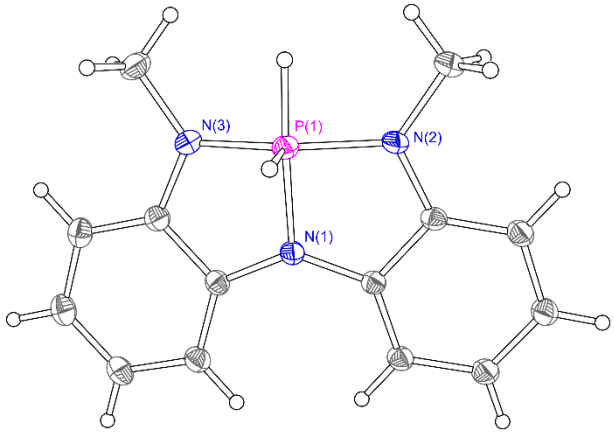


**Figure 2-1**. Solid state structure of **2.2**. Thermal ellipsoid plots rendered at the 50% probability level.

Despite the apparent $C_{2v}$ symmetry of **2.2** in solution, X-ray diffraction of a colorless single crystal of **2.2** displayed a solid−state structure of approximate $C_s$ symmetry (Figure 2-1). The structure about the pentacoordinate phosphorus may be described as quasi-square pyramidal ($\tau_5$ = 0.33),[17] where the two hydride ligands occupy inequivalent apical and basal positions ($\angle H_1–P–N_2$ = 98.3° and $\angle H_2–P–N_2$ = 165.7°) and the chelating triamide binds at the remaining basal vacancies. The apparent discrepancy between the solution and solid-state structures for **2.2** can be rationalized by reference to DFT calculations. While the global minimum for **2.2** is predicted at the B3LYP/6-31G** level of theory to exhibit a $C_s$ symmetric molecular structure in accord with the X-ray diffraction structure, a putative $C_{2v}$ symmetric structure for **2.2** was located as a first order saddle point along the wagging coordinate connecting degenerate $C_s$ ground states. The relatively low

energy of this stationary point ($E_{rel}$ = 5.76 kcal/mol) is consistent with rapid interconversion and time-averaging on the NMR timescale.

## 2-4. Electronic Structure Analysis of Molecular Phosphorus Compounds

*2-4-1. X-ray absorption spectra for molecular phosphorus compounds.*

Phosphorus K-edge XANES data were collected for $P(NMePh)_3$ and **2.1** to quantify the change in unoccupied frontier orbital energies in response to the nontrigonal structure of **2.1** (Figure 2-2). The spectrum of $P(NMePh)_3$ in canonical $C_3$ symmetry revealed an intense pre-edge feature at 2147.0 eV that was subsequently assigned as P 1s → P-N σ* based on DFT and TDDFT calculations. Using $P(NMePh)_3$ as a benchmark for comparisons, the spectrum of **2.1** revealed marked differences, the most notable being a 1.1 eV decrease in pre-edge peak energy. The first pre-edge peak for **2.1** was observed at 2145.9 eV and a second higher energy feature was observed at 2147.5 eV. As described for $P(NMePh)_3$, the first pre-edge feature in **2.1** is assigned as P 1s → P-N σ*, indicating that the $C_3 \rightarrow C_s$ structure change yields a pronounced decrease in P-N σ* energy. As we will show, the P-N σ* MOs involved in the pre-edge transitions represent the Lewis-acidic acceptor orbitals that participate in biphilic reactions at phosphorus.

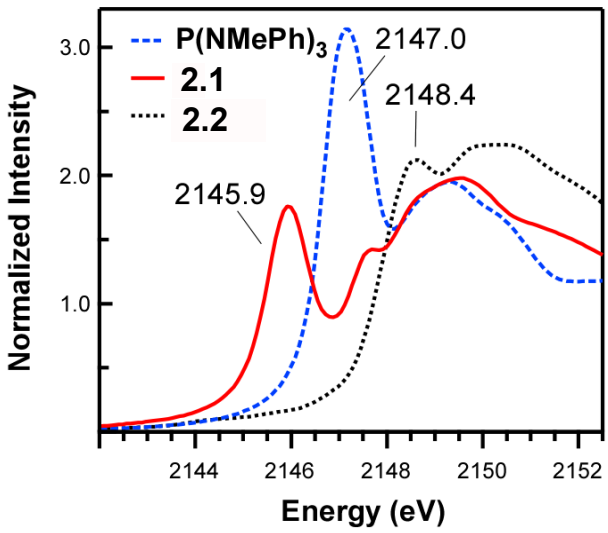


**Figure 2-2.** Comparison of P K-edge XANES spectra for $P(NMePh)_3$, **2-1** and **2-2**.

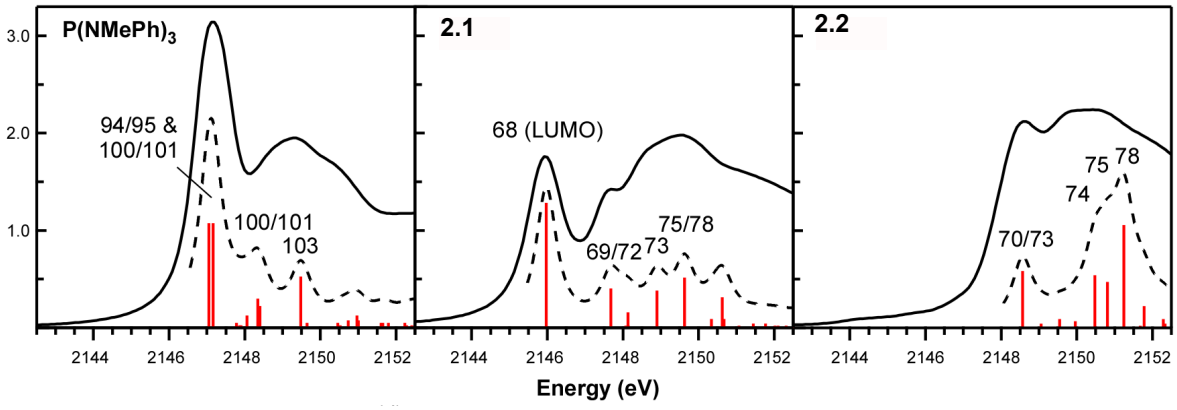


**Figure 2-3.** Comparison of experimental (solid line) and simulated (dashed line) P K-edge XANES spectra for $P(NMePh)_3$, **2.1** and **2.2**. Individual transitions are represented by red bars and indicate relative differences in calculated oscillator strength. The transitions are labeled according to the predominant calculated MOs mixing in the excited states. The labels correspond to those provided in Figure 2-4.

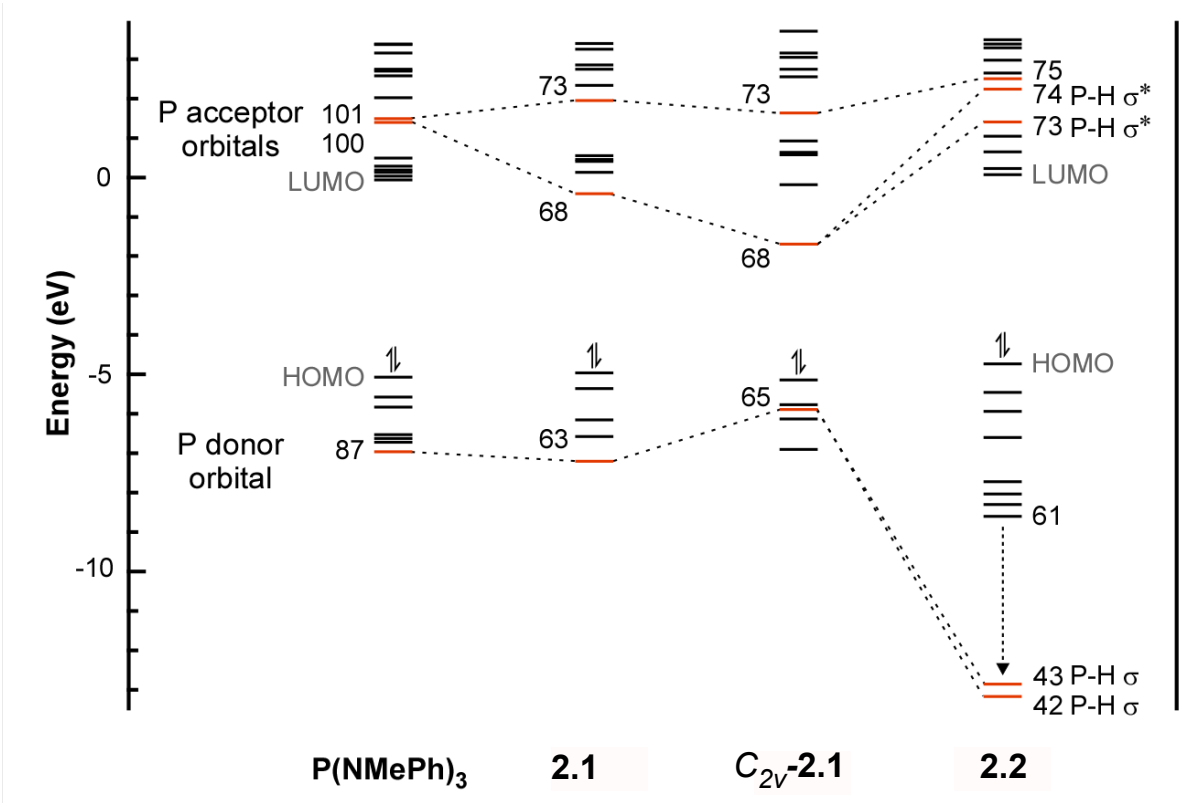


**Figure 2-4.** Truncated MO correlation diagram of molecular P(NNN) complexes. Frontier orbitals relevant to the XAS results and reactivity at phosphorus are highlighted in red and connected by dashed lines to show how they transform across the series.

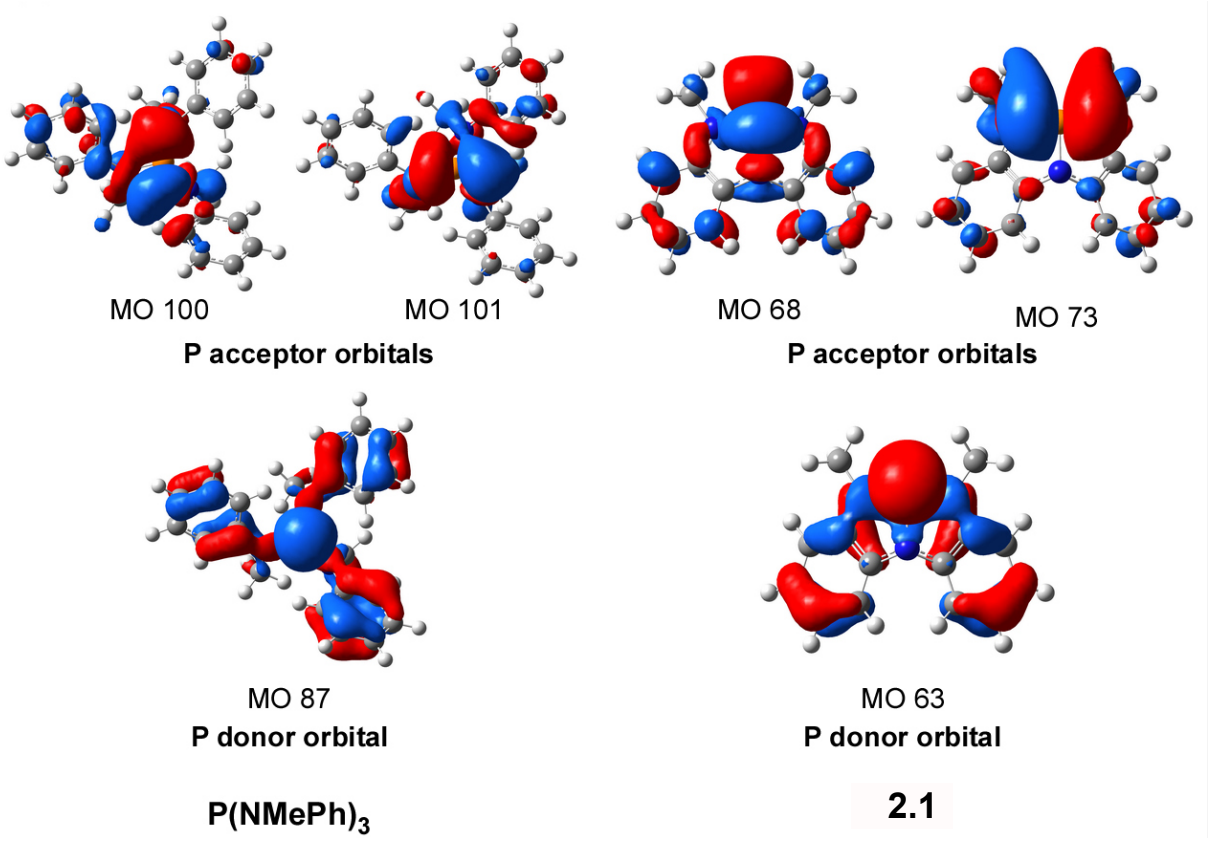


**Figure 2-5.** Selected donor-acceptor Kohn-Sham orbitals from DFT calculations of $P(NMePh)_3$ and **2.1**.

We next analyzed **2.2** to determine how formation of P–H bonds by formal oxidative addition of **2.1** with $H_2$ affects its electronic structure. The pre-edge feature observed at 2145.9 eV for **2.1** is not present in the spectrum of **2.2**; the first feature instead appeared at much higher energy (2148.4 eV). In our initial assumption, this higher-energy feature was associated with the newly formed P-H bonds, which was confirmed by our TDDFT calculations described below. The large energy increase for the first feature in **2.2** relative to **2.1** is consistent with oxidation of P(III) to P(V), which lowers the energy of the P 1s orbital due to the increased effective nuclear charge ($Z_{eff}$) at phosphorus.

*2-4-2. DFT electronic structure analysis of molecular phosphorus compounds.*

DFT and TDDFT calculations were performed on $P(NMePh)_3$, **2.1**, and **2.2** to help assign the observed spectral features and identify the composition of the participating MOs. For completeness, we also performed calculations on the planar T-shaped structure of **2.1** in order to evaluate how symmetry differences in the bent ($C_s$) and planar structure ($C_{2v}$) affect orbital energies and electronic structure at phosphorus. To distinguish between the two structures of **2.1** in the following discussion, we refer to the planar structure as $C_{2v}$-**2.1**, which is calculated to be 2.5 kcal/mol higher than **2.1**. While $C_{2v}$-**2.1** is not observed experimentally, consistent with our calculations, **2.1** can adopt $C_s$ or $C_{2v}$ structures upon reacting with substrates, and the preferred P(NNN) structure depends on the identity of the bound groups, as shown for **2.2**.

An MO correlation diagram was constructed to facilitate our analysis and visualize changes in MO energies as a function of structure and P oxidation state (Figure 2-4). For convenience, frontier orbitals relevant to the XAS results and reactivity at phosphorus are highlighted in red in Figure 2-4 and connected by dashed lines to show how they transform across the series.

The MO diagram for $P(NMePh)_3$ provides a representative benchmark for phosphines in their common three-fold symmetry, so that the effect of the nontrigonal geometric distortions on orbital energies and compositions can be compared. The MO associated with the P lone pair in $P(NMePh)_3$ (MO 87) was identified by analysis of the calculated Kohn Sham orbitals and P 3s and 3p character mixing in the MO (10.7% and 18.4%, respectively; Figure 2-5). This MO is located at lower energy relative to the HOMO, HOMO-1, and HOMO-2, which are best described as N-aryl π* with limited P 3p character (< 5%). The LUMO and LUMO + 1 are also best described as aryl π* with similar amounts of P 3p character (5.6% and 7.7%, respectively). The unoccupied frontier orbitals

with the largest amount of P 3p character are MOs 100 (47.4%) and 101 (53.2%). These are assigned as P-N σ* with the nearly degenerate P $3p_x$ and $3p_y$ orbitals (Figure 2-5) and are important because they represent the acceptor orbitals on phosphorus.

With the $P(NMePh)_3$ MO diagram for reference, we can evaluate how changing the geometry to nontrigonal $C_{2v}$-**2.1** and **2.1** affects the energies of the P donor and acceptor MOs. As shown in Figure 2-4, the most pronounced change occurs with the nearly degenerate P acceptor MOs in $P(NMePh)_3$ that split in $C_{2v}$-**2.1** and **2.1** to yield a new LUMO at lower energy (MO 68; Figure 2-5). The energy of the remaining P acceptor orbital (MO 73) is relatively unaffected by comparison. Deformation from $C_{2v}$ to $C_s$ symmetry in **2.1** causes the LUMO energy to increase by 1.3 eV compared to $C_{2v}$-**2.1**, and increases the amount of P 3p character from 43.8% ($C_{2v}$-**2.1**) to 56.6% (**2.1**). This increase in P 3p character is notable because it suggests that the P acceptor orbital becomes more accessible for reactions with substrates upon distortion from nontrigonal $C_{2v}$ to $C_s$ symmetry.

We next evaluated changes in the calculated MOs in response to P–H bond formation in **2.2**. As expected, MOs associated with the P donor and acceptor orbitals in **2.1** are transformed upon formation of the new axial and equatorial P-H bonds, resulting in two pairs of P-H σ and σ* MOs that appear at lower and higher energy, respectively. While not shown in the MO diagram in Figure 2-4, oxidation to P(V) caused the energy of the calculated P 1s orbitals to decrease by 1.2 – 1.3 eV compared to the P(III) complexes $P(NMePh)_3$ and **2.1**. This is attributed to the increase in $Z_{eff}$ at P upon oxidation, and accounts for part of the 2.5 eV difference in first peak energies in the spectrum of **2.1** and **2.2** (see Appendix A for detail).

The simulated spectrum for $P(NMePh)_3$ from TDDFT revealed that the first pre-edge peak at 2147.0 eV can be assigned to two transitions arising from mixing of MOs 94/95 and 100/101 in the excited state. Both MO sets are approximately *e* symmetry in the $C_3$ point group and the intensity of the calculated oscillator strength for each transition stems from the large P 3p character mixing in P acceptor MOs 100 and 101 (47.4% and 53.2% calculated P 3p, respectively). For comparison, MOs 94 and 95 have smaller amounts of P 3p character (5.6% and 7.7%).

The distortion from trigonal symmetry in $P(NMePh)_3$ to nontrigonal symmetry in **2.1** results in a single P 1s → LUMO (MO 68) transition assigned to the first pre-edge feature at 2145.9 eV. The lower energy of this transition can be traced back to the splitting of the P acceptor orbitals upon distortion to nontrigonal symmetry, as shown in the MO correlation diagram provided in Figure 2-4. TDDFT calculations of **2.2** revealed that the first peak at 2148.4 eV involves an excited state that contains mixtures of MOs 70 and 73. Both of these orbitals have appreciable P-H σ* character, so the transition is assigned as P 1s → P-H σ*.

## 2-5. Discussion on Biphilic Hypothesis

These spectroscopic and computational results can be contextualized by a qualitative molecular orbital diagram tracing the nontrigonal distortion coordinate, as presented in Figure 2-6. The typical trigonal pyramidal $C_{3v}$ ground state geometry for $\sigma^3$-P gives the lone pair as HOMO ($2a_1$) and LUMO as a doubly degenerate (2e) set of orbitals describing phosphorus-substituent antibonding (Figure 2-6, *left*). Descent to $C_s$ molecular symmetry as depicted (Figure 2-6, *center*) does not dramatically alter the lone pair energy but lifts the degeneracy of the unfilled orbitals by decreasing destructive overlap of the substituents with respect to $p_x$ and increasing destructive overlap with respect to $p_y$. Further transit along this distortion coordinate culminates at a $C_{2v}$-symmetric T-shaped structure (Figure 2-6, *right*) possessing orthogonal frontier orbitals, the precise ordering of which depends on the nature of the substituent and its electronegativity.

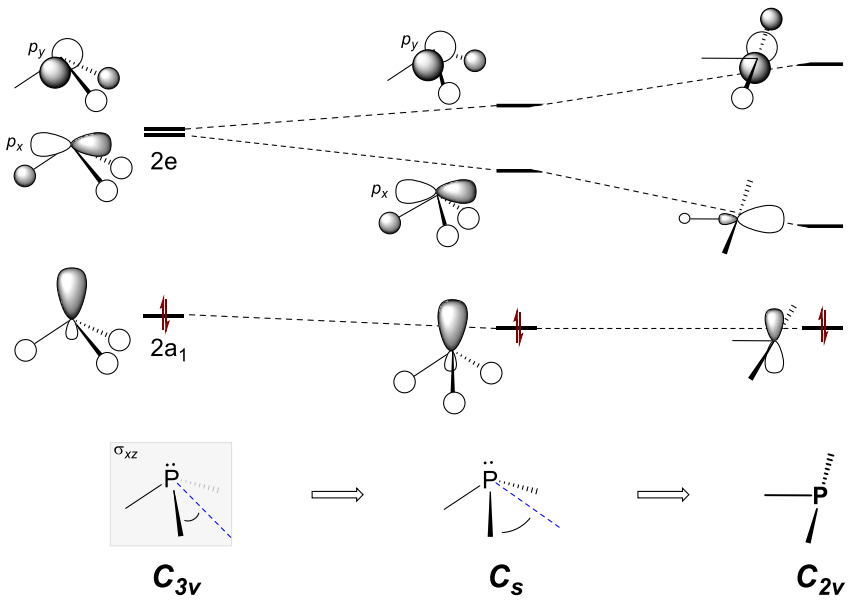


**Figure 2-6.** Qualitative frontier molecular orbital diagrams depicting the electronic structure arising from nontrigonal perturbation of a model $\sigma^3$-P compound.

According to this analysis, we formulate the hypothesis that nontrigonal $\sigma^3$–P will inherently exhibit lower LUMO energies and lower HOMO-LUMO energy gaps than typical trigonal $\sigma^3$–P. And insofar as oxidative addition is facilitated by synergistic donor/acceptor orbital interactions, the colocalization of energetically accessible frontier orbitals within such nontrigonal $\sigma^3$–P structures would be expected to enhance biphilic reactivity at tricoordinate phosphorus.

To provide context for this biphilic hypothesis, we used computational tools to ascertain in a more general fashion the effect of geometrical deformation on the frontier orbital energies of tricoordinate phosphorus for any nontrigonal geometry, not just at discrete structures such as **1** and $C_{2v}$-**2.1**. To this end, the $PN_3$ framework of a model tricoordinate phosphorous triamide $P(NH_2)_3$ was parameterized within local $C_s$ symmetry as illustrated in Figure 2-7, where $P_1$ defines the coordinate origin, $N_1$ resides on the $\sigma_v$ plane, and $N_2$/$N_3$ are symmetry-related by $\sigma_v$ reflection. This model provides two independent driving coordinates corresponding to a bond angle $\theta$ (i.e. $\angle N_1–P_1–N_2 = \angle N_1–P_1–N_3$) and a dihedral angle $\varphi$ (between two planes determined by atoms $N_1$, $P_1$ and $N_2$ and by $N_1$, $P_1$ and $N_3$).

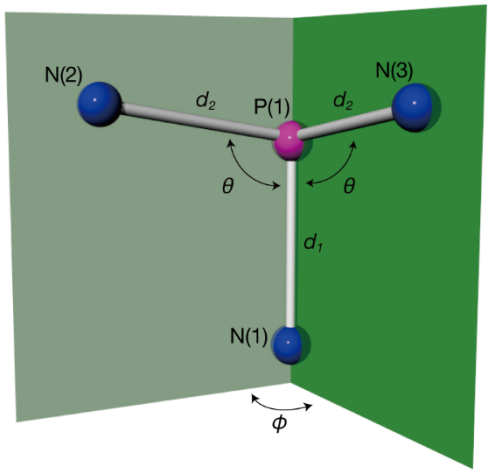


**Figure 2-7.** Definition of geometrical parameters used to index the computational structures of $P(NH_2)_3$

within local $C_s$ symmetry. Hydrogens are omitted for clarity.

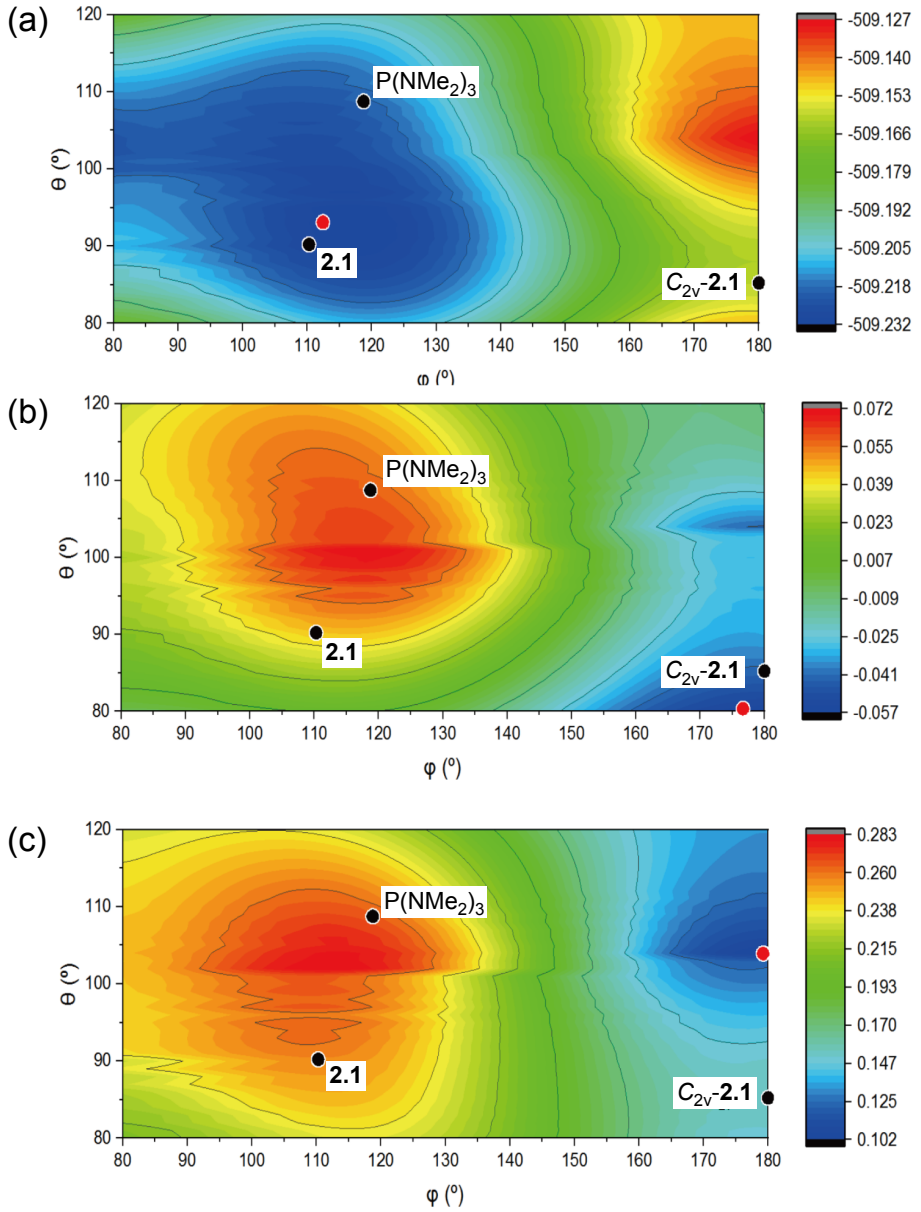


**Figure 2-8**. Contour maps depicting the orbital of (a) Total electronic energy, (b) LUMO energies, (c) ΔHOMO–LUMO for all $P(NH_2)_3$ structures with $C_s$-symmetry. Energies are shown in a units of Hartrees. Points corresponding to the structures of $P(NMePh)_3$, **2.1** and $C_{2v}$-**2.1** are superimposed as black points.

By incrementing the values of $\theta$ and $\varphi$ in 1° intervals throughout the range 80° ≤ $\theta$ ≤ 120° and 80° ≤ $\varphi$ ≤ 180°, 4141 discrete input structures within local $C_s$ space were computationally generated. A geometry optimization of P–N bond lengths ($d_1$ = $d$($P_1$–$N_1$), $d_2$ = $d$($P_1$–$N_2$) = $d$($P_1$–

$N_3$)) and hydrogen positions within the constraints ($\theta$,$\varphi$) provide a local minimum for each structure, from which (a) total electronic energy $E_{tot}$, (b) LUMO energy $E_{LUMO}$, and (c) frontier orbital energy gap between HOMO and LUMO $\Delta E_{HOMO/LUMO}$ were extracted and plotted as contour maps (Figure 2-8a-c).

At the B3LYP/6-31g* level of theory, the overall electronic energy plot (Figure 2-8a) describes a minimum for $P(NH_2)_3$ that is nearly trigonal ($\theta$=93°, $\varphi$=113°), with electronic energy increasing upon planarization ($\varphi \rightarrow 180°$) but varying only modestly for excursions of $\theta$ from equilibrium. For reference, points corresponding to values of ($\theta$,$\varphi$) exhibited by **2.1**, $C_{2v}$-**2.1**, and $P(NMePh)_3$ are overlain on the electronic potential energy surface for $P(NH_2)_3$.

In terms of frontier orbital energies, HOMO energies largely correlate with the total electronic energy in accord with predictions from Walsh's rules. However, an inspection of the plot of LUMO energies (Figure 2-8b) show an inversion in energetic ordering with respect to total electronic energy. Specifically, structures close to the trigonal minimum for $P(NH_2)_3$ exhibit the energetically highest-lying LUMOs. By contrast, the lowest-lying LUMO energies are found for planarized structures ($\varphi \rightarrow 180°$). This data reinforces the experimental observations from XAS spectroscopy and suggests that nontrigonal deformation of phosphorous triamides, especially toward $C_{2v}$ symmetry (e.g. $C_{2v}$–**2.1**), provides for higher phosphorus-based electrophilic reactivity.

As a corollary to the individual frontier orbital trends, a consideration of the frontier orbital energy gap $\Delta E_{HOMO/LUMO}$ plotted in Figure 2-8c is instructive. Trigonal structures, as exemplified by $P(NMePh)_3$, are those evidently that maximize $\Delta E_{HOMO/LUMO}$. In terms of reactivity, this large gap in frontier orbital energies diminishes the propensity for biphilic reactivity, instead accentuating 'monophilic' phosphorus-based nucleophilic reactivity via the HOMO lone pair. By

complement, nontrigonal structures such as **2.1**, but even more so $C_{2v}$–**2.1**, express decreased energy gaps $\Delta E_{HOMO/LUMO}$ consistent with an increased biphilicity for these species relative to compositionally related trigonal phosphorous triamides. The difference in $\Delta E_{HOMO/LUMO}$ between **2.1** and $C_{2v}$–**2.1** coincides with the orbital analysis in Figure 2-4, suggesting that further gains in biphilic reactivity of nontrigonal tricoordinate phosphorus through planarization. Such a realization motivates us to design an appropriate molecular framework to support a phosphorous triamide with molecular $C_{2v}$ symmetry. At present, Arduengo's 5-aza-2,8-dioxa-3,7-di-*tert*-butyl-1-phosphabicyclo[3.3.0]octa-3,6-diene [18] and Wang's phosphorus triamide [19] represent only examples of isolable planar nontrigonal tricoordinate phosphorus compounds. That said, because the barrier to interconversion of **2.1** and $C_{2v}$-**2.1** is known both experimentally and computationally to be low, it is plausible the reported biphilic reactivity of **2.1** is expressed through a preequilibrium deformation to $C_{2v}$-**2.1**.

Another notable feature of Figure 2-8c is that despite the low $\Delta E_{HOMO/LUMO}$ for $C_{2v}$-**2.1**, it does not represent the minimum within the range ($\theta$, $\varphi$) surveyed. Rather, a planar structure with slightly obtuse values of $\theta$ (i.e., $\theta$=104°, $\varphi$=180°) defines the absolute minimum for $\Delta E_{HOMO/LUMO}$. Consequently, if one were able to access such a structure (presumably through appropriate molecular constraint), then presumably the biphilicity of the phosphorus center would be maximized within this local $PN_3$ substitution pattern. This conjecture awaits further experimental exploration.

## 2-6. Conclusion and Outlook

We have provided a combined experimental spectroscopic and theoretical arguments of the electronic structure of geometrically constrained phosphorus compounds both in the tricoordinate and pentacoordinate states. The work provides a rare example where a nontrigonally distorted $\sigma^3$-P compound is interrogated side-by-side with a compositionally related trigonal analogue, allowing a direct comparison of their electronic structures in a way that illuminates aspects of their differential reactivity.

P K-edge analysis has quantified the electronic changes in nontrigonally distorted $\sigma^3$-P compounds and these changes in frontier orbital energy are reproduced by DFT and TDDFT calculations with excellent agreement, allowing the spectral features to be assigned. The combined experimental and theoretical interpretation permit the following specific conclusions to be enumerated regarding the systems studied here: (1) The symmetry-lowering nontrigonal distortion for $\sigma^3$-P leads to a pronounced lowering of a phosphorus-based unoccupied orbital. (2) The unoccupied orbital lowering enables nontrigonal $\sigma^3$-P compounds to behave not only as electron donors (i.e., canonical reactivity for $PR_3$) but also as acceptors of electron density at the same site. (3) The low-lying unfilled orbital is chemically reactive and can become engaged in bonding at phosphorus in the pentacoordinate state.

In sum, this study substantiates the contribution of constrained geometry of nontrigonal $\sigma^3$-P phosphorus compounds to colocalized electron–donor and –acceptor behavior at a single phosphorus site and represents the solid foundation for the expansion of the ‘biphilic’ hypothesis to transition metal complexes, which will be discussed in the following chapters.

## 2-7. Experimental Section

### *2-7-1. General consideration and methods*

**General Considerations.** All reagents were purchased from commercial vendors and used as received unless otherwise noted. Diethyl ether ($Et_2O$), methylene chloride ($CH_2Cl_2$), tetrahydrofuran (THF), and pentane were dried according to the method of Grubbs[20] as modified by Bergman[21] using a Glass Contour Solvent Purification System. All glassware was oven-dried at 120 °C prior to use. All reactions were carried out under dry nitrogen atmosphere (Schlenk line or glovebox) unless otherwise noted. Compounds $P(NMePh)_3$ [22] and **2.1** [23] were synthesized according to the literature procedures and characterized by $^1H$ and $^{31}P$ NMR spectroscopy prior to use. The crystal structure of $P(NMePh)_3$ was determined to allow for comparison of its metrical parameters with cyclic analogues. Solution NMR spectra were recorded on a VARIAN Inova-500 (500 MHz) spectrometer and processed with a MestReNova software. $^1H$ NMR chemical shifts (δ in ppm) were calibrated to the residual solvent peak ($C_6D_6$, δ 7.16 ppm). $^{13}C\{^1H\}$ NMR shifts are given in ppm with respect to solvent residual peak ($C_6D_6$, δ 128.06 ppm). Coupling constants are reported as *J*-values in Hz. High resolution ESI mass spectra were obtained from the Mass Spectrometry Laboratory at the School of Chemical Sciences, University of Illinois at Urbana-Champaign. X-ray diffraction data was collected on a Bruker SMART APEX CCD area detector system equipped with a graphite monochromator and a MoKα fine-focus sealed tube (λ = 0.71073 Å). Raw data integration and reduction were performed with the SAINT [24] and SADABS [25] programs. Structures were solved by direct methods using SHELXT[26] and refined by least-squares methods on $F^2$ using the SHELXL software package. All non-hydrogen atoms were refined with anisotropic displacement parameters. The hydrogen atoms attached to phosphorus were located in

Fourier maps and were refined isotropically without constraints. All other hydrogen atoms were fixed in their ideal geometries. Graphical representations were generated in XP.

**XANES Sample Preparation.** P K-edge XANES samples were prepared in an $N_2$-filled glovebox with <1.0 ppm $O_2$ by grinding crystalline $P(NMePh)_3$, **2.1** and **2.2** (ca. 10 mg) for 2 min using a Wig-L-Bug grinder and polystyrene capsules containing a Plexiglas pestle. The resulting powder for **2.1** and **2.2** was dusted onto single-sided tape (40 μm) exposed through a 5 x 20 x 1 mm window on an aluminum plate using a series 237 Winsor & Newton University Bright brush. P K-edge XANES analysis of the tape, brush fibers, and Wig-L-Bug materials confirmed them to have no measurable phosphorus impurities. The samples were sealed behind two layers of polypropylene film (4 μm, SPEX CertiPrep) separated by an aluminum spacer (1 μM) and transported to the beamline in a sealed container under $N_2$.

**XANES Data Collection and Analysis.** All P K-edge XANES data were collected as previously described on BL 14-3 at the Stanford Synchrotron Radiation Lightsource (SSRL) in Menlo Park, CA under dedicated operating conditions of 3.0 GeV and 500 mA.[27-30] BL 14-3 is equipped with a bending magnet source and a water-cooled double crystal Si(111) monochromator. The sample chamber and gas-flow cell (when used) were maintained under a slow purge of He during data collection. Data were collected in fluorescence mode using a PIPS detector in triplicate sets for each sample over three energy regions, as described previously. The step sizes over the pre-edge (~2106-2140 eV), edge (~2140-2180 eV), and post-edge (~2180-2380 eV) were 1.0, 0.08, and 1.5 eV, respectively. A calibration scan was collected before and after each set of scans on $Na_4P_2O_7$ (2152.40 eV) or $PPh_4Br$ (2146.96 eV).[31] Calibrations, background subtraction, normalization, and averaging of individual scans were completed using the Athena program in the IFFEFIT XAS

software package.[32] A first order polynomial was fit to the pre-edge region to remove the background from each scan. The background-subtracted scans were normalized by fitting a second or third order polynomial to the post-edge regions and setting the step function to an intensity of 1.0 at a set point of 2165 eV.

**DFT and TDDFT Calculations.** All species were modeled as previously described with the B3LYP-D3 flavor of density functional theory as implemented by Gaussian09.[33] This functional combines Becke's three-parameter exchange functional[34] with the correlation functional of Lee, Yang and Parr.[35] Empirical dispersion corrections were added with Grimme's D3 protocol.[36] Nonmetals were modeled with Pople's split-valence double-ζ plus polarization basis set 6-31G(d,p).[37, 38] All species were modeled in the gas phase. Time-dependent density functional theory (TDDFT) calculations were subsequently performed as described previously in order to approximate excitation energies and amplitudes (oscillator strengths) for specific excited states, as well as to simulate the P K-edge XAS data. As previously discussed, an energy shift of +49.6 eV was applied to the calculated spectra to account for the errors in the accuracy of the simulated spectra in including these errors as well as errors associated with relativistic effects and general inaccuracy of the functional. The scalar energy shift was determined by comparing the experimental and calculated energies of the first feature in each spectrum.

*2-7-2. Synthetic procedures*

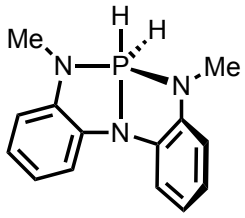


**Synthesis of 2.2.** To a solution of **2.3** (dichloride adduct of **2.1**, 20 mg, 0.061 mmol) in tetrahydrofuran (5 mL) at –35 °C was added sodium cyanoborohydride (77 mg, 0.12 mmol) in one portion. The reaction mixture was stirred 1 h, then warmed to ambient temperature. The solvent was subsequently removed in vacuo. The solid residue was triturated with pentane, and the suspension was filtered over celite. The colorless filtrate was evaporated to give the product **2.2** as a white solid (13 mg, 80 %). A single crystalline sample of **2.2** was obtained from a concentrated pentane solution at –35°C. $^{1}$H NMR (500 MHz, $C_6D_6$) δ 7.40 (d, $J$ = 7.6 Hz, 2H), 7.07 (d, $J$ = 523 Hz, 2H), 7.03 – 6.93 (m, 4H), 6.51 (d, $J$ = 7.2 Hz, 2H), 2.44 (d, $J$ = 16.7 Hz, 6H). $^{31}$P NMR (203 MHz, $C_6D_6$) δ –67.7 (triplet of septets, $J$ = 523, 16.6 Hz). $^{13}$C NMR (126 MHz, $C_6D_6$) δ 133.9 (d, $J$ = 13.1 Hz), 131.8 (d, $J$ = 14.6 Hz), 120.5, 119.8, 110.6 (d, $J$ = 9.2 Hz), 108.7 (d, $J$ = 7.2 Hz), 28.1 (d, $J$ = 14.9 Hz). MS (ESI) calculated for $C_{14}H_{16}N_3P$ (M+): 257.1082, found: 257.1078.

## 2-8. References


1. Rauk, A.; Allen, L. C.; Mislow, K. Pyramidal Inversion. *Angew. Chem. Int. Ed.* **1970**, *9*, 400–414.
2. Levin, C. C. Qualitative Molecular Orbital Picture of Electronegativity Effects on $XH_3$ Inversion Barriers. *J. Am. Chem. Soc.* **1975**, *97*, 5649–5655.
3. Burdett, J. K. Molecular Shapes: *Theoretical Models of Inorganic Stereochemistry*; Wiley: New York, **1980**.
4. Adhikari, D.; Mossin, S.; Basuli, F.; Huffman, J. C.; Szilagyi, R. K.; Meyer, K.; Mindiola, D. J. Structural, Spectroscopic, and Theoretical Elucidation of a Redox-Active Pincer-Type Ancillary Applied in Catalysis. *J. Am. Chem. Soc.* **2008**, *130*, 3676–3682.
5. Harkins, S. B.; Mankad, N. P.; Miller, A. J. M.; Szilagyi, R. K.; Peters, J. C. Probing the Electronic Structures of $[Cu_2(\mu\text{-}XR_2)]^{n+}$ Diamond Cores as a Function of the Bridging X Atom (X = N or P) and Charge (n = 0, 1, 2). *J. Am. Chem. Soc.* **2008**, *13*, 3478–3485.
6. Mankad, N. P.; Antholine, W. E.; Szilagyi, R. K.; Peters, J. C. Three-Coordinate Copper(I) Amido and Aminyl Radical Complexes. *J. Am. Chem. Soc.* **2009**, *131*, 3878–3880.
7. Mossin, S.; Tran, B. L.; Adhikari, D.; Pink, M.; Heinemann, F. W.; Sutter, J.; Szilagyi, R. K.; Meyer, K.; Mindiola, D. J. A Mononuclear Fe(III) Single Molecule Magnet with a 3/2↔5/2 Spin Crossover. *J. Am. Chem. Soc.* **2012**, *134*, 13651–13661.
8. Solomon, E. I.; Hedman, B.; Hodgson, K. O.; Dey, A.; Szilagyi, R. K. Ligand K-edge X-ray Absorption Spectroscopy: Covalency of Ligand-Metal Bonds. *Coord. Chem. Rev.* **2005**, *249*, 97-129.
9. MacMillan, S. N.; Lancaster, K. M. X-ray Spectroscopic Interrogation of Transition-Metal-Mediated Homogeneous Catalysis: Primer and Case Studies. *ACS Catal.* **2017**, *7*, 1776-1791.
10. Donahue, C. M.; Daly, S. R. Ligand K-edge XAS Studies of Metal-Phosphorus Bonds: Applications, Limitations, and Opportunities. *Comments Inorg. Chem.* **2018**, *38*, 54-78.
11. Donahue, C. M.; McCollum, S. P.; Forrest, C. M.; Blake, A. V.; Bellott, B. J.; Keith, J. M.; Daly, S. R. Impact of Coordination Geometry, Bite Angle, and Trans Influence on Metal–Ligand Covalency in Phenyl-Substituted Phosphine Complexes of Ni and Pd. *Inorg. Chem.* **2015**, *54*, 5646-5659.
12. Lee, K.; Wei, H.; Blake, A. V.; Donahue, C. M.; Keith, J. M.; Daly, S. R. Ligand K-edge XAS, DFT, and TDDFT Analysis of Pincer Linker Variations in Rh(I) PNP Complexes: Reactivity Insights from Electronic Structure. *Dalton Trans.* **2016**, *45*, 9774-9785.
13. Blake, A. V.; Wei, H.; Lee, K.; Donahue, C. M.; Keith, J. M.; Daly, S. R. Solution and Solid Ligand K-edge XAS Studies of PdCl2 Diphosphine Complexes with Phenyl and Cyclohexyl Substituents. *Eur. J. Inorg. Chem.* **2018**, 2267-2276.
14. Lee, K.; Wei, H.; Blake, A. V.; Donahue, C. M; Keith, J. M.; Daly, S. R. Measurement of Diphosphine σ-Donor and π-Acceptor Properties in d0 Titanium Complexes Using Ligand K-edge XAS and TDDFT. *Inorg. Chem.* **2018**, *57*, 10277-10286.
15. Mitzel, N. W.; Smart, B. A.; Dreihäupl, K.-H.; Rankin, D. W. H.; Schmidbaur, H. Low Symmetry in $P(NR_2)_3$ Skeletons and Related Fragments: An Inherent Phenomenon. *J. Am. Chem. Soc.* **1996**, *118*, 12673–12682.

16. Zhao, W.; McCarthy, S. M.; Lai, T. Y.; Yennawar, H. P.; Radosevich, A. T. Reversible Intermolecular E-H Oxidative Addition to a Geometrically Deformed and Structurally Dynamic Phosphorous Triamide. *J. Am. Chem. Soc.* **2014**, *136*, 17634–17644.

17. Trans, D.; Addison, A. W.; Rao, T. N. Synthesis, Structure, and Spectroscopic Properties of Copper(II) Compounds Containing Nitrogen-Sulphur Donor Ligands ; the Crystal and Molecular Structure of Aqua[l,7-Bis(N-Methylbenzimidazol-2'-Yl)- 2,6-Dithiaheptane]Copper(II) Perchlorate. *J. Chem. Soc. Dalton. Trans.* **1984**, 1349.

18. Culley, S. A.; Arduengo, A. J. Synthesis and Structure of the First 10-P-3 Species. *J. Am. Chem. Soc.* **1984**, *106*, 1164–1165.

19. Mondal, M. K.; Zhang, L.; Feng, Z.; Tang, S.; Feng, R.; Zhao, Y.; Tan, G.; Ruan, H.; Wang, X. Tricoordinate Nontrigonal Pnictogen-Centered Radical Anions: Isolation, Characterization, and Reactivity. *Angew. Chem. Int. Ed.* **2019**, *58*, 15829–15833.

20. Pangborn, A. B.; Giardello, M. A.; Grubbs, R. H.; Rosen, R. K.; Timmers, F. J. Safe and Convenient Procedure for Solvent Purification. *Organometallics* **1996**, *15*, 1518–1520.

21. Alaimo, P. J.; Peters, D. W.; Arnold, J.; Bergman, R. G. Suggested Modifications to a Distillation-Free Solvent Purification System. *J. Chem. Educ.* **2001**, *78*, 64.

22. Rydon, H. N.; Tonge, B. L. The Organic Chemistry of Phosphorus. Part VI. Some Phosphorus-containing Derivatives of 2,2,2-Trichloroethanol and N-Methylaniline. *J. Chem. Soc.* **1957**, 4862.

23. Zhao, W.; McCarthy, S. M.; Lai, T. Y.; Yennawar, H. P.; Radosevich, A. T. Reversible Intermolecular E–H Oxidative Addition to a Geometrically Deformed and Structurally Dynamic Phosphorous Triamide. *J. Am. Chem. Soc.* **2014**, *136*, 17634–17644.

24. Bruker, *SAINT*, 2012, Bruker AXS Inc., Madison, Wisconsin, USA.

25. Bruker, *SADABS,* 2001, Bruker AXS Inc., Madison, Wisconsin, USA.

26. Sheldrick, G. M. A Short History of SHELX. *Acta. Cryst.* **2008**, *A64*, 112-122.

27. Donahue, C. M.; McCollum, S. P.; Forrest, C. M.; Blake, A. V.; Bellott, B. J.; Keith, J. M.; Daly, S. R. Impact of Coordination Geometry, Bite Angle, and Trans Influence on Metal–Ligand Covalency in Phenyl-Substituted Phosphine Complexes of Ni and Pd. *Inorg. Chem.* **2015**, *54*, 5646-5659.

28. Lee, K.; Wei, H.; Blake, A. V.; Donahue, C. M.; Keith, J. M.; Daly, S. R. Ligand K-edge XAS, DFT, and TDDFT Analysis of Pincer Linker Variations in Rh(I) PNP Complexes: Reactivity Insights from Electronic Structure. *Dalton Trans.* **2016**, *45*, 9774-9785.

29. Blake, A. V.; Wei, H.; Lee, K.; Donahue, C. M.; Keith, J. M.; Daly, S. R. Solution and Solid Ligand K-edge XAS Studies of $PdCl_2$ Diphosphine Complexes with Phenyl and Cyclohexyl Substituents. *Eur. J. Inorg. Chem.* **2018**, 2267-2276.

30. Blake, A. V.; Wei, H.; Donahue, C. M.; Lee, K.; Keith, J. M.; Daly, S. R. Solid Energy Calibration Standards for P K-edge XANES: Electronic Structure Analysis of $PPh_4Br$. *J. Synchrotron Radiat.* **2018**, *25*, 529-536.

31. Minasian, S. G.; Keith, J. M.; Batista, E. R.; Boland, K. S.; Kozimor, S. A.; Martin, R. L.; Shuh, D. K.; Tyliszczak, T.; Vernon, L. J. Carbon K-Edge X-ray Absorption Spectroscopy and Time-Dependent Density Functional Theory Examination of Metal-Carbon Bonding in Metallocene Dichlorides. *J. Am. Chem. Soc.* **2013**, *135*, 14731-14740.

32. Ravel, B.; Newville, M. ATHENA, ARTEMIS, HEPHAESTUS: data analysis for x-ray absorption spectroscopy using IFEFFIT. *J. Synchrotron Radiat.* **2005**, *12*, 537-541.

33. Gaussian 09, Revision B.01, Frisch, M.J.; Trucks, G.W.; Schlegel, H.B.; Scuseria, G.E.; Robb, M.A.; Cheeseman, J.R.; Scalmani, G.; Barone, V.; Mennucci, B.; Petersson, G.A.; Nakatsuji, H.; Caricato, M.; Li,X.; Hratchian, H.P.; Izmaylov, A.F.; Bloino, J.; Zheng, G.; Sonnenberg, J.L.; Hada, M.; Ehara, M.; Toyota, K.; Fukuda, R.; Hasegawa, J.; Ishida, M.; Nakajima, T.; Honda, Y.; Kitao, O.; Nakai, H.; Vreven, T.; Montgomery, J.A., Jr.; Peralta, J.E.; Ogliaro, F.; Bearpark, M.; Heyd, J.J.; Brothers, E.; Kudin, K.N.; Staroverov, V.N.; Kobayashi, R.; Normand, J.; Raghavachari, K.; Rendell, A.; Burant, J.C.; Iyengar, S.S.; Tomasi, J.; Cossi, M.; Rega, N.; Millam, N.J.; Klene, M.; Knox, J.E.; Cross, J.B.; Bakken, V.; Adamo, C.; Jaramillo, J.; Gomperts, R.; Stratmann, R.E.; Yazyev, O.; Austin, A.J.; Cammi, R.; Pomelli, C.; Ochterski, J. W.; Martin, R.L.; Morokuma, K.; Zakrzewski, V.G.; Voth, G.A.; Salvador, P.; Dannenberg, J.J.; Dapprich, S.; Daniels, A.D.; Farkas, Ö.; Foresman, J.B.; Ortiz, J.V.; Cioslowski, J.; Fox, D.J. Gaussian, Inc., Wallingford CT, 2009.

34. Becke, A. D. Density-Functional Thermochemistry. III. The Role of Exact Exchange. *J. Chem. Phys.* **1993**, *98*, 5648-5652.

35. Lee, C.; Yang, W.; Parr, R. G. Development of the Colle-Salvetti Correlation-Energy Formula into a Functional of the Electron Density. *Phys. Rev. B Condens. Matter* **1988**, *37*, 785-789.

36. Grimme, S.; Antony, J.; Ehrlich, S.; Krieg, H. A Consistent and Accurate Ab Initio Parametrization of Density Functional Dispersion Correction (DFT-D) for the 94 Elements H-Pu. *J. Chem. Phys.* **2010**, *132*, 154104/154101-154104/154119.

37. Hehre, W. J.; Ditchfield, R.; Pople, J. A. Self-Consistent Molecular Orbital Methods. XII. Further Extensions of Gaussian-Type Basis Sets for Use in Molecular Orbital Studies of Organic Molecules. *J. Chem. Phys.* **1972**, *56*, 2257-2261.

38. Hariharan, P. C.; Pople, J. A. Influence of Polarization Functions on MO Hydrogenation Energies. *Theor. Chim. Acta* **1973**, *28*, 213-222.

# Chapter 3 Synthesis of Ruthenahydrophosphoranes via Nonspectator Reactivity of Nontrigonal P(III) Ligands: Net insertion, Intramolecular α-H-Migration and Hydride Addition

A significant portion of the work described in this chapter has been published in:

Tanushi, A.; Radosevich, A. T. Insertion of a Nontrigonal Phosphorus Ligand into a Transition Metal-Hydride: Direct Access to a Metallohydrophosphorane. *J. Am. Chem. Soc.* **2018**, *140*, 8114–8118.

Lee, K.; Blake, A.; Tanushi, A.; McCarthy, S.; Kim, D.; Loria, S.; Donahue, C.; Spielvogel, K.; Keith, J.; Daly, S.; et al. Validating the Biphilic Hypothesis of Nontrigonal P(III) Compounds. *Angew. Chem. Int. Ed.* **2019**, *58*, 6993–6998.

## 3-1. Introductory Remarks: Access to Group 8 Metallohydrophosphoranes

Tricoordinate phosphorus (8-P-3) compounds[1,2] are essential donor ligands in transition metal chemistry.[3-6] Within typical (pseudo)threefold symmetry, the Lewis basicity and nucleophilicity of trigonal pyramidal 8-P-3 compounds makes the mixture of a transition metal fragment (M–X) and a phosphine ($R_3P$) a robust and reliable route to the formation of $R_3P$–M–X complexes (Figure 3-1, *left*).

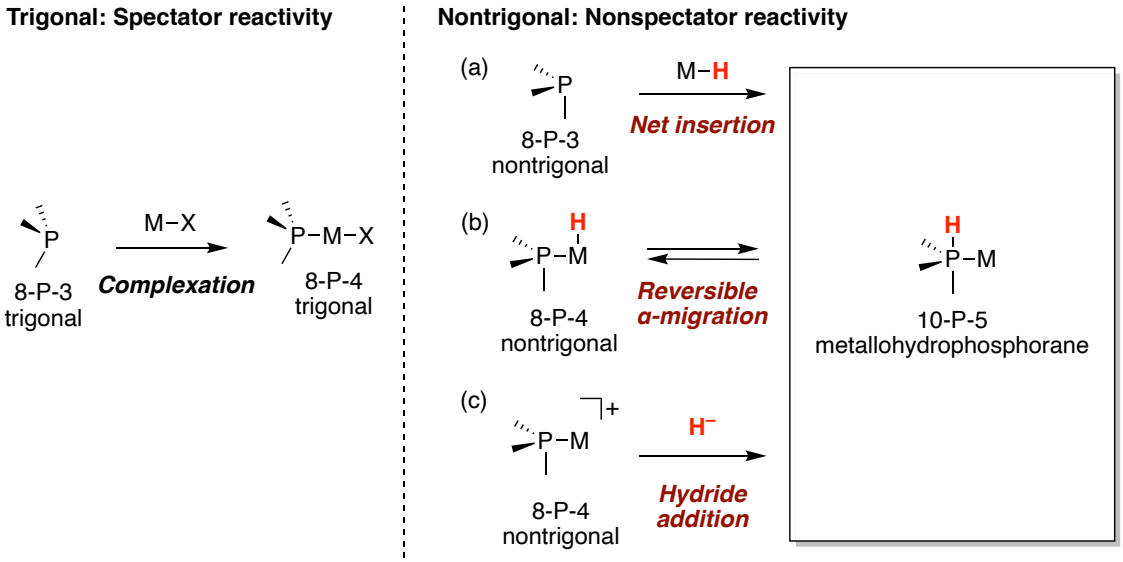


**Figure 3-1.** Divergent metalation of trigonal and nontrigonal 8-P-3 compounds.

In Chapter 2, we quantitatively demonstrated the biphilicity[7] of nontrigonal tricoordinate phosphorus ligands that enhances the access to higher coordinate P species. In Chapter 3, using the nontrigonal biphilic P(III) compounds as ligands coordinating to Group 8 Ru centers, we will show various 'nonspectator' reactivities that diverge from the traditional view of phosphines as spectator ligands with a particular focus on the chemistry of hydrides (Figure 3-1, *right)*.

In the first part (**Sections 3-2 and 3-3**), we will show a noncanonical ligation event arising from metalation of a nontrigonal 8-P-3 compound. The net insertion of a distorted 8-P-3

phosphorous triamide center into a transition metal-hydride bond to form a 10-P-5 metallophosphorane (Figure 3-1a) in preference to the typical 8-P-4 complex. The properties of the resulting metallophosphoranes are investigated by various methods, including the XANES analysis we used for nonmetal phosphorus species in Chapter 2. In the second part (**Sections 3-4 and 3-5**), using an isolated intermediate 8-P-4 complex of the net insertion, we show an α-H-migration from Ru to P and investigate its mechanism process experimentally and computationally. We will also demonstrate that the α-H-migration is bidirectional, reversible and can be controlled by perturbation of Ru coordination environment (Figure 3-1b). In the third part (**Sections 3-6 and 3-7**), we will expand the synthetic routes to the metallohydrophosphoranes to exogenous hydride addition to 8-P-4 complexes (Figure 3-1c). Through these results, we realize the merger of phosphorus-based biphilic reactivity[8] with transition metal ligancy and thereby provide a new entry point for the study of supporting ligands based on higher coordination number phosphorus fragments.

## 3-2. Synthesis of Tridentate Ligand L1

A novel tridentate ligand **L1** with a nontrigonal phosphorus triamide moiety with two pyridyl side arms was newly designed and synthesized from bis(2-aminophenyl)amine [9] by twofold electrophilic heteroarylation with 2-chloropyridine, followed by insertion of $PCl_3$ in the presence of $NEt_3$.[10]

**Scheme 3-1.** (a) Synthesis of tridentate ligand **L1**. (b) Structure of nontrigonal phosphorus triamide **2.1**.

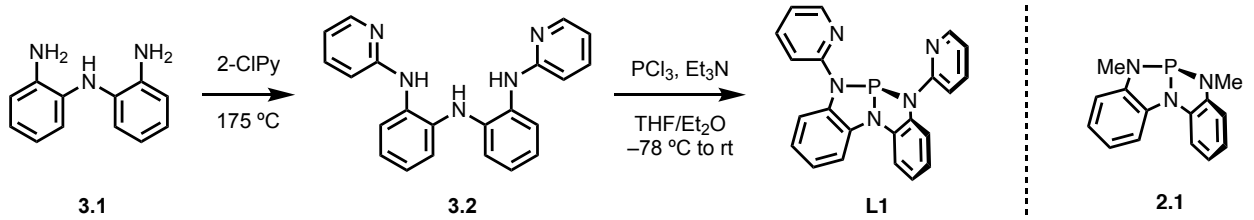


**3.1** **3.2** **L1** **2.1**

In the solution phase, $^1$H NMR spectra of **L1** exhibit a twofold equivalence of resonances ($\delta$ 8.26–6.92 ppm), indicating a time-averaged $C_s$ molecular symmetry or higher. A $^{31}P\{^1H\}$ NMR spectrum of **L1** displays a singlet at δ 141.7 ppm (Figure 3-2a), residing upfield as compared to **2.1** (δ 159.8 ppm). Structural analysis suggests the origin of this spectral distinction. X-ray diffraction of a colorless single crystal of the ligand **L1** revealed a solid state structure of approximate $C_s$ local symmetry (Figure 3-3) marked by folding of the phosphorous triamide moiety along the $P_1$–$N_1$ axis, in line with previous observations for **2.1**. However, in contrast to **2.1**, the $\angle N_2$–$P_1$–$N_3$ angle for **L1** is decidedly more acute (cf. 108.67(4)° vs. 115.21(7)°) while the bond lengths $d(P_1$–$N_{2/3})$ are somewhat longer (cf. 1.7341(8)° vs. 1.7190(13)° for $d(P_1$–$N_2)$ and 1.7786(8)° vs. 1.7014(14)° for $d(P_1$–$N_3)$). These structural features can be rationalized qualitatively by reference to Bent's rule, [11] where the electron-withdrawing 2-pyridyl *N*-substituents attract phosphorus *p*-character to the $P_1$–$N_{2/3}$ bonds, resulting in elongated $d(P$–$N_{2/3})$ distances and contracted $\angle N_2$–$P_1$–$N_3$ angles. The complementary accrual of *s*-character in the

nonbonding *P*-based lone pair therefore increases nuclear shielding for **L1** as observed in the $^{31}P\{^{1}H\}$ NMR chemical shift.

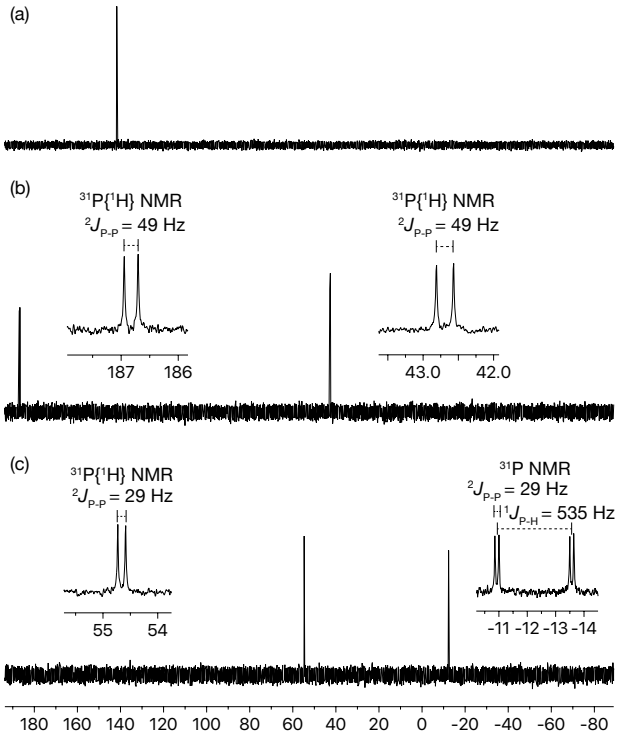


**Figure 3-2.** $^{31}P$ NMR spectra of (a) **L1** (b) **3.3** (c) **3.4** in $CDCl_3$. Units are ppm relative to 85% $H_3PO_4$.

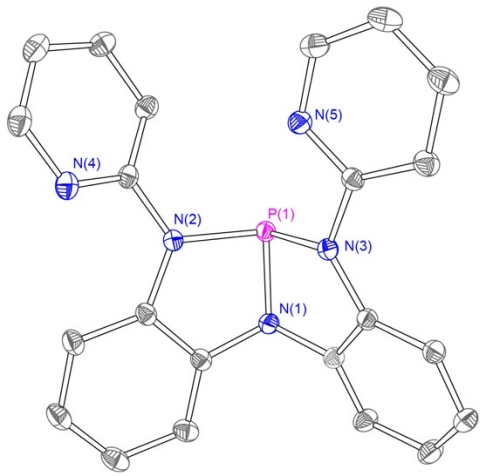


**Figure 3-3.** Thermal ellipsoid plots rendered at the 50% probability level for **L1**. Hydrogens are omitted for clarity.

## 3-3. Insertion of Nontrigonal P(III) Ligand into Ru–H

### *3-3-1. Metalation of **L1** with $RuCl_2(PPh_3)_3$*

**Scheme 3-2.** Metalation of **L1** with Ru precursors.

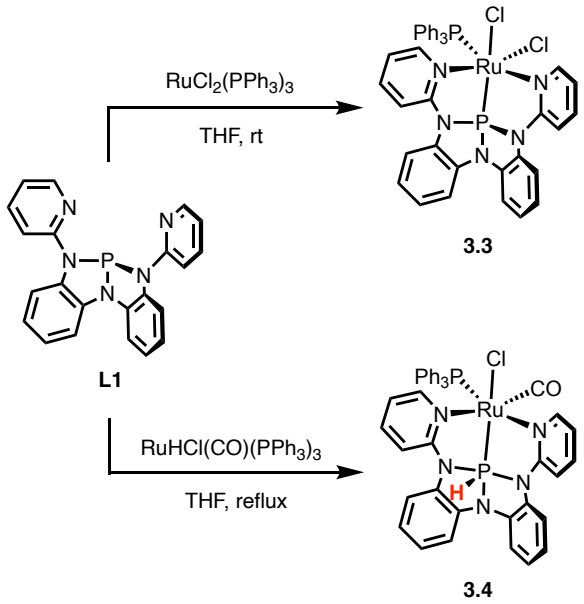


Metalation of **L1** by treatment with $RuCl_2(PPh_3)_3$ [12] was achieved in THF at ambient temperature to afford an octahedral complex $RuCl_2(PPh_3)$(**L1**) (**3.3**) (Scheme 3-2). In the resulting $^{31}P\{^1H\}$ NMR spectra, the resonance corresponding to the phosphorus nucleus of **L1** is found downfield (relative to free ligand **L1**) as a doublet at $\delta$ 186.8 ppm with $J = 49$ Hz; the corresponding coupling partner arising from the phosphorus nucleus of $PPh_3$ resonates at δ 42.7 ppm with complementary $J = 49$ Hz coupling (Figure 3-2b). The $\kappa_3$-chelating mode is confirmed by X-ray diffraction of a single crystal sample, where the facial coordination of the tridentate **L1** ligand is evident (Figure 3-4). The $Ph_3P$ ligand is found *cis* with respect to the phosphorus atom in the **L1** fragment, giving a complex of overall $C_1$ symmetry. The high number of complex overlapping resonances in the aryl region of the solution phase $^1H$ NMR spectra for **3.3** are congruent with the elimination of the symmetry element about the central $P_1$–$N_1$ axis of **L1** upon ligation. The $\angle N_2$–

$P_1$–$N_3$ angle is broadened (113.94(4°) as compared to free **L1**, braced by the constraint imposed by the chelation of the pyridyl arms to Ru. A distinctive feature of the structure for **3.3** is the exceptionally short *d*($Ru_1$–$P_1$) bond distance (2.1262(3) Å), which is significantly shorter than the typical range for $\sigma^3$-P–Ru bonds (2.20 Å < *d* < 2.45 Å) and only modestly longer than the shortest characterized $\sigma^3$-P–Ru distance (2.0883(6) Å),[13] found for a NPN $\kappa^3$-chelate containing a central $\sigma^3$-P site substituted with electronegative heteroatoms similar to **2** (Chart 3-1).

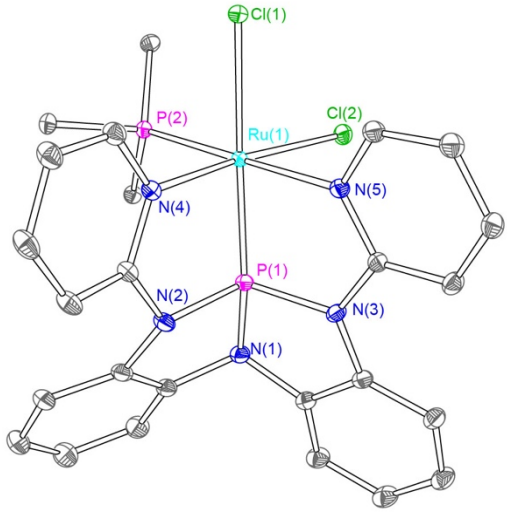


**Figure 3-4.** Thermal ellipsoid plots rendered at the 50% probability level for **3.3**. Hydrogens, solvent molecules of crystallization and phenyl rings of $PPh_3$ ligands are omitted for clarity.

**Chart 3-1.** Shortest characterized $\sigma^3$-P–Ru bond reported by Braustein and co-workers (Ref. 13).

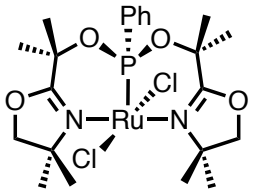

*3-3-2. Metalation of **L1** with RuHCl(CO)(PPh$_3$)$_3$*

Metalation of **L1** with RuHCl(CO)(PPh$_3$)$_3$[14] was similarly attempted; however, the expected congener of **3.3** was not returned. Instead, $^{31}P\{^1H\}$ NMR spectra (Figure 3-2c) showed formation of a new complex with a large upfield shift for the phosphorus atom of **L1** at $\delta$ –12.3 ppm and coupling (doublet, $J$ = 29 Hz) to one remaining PPh$_3$ ligand ($\delta$ 54.7 ppm, $^2J_{P\text{-}P}$ = 29 Hz). In the $^1$H-coupled $^{31}$P NMR spectrum, the signal at $\delta$ –12.3 ppm is further split into a doublet with a large coupling constant ($J$ = 535 Hz). The magnitude of this coupling constant suggests the formation of a direct P–H bond. Indeed, the corresponding proton coupling partner is found in the $^1$H NMR spectrum as a doublet at $\delta$ 7.52 ppm ($J$ = 535 Hz), well downfield from the typical range for a Ru(II)–H (i.e. $\delta < 0$ ppm). The formation of P–H bond is also supported by an absorption at 2226 cm$^{-1}$ in the IR spectrum, which can be assigned to a P–H stretching mode. Together, these spectra suggest that reaction of **L1** with RuHCl(CO)(PPh$_3$)$_3$ affords a stable complex in which the hydrido ligand of Ru is transferred to the phosphorus atom, which we formulate as RuCl(CO)(PPh$_3$)(**L1**$^H$) (**3.4**, Scheme 3-2).

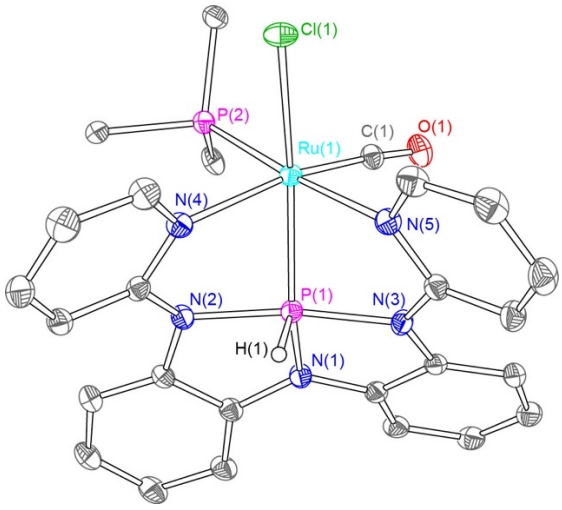


**Figure 3-5.** Thermal ellipsoid plots rendered at the 50% probability level for **3.4**. Hydrogens except H(1) and phenyl rings of PPh$_3$ ligands are omitted for clarity. Only one of the three independent molecules in the

unit cell is shown.

The solid-state structure of **3.4**, determined by X-ray diffraction on a single crystal confirms this assignment (Figure 3-5). Indeed, the 10-P-5 nature of the phosphorus environment is evident. The geometry about P is described by a distorted trigonal bipyramid ($\tau_5 = 0.50$)[15] with the H and Ru substituents occupying equatorial positions; by consequence, the phosphorous triamide framework is greatly planarized as compared to **3.3** with the 2-pyridylamides occupying the *trans* diapical sites ($\angle N_2–P_1–N_3 = 170.74(7)°$). The ruthenium-phosphorus bond distance ($d(Ru_1–P_1)$ = 2.2509(4) Å) is ca. 0.12 Å longer than in **3.3**. The origin of this change is given at least in part by the ring constraints imposed by the chelating pyridyl arms, which draw the pentacoordinate phosphorus away from an idealized axial octahedral coordination site about ruthenium (compare $\angle P_1–Ru–Cl_1 = 168.85(1)°$ vs. 160.57(2)° for **3.3** and **3.4**, respectively).

*3-3-3. Structure of metallophosphorane **3.4** and comparison to metal–hydride species*

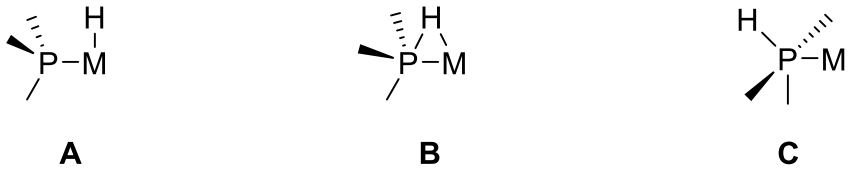


**Figure 3-6.** Canonical structures corresponding to hydride transfer from M→P.

In view of the apparent transferal of hydride from Ru to P in **3.4**, it is instructive to consider the suite of isomeric canonical structures in Figure 3-6.

While examples of the type **A** (metal-bound terminal hydride) are legion,[16-19] complexes of the type **B** (bridging hydride) are less common; Schrock has characterized such complexes of Re[20] and Mo[21] formed by protonation of the progenitor metal-phosphine (Scheme 3-3).[22,23] Specifically, treatment of rhenium diphenylphosphine complex **3.S1** with an equimolar amount of $[H(OEt_2)_2]BAr^F{}_4$ in $CH_2Cl_2$ at –40 °C afforded monoprotonated cationic complex **3.S2**. The $^1H$ NMR spectrum showed a doublet of doublets signal for the newly introduced proton ($H_a$) at δ 3.36 ppm ($J_{PH}$ = 54 Hz, $J_{HH}$ = 15 Hz). The coupling partner hydrogen ($H_b$) was found as a doublet of doublets at δ 6.75 ppm ($^2J_{PH}$ = 375 Hz, $^2J_{HH}$ = 15 Hz), corresponding to the P–H of the $HPPh_2$ ligand. The downfield chemical shift (δ 3.36 ppm) and relatively large coupling constant ($J_{PH}$ = 54 Hz) showed a stronger interaction between $H_a$ and P, suggesting a metallophosphorane structure. In the obtained crystal structure of **3.S2**, $H_a$ was successfully located between Re–P and in the Re–P–N plane under constraints on Re–$H_a$ and P–$H_a$ distances. Relatedly, protonation of anionic Mo–nitride complex **3.S3** by $[Et_3NH]BAr^F{}_4$ in benzene, which resulted in a doublet of doublets resonance at δ 3.94 ppm ($J_{PH}$ = 133 Hz, 6 Hz) for the newly attached proton. The authors proposed the metallophosphorane **3.S1** with a bridging H as the structure of the product.

**Scheme 3-3.** Synthesis of Re and Mo complexes with bridging hydrides over M–$PR_3$ bonds by Schrock.

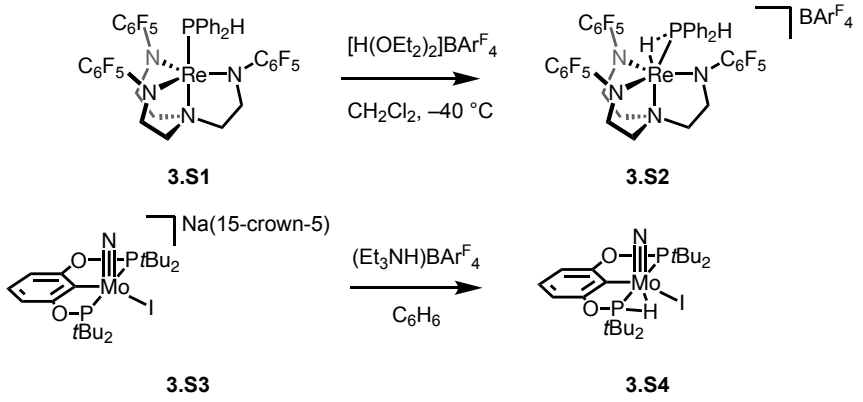


By contrast, examples of the type **C** (phosphorus-bound terminal hydride) have not been isolated or structurally characterized. The only reports were by Ebsworth and coworkers; they synthesized mixtures of complexes containing *trans*-$PtX(PEt_3)_2(PH_2X_2)$ by reactions of $PtX(PEt_3)_2$ and $PX_3$ (X = Cl, Br) (Scheme 3-4).[24] Due to the lack of isolated products, however, the authors noted that they could not completely exclude the possibilities that the products are anionic six-coordinate phosphorus species $[PtX(PEt_3)_2(PH_2X_3)]^-$. They also reported the synthesis of $Ir(CO)BrH(PEt_3)_2(PH_2F_2)$ by reaction of $Ir(CO)BrH(PEt_3)_2(PH_2)$ with $XeF_2$.[25]

**Scheme 3-4.** Synthesis of metallohydrophosphoranes reported by Ebsworth *et al*.

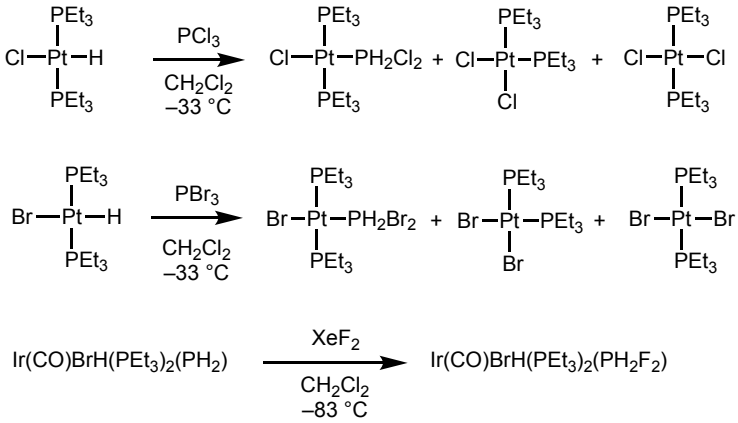

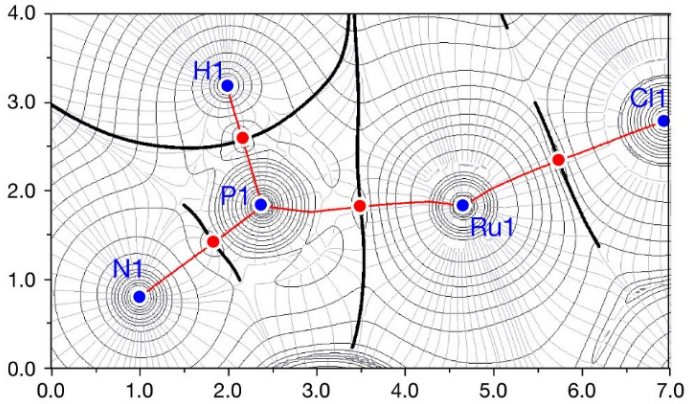


**Figure 3-7.** Calculated electron density for **3.3** in the plane defined by Ru–P–H coordinates. Electron density contours (—), gradient vector field (—), bond paths (—), bond critical points (•), and atomic basins (▬) are depicted. Units are Å.

Neither the downfield $^{1}$H NMR chemical shift of the hydrido ligand ($\delta$ 7.52 ppm) nor the long $d$(Ru$_1$-H$_1$) experimental distances (2.980–2.998 Å) seem to indicate significant Ru···H interaction for **3.4**, disfavoring depictions **A** and **B**. As a further point of adjudication, the topological properties of the electron density were analyzed within the QTAIM framework.[26] A geometry-optimized DFT model (B3LYP/def2-TZVP) of **3.4** reproduces the experimental structure with good agreement (see Experimental Section), and an all-electron single point calculation (B3PW91/def2-TZVP with zero-order regular approximation (ZORA)[27,28] for relativistic effects) was executed. As depicted in the plot of the electron density in the plane containing the Ru, P, and H nuclei (Figure 3-7), bond paths defined by (3,–1) critical points are found for Ru–P and P–H, but not for Ru···H. Moreover, the atomic basins for Ru and H do not abut. Consequently, complex **3.4** is well-formulated as the first isolated and structurally characterized example of ruthenahydrophosphorane with a terminal, nonbridging P-bound hydride (type **C**).

*3-3-4. Hydridic Reactivity of P–H bonds*

With respect to reactivity, complex **3.4** exhibits hydridic character; treatment with triphenylcarbenium hexafluorophosphate ($Ph_3CPF_6$) leads to hydride abstraction and conversion to [RuCl(CO)($PPh_3$)(**L1**)]$PF_6$ (**3.5**) (Scheme 3-5). The abstraction of hydride was confirmed by the disappearance of the IR band corresponding to P–H stretching and a hypsochromic shift of the C=O stretching band ($\Delta\nu_{CO}$ = 70 $cm^{-1}$). Moreover, the $^{31}P$ NMR spectra for **3.5** (δ 187.3 ppm (**L1**); δ 42.5 ppm ($PPh_3$); $^2J_{P-P}$ = 43 Hz for the couple) no longer exhibit $^1J_{P-H}$ coupling. However, the treatment of **3.5** with an exogenous hydride donor ($NaBH_4$) returns **3.4**, indicating the bidirectionality of the phosphorus-centered hydride reactivity and the pronounced electrophilicity of the distorted phosphorous triamide center. All attempts to deprotonate the P–H in **3.4** by treatment with base (e.g. KHMDS, KH/18-crown-6) have been unsuccessful to date; the acidity of P–H moiety is apparently quite low.

**Scheme 3-5**. Reversible hydride abstraction from **3.4**.

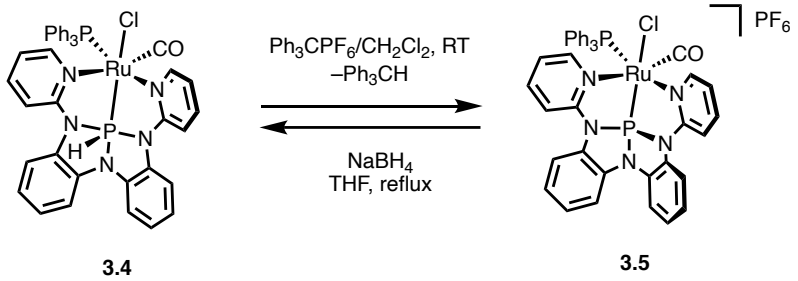


**3.4** **3.5**

### *3-3-5. Electronic structure analysis of complexes **3.3** and **3.4** by P K-edge XANES with TDDFT calculation*

We next evaluated the XANES spectra of **3.3** and **3.4** to determine how metalation of **L1** and phosphorus insertion into a Ru-H bond compared to electronic structure data collected for tricoordinate nontrigonal phosphorus triamide **2.1** and its derivative in Chapter 2. The P K-edge XANES spectrum of **3.3** revealed three features: a shoulder at 2145.9 eV and two prominent peaks at 2146.8 and 2148.1 eV (Figure 3-8). The P K-edge XANES spectrum of **3.4** yielded similar features at 2145.9 and 2148.2 eV, but the intense peak at 2146.8 eV in **3.3** was no longer present.

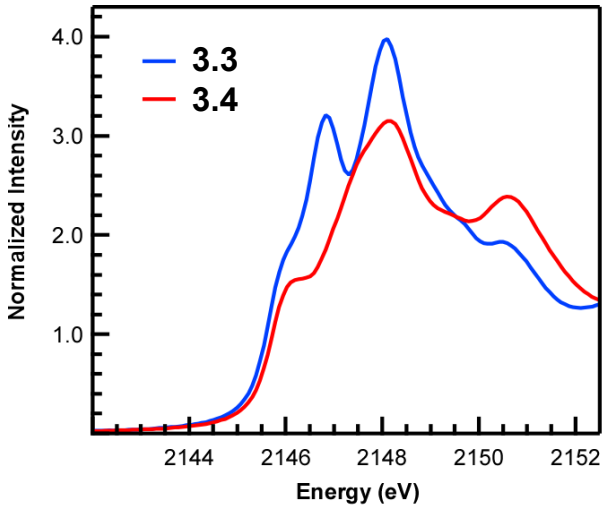


**Figure 3-8.** Comparison of P K-edge XANES spectra for **3.3** (blue) and **3.4** (red).

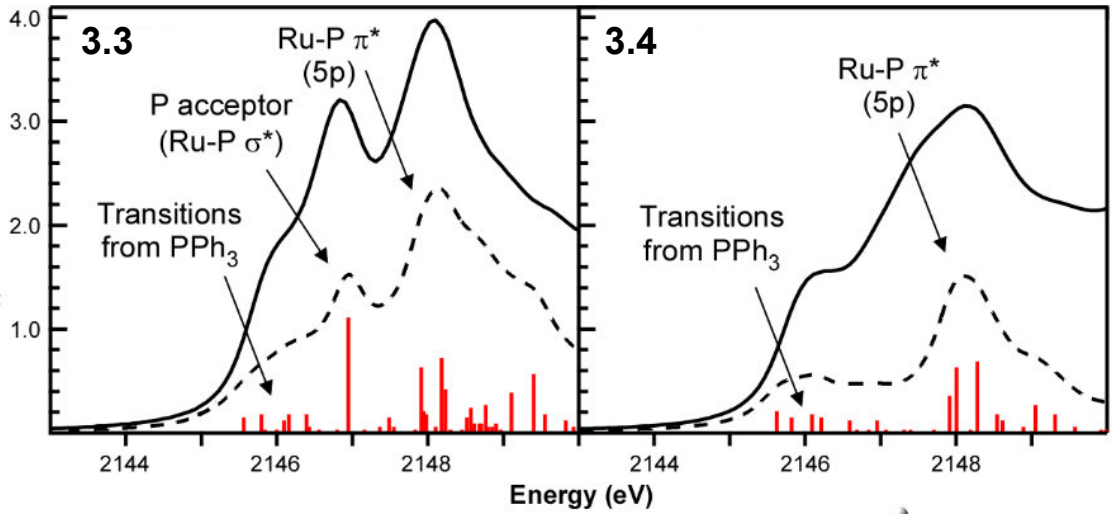


**Figure 3-9.** Comparison of experimental (solid line) and simulated (dashed line) P K-edge XANES spectra for **3.3** and **3.4**. Individual transitions are represented by red bars and indicate relative differences in calculated oscillator strength. The transitions are labeled with calculated MOs mixing in the excited states.

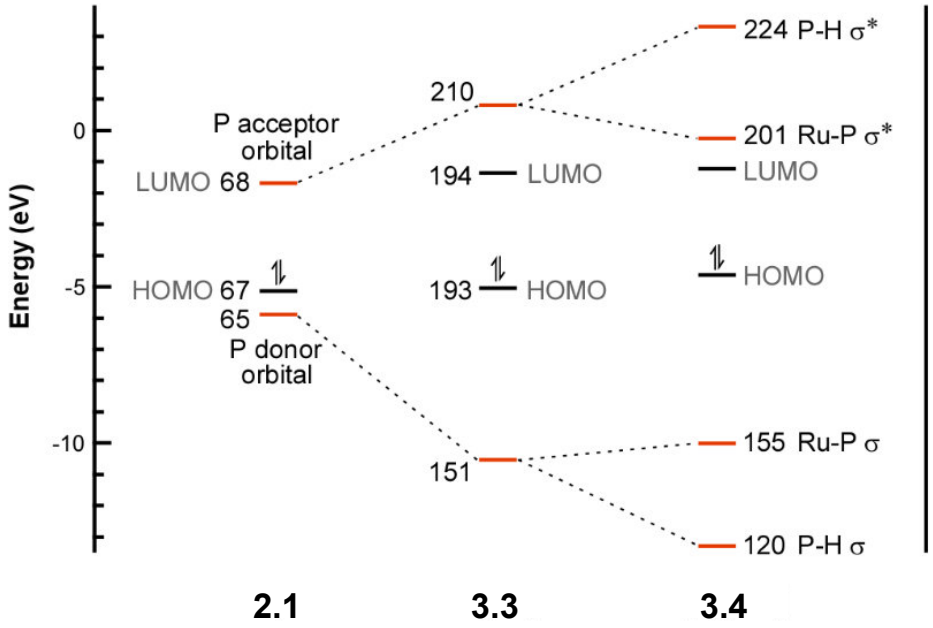


**Figure 3-10.** Truncated MO correlation diagram of **2.1**, **3.3**, **3.4**. Frontier orbitals relevant to the XAS results and reactivity at phosphorus are highlighted in red and connected by dashed lines to show how they transform across the series.

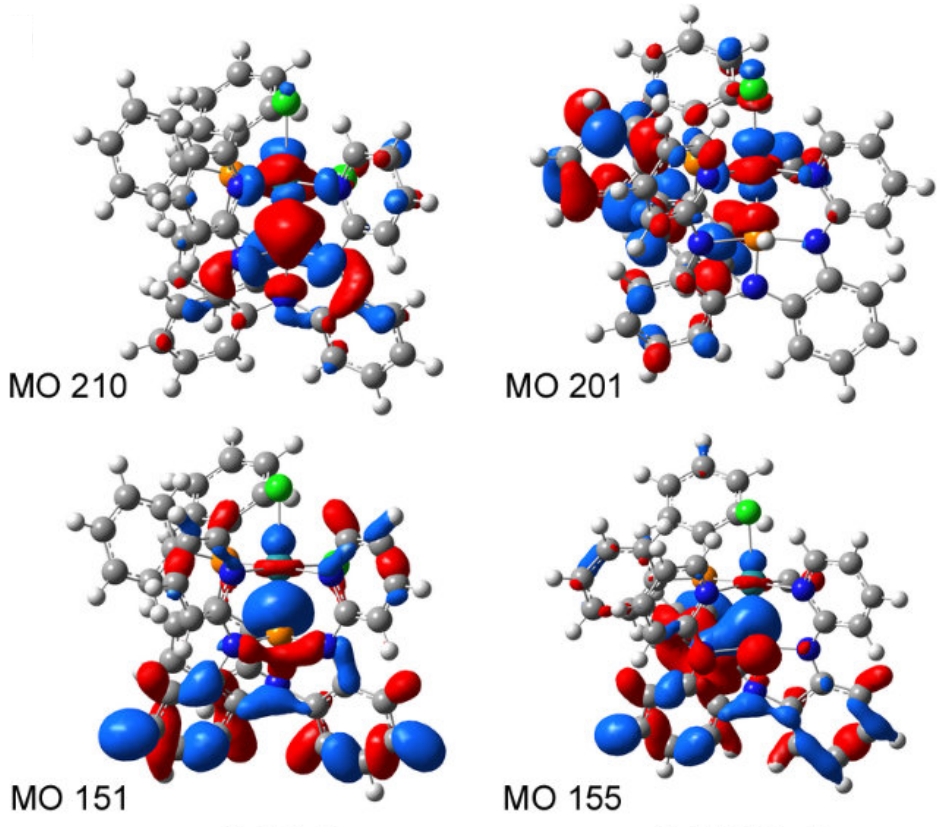


**Figure 3-11.** Selected donor-acceptor Kohn-Sham orbitals from DFT calculations of **3.3**, and **3.4**.

DFT and TDDFT calculations were once again used to assign the spectral features and account for the electronic structure differences in **3.3** and **3.4** (Figure 3-9a). DFT calculations revealed that the phosphorus acceptor orbital on the free ligand **L1** mixes with the empty $4d_{z2}$ on Ru to form a new MO that has some Ru-P σ* character and a large amount of P acceptor character (MO 210; Figure 3-10 and Figure 3-11), as reflected in the calculated MO composition (43.3% P 3p and 11.2% Ru 4d;). For comparison, a complementary Ru-P σ bonding MO was identified at lower energy (MO 151; Figure 3-10) with lower P 3p mixing due to the absence of P acceptor character (9.7% P 3p and 5.4% Ru 4d).

Inserting P into the Ru-H bond in **3.4** yields Ru-P σ and σ* orbitals at similar energies to those calculated for **3.3** (MOs 155 and 201; Figure 3-10), but the P acceptor character in the unoccupied orbital is extinguished (MO 201 has only 2.5% P 3p compared to 43.3% in **3.3**). The complementary Ru-P σ orbital in **3.4** (MO 155) has 8.3% P 3p and 3.4% Ru 4d character – slightly less than that observed in **3.3**. Two new MOs assigned to P-H σ and $\sigma^*$ (MOs 120 and 224, respectively) were also identified for **3.4**, as expected.

TDDFT calculations revealed that the large amount of P 3p acceptor character in MO 210 for **3.3** gives rise to the intense transition at 2146.8 eV in the P K-edge XANES spectrum shown in Figure 3b. Weaker transitions centered around 2146 eV are associated with unoccupied frontier orbitals containing smaller amounts of P 3p character from $PPh_3$, whereas at higher energy (ca. 2148 eV) are transitions best described as 1s → Ru-P π*. These latter transitions arise from higher energy MOs that contain significant amounts of Ru 5p mixing (MOs 212, 215, and 216; see Experimental Section for details)

Metalation of **L1** to form **3.3** yields a prototypical dative P→Ru bond with the P lone pair, but the P acceptor orbital remains available as indicated by an intense P K-edge XANES transition at 2146.8 eV. However, in the presence of a Ru-bound hydride, phosphorus inserts into the Ru-H bond and fills the low-lying P acceptor orbital, thereby causing the intense pre-edge transition to disappear. Furthermore, the MO correlation diagrams provided the same qualitative electronic structure variations regardless if P in **2.1** or **L1** is formally inserted into H-H or Ru-H bonds.

## 3-4. Direct Observation of Intramolecular H-migration from Ru to P and Mechanistic Investigation

### *3-4-1. Metalation of **L1** with $RuHCl(PPh_3)_3$*

Whereas the insertion reactivity and the hydridic character of P–H in metallophosphorane **3.4** strongly indicate an α-H-migration from Ru to P, there remain unanswered questions. We did not show: (i) the intermediates in the multistep reaction sequence that shows the direct α-H-migration is involved, and (ii) the mechanism and transition state of H-migration (for instance, whether there is a three-membered transition state similar to that for CO insertion).

In order to detect the α-migration directly, the synthesis of a Ru–H complex featuring ligand **L1** was first attempted. A metalation of **L1** by treatment with $RuHCl(PPh_3)_3$[29] in THF at ambient temperature afforded an octahedral complex *fac*-$RuHCl(PPh_3)$(**L1**) (**3.6**) (Scheme 3-6).

**Scheme 3-6.** Metalation of **L1** with $RuHCl(PPh_3)_3$.

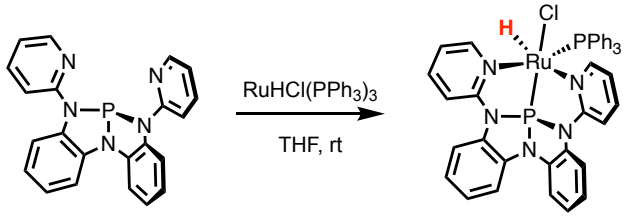


$^{31}P\{^1H\}$ NMR spectra displayed a signal corresponding to the phosphorus triamide P as a doublet at δ 190.1 ppm ($J_{P\text{-}P}$ = 54 Hz), which is found downfield relative to **L1** (δ 141.7 ppm) and is similar value to that of $RuCl_2(PPh_3)$(**L1**) (δ 186.8 ppm) (Figure 3-12a). The corresponding coupling partner arising from the $PPh_3$ ligand resonates at δ 66.6 ppm. In the H-coupled $^{31}P$ NMR spectrum, the signal at δ 190.1 ppm was further split into a doublet ($J_{P\text{-}H}$ = 31 Hz). In $^1H$ NMR spectra, the corresponding coupling partner was found as a double doublet at δ –12.05 ppm, which

was split by the couplings with two phosphorus nuclei ($^2J_{P-H}$ = 31 Hz, 28 Hz). The $^1$H NMR chemical shift below 0 ppm indicates the H atom corresponds to a ruthenium hydride. In contrast to the previously reported reaction of **L1** with $RuHCl(CO)(PPh_3)_3$, the hydride migration from Ru to P was not observed in this case even at high temperature.

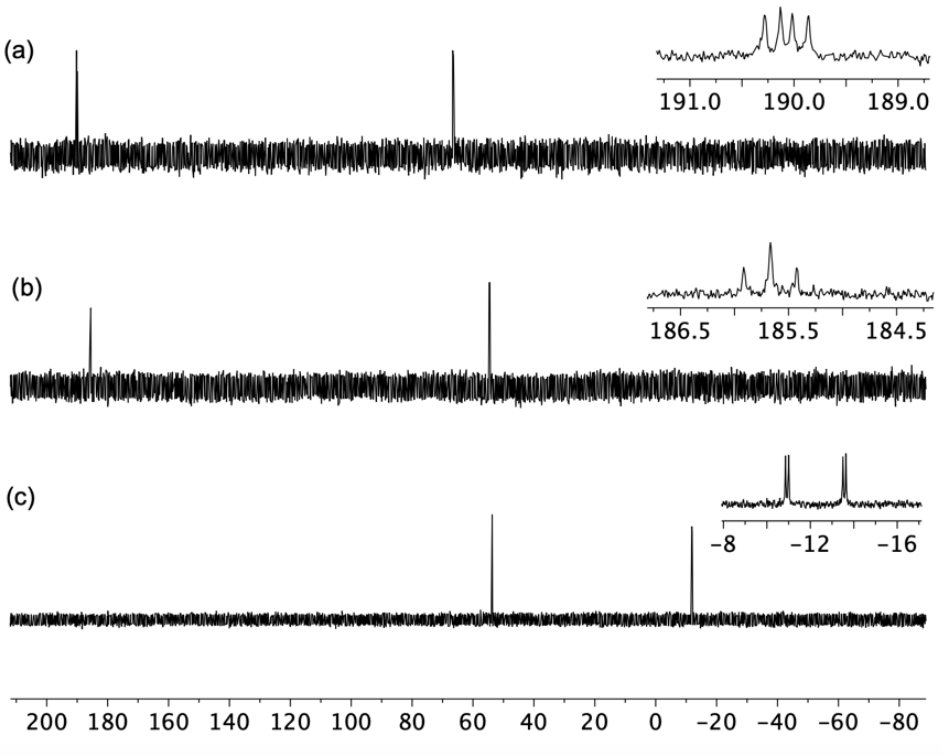


**Figure 3-12.** $^{31}P\{^1H\}$ NMR spectra of (a) **3.6**, (b) **3.7** and (c) **3.4** in $C_6D_6$. Units are in ppm. Inset figures show $^1$H -coupled $^{31}$P NMR spectra.

*3-4-2. Reaction of **3.6** and CO*

Next, the Ru–H complex **3.6** was treated with CO to see if an intramolecular H-migration is induced. However, a reaction of compound **3.6** with CO (1 atm) at ambient temperature did not return the expected metallophosphorane immediately. Instead, the reaction afforded another metal-

phosphine type complex **3.7** with a $\kappa^2$-*P,N*-chelation mode by a substitution of one of the pyridyl moeities (Scheme 3-7).

**Scheme 3-7.** Reaction of CO with **3.6** followed by intramolecular H-transfer.

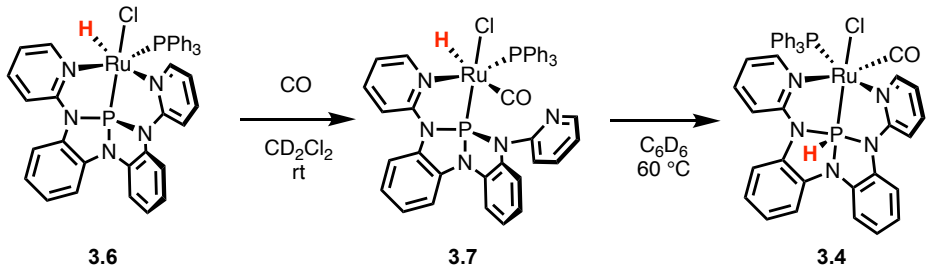


The assignment of **3.7** was based on the observation that the resonance corresponding to the triamide phosphorous was found at $\delta$ 185.7 ppm, coupled to the $^{31}$P nucleus of $PPh_3$ (δ 54.6 ppm) by 38 Hz (Figure 3-12b), suggesting that there are no drastic changes in the environment of two phosphorus nuclei upon reaction. In contrast to the minor changes in the $^{31}$P NMR spectra, $^{1}$H NMR spectra displayed a significant effect of the substitution. The Ru–H resonance appeared at δ –4.53 ppm, significantly shifted downfield from that of **3.6** (δ –12.03 ppm) and coupled to two $^{31}$P nuclei ($^2J_{P-H}$ = 38 Hz, 20Hz) . In addition, the signals corresponding to the hydrogens of substituted pyridyl ring were found significantly upfield relative to **3.7**, which agrees with the increase of shielding due to the dissociation of pyridyl nitrogen atom from Ru center.

The κ$^2$-chelating mode of **3.7** was further confirmed by the solid-state structure determined by X-ray diffraction on a single crystal obtained from a slow diffusion of pentane into a dichloromethane solution via layering at –35ºC (Figure 3-13). Distinctively, the $d$(Ru$_1$-P$_1$) bond distance (2.1758(7) Å) is significantly shorter than the typical range for $R_3P$–Ru bonds (2.20 Å < $d$ < 2.45 Å). In $RuCl_2(PPh_3)$(**L1**) (**3.3**), a metal–phosphine type complex with a $\kappa^3$-chelating mode, the $d$(Ru$_1$-P$_1$) bond distance (2.1262(3) Å) is shorter and the angles ∠N$_1$–P$_1$–N$_3$ (113.95º) and

$\angle N_1–P_1–N_3$ (147.62°) are larger than **3.3**, indicating the position of Ru atom relative to **L1** and the geometry of phosphorus triamide framework are strongly constrained by the chelation of pyridyl rings. Additionally, the NMR and solid-structure data both display that the pyridyl ring *trans* to the Ru–H bond is selectively substituted by CO, probably due to the strong *trans* effect of $H^-$ ligands.[30,31]

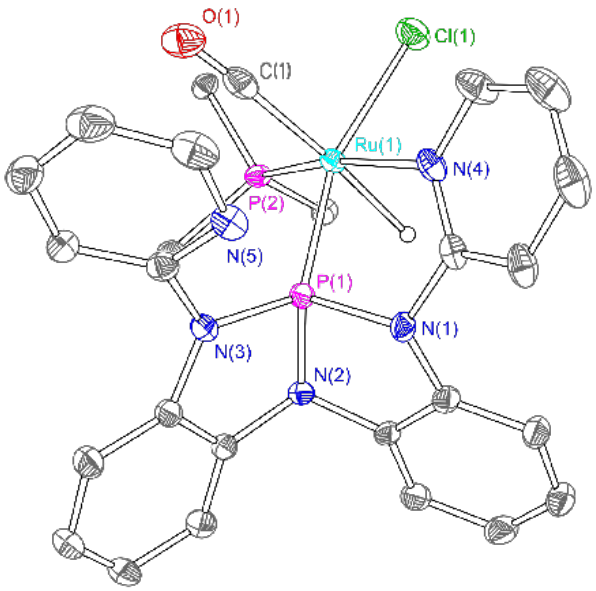


**Figure 3-13**. Thermal ellipsoid plots rendered at the 50% probability level for **3.7**. Hydrogen atoms except H(1), carbon atoms in phenyl groups of $PPh_3$ and solvent molecules of crystallization are also omitted for clarity. Only one of the two independent molecules contained in the unit cell is shown.

**Table 3-1.** Selected bond distances (Å) and Angles (º) for **L1**, **3.7** and **3.3**.

| metric | **L1** | **3.7** | **3.3** |
|---|---|---|---|
| $d(Ru_1–P_1)$ | | 2.1758(7) | 2.1262(3) |
| $d(Ru_1–P_2)$ | | 2.3041(7) | 2.3329(3) |
| $d(Ru_1–Cl_1)$ | | 2.4801(7) | 2.4836(3) |
| $d(P_1–N_1)$ | 1.7786(8) | 1.736(2) | 1.7135(9) |
| $d(P_1–N_2)$ | 1.7485(8) | 1.730(2) | 1.7085(9) |
| $d(P_1–N_3)$ | 1.7341(8) | 1.706(2) | 1.7280(9) |
| $\angle Ru_1–P_1–N_2$ | | 129.11(8) | 147.62(3) |
| $\angle P_1–Ru_1–Cl_1$ | | 162.08(3) | 168.851(10) |
| $\angle N_1–P_1–N_3$ | 108.67(4) | 111.12(11) | 113.94(4) |
| $\angle N_1–P_1–N_2$ | 89.45(4) | 92.47(11) | 92.04(4) |
| $\angle N_2–P_1–N_3$ | 90.56(4) | 91.79(10) | 91.40(4) |

*3-4-3. Intramolecular H-transfer reactivity of **3.7***

When the $C_6D_6$ solution of **3.7** was heated at 60 °C, an immediate color change from pale yellow to orange was observed. The $^{31}P\{^1H\}$ NMR spectrum showed the formation of single species with a significant upfield chemical shift for phosphorus triamide at δ –11.9 ppm, which is coupled to the other phosphorus atom of $PPh_3$ ligand at δ 53.8 ppm ($^2J_{P\text{-}P}$ = 29 Hz) (Figure 3-12c). The formation of P–H bond was suggested by the $^1H$-coupled $^{31}P$ NMR, which showed an additional larger scale coupling of the signal at δ –11.9 ppm ($^1J_{P–H}$ = 531 Hz). In $^1H$ NMR spectrum, the coupling partner was found at δ 7.51 ppm and there was no signal observed in the upfield metal–hydride range (δ < 0 ppm). These spectroscopic results are all consistent with the previously characterized metallophosphorane **3.4**. In effect, upon heating complex **3.7** undergoes an intramolecular H-transfer from Ru to P with coordination of the free pyridyl arm to yield the metallophosphorane **3.4** with $\kappa^3$-*N,P,N*-chelation mode (Scheme 3-7, *right*).

*3-4-4. Kinetic Study of the Intramolecular H-transfer*

Next, the intramolecular H-transfer of **3.7** to form **3.4** in $C_6D_6$ (Scheme 3-7, *right*) was monitored by $^1$H NMR at variable temperatures to obtain kinetic data and investigate the mechanism. The reaction rate was revealed to follow a first-order decay with respect to consumption of **3.7** (eq 1). The result suggests that a bimolecular H-transfer process involving two molecules of **3.7** is not likely. Transition state parameters ($\Delta G^{\ddagger}$ = 25 kcal·mol$^{-1}$, $\Delta H^{\ddagger}$ = 28 kcal·mol$^{-1}$, $\Delta S^{\ddagger}$ = 13 cal·mol$^{-1}$·K$^{-1}$) were obtained from Eyring analysis (Figure 3-14).

$$-d[\mathbf{3.7}]/dt = -k_{obs}\,[\mathbf{3.7}] \quad (1)$$

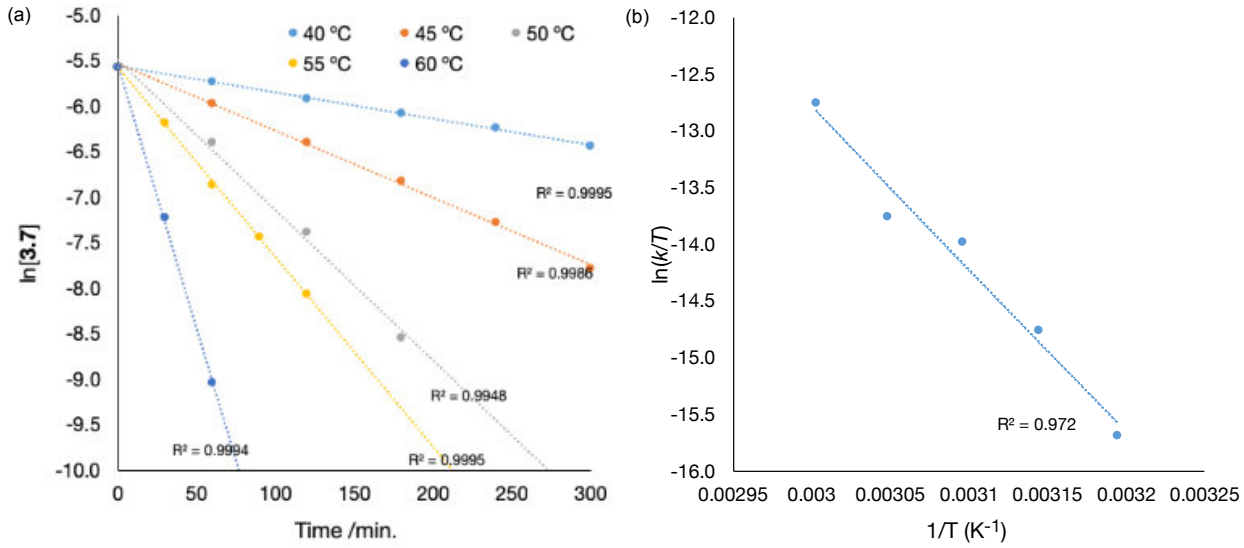


**Figure 3-14.** (a) Kinetic experiments of intramolecular H-transfer. Plot of ln[**3.7**] vs time monitored ([**3.7**]$_0$ = 2.6 mM, $C_6D_6$) at 313 K – 333 K. (b) Eyring plot of ln($k$/T) versus 1/T ($k$ = first-order rate constant, T = temperature in Kelvin) for the reaction of **3.7** to give **3.4**.

*3-4-5. DFT Mechanistic Studies*

In collaboration with Prof. S. Grimme and coworkers at the University of Bonn, the hydride transfer mechanism from **3.7** to **3.4** was further investigated by DFT at the ZORA-PBE0-D4[32-

[35]+COSMO-RS($C_6H_6$)[36, 37] /ZORA-def2-QZVPP[38]//PBEh-3c[39] level of theory (Figure 3-15 and Figure 3-16). Two unimolecular pathways for the exergonic transfer reaction ($\Delta G_R = -12.3$ kcal·mol$^{-1}$) were evaluated: (A) hydride transfer after prior isomerization and (B) hydride transfer via a pyridyl intermediate.

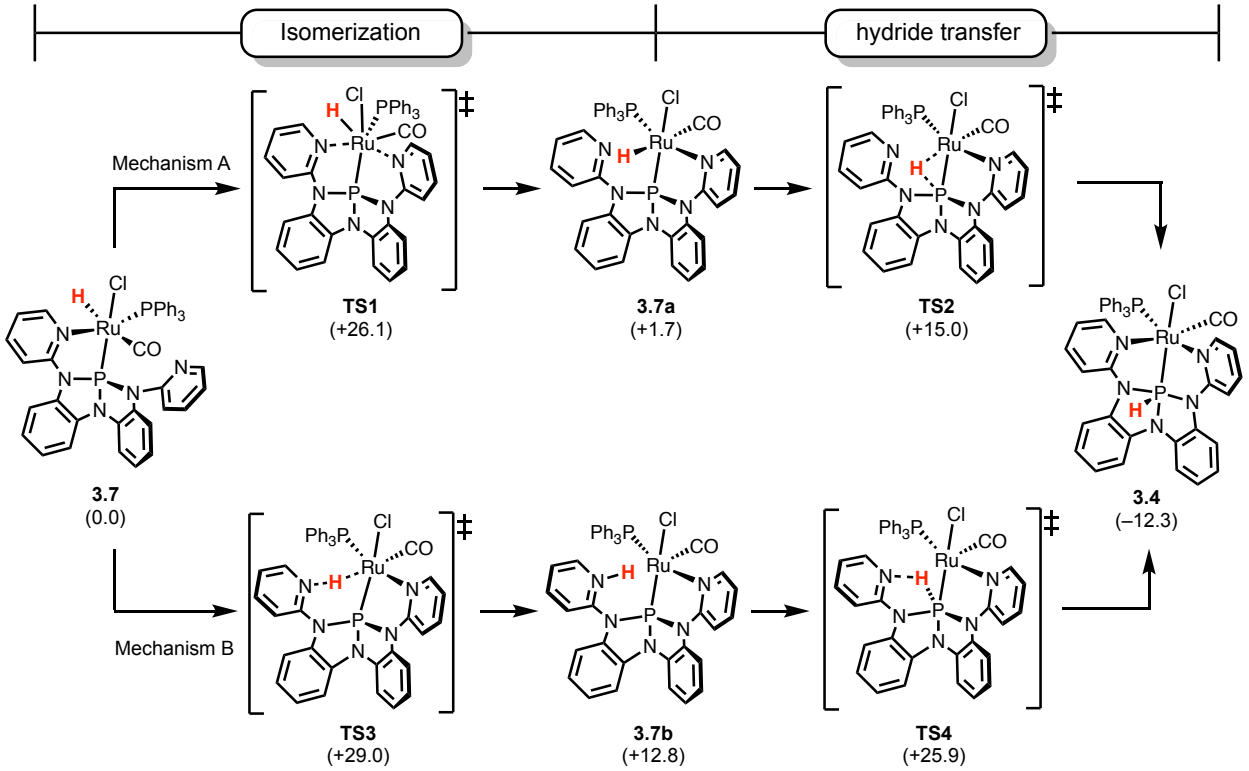


**Figure 3-15.** Computed reaction and activation free energies at the ZORA-PBE0-D4/ZORA-def2-QZVPP/PBEh-3c level of theory for the hydride transfer from **3.7** to **3.4** for two mechanisms. All values are given in kcal·mol$^{-1}$.

The first pathway A involves an initial isomerization of **3.7** via **TS1** ($\Delta G^{\ddagger}$(**TS1**) = 26.1 kcal·mol$^{-1}$) yielding intermediate **3.7a** ($\Delta G$ (**3.7a**) = 1.7 kcal·mol$^{-1}$). Subsequent hydride transfer via **TS2** ($\Delta G^{\ddagger}$(**TS2**) = 15.0 kcal·mol$^{-1}$) yields product **3.4**. The pyridyl-mediated pathway B involves the hydride transfer from Ru to the pyridyl moiety ($\Delta G^{\ddagger}$(**TS3**) = 29.0 kcal·mol$^{-1}$) forming intermediate **3.7b** ($\Delta G$(**3.7b**) = 12.8 kcal·mol$^{-1}$) followed by the transfer from the pyridyl moiety

to P via **TS4** ($\Delta G^{\ddagger}$(**TS4**) = 25.9 kcal·mol$^{-1}$). The pathway A is preferred over pathway B with an overall reaction barrier of 29.0 kcal·mol$^{-1}$ resulting from the rate-determining initial isomerization step. The calculated activation free energy of $\Delta G^{\ddagger}$(**TS1**) = 26.1 kcal·mol$^{-1}$ ($\Delta H^{\ddagger}$(**TS1**) = 26.6 kcal·mol$^{-1}$, $\Delta S^{\ddagger}$(**TS1**) = 1.3 cal·mol$^{-1}$·K$^{-1}$) matches well the experimental value obtained by Eyring analysis. We note that a direct pathway where the hydride transfer occurs first followed by isomerization was also investigated, but yielded a much larger activation free energy for the rate determining step and will not be discussed in detail here.

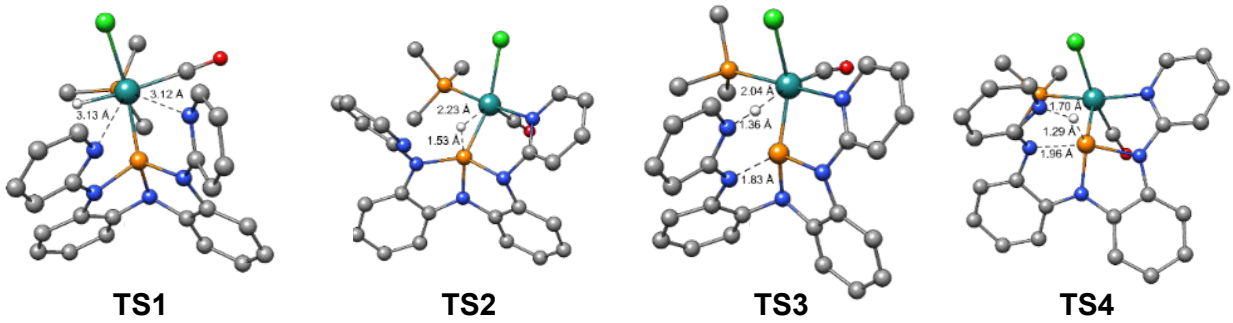


**Figure 3-16**. Couputed structures for Transition states **TS1**-**TS4**. Hydrogen atoms except H(1) and phenyl rings of $PPh_3$ ligand are omitted for clarity.

*3-4-6. Discussion: hydride transfer mechanism*

The mechanistic investigation showed the α-H-migration has the character of a hydride migration. In particular, the transition state with the three-membered Ru–P–H metallacycle (**TS2**) is reminiscent of the classic 1,1- and 1,2-migratory insertions of CO and alkenes, respectively, into metal hydrides. Based on the similarity, it seemed reasonable to attempt to investigate directional control in the migration reactivity by external stimulus, such as coordinative unsaturation.

## 3-5. Effect of Perturbation of the Ru Coordination Environment on Reversible Intramolecular α-H-migration

### *3-5-1. Chloride abstraction from Complex **3.6** to prevent intramolecular H-migration*

In focusing on the possible reversibility of migration, we attempted to control the migration reactivity by modifying the coordination environment first through chloride abstraction. $NaBAr^F_4$ (1.1 eq) was added to an acetonitrile-$d_3$ solution of **3.6** and the mixture was stirred at 60 ºC for 2 hours. The resulting solution was filtered and placed under a CO atmosphere to yield cationic Ru complex **3.8** (Scheme 3-8, *left*).

**Scheme 3-8.** Prevention of metallophosphorane formation by Cl abstraction.

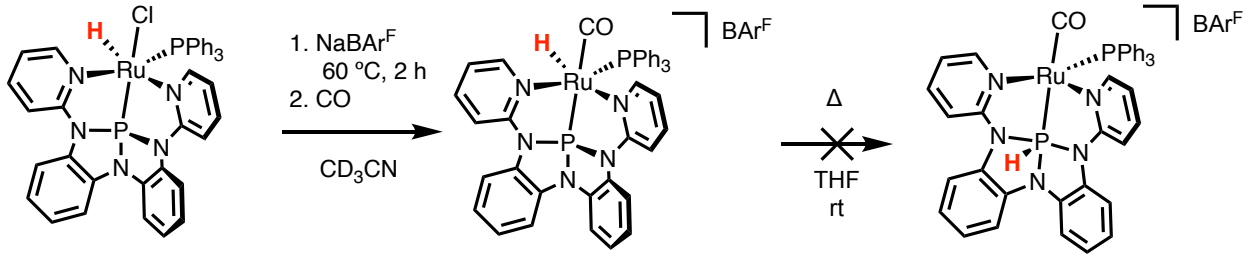


**3.6** **3.8** **3.9**

The incorporation of CO ligand is confirmed by a singlet signal at δ 185.2 ppm in $^{13}C$ NMR spectrum. The $^{31}P\{^1H\}$ NMR spectrum displays two doublet signals at δ 181.6 ppm (triamide phosphorus) and δ 54.4 ppm ($PPh_3$), coupled to each other with $^2J_{P\text{-}P}$ = 42 Hz. In $^1H$-coupled $^{31}P$ NMR spectra, the signal of triamide phosphorus nucleus is further split into a doublet ($^2J_{P\text{–}H}$ = 35 Hz). The corresponding coupling partner is found as a double of doublets in $^1H$ NMR spectra at δ –5.03 ppm, indicative of a ruthenium–hydride signal. The relatively small coupling constants ($^2J_{P\text{–}P}$ = 42 Hz, $^2J_{P\text{–}H}$ = 35 Hz and 20 Hz) indicates that all hydride and phosphorus ligands are mutually related by *cis* stereochemistry (i.e. *fac*-configuration). This observation suggests that the CO ligand

of **3.8** is located at the position *trans* to triamide phosphorus and there is no other stereoisomerization in the conversion from **3.6** to **3.8**.

Notably, and in contrast to complex **3.7**, complex **3.8** does not undergo an intramolecular H-transfer reaction to form a corresponding metallophosphorane **3.9** when heated (Scheme 3-8, *right*). Density Functional Theory (DFT) calculations at the ZORA-PBE0-D4+COSMO-RS(THF)/ZORA-def2-QZVPP//PBEh-3c level of theory revealed **3.9** to be 3.7 kcal·mol$^{-1}$ higher in Gibbs free energy than **3.8**. Qualitatively, the reaction is thermodynamically unfavorable, probably due to the formation of a formal 16e$^-$ complex from an 18e$^-$ complex.

**Scheme 3-9.** Induction of intramolecular H-transfer by external halide addition.

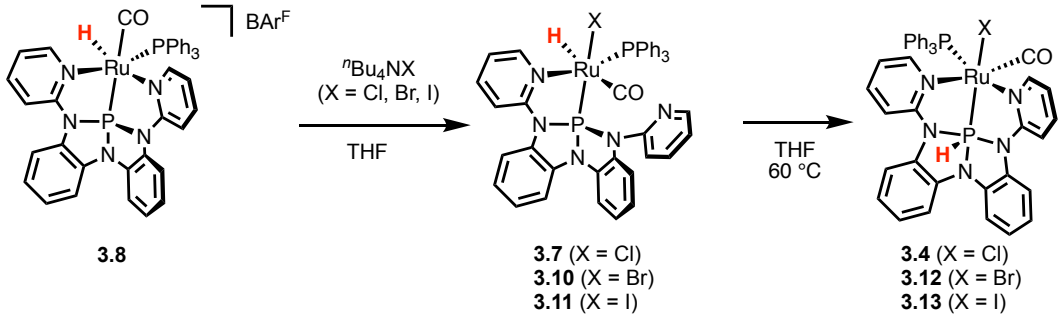


Treatment of **3.8** with $^n$Bu$_4$NCl results in the formation of the $\kappa^2$-(P,N)-chelating species **3.7** by ligand substitution of one of the pyridyl moieties for chloride. As previously demonstrated, complex **3.7** can be further converted into metallophosphorane **3.4** upon heating (Scheme 3-9). Indeed, the corresponding metallophosphoranes with Ru–Br (**3.12**) and Ru–I (**3.13**) bonds could be synthesized by analogous reactions of **3.8** with $^n$Bu$_4$NBr and $^n$Bu$_4$NI, respectively (spectral data are in Table 3-2), where the intermediacy of **3.10** and **3.11** are assumed by analogy.

**Table 3-2.** Selected NMR spectroscopic data for RuX(CO)($PPh_3$)(**L1**) (**3.4, 3.12, 3.13**).

| Entry | $^{31}$P NMR $\delta_{P(N)3}$ /ppm | $^{31}$P NMR $\delta_{PPh3}$ /ppm | $^{1}$H NMR $\delta_{PH}$ / ppm | $^{2}J_{P-P}$ /Hz | $^{1}J_{P-H}$ /Hz |
|---|---|---|---|---|---|
| **3.4 (X = Cl)** | –12.3 | 54.7 | 7.66 | 29 | 535 |
| **3.12 (X = Br)** | –12.0 | 54.9 | 7.63 | 27 | 537 |
| **3.13 (X = I)** | –11.3 | 56.1 | 7.48 | 25 | 538 |

*3-5-2. Chloride Abstraction from Metallophosphorane **3.4**: Intramolecular H-back-migration from P to Ru*

**Scheme 3-10**. Intramolecular back-migration of hydride by Cl abstraction from **3.4**.

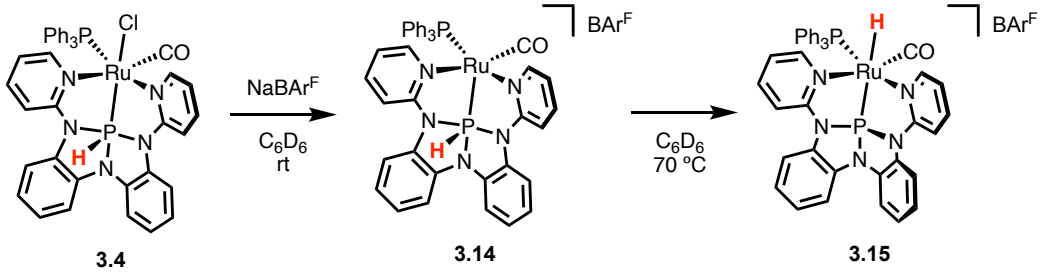


Based on the results, we expected it might be possible to recover a Ru–H bond from a metallophosphorane by changing the coordination environment of Ru. When a $C_6D_6$ solution of **3.4** with $NaBAr^F{}_4$ (1.1 eq) was stirred at ambient temperature, precipitation of NaCl as a white powder was observed. The $^{31}P\{^1H\}$ NMR spectrum of this solution following filtration shows formation of a new species **3.14** with a phosphorus triamide resonance at δ –21.6 ppm (Scheme 3-10, *left*). A $^1H$ NMR signal in the downfield region (δ 6.62 ppm) with large $^1J_{P–H}$ coupling constant (569 Hz) suggests the P–H bond still remains in **3.14**. However, when the solution of **3.14** was heated at reflux overnight, the color was observed to change from yellow to to deep orange. At this time, the $^{31}P$ NMR displays a resonance for triamide phosphorus nucleus at δ 187.7 ppm, significantly downfield from **3.4** and **3.14** and out of the pentacoordinate phosphorus region. The signal is coupled to the other phosphorus nucleus of triphenylphosphine at δ 59.1 ppm ($^2J_{P–P}$ = 20 Hz) and a hydrogen nucleus ($J_{P–H}$ = 202 Hz). In $^1H$ NMR spectra, a drastic upfield shift is observed for the coupling partner of the triamide phosphorus nucleus, which resonates at δ –2.90 ppm in the Ru–H region. The $^2J_{P–H}$ coupling constant (202 Hz) is relatively large, indicating that the triamido phosphorus and the new hydride ligand are mutually in a *trans* configuration. These spectroscopic

results suggest formation of ruthenium–phosphine type complex **3.15** (Scheme 3-10, *right*) in which the hydride formerly bound to P has migrated to Ru and now occupies the site initially housing the abstracted Cl ligand. Although complex **3.15** is a stereoisomer of **3.8**, the interconversion between the two species was not observed, suggesting the stereoisomerization has a high reaction barrier. Notably, a reaction of **3.15** with tetrabutylammonium chloride at 60 ºC recovers the original metallophosphorane **3.4** via another intramolecular H-transfer from Ru to P.

## 3-6. Synthesis of Metallohydrophosphorane from Metal–phosphine by Reactions with Exogenous Hydride Sources

*3-6-1. Reactions of complex **3.3** and sodium borohydride*

In previous sections, we demonstrated the metallophosphoranes can be synthesized by (i) a net insertion of P(III) into P–H or (ii) an α-H-migration from Ru to P. Based on the hydridic property of the formed P–H bond of metallohydrophosphorane **3.4** (Scheme 3-5), we also hypothesized that reactions of metal–phosphines with exogenous hydride nucleophiles would yield metallohydrophosphoranes.

Previously, Nakazawa, Miyoshi and co-authors used a similar approach of nucleophilic attack; the reaction of $[Cp(CO)_2Fe(PPh_2H)]PF_6$ and $NaBH_4$ in ethanol yielded $Cp(CO)_2FeH$ and free $PPh_2H$ (Scheme 3-11). [40] The authors proposed a mechanism with metallophosphorane intermediate, formed by initial nucleophilic attack of $H^-$ to the phosphorus center.[41]

**Scheme 3-11.** Proposed formation of metallophosphorane via nucleophilic halide addition by Nakazawa and Miyoshi.

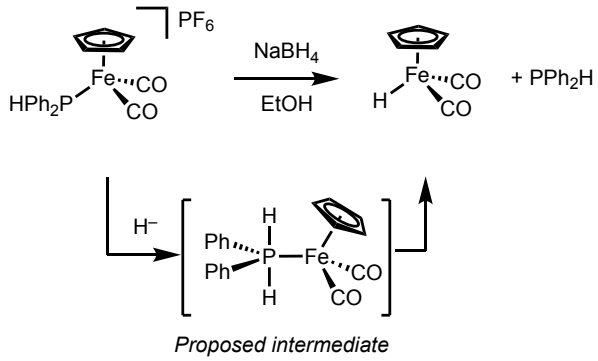


Treatment of metal–phosphine type complex **3.3** with $NaBH_4$ in tetrahydrofuran at 60 ºC afforded a single product (**3.16**) cleanly (Scheme 3-12). $^{31}P\{^1H\}$ NMR spectra indicated the formation of a new metallophosphorane complex with a large upfield-shifted resonance of the

phosphorus triamide at δ –7.6 ppm, coupled to remaining $PPh_3$ ligand at δ 62.8 ppm ($^2J_{P\text{-}P}$ = 66 Hz) (Figure 3-17b). The $^1H$ NMR spectrum showed a doublet of doublets at δ 8.96 ppm ($^2J_{PH}$ = 535 Hz, 5.0 Hz), which suggests the formation of P–H bond.

**Scheme 3-12.** Reaction of **3.3** and $NaBH_4$.

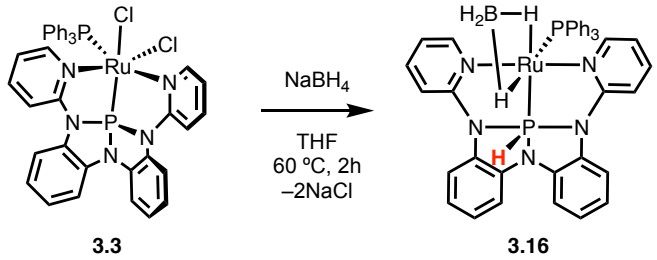


**3.3** **3.16**

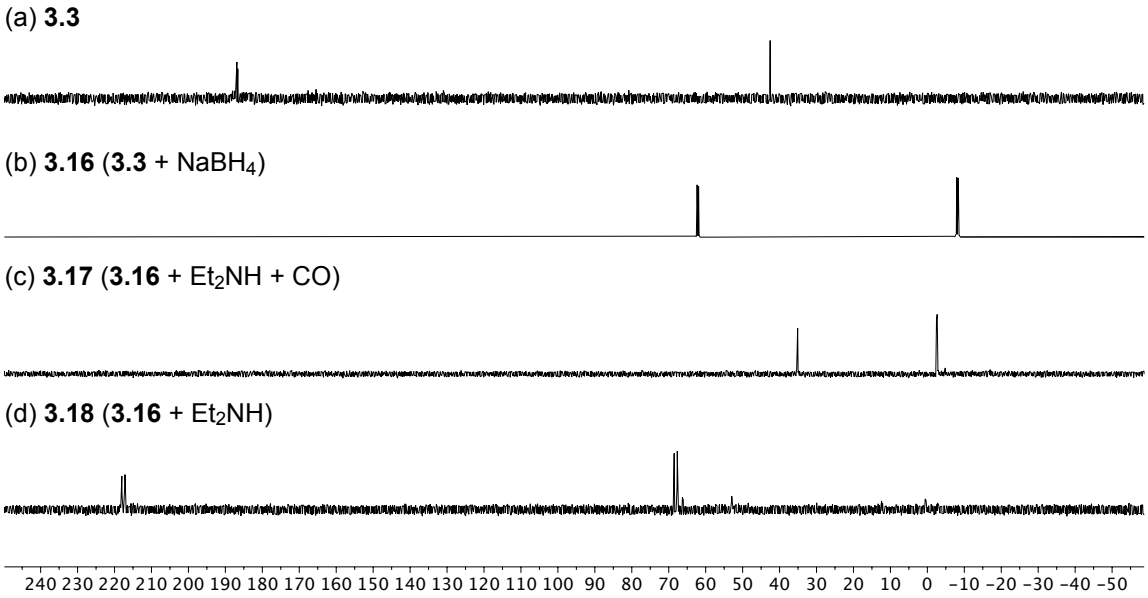


**Figure 3-17**. $^{31}P$ NMR spectra of (a) **3.3**, (b) **3.16** (c) **3.17** (d) **3.18**. Units are in ppm relative to 85% $H_3PO_4$.

The solid-state structure of **3.16** determined by X-ray diffraction on a single crystal grown from a $CH_2Cl_2$ solution layered with pentane revealed the identity of metallohydrophosphorane **3.16** as $Ru^{II}(\eta^2\text{-}BH_4)(PPh_3)(\mathbf{L1}^H)$ (Figure 3-18, Scheme 3-12). The formation of P–H bond was accompanied by the substitution of two Cl ligands with $\eta^2$-$BH_4$ ligand and the isomerization of tridentate ligand **L1** from *facial* to *meridional* configuration. The planarization of the phosphorus

triamide framework was observed ($\angle N_1–P_1–N_3$ = 168.23(4)°) to result the pentacoordinate phosphorus center with the H and Ru substituents at equatorial positions.

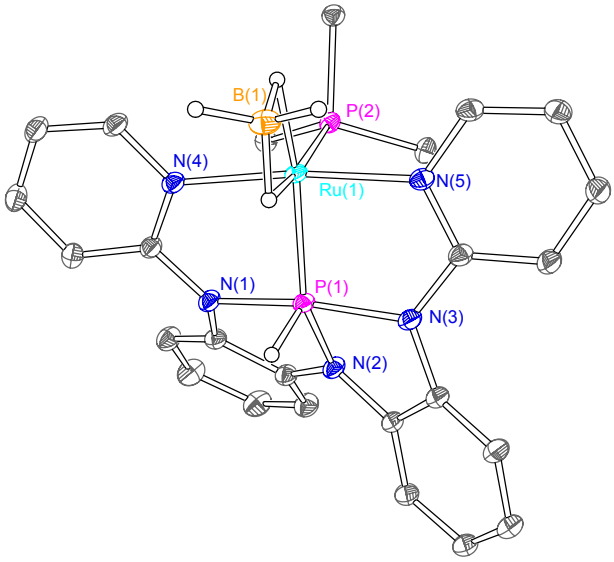


**Figure 3-18.** Thermal ellipsoid plots rendered at the 50% probability level for **3.16**. Hydrogen atoms except H(1) and ones in $BH_4$ ligand, carbon atoms in phenyl groups of $PPh_3$ are omitted for clarity.

**Table 3-3.** Selected bond distances (Å) and Angles (º) for **3.16** and **3.4**.

| metric | **3.16** | **3.4** |
|---|---|---|
| $d(Ru_1–P_1)$ | 2.2161(3) | 2.2509(4) |
| $d(Ru_1–P_2)$ | 2.2900(3) | 2.3359(4) |
| $d(P_1–N_1)$ | 1.8802(10) | 1.8362(14) |
| $d(P_1–N_2)$ | 1.7423(10) | 1.7178(14) |
| $d(P_1–N_3)$ | 1.8691(10) | 1.8162(14) |
| $\angle Ru_1–P_1–N_2$ | 148.19(4) | 140.14(6) |
| $\angle N_1–P_1–N_3$ | 168.23(4) | 170.74(7) |
| $\angle N_1–P_1–N_2$ | 84.01(4) | 86.59(7) |
| $\angle N_2–P_1–N_3$ | 84.22(4) | 87.25(7) |
| $\tau_5$ | 0.33 | 0.50 |

The $^1$H NMR spectrum of **3.16** only showed a broad signal at $\delta$ –7.81 ppm at ambient temperature for one proton of $BH_4^-$, probably due to a fluxional behavior of the ligand. At 193 K, signals for all four hydrogens were visible in the spectrum; two doublets are observed at δ –2.77 and –7.63 ppm for the bridging hydrides and a broad singlet at δ 3.75 ppm corresponding to two terminal hydrogens (Figure 3-19). Upon rising temperatures, the signals collapse. As a point of reference, similar fluxional behavior of $\eta^2$-$BH_4^-$ is reported for a (PNP)RuH($BH_4$) complex by Milstein.[42]

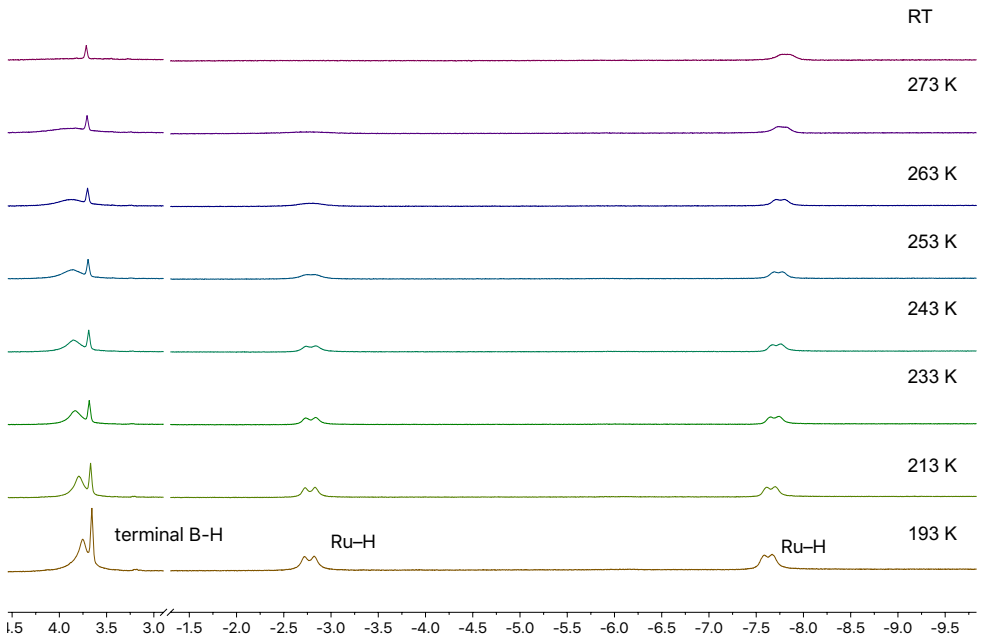


**Figure 3-19**. Variable-temperature (193 K – room temperature) $^1$H NMR spectra of complex **3.16** in the region of $BH_4$ ligand. (solvent: $CD_2Cl_2$)

*3-6-2. Reaction of tetrahydroborate complex **3.16** with diethylamine*

**Scheme 3-13**. Reaction of **3.16** with base under CO atmosphere.

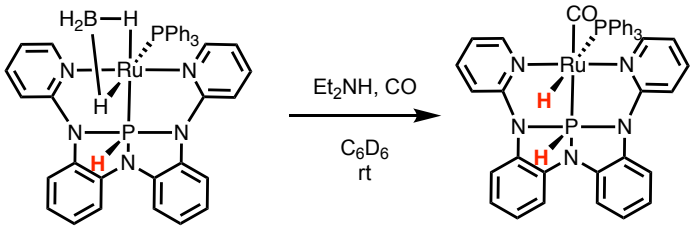


Treatment of complex **3.16** with diethylamine under CO atmosphere affords a Ru–H complex **3.17** (Scheme 3-13). The neutral CO ligand fills the vacant coordination site upon removal of $BH_3$. The assignment was based on $^{1}H$ and $^{31}P$ NMR spectroscopy (Figure 3-18, Figure 3-20). The $^{1}H$ NMR spectra show two hydride signals at δ 9.24 ppm (P–H, $H_a$) and at δ –6.50 ppm (Ru–H, $H_b$). In the $^{31}P$ NMR spectra, the triamidophosphorus resonates in low-field region at δ –2.8 ppm ($P_a$) and the $PPh_3$ ($P_b$) at δ 35.2 ppm. The coupling constants among these four nuclei are shown in Figure 3-20.

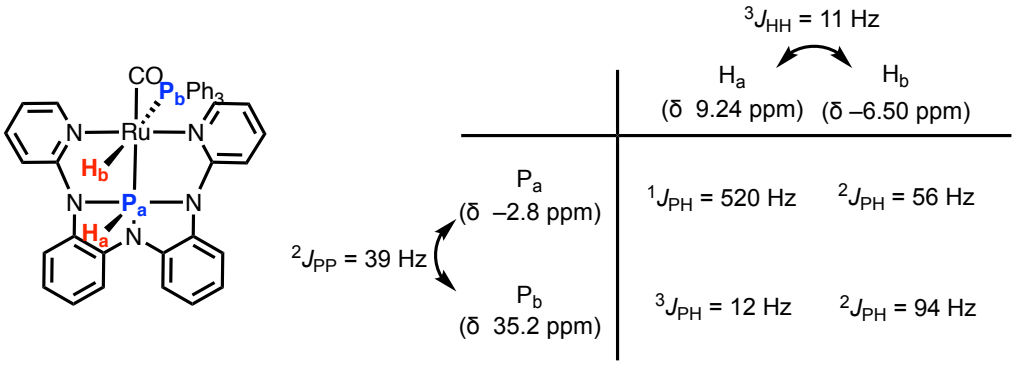


**Figure 3-20**. Important $^{1}H$ NMR and $^{31}P$ NMR signals and couplings in **3.17**.

Compound **3.17** gradually decomposes in solution and the formation of free $H_2$ is detected in $^{1}H$ NMR spectra (δ 4.47 ppm in $C_6D_6$), suggesting a reductive elimination from **3.17**. Additionally, treatment of **3.17** and acetophenone in $C_6D_6$ at 80 ºC yields a trace amount of 1-phenylethanol,

indicating C=O hydrogenation by **3.17**. However, the fate of the Ru complex in these reactions was not clear; the decomposition is accompanied by dissociation of free $PPh_3$ and an uncharacterized product with a $^{31}P$ NMR signal at δ 23 ppm.

**Scheme 3-14.** Decomposition of two metallohydrophosphoranes **3.16** and **3.19** yielding same uncharacterized product **3.18**.

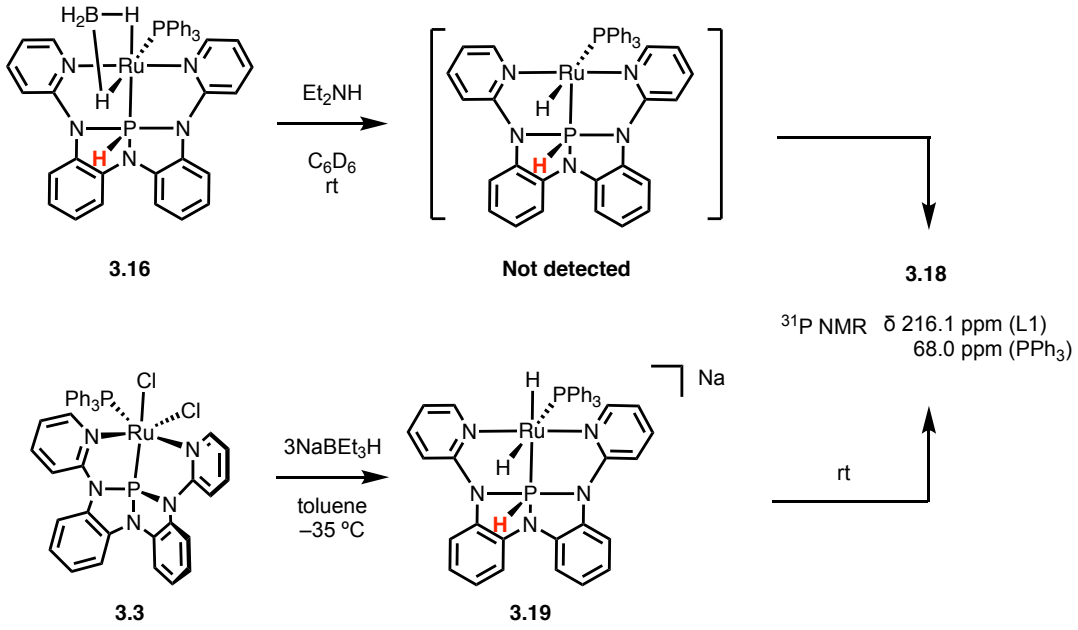


Distinct reactivity was observed when addition of $Et_2NH$ was performed without CO. Under an $N_2$ atmosphere, complex **3.16** slowly reacts with $Et_2NH$ in $C_6D_6$ to afford complex **3.18**, with $^{31}P$ NMR resonances at δ 217.6 ppm and 68.1 ppm with relatively strong mutual coupling ($^2J_{P-P}$ = 170 Hz, Figure 3-18). Based on the significant downfield shift and absence of low-field signals (δ < 0 ppm) in $^1H$ NMR, we initially anticipated product **3.18** is $Ru^0(PPh_3)(\kappa^3$-**L1**), formed by a dissociation of $Et_2NH{\bullet}BH_3$ followed by a reductive elimination of $H_2$. However, the $^{31}P$ NMR signal at δ 217.6 ppm still has a coupling with a H atom ($J_{P-H}$ = 180 Hz). The coupling partner was not identified in $^1H$ NMR and possibly in the complex aryl region. We also suspected the formation of lower coordinate P ligand via P–N bond cleavage, but it is not likely because of the twofold

equivalence of $^{1}$H NMR spectrum suggesting a $C_s$-symmetry in the solution state. Until now, the identity of **3.18** has been unknown and its characterization is still in progress.

### *3-6-3. Reactions of complex **3.3** and sodium triethylborohydride*

Considering the formation of borohydride complex **3.16**, $NaBEt_3H$ was also used as a hydride source. Treatment of **3.3** with $NaBEt_3H$ (5 eq) in toluene at –35 ºC afforded a different product assigned as **3.19**. $^{31}$P NMR spectra of **3.19** displayed two resonances of triamidophosphorus to δ 10.4 ppm, whose upfield shift from **3.3** suggests metallophosphorane formation, the $PPh_3$ nucleus at δ 61.9 ppm with mutual coupling ($^{2}J_{P–P}$ = 33 Hz). In $^{1}$H-coupled $^{31}$P NMR, ($J$ = 469 Hz, 140 Hz, 33 Hz). The three coupling partner hydrogens all appeared in the $^{1}$H NMR spectrum; one is a P–H signal in high-field region ($\delta$ 9.57 ppm, $^{1}J_{P–H}$ = 140 Hz) and the other two signals in low-field Ru–H region (δ –4.10 ppm, $^{2}J_{P–H}$ = 469 Hz and δ –7.11 ppm, $^{2}J_{P–H}$ = 469 Hz). These data indicate that three-fold addition $NaBEt_3H$ to **3.3** affords anionic trihydride complex **3.19** (Scheme 3-14). Even when fewer equivalents of $NaBEt_3H$ were added, however, the reaction affords **3.19** albeit with lower conversion**.** When the solution of **3.19** was warmed to ambient temperature, all low-field $^{1}$H NMR signals (δ < 0 ppm) corresponding to Ru–H disappear to yield complex **3.18**, the uncharacterized product of the reaction of **3.16** and $Et_2NH$ under $N_2$ atmosphere (Scheme 3-14).

### *3-6-4. Reactions of **3.6** with hydride sources*

Metal–phosphine type complex **3.6** was also reacted with these hydride sources. While treatment of **3.6** with $NaBH_4$ afforded the same product **3.16**, a novel complex **3.20** was produced when $NaBEt_3H$ (1 equiv.) was added to a toluene solution of **3.6** at –35 ºC (Scheme 3-15). An

increase in P-coordination number is not likely based on small changes in the chemical shifts of $^{31}$P NMR signals (δ 182.5 ppm and 77.3 ppm, $^{2}J_{P-P}$ = 26 Hz) for **3.20** compared to **3.6**. In $^{1}$H NMR spectra of **3.20**, a set of low-field signals are found at δ -2.66 ppm ($J$ = 174, 23, 10 Hz) and -–14.11 ppm ($J$ = 27, 17, 10 Hz), corresponding to *trans*- and *cis*-hydride ligands to triamidophosphorus, respectively. Thus complex **3.20** was assigned as $RuH_2(PPh_3)$(**L1**), formed by a monosubstitution of $Cl^-$ in **3.6** by $H^-$ (Scheme 3-15).

**Scheme 3-15.**Reactions of **3.6** with hydride sources.

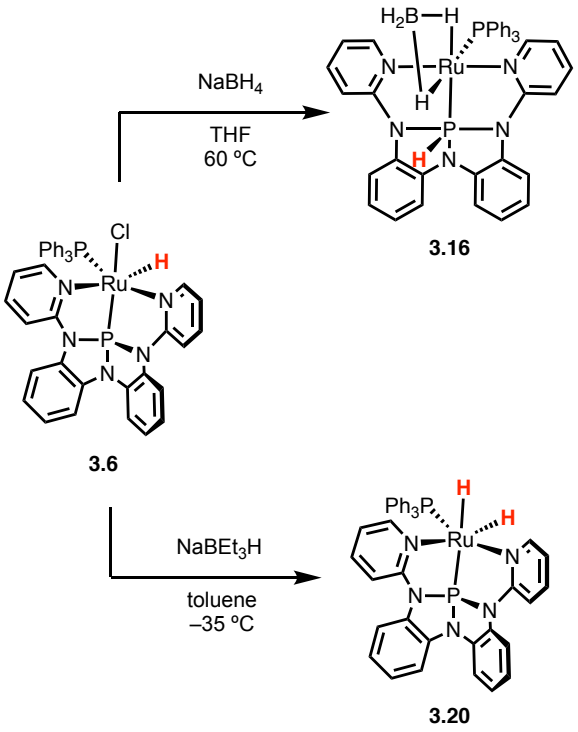

## 3-7. Nonspectator L/X Switching of Cationic Cyclopentadienylruthenium(II) Complexes with Nontrigonal Phosphorus(III) Ligands

### *3-7-1. Metalation of **L1** with [CpRu(CH$_3$CN)$_3$]PF$_6$ and [Cp*Ru(CH$_3$CN)$_3$]PF$_6$*

In previous sections, the reactions of the electrophilic P center with hydride sources were complicated by the simultaneous $H^-$-substitution of Cl ligands. Consequently, we attempted to achieve a simpler P-centered reactivity by using coordinatively saturated and inert ruthenium fragments instead. In related prior work of our laboratory, monodentate phosphorus triamide **2.1** was metalated with cationic cyclpentadienyliron(II) dicarbonyl fragment ($Fp^+$) to give complex **3.21**. Complex **3.21** was cleanly converted to metallofluorophosphorane **3.22** via nucleophilic addition of exogeneous fluoride to the electrophilic P center, without the change in substitution at the metal center (Scheme 3-16).[43]

**Scheme 3-16**. Previous work of nucleophilic fluoride addition to electronic P(III) ligand.

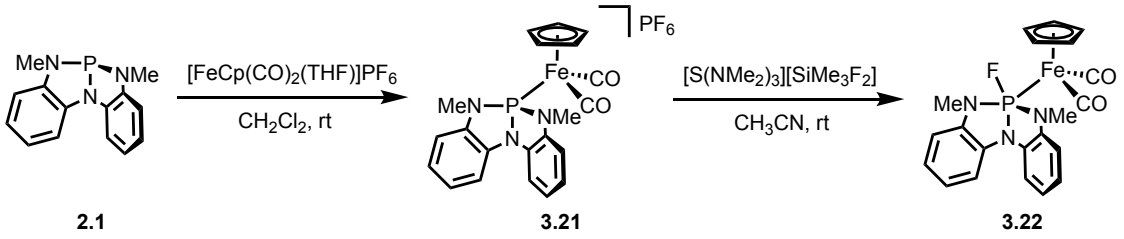


Inspired by this work, tridentate ligand **L1** was metalated with the 'CpRu(II)' fragment to similarly access a coordinatively saturated cationic metal complex bearing a nontrigonal $\sigma_3$-P ligand. Specifically, treatment of **L1** with [CpRu(CH$_3$CN)$_3$]PF$_6$ in THF at ambient temperature cleanly afforded novel complex **3.23** (Scheme 3-17). A singlet resonance at low-field (δ 210.2 ppm) in $^{31}$P NMR spectra and twofold equivalence of the aryl region of $^1$H NMR spectra support the formation of tridentate NPN complex. Analogous metalation with [Cp$^*$Ru(CH$_3$CN)$_3$]PF$_6$ (Cp*

= pentamethylcyclopentadienyl) yielded a $Cp^*$ congener **3.24** with a $^{31}P$ NMR resonance at δ 207.6 ppm.

**Scheme 3-17**. Synthesis of cationic complexes **3.23** and **3.24**.

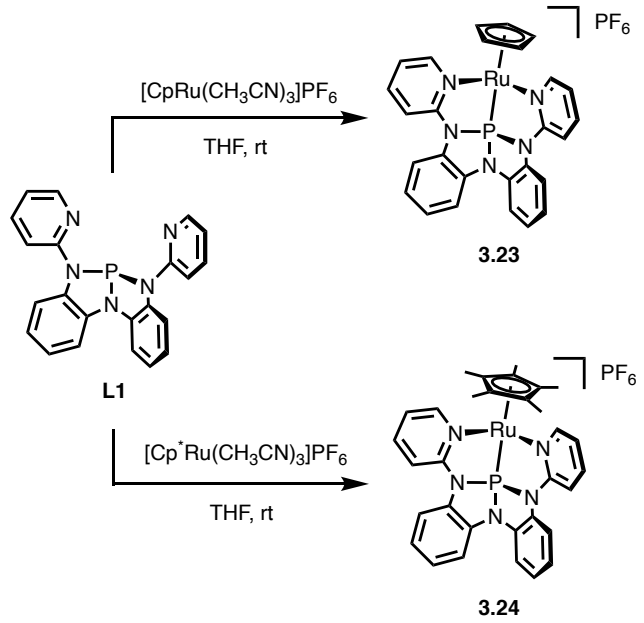


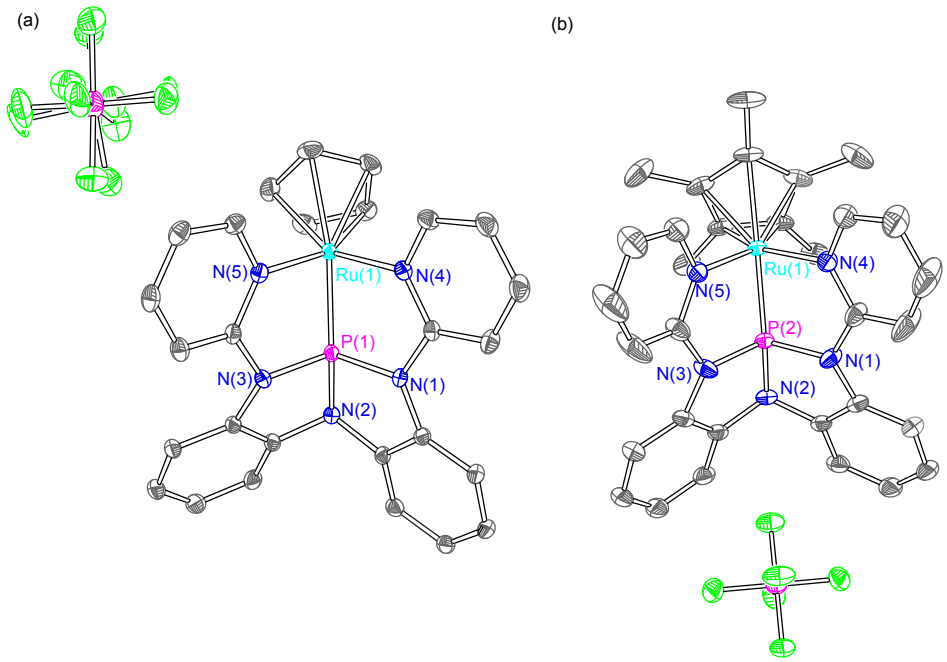


**Figure 3-21.** Thermal ellipsoid plots rendered at the 50% probability level for (a) **3.23** (b) **3.24**. Recrystallization solvents and Hydrogen atoms are omitted for clarity.

X-ray diffraction analysis of a single crystal of **3.23** grown in chloroform solution revealed a facial $\kappa^3$-chelation mode of **L1**. The solid-state structure of **3.24** was also revealed by single-crystal X-ray diffraction, showing mostly analogous structure to **3.23**. Notably, the $d(Ru_1–P_1)$ bond distance (2.1678(5) Å for **3.23** and 2.1560(5) Å for **3.24**) are rather short for ($\sigma^3$-P)–Ru bonds (2.20 Å < $d$ < 2.45 Å), albeit slightly longer than that found in **3.3** ($RuCl_2(PPh_3)$(**L1**)) ($d$ = 2.1262(3) Å).

### *3-7-2. Hydride addition to **3.23***

**Scheme 3-18**. Synthesis of metallophosphoranes by nucleophilic addition of hydride and fluoride.

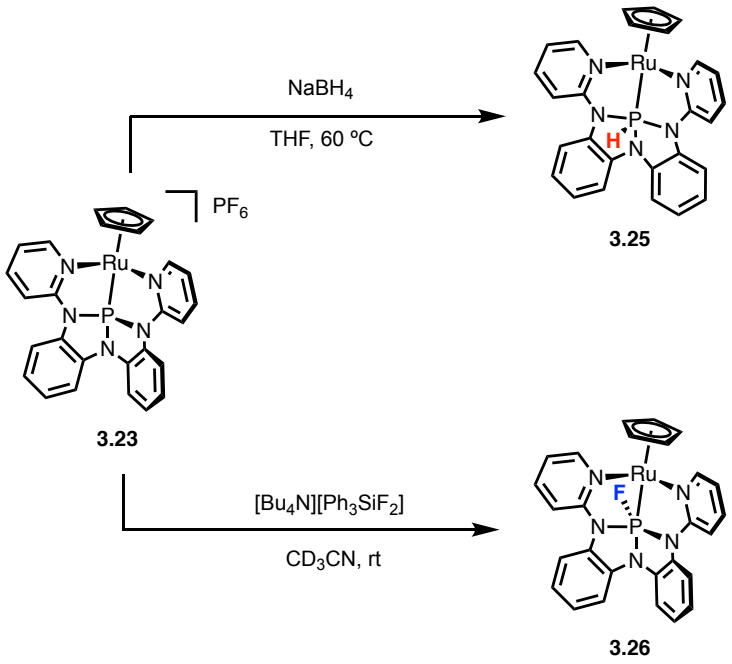


When cationic complex **3.23** was treated with $NaBH_4$ in THF at 60 ºC, an immediate color change of the solution from pale yellow to red was observed (Scheme 3-18, *top*). $^{31}P\{^1H\}$ NMR spectra of the product (**3.25**) displays a singlet at δ 16.3 ppm, a dramatic upfield shift compared to **3.23** (Δδ = –193.9 ppm) (Figure 3-22a,b). Furthermore, the signal was split into a doublet in $^1H$-coupled $^{31}P$ NMR spectra, with a large coupling constant of $J$ = 476 Hz. In $^1H$ NMR spectra, the

corresponding coupling partner is found as a doublet in high-region at δ 8.22 ppm ($J$ = 476 Hz), suggesting the formation of P–H bond. As expected, novel metallohydrophosphorane **3.25** was produced by an exogenous hydride addition to the P center. Notably, the hydridicity of **3.25** is significantly stronger than the previously synthesized metallophosphorane **3.4**. When complex **3.25** was redissolve in $CDCl_3$, immediate hydrodechlorination proceeds to recover the original cation CpRu(**L1**)$^+$, confirmed by the observation of analogous $^{31}$P NMR and $^1$H NMR signal to **3.23**. Similar hydrodechlorination of chloroform was reported by our group for a P–H bond in HBpin adduct of nontrigonal phosphorus triamide **2.1**.[44]

*3-7-3. Fluoride addition to **3.23***

Lastly, an analogous fluoride addition was attempted for **3.23** (Scheme 3-18, *bottom*). Upon addition of tetrabutylammonium diflurotriphenylsilicate in $CD_3CN$ at ambient temperature, the pale yellow solution turned to thick yellow. The formation of a P–F bond in the product (**3.26)** was indicated by a doublet resonance at δ 84.0 ppm with a large scalar coupling ($^1J_{P–F}$ = 1003 Hz) (Figure 3-22c). The doublet signal in $^{19}$F NMR spectra at 58.0 ppm has the complementary coupling ($^1J_{P–F}$ = 1004 Hz). Thus complex **3.26** was assigned as a metallofluorophosphorane, formed by an exogenous fluoride addition to the P center.

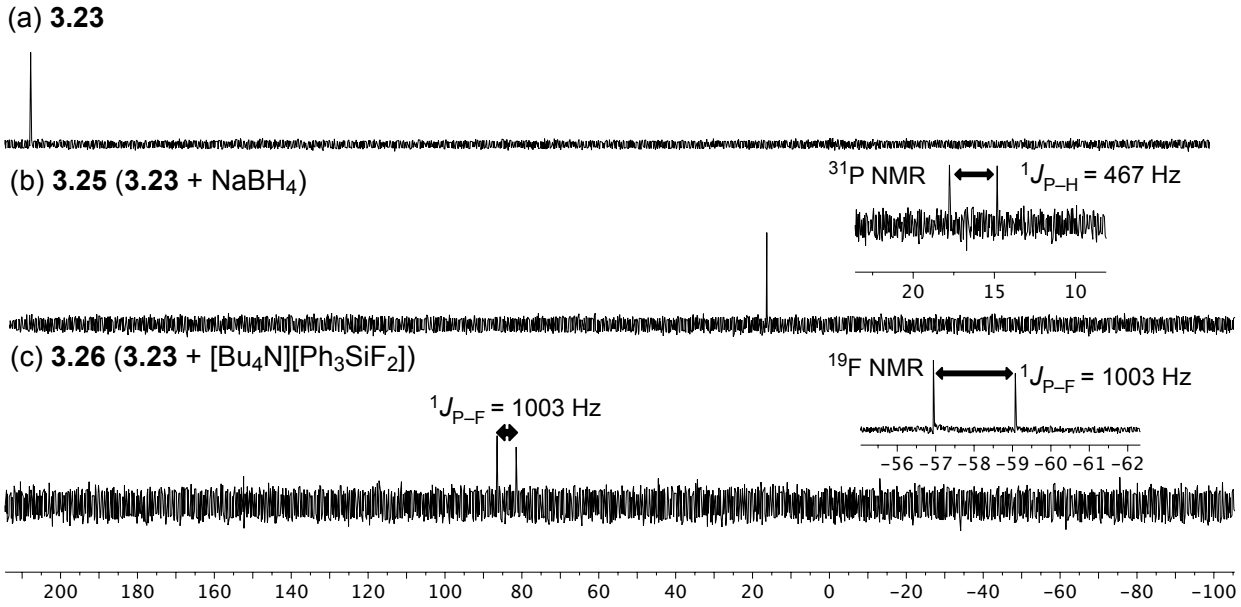


**Figure 3-22.** $^{31}P\{^{1}H\}$ spectra of (a) **3.23** (b) **3.25** (c) **3.26**. Units are in ppm relative to 85% $H_3PO_4$. Inset spectra are (b) $^{1}H$-coupled $^{31}P$ NMR spectra of **3.25**, (c) $^{19}F$ NMR spectra of **3.26**.

## 3-8. Conclusion and Outlook

Taken together, the results in Chapter 3 demonstrate that geometrically deformed tricoordinate phosphorus ligands exhibit properties that diverge from the traditional view of phosphines as spectator ligands. The relative ease-of-access to higher-coordinate organophosphorus substituents makes them viable entities in late transition metal organometallic chemistry arising from 'nonspectator' $\sigma^3$–P ligand reactivity. A growing awareness of the ease with which metallophosphoranes are accessed motivates us therefore to pursue additional study on higher coordination number phosphorus-based chelating ligands.

Moreover, the flexibility of the phosphorus center in nontrigonal phosphorous triamide **L1** to adopt various geometries and coordination numbers calls to mind a connection to the active participation of ligands as found in metal-ligand cooperative chemistry. In Chapter 3, the high preference of ruthenium for single oxidation state ($Ru^{II}$) and geometry (6-coordinate octahedral) made it easier to simplify the systems and to analyze the products. However, metals with higher coordinative and redox flexibility would seem to be ideal if we wish to target metal–ligand cooperative transformation accompanied by changes of oxidation states and/or coordination number of the metals too. In this vein, we will show novel metal–ligand cooperative reactivity of M–P bonds in Group 9 metal complexes in Chapter 4.

## 3-9. Experimental Section

### *3-9-1. General consideration and Methods*

**General consideration.** All reagents were purchased from Sigma-Aldrich, Alfa Aesar, ACROS, TCI, Oakwood Chemical, or Strem Chemicals and used as received unless otherwise noted. Diethyl ether ($Et_2O$), methylene chloride ($CH_2Cl_2$), tetrahydrofuran (THF), toluene and pentane were dried according to the method of Grubbs[45] as modified by Bergman[46] using a Glass Contour Solvent Purification System. All glassware was oven-dried at 120°C prior to use. All reactions were carried out under dry nitrogen atmosphere (Schlenk line or glovebox) unless otherwise noted. NMR spectra were recorded on a Bruker-400 (400 MHz) or Bruker-500 (500 MHz) spectrometer and processed with a MestReNova software. $^1$H NMR chemical shifts are given in ppm with respect to solvent residual peak ($CDCl_3$, δ 7.26 ppm; $CD_2Cl_2$, δ 5.32 ppm; $C_6D_6$, δ 7.16 ppm), $^{13}C\{^1H\}$ NMR shifts are given in ppm with respect to ($CDCl_3$ δ 77.16 ppm, $CD_2Cl_2$ δ 53.84 ppm, $C_6D_6$ δ 128.06 ppm). Coupling constants are reported as *J*-values in Hz. High resolution ESI mass spectra were obtained from the Mass Spectrometry Laboratory at the School of Chemical Sciences, University of Illinois at Urbana-Champaign or at the Mass Spectrometry Laboratory in the Department of Chemistry Instrumentation Facility, MIT, using either Agilent QTOF 6545 with ESI ionization source or a JEOL AccuTOF-DART (JMST100LP, ionSense DART source). X-ray diffraction data was collected on a Bruker SMART APEX CCD area detector system equipped with a graphite monochromator and a MoKα fine-focus sealed tube (λ = 0.71073 Å). Raw data integration and reduction were performed with the SAINT[47] and SADABS[48] programs. Structures were solved by direct methods using SHELXT[49] and refined by least-squares methods on $F^2$ using SHELXL software package. All non-hydrogen atoms were refined with anisotropic displacement

parameters. The hydrogen atoms at phosphorus atoms of compound **3.4** and **3.16** were located in Fourier maps and were refined isotropically without constraints. All other hydrogen atoms were fixed in their ideal geometries. XP was used for graphical representations.

**XANES Sample Preparation.** P K-edge XANES samples were prepared in an $N_2$-filled glovebox with <1.0 ppm $O_2$ by grinding crystalline **3.3** and **3.4** (ca. 10 mg) for 2 min using a Wig-L-Bug grinder and polystyrene capsules containing a Plexiglas pestle. Samples were prepared similarly to Chapter 2, but their data were first collected using a gas-flow cell designed at Iowa for air-sensitive XAS measurements in the tender X-ray region. Subsequent P K-edge XANES data collected on **3.3** and **3.4** after brief exposure to air revealed no differences when compared to samples handled under rigorously air-free conditions.

**Determination of rate constant and Eyring analysis.** In an inert-atmosphere glovebox, compound **3.7** was dissolved in . The sample was then transferred to a sealable J. Young NMR tube.

*3-9-2. Synthetic Procedures*

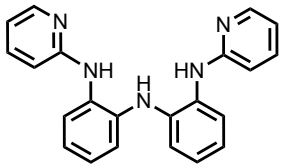

3.2

**Synthesis of triamine 3.2**. Bis(2-aminophenyl)amine **3.1**[50] (5.76 g, 28.9 mmol) was dissolved in 2-chloropyridine (11.5 mL, 122 mmol) and stirred under reflux overnight. After being cooled to RT, the mixture was dissolved in dichloromethane and washed three times with 1 M NaOH solution. The organic phase was dried over sodium sulfate and filtered. The solution was concentrated under vacuum. To the dark mixture was added $Et_2O$ and the resulting purple solid was filtered, thoroughly washed with $Et_2O$ and dried *in vacuo* to give product as purple powder (6.66 g, 65.1 %). $^1$H NMR (500 MHz, $CDCl_3$) δ 8.08 (ddd, *J* = 5.0, 2.0, 0.9 Hz, 2H), 7.52 (dd, *J* = 7.8, 1.5 Hz, 2H), 7.38 (ddd, *J* = 8.3, 7.2, 1.9 Hz, 2H), 7.11-6.95 (m, 6H), 6.86 (br s, 2H), 6.63 (ddd, *J* = 7.2, 5.0, 0.9 Hz, 2H), 6.50 (d, *J* = 8.4 Hz, 2H), 6.20 (br s, 1H) ppm. $^{13}$C{$^1$H} NMR (126 MHz, $CDCl_3$) δ 157.0, 148.3, 137.8, 137.6, 131.3, 125.5, 124.5, 122.3, 119.5, 114.8, 108.5 ppm. MS (ESI) calcd for $C_{22}H_{20}N_5$ (M+H): 354.1719, found: 354.1713

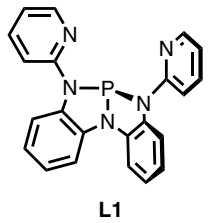

L1

**Synthesis of tridentate ligand L1.** Triamine **3.2** (405 mg, 1.15 mmol) and triethylamine (1.60 mL, 11.5 mmol) was dissolved in THF/$Et_2O$ (1/2, 18 mL). To the solution was added phosphorus trichloride (0.100 mL, 1.15 mmol) dropwise via syringe. The reaction mixture was stirred at –78°C for 1h and then warmed to room temperature. After 4h of stirring at room temperature, the suspension was filtered through Celite under $N_2$ atmosphere and the filtrate was concentrated *in vacuo,* and the resulting solid mixture was brought into a nitrogen-filled glovebox. The resulting solid mixture was recrystallized via slow diffusion of pentane into a benzene solution. The resulting crystalline solid was filtered and dried to give pure product of **L1** as off-white crystals (124 mg, 28.2 %). $^1$H NMR (500 MHz,

$CDCl_3$) δ 8.27 (dt, *J* = 4.9, 1.5 Hz, 1H), 7.78 – 7.62 (m, 2H), 7.52 (d, *J* = 1.4 Hz, 1H), 7.50 (d, *J* = 1.2 Hz, 1H), 7.06 (td, *J* = 7.8, 1.3 Hz, 1H), 7.02 – 6.92 (m, 3H) ppm.$^{13}C\{^1H\}$ NMR (126 MHz, $CDCl_3$) δ 154.6 (d, *J* = 15.7 Hz), 148.0, 141.9 (d, *J* = 6.4 Hz), 138.1, 135.2 (d, *J* = 3.5 Hz), 124.6, 121.6, 119.0 (d, *J* = 5.1 Hz), 118.6, 114.7 (d, *J* = 5.0 Hz), 113.8 ppm. $^{31}P\{^1H\}$ NMR (203 MHz, $CDCl_3$) δ 141.7 ppm. MS (ESI) calcd for $C_{22}H_{17}N_5P$ (M+H): 382.1222, found: 382.1216.

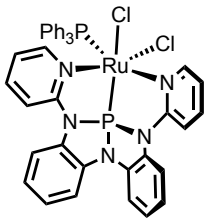

**3.3**

**Synthesis of 3.3**. Under a $N_2$ atmosphere, tris(triphenylphosphine)ruthenium(II) dichloride (55 mg, 0.057 mmol) was suspended in THF (6 mL). To the solution was added dropwise a solution of ligand **L1** (22 mg, 0.057 mmol) in THF (6 mL) at room temperature. The resulting yellow solution was stirred overnight at room temperature and a yellow precipitate was gradually formed. The solvent was removed under vacuum and the resulting solid was washed with $Et_2O$. Recrystallization from dichloromethane/pentane afforded pure product of **3.3** as orange crystals (35 mg, 76 %).$^1H$ NMR (500 MHz, $CDCl_3$) δ 9.98 (dt, *J* = 5.5, 2.3 Hz, 1H), 9.45 (dd, *J* = 6.4, 1.4 Hz, 1H), 7.82 – 7.72 (m, 1H), 7.67 – 7.56 (m, 9H), 7.39 – 7.30 (m, 1H), 7.30 – 7.22 (m, 2H), 7.20 – 7.02 (m, 14H), 7.01 (d, *J* = 8.1 Hz, 1H), 6.91 (td, *J* = 7.7, 1.2 Hz, 1H), 6.38 (ddd, *J* = 7.4, 6.1, 1.3 Hz, 1H). $^{13}C\{^1H\}$ NMR (126 MHz, $CDCl_3$) δ 154.6, 153.6 (d, *J* = 14.8 Hz), 151.9, 138.7, 138.1, 137.3, 136.2, 134.1 (d, *J* = 9.7 Hz), 134.1 (d, *J* = 45.1 Hz), 133.5 (t, *J* = 8.2 Hz), 129.1, 128.9, 128.7, 127.5 (d, *J* = 9.6 Hz), 124.9, 124.6, 123.0, 122.7, 119.5 (d, *J* = 9.0 Hz), 119.2, 118.6, 118.2 (d, *J* = 8.7 Hz), 113.0, 113.0 (d, *J* = 11.6 Hz), 110.8, 108.3. $^{31}P\{^1H\}$ NMR (203 MHz, $CDCl_3$) δ 186.8 (d, *J* = 49.2 Hz), 42.7 (d, *J* = 49.2 Hz) ppm. MS (ESI) calcd for $C_{40}H_{31}ClN_5P_2Ru$ (M–Cl): 780.0787, found: 780.0792.

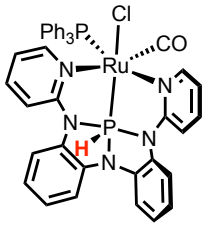


3.4

**Synthesis of 3.4**. Carbonylchlorohydridotris(triphenylphosphine)ruthenium(II) (50 mg, 0.052 mmol) was suspended in THF (5 mL) under a $N_2$ atmosphere. To the solution was added dropwise a solution of ligand **L1** (20 mg, 0.052 mmol) in THF (5 mL) at reflux. The resulting yellow solution was stirred overnight at room temperature to afford an orange solution. The solvent was removed under vacuum and the resulting solid was washed with $Et_2O$ and acetonitrile to give pure product of **3.4** as a yellow powder (20 mg, 48 %). $^1$H NMR (500 MHz, $CDCl_3$) δ 9.47 (dd, *J* = 5.6, 2.6 Hz, 1H), 9.32 (dd, *J* = 5.9, 1.9 Hz, 1H), 7.80 (dd, *J* = 7.5, 1.6 Hz, 1H), 7.68 (ddd, *J* = 8.6, 7.1, 1.8 Hz), 7.67 (dd, *J* = 534.7, 1.8 Hz, 1H), 7.61 (dd, *J* = 7.9, 1.3 Hz, 1H), 7.51 – 7.24 (m, 7H), 7.21 – 7.15 (m, 4H), 7.12 – 7.03 (m, 6H), 7.03 – 6.88 (m, 4H), 6.79 (t, *J* = 7.7 Hz, 1H), 6.74 (td, *J* = 7.7, 1.3 Hz, 1H), 6.63 (t, *J* = 6.5 Hz, 1H), 6.59 (dd, *J* = 7.7, 1.4 Hz, 1H) ppm. $^{13}$C{$^1$H} NMR (126 MHz, $CDCl_3$) δ 202.9 (t, *J* = 16.7 Hz), 151.7 (d, *J* = 4.0 Hz), 151.6, 151.5, 150.6, 138.8 (d, *J* = 20.6 Hz), 133.9, 133.7 (d, *J* = 10.5 Hz), 133.0, 132.4 (d, *J* = 6.1 Hz), 132.0, 131.2 (d, *J* = 8.0 Hz), 129.4, 128.8, 128.6 (d, *J* = 7.5 Hz), 127.7 (d, *J* = 9.7 Hz), 122.3, 120.5, 120.1 (d, *J* = 13.4 Hz), 116.5, 115.8, 113.7 (d, *J* = 7.7 Hz), 112.4 (d, *J* = 7.7 Hz), 111.4, 110.1, 110.0, 108.6 ppm.$^{31}$P{$^1$H} NMR (203 MHz, $CDCl_3$) δ 54.7 (d, *J* = 29.0 Hz), -12.3 (d, *J* = 29.1 Hz) ppm. IR (KBr pellet) *ν*(CO) = 1956.6 cm$^{-1}$, *ν*(PH) = 2226.4 cm$^{-1}$. MS (ESI) calcd for $C_{41}H_{32}N_5OP_2Ru$ (M–Cl): 774.1126, found: 774.1125.

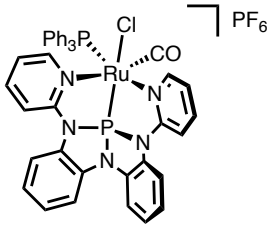


3.5

**Synthesis of 3.5**. Under a $N_2$ atmosphere, complex **3.3** (2.7 mg, 3.3 μmol) was dissolved in dichloromethane (1 mL). To the solution was added triphenylcarbenium hexafluorophosphate (1.3 mg, 3.3 μmol) and stirred for 15 min. The solvent was removed under vacuum and the resulting solid

was washed with pentane. Recrystallization from chloroform/pentane afforded pure product of **3.5** as a white powder (2.9 mg, 91 %). $^{1}$H NMR (500 MHz, $CD_2Cl_2$) δ 9.51 (dt, *J* = 5.8, 2.2 Hz, 1H), 8.86 (dd, *J* = 6.1, 1.7 Hz, 1H), 8.08 (t, *J* = 7.1 Hz, 1H), 7.93 (t, *J* = 7.4 Hz, 1H), 7.77 (d, *J* = 8.7 Hz, 2H), 7.63 (dd, *J* = 7.6, 1.7 Hz, 1H), 7.51 (d, *J* = 8.2 Hz, 1H), 7.45 – 7.26 (m, 9H), 7.23 (td, *J* = 7.8, 2.7 Hz, 7H), 7.09 (dd, *J* = 7.8 Hz, 1H), 6.87 (dd, *J* = 7.4, 5.9 Hz, 1H). $^{13}$C{$^{1}$H} NMR (126 MHz, $CD_2Cl_2$) δ 150.4, 149.50, 149.46, 141.9 (d, *J* = 29.5 Hz), 136.5, 135.7, 133.3 (d, *J* = 10.0 Hz), 132.0 (d, *J* = 9.8 Hz), 131.3, 130.8, 130.4, 128.6 (d, *J* = 10.6 Hz), 126.4, 126.3, 124.8, 124.2, 121.7, 121.6, 120.4, 120.3, 119.2, 119.1, 115.3 (d, *J* = 6.9 Hz), 115.0 (d, *J* = 6.2 Hz), 111.0 (d, *J* = 4.5 Hz), 109.37 (d, *J* = 4.2 Hz). (A signal corresponding to carbonyl group was not resolved.) $^{31}$P{$^{1}$H} NMR (203 MHz, $CD_2Cl_2$) δ 187.3 (d, *J* = 35.0 Hz), 42.6 (d, *J* = 34.0 Hz). -145.7 (hept). IR (KBr pellet) *ν*(CO) = 2026.8 cm$^{-1}$. Mass spectrometry was performed for [RuCl(CO)($PPh_3$)(L1)]B($C_6F_5$)$_4$. MS (ESI) calcd for $C_{41}H_{31}ClN_5OP_2Ru$ (M–B($C_6F_5$)$_4$): 808.0736, found: 808.0740.

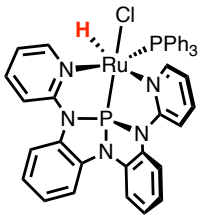

**3.6**

**Synthesis of 3.6**. Under a $N_2$ atmosphere, chlorohydridotris(triphenylphosphine) ruthenium(II)[51] (220 mg, 0.24 mmol) was suspended in THF (3 mL). To the solution was added dropwise a solution of ligand **L1** (90 mg, 0.24 mmol) in THF (3 mL) at room temperature. The resulting orange suspension was stirred overnight at room temperature and a yellow precipitate was gradually formed. The yellow solid was collected by filtration and washed with $Et_2O$ three times then dried in vacuo to yield desired product of **3.6** as yellow solid (121 mg, 65 %). Complex **3.6** slowly reacts with chlorinated solvents such as $CH_2Cl_2$ or $CHCl_3$ to form dichloride complex $RuCl_2(PPh_3)$(**L1**), which prevents the

crystallization of pure product of **3.6**. $^{1}$H NMR (500 MHz, $CD_2Cl_2$) δ 9.82 (dd, J = 5.8, 2.3 Hz, 1H)After, 9.00 (dd, J = 5.7, 1.8 Hz, 1H), 7.72 (td, J = 7.8, 1.8 Hz, 1H), 7.53 (dd, J = 7.7, 1.5 Hz, 1H), 7.51 – 7.40 (m, 9H), 7.23 – 6.97 (m, 16H) 6.94 – 6.77 (m, 1H), 6.66 (dd, J = 7.2, 5.7 Hz, 1H), -13.11 (dd, J = 31, 28 Hz, 1H). $^{13}$C NMR (126 MHz, $CD_2Cl_2$) δ 153.92, 153.78, 152.25 (d, J = 13.9 Hz), 151.68, 150.25, 138.57, 138.00, 137.34, 136.98, 136.77, 136.62, 134.38 (dd, J = 22.8, 8.2 Hz), 133.83 (d, J = 10.5 Hz), 128.79 (d, J = 2.3 Hz), 127.56 (d, J = 9.5 Hz), 124.70 (d, J = 36.4 Hz), 122.71, 121.94, 119.19 (d, J = 9.0 Hz), 119.01 (d, J = 9.0 Hz), 118.72 (d, J = 2.3 Hz), 118.65, 113.40 (d, J = 5.8 Hz), 113.24 (d, J = 5.3 Hz), 110.21 (d, J = 3.3 Hz), 109.05 (d, J = 3.5 Hz). $^{31}$P NMR (203 MHz, $CD_2Cl_2$) δ 191.8 (d, *J* = 55 Hz), 67.5 (d, *J* = 55 Hz). MS (DART) calcd for $C_{40}H_{31}ClN_5P_2Ru$ (M–H): 780.0787, found: 780.0781.

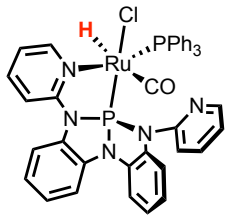


**3.7**

**Synthesis of 3.7**. In a J-young tube, complex **3.6** (25.0 mg, 0.032 mmol) was suspended in dichloromethane (1 mL). The tube was subjected to three freeze–pump–thaw cycle and then filled with 1 atom of carbon monoxide gas at room temperature. The mixture turned to a pale yellow solution. After 15 min, the solution was filtered and the filtrate was layered with pentane and left at –35 ºC, affording complex **3.7** as a yellow crystalline solid (12.1 mg, 46 %). $^{1}$H NMR (400 MHz, $CD_2Cl_2$) δ 9.42 (dd, J = 5.5, 2.6 Hz, 1H), 7.97 (t, J = 7.7 Hz, 1H), 7.91 (dd, J = 5.0, 1.9 Hz, 1H), 7.75 (td, J = 7.8, 1.9 Hz, 1H), 7.55 – 7.40 (m, 9H), 7.34 (d, J = 8.4 Hz, 1H), 7.29 (t, J = 6.6 Hz, 1H), 7.15 (d, J = 3.5 Hz, 8H), 7.12 – 7.07 (m, 3H), 7.07 – 7.01 (m, 2H), 6.95 (d, J = 7.9 Hz, 1H), 6.87 (t, J = 7.6 Hz, 1H), 6.78 (t, J = 7.7 Hz, 1H), -4.53 (dd, J = 39, 20 Hz, 1H). $^{13}$C NMR (101 MHz, $CD_2Cl_2$) δ 155.29 (d, *J* = 11.7 Hz), 153.55, 150.79 (d, *J* = 8.3 Hz), 149.35, 138.88 (d, *J* = 4.1 Hz), 138.81, 137.16 (d, *J* =

11.0 Hz), 136.99, 136.94, 136.51, 135.14 (d, $J$ = 6.4 Hz), 134.11 (d, $J$ = 10.8 Hz), 133.92 (d, $J$ = 10.8 Hz), 129.76 (d, $J$ = 2.4 Hz), 127.88 (d, $J$ = 10.0 Hz), 126.11, 123.00, 122.56, 121.38, 121.33, 121.27, 120.89 (d, $J$ = 2.3 Hz), 118.62 (d, $J$ = 6.1 Hz), 118.16 (d, $J$ = 4.0 Hz), 116.41 (d, $J$ = 8.7 Hz), 110.17 (d, $J$ = 4.7 Hz), 109.26 (d, $J$ = 4.3 Hz).. $^{31}P\{^{1}H\}$ NMR (162 MHz, $CD_2Cl_2$) **δ 184.5 (d, $J$ = 40 Hz), 54.1 (d, $J$ = 40 Hz).** MS (DART) calcd for $C_{41}H_{31}ClN_5OP_2Ru$ (M–H): 808.0730, found: 808.0853.

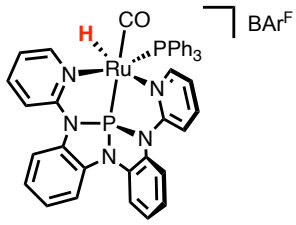

**3.8**

**Synthesis of 3.8**. Under a $N_2$ atmosphere, complex **3.6** (26.4 mg, 0.0334 mmol) and was suspended in acetonitrile (1 mL). To the suspension was added sodium tetrakis[3,5-bis(trifluoromethyl)phenyl]borate (33.0 mg, 0.372 mmol, 1.1 eq) and stirred for 2 h at 60 ºC. The white precipitate of NaCl was filtered and the filtrate was poured into a J-young tube, to which 1 atm of CO was introduced. After 30 min, the solvent was removed in vacuo and the pale-yellow residue was washed with pentane and dried in vacuo to afford complex **3.8** as a product. (40.8 mg, 92%). $^{1}H$ NMR (500 MHz, $CD_3CN$) δ 8.84 (dt, $J$ = 4.9, 2.2 Hz, 1H), 8.18 (td, $J$ = 7.9, 1.8 Hz, 1H), 7.89 (td, $J$ = 7.8, 1.9 Hz, 1H), 7.79 – 7.74 (m, 1H), 7.71 (dt, $J$ = 5.0, 2.2 Hz, 16H), 7.67 (s, 4H), 7.62 – 7.53 (m, 2H), 7.46 (ddd, $J$ = 7.3, 5.7, 1.3 Hz, 1H), 7.11 – 7.07 (m, 1H), 6.98 (td, $J$ = 7.7, 1.3 Hz, 1H), 6.88 (td, $J$ = 7.8, 1.2 Hz, 1H), -5.05 (dd, $J$ = 34.9, 19.7 Hz, 1H). $^{13}C$ NMR (101 MHz, $CD_3CN$) $^{13}C$ NMR (101 MHz, $CD_3CN$) δ 185.18, 163.36, 162.87, 162.37, 161.87, 153.52, 149.41, 141.45, 140.50, 138.67, 135.66, 135.35, 134.86, 134.09 (d, $J$ = 10.9 Hz), 131.41 (d, $J$ = 2.5 Hz), 130.09 (dd, $J$ = 5.8, 2.9 Hz), 129.78 (dd, $J$ = 5.8, 2.9 Hz), 129.28 (d, $J$ = 10.2 Hz), 127.20, 126.83, 124.54, 124.13, 124.00, 123.01 (d, $J$ = 2.3 Hz), 122.97, 122.41, 122.31, 121.42, 120.88 (d, $J$ = 6.1 Hz),

117.19 (d, $J$ = 9.0 Hz), 111.11 (d, $J$ = 5.2 Hz), 110.62 (d, $J$ = 5.1 Hz).$^{31}$P NMR (162 MHz, $CD_3CN$) δ 181.6 (d, $J$ = 42 Hz), 54.4 (d, $J$ = 42 Hz). MS (DART) calcd for $C_{41}H_{32}N_5OP_2Ru$ (M–$BAr^F{}_4$): 774.1120, found: 774.1159.

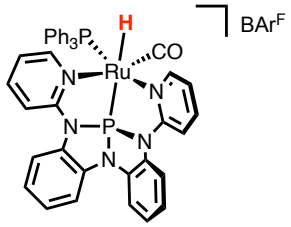

3.15

**Synthesis of 3.15.** Under a $N_2$ atmosphere, complex **3.4** (5.0 mg, 0.0062 mmol, 1.0 eq) and was suspended in $C_6D_6$ (1 mL). To the suspension was added sodium tetrakis[3,5-bis(trifluoromethyl)phenyl]borate (7.0 mg, 0.0079 mmolm, 1.3 eq) and the mixture was stirred for 4 h at ambient temperature. The white precipitate of NaCl was filtered and the filtrate containing complex **3.14** was heated at 80 ºC overnight. The formation of desired product was confirmed by NMR spectroscopy. $^1$H NMR (400 MHz, $C_6D_6$) δ 8.73 (d, $J$ = 5.7 Hz, 1H), 8.35 (s, 8H), 8.09 (d, $J$ = 5.9 Hz, 1H), 7.58 (s, 4H), 7.28 (d, $J$ = 7.5 Hz, 1H), 7.26 – 7.23 (m, 2H), 7.23 – 7.20 (m, 3H), 7.12 – 7.06 (m, 1H), 6.92 – 6.85 (m, 4H), 6.85 – 6.77 (m, 9H), 6.73 (d, $J$ = 8.4 Hz, 1H), 6.69 – 6.59 (m, 2H), 6.56 – 6.37 (m, 2H), 6.25 (d, $J$ = 8.3 Hz, 1H), 6.13 (t, $J$ = 6.6 Hz, 1H), 5.62 (t, $J$ = 6.7 Hz, 1H), 5.53 (d, $J$ = 5.2 Hz, 1H), -2.90 (dd, $J$ = 203.3, 24.5 Hz, 1H). $^{31}$P NMR (162 MHz, $C_6D_6$) δ 187.6 (d, $J$ = 20 Hz), 59.1 (d, $J$ =20 Hz). MS (DART) calcd for $C_{41}H_{32}N_5OP_2Ru$ (M–$BAr^F{}_4$): 774.1120, found: 774.1137.

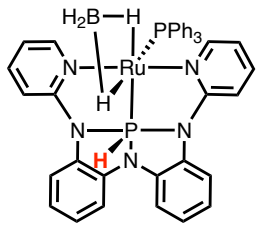

3.16

**Synthesis of 3.16**. Under a $N_2$ atmosphere, complex **3.3** (30.0 mg, 0.0367 mmol, 1 eq) and sodium borohydride (13.9 mg, 0.367 mmol, 10 eq) was suspended in tetrahydrofuran (8 mL) and heated at 70 ºC for 2 h. The unreacted sodium borohydride was filtered, and the orange filtrate was dried

in vacuo. The resulting orange residue was washed with pentane and dried in vacuo to afford **3.16** as a yellow solid (22.8 mg, 82 %). Recrystallization from dichloromethane/pentane afforded a single crystal suitable for X-ray diffraction study. $^{1}$H NMR (400 MHz, $CD_2Cl_2$, 298 K) δ 9.00 (dd, *J* = 534.6, 5.2 Hz, 1H), 8.54 (dd, *J* = 6.0, 1.8 Hz, 2H), 7.76 – 7.53 (m, 2H), 7.28 (ddd, *J* = 8.6, 6.9, 1.8 Hz, 2H), 7.13 – 7.00 (m, 9H), 6.98 (d, *J* = 8.5 Hz, 2H), 6.91 (ddd, *J* = 10.2, 6.1, 2.3 Hz, 10H), 6.81 – 6.72 (m, 2H), 6.50 – 6.30 (m, 2H), -7.84 (br, 1H). $^{13}$C NMR (101 MHz, $CD_2Cl_2$) δ 157.0 (d, *J* = 11.2 Hz), 154.0, 136.3, 134.5, 134.0 (d, *J* = 3.0 Hz), 133.5 (d, *J* = 9.7 Hz), 132.9 (d, *J* = 10.6 Hz), 131.7 (d, *J* = 2.4 Hz), 129.5 (d, *J* = 2.3 Hz), 129.2 (d, *J* = 10.2 Hz), 128.1 (d, *J* = 9.5 Hz), 121.3, 120.5, 114.1, 112.8 (d, *J* = 7.0 Hz), 111.9 (d, *J* = 2.3 Hz), 110.3. $^{31}$P NMR (162 MHz, $CD_2Cl_2$) δ 62.1(d, *J* = 66 Hz), -8.2 (d, *J* = 66 Hz). MS (DART) Calcd for $C_{40}H_{35}BN_5P_2Ru$ (M–H): 760.1499, found: 760.1557.

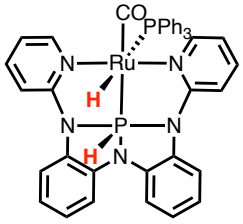


**3.17**

**Synthesis of 3.17**. Under a $N_2$ atmosphere, complex **3.3** (20 mg, 0.025 mmol, 1 eq) and sodium borohydride (5.5 mg, 0.15 mmol, 6 eq) was suspended in tetrahydrofuran (8 mL) and heated at 70 ºC for 2 h. The unreacted sodium borohydride was filtered, and the orange filtrate was dried in vacuo. The resulting orange residue was dissolved in $C_6D_6$ under a 1 atm of CO atmosphere, complex **3.16** was dissolved in $C_6D_6$ (1 mL). To the solution was added diethylamine (0.030 mL, 0.29 mmol, 12 eq) dropwise and the mixture was stirred for 30 minutes at room temperature. After removing the solvent from the yellow solution in vacuo, the obtained solid was washed with pentane to afford **3.17** as a yellow solid (8.0 mg, 42 %). $^{1}$H NMR (500 MHz, $C_6D_6$) δ 9.25 (dt, *J* = 520, 12 Hz, 1H), 8.44 (dd, *J* = 6.0, 1.8 Hz, 2H), 7.61 (dd, *J* = 7.8, 1.3 Hz, 2H), 7.22 – 7.17 (m, 6H), 6.93 – 6.84 (m, 6H), 6.83 – 6.72 (m, 10H), 6.62 (ddd, *J* = 8.6, 6.9, 1.8 Hz, 2H), 5.57 (ddd, *J* = 7.1, 5.8, 1.4 Hz,

2H), -6.48 (ddd, $J$ = 93.6, 56.3, 11.0 Hz, 1H). $^{13}$C NMR (126 MHz, $C_6D_6$) δ 156.9 (d, $J$ = 15 Hz), 155.19 (d, $J$ = 3.4 Hz), 135.92, 135.83, 135.51, 135.27 (d, $J$ = 3.0 Hz), 134.9, 134.3, 134.1, 133.1 (d, $J$ = 11.9 Hz), 128.9 (d, $J$ = 1.8 Hz), 120.9 (d, $J$ = 14.3 Hz), 113.6, 113.1 (d, $J$ = 6.1 Hz), 112.5 (d, $J$ = 2.9 Hz), 110.7. $^{31}$P NMR (203 MHz, THF-$d_8$) δ 35.2 (d, $J$ = 39 Hz), -2.6 (d, $J$ = 38 Hz). MS (DART) Calcd for $C_{41}H_{32}N_5OP_2Ru$ (M–H): 774.1120, found: 774.1264.

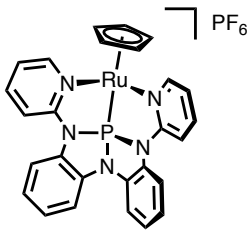

**3.23**

**Synthesis of 3.23**. Tris(acetonitrile)cyclopentadienylruthenium hexafluorophosphate (22.8 mg, 0.052 mmol) was suspended in dichloromethane (5 mL) under a $N_2$ atmosphere. To the solution was added dropwise a solution of ligand **L1** (20 mg, 0.052 mmol) in $CH_2Cl_2$ (5 mL). The resulting orange solution was stirred overnight at room temperature to afford an orange solution. The solvent was removed under vacuum and dissolved in chloroform. Yellow plate crystals of pure product of **3.23** were obtained from a chloroform solution. The crystal was suitable for X-ray diffraction. $^1$H NMR (500 MHz, $CD_2Cl_2$) δ 9.38 – 9.15 (m, 2H), 7.97 – 7.79 (m, 4H), 7.61 (d, $J$ = 8.4 Hz, 2H), 7.56 – 7.32 (m, 2H), 7.13 – 6.85 (m, 2H), 4.93 (s, 4H). $^{13}$C NMR (126 MHz, $CD_2Cl_2$) δ 157.9 (d, $J$ = 3.4 Hz), 153.4 (d, $J$ = 19.6 Hz), 139.6, 138.2, 133.2 (d, $J$ = 8.4 Hz), 126.3, 124.3, 120.4 (d, $J$ = 10.0 Hz), 120.3, 114.7 (d, $J$ = 6.1 Hz), 111.2 (d, $J$ = 3.8 Hz), 80.6 (d, $J$ = 4.1 Hz). $^{31}$P NMR (203 MHz, $CD_2Cl_2$) δ 210.2 (s). MS (ESI) Calcd for $C_{27}H_{21}N_5PRu$ (M–PF6): 548.0585, found: 548.0583.

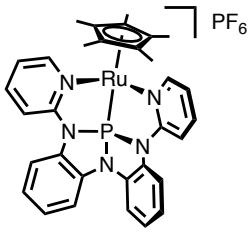


3.24

**Synthesis of 3.24**. Tris(acetonitrile)pentamethylcyclopentadienylruthenium hexafluorophosphate (26.4 mg, 0.052 mmol) was suspended in dichloromethane (5 mL) under a $N_2$ atmosphere. To the solution was added dropwise a solution of ligand **L1** (20 mg, 0.052 mmol) in $CH_2Cl_2$ (5 mL). The resulting orange solution was stirred overnight at room temperature to afford an orange solution. The solvent was removed under vacuum and recrystallized from $CHCl_3$/pentane to give yellow crystals of pure product of **3.24**. The crystal was suitable for X-ray diffraction. $^1$H NMR (500 MHz, $CDCl_3$) δ 9.03 – 8.84 (m, 2H), 7.89 – 7.72 (m, 4H), 7.55 (d, $J$ = 8.3 Hz, 2H), 7.49 (dd, $J$ = 7.6, 1.6 Hz, 2H), 7.29 – 7.15 (m, 6H), 1.68 (d, $J$ = 3.5 Hz, 15H). $^{31}$P NMR (203 MHz, $CDCl_3$) δ 208.5 (s). MS (ESI) Calcd for $C_{32}H_{31}N_5PRu$ (M–PF6): 618.1361, found: 618.1395.

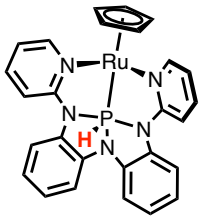


3.25

**Synthesis of 3.25**. Under a $N_2$ atmosphere, complex **3.23** (3.5 mg, 5.1 μmol) was dissolved in tetrahydrofuran (1 mL). To the solution was added sodium borohydride (1.0 mg, 26 μmol) and heated at 60 ºC for 15 min. The solvent was removed under vacuum and the resulting solid was dissolved in $C_6D_6$. $^1$H NMR (400 MHz, $C_6D_6$) δ 8.94 (dt, $J$ = 5.7, 1.0 Hz, 2H), 8.22 (d, $J$ = 476.9 Hz, 1H), 7.88 – 7.79 (m, 2H), 7.02 – 6.96 (m, 2H), 6.96 – 6.89 (m, 4H), 6.89 – 6.83 (m, 4H), 6.10 (ddd, $J$ = 7.1, 5.7, 1.5 Hz, 2H), 4.00 (d, $J$ = 0.9 Hz, 4H). $^{31}$P NMR (162 MHz, $C_6D_6$) δ 16.3 (s).

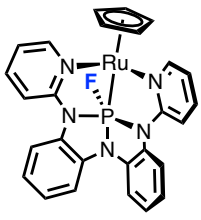


3.26

**Synthesis of 3.26**. To a J-young tube, complex **3.23** (3.5 mg, 5.1 μmol) was dissolved in $CD_3CN$ (0.8 mL). To the solution was added tetrabutylammonium difluorotriphenuylsilicate (3.5 mg, 5.1 μmol, 1 eq). After 15 min, the product **3.26** was characterized by NMR spectroscopy. $^1$H NMR (500 MHz, $CD_3CN$) δ

9.28 (d, $J$ = 5.6 Hz, 2H), 7.93 (d, $J$ = 7.7 Hz, 2H), 7.59 (ddd, $J$ = 8.6, 5.1, 1.6 Hz, 2H), 7.31 – 7.09 (m, 4H), 7.02 – 6.86 (m, 4H), 6.69 (t, $J$ = 6.5 Hz, 2H), 4.07 (s, 1H).$^{19}$F NMR (471 MHz, $CD_3CN$) δ -58.0 (d, $J$ = 1004 Hz), -72.9 (d, $J$ = 706.5 Hz, $PF_6$).$^{31}$P NMR (203 MHz, $CD_3CN$) δ 84.0 (d, $J$ = 1003 Hz), -144.04 ($PF_6$).

## 3-10. References


1. For N-X-L nomenclature, see: Perkins, C. W.; Martin, J. C.; Arduengo, A. J.; Lau, W.; Alegria, A.; Kochi, J. K.; An Electrically Neutral a-Sulfuranyl Radical from the Homolysis of a Perester with Neighboring Sulfenyl Sulfur: 9-S-3 species *J. Am. Chem. Soc.* **1980**, *102*, 7753–7759.
2. We adopt the naming convention, consistent with IUPAC recommendations, whereby "phosphorus" refers to the element name and "phosphorous" denotes the P(III) oxidation state (i.e. derivatives of phosphorous acid $(HO)_3P$). See: Hartshorn, R.M.; Hellwich, K.-H.; Yerin, A.; Damhus, T.; Hutton, A.T. "Brief Guide to the Nomenclature of Inorganic Chemistry." *Pure Appl. Chem.* **2015**, *87*, 1039-1049, and references therein.
3. Kamer, P. C. J.; Leeuwen, P. W. N. M. van *Phosphorus(III) Ligands in Homogeneous Catalysis: Design and Synthesis*; 1st Ed.; Wiley: Hoboken, N.J, 2012.
4. Tolman, C. A. Steric Effects of Phosphorus Ligands in Organometallic Chemistry and Homogeneous Catalysis. *Chem. Rev.* **1977**, *77*, 313–348.
5. Crabtree, R. H. Carbonyls, Phosphine Complexes, and Ligand Substitution Reactions. In *The Organometallic Chemistry of the Transition Metals*; John Wiley & Sons, Inc., **2005**; pp. 87–124.
6. Grabulosa, A. *P-Stereogenic Ligands in Enantioselective Catalysis*; RSC catalysis series; Royal Society of Chemistry: Cambridge, **2011**.
7. Pearson, R. G.; Gray, H. B.; Basolo, F. Mechanism of Substitution Reactions of Complex Ions. XVI. Exchange Reactions of Platinum(II) Complexes in Various Solvents. *J. Am. Chem. Soc.* **1960**, *82*, 787–792.
8. Kirby, A. J.; Warren, S. G. *The Organic Chemistry of Phosphorus*; Elsevier: Amsterdam, **1967**; p 20.
9. Ren, P.; Vechorkin, O.; Von Allmen, K.; Scopelliti, R.; Hu, X. A Structure-Activity Study of Ni-Catalyzed Alkyl-Alkyl Kumada Coupling. Improved Catalysts for Coupling of Secondary Alkyl Halides. *J. Am. Chem. Soc.* **2011**, *133*, 7084–7095.
10. Zhao, W.; McCarthy, S. M.; Lai, T. Y.; Yennawar, H. P.; Radosevich, A. T. Reversible Intermolecular E-H Oxidative Addition to a Geometrically Deformed and Structurally Dynamic Phosphorous Triamide. *J. Am. Chem. Soc.* **2014**, *136*, 17634–17644.
11. Bent, H. A. An Appraisal of Valence-bond Structures and Hybridization in Compounds of the First-row elements. *Chem. Rev.* **1961**, *61*, 275-311.
12. Hallman, P. S.; Stephenson, T. A.; Wilkinson, G. Tetrakis-(Triphenylphosphine)Dichloro-Ruthenium(II) and Tris-(Triphenylphosphine)-Dichlororuthenium(II). *Inorg. Synth.* **2007**, *12*, 237−240.
13. Braunstein, P.; Naud, F.; Pfaltz, A.; Rettig, S. J. Ruthenium Complexes with Novel Tridentate N,P,N Ligands Containing a Phosphonite Bridge between Two Chiral Oxazolines. Catalytic Activity in Cyclopropanation of Olefins and Transfer Hydrogenation of Acetophenone. *Organometallics* **2000**, *19*, 2676–2683.
14. Ahmad, N.; Levison, J. J.; Robinson, S. D.; Uttley, M. F.; Wonchoba, E. R.; Parshall, G. W. Complexes of Ruthenium, Osmium, Rhodium, and Iridium Containing Hydride Carbonyl, or Nitrosyl Ligands. *Inorg. Synth.* **2007**, *15*, 45−64

15. Trans, D.; Addison, A. W.; Rao, T. N. Synthesis, Structure, and Spectroscopic Properties of Copper(II) Compounds Containing Nitrogen-Sulphur Donor Ligands ; the Crystal and Molecular Structure of Aqua[l,7-Bis(N-Methylbenzimidazol-2'-Yl)- 2,6-Dithiaheptane]Copper(II) Perchlorate. *J. Chem. Soc. Dalton. Trans.* **1984**, 1349.

16. Kaesz, H. D.; Saillant, R. B. Hydride Complexes of the Transition Metals. *Chem. Rev.* **1972**, *72*, 231–281.

17. McCue, J. P. Transition Metal Hydrides. *Coord. Chem. Rev.* **1973**, *10*, 265–333.

18. Moore, D. S.; Robinson, S. D. Hydrido Complexes of the Transition-Metals. *Chem. Soc. Rev* **1983**, *12*, 415–452.

19. McGrady, G. S.; Guilera, G. The Multifarious World of Transition Metal Hydrides. *Chem. Soc. Rev.* **2003**, *32*, 383–392.

20. Reid, S. M.; Neuner, B.; Schrock, R. R.; Davis, W. M. Synthesis of Rhenium Complexes That Contain the $[(C_6F_5NCH_2CH_2)_3N]^{3-}$ Ligand. *Organometallics* **1998**, *17*, 4077–4089.

21. Hebden, T. J.; Schrock, R. R.; Takase, M. K.; Müller, P. Cleavage of Dinitrogen to Yield a (t-BuPOCOP)Molybdenum(IV) Nitride. *Chem. Commun.* **2012**, *48*, 1851.

22. Albinati, A.; Lianza, F.; Pasquali, M.; Sommovigo, M.; Leoni, P.; Pregosin, P. S.; Rüegger, H. Pd-H-P Bridging in a Palladium(I) Dimer. *Inorg. Chem.* **1991**, *30*, 4690–4692.

23. Leoni, P.; Pasquali, M.; Sommovigo, M.; Laschi, F.; Zanello, P.; Albinati, A.; Lianza, F.; Pregosin, P. S.; Rüegger, H. Chemistry of Phosphido-Bridged Palladium(I) Dimers. $H_2$Pd-H-P Interactions: A New Bonding Mode for Secondary Phosphines. *Organometallics* **1993**, *12*, 1702–1713.

24. Allen, C. W.; Ebsworth, E. A. V.; Henderson, S. G.; Rankin, D. W. H.; Robertson, H. E.; Whitelock, J. D. Reactions of Halogenohydridobis(Triethylphosphine)Platinum Trihalogenophosphines:Some Unusual Complexes of Pt" Containing Five-Co- Ordinated Phosphorus. *J. Chem. Soc. Dalton Trans.* **1986**, 1333-1338.

25. Blake, A. J.; Cockman, R. W.; Ebsworth, E. A. V.; Henderson, S. G. D.; Holloway, J. H.; Pilkington, N. J.; Rankin, D. W. H. Complexes of Iridium and Platinum Containing 5-Coordinated Phosphorus. *Phosphorous and Sulfur and the Related Elements* **1987**, *30*, 143–146.

26. Bader, R. F. W. in *Atoms in Molecules: A Quantum Theory*, Oxford University Press, Oxford, 1990.

27. van Lenthe, E.; Baerends, E. J.; Snijders, J. G. Relativistic Regular Two Component Hamiltonians. *J. Chem. Phys.* **1993**, *99*, 4597–4610.

28. Pantazis, D. A.; Chen, X.-Y.; Landis, C. R.; Neese, F. All-Electron Scalar Relativistic Basis Sets for Third-Row Transition Metal Atoms. *J. Chem. Theory Comput.* **2008**, *4*, 908–919.

29. Hallman, P. S.; McGarvey, B. R.; Wilkinson, G. *J. Chem. Soc. A*, **1968**, 3143-3150.

30. Basolo, F.; Chatt, J.; Gray, B.; Pearson, R. G.; Shaw, B. L.; *J. Chem. Soc.* **1961**, 2207.

31. Kaesz, H. D.; Saillant, R. B. Hydride Complexes of the Transition Metals. *Chem. Rev.* **1972**, *72*, 231–281.

32. Adamo, C.; Barone, V. Toward Reliable Density Functional Methods without Adjustable Parameters: The PBE0 Model. *J. Chem. Phys.* **1999**, *110*, 6158–6170.

33. Caldeweyher, E.; Bannwarth, C.; Grimme, S. Extension of the D3 Dispersion Coefficient Model. *J. Chem. Phys.* **2017**, *147*, 34112.

34. Caldeweyher, E.; Ehlert, S.; Hansen, A.; Neugebauer, H.; Spicher, S.; Bannwarth, C.; Grimme, S. A Generally Applicable Atomic-Charge Dependent London Dispersion Correction. *J. Chem. Phys.* **2019**, *150*, 154122.

35. Van Lenthe, E.; Baerends, E. J.; Snijders, J. G. Relativistic Regular Two-Component Hamiltonians. *J. Chem. Phys.* **1993**, *99*, 4597–4610.

36. Klamt, A. Conductor-like Screening Model for Real Solvents: A New Approach to the Quantitative Calculation of Solvation Phenomena. *J. Phys. Chem.* **1995**, *99*, 2224–2235.

37. Klamt, A.; Jonas, V.; Bürger, T.; Lohrenz, J. C. W. Refinement and Parametrization of COSMO-RS. *J. Phys. Chem. A* **1998**, *102*, 5074–5085.

38. Weigend, F.; Ahlrichs, R. Balanced Basis Sets of Split Valence, Triple Zeta Valence and Quadruple Zeta Valence Quality for H to Rn: Design and Assessment of Accuracy. *Phys. Chem. Chem. Phys.* **2005**, *7*, 3297–3305.

39. Grimme, S.; Brandenburg, J. G.; Bannwarth, C.; Hansen, A. Consistent Structures and Interactions by Density Functional Theory with Small Atomic Orbital Basis Sets. *J. Chem. Phys.* **2015**, *143*, 54107.

40. Nakazawa, H.; Kubo, K.; Kai, C.; Miyoshi, K. A New Reaction of $[Cp(CO)_2Fe(PPh_2H)]PF_6$ with $NaBH_4$ to Give $Cp(CO)(H)Fe(PPh_2H)$ via $Cp(CO)_2FeH$ and PPh2H. *J. Organomet. Chem.* **1992**, *439*, C42–C45.

41. A later computational study was performed for this reaction by Brown, Fitzpatrick and Glass that suggested the mechanism with formyl intermediate $Cp(CO)Fe(CHO)(PPh_2H)$ is more likely. Brown, D. A.; Deignan, J. P.; Fitzpatrick, N. J.; Fitzpatrick, G. M.; Glass, W. K. Theoretical and Experimental Studies of Hydride Addition to Iron Carbonyl Phosphine and Phosphite Complexes. *Organometallics* **2001**, *20* (8), 1636–1645.

42. Zhang, J.; Balaraman, E.; Leitus, G. and Milstein D. *Organometallics*, **2011**, *30*, 5716-5724.

43. Cleveland, G. T.; Radosevich, A. T. A Nontrigonal Tricoordinate Phosphorus Ligand Exhibiting Reversible "Nonspectator" L/X-Switching. *Angew. Chem. Int. Ed.* **2019**, *58*, 15005–15009.

44 . Lin, Y. C.; Hatzakis, E.; McCarthy, S. M.; Reichl, K. D.; Lai, T. Y.; Yennawar, H. P.; Radosevich, A. T. P-N Cooperative Borane Activation and Catalytic Hydroboration by a Distorted Phosphorous Triamide Platform. *J. Am. Chem. Soc.* **2017**, *139*, 6008–6016.

45. Pangborn, A. B.; Giardello, M. A.; Grubbs, R. H.; Rosen, R. K.; Timmers, F. J. *Organometallics* **1996**, *15*, 1518–1520.

46. Alaimo, P. J.; Peters, D. W.; Arnold, J.; Bergman, R. G. *J. Chem. Educ.*, **2001**, *78*, 64.

47. Bruker, *SAINT*, 2012, Bruker AXS Inc., Madison, Wisconsin, USA.

48. Bruker, *SADABS,* 2001, Bruker AXS Inc., Madison, Wisconsin, USA.

49. Sheldrick, G. M. *Acta. Cryst.*, **2008**, *A64*, 112-122.

50. Ren, P.; Vechorkin, O.; Von Allmen, K.; Scopelliti, R.; Hu, X. *J. Am. Chem. Soc.* **2011**, *133*, 7084–7095.

51. Snelgro, J. L.; Conrad, J. C.; Yap, G. P. A.; Fogg, D. E. The Kinetic Instability of σ-Bound Aryloxide in Coordinatively Unsaturated or Labile Complexes of Ruthenium. *Inorg. Chem. Acta* **2003**, *345*, 268–278.

# Chapter 4 Metal–Ligand Cooperative Reactivity of Group 9 Complexes of Nonspectator Phosphosrus(III) Ligands

## 4-1. Introductory remark: Metal–Ligand Cooperation with Electrophilic Ligands

Metal–ligand cooperation (MLC), in which both the metal and the ligand are actively and directly involved in bond activation processes, has been an emerging concept in transition metal catalysis recently.[1] Among diverse modes of MLC, here we only focus on the systems using a polarized $M^{\delta-}$–$L^{\delta+}$ (M: electron-rich late transition metal, L: π-acceptor ligands) bond as a platform of bond activation, which are most strongly related to our systems.[2] As shown in a simplified frontier MO diagram in Figure 4-1, there coexist the nucleophilicity of the electron-rich metal and the electrophilicity of the Lewis-acidic ligand, if the backdonation from the electron-rich metal is not strong enough to cancel these.

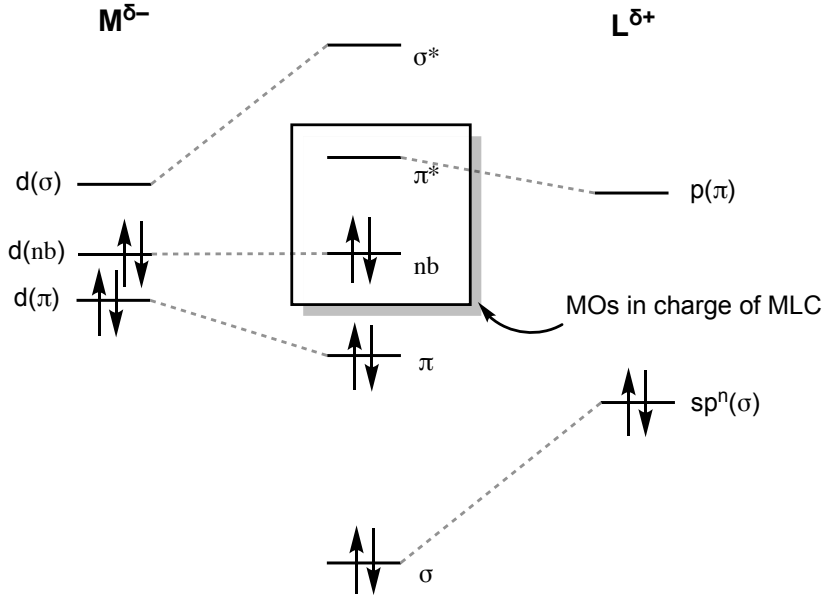


**Figure 4-1**. Simplified frontier MO diagrams for MLC system with poralized $M^{\delta-}$–$L^{\delta+}$ bond.

For instance, a cationic ruthenium silylene complex studied by Tilley has a high partial positive charge on the Si and forms a polarized $Ru^{\delta-}$–$Si^{\delta+}$ bond (**Scheme 4-1.** Formal [2+2] cycloaddition of isocyanates to ruthenium silylene complex reported by (a) Tilley and (b) Whited.Scheme 4-1a).[3] While the complex does not readily react with nonpolar substrates, the authors reported a formal

[2+2] cycloaddition of isocyanates to the Ru=Si bond. The overall cycloaddition proceeds through initial nucleophilic attack at an electrophilic silylene. Similar dipolar addition to M=Si bonds are also reported by Whited (**Scheme 4-1.** Formal [2+2] cycloaddition of isocyanates to ruthenium silylene complex reported by (a) Tilley and (b) Whited.Scheme 4-1b).[4,5] Other known examples of ligands affording similar electronic structures are Fisher carbenes,[6 - 10] borylene[11 - 13] and phosphenium.[14]

**Scheme 4-1.** Formal [2+2] cycloaddition of isocyanates to ruthenium silylene complex reported by (a) Tilley and (b) Whited.

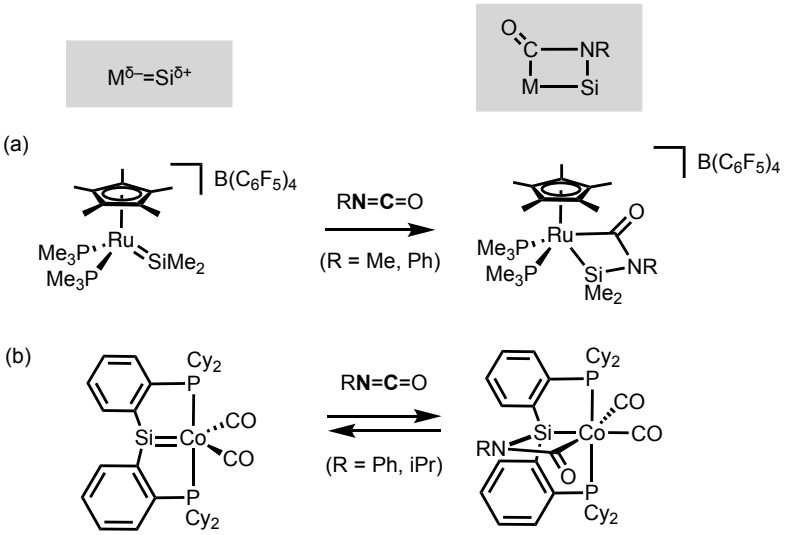


In Chapter 3, we demonstrated that the highly electrophilic nontrigonal phosphorus ligand functions as a hydride acceptor affording metallohydrophosphoranes by nonspectator reactivities. In this chapter, we will expand the nonspectator reactivities of the electrophilic P(III) ligand by combining it with electron-rich nucleophilic metal centers to target a bifunctional electronic structure of the resulting M–P bonds. The transition from Group 8 to Group 9 metals enables unique cooperative activation of C=E and E–H bonds across the M–$PR_3$ bonds, in which an increase in P-coordination number is accompanied by a $2e^-$ redox process at the metal (Figure 4-2).

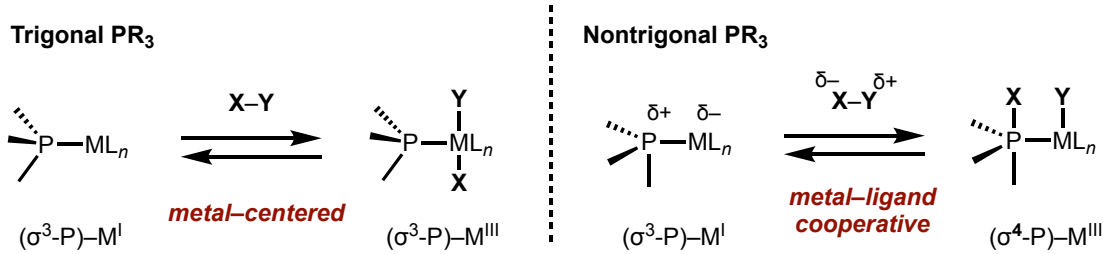


**Figure 4-2**. (left) classic metal–centered activation (right) proposed metal–ligand cooperative activation

## 4-2. Synthesis of Low-valent Rh(I)/Ir(I) $PR_3$ Complexes

### *4-2-1. Synthesis of RhCl(PPh3)(κ²-**L1**)*

Based on the electronic structure discussion in the previous section, we first targeted monovalent Group 9 complexes with square planar geometries as a platform of metal–ligand cooperative bond activation. Metalation of **L1** with $[Rh(cod)Cl]_2$ (0.5 eq) and $PPh_3$ in THF at ambient temperature yielded the expected square planar Rh(I) complex **4.1**, in which **L1** coordinates to the metal as a bidentate $\kappa^2$ ligand (Scheme 4-2). Complex **4.1** can also be synthesized through metalation of **L1** with $RhCl(PPh_3)_3$ (Wilkinson's catalyst).

**Scheme 4-2**. Synthesis of square planar $Rh^I$ and $Ir^I$ complexes of **L1**.

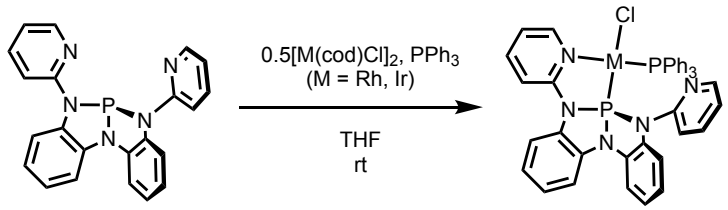


**L1** **4.1** (M=Rh) **4.2** (M=Ir)

In the $^{31}P$ NMR spectra, the complex **4.1** exhibits two doublet of doublet signals; one at δ 151.9 ppm ($^1J_{RhP}$ = 292 Hz, $^2J_{PP}$ =52 Hz) corresponding to the triamido phosphorus nucleus and the other at δ 43.7 ppm ($^1J_{RhP}$ = 170, $^2J_{PP}$ = 52 Hz) for the $PPh_3$ ligand. Contrary to the depicted chemical structure of **4.1**, the $^1H$ NMR spectra show a twofold equivalence of resonances in the aryl region, suggesting the time-average $C_s$ symmetry in the solution phase. This observation can be explained by a fluxional behavior of tridentate ligand **L1** by degenerate interchange of the two pyridyl side arms. A broadened signal at δ 8.92 ppm corresponding to the protons at the 2-position of pyridyl moieties supports this assumption. The κ²-chelating mode is confirmed by X-ray diffraction of a single crystal obtained from dichloromethane/pentane solution at –35 ºC (Figure 4-3). The

rhodium atom in the solid-state structure of complex **4.1** adopts an approximate square planar geometry ($\tau_4 = 0.10$)[15] with the chloride ligand positioned *trans* to the triamidophosphorus atom. The most noticeable features of the structure are the Rh(1)−P(1) bond distance of 2.120(4) Å to the triamidophosphorus which is markedly shorter than that found to triphenylphosphine ($d$(Rh(1)−P(2)) = 2.251 Å). The local structure of the phosphorus triamide framework is slightly affected by the coordination; there is an increase in the angle $\angle_{N1-P1-N3}$ (113.63(7)° in **4.1** and 108.67(4)° in free **L1**) upon ligation.

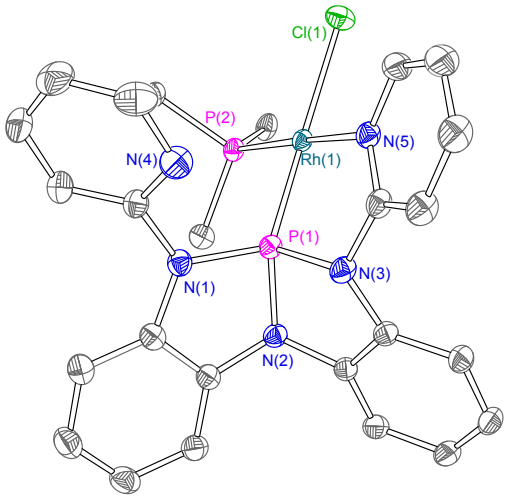


**Figure 4-3**. Thermal ellipsoid plots rendered at the 50% probability level for **4.1**. Hydrogens, solvent molecules of crystallization and phenyl rings of $PPh_3$ ligands are omitted for clarity

*4-2-2. Synthesis of IrCl(PPh3)(κ²-**L1**)*

Analogous metalation of **L1** by treatment with $[Ir(cod)Cl]_2$ (0.5 eq) and $PPh_3$ (1 eq) affords the corresponding Ir(I) complex **4.2**. Complex **4.2** exhibits a set of $^{31}P$ NMR resonances corresponding to the triamido phoshorus nucleus at δ 111.6 ppm ($^2J_{P-P}$ = 37 Hz) and to the $PPh_3$ nucleus at δ 13.0 ppm ($^2J_{P-P}$ = 37 Hz).

**Scheme 4-3**. Dimerization of complex **4.2**.

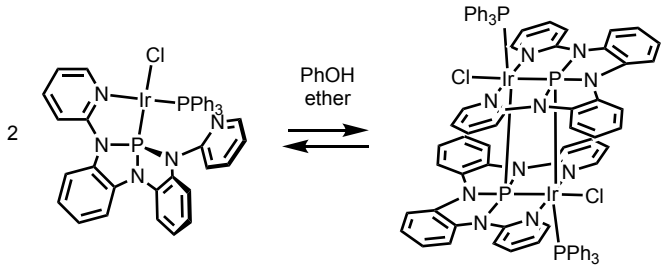


**4.2** **4.3**

Although the several attempts to recrystallize **4.2** did not afford a single crystal of sufficient quality for X-ray diffraction, diiridium complex **4.3**, a dimer of **4.2**, was serendipitously obtained from a solution of **4.2** with phenol and ether (Scheme 4-3). The solid state structure of **4.3** showed the dimerization occurs via the interaction between two Ir–$P(N)_3$ bonds resulting in a four-membered diamond-core dimetallacycle containing two triamidophosphorus atoms bridging two Ir centers (Figure 4-4 and Figure 4-5).

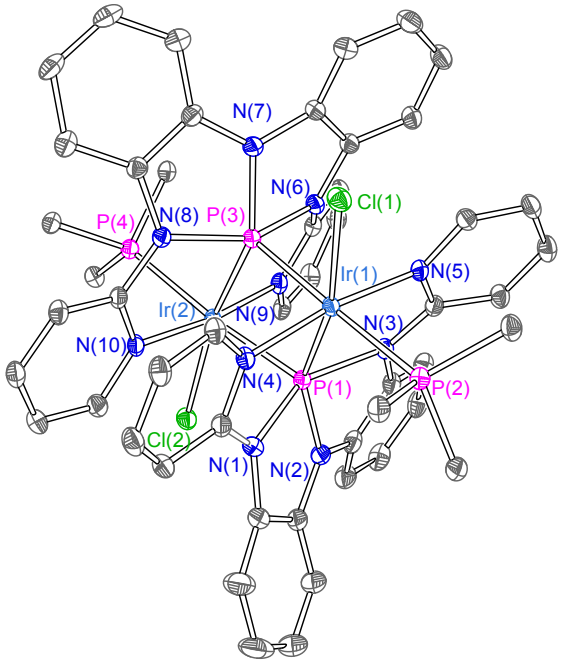


**Figure 4-4**. Thermal ellipsoid plots rendered at the 50% probability level for **4.3**. Hydrogens and phenyl rings of $PPh_3$ ligands are omitted for clarity.

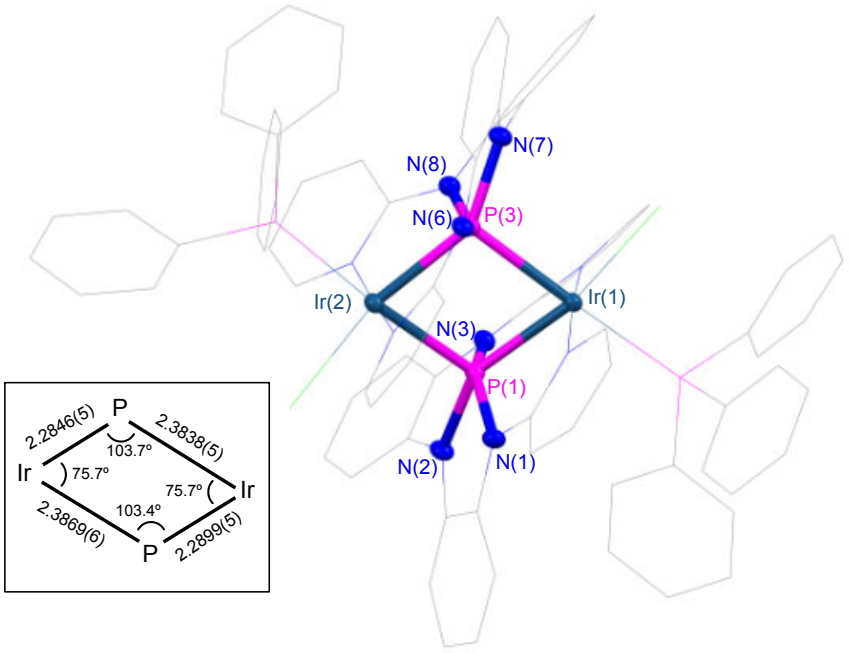


**Figure 4-5.** Structure of **4.3**, with hydrogen atoms omitted for clarity. Two phosphorus atoms and their substituent atoms are depicted with thermal ellipsoids at 50% probability (inset: selected structural parameters).

The two triamidophosphorus ligand takes on an unusual $\mu_2$-bridging role in this complex. The formation of pentacoordinate phosphorus centers with an approximate square pyramidal geometry ($\tau_5$[16] is 0.06 for P(1), 0.10 for P(3)) is accompanied by the planarization of $PN_3$ framework ($\angle_{N(1)–P(1)–N(3)}$ = 151.17(8)º, $\angle_{N(6)–P(3)–N(8)}$ = 152.45(8)º, compared to 108.67(4)º for free **L1**). The Ir–P distances show largely asymmetric features ($d_{Ir(1)–P(1)}$ = 2.2899(5) Å, $d_{Ir(2)–P(1)}$ = 2.3869(6) Å, $d_{Ir(1)–P(3)}$ = 2.2846(5) Å, $d_{Ir(2)–P(3)}$ = 2.3838(5) Å). The two nitrogen atoms N(2) and N(7) are on the same plane of the Ir(1)–P(1)–Ir(2)–P(3) cycle, but not on the line P(1)–P(3), shown by the asymmetric Ir–P–N angles ($\angle_{Ir(1)–P(1)–N(2)}$ = 147.66(7)º, $\angle_{Ir(1)–P(1)–N(2)}$ = 108.84(7)º, $\angle_{Ir(2)–P(3)–N(7)}$ = 146.74(7)º, $\angle_{Ir(1)–P(3)–N(7)}$ = 109.52(6)º).

Different from other ligands such as halides, hydride or CO, $\mu_2$-bridging is a strikingly sparce coordination mode for tricoordinate phosphorus ligands.[17, 18] As a similar example, Arduengo reported that a reaction of $C_{2v}$ symmetric 'biphilic'[19] phosphoramidite **4.4** and equimolar $Ag(CH_3CN)_4$ affords a crystalline polymeric species **4.5** with a [–Ag(CH3CN)$_2$($\mu_2$-**4.4**)–] repeat unit (Scheme 4-4). Attempts to synthesize a monomeric dinuclear complex of $\mu_2$-bridging **4.4** were not successful. The structure of **4.5** shares similar features to **4.3** in its approximate planar P(ONO) framework ($\angle_{OPO}$ = 167.7(6)º) and unsymmetrical M–$PR_3$–M coordination ($d_{P-Ag}$ = 0.2434 (5) and 0.2574(5) Å).

**Scheme 4-4.** Arduengo's report of polymeric linear chain Ag complex with $\mu_2$-$PR_3$ ligands.

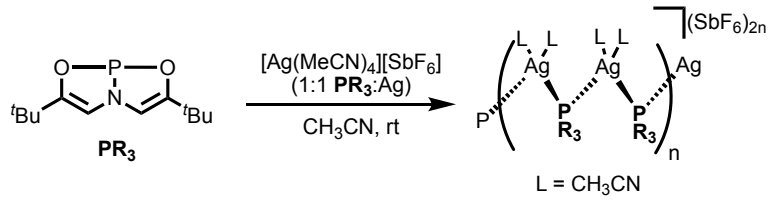


**4.4** **4.5**

Syntheses of dimeric complexes with bridging $\mu$-$PR_2$ from metal–phosphenium or metal–phosphide complexes are more common than bridging $\mu$-$PR_3$ congeners, and have been reported by Peters,[20,21] Gudat,[22] Thomas[23-25] and others. While the crystallographic characterization of **4.3** is secure, a reproducible preparation of this remarkable complex has regrettably not been achieved. Notwithstanding the aleatory synthesis, the crystal structure strongly suggests that an intermolecular donor–acceptor interaction centered on Ir and P atoms can be formed between two molecules of **4.2**. This interpretation indicates that **4.2** has the desired bifunctional electronic structure with the coexistence of a Lewis-basic Ir and Lewis-acidic P(N)$_3$.

## 4-3. Cooperative Activation of C=E Bonds by IrCl(PPh$_3$)(L1)

### *4-3-1. Reactions of **4.2** with isocyanates*

Based on the potential bifunctional feature of **4.2**, we attempted metal–ligand cooperative bond activation over the Ir–PR$_3$ bond. Inspired by previous work by Tilley and Whited (Scheme 4-1), we first treated **4.2** with ethyl isocyanate to target a [2+2] cycloaddition of C=N bond to the Ir–P bond. The reaction proceeds cleanly at ambient temperature to afford a single product **4.6** (Scheme 4-5, *top*).

**Scheme 4-5**. Treatment of Ir complex **4.2** with isocyanates.

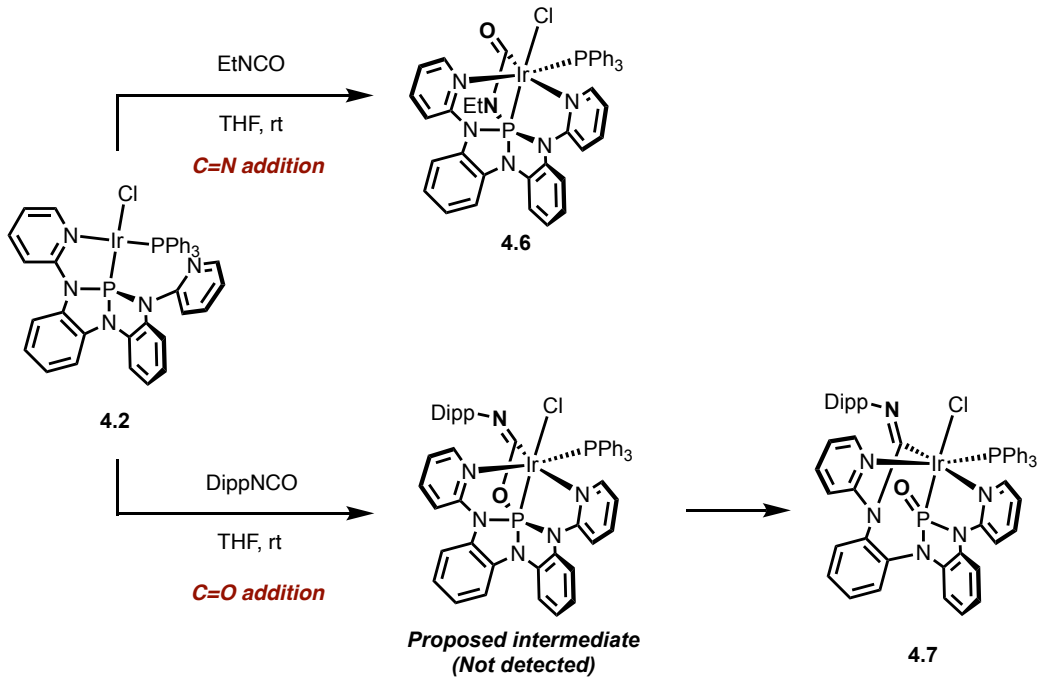


The $^{31}P\{^1H\}$ NMR spectrum displayed two low field doublets at δ –0.7 and –74.8 ppm with mutual coupling ($^2J_{P–P}$ = 17 Hz). The significant upfield shift of the triamidophosphorus signal at δ –74.8 ppm indicates the increase in P coordination number. In the $^1$H-coupled $^{31}$P NMR spectrum, the signal at δ –74.8 ppm is further split into a triplet ($J_{P–H}$ = 13 Hz), suggesting two protons have

close contact with the spin system of the P. The corresponding coupling partners are found in $^{1}$H NMR spectrum; the resonances arising from the diastereotopic methylene protons are observed with the same coupling constant at δ 2.06 and 1.65 ppm ($J_{P–H}$ = 13 Hz). In the $^{13}$C NMR spectrum, the resonance corresponding to the methylene is found as a doublet at 41.5 ppm with a coupling with the triamido phosphorus nucleus ($J_{P–C}$ = 14 Hz). The $^{1}$H NMR signals in the aryl region suggest the overall $C_1$ symmetry. Taken together, complex **4.6** is assigned as a metallophosphorane depicted in Scheme 4-5, formed by the expected [2+2] cycloaddition between C=N and Ir–P bonds.

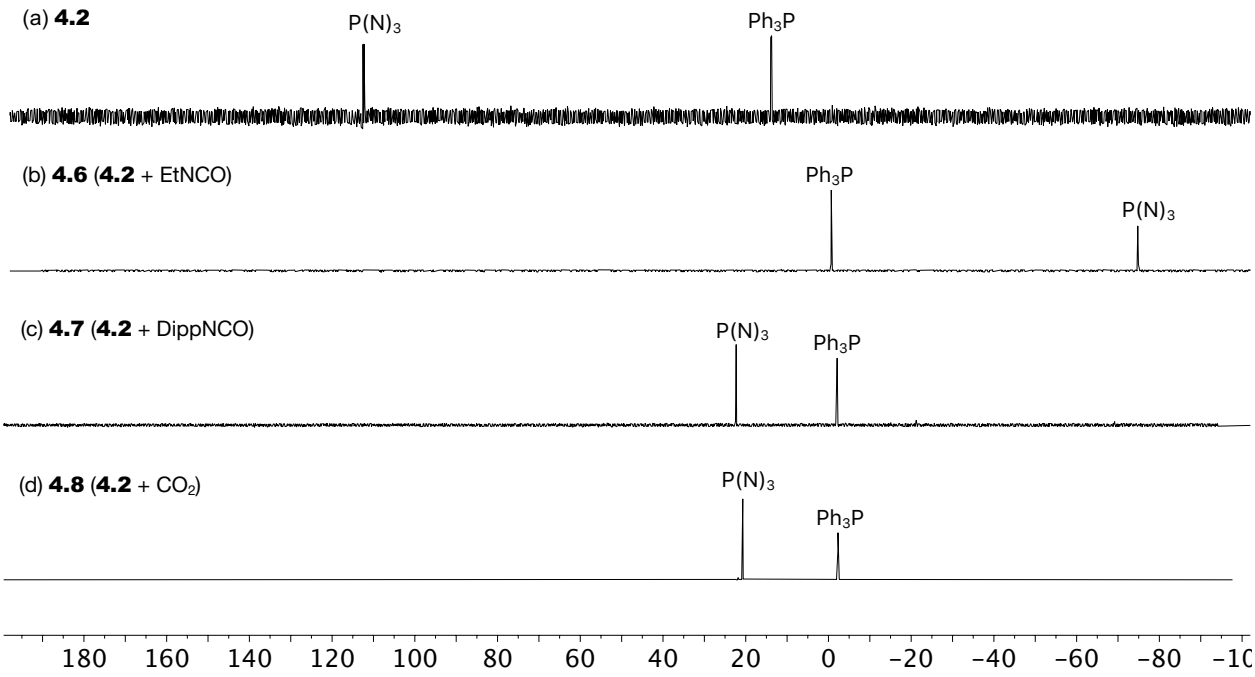


**Figure 4-6.** $^{31}$P{$^{1}$H} NMR spectra of (a) **4.2** (b) **4.6** (c) **4.7** (d) **4.8**. Units are ppm relative to 85% $H_3PO_4$.

In contrast, when complex **4.2** was treated with DippNCO (Dipp = 2,6-diisopropylphenyl) under otherwise identical conditions, the reaction did not return the expected [2+2] cycloaddition product. The $^{31}$P NMR spectra of product **4.7** show a triamidophosphorus resonance at δ 22.4 ppm (d, $^{2}J_{PP}$ = 27 Hz), drastically downfield-shifted compared to **4.6** (Δδ = 97.2 ppm). The

corresponding coupling partner is a triphenylphosphine nucleus found at δ –2.2 ppm in $^{31}$P NMR. Although neither $^{1}$H NMR nor the $^{13}$C NMR spectra provide sufficient data for an unambiguous structural assignment, the identity of **4.6** was characterized by X-ray diffraction of a single crystal obtained from a slow diffusion of pentane into a dichloromethane solution at –35 ºC. The solid-state structure of **4.7** reveals the formation of phosphoryl species (Figure 4-7).[26] The C=O bond of DippNCO is completely cleaved to result the P=O bond formation and the coordination of the remaining DippN=C moiety to the Ir center at the *trans* position to a pyridyl ligand. Notably, the C=O bond splitting is accompanied by the cleavage of P(1)–N(3) bond ($d_{P(1)–N(3)}$ = 3.325 Å in **4.7**) and N(3) forms a new C–N bond with the coordinating C(1) atom of DippN=C–Ir moiety, resulting in a $\kappa^4$-*P, N, N',C*-chelate. The resulting phosphoryl ligand has an approximate symmetric framework ($d_{P(1)–N(1)}$ = 1.7372(13) Å, $d_{P(1)–N(2)}$ = 1.7136(12) Å, $\angle_{O(1)–P(1)–N(1)}$ = 110.44(6)º, $\angle_{O(1)–P(1)–N(2)}$ = 113.16(6)º).

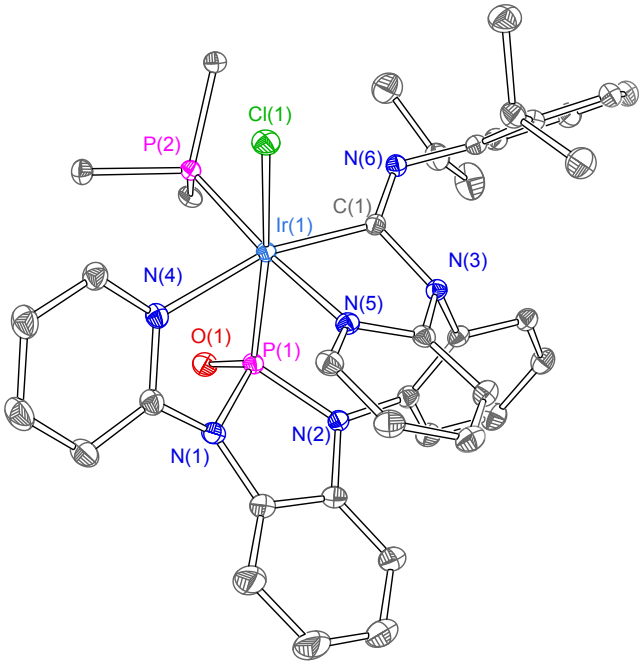


**Figure 4-7.** Thermal ellipsoid plots rendered at the 50% probability level for **4.7**. Hydrogens and phenyl rings of $PPh_3$ ligands are omitted for clarity.

The formation of complex **4.7** can be explained by a mechanism in which [2+2] cycloaddition of C=O is followed by the rearrangement around the P center (Scheme 4-6). Although the proposed intermediate of [2+2] cycloaddition of C=O and Ir–P was not directly detected, the observed stereoselectivity in the crystal structure agrees with the proposed mechanism.

**Scheme 4-6**. Proposed mechanism for the formation of phosphoryl complex **4.7**.

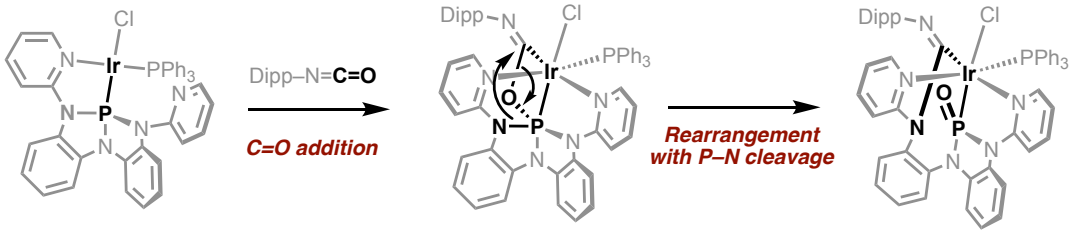


It is known that the cleavage of P–N bonds often leads to the formation of phosphoryl complexes. For instance, Kirchner and coworkers reported Group 10 complexes of pincer-type PNP ligand can be converted into phosphoryl complexes by cleavages of P–N bonds (Scheme 4-7).[27,28] Similar hydrolytic P–N bond cleavages to afford phosphoryl palladium complexes are reported by Barakrishna[29] and Krisunamurthy.[30] As for structurally close systems, Thomas synthesized two *N*-heterocyclic phosphoryl species by oxidizing the phosphenium P with trimethylamine *N*-oxide[31] or by heterolytic addition of RO–H bond to Pt–P bond followed by an Arbuzov-type process[32] to dissociate RCl[33] (Scheme 4-8).

**Scheme 4-7**. Kirchner's phosphoryl complexes formed *via* P–N bond cleavage of pincer-type PNP ligand

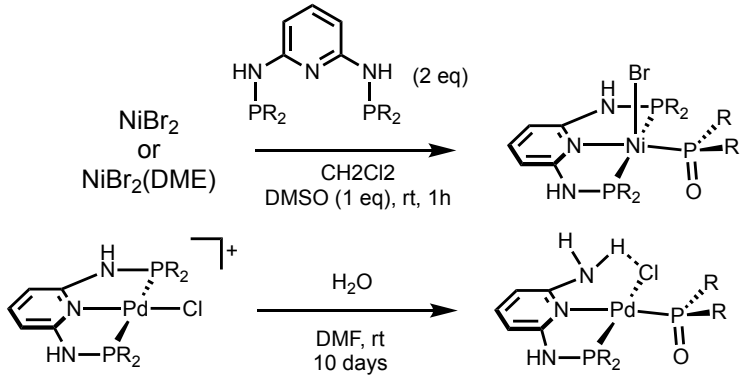

**Scheme 4-8**. Synthesis of *N*-heterocyclic phosphoryl complexes reported by Thomas.

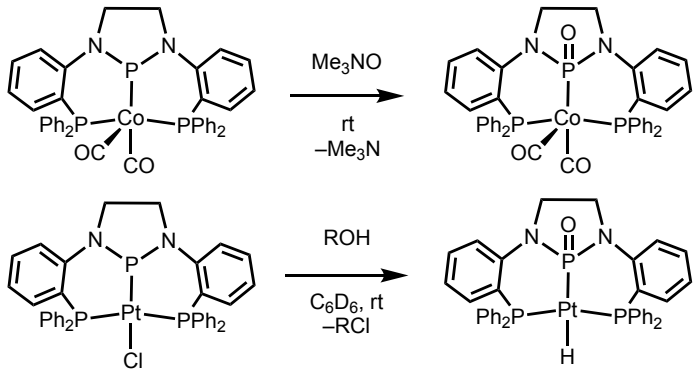


We hypothesized the distinct reactivity of **4.2** with DippNCO is due to the bulky Dipp *N*-substituent, which prevents the [2+2] cycloaddition of C=N bond otherwise observed in the reaction with EtNCO. To support this, we conducted ground state geometry optimization and electronic energy calculations for regioisomeric C=N and C=O cycloaddition products of both EtNCO and DippNCO at B3LYP/def2-TZVP level (Figure 4-8). All cycloaddition reactions are calculated to be thermodynamically downhill, but when EtNCO is used, cycloaddition to the C=N moeity is much more favorable than the regioisomeric addition to the C=O moiety ($\Delta G_{C=N}$ = –19.9 kcal/mol vs $\Delta G_{C=O}$ = –6.7 kcal/mol). Complementarily, when DippNCO is used the C=O addition is computed to have a stronger driving force ($\Delta G_{C=N}$ = –14.2 kcal/mol vs $\Delta G_{C=O}$ = –16.4 kcal/mol). In this way, the computational results reinforce a thermodynamic rationale for the experimental observations.

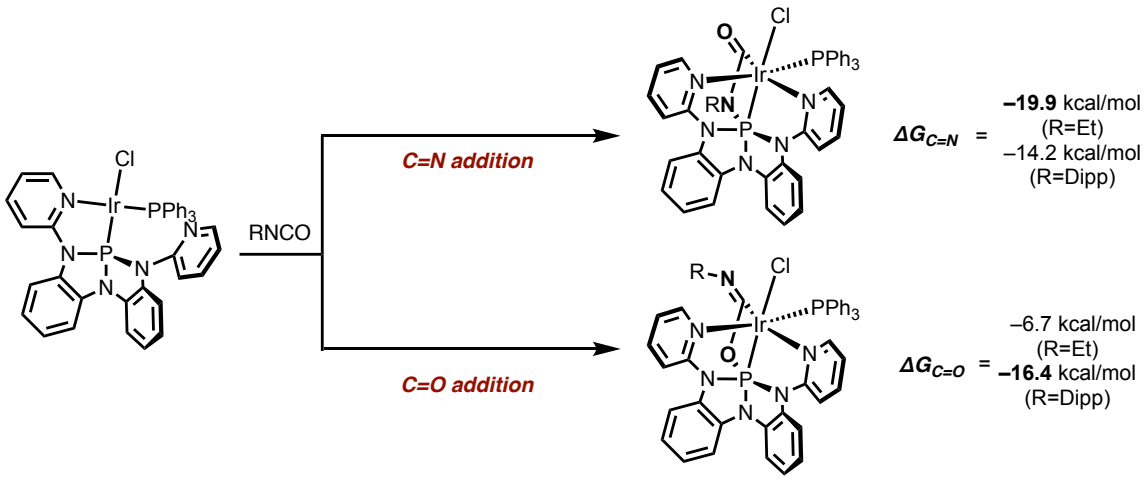


**Figure 4-8.** Calculated energy differences of C=N and C=O cycloaddition to **4.2** for EtNCO and DippNCO.

In both cases, the formation of phosphoryl complex from the C=O cycloaddition product is computed to be highly exothermic ($\Delta G$ = –31.1 kcal/mol for R=Et, $\Delta G$ = –31.5 kcal/mol for R=Dipp). Based on this result, a THF solution of **4.6** was heated at reflux to see if the conversion into a phosphoryl product proceeds. Although the reaction was not clean, a main product **4.8** shows a set of $^{31}$P NMR resonances at δ 23.7 and –4.0 ppm with mutual coupling of $J$ = 29 Hz. Based on the values of chemical shifts and coupling constant of **4.8** close to **4.7**, the formation of stable phosphoryl product was confirmed, as predicted by the calculation (Scheme 4-9).

**Scheme 4-9**. Conversion from C=N cycloaddition product to phosphoryl complex.

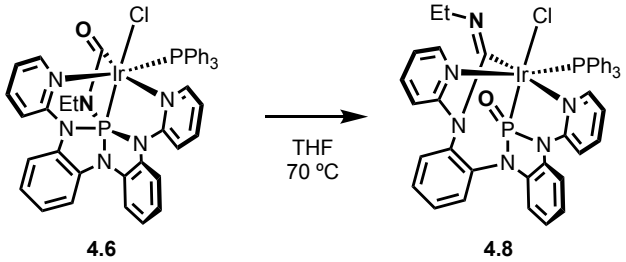

*4-3-2. Cooperative heterolytic splitting of carbon dioxide by **4.2***

**Scheme 4-10**. Metal–ligand cooperative splitting of carbon dioxide by **4.2**

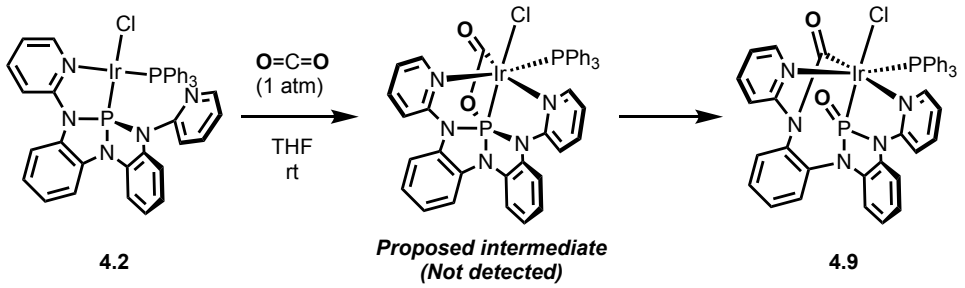


**4.2** **4.9**

Treatment of **4.2** with carbon dioxide afforded analogous phosphoryl complex **4.9** by splitting of the C=O bond (Scheme 4-10). When a THF solution of **4.2** was exposed to $CO_2$ atmosphere (1 atm), an off-white powder of **4.9** immediately precipitated. In the resulting $^{31}P\{^{1}H\}$ NMR spectra of **4.9**, the resonance corresponding to P(NNO) nucleus is found as a doublet at δ 20.8 ppm, which is coupled with a signal at δ –2.4 ppm of triphenylphosphine nucleus with $^{2}J_{P-P} = 25$ Hz. (Figure 4-6d). The P–O bond formation and $\kappa^4$-*P,N,N,C*-chelating mode are confirmed by X-ray diffraction of a single crystal sample. As a result of heterolytic splitting of $CO_2$ by Ir–P bond, an iridium-amide moiety is generated by a newly formed C(1)–N(3) bond as a result of P(1)–N(3) cleavage. The structures of **4.6** and **4.9** are almost analogous except for the substituents of C(1).

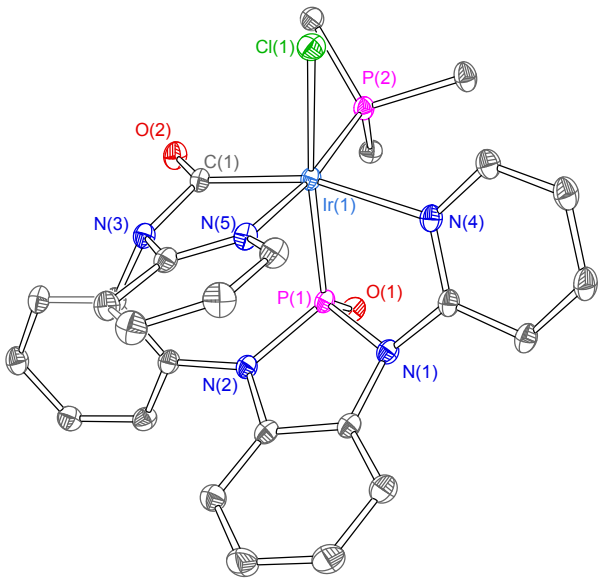


**Figure 4-9.** Thermal ellipsoid plots rendered at the 50% probability level for **4.8**. Hydrogens and phenyl rings of $PPh_3$ ligands are omitted for clarity.

Most of the previous attempts to cleave C=O bonds in $CO_2$ have utilized the large $C^{\delta+}=O^{\delta-}$ polarization due to the high C=O bond strength (127 kcal/mol). Along with 1,2-addition of frustrated Lewis pairs (FLPs) to the C=O bond,[34] there have been increasing number of metal–ligand cooperative approaches to activate C=O bonds. Cycloaddition products with four-membered metallacycle such as described in Scheme 4-10 have been proposed as intermediates in these studies (Scheme 4-11). Grubbs reported a reaction of a pincer-type iridium carbene complex and $CO_2$ to provide a formate ester and an iridium carbonyl.[35] Whited reported an insertion of $CO_2$ into a Rh–Si bond followed by a splitting of C=O bond to form of Rh–CO and Si–O–Rh moieties.[36] Such heterolytic splitting of $CO_2$ has also been reported recently for polarized heterobimetallic systems.[37-39]

**Scheme 4-11**. Reported metal–ligand cooperative splitting of carbon dioxide through proposed four-membered metallacycle intermediates.

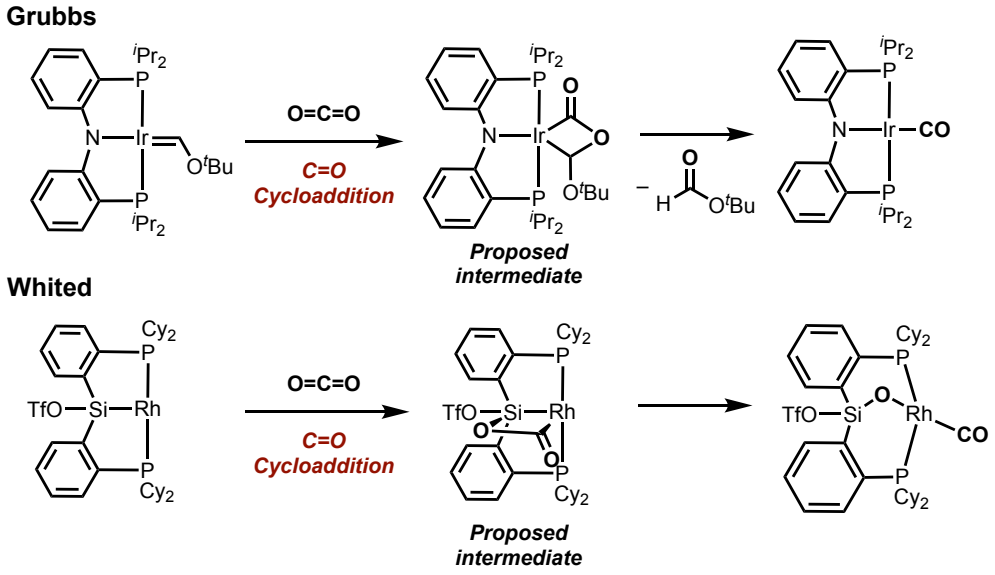


However, there have been fewer examples of using polarized metal–phosphorus bonds to split C=O bond (Scheme 4-12). The reactivity of **4.2** is most close to a report by Langer and coworkers, where they demonstrated a Ir(I) complex activates 2 equivalents of $CO_2$ to form a Ir(III)–phosphoryl complex via a P–C bond cleavage.[40] Milstein reported a similar complicated $CO_2$ activation by two molecules of PNP–Ni(II) complexes.[41] In these reactions, the mechanism of P–C bond cleavage and phoshoryl complex formation is unknown. For lower coordinate phosphorus ligands, Müller and Wolf recently reported a cooperative $CO_2$ splitting by an iron(0) phosphinine complex.[42] Taken together, the $CO_2$ splitting by complex **4.2** represents a clean, well-defined splitting of $CO_2$ by an equimolar M–$PR_3$ bond.

**Scheme 4-12**. Reported metal–ligand cooperative splitting of carbon dioxide by M–P bonds

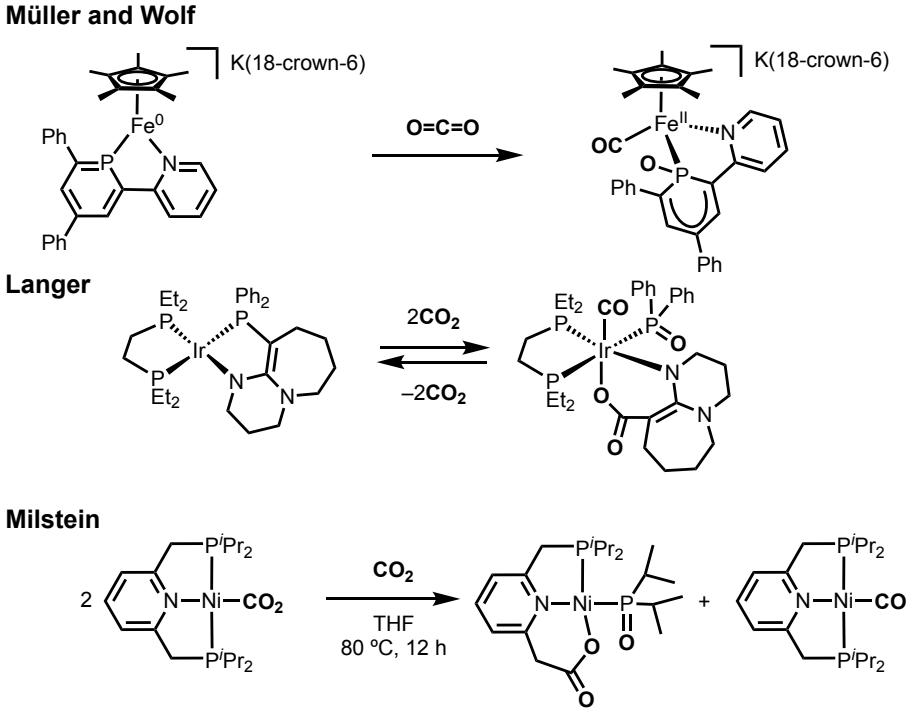


*4-3-3. Cooperative reaction with isothiocyanates*

Analogous treatment of **4.2** with methyl isothiocyanate (MeNCS) affords corresponding thiophosphoryl complex **4.10** (Scheme 4-13). $^{31}P\{^{1}H\}$ NMR spectra of **4.10** showed a set of resonances at δ 71.6 and –6.8 ppm with a mutual coupling ($^{2}J_{P–P}$ = 18 ppm).

**Scheme 4-13**. Treatment of **4.2** with isothiocyanates.

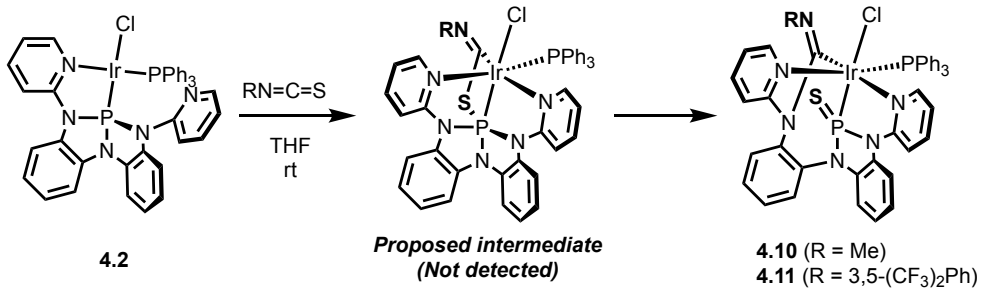

Complex **4.11**, a reaction product of **4.2** and 3,5-trifluoromethylphenyl isothiocyanate, showed similar $^{31}$P NMR spectroscopic features (δ 70.0 and –7.8 ppm, $^{2}J_{P-P}$ = 17 ppm). A single crystal of **4.11** suitable for X-ray diffraction was obtained from recrystallization from a slow diffusion of pentane into a dichloromethane solution. The solid-state structure of **4.11** confirms the C=S bond splitting and shows the formation of P=S bond by an analogous rearrangement of phosphorus triamide framework (Figure 4-10). While P-bound S atoms often coordinate to another metal center in structurally characterized thiophosphoryl complexes, **4.11** is classified as a terminal thiophosphoryl complex; based on the large Ir(1)–P(1)–S(1) angle ($\angle_{Ir(1)-P(1)-S(1)}$ = 127.72(3)º) suggests the S atm does not bridge over Ir–P bond but form a terminal thiophosphoryl complex. The P–S bond length ($d_{P(1)-S(1)}$ = 1.9473(7) Å) is within the region of terminal P=S bonds in the reported terminal thiophosphoryl complexes (1.93 Å < $d$ < 2.18 Å).[43-53] Different from the reactivity with isocyanates, the product proceeds regardless of the bulkiness of R group, suggesting the [2+2] cycloaddition of C=S is more favorable than that of C=O.

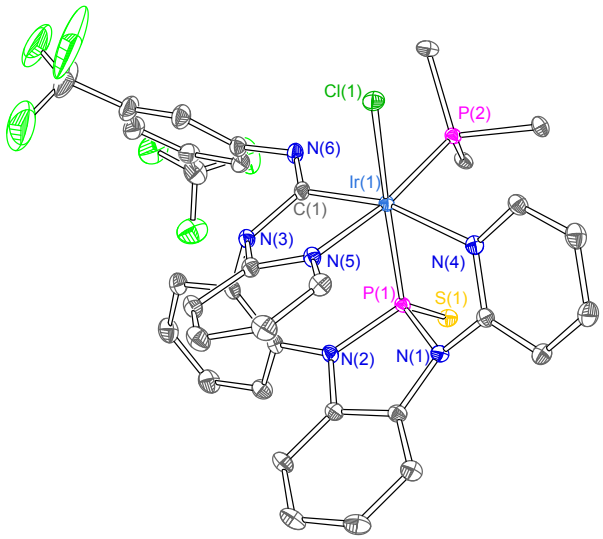


**Figure 4-10.** Thermal ellipsoid plots rendered at the 50% probability level for **4.11**. Hydrogens and phenyl rings of $PPh_3$ ligands are omitted for clarity

## 4-4. Cooperative Activation of E–H Bonds by $IrCl(PPh_3)(L1)$

### *4-4-1. Cooperative addition of O–H bonds to **4.2***

We next targeted cooperative activation of polar E–H bonds (E: electronegative substituents) on the Ir–P bond of **4.2**. Treatment of **4.2** with excess phenol in THF at ambient temperature afforded a single complex **4.12**, which lacked the nontrigonal triamido phosphorus $^{31}P$ NMR resonance in high-field region of the spectrum. Instead, the $^{31}P\{^1H\}$ spectrum of **4.12** displayed two low-field doublets at δ 12.8 and –50.9 ppm and with mutual coupling ($^2J_{P–P}$ = 18 Hz) (Figure 4-11). In the $^1H$-coupled $^{31}P$ NMR spectrum, the signal at δ 12.8 ppm was further split into a doublet with a coupling constant ($J_{P–H}$ = 18 Hz).

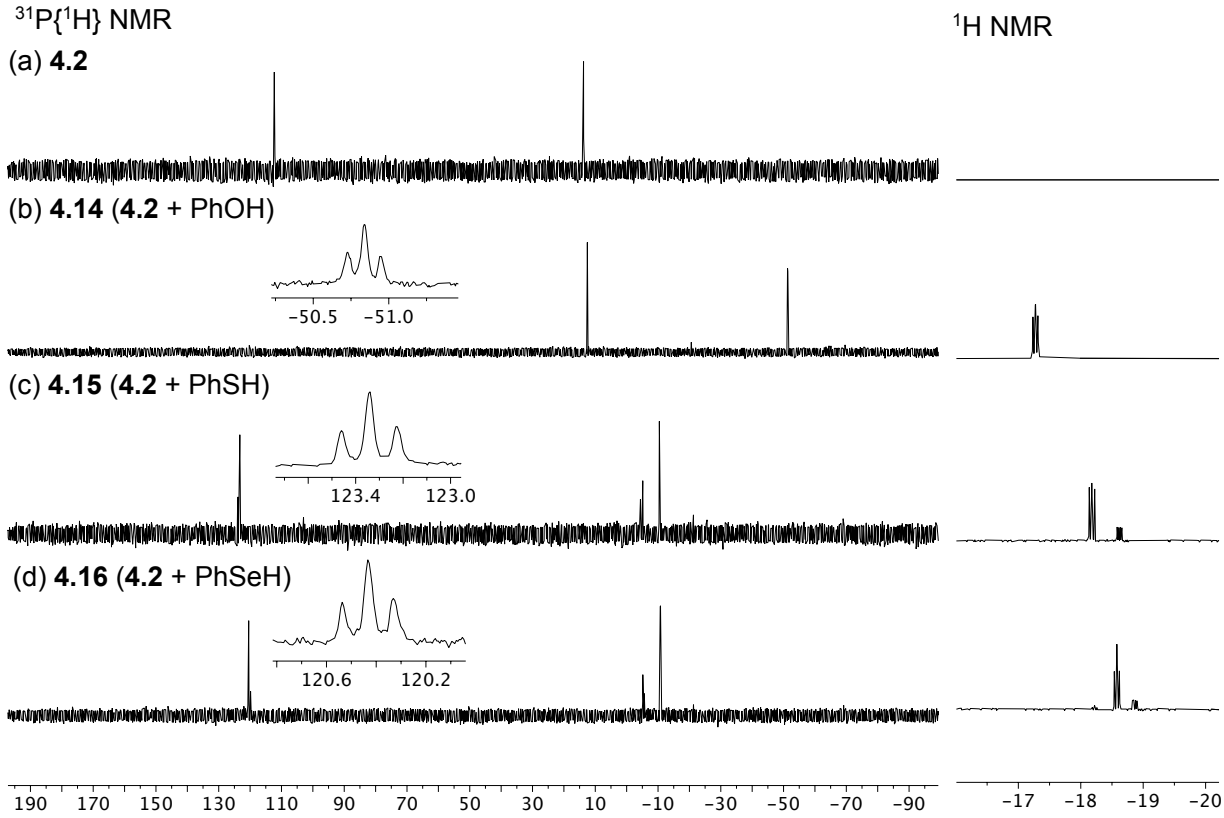


**Figure 4-11.** $^{31}P\{^1H\}$ NMR spectra and $^1H$ NMR (only low-field region) of (a) **4.2** (b) **4.14** (c) **4.15** (d) **4.16**. Units are ppm relative to 85% $H_3PO_4$. Insets show $^1H$-coupled $^{31}P$ NMR spectra.

The corresponding coupling partner was found in the $^{1}$H NMR spectrum in the low-field region at δ –17.26 ppm (dd, $^{2}J_{P–H}$ = 18 Hz, 14 Hz), which can be assigned to an Ir–H fragment, which is probably formed by a proton abstraction of alcohol by the basic Ir. Additionally, based on the increase in P-coordination number suggested by the significant upfield shift of the triamidophosphorus signal in $^{31}$P NMR (Δδ = 161.5 ppm from **4.2** to **4.12**), the remaining $RO^{–}$ group is considered to form a bond with the electrophilic P center. Taken together, product **4.12** was assigned as an $Ir^{III}$ metallophosphorane formed by a cooperative dipolar addition of the $O^{\delta–}$–$H^{\delta+}$ bond to the $P^{\delta+}$–$Ir^{\delta–}$ bond (Scheme 4-14, *top*). Complex **4.2** was also reacted with O–H bonds in benzoic acid and water under the same condition to yield analogous metallophosphoranes **4.13** and **4.14**, respectively. Different from stable **4.12** and **4.13**, water adduct **4.14** undergoes a fast decomposion probably due to the reactive P–OH moiety.

**Scheme 4-14**. Reactivity of **4.2** with E–H bonds (E = O, S, Se)

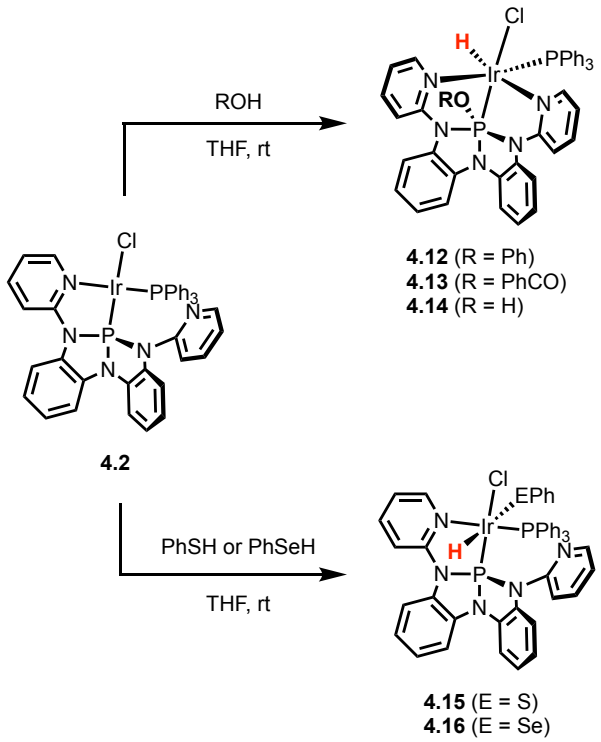

*4-4-2. Metal–centered oxidative addition of S–H and Se–H bonds to **4.2***

Considering the success of cooperative activation of phenol, **4.2** was also treated with benzenethiol and benzeneselenol, affording compounds **4.15** and **4.16** as main products, respectively. Interestingly, the $^{31}$P NMR signals corresponding to triamidophosphorus moieties appear in the high-field in the spectra for these products at δ 123.9 ppm (doublet coupled to a signal at δ –10.5 ppm with $^{2}J_{P–P}$ = 20 Hz) for **4.15** and δ 121.2 ppm (doublet coupled to a signal at δ –10.8 ppm with $^{2}J_{P–P}$ = 16 Hz) for **4.16** (Figure 4-11). In the $^{1}$H-coupled $^{31}$P NMR spectra, both products showed additional P–H coupling with corresponding Ir–H nuclei, found at δ –18.18 ppm ($^{2}J_{P–H}$ = 19 Hz) for **4.15** and δ –18.58 ppm ($^{2}J_{PH}$ = 16 Hz) for **4.16** in the $^{1}$H NMR, respectively. Considering each product showed a single resonance in the high-field region (δ > 8 ppm) of the NMR spectrum, one of the pyridyl ring does not seem to coordinate to the Ir center. Taken together, the products are assigned as ($\sigma^3$–P)–Ir$^{III}$ complexes formed by the metal–centered oxidative addition of S–H or Se–H bonds (Scheme 4-14, *bottom*). Observation of several side products with similar $^{31}$P NMR and $^{1}$H NMR characteristics to the main products suggests formation of Ir-centered stereoisomers.

*4-4-3. DFT calculations to understand different reactivities with O–H, S–H and Se–H*

To understand the distinct reactivities above, we performed DFT calculations (B3LYP/def2-TZVP) to evaluate the relative energies of metal–centered addition products and cooperative addition products for PhOH, PhSH and PhSeH. For the metal–centered addition products, products with the lowest electronic energy among all possible stereoisomers based on NMR are used (see Appendix C for detail). The computational results fully support the observed products;

while the cooperative addition is more favorable by 4.3 kcal•mol$^{-1}$ for PhOH, the metal–centered addition has larger driving forces for PhSH and PhSeH by 9.5 kcal•mol$^{-1}$ and 11.7 kcal•mol$^{-1}$, respectively. Qualitatively, this observation can be correlated with the relative affinity of P and PhE$^{-}$ groups (bond dissociation energies are P–O > P–S ≒ P–Se).[54]

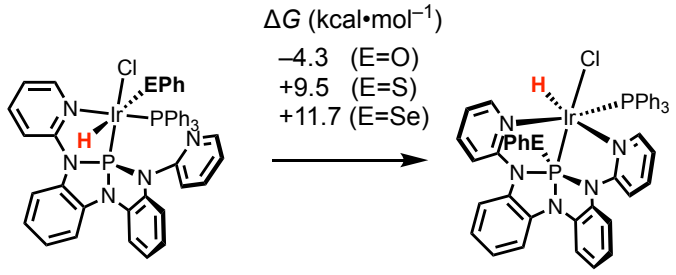


**Figure 4-12.** Driving force of cooperative addition compared to metal–centered addition products calculated at B3LYP.def2-TZVP level of theory.

*4-4-4. Reaction of **4.2** with Ammonia Borane*

**Scheme 4-15**. Reaction of **4.2** with ammonia borane

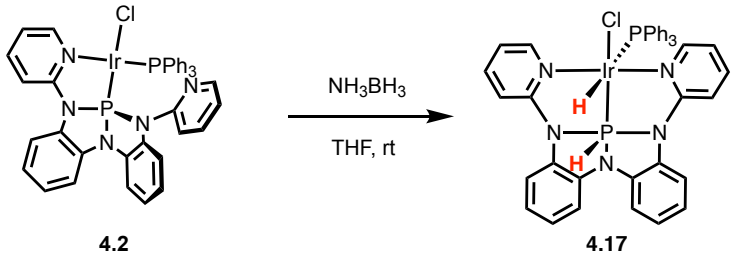


Motivated by the success of O–H cooperative activation, we attempted a dehydrogenation of ammonia borane by complex **4.2**. Reaction of **4.2** with ammonia borane in tetrahydrofuran solution results in conversion to a single new product **4.17** with a set of $^{31}P\{^{1}H\}$ NMR resonances at $\delta$ –10.9 ppm and –89.6 ppm with mutual coupling ($^{2}J_{P-P}$ = 13 Hz). In the $^{1}$H-coupled $^{31}$P NMR spectrum, the signal at δ –89.6 ppm is further split into a doublet of doublets by large and small coupling constants ($J_{P-H}$ = 581 Hz and 35 Hz), suggesting a P–H bond formation. The other signal

at δ –10.9 ppm corresponding to the $Ph_3P$ nucleus also had a relatively large coupling ($J_{P–H}$ = 186 Hz) indicating a hydride ligand in *trans*-configuration with the $Ph_3P$. The coupling partners were characterized in the $^1H$ NMR spectrum; a signal corresponding to P–*H* nucleus resonates at δ 9.13 ppm ($^1J_{P–H}$ = 586 Hz) and one for Ir–*H* nucleus at δ –11.49 ppm ($^2J_{P–H}$ = 186 Hz, 35 Hz). These two H nuclei had mutual coupling too ($^3J_{HH}$ = 8 Hz). Combined with the twofold equivalence of the aryl region of the $^1H$ NMR spectrum, product **4.17** was assigned to the desired hydrogenation product of **4.2**, in which the tridentate **L1** coordinates with the *mer*-$\kappa^3$-chelation mode. The formation of meridional isomer was similar to our previous treatment of $RuCl_2(PPh_3)$(*fac*-**L1**) with sodium borohydride to yield Ru($\eta^2$-$BH_4$)($PPh_3$)(*mer*-**L1**) (see section *3-6-1* in Chapter 3). There may be shared mechanisms or transition states between these reactions for the processes of M–H and P–H bonds formation.

Complex **4.2** was also exposed to gaseous hydrogen atmosphere to see if cooperative addition of $H_2$ was viable. The messy reaction yielded a mixture of multiple products, but metallohydrophosphorane **4.17** was not observed. This significant difference in reactivity with ammonia borane and $H_2$ suggest that the cooperative bond activation requires a highly polarized chemical bond.

This reaction provides the first example of cooperative dehydrogenation of ammonia borane by a ($\sigma^3$-P)–M bond. Cooperative hydrogenation of M–P bonds by ammonia borane or $H_2$ has been known for only lower-coordinate phosphorus ligands such as in metal–phosphide or metal–phosphenium complexes. While the 2nd or 3rd low transition metal systems have been known for long,[55-58] the 3d metal complexes capable of activating $H_2$ have been reported only recently (Scheme 4-16). Thomas discovered the 1,2-addition of $H_2$ across the Co–P bond of a PPP-pincer

cobalt phosphenium complex.[59] Gudat also reported the dehydrogenation of ammonia borane catalyzed by a s sequential addition of a hydride and a proton to the manganese phosphenium complex Although this Mn complex did not activate $H_2$, they recently succeeded in cooperative $H_2$ addition in a Cr–phosphenium system.

**Scheme 4-16**. Reported examples of hydrogenation of 3d metal–phosphenium bonds.

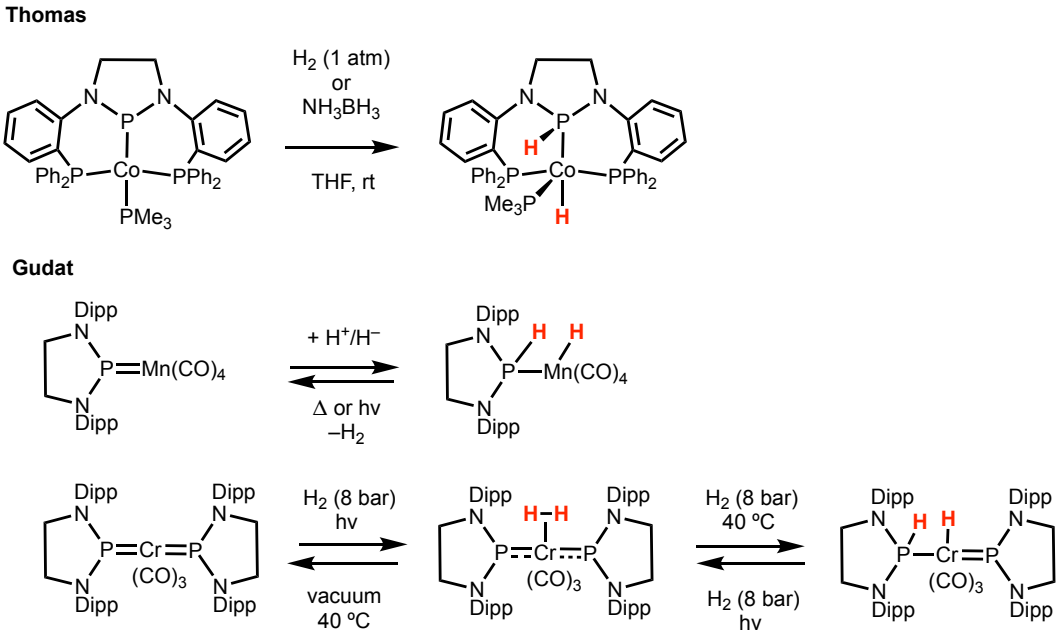

## 4-5. Sequential Cooperative Reactivity of RhCl(PPh$_3$)(L1)

*4-5-1. Metallohydrophosphorane synthesis by cooperative HCl addition*

The cooperative reactivity of complex **4.1**, the Rh$^{I}$ congener of Ir$^{I}$ complex **4.2**, was also investigated. To a $CDCl_3$ solution of **4.1** was added equimolar amount of HCl dissolved in THF (Scheme 4-17). Initially a protonation at the Rh occurred to give an intermediate **4.18**, which was monitored by $^{1}$H NMR that displays resonance in the low-field region at δ –13.28 ppm, without a change in P-coordination number. The *in-situ* $^{31}$P NMR spectrum shows a resonance at δ 167.9 ppm for the triamidophosphorus nucleus. However, this intermediate **4.19** was soon converted to a single complex **4.20**. The $^{31}$P NMR spectrum of **4.20** displayed a significant upfield shift of the chemical shift of the triamidophosphorus nucleus to δ 24.9 ppm as a doublet of doublet signal due to coupling to the $PPh_3$ nucleus (δ 20.3 ppm, $^{2}J_{PP}$ = 12 Hz) and the Rh ($^{1}J_{Rh–P}$ = 145 Hz). Moreover, in the H-coupled $^{31}$P NMR spectrum, the signal at δ 24.9 ppm is further split into a doublet with $J_{P–H}$ =639 Hz, due to the directly bound H nucleus (δ 8.82 ppm in $^{1}$H NMR).

**Scheme 4-17**. Two routes to metallophosphorane **4.19**. (*left*) reversible addition of HCl and (*right*) net insertion of P(III) into Rh–H.

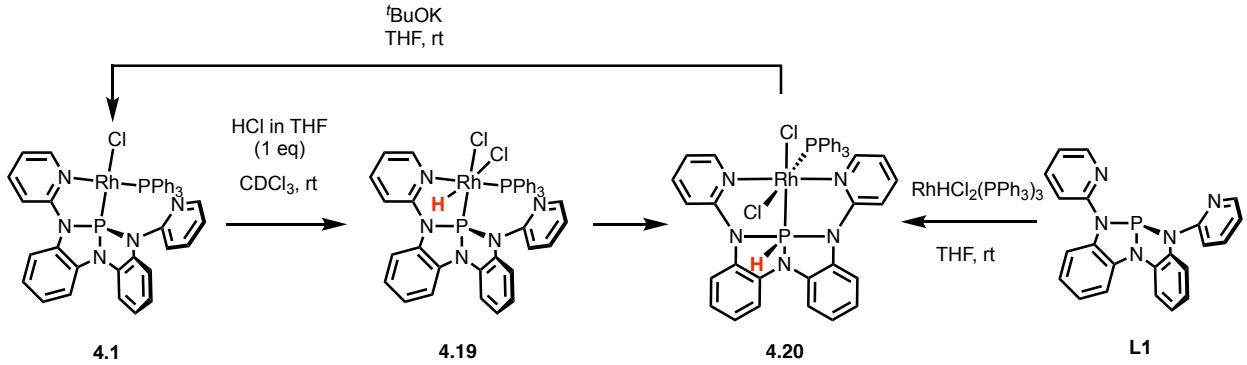


These spectroscopic features strongly indicate the formation of Rh$^{III}$ metallohydrophosphorane formed by an α-H migration from Rh to P (Scheme 4-17). Alternatively, product **4.20** can be

synthesized by a metalation of **L1** with $Rh^{III}HCl_2(PPh_3)_3$ via net insertion of the P(III) ligand, which supports the assignment.

X-ray diffraction of a yellow single crystal obtained by slow diffusion of pentane into a $CDCl_3$ solution revealed the meridional $\kappa^3$-chelation mode of **L1** in the solid-state structure of **4.20** (Figure 4-13). The planarization of the phosphorus triamide framework was observed ($\angle N_1–P_1–N_3$ = 168.0(2)°) to result the pentacoordinate phosphorus center ($\tau_5$ = 0.34) with the H and Rh substituents at equatorial positions. The Rh–P bond distance ($d$(Rh(1)–P(1)) = 2.2404(14) Å) is shorter than Rh(I) complex **4.1** by 0.011 Å, which may be due to the changes in the Rh oxidation state from +1 to +3 or in the coordination mode from $\kappa^2$ to $\kappa^3$.

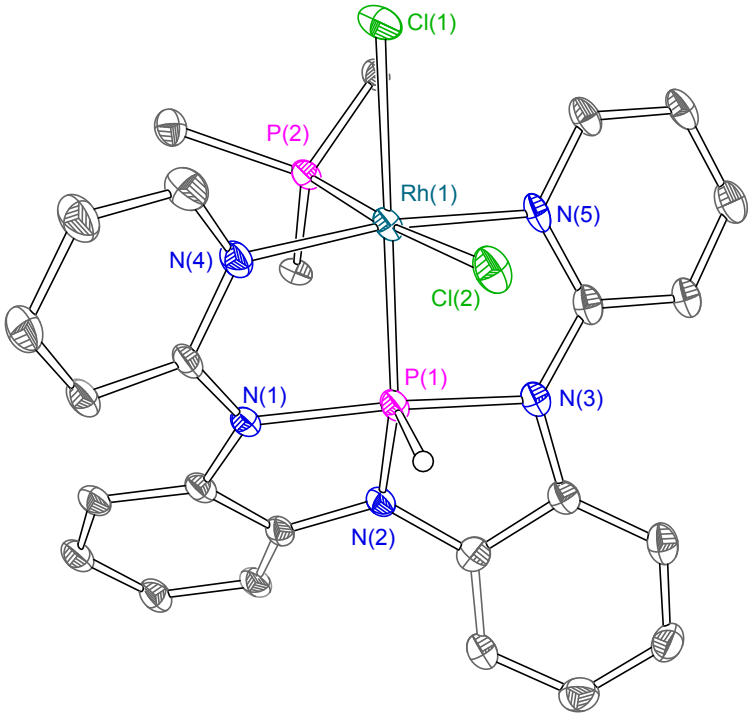


**Figure 4-13**. Thermal ellipsoid plots rendered at the 50% probability level for **4.20**. Hydrogens atoms except *P*–H, phenyl rings of $PPh_3$ ligands and recrystallization solvents are omitted for clarity. Only one of the four molecules in the unit cell is displayed,

While the P–H bond of ruthenahydrophosphoranes was not cleanly deprotonated by base addition (see section *3-3-4* in **Chapter 3**), this HCl addition to **4.1** was reversible; treatment of **4.20** with potassium tert-butoxide in THF returns the original $Rh^{I}$ complex **4.1** (Scheme 4-17). Metallohydrophosphorane **4.20** also exhibits hydridic character (Scheme 4-18); treatment with triphenylcarbenium hexafluorophosphate ($Ph_3CPF_6$) leads to hydride abstraction to yield ($\sigma^3$-P)–Rh complex **4.21**, with a high-field $^{31}P$ NMR resonance at δ 151.2 ppm without $^{1}J_{P-H}$ coupling.

**Scheme 4-18.** Hydride abstraction from metallohydrophosphorane **4.20**.

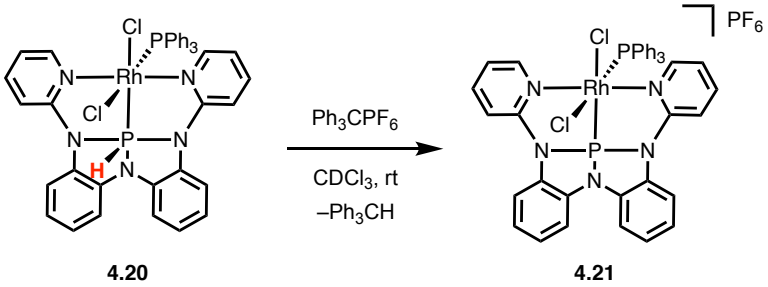


**4.20** **4.21**

*4-5-2. Stepwise cooperative activation of allyl chloride by **4.1***

The reactivity of **4.1** and HCl suggested two-step processes of metal–centered oxidative addition followed by α-H-migration from Rh to P. While the intermediate **4.19** was not isolable, analogous treatment of **4.1** with allyl chloride at ambient temperature yields corresponding stable metal–centered oxidation product **4.22** cleanly (Scheme 4-19).

**Scheme 4-19.** Stepwise cooperative addition of allyl chloride to **4.1**.

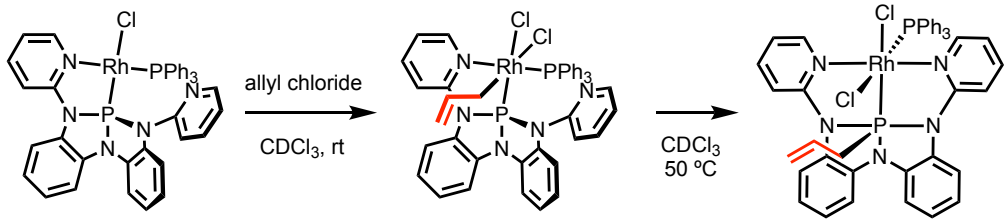


**4.1** **4.22** **4.23**

The $^{31}$P NMR spectrum of **4.22** displays a set of doublet of doublets resonances at δ 160.2 ppm and δ 27.4 ppm with mutual coupling ($^{2}J_{P–P}$ = 22 Hz) and with direct Rh-P coupling ($^{1}J_{Rh–P}$ = 193 and 133 Hz, respectively). The asymmetric resonances in the aryl region of $^{1}$H NMR suggests that only one of two pyridyl side arms of **L1** coordinates to the metal.

Upon heating the solution at 50 ºC, $Rh^{III}$ complex **4.2**2 was gradually converted to a single new product **4.23**. In the $^{31}$P NMR spectrum of **4.23**, the triamidophosphorus signal drastically shifted upfield to δ –7.1 ppm (Δδ = 167.3 ppm), coupled to the $PPh_3$ nucleus at δ 19.7 ppm ($^{2}J_{P–P}$ = 12 Hz). In the $^{1}$H-coupled $^{31}$P NMR spectrum, the signal at δ –7.1 ppm is further split into triplet by small coupling value $^{1}J_{P–H}$ = ~5 Hz. More importantly, the $^{13}$C NMR spectrum displayed a resonance at δ 46.6 ppm corresponding to the $CH_2$=CH–$\underline{C}H_2$ nucleus, which was found as a doublet with a large coupling value $J$ = 85 Hz. This suggests the formation of P–C bond in **4.22** via the α-allyl group migration from Rh to P, which is an analogous process of H-transfer observed in HCl addition (Scheme 4-19).

For the C-based group migration within M–$PR_3$ bonds, the decomposition of metallophosphoranes by hydrocarbyl group transfer from P to M was reported by Riess[60] and Miyamoto[61] independently. More recently, we reported net insertion of P(III) ligands into Group 10 M–Me bonds to yield metallocarbylphosphoranes (see Chapter 5).[62] However, the direct observation of the α-migration of hydrocarbyl fragment from M to P was unprecedent. The mechanistic investigation of the formation of **4.23** from **4.22** process is underway.

## 4-6. Conclusion and Outlook

Chapter 4 provided various metal–ligand cooperative reactivities enabled by Group 9 metal complexes of nonspectator tricoordinate phosphorus ligands. The designed ($\sigma^3$-P)–Ir bond between a nucleophilic Ir and an electrophilic P enabled (i) heterolytic cleavage of C=O and C=S bonds (ii) [2+2] cycloaddition of a C=N bond (iii) cooperative oxidative addition of O–H bonds. In the Rh congener, apparent cooperative addition of HCl and allyl chloride was achieved by a stepwise metal–centered oxidative addition followed by α-migration within the Rh–P bond.

Although such metal–ligand cooperative bond activation by ($\sigma^3$-P)–M complexes has been proposed in many literatures, the resulting metallophosphorane intermediates have never been isolated or directly characterized (see **section 1-5** in Chapter 1).[63] Our results provide the first well-defined examples of the predicted cooperative reactivity of ($\sigma^3$-P)–M complexes and open a door to wider application of higher coordination P ligands as viable synthetic intermediates to target. Along this line, the development of stoichiometric and catalytic transformation based on the concept is ongoing.

## 4-7. Experimental Section

### *4-7-1. General consideration and Methods*

**General Consideration**. All reagents were purchased from Sigma-Aldrich, Alfa Aesar, ACROS, TCI, Oakwood Chemical, or Strem Chemicals and used as received unless otherwise noted. Diethyl ether ($Et_2O$), methylene chloride ($CH_2Cl_2$), tetrahydrofuran (THF), toluene and pentane were dried according to the method of Grubbs[64] as modified by Bergman[65] using a Glass Contour Solvent Purification System. All glassware was oven-dried at 120 °C prior to use. All reactions were carried out under dry nitrogen atmosphere (Schlenk line or glovebox) unless otherwise noted. NMR spectra were recorded on a Bruker-400 (400 MHz) or Bruker-500 (500 MHz) spectrometer and processed with a MestReNova software. $^1$H NMR chemical shifts are given in ppm with respect to solvent residual peak ($CDCl_3$, δ 7.26 ppm; $CD_2Cl_2$, δ 5.32 ppm; $C_6D_6$, δ 7.16 ppm), $^{13}C\{^1H\}$ NMR shifts are given in ppm with respect to ($CDCl_3$ δ 77.16 ppm, $CD_2Cl_2$ δ 53.84 ppm, $C_6D_6$ δ 128.06 ppm). $^{31}$P NMR shifts are given in ppm with respect to 85 % $H_3PO_4$. Coupling constants are reported as *J*-values in Hz. High resolution ESI mass spectra were obtained from the Mass Spectrometry Laboratory in the Department of Chemistry Instrumentation Facility, MIT, using either Agilent QTOF 6545 with ESI ionization source or a JEOL AccuTOF-DART (JMST100LP, ionSense DART source).

**X-ray diffraction**. X-ray structures data were collected on a Bruker three-circle platform goniometer equipped with an Apex II CCD and an Oxford cryostream cooling device operating at 100 K. Radiation was from a graphite fine focus sealed tube Mo Kα (0.71073 Å) source. Crystals were mounted on a glass fiber pin using Paratone N oil. Data was collected as a series of φ and/or ω scans. Data was integrated using SAINT and scaled with multi-scan absorption correction using

SADABS.[66] The structures were solved by intrinsic phasing using SHELXT (Apex3 program suite v2016.1.0) and refined against F2 on all data by full matrix least squares with SHELXL-97.[67] All non-hydrogen atoms were refined anisotropically. H atoms were placed at idealized positions and refined using a riding model. Olex 2[68] was used for the solution of structures. The hydrogen atoms at phosphorus atoms were located in Fourier maps and were refined isotropically without constraints. XP was used for graphical representations.

*4-7-2. Synthetic Procedures*

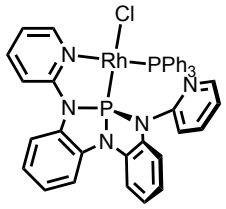

**4.1**

**Synthesis of 4.1**. To a solution of bis(1,5-cyclooctadiene)dirhodium(I) dichloride (12.9 mg, 0.0263 mmol , 1.0 eq) and triphenylphosphine (13.8 mg, 0.526 mmol, 2.0 eq) in tetrahydrofuran (3 mL) was added a THF solution (2 mL) of **L1** (20.0 mg, 0.0526 mmol, 2.0 eq) dropwise. The resulting orange solution was stirred for 30 min. After the solvent was removed *in vacuo* from the resulting yellow suspension, the yellow residue was thoroughly washed with ether and dried *in vacuo* to afford a pure product of **4.1** as yellow solids (29.4 mg, 71.7 %). A crystal suitable for single-crystal X-ray diffraction was obtained from a slow diffusion of pentane into a dichloromethane solution at –35 ºC. $^{1}$H NMR (400 MHz, $CD_2Cl_2$) δ 8.92 (br, 2H), 7.84 (t, $J$ = 7.8 Hz, 2H), 7.41 – 7.28 (m, 8H), 7.26 (t, $J$ = 6.3 Hz, 2H), 7.22 – 7.13 (m, 5H), 7.13 – 6.99 (m, 6H), 6.99 – 6.79 (m, 6H). $^{31}$P NMR (162 MHz, $CD_2Cl_2$) δ 151.9 (dd, $^{1}J_{RhP}$ = 292 Hz, $^{2}J_{PP}$ =52 Hz), 43.7 (dd, $^{1}J_{RhP}$ = 170, $^{2}J_{PP}$ = 52 Hz).

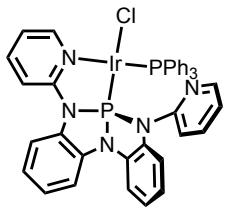

**4.2**

**Synthesis of 4.2**. To a solution of bis(1,5-cyclooctadiene)diiridium(I) dichloride (17.6 mg, 0.0263 mmol , 1.0 eq) and triphenylphosphine (13.8 mg, 0.263 mmol, 2.0 eq) in tetrahydrofuran (3 mL) was added a THF solution (2 mL) of **L1** (20.0 mg, 0.0526 mmol, 2.0 eq) dropwise. The resulting orange solution was stirred for 30 min. After the solvent was removed *in vacuo* from the resulting brown solution, the orange residue was thoroughly washed with ether and dried *in vacuo* to afford complex **4.2** as pale orange solids (34.2 mg, 74.8 %). Due to the low stability or solubility of **4.2** in the solution state, the $^{13}$C NMR spectrum is not given. $^{1}$H NMR (400 MHz, THF-$d_8$) δ 10.09 (s, 1H), 8.17 (s, 1H), 8.09 – 7.96 (m, 1H), 7.69 – 7.63 (m, 1H), 7.61 – 7.51 (m, 2H), 7.43 – 7.30 (m,

9H), 7.25 – 7.17 (m, 3H), 7.11 – 7.03 (m, 4H), 7.03 – 6.86 (m, 10H), 6.76 – 6.63 (m, 3H).$^{31}$P NMR (162 MHz, THF-$d_8$) δ 112.2 (d, *J* = 37 Hz), 13.7 (d, *J* = 37 Hz). MS (DART) Calcd for $C_{40}H_{32}ClN_5P_2Ir$ (M–H): 872.1456, found: 872.1542.

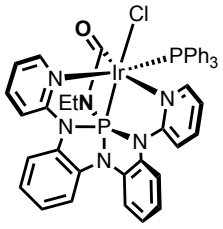

**4.6**

**Synthesis of 4.6**. Under a $N_2$ atmosphere, to a suspension of **4.2** (26 mg, 0.030 mmol) in THF (3 mL) was added ethyl isocyanate (0.050 mL,0.63 mmol, 21 eq) at room temperature. After 15 min, the solvent was removed *in vacuo*. The resulting orange residue was thoroughly washed with pentane and dried *in vacuo*. to give **4.6** as yellow solid. $^1$H NMR (400 MHz, $CD_2Cl_2$) δ 10.09 (ddd, *J* = 5.7, 3.3, 1.8 Hz, 1H), 8.72 (dd, *J* = 5.8, 1.8 Hz, 1H), 7.78 – 7.67 (m, 2H), 7.66 – 7.53 (m, 1H), 7.53 – 7.45 (m, 2H), 7.39 – 7.24 (m, 8H), 7.22 – 7.04 (m, 11H), 7.00 – 6.90 (m, 2H), 6.65 (t, *J* = 6.4 Hz, 1H), 2.06 (ddq, *J* = 14.0, 11.2, 7.0 Hz, 1H), 1.65 (tq, *J* = 14.2, 7.1 Hz, 1H), -0.13 (t, *J* = 7.1 Hz, 3H).$^{31}$P NMR (162 MHz, $CD_2Cl_2$) δ -0.7 (d, *J* = 17 Hz), -74.8 (d, *J* = 17 Hz). $^{13}$C NMR (101 MHz, $CD_2Cl_2$) δ 152.97, 150.09, 148.11, 139.56, 138.33, 136.91 (d, *J* = 7.0 Hz), 133.53, 132.59 (d, *J* = 7.0 Hz), 130.28, 129.37, 127.99, 124.45, 123.22, 121.47, 119.82 (d, *J* = 13.8 Hz), 118.14 (d, *J* = 14 Hz), 117.90 (d, *J* = 2.9 Hz), 116.81, 112.79 – 112.50 (m), 111.15, 111.09, 110.13, 41.9 (d, *J* = 14 Hz), 14.71.

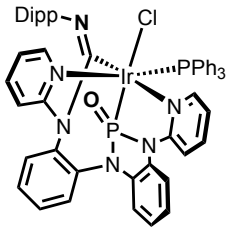

**4.7**

**Synthesis of 4.7**. Under a $N_2$ atmosphere, to a suspension of **4.2** (8.7 mg, 0.010 mmol) in THF (1 mL) was added 2,6-bis(diisoproypl)phenyl isocyanate (0.050 mL, 0.23 mmol, 23 eq) at room temperature. After 15 min, the solvent was dried *in vacuo*. The resulting orange residue was thoroughly washed with pentane and dried *in vacuo*. to give **4.7** as yellow solid. Recrystallization from

dichloromethane/pentane at –35 ºC afforded a single crystal suitable for X-ray diffraction study. $^{31}P\{^{1}H\}$ NMR (203 MHz, THF) δ 22.4 (d, *J* = 27 Hz), -2.2 (d, *J* = 26.8 Hz).

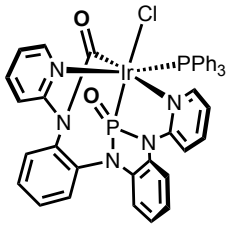

4.9

**Synthesis of 4.9**. In a seled J. Young tube, Complex **4.2** (8.7 mg, 0.010 mmol) was suspended in THF (1 mL). The suspension was degassed (freeze–pump–thaw method) and the tube was filled with $CO_2$ (1 atm). After 15 min, the yellow precipitate was collected by decantation, washed with pentane thoroughly and dried *in vacuo* to afford 4.9 as a yellow solid. A crystal suitable for X-ray diffraction was obtained from Recrystallization from dichloromethane/pentane at –35 ºC afforded a single crystal suitable for X-ray diffraction study. $^{1}H$ NMR (400 MHz, $CD_2Cl_2$) δ 7.94 (dd, *J* = 5.8, 1.8 Hz, 1H), 7.87 (dd, *J* = 5.8, 3.0 Hz, 1H), 7.82 (td, *J* = 7.8, 1.9 Hz, 1H), 7.69 (d, *J* = 7.7 Hz, 6H), 7.61 – 7.52 (m, 3H), 7.47 (d, *J* = 8.2 Hz, 1H), 7.28 (t, *J* = 7.4 Hz, 3H), 7.15 (t, *J* = 7.7 Hz, 7H), 6.96 (dd, *J* = 6.9, 2.2 Hz, 1H), 6.74 (d, *J* = 8.3 Hz, 1H), 6.69 (t, *J* = 6.4 Hz, 2H), 6.55 (tt, *J* = 7.6, 5.9 Hz, 2H), 6.26 (dd, *J* = 6.9, 2.3 Hz, 1H), 6.20 (t, *J* = 6.6 Hz, 1H). $^{31}P\{^{1}H\}$ NMR (162 MHz, $CD_2Cl_2$) δ 20.8 (d, *J* = 25 Hz), -2.4 (d, *J* = 25 Hz)..

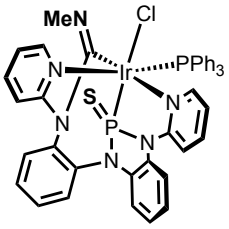

4.10

**Synthesis of 4.10**. Under a $N_2$ atmosphere, to a suspension of **4.2** (8.7 mg, 0.010 mmol) in THF (1mL) was added methyl isothiocyanate (0.010 mL, 0.15 mmol, 15 eq) at room temperature. The *in-situ* recorded NMR spectra of the reaction mixture indicated the quantitative formation of complex **4.10** based on the comparison to the spectra of **4.11**. $^{31}P\{^{1}H\}$ NMR (162 MHz, THF) δ 71.6 (d, *J* = 18 Hz), -6.8 (d, *J* = 18 Hz).

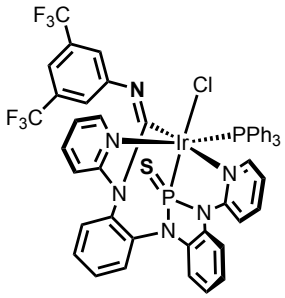


4.11

**Synthesis of 4.11**. Under a $N_2$ atmosphere, to a suspension of **4.2** (8.7 mg, 0.010 mmol) in THF (1 mL) was added 3,5-bis(trifluoromethyl)phenyl isothiocyanate (0.010 mg, 0.050 mmol, 5.0 eq) at room temperature. After 15 min, the solvent was dried *in vacuo*. The resulting orange residue was thoroughly washed with pentane and dried *in vacuo*. to give **4.11** as yellow solid. Recrystallization from dichloromethane/pentane at –35 ºC afforded a single crystal suitable for X-ray diffraction study. $^1$H NMR (500 MHz, $CD_2Cl_2$) δ 8.07 (dd, $J$ = 5.7, 1.9 Hz, 1H), 7.88 (td, $J$ = 8.0, 1.7 Hz, 1H), 7.63 – 7.49 (m, 2H), 7.49 – 7.40 (m, 2H), 7.33 (td, $J$ = 7.3, 1.6 Hz, 3H), 7.24 (ddd, $J$ = 8.7, 7.2, 1.7 Hz, 1H), 7.18 (s, 6H), 7.07 (dd, $J$ = 8.0, 1.3 Hz, 1H), 7.05 – 6.94 (m, 1H), 6.70 (dddd, $J$ = 13.8, 7.1, 3.3, 1.5 Hz, 3H), 6.54 (dtd, $J$ = 29.0, 7.6, 1.3 Hz, 2H), 6.24 (ddt, $J$ = 7.3, 6.0, 1.3 Hz, 1H), 6.19 (dd, $J$ = 8.0, 1.4 Hz, 1H), 6.00 (dd, $J$ = 7.9, 1.4 Hz, 1H). $^{31}$P NMR (203 MHz, $CD_2Cl_2$) δ 69.0 (d, $J$ = 18 Hz), -8.3 (d, $J$ = 18 Hz).

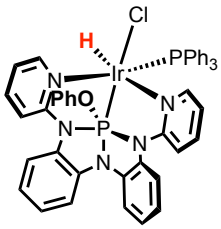


4.12

**Synthesis of 4.12**. Under a $N_2$ atmosphere, to a suspension of **4.2** (8.7 mg, 0.010 mmol) in THF (1 mL) was added phenol (1.0 mg, 0.011 mmol, 1.1 eq) at room temperature. The yellow precipitate of **4.2** immediately dissolved and the resulting solution was stirred for 2 h at room temperature. The solvent was removed *in vacuo* and the orange residue was washed with ether and dried *in vacuo* to give **4.12** as an orange solid. $^1$H NMR (400 MHz, $C_6D_6$) δ 10.05 (t, $J$ = 4.1 Hz, 1H), 9.60 (d, $J$ = 5.7 Hz, 1H), 7.92 – 7.62 (m, 7H), 7.49 (d, $J$ = 7.9 Hz, 1H), 6.98 (d, $J$ = 2.7 Hz, 3H), 6.85 – 6.77 (m, 8H), 6.53 (d, $J$ = 8.4 Hz, 1H), 6.48 (d, $J$ = 8.3 Hz, 1H), 6.33 (t, $J$ = 6.5 Hz, 1H), 6.17 (t, $J$ = 6.4 Hz, 1H), 5.97

(t, $J$ = 4.7 Hz, 2H), -17.26 (dd, $J$ = 17.6, 14.4 Hz, 1H). $^{31}$P NMR (162 MHz, $C_6D_6$) δ 12.6 (d, $J$ = 15 Hz), -51.3 (d, $J$ = 17 Hz).

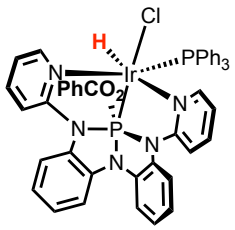


**4.13**

**Synthesis of 4.13**. Under a $N_2$ atmosphere, to a suspension of **4.2** (8.7 mg, 0.010 mmol) in THF (1 mL) was added benzoic acid (1.0 mg, 0.011 mmol, 1.1 eq) at room temperature. The yellow precipitate of **4.2** immediately dissolved and the resulting solution was stirred for 2 h at room temperature. The solvent was removed *in vacuo* and the orange residue was washed with ether and dried *in vacuo* to give **4.13** as an orange solid $^1$H NMR (400 MHz, $C_6D_6$) δ 10.11 – 10.00 (m, 1H), 9.53 (d, $J$ = 5.7 Hz, 1H), 9.29 (d, $J$ = 6.2 Hz, 1H), 8.11 (t, $J$ = 8.3 Hz, 3H), 7.80 – 7.61 (m, 8H), 7.46 – 7.34 (m, 2H), 7.10 – 6.96 (m, 6H), 6.94 – 6.84 (m, 3H), 6.82 – 6.72 (m, 12H), 6.72 – 6.65 (m, 3H), 6.62 – 6.53 (m, 4H), 6.39 – 6.19 (m, 3H), -17.30 – -18.70 (m, 1H). $^{31}$P{$^1$H} NMR (162 MHz, THF) δ 12.7 (d, $J$ = 20 Hz), -45.5 (d, $J$ = 20 Hz).

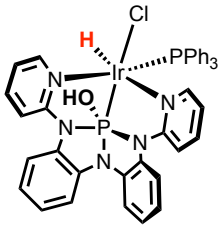


**4.14**

**Synthesis of 4.14**. Under a $N_2$ atmosphere, to a suspension of **4.2** (8.7 mg, 0.010 mmol) in THF-$d_8$ (1.0 mL) was added water (0.010 mL, 0.56 mmol) at room temperature. The *in-situ* recorded NMR spectra of the reaction mixture indicated the quantitative formation of complex **4.14** based on the comparison to the specta of **4.12**. Due to the low stability of the product, the isolation of **4.14** was not possible. $^1$H NMR (400 MHz, THF) δ 9.68 (dt, $J$ = 5.6, 2.2 Hz, 1H), 9.19 (d, $J$ = 5.6 Hz, 1H), 7.84 – 7.69 (m, 4H), 7.60 – 7.49 (m, 7H), 7.45 (q, $J$ = 8.5 Hz, 4H), 7.41 – 7.35 (m, 2H), 7.18 – 7.07 (m, 5H), 7.07 – 6.91 (m, 2H), 6.78 (t, $J$ = 7.5 Hz, 1H), 6.65 (t, $J$ = 7.8 Hz, 1H), 6.58 (t, $J$ = 6.4 Hz, 1H). -18.19 (t, $J$ = 16.1 Hz, 1H). $^{31}$P NMR (162 MHz, THF) δ 13.2 (d, $J$ = 19 Hz), -60.0 (d, $J$ = 19 Hz).

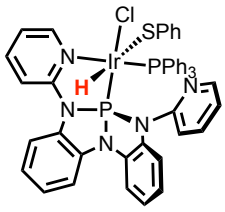


**4.15**

**Synthesis of 4.15**. Under a $N_2$ atmosphere, to a suspension of **4.2** (8.7 mg, 0.010 mmol) in THF (1.0 mL) was added benzenethiol (0.010 mL, 0.10 mmol) at room temperature. After 2 h, the solvent was removed in vacuo. The reaction mixture was dissolved in toluene-$d_8$ and the recorded crude NMR spectra indicated the formation of complex **4.15**. $^1$H NMR (400 MHz, Tol) δ 10.05 (ddd, $J$ = 5.8, 3.2, 1.8 Hz, 1H), 7.92 – 7.75 (m, 5H), 7.58 – 7.52 (m, 2H), 7.40 – 7.28 (m, 2H), 6.95 – 6.87 (m, 8H), 6.87 – 6.72 (m, 7H), 6.70 – 6.63 (m, 4H), 6.54 – 6.49 (m, 2H), -18.18 (dd, $J$ = 18.7, 16.0 Hz, 1H).$^{31}$P NMR (162 MHz, None) δ 123.3 (d, $J$ = 19 Hz), -10.5 (d, $J$ = 19 Hz).

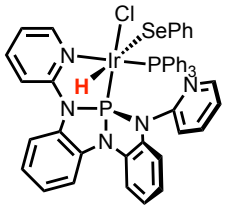


**4.16**

**Synthesis of 4.16**. Under a $N_2$ atmosphere, to a suspension of **4.2** (8.7 mg, 0.010 mmol) in THF (1.0 mL) was added benzeneselenol (0.010 mL, 0.094 mmol) at room temperature. After 2 h, the solvent was removed in vacuo. The reaction mixture was dissolved in toluene-$d_8$ and the recorded crude NMR spectra indicated the formation of complex **4.16**. $^1$H NMR (400 MHz, Tol) δ 10.22 – 10.07 (m, 1H), 7.81 (ddt, $J$ = 11.3, 6.1, 1.4 Hz, 5H), 7.55 – 7.41 (m, 2H), 7.30 – 7.24 (m, 1H), 7.24 – 7.19 (m, 1H), 6.85 (dddd, $J$ = 6.3, 5.1, 3.5, 1.9 Hz, 8H), 6.78 – 6.68 (m, 2H), 6.66 – 6.54 (m, 3H), 6.55 – 6.48 (m, 1H), 6.43 (t, $J$ = 7.6 Hz, 2H), -18.63 (t, $J$ = 16.4 Hz, 1H).$^{31}$P NMR (162 MHz, THF) δ 120.5 (d, $J$ = 16 Hz), -10.7 (d, $J$ = 16 Hz).

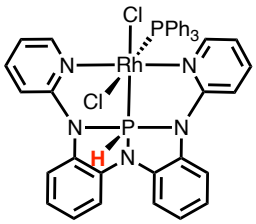

4.20

**Synthesis of 4.20**. Under a $N_2$ atmosphere, a solution of **4.1** (7.8 mg, 0.010 mmol) in $CDCl_3$ (2 mL) was added a dioxane solution of HCl (4 M, 2.5 µL, 0.010 mmol, 1 eq) diluted in THF (0.050 mL) dropwise at room temperature. The reaction mixture was left overnight to give an orange solution of pure product **4.20**. The crystal suitable for single crystal XRD study was obtained from recrystallization from slow diffusion of pentane into a $CDCl_3$ solution. $^1$H NMR (500 MHz, $CDCl_3$) δ 9.50 (dd, $J$ = 6.2, 1.7 Hz, 2H), 8.75 (dt, $J$ = 639.4, 1.8 Hz, 1H), 7.51 (ddd, $J$ = 8.7, 6.9, 1.7 Hz, 2H), 7.41 – 7.38 (m, 2H), 7.37 – 7.32 (m, 2H), 7.25 – 7.22 (m, 2H), 7.20 – 7.10 (m, 9H), 6.99 – 6.76 (m, 10H), 6.61 – 6.45 (m, 2H). $^{31}$P NMR (203 MHz, $CDCl_3$) δ 20.2 (dd, $^1J_{RhP}$ = 123 Hz, $^2J_{PP}$ = 12 Hz), -24.86 (dd, $^1J_{RhP}$ = 145 Hz, $^2J_{PP}$ = 12 Hz).

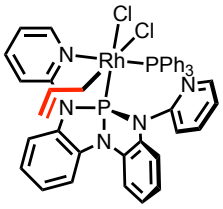

4.22

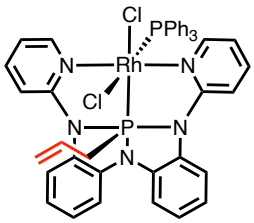

4.23

**Synthesis of 4.22**. and **4.23**. Under a $N_2$ atmosphere, a solution of **4.1** (7.8 mg, 0.010 mmol) in $CDCl_3$ (2 mL) was added allyl chloride (0.010 mL, 0.12 mmol) at room temperature. The reaction mixture was stirred for 30 min. to give an orange solution of pure product of **4.22**. The quantitative formation of **4.22** was indicated by the *in-situ* recorded NMR spectroscopy and the solution was used for the synthesis of **4.23** without further purification. The resulting $CDCl_3$ solution in the synthesis of **4.22** was heated at 50 ºC overnight. The *in-situ* recorded NMR spectra of the reaction mixture indicated the formation of complex **4.23**. **4.22**: $^1$H NMR (400 MHz, $CDCl_3$) δ 9.73 (t, $J$ = 5.1 Hz, 1H), 8.55 (dd, $J$ = 5.7, 1.7 Hz, 1H), 8.26 (t, $J$ = 7.8 Hz, 2H), 8.00 (t, $J$ = 9.0 Hz, 2H), 7.72 (dd, $J$ = 7.9, 1.4 Hz, 1H), 7.65 (t, $J$ = 7.7 Hz, 2H), 7.43 – 7.28 (m, 11H), 7.25 – 7.14 (m, 6H), 7.02 (t, $J$ = 7.8 Hz, 1H),

6.87 (t, $J$ = 6.5 Hz, 1H), 5.97 (ddt, $J$ = 16.7, 10.0, 6.6 Hz, 1H), 5.50 – 5.35 (m, 2H), 4.29 (d, $J$ = 16.7 Hz, 1H), 3.98 (d, $J$ = 9.8 Hz, 1H). $^{31}$P NMR (162 MHz, $CDCl_3$) δ 160.2 (dd, $^1J_{RhP}$ = 193 Hz, $^2J_{PP}$ = 22 Hz), 27.4 (dd, $^1J_{RhP}$ = 133 Hz, $^2J_{PP}$ = 22 Hz). **4.23**: $^{31}$P NMR (162 MHz, $CDCl_3$) δ 19.7 (dd, $J$ = 123, 12 Hz), -7.1 (dd, $J$ = 150, 12 Hz).

## 4-8. References


1. Khusnutdinova, J. R.; Milstein, D. Metal-Ligand Cooperation. *Angew. Chem. Int. Ed.* **2015**, *54*, 12236–12273.
2. Whited, M. T. Metal-Ligand Multiple Bonds as Frustrated Lewis Pairs for C-H Functionalization. *Beilstein J. Org. Chem.* **2012**, *8*, 1554–1563.
3. Mitchell, G. P.; Tilley, T. D. Reversible Cycloaddition of Isocyanates to Ruthenium Silylene Complexes. *J. Am. Chem. Soc.* **1997**, *119*, 11236–11243.
4. Whited, M. T.; Zhang, J.; Ma, S.; Nguyen, B. D.; Janzen, D. E. Silylene-Assisted Hydride Transfer to $CO_2$ and $CS_2$ at a $[P_2Si]$Ru Pincer-Type Complex. *Dalton. Trans.* **2017**, *46*, 14757–14761.
5. Whited, M. T.; Zhang, J.; Conley, A. M.; Ma, S.; Janzen, D. E.; Kohen, D. Bimetallic, Silylene-Mediated Multielectron Reductions of Carbon Dioxide and Ethylene. *Angew. Chem. Int. Ed.* **2021**, *60*, 1615–1619.
6. Whited, M. T.; Grubbs, R. H. Oxygen-Atom Transfer from Carbon Dioxide to a Fischer Carbene at (PNP)Ir. *J. Am. Chem. Soc.* **2008**, *130*, 5874–5875.
7. Whited, M. T.; Grubbs, R. H. A Catalytic Cycle for Oxidation of Tert-Butyl Methyl Ether by a Double C-H Activation-Group Transfer Process. *J. Am. Chem. Soc.* **2008**, *130*, 16476–16477.
8. Brookes, N. J.; Ariafard, A.; Stranger, R.; Yates, B. F. Cleavage of Carbon Dioxide by an Iridium-Supported Fischer Carbene. A DFT Investigation. *J. Am. Chem. Soc.* **2009**, *131*, 5800–5808.
9. Whited, M. T.; Grubbs, R. H. Late Metal Carbene Complexes Generated by Multiple C−H Activations: Examining the Continuum of M═C Bond Reactivity. *Acc. Chem. Res.* **2009**, *42*, 1607–1616.
10. Van Der Boom, M. E. Oxygen Atom "Cut and Paste" from Carbon Dioxide to a Fischer Carbene Complex. *Angew. Chem. Int. Ed.* **2009**, *48*, 28–30.
11. Laitar, D. S.; Müller, P.; Sadighi, J. P. Efficient Homogeneous Catalysis in the Reduction of $CO_2$ to CO. *J. Am. Chem. Soc.* **2005**, *127*, 17196–17197.
12. Pierce, G. A.; Vidovic, D.; Kays, D. L.; Coombs, N. D.; Thompson, A. L.; Jemmis, E. D.; De, S.; Aldridge, S. Half-Sandwich Group 8 Borylene Complexes: Synthetic and Structural Studies and Oxygen Atom Abstraction Chemistry. *Organometallics* **2009**, *28*, 2947–2960.
13. De, S.; Pierce, G. A.; Vidovic, D.; Kays, D. L.; Coombs, N. D.; Jemmis, E. D.; Aldridge, S. Reactivity of Cationic Terminal Borylene Complexes: Novel Mechanisms for Insertion and Metathesis Chemistry Involving Strongly Lewis Acidic Ligand Systems. *Organometallics* **2009**, *28*, 2961–2975.
14. While metal–phospenium bond can act as the polarized bond, according to Thomas, phosphenium ligands ($PR_2^+$) are often reduced to phosphido ($PR_2^-$) ligands upon coordination to low-valent metals, See Pan, B.; Bezpalko, M. W.; Foxman, B. M.; Thomas, C. M. Heterolytic Addition of E-H Bonds across Pt-P Bonds in Pt N-Heterocyclic Phosphenium/Phosphido Complexes. *Dalton. Trans.* **2012**, *41* (30), 9083–9090.
15. Yang, L.; Powell, D. R.; Houser, R. P. Structural variation in copper(I) complexes with pyridylmethylamide ligands: structural analysis with a new four-coordinate geometry index, $\tau_4$. *Dalton Trans*. **2007**, 955−964.

16. Addison, A. W.; Rao, T. N.; Reedijk, J.; van Rijn, J.; Verschoor, G. C. Synthesis, structure, and spectroscopic properties of copper(II) compounds containing nitrogen–sulphur donor ligands; the crystal and molecular structure of aqua[1,7-bis(N-methylbenzimidazol-2′-yl)-2,6-dithiaheptane]copper(II) perchlorate. *J. Chem. Soc., Dalton Trans*. **1984**, 1349−1356.

17. Cotton, F. A.; Wilkinson, G.; Murillo C. A.; Bochmann, M. The Group 15 Elements: P, As, Sb, Bi. In *Advanced Inorganic Chemistry*, Wiley, New York, 6th ed., **1999**, 380-443.

18. Green, J. C.; Green, M. L. H.; Parkin, G. The Occurrence and Representation of Three-Centre Two-Electron Bonds in Covalent Inorganic Compounds. *Chem. Comm.* **2012**, *48*, 11481–11503.

19. Pearson, R. G.; Gray, H. B.; Basolo, F. *J. Am. Chem. Soc.* **1960**, *82*, 787−792.

20. Harkins, S. B.; Mankad, N. P.; Miller, A. J. M.; Szilagyi, R. K.; Peters, J. C. Probing the Electronic Structures of $[Cu2(\mu\text{-}XR_2)]^{n+}$ Diamond Cores as a Function of the Bridging X Atom (X = N or P) and Charge (n = 0, 1, 2). *J. Am. Chem. Soc.* **2008**, *130*, 3478–3485.

21. Mankad, N. P.; Harkins, S. B.; Antholine, W. E.; Peters, J. C. Multifrequency EPR Studies of $[Cu^{1.5}Cu^{1.5}]^{+}$ for $Cu_2(\mu\text{-}NR_2)_2$ and $Cu_2(\mu\text{-}PR_2)_2$ Diamond Cores. *Inorg. Chem.* **2009**, *48*, 7026–7032.

22. Gediga, M.; Feil, C. M.; Schlindwein, S. H.; Bender, J.; Nieger, M.; Gudat, D. N-Heterocyclic Phosphenium Complex of Manganese: Synthesis and Catalytic Activity in Ammonia Borane Dehydrogenation. *Chem. A Eur. J.* **2017**, *23*, 11560–11569.

23. Hatzis, G. P.; Oliemuller, L. K.; Dickie, D. A.; Thomas, C. M. N-Heterocyclic Phosphido Complexes of Rhodium Supported by a Rigid Pincer Ligand. *Eur. J. Inorg. Chem.* **2020**, 2873–2881.

24. Poitras, A. M.; Bezpalko, M. W.; Moore, C. E.; Dickie, D. A.; Foxman, B. M.; Thomas, C. M. A Series of Dimeric Cobalt Complexes Bridged by N-Heterocyclic Phosphido Ligands. *Inorg. Chem.* **2020**, *59*, 4729–4740.

25. Poitras, A. M.; Oliemuller, L. K.; Hatzis, G. P.; Thomas, C. M. Highly Selective Hydroboration of Terminal Alkenes Catalyzed by a Cobalt Pincer Complex Featuring a Central Reactive N-Heterocyclic Phosphido Fragment. *Organometallics* **2021**, *40*, 1025-1031.

26. Sutra, P.; Igau, A. Anionic Phosph(in)Ito ("Phosphoryl") Ligands: Non-Classical "Actor" Phosphane-Type Ligands in Coordination Chemistry. *Coord. Chem. Rev.* **2016**, *308*, 97–116.

27. Benito-Garagorri, D.; Mereiter, K.; Kirchner, K. Selective Phosphoramidite Cleavage as a Route to Novel Chiral and Achiral Pentacoordinated Nickel(II) PNP Pincer Complexes. *Eur. J. Inorg. Chem.* **2006**, *21*, 4374–4379.

28. Benito-Garagorri, D.; Kirchner, K. Modularly Designed Transition Metal PNP and PCP Pincer Complexes Based on Aminophosphines: Synthesis and Catalytic Applications. *Acc. Chem. Res.* **2008**, *41*, 201–213.

29. Punji, B.; Mague, J. T.; Balakrishna, M. S. Synthesis of Neutral ($Pd^{II}$, $Pt^{II}$), Cationic ($Pd^{II}$), and Water-Induced Anionic ($Pd^{II}$) Complexes Containing New Mesocyclic Thioether-Aminophosphonite Ligands and Their Application in the Suzuki Cross-Coupling Reaction0. *Inorg. Chem.* **2006**, *45*, 9454–9464.

30. Krishna, H.; Krishnamurthy, S. S.; Nethaji, M.; Murugavel, R.; Prabusankar, G. Unusual Reactivity of a Sterically Hindered Diphosphazane Ligand, $EtN(P(OR)_2)_2$, (R = $C_6H_3(i\text{Pr})_2$-2,6) towards ($H_3$-Allyl)Palladium Precursors. *J. Chem. Soc. Dalt. Trans.* **2007**, *3*, 2908–2914.

31. Pan, B.; Bezpalko, M. W.; Foxman, B. M.; Thomas, C. M. Heterolytic Addition of E-H Bonds across Pt-P Bonds in Pt N-Heterocyclic Phosphenium/Phosphido Complexes. *Dalton Trans.* **2012**, *41*, 9083–9090.

32. Brill, T.B.; Landon, S. J. Arbuzov-like dealkylation reactions of transition-metal-phosphite complexes. *Chem. Rev.* **1984**, *84*, 577–585

33. Pan, B.; Bezpalko, M. W.; Foxman, B. M.; Thomas, C. M. Coordination of an N-Heterocyclic Phosphenium Containing Pincer Ligand to a Co(CO)2 Fragment Allows Oxidation to Form an Unusual N-Heterocyclic Phosphinito Species. *Organometallics* **2011**, *30*, 5560–5563.

34. Stephan, D. W.; Erker, G. Frustrated Lewis Pair Chemistry: Development and Perspectives. *Angew. Chem., Int. Ed.* **2015**, *54*, 6400−6441.

35. Whited, M. T.; Grubbs, R. H. Oxygen-Atom Transfer from Carbon Dioxide to a Fischer Carbene at (PNP)Ir. *J. Am. Chem. Soc.* **2008**, *130*, 5874–5875.

36. Whited, M. T.; Zhang, J.; Donnell, T. M.; Eng, V. H.; Peterson, P. O.; Trenerry, M. J.; Janzen, D. E.; Taylor, B. L. H. Cooperative $CO_2$ Scission by Anomalous Insertion into a Rh-Si Bond. *Organometallics* **2019**, *38*, 4420–4432.

37. Krogman, J. P.; Foxman, B. M.; Thomas, C. M. Activation of $CO_2$ by a Heterobimetallic Zr/Co Complex. *J. Am. Chem. Soc.* **2011**, *133*, 14582−14585. (57)

38. Cooper, O.; Camp, C.; Pécaut, J.; Kefalidis, C. E.; Maron, L.; Gambarelli, S.; Mazzanti, M. Multimetallic Cooperativity in Uranium- Mediated $CO_2$ Activation. *J. Am. Chem. Soc.* **2014**, 136, 6716− 6723.

39. Escomel, L.; Del Rosal, I.; Maron, L.; Jeanneau, E.; Veyre, L.; Thieuleux, C.; Camp, C. Strongly Polarized Iridiumδ--Aluminumδ+ Pairs: Unconventional Reactivity Patterns Including $CO_2$ Cooperative Reductive Cleavage. *J. Am. Chem. Soc.* **2021**, *143*, 4844-4856.

40. Langer, J.; Hamza, A.; Pápai, I. RuBisCO-Inspired $CO_2$ Activation and Transformation by an Iridium(I) Complex. *Angew. Chem. Int. Ed.* **2018**, *57*, 2455–2458.

41. Oren, D.; Diskin-Posner, Y.; Avram, L.; Feller, M.; Milstein, D. Metal–Ligand Cooperation as Key in Formation of Dearomatized $Ni^{II}$–H Pincer Complexes and in Their Reactivity toward CO and $CO_2$. *Organometallics* **2018**, *37*, 2217-2221.

42. Leitl, J.; Marquardt, M.; Coburger, P.; Scott, D. J.; Streitferdt, V.; Gschwind, R. M.; Müller, C.; Wolf, R. Facile C=O Bond Splitting of Carbon Dioxide Induced by Metal–Ligand Cooperativity in a Phosphinine Iron(0) Complex. *Angew. Chem. Int. Ed.* **2019**, *58*, 15407–15411.

43. Lindner, E.; Bouachir, F.; Weishaupt, M.; Hoehne, S.; Schilling, B. Das Verhalten von Mono- Und Diorganylphosphansulfiden Gegenüber Metallcarbonylsystemen. XX. Darstellung, Eigenschaften Und Kristallstruktur von Ammin(Tetracarbonyl) (Dimethylthiophosphinito) Rhenium. *Zeitschrift fur Anorg. und Allg. Chemie* **1979**, *456*, 163–168.

44. Anderson, D. M.; Ebsworth, E. A. V; Stephenson, T. A.; Walkinshaw, M. D. Metal Complexes of Sulphur Ligands. Part 22. Reaction of Platinum(II) and Palladium(II)NN-Dialkyldithiocarbamates with Diphenylphosphine Chalcogenides. *J. Chem. Soc. Dalt. Trans.* **1982**, *12*, 2343.

45. Pinillos, M. T.; Jarauta, M. P.; Carmona, D.; Oro, L. A.; Apreda, M. C.; Foces-Foces, C.; Cano, F. H. Formation of a Dithiophosphinate Rhodium(III) Complex from the Unstable Three-Membered Ring

Species [($\eta^5$-$C_5Me_5$)( $\eta^1$-$PSPh_2$)$RhPh_2PS$]. Crystal Structure of [($\eta^5$-C5Me5)($\eta^1$-PSPh2)$RhPh_2SPS$]. *J. Organomet. Chem.* **1988**, *345*, 6–9.

46. Lorenz, I. -P; Mürschel, P.; Pohl, W.; Polborn, K. Mono- Und Diferriophosphane Und -thioxophosphorane. *Chem. Ber.* **1995**, *128*, 413–416.
47. Lindner, E.; Kneißle, W.; Fawzi, R.; Steimann, M.; Mayer, H. A.; Gierling, K. Preparation, Properties, and Reactions of Metal-Containing Heterocycles, XCI. Insertion of Activated Alkynes and Sulfur into the P-P Bond of Diphosphamolybdacyclopropanes. *Chem. Ber.* **1995**, *128*, 973–982.
48. Brym, M.; Jones, C.; Waugh, M. The Reactivity of an Iridaphosphirene Complex, [Ir(═C(But)P(Cy))(CO)($PPh_3$)$_2$], Cy = Cyclohexyl, toward Electrophiles. *J. Chem. Soc. Dalt. Trans.* **2003**, *3*, 2889–2893.
49. Shafaei-Fallah, M.; Shi, W.; Fenske, D.; Rothenberger, A. Synthesen Und Strukturen von Übergangsmetall-Komplexen Mit Dithiophosphinato- Und Trithiophosphonato-Liganden. *Zeitschrift fur Anorg. und Allg. Chemie* **2006**, *632*, 1091–1096.
50. Graham, T. W.; Udachin, K. A.; Zgierski, M. Z.; Carty, A. J. Remarkable Two-Step, Four-Electron Oxidative Addition Reactions at Phosphorus [P(I)–P(V)] in Terminal Electrophilic Phosphinidene Complexes. *Can. J. Chem.* **2007**, *85*, 885–888.
51. Sues, P. E.; Forbes, M. W.; Lough, A. J.; Morris, R. H. Ligand-Based Molecular Recognition and Dioxygen Splitting: An Endo Epoxide Ending. *Dalt. Trans.* **2014**, *43*, 4137–4145.
52. Albuerne, I. G.; Alvarez, M. A.; García, M. E.; García-Vivó, D.; Ruiz, M. A. Chemistry of $CS_2$- and SCNPh-Adducts of the Pyramidal Phosphinidene-Bridged Complex [$Mo_2Cp$(μ-$\kappa^1$:$\kappa^1$,$HPC_5H_4$)(CO)$_2$($\eta^6$-HMes*)(PMe3)]. *Dalton Trans.* **2017**, *46*, 3510–3525.
53. Li, J. P.; Luo, S. P.; Zhan, S. Z.; Shi, Y. C. Synthesis, Characterization and Electrocatalytic $H_2$ Production of Phosphine-Substituted CpFe Complexes. *Polyhedron* **2018**, *152*, 94–101.
54. Luo, Y . R ., *Comprehensive Handbook of Chemical Bond Energies*, CRC Press, Boca Raton, FL, **2007**.
55. Roddick, D. M.; Santarsiero, B. D.; Bercaw, J. E. Synthesis and Reactivity of Cyclopentadienylhafnium Phosphido Complexes. Hydrogenolysis and Carbon Monoxide Insertion for Hf-$PR_2$ Bonds. *J. Am. Chem. Soc.* **1985**, *107*, 4670–4678.
56. Fryzuk, M. D.; Bhangu, K. Activation of Dihydrogen by Organo-Iridium-Phosphido Complexes. Evidence for .Alpha.-Hydrogen Abstraction by a Terminal Phosphide Ligand. *J. Am. Chem. Soc.* **1988**, *110*, 961–963.
57. Derrah, E. J.; Pantazis, D. A.; McDonald, R.; Rosenberg, L. A Highly Reactive Ruthenium Phosphide Complex Exhibiting Ru-P π-Bonding. *Organometallics* **2007**, *26*, 1473–1482.
58. Hoyle, M. A. M.; Pantazis, D. A.; Burton, H. M.; McDonald, R.; Rosenberg, L. Benzonitrile Adducts of Terminal Diarylphosphido Complexes: Preparative Sources of "Ru=$PR_2$." *Organometallics* **2011**, *30*, 6458–6465.
59. Poitras, A. M.; Knight, S. E.; Bezpalko, M. W.; Foxman, B. M.; Thomas, C. M. Addition of H2 Across a Cobalt-Phosphorus Bond. *Angew. Chem. Int. Ed.* **2018**, *57*, 1497–1500.
60. Vierling, P.; Riess, J. G. New Molybdenum and Iron Phospho- ranides. Mechanism and Stereochemistry of the Rearrangement and Migration of a Phosphorus-Bound Allylic Group into an Iron-Bound Vinylic Group. *Organometallics* **1986**, *5*, 2543–2550.

61. Kajiyama, K.; Nakamoto, A.; Miyazawa, S.; Miyamoto, T. K. *Chem. Lett.* **2003**, *32*, 332−333.

62. Hwang, S. J.; Tanushi, A.; Radosevich, A. T. Enthalpy-Controlled Insertion of a "Nonspectator" Tricoordinate Phosphorus Ligand into Group 10 Transition Metal-Carbon Bonds. *J. Am. Chem. Soc.* **2020**, *142*, 21285–21291.

63. Goodman, J.; Macgregor, S. A. Metallophosphoranes: The Hidden Face of Transition Metal-Phosphine Complexes. *Coord. Chem. Rev.* **2010**, *254*, 1295–1306.

64. Pangborn, A. B.; Giardello, M. A.; Grubbs, R. H.; Rosen, R. K.; Timmers, F. J. *Organometallics*, **1996**, *15*, 1518–1520.

65. Alaimo, P. J.; Peters, D. W.; Arnold, J.; Bergman, R. G. *J. Chem. Educ.*, **2001**, *78*, 64.

66. Bruker AXS (2009). Apex II. Bruker AXS, Madison, Wisconsin.

67. Sheldrick, G. M. *Acta Cryst.* **2010**, *D66*, 479–485.

68. Dolomanov, O.V., Bourhis, L.J., Gildea, R.J, Howard, J.A.K. & Puschmann, H. *J. Appl. Cryst.* **2009**, *42*, 339-341.

# Chapter 5 Insertion of Nonspectator Phosphorus Ligands into Group 10 Transition Metal–Carbon Bonds

A significant portion of the work described in this chapter has been published in:

Hwang, S. J.;† Tanushi, A.;† Radosevich, A. T. Enthalpy-Controlled Insertion of a "Nonspectator" Tricoordinate Phosphorus Ligand into Group 10 Transition Metal-Carbon Bonds. *J. Am. Chem. Soc.* **2020**, *142*, 21285–21291.

## 5-1. Introductory Remarks: Spectator and Nonspectator Roles of Tricoordinate Phosphorus Ligands in Chemistry of Group 10 Metal–Carbon Bonds

Cross-coupling reactions based on group 10 metal-carbon bond formation is undoubtedly one of the most important discoveries in organometallic chemistry. The original foundation of the work found in 1970's has evolved into versatile, useful and reliable methods in the organic syntheses in both academia and industry, leading to the awarding of the Nobel Prize in Chemistry in 2010.[1] Significant contributions to this process arise from the enhancement of catalytic activity because of the development of phosphine ligands. They have been optimized as 'spectator' ligands, which tune the electronic and steric properties of the metal center without directly participating in the bond activation.

For 'nonspectator' reactivity of phosphorus ligands with metal–carbon bonds, the low coordination and electronic unsaturation of the P fragment enabled insertion reactions of phosphenium,[2-4] phosphide,[5,6] and phosphinidene[7-10] ligands into transition metal alkyls. By contrast, well-defined examples of analogous reactions with $\sigma^3$–P ligands have been scarce. Bernskoetter has inferred that methyl exchange in $(Me_3P)_3Co(CH_3)_2I$ involves such a step.[11] As initially proposed by Green, Felkin, and Swierczewski,[12] P-substituent scrambling/redistribution during group 10 metal-phosphine-catalyzed coupling have been proposed in some cases to evolve via higher P-coordinate metallophosphorane intermediates.[13,14] Structurally well-defined examples validating such proposed intermediates, however, are lacking.

Nontrigonal tricoordinate phosphorus compounds have shown the ability to access higher coordinate phosphorus species by cleaving various metal–ligand σ-bonds. In Chapter 3, formation of metallohydrophosphorane *via* a net insertion of nontrigonal P(III) ligand into Ru–H bond was

discussed and investigated. In Chapter 4, a Rh(III) metallophosphorane with a P–C bond was synthesized by a stepwise Rh(I)–centered oxidation of allyl chloride followed by an intramolecular migration of allyl group from Rh to P. Herein Chapter 5 will discuss another 'nonspectator' reactivity of a tricoordinate phosphorus ligand with Group 10 metal–carbon bonds, which is an unprecedented insertion into M–$CH_3$ bonds. In the former part, we will design a novel bidentate ligand **L2** with both nontrigonal and trigonal phosphorus coordination sites, which directly demonstrates the contribution of nontrigonal deformation to the insertion reactivity. Based on the M–C bond enthalpies, the complexes span the intramolecular Me-group transfer reaction coordinate from (hydrocarbyl)metal phosphine to hydrocarbylmetallophosphorane within the group 10 triad. In the latter part, we will expand the chemistry to tridentate ligand **L1**, which affords more stable metallocarbylphosphoranes *via* net insertions into M-C bonds, and investigate the metalation with Pd(II) or Pt(II) dialkyl complexes. The different behaviors of Pd(II) and Pt(II) systems upon oxidative addition reflect the periodic trend of insertion reactivity into M–C bonds.

## 5-2. Synthesis of Bidentate P^P–Chelate Ligand L2 and L3

To directly demonstrate the contribution of nontrigonal P(III) center to unusual reactivity, a bidentate P^P-chelate (**L2**) containing both trigonal and nontrigonal tricoordinate phosphorus centers was prepared on multigram scale (Scheme 5-1). Bis(2-aminophenyl)amine **5.1** [15] is transformed by three-steps Pd-catalyzed C-N and C-P coupling reactions to give **5.4**, followed by treatment with $PCl_3$ in the presence of $Et_3N$ to afford the $\kappa^2$-chelating framework. The $^{31}P\{^1H\}$ NMR spectra of ligand **L2** show two doublet resonances (δ 154.3 ppm, −8.0 ppm), in which the downfield resonance falls within the range of previously reported nontrigonal phosphorous triamides.[16] The magnitude of the observed spin-spin interaction between the two $^{31}P$ nuclei ($J$ = 86 Hz) is large and may arise via a through-space coupling mechanism.[17,18]

**Scheme 5-1.** Synthesis of ligands **L2** and **L3**.

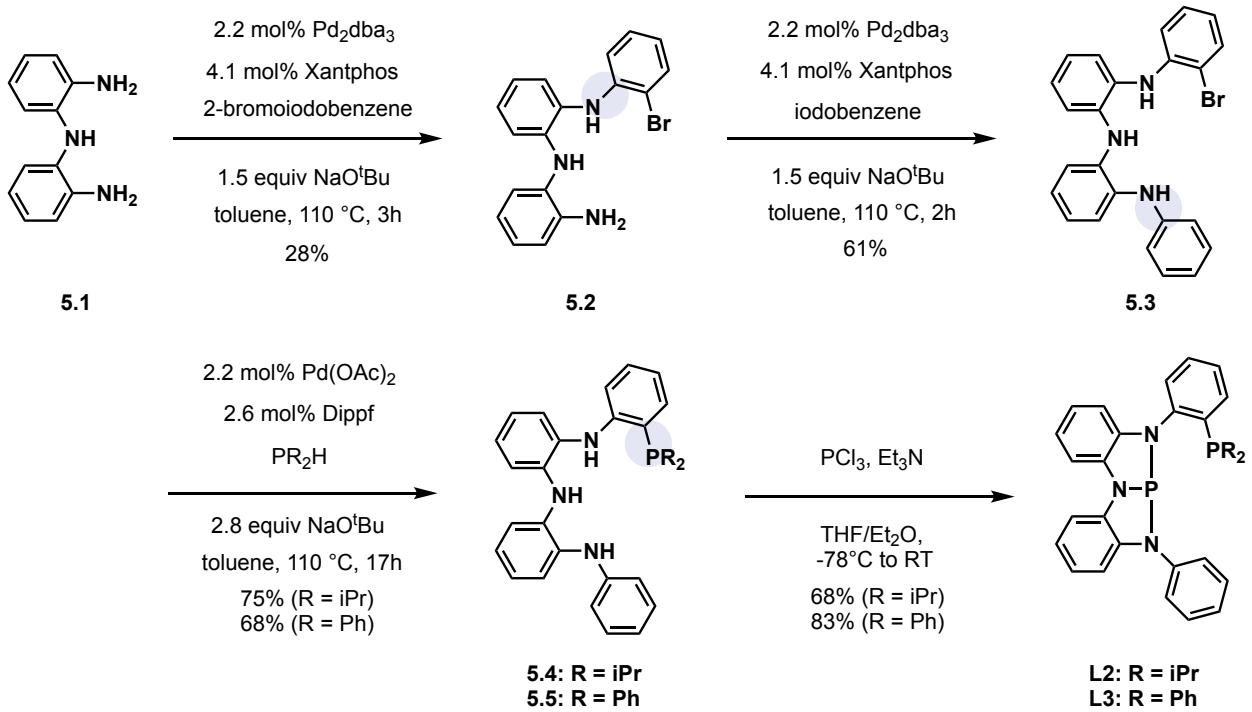

The experimentally determined structure for *P*,*P*-diphenyl congener **L3** (Figure 5-1) from X-ray diffraction reports a distance between phosphorus atoms ($d_{P\text{-}P}$ = 3.870 Å) that falls within a range that is both consistent with through-space spin coupling ($J_{PP}$) in $^{31}$P NMR spectra[19] and suitable for accommodation of a transition metal guest through bidentate chelation.

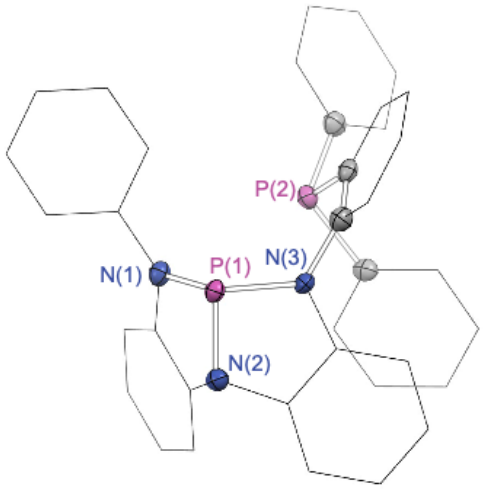


**Figure 5-1.** Structure for **L3**, with hydrogen atoms and solvent molecules omitted for clarity. Two phosphorus atoms and their substituent atoms are depicted with thermal ellipsoids at 50% probability.

## 5-3. Metalation of L2 with Group 10 M–Me Precursors

### *5-3-1. Metalation with (cod)Pt(Me)(Cl)*

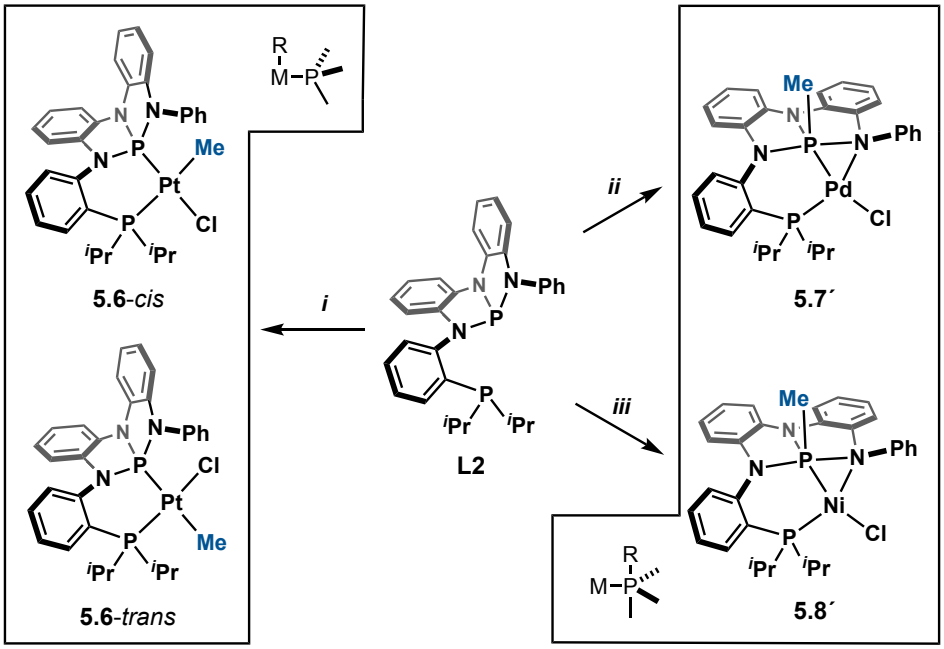


**Figure 5-2.** Metalation of **L2** with group 10 complexes of the formula $L_2M(Cl)(Me)$. Reaction conditions: (*i*) (cod)Pt(Cl)(Me), benzene, RT, 90% (*ii*) (cod)Pd(Cl)(Me), benzene, RT, 99%. (*iii*) $(Me_3P)_2Ni(Cl)(Me)$, benzene, RT, 37%.

Metalation of **L2** with (cod)PtClMe in $C_6H_6$ at ambient temperature afforded the expected $\kappa^2$-chelated complexes (**L2**)PtClMe as an apparent 5:1 mixture of geometrical isomers (i.e. **5.6**-*cis* and **5.6**-*trans*, Figure 5-2). The major isomer exhibits $^{31}P$ NMR resonances (Figure 5-3b) corresponding to the triamido phosphorus nucleus at δ 100.2 ppm ($^2J_{P-P}$ = 28 Hz, $^{195}Pt$ satellite $^1J_{Pt-P}$ = 6700 Hz) and the $(^iPr)_2ArP$ nucleus at δ 17.4 ppm ($^2J_{P-P}$ = 28 Hz, $^{195}Pt$ satellite $^1J_{Pt-P}$ = 1695 Hz). The $^{31}P$ NMR spectrum of the minor isomer features an analogous set of resonances at δ 142.3 ppm ($^2J_{P-P}$ = 27 Hz, $^{195}Pt$ satellite $^1J_{Pt-P}$ = 2601 Hz) and δ 15.9 ppm ($^2J_{P-P}$ = 27 Hz, $^{195}Pt$ satellite $^1J_{Pt-P}$ = 4048 Hz).

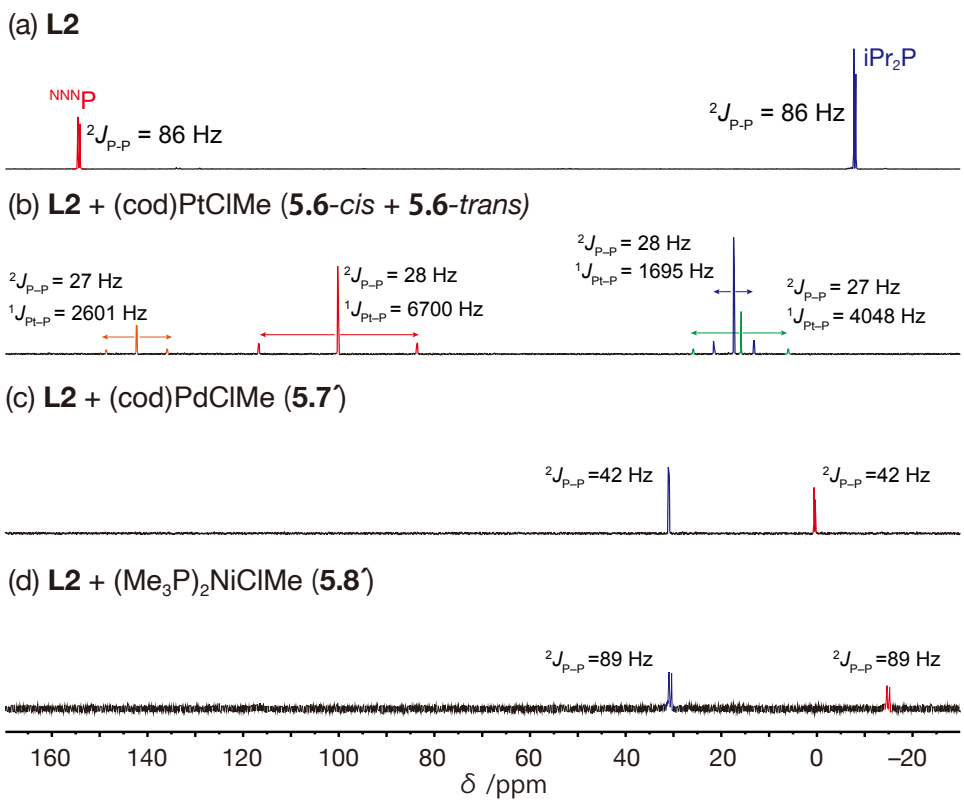


**Figure 5-3.** $^{31}$P NMR spectra of (a) **L2**, (b) **5.6**, (c) **5.7**, (d) **5.8** in $CD_2Cl_2$. Units are ppm relative to 85% $H_3PO_4$.

Diffusion of *n*-pentane into a $CHCl_3$ solution of complexes **5.6** at room temperature deposited colorless single crystals confirms the asymmetric bisphosphine unit coordinated to the platinum center as the $\kappa^2$-chelating mode (Figure 5-4). The platinum atom in the solid-state structure of complex **5.6** adopts a nearly perfect square planar geometry ($\tau_4 = 0.06$)[20] with the chloride ligand positioned *trans* to the triamide phosphorous atom. The most noticeable features of the structure are the Pt(1)−P(1) bond distance of 2.165 Å for the triamide phosphorous which is notably contracted when compared to that found for trigonal phosphorous, P($^i$Pr)$_2$ (*d*(Pt(1)−P(2)) = 2.341 Å) in complex **5.6**. The asymmetry in the Pt−P distances is consistent with the different magnitude of coupling constants between Pt and two phosphorus atoms, inferring the strong *trans* influence

of the nontrigonal phosphorous ligand as compared to the trigonal phosphorus ligand. The crystallographically observed isomer **5.6**-*cis* is assigned as major isomer in solution by reference to the correlation between Pt−P bond lengths and coupling constants reported by Woollins and co-workers (i.e. $d_{Pt-P}$ (Å) = 2.421 – $^{1}J_{Pt-P}$/24255, Table 5-1).[21] Additionally, DFT geometry optimization calculations for both **5.6**-*cis* and **5.6**-*trans* at B3LYP/def2-TZVP level was performed. Total energies for the two isomers suggested **5.6**-*cis* is energetically more stable than **5.6**-*trans* by 4.1 kcal/mol and reproduce the calculated Pt(1)−P(1) bond distance of **5.6**-*cis* of 2.171 Å is significantly shorter than that of **5.6**-*trans* (2.286 Å), supporting the strong *trans*-influence of the nontrigonal phosphorus ligand.

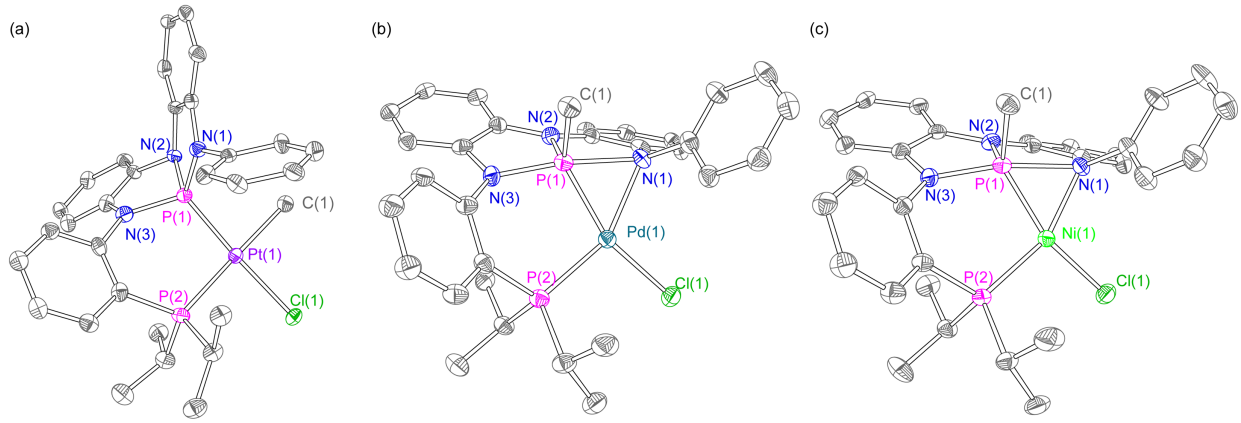


**Figure 5-4.** Thermal ellipsoids rendered at the 50% level for (a) **5.6**-*cis*, (b) **5.7′** and (c) **5.8′**. Hydrogen atoms and solvent molecules are omitted for clarity.

**Table 5-1**. Relationships between $J_{Pt-P}$ values and Pt–P bond lengths in **5.6**-*cis* and **5.6**-*trans*.

| | **5.6**-*cis* | | | **5.6**-*trans* | | |
|---|---|---|---|---|---|---|
| | $^{1}J_{Pt-P}$ (Hz)[a] | $d_{derived}$[b] | $d_{calc}$ | $^{1}J_{Pt-P}$ (Hz)[a] | $d_{derived}$[b] | $d_{calc}$[c] |
| Pt(1)–P(1) | 2601 | 2.314 | 2.286 | 6700 | 2.145 | 2.171 |
| Pt(1)–P(2) | 4048 | 2.254 | 2.265 | 1695 | 2.351 | 2.399 |

[a] Experimental values in $^{31}$P NMR spectra. [b] Bond distance derived from $^{1}J_{Pt\text{-}P}$ based on the correlation in Ref. 21. [c] Bond distance calculated by DFT calculation at B3LYP/def2-TZVP level.

*5-3-2. Metalation with (cod)Pd(Me)(Cl)*

Despite the periodic similarities between Pt and Pd, an analogous metalation of **L1** by (cod)Pd$^{II}$(Me)(Cl) did not return the anticipated κ$^2$-chelate congeners of **5.6**-*cis* and **5.6**-*trans*. Instead, a single new diamagnetic Pd complex was obtained which lacked the characteristic nontrigonal triamidophosphorus $^{31}$P NMR resonance in the high field region of the spectrum (Figure 5-3c). The $^{31}$P{$^{1}$H} NMR spectrum displayed two low field doublets (δ 31.0, 0.5 ppm) with mutual coupling ($^{2}J_{P–P}$ = 42 Hz). In the $^{1}$H-coupled $^{31}$P NMR spectrum, the signal at δ 0.5 ppm is further split into a quartet ($J_{P–H}$ = 11 Hz). The corresponding coupling partner is found in the $^{1}$H NMR spectrum; the resonance arising from the –Me moiety is observed as a doublet at δ 1.12 ppm ($J$ = 11 Hz). The magnitude of this coupling is inconsistent with typical $^{3}J$ constants for $R_3P$–Pd–$CH_3$ connectivity, but rather suggests closer contact between the spin systems.

X-ray diffraction of single crystals obtained from a benzotrifluoride/pentane solution at −35 °C resolves the spectral discrepancy. The structure (Figure 5-4b) clearly shows the absence of a palladium-methyl, but instead apparent migration of the methyl from Pd to the nontrigonal P center to furnish a palladamethylphosphorane complex **5.7′** (Figure 5-2). As a consequence of methyl group migration to the triamidophosphorus center, the X-ray crystal structure of complex **5.7′** revealed a distorted trigonal bipyramidal geometry around the phosphorus center ($\tau_5$ = 0.67)[22] with Me and Pd substituents occupying equatorial positions with respective bond distances $d_{P1–C1}$ = 1.815(6) Å and $d_{P1–Pd1}$ = 2.1435(18) Å, and an angle $\angle_{C1–P1–Pd1}$ = 126.8(2)°. The nontrigonal phosphorus accommodates the additional methyl substituent by planarization of the triamide

framework (i.e. increase in the angle $\angle_{N1-P1-N3}$ from 110.55(18)° to 166.7(2)°). Coincident with this planarization process, the distal N1 atom in **L2** is brought into bonding proximity of the metal, rendering the four-coordinated $Pd^{II}$ complex in a distorted square planar geometry ($\tau_4 = 0.37$). In effect, **L2** takes on ($P^1,N^1$-η, κ$P^2$)–binding to palladium. A significant dissymmetry in P–N bond distances results; P1−N1 bond distance is significantly longer (*d* 2.2002(5) Å) than either P1−N2 or P1−N3 (*d* 1.716(5) and 1.766(5) Å, respectively) but well-below the sum of the van der Waals radii.

*5-3-3. Metalation with $Ni(PMe_3)_2(Me)(Cl)$*

Metalation of **L1** with $(Me_3P)_2Ni^{II}(Cl)(Me)$ similarly yielded a corresponding nickelamethylphosphorane complex **5.8′**. The $^{31}P\{^1H\}$ NMR spectrum displayed two signals; the triamidophosphorus moiety with its characteristic large upfield shift is found at δ –12.2 ppm and the remaining diisopropylphosphine at δ 31.0 ppm. The single crystal X-ray structure of complex **5.8′** obtained from a toluene/pentane solution at −35°C confirms the formation of metallophosphorane complex with the ($P^1,N^1$-η, κ$P^2$)–binding by insertion of $\sigma^3$–P to the Ni-methyl bond. Apart from the shorter bonds between the metal and primary ligands (i.e. Ni–P, Ni–N, Ni–Cl) in nickel complex **6′**, the structures of the compounds **5.7′** and **5.8′** are analogous.

In contrast to the stable $Pd^{II}$ complex **5.7′**, $Ni^{II}$ complex **5.8′** gradually decomposed in solution to yield a metal-phosphine type complex **5.9**. The $^{31}P\{^1H\}$ NMR spectrum displayed a signal at 149.4 ppm, which is coupled to diisopropylphosphine signal at δ 45.5 ppm with a coupling constant $^2J_{PP} = 425$ Hz. Considering the drastic downfield shift and the large coupling constant, we assigned complex **5.9** as an amide complex with two tricoordinate phosphorus side arms, which is formed

by a cleavage of P(1)−N(3) bond. This type of P-N bond cleavage reactions in $\eta^2$-(*P,N*)-metallophosphorane were previously reported by Riess. [23]

**Scheme 5-2.** Decomposition of **5.8´**.

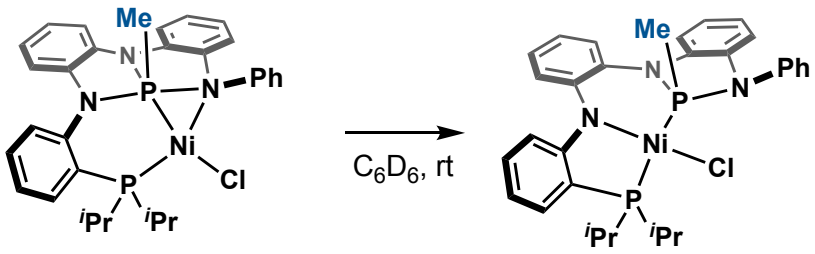


**5.8´** **5.9**

## 5-4. DFT Calculation to Understand the Different Reactivity within Group 10 Triad

### *5-4-1. Gibbs free energy calculation*

While metallamethylphosphorane complexes **5.7′** and **5.8′** appear to be the thermodynamically favored products in the case of Pd and Ni system, efforts to convert the Pt-phosphine complex **5.6** into the analogous platinamethylphosphorane complex have been unsuccessful. To understand the factors governing speciation of the complexes above, DFT calculations (B3LYP/def2-TZVP) were conducted to evaluate the relative energies of the metal phosphine (**5.6-5.8**) and metallophosphorane (**5.6′-5.8′**) isomers (Figure 5-5).

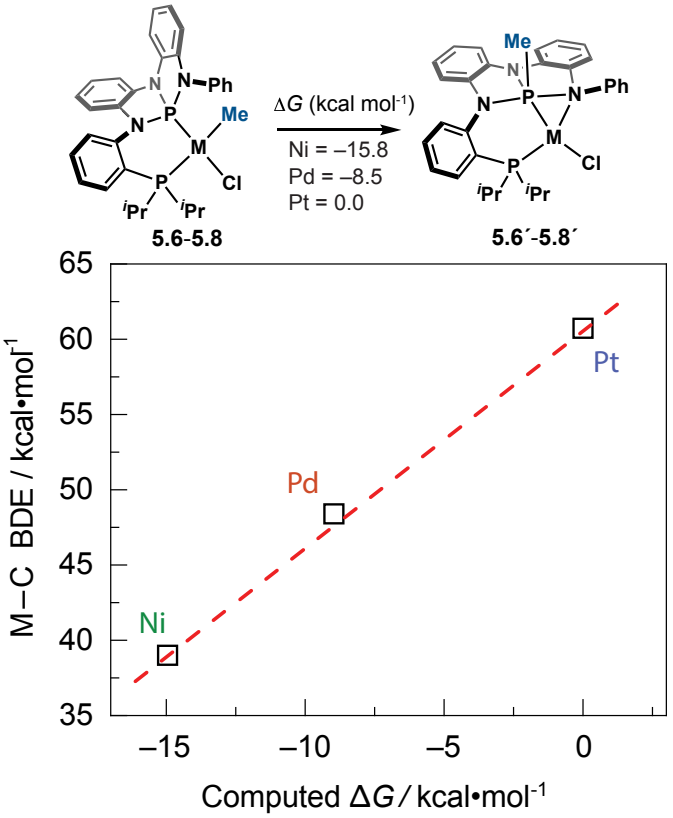


**Figure 5-5.** Calculated Gibbs free energy of methyl α-migration for Ni, Pd and Pt complexes at the B3LYP/def2-TZVP level of theory.

Where available, the computed metrics for complexes are in good agreement with the experimentally determined values. The computed free energy of methyl migration displays a monotonic trend in which the driving force decreases down the group 10 triad ($\Delta G$ = −15.8 (Ni), −8.5 (Pd), and 0.0 (Pt) kcal mol$^{-1}$). Qualitatively, this observation correlates inversely with the known trend in group 10 metal-carbon (M−C) bond strengths (i.e. BDE: Ni−C < Pd−C < Pt−C) and is predicted semiquantitatively by reference to reported P−C (63 kcal/mol) and M−C (38.0−66.5 kcal/mol)[24] bond dissociation energies. In effect, the methyl ligand migration to phosphorus is less energetically costly for Pd and Ni complexes than for the Pt compound, implying an increased stability of the metallomethylphosphorane complex for the first and second row metals relative to the third.[25]

*5-4-2. Intrinsic bond orbital analysis*

Analysis of the DFT (B3LYP/def2-TZVP) wavefunctions for metal-phosphines **5.6**-**5.8** and metallophosphoranes **5.6´**-**5.8´** by the intrinsic bond orbital (IBO)[26,27] method provides additional insight into the local M–P bonding. The triad of standard $\kappa^2$-chelated isomers **5.6**-**5.8** (Figure 5-6A-C*, top*) show ($\sigma^3$–P)–M IBOs consistent with a typical L-type dative σ-interaction, expressed as partial charges assigned mainly to P (e.g. Figure 5-6b, *left*: P=1.533, Pd=0.378). In each case, the IBO corresponding to the analogous interaction in the metallophosphophorane isomers **5.6´**-**5.8´** (Figure 5-6A-C, *bottom*) indicates an increased parity of distribution across the P–M bond (e.g. Figure 6B, *left*: P=1.154, Pd=0.815) as in a X-type normal covalent bond. Additionally, localized orbital bonding analysis (LOBA)[28] was performed to assign the intuitive oxidation states (OS) of the metal centers.[29] For all compounds in Figure 6, four doubly occupied metal-based orbitals

corresponding to the nonbonding *d* valence set are identified. Consequently, the formal oxidation state for all compounds remains +2.

.

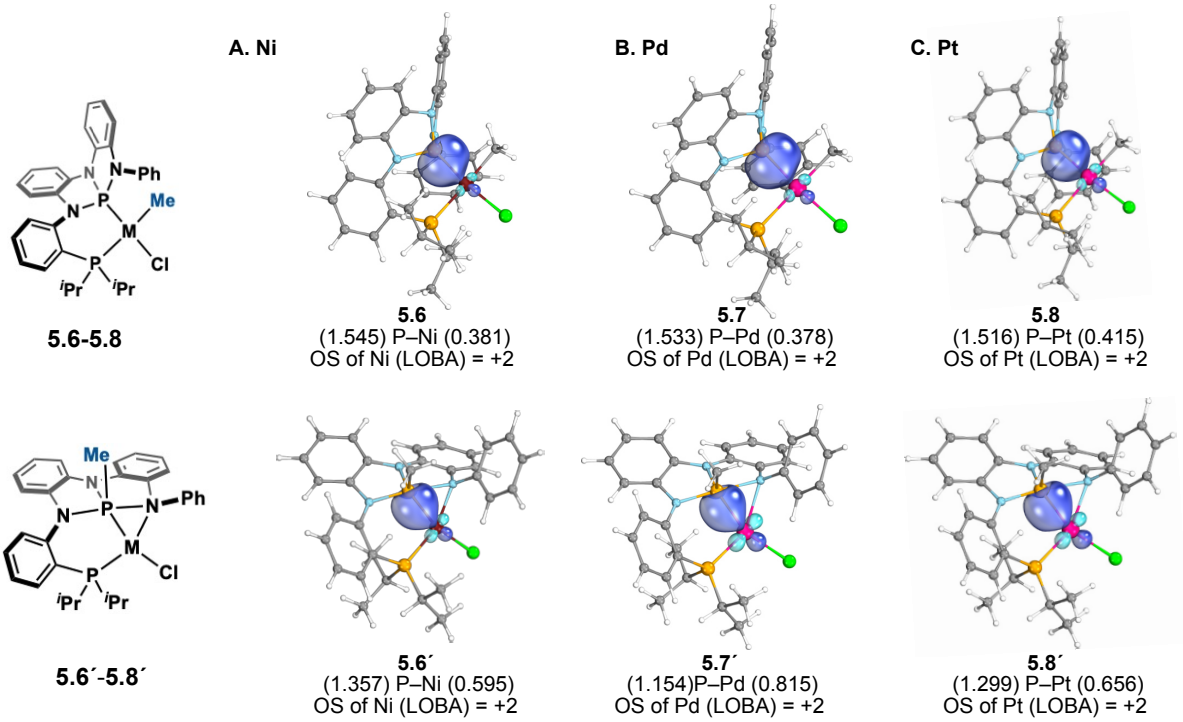


**Figure 5-6.** IBO depictions of M–P bonds and LOBA oxidation states. Numbers in parentheses correspond to the partial charge distributions of IBO. Orbital isosurface contains 80% of the integrated electron density of the orbital.

### *5-4-3. Discussion: arrested reductive elimination*

Whereas metathetical sequences involving P–C bond formation/cleavage by oxidative addition/reductive elimination of phosphonium ions at late metals are well-known,[30] the observed nonspectator insertion of **L2** to $Pd^{II}$–Me and $Ni^{II}$–Me occurs without formal oxidation state change of the metal. In effect, compounds **5.7´** and **5.8´** can be viewed as exemplars of an arrested reductive elimination (i.e P–C bond formation without release from the metal coordination sphere). Through this lens, the current results connect to prior proposals of metallophosphorane-mediated

catalyst (de)activation via *in situ* $M^{II}/M^{0}$ redox. Verkade has proposed that fluoride addition to Pd(II)-(bis)phosphines initially forms metallofluorophosphorane followed by the reductive elimination of the P fragment to give $Pd^{0}$.[31-33] Ozawa has investigated the reductive P–C bond elimination from styrylpalladium(II)–phosphine complexes via metallophosphorane intermediates,[34] Furthermore, the resemblance to known metal–ligand cooperative systems[35] (e.g. CO/acyl,[36-40] carbene/alkyl,[41] silylene/silyl,[42] amide/amine,[43-47] and stibine/stiborane[48]) suggests new opportunities for such metallophosphorane intermediates in organometallic chemistry by intentional design.

## 5-5. Metalation of Tridentate Ligand L1 with Group 10 Metal–Alkyl Precursors

### *5-5-1. Metalation of **L1** with (cod)PdCl(Me) and PdMe$_2$(tmeda)*

Considering the decomposition pathway of **5.8′** through P–N bond cleavage, the ($P^1$,$N^1$-η, κ$P^2$)–binding of ligand **L2** is not desirable if we wish to synthesize stable metallophosphoranes or to investigate the further reactivity of metallophosphoranes. To prevent this coordination mode by an additional coordination moiety, tridentate dipyridyl ligand **L1** (used in Chapters 3 and 4) was metalated with Group 10 metal–alkyl precursors. Metalation of **L1** with (cod)PdClMe in $C_6D_6$ afforded a single diamagnetic Pd complex **5.10′** (Scheme 5-3).

**Scheme 5-3**. Metalation of **L1** with (cod)PdClMe and (tmeda)PdMe$_2$

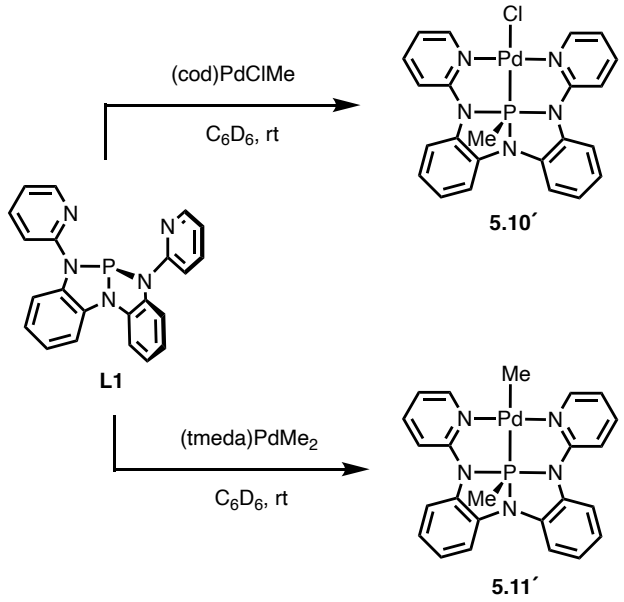


A $^{31}P\{^1H\}$ NMR spectrum of **5.10′** displays a low field singlet at δ –17.2 ppm, suggesting the formation of metallophosphorane by an insertion of the P(III) ligand into a Pd–Me bond. In the $^1$H-coupled $^{31}$P NMR spectrum, the signal is further split into a quartet ($J_{P–H}$ = 9.7 Hz). The corresponding $^1$H NMR spectrum resolves the complementary coupling partner, with a doublet at δ 1.77 ppm (6H, $J$ = 17 Hz) assigned to the *P*–methyl group. Notably, the $^1$H NMR spectrum

indicates an approximate $C_s$ symmetry in the solution state. X-ray diffraction of a yellow crystal of metallophosphorane **5.10′** confirmed the insertion reactivity by clearly showing a P–Me bond instead of a Pd–Me bond (Figure 5-7). The four-coordinated $Pd^{II}$ complex is in an approximate square planar geometry ($\tau_4 = 0.10$). Both of the pyridyl side arms in **L1** coordinate to the palladium to form a $\kappa^3$-*N,P,N*-coordination fashion, which is distinct from the ($P^1,N^1$-η, $\kappa P^2$)–binding mode in **L2** congener **5.7′**. The geometry around the phosphorus is rather closer to square pyramidal ($\tau_5 = 0.25$) compared to **5.7′** ($\tau_5 = 0.67$). The bond distance $d_{P(1)–Pd(1)} = 2.2342\ (18)$ Å is significantly longer than that of **5.7′** ($d_{P(1)–Pd(1)} = 2.1435(18)$ Å), probably due to the constraint applied by the tridentate chelate. The P–C bond length is not largely different between the two complexes ($d_{P(1)–C(1)} = 1.825(7)$ Å in **5.10′** and $d_{P(1)–C(1)} = 1.815(6)$ Å in **5.7′**). The formation of 3c-4e bonding in N1–P1–N3 is suggested by the long P–N bond lengths in the linearly positioned N1–P1–N3 moiety ($d_{P(1)–N(1)} = 1.865(5)$ Å, $d_{P(1)–N(2)} = 1.744(5)$ Å, $d_{P(1)–N(3)} = 1.839(5)$ Å).

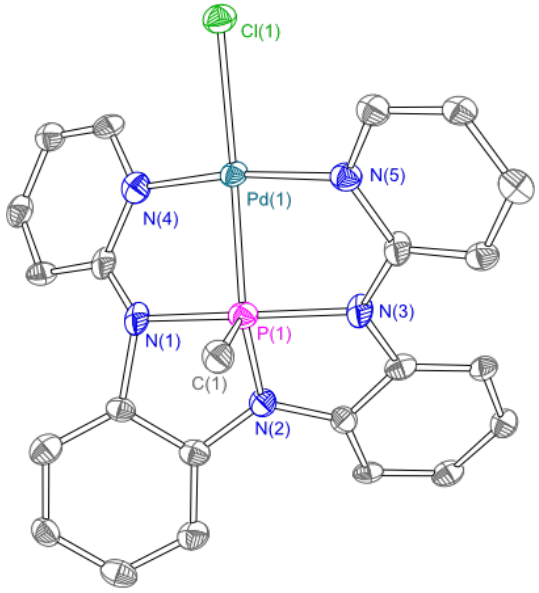


**Figure 5-7.** Thermal ellipsoids rendered at the 50% level for **5.10′**. Hydrogen atoms are omitted for clarity.

The insertion of the P(III) center into a Pd–Me bond was also observed when **L1** was metalated with dimethyl precursor (tmeda)$PdMe_2$ (tmeda = tetramethylethylenediamine). In the $^{31}P\{^{1}H\}$ NMR spectrum of the product **5.11´**, the triamidophosphorus moiety resonates at δ 20.7 ppm with a significant upfield shift from typical region of metal–phosphine type complexes. The downfield chemical shift of **5.11´** (δ 20.7 ppm) compared to **5.10´** (δ –17.2 ppm) is probably due to the substitution of the *trans* ligand of the pentacoordinate phosphorus by Me group, a strong σ-donor ligand. The $^{1}H$ NMR spectrum shows two doublet signals with different coupling values; one at δ 1.44 ppm (d, $^{3}J_{P-H}$ = 3.4 Hz) can be assigned to *Pd*–Me and one at δ 0.86 ppm (d, $^{2}J_{P-H}$ = 13.4 Hz) to *P*–Me, respectively. The aromatic signals suggested an approximate $C_s$ symmetry in the solution state. In the H-coupled $^{31}P$ NMR spectrum, only the larger coupling ($^{2}J_{P-H}$ = 13.4 Hz) was observed in the resolution.

### *5-5-2. Metalation of **L1** with (cod)Pd($CH_2TMS$)$_2$*

**Scheme 5-4.** Metalation of **L1** with (cod)Pd($CH_2TMS$)$_2$

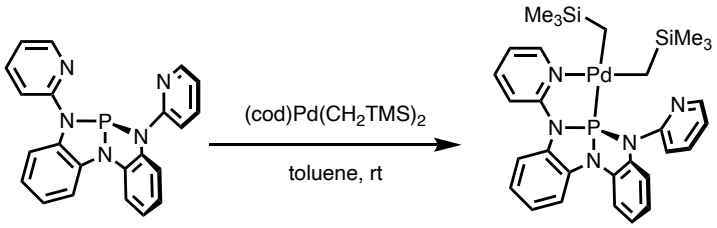


**L1** **5.12**

In contrast, an analogous metalation of **L1** with (cod)Pd($CH_2TMS$)$_2$ yielded a $\kappa^2$-chelate complex **5.12** instead of an anticipated metallophosphorane congener of **5.11** (Scheme 5-4). Compound **5.12** showed a singlet $^{31}P$ NMR resonance at δ 154.0 ppm, in the high field region of

the spectrum. A colorless crystal of **5.12** suitable for X-ray diffraction was obtained from a toluene solution layered with pentane at –35 ºC. The solid-state structure of **5.12** shows the **L1** coordinates to the palladium center as the $\kappa^2$-chelating mode to form an approximate square-planar geometry ($\tau_4$ = 0.09) (Figure 5-8). The phosphorus triamide framework is slightly affected by the coordination; there is an increase in the angle $\angle_{N1-P1-N3}$ (111.59(4)° in **5.12** and 108.67(4)° in free **L1**). The three P–N bond lengths are analogous ($d_{P(1)-N(1)}$ = 1.7368(8) Å, $d_{P(1)-N(2)}$ = 1.7366(8) Å, $d_{P(1)-N(1)}$ = 1.7316(8) Å), which is distinct from the metallophosphoranes **5.7′** or **5.10**.

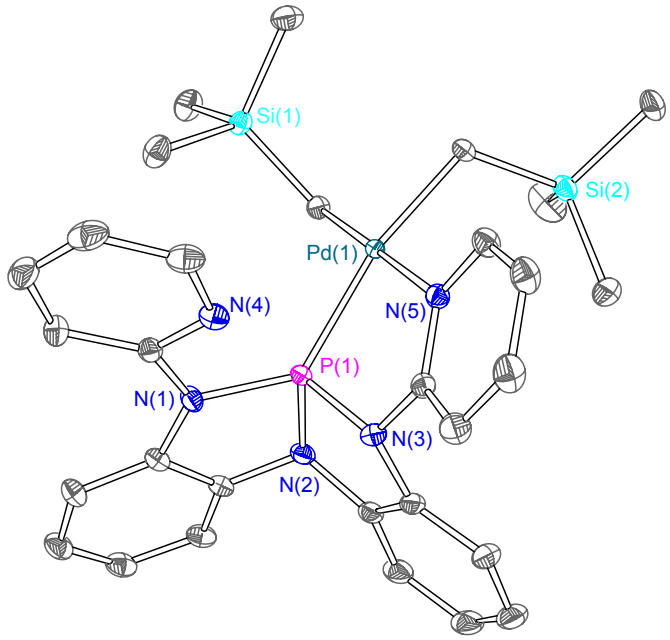


**Figure 5-8** Thermal ellipsoids rendered at the 50% level for **5.12**. Hydrogen atoms are omitted for clarity.

**Scheme 5-5.** Proposed dynamic solution behavior of **5.12**.

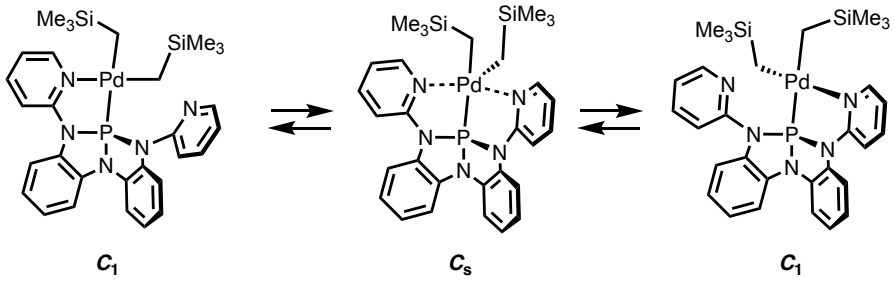

Contrary to expectation for the $C_1$-symmetric structure determined for **5.12** in the solid state, the $^1$H NMR spectrum at ambient temperature shows apparent $C_s$ symmetry in solution. The broadened $^1$H NMR signals suggest the tridentate ligand **L1** is fluxional and switches its metal coordination between two pyridyl groups (Scheme 5-5). Similar fluxional shifts of pyridyl ligands are observed and in Pd(II) $\kappa^2$-terpyridine derivatives and investigated by Orrell and coworkers.[49,50] Similar fluxional behavior was also observed in RhCl($PPh_3$)(**L1**) (**4.1**) with a $\kappa^2$-**L1** coordination (see Chapter 4).

### *5-5-3. Discussion of the distinct reactivity of **L1** with (L)PdMe$_2$ and (L)Pd(CH$_2$TMS)$_2$*

To understand the factors governing speciation of the complexes above, DFT calculations (B3LYP/def2-TZVP) were conducted to evaluate the relative energies of the metal phosphine (**5.11** and **5.12**) and metallophosphorane (**5.11´** and **5.12´**) isomers . As expected, the substitution of two carbon substituents from H to $CH_2TMS$ groups did not affect the relative energies between metal phosphine and metallophosphorane dramatically. In both cases, the computed driving force of metallophosphorane formation is large (–21.4 kcal/mol for R=Me, –19.5 kcal/mol for R=$CH_2TMS$) (Table 5-2).

**Table 5-2.** Driving force of metallophosphorane formation from **5.11** and **5.12** calculated at B3LYP/def2-TZVP level.

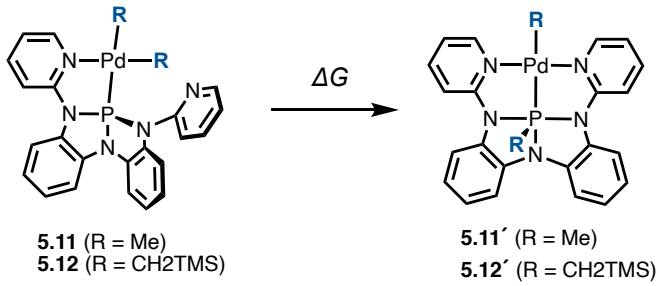


| | Δ*G* (kcal/mol) |
|---|---|
| **5.11** → **5.11´** (R=Me) | –21.4 |
| **5.12** → **5.12´** (R=$CH_2TMS$) | –19.5 |

Therefore, the selective formation of **5.12** is probably because of a high-energy transition state in the α-carbyl-transfer between **5.12** and **5.12′**. Based on this hypothesis, a $C_6D_6$ solution of **5.12** was heated at 80 ºC to induce the metallophosphorane formation. However, a decomposition proceeds to give an uncharacterized complex with a single resonance at δ 39.0 ppm in $^{31}P$ NMR and metallophosphorane **5.12′** was not observed.

### *5-5-4. Metalation of **L1** with (cod)PtMe$_2$*

**Scheme 5-6.** Metalation of **L1** with (cod)PtMe$_2$

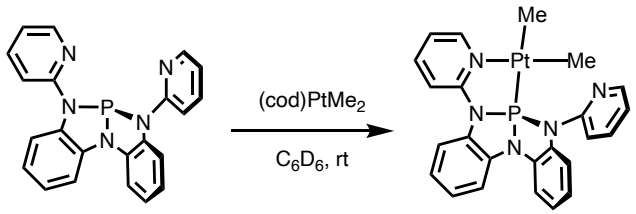


**L1** **5.13**

As observed in the case of bidentate ligand **L2**, the substitution of palladium with platinum also inhibited the P(III) insertion of **L1**. Metalation of **L1** with (cod)PtMe$_2$ in $C_6D_6$ afforded a diamagnetic complex **5.13** (Scheme 5-6). Complex **5.13** exhibits a $^{31}P$ NMR resonance corresponding to the triamido phosphorus nucleus at δ 160.5 ppm ($^{195}Pt$ satellite $^1J_{Pt–P}$ = 3044 Hz). This $^1J_{Pt–P}$ value is closer to **5.6**-*trans* ($^1J_{Pt–P}$ = 2600 Hz), in which the triamidophosphorus is in *trans* configuration to the Me ligand ($^1J_{Pt–P}$ = 6700 Hz for **5.6**-*cis*). In a $^1H$-coupled $^{31}P$ NMR spectrum of **5.13**, the signal at 160.5 ppm was observed as heptet with a coupling value of ~10 Hz. The corresponding coupling partners were found in the $^1H$ NMR spectrum; the resonances arising from six H nuclei of two Pt–Me moieties are observed as doublets at δ 0.43 ppm ($^3J_{P–H}$ = 10.7 Hz) and 0.40 ppm ($^3J_{P–H}$ = 9.9 Hz). The $^1H$ NMR spectrum suggests the $C_1$-symmetric structure in a

solution state and broadening of the $^{1}$H NMR signals is not observed in **5.13** at ambient temperature, probably due to the relatively robust metal–ligand bonding in Pt compared to Pd.

## 5-6. Reactivity of Dialkyl Group 10 Metal–phosphine Complexes

*5-6-1. Oxidative addition of RX to palladium complex **5.12***

The Pd or Pt center of these dialkyl complexes are expected to be electron-rich due to the strong σ-donor property of alkyl ligands. Therefore, we attempted to utilize the metal–phosphine type complexes **5.12** and **5.13** for bond activation chemistry analogous to the Rh(I) or Ir(I) complexes discussed in Chapter 4.

**Scheme 5-7.** Two-step transformation of **5.12** into **5.12´**

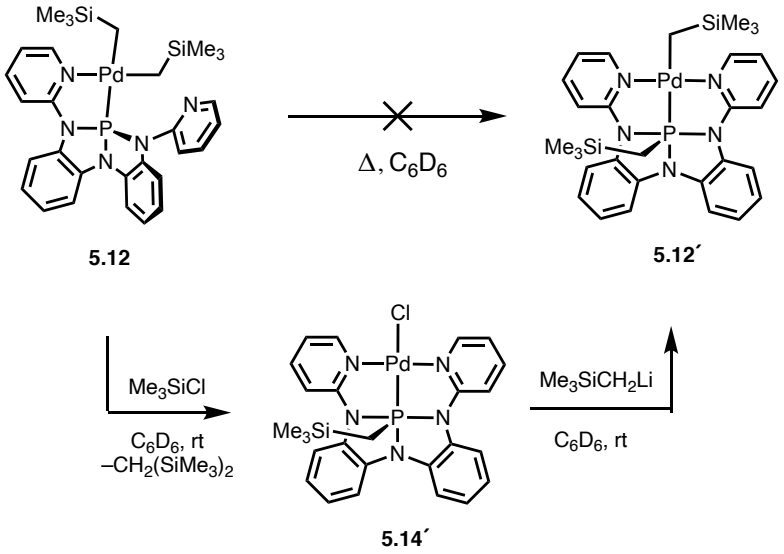


Treatment of **5.12** with trimethylsilyl chloride afforded a single diamagnetic product **5.14´** (The Pd or Pt center of these dialkyl complexes are expected to be electron-rich due to the strong σ-donor property of alkyl ligands. Therefore, we attempted to utilize the metal–phosphine type complexes **5.12** and **5.13** for bond activation chemistry analogous to the Rh(I) or Ir(I) complexes discussed in Chapter 4.

**Scheme 5-7**, *left*). The $^{31}$P NMR spectrum of **5.14´** showed a singlet resonance at δ –12.4 ppm. The dramatic upfield shift (Δδ = –166 ppm) suggested the formation of metallophosphorane. In the $^{1}$H-coupled $^{31}$P NMR spectrum, the signal at δ –12.4 ppm was further split into a triplet ($J_{P–H}$ = 15 Hz). The corresponding $^{1}$H NMR spectrum resolves the complementary coupling partner, with a doublet at δ 1.28 ppm ($^{2}J_{P–H}$ = 15 Hz) assigned to the *P*–methylene group. In addition, the chemical shifts of aromatic protons are almost identical between **5.14´** and **5.10´**. Taken together, compound **5.14´** was assigned as PdCl(**L1**$^{CH2TMS}$) formed by an intramolecular migration of a $CH_2TMS$ group from Pd to P. In a proposed mechanism of the formation of **5.14´**, an initial oxidative addition of trimethylsilyl chloride to **5.12** yields a $Pd^{IV}$–$PR_3$ complex followed by an intramolecular transfer of $CH_2TMS$ group, and then the reductive elimination of $CH_2(SiMe_3)_2$ gives the final $Pd^{II}$ metallophosphorane **5.14´** (**Error! Not a valid bookmark self-reference.**). However, there are many other possible mechanisms and the mechanistic investigation is underway. Treatment of **5.12** with other RX (allyl bromide, benzyl bromide, iodomethane, iodobenzene, methyl triflate, trimethylsilyl acetate, trimethylsilyl cyanide trimethyl(thiophenyl)silane) also yielded corresponding metallophosphoranes PdX(**L1**$^{CH2TMS}$) *via* intramolecular $CH_2TMS$ migration. The intramolecular migration of R groups from Pd to $PR_3$ provides another important method to access metallophosphoranes with various P–substituents and *trans*-ligands.

**Scheme 5-8**. Proposed mechanism of formation of **5.14´**

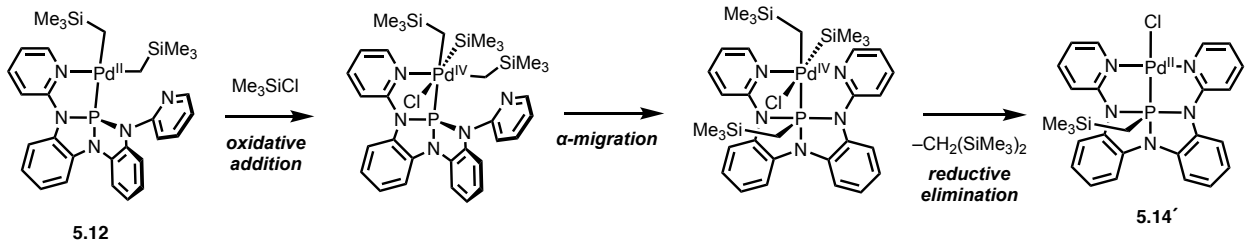

Metallophosphorane **5.12′**, which was not accessible by an intramolecular $CH_2TMS$ transfer from **5.12**, can be synthesized by transmetalation of **5.14′** (The Pd or Pt center of these dialkyl complexes are expected to be electron-rich due to the strong σ-donor property of alkyl ligands. Therefore, we attempted to utilize the metal–phosphine type complexes **5.12** and **5.13** for bond activation chemistry analogous to the Rh(I) or Ir(I) complexes discussed in Chapter 4.

**Scheme 5-7**, *right*). Treatment of **5.14′** with excess $TMSCH_2Li$ gives a single product, which shows a singlet resonance corresponding to the triamidophosphorus nucleus at δ 23.6 ppm. The product was assigned to **5.12′** based on the chemical shift value close to **5.11′** (δ 20.7 ppm) and the observation of a triplet of triplet signal ($J_{P–H}$ = 21 Hz, 13 Hz) in the $^{1}H$-coupled $^{31}P$ NMR spectra. The fact that the transmetalation did not return the starting material **5.12** supports the computational result that **5.14′** is significantly more stable than **5.14**.

We also investigated the formed P–C bonds of these metallophosphoranes. However, different from the rich reactivity of P–H bonds of the metallohydrophosphoranes synthesized in Chapter 3 or 4, all attempts to cleave the formed P–C bonds have not been successful, particularly because the cleavage of P–N bonds (weaker than P–C bonds) in triamidophosphorus frameworks are prioritized.

### *5-6-2. Stepwise and cooperative oxidative addition to platinum complex **5.13***

Considering the general stability of Pt(IV) species compared to Pd(IV), analogous reaction was attempted for platinum dimethyl complex **5.13** to isolate the oxidative addition product. Treatment of **5.13** with excess methyl triflate in $C_6D_6$ immediately afforded precipitates of formal $Pt^{IV}$ complex **5.15** (Scheme 5-9).

**Scheme 5-9.** Addition of MeOTf to **5.13** followed by fluoride addition.

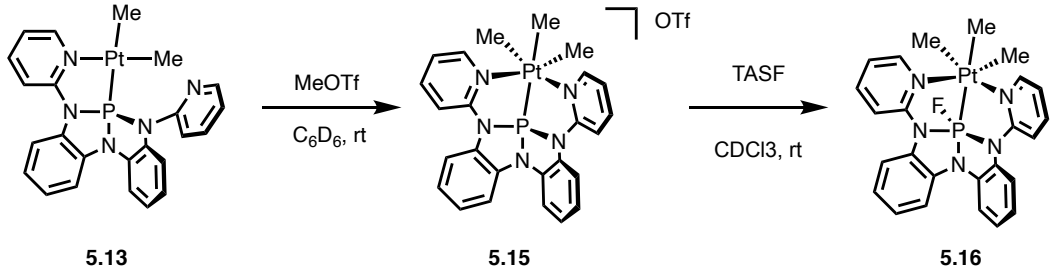


Importantly, the triamidophosphorus moiety resonates in high-field region at δ 160.5 ppm in the $^{31}$P NMR, suggesting there was no increasing in P coordination number (Figure 5-9b). In the $^{1}$H NMR spectrum, two distinct doublet signals at δ 1.36 ppm and the other at δ 1.05 ppm (the ratio of the signal areas is 1:2) suggests three Pt–Me groups in $C_s$ symmetry. Taken together, a nucleophilic attack of Pt to MeOTf forms a cationic octahedral $Pt^{IV}$ trimethyl complex with a counter anion $OTf^{-}$, without an intramolecular migration of any Me groups.

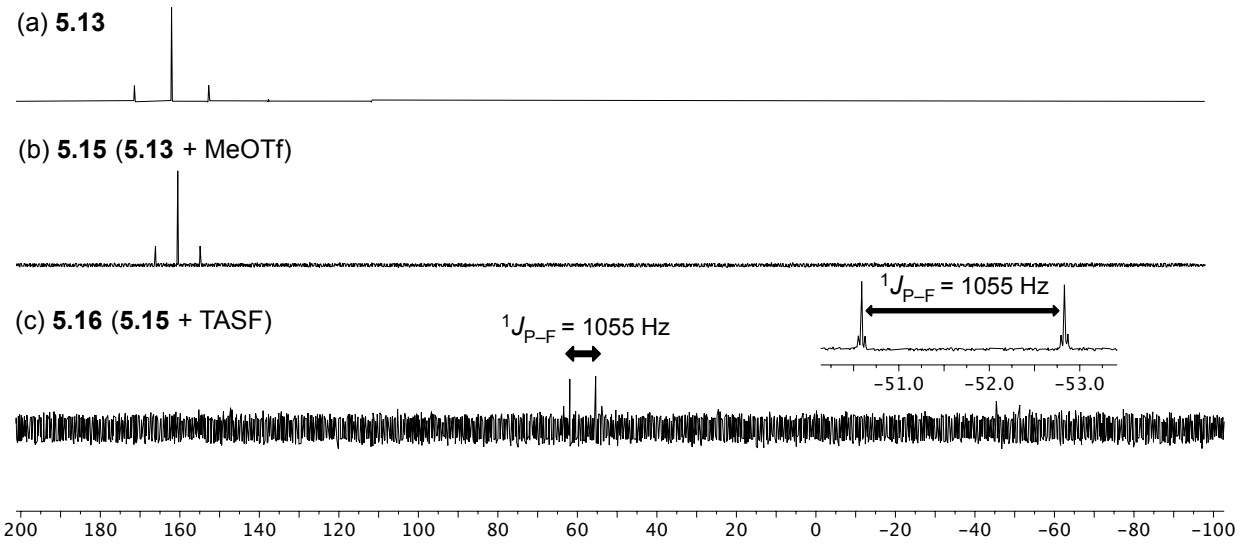


**Figure 5-9.** $^{31}$P NMR spectra of (a) **5.13** in $C_6D_6$ and (b) **5.5**, (c) **5.16** in $CDCl_3$. Units are ppm relative to 85% $H_3PO_4$. (Inset) $^{19}$F NMR spectrum of **5.16** in $CDCl_3$.

Since compound **5.15** is a cationic complex with a saturated metal center with a nontrigonal P(III) ligand, a fluoride addition to the phosphorus was attempted as previously reported in our

group.[51] Treatment of **5.15** with tris(dimethylamino)sulfonium trimethyldifluorosilicate (TASF) in chloroform resulted in formation of a single new complex **5.16**, indicated by a doublet resonance at δ 58.7 ppm in the $^{31}$P NMR spectrum (Figure 5-9c). A large coupling constant ($J$ = 1055 Hz) is due to a single fluorine bound to the phosphorus and the corresponding coupling partner is found as a doublet in the $^{19}$F NMR spectrum at δ –51.7 ppm ($J$ = 1055 Hz. Figure 5-9 inset). Considering the little difference in the $^{1}$H NMR signals from **5.15**, complex **5.16** is tentatively assigned to the desired metallofluorophosphorane. The stepwise synthesis of **5.16** from **5.13** demonstrates the bifuncionality of the Pt–P bond of **5.13**; the nucleophilic attack by the Lewis-basic Pt center to MeOTf yields **5.15**, followed by a $F^-$ addition to the Lewis-acidic P center. Different from Pd systems, the migration of Me from M to P does not proceed easily in Pt complexes, keeping the acceptor property of P center available.

Then we also attempted a one-step, metal–ligand cooperative bond activation by **5.13** and targeted $B^{\delta+}$–$H^{\delta-}$ bond as an initial target, inspired by our previous work of cooperative addition of HBpin by a P–N bond of our nontrigonal phosphorus triamide **2.1** (Scheme 5-10).[52]

**Scheme 5-10**. Activation of pinacolborane by nontrigonal phosphorus triamide **2.1**.

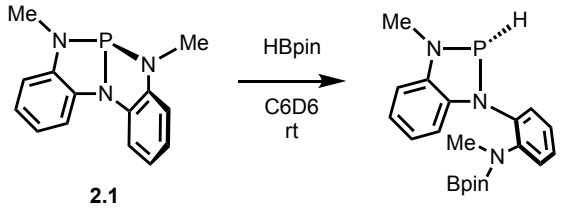


**2.1**

**Scheme 5-11**. Cooperative B–H activation by **5.13**.

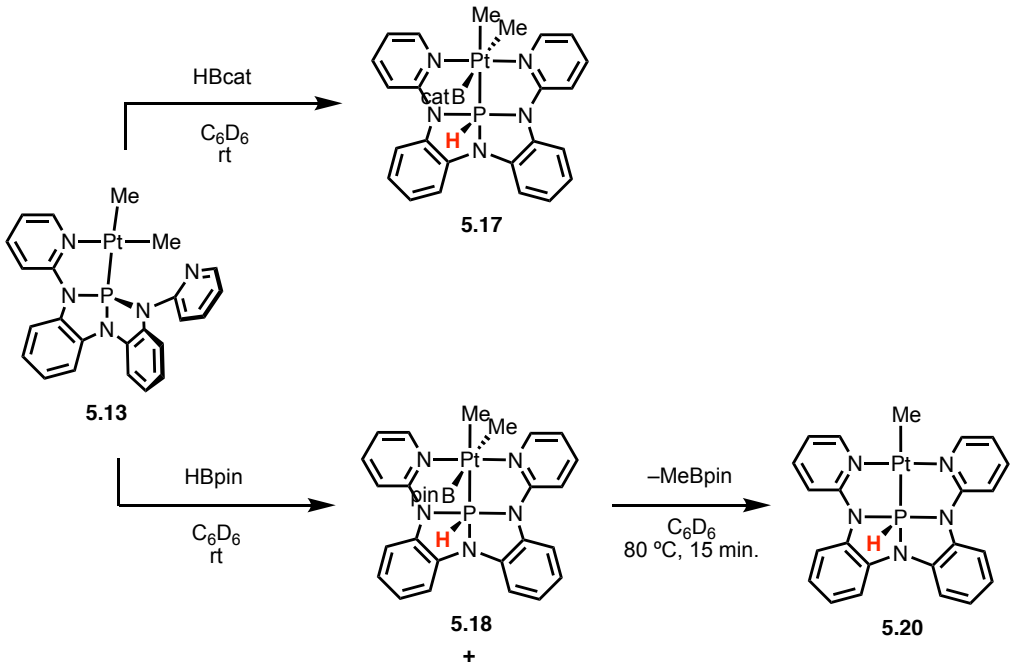


Treatment of **5.13** with excess catecholborane in $C_6D_6$ at ambient temperature affords a single product **5.17** with a $^{31}P\{^1H\}$ NMR resonance at δ 104.9 ppm ($^1J_{Pt–P}$ = 2185 Hz) (Figure 5-10b). In fully-coupled $^{31}P$ NMR spectrum, the signal is further split with a large coupling constant ($J$ = 350 Hz), suggesting formation of a P–H bond. The coupling partner was found in $^1H$ NMR as a doublet at 7.81 ppm ($^1J_{P–H}$ = 2185 Hz). The $^1H$ NMR spectra also showed two-fold equivalence of resonances for aryl region and two doublet signals at 1.25 ppm and 1.46 ppm corresponding to two Pt–Me groups. Given the following: (1) the presence of a P–H bond. (2) $C_s$ symmetry in solution state, and (3) the presence of two distinct Pt–Me groups, complex **5.17** was tentatively assigned as a cooperative B–H activation product described in Scheme 5-11.

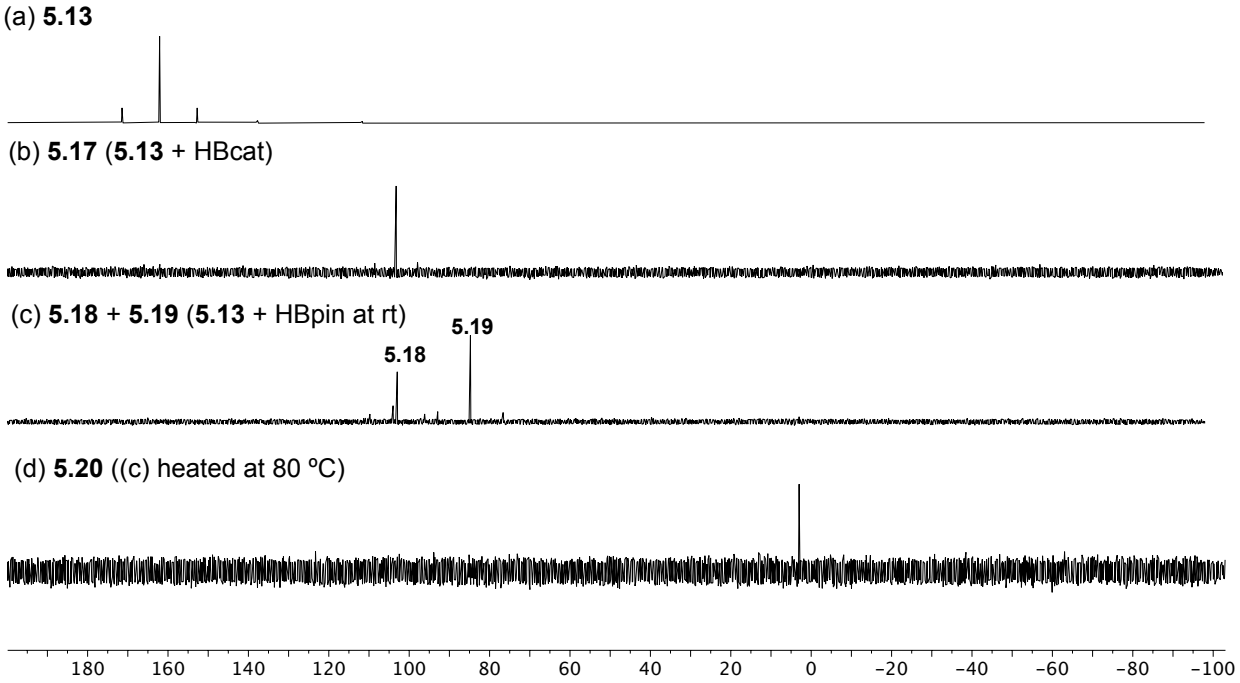


**Figure 5-10.** $^{31}P$ NMR spectra of (a) **5.13** (b) **5.17**, (c) **5.18** + **5.19** (d) **5.20** in $C_6D_6$. Units are ppm relative to 85% $H_3PO_4$.

Analogous treatment of **5.13** with pinacolborane initially yields a mixture of two products **5.18** (minor) and **5.19** (major) with similar spectroscopic features to **5.17**; $^{31}P$ NMR spectra show resonances at δ 104.9 ppm ($^1J_{Pt-P}$ = 2209 Hz, $^1J_{P-H}$ = 341 Hz) for **5.18** and δ 84.8 ppm ($^1J_{Pt-P}$ = 2635 Hz, $^1J_{P-H}$ = 325 Hz) for **5.19**, respectively (Figure 5-10c). Corresponding coupling partners in $^1H$ NMR spectra are also found at δ 8.00 ppm ($^1J_{P-H}$ = 341 Hz) for **5.18** and δ 9.54 ppm ($^1J_{P-H}$ = 325 Hz) for **5.19**, respectively. Identity of minor product **5.19** was not determined but considered to be a stereoisomer of **5.18**. Upon heating the mixture at 80 ºC for 15 min., decomposition of both products yields a single product **5.20** with a resonance in $^{31}P$ NMR at 3.0 ppm ($^1J_{Pt-P}$ = 2528 Hz, $^1J_{P-H}$ = 481 Hz) (Figure 5-10d). Formation of $CH_3Bpin$ was observed with the *in-situ* recorded NMR spectra, indicating the process is a Pt-centered reductive elimination to give Pt(II) metallophosphorane **5.20**.

Unfortunately, the low stability of **5.17**-**5.20** prevented further characterization of these products. Yet, the result supports the expected cooperative bond activation based on the polarized Pt–P bond of **5.13**, which is distinct from the intramolecular migration-based reactivity of Pd(II) systems.

## 5-7. Conclusion and Outlook

In this chapter, the net insertion of geometrically distorted phosphorus center into Group 10 metal–carbon bonds will be presented. The insertion reactivity can be rationalized by periodic variation in M–C bond enthalpies within Group 10 triads. The work demonstrates direct and general access to unusual metal complexes with higher-coordinate ligands and opens a door to the development of novel types of bond activation and group transfer processes. The periodic trend of insertion reactivity into M–C bonds affects other reactivity, such as oxidative addition, as demonstrated by the distinct reactivity of Pd(II) and Pt(II) dialkyl complexes. In Pd(II) systems, the facile migration of an R group from Pd to P yields stable metallophosphoranes and blocks the P-acceptor character. In Pt(II) systems without intramolecular R-group migration, however, the phosphorus atom remains available as a Lewis-acidic ligand upon oxidative addition, enabling the cooperative addition to the Pt–P bond.

The observed reactivity trend of the Pd(II) and Pt(II) systems is reminiscent of the Rh(I) and Ir(I) complexes discussed in Chapter 4. The group 9 complexes are easier systems to investigate and understand the cooperative reactivity due to the bistability of low and high oxidation states ($Rh^{I}/Rh^{III}$ or $Ir^{I}/Ir^{III}$). However, group 10 systems discussed in Chapter 5 show the faster reductive elimination to recover the original oxidation states ($Pd^{IV}$ to $Pd^{II}$ or $Pt^{IV}$ to $Pt^{II}$), which is also essential to design catalytic transformation based on these systems. Investigation along this line is currently underway.

## 5-8. Experimental Section

### *5-8-1. General Consideration and Methods*

**General Consideration.** All reactions were carried out on the benchtop inside a fume hood. All reagents were purchased from Sigma-Aldrich, Alfa Aesar, ACROS, TCI, or Oakwood Chemical, and used as received unless otherwise noted. Bis(2-aminophenyl)amine[53] (cod)Pt(Me)(Cl)[54], Ni(Me)(Cl)$(PMe_3)_2$[55] and **L1**[56] were prepared as previously reported. Cross couplings were carried out in sealed heavy-walled reaction flasks (Chemglass Part # CG-1880-R-03) fitted with perfluoro O-rings (Chemglass part #CG-309-220). Column chromatography was carried out on silica gel (SiliFlash® Irregular Silica Gel, P60 40-63μm). Thin layer chromatography was performed using Analtech aluminum backed fluorescent silica gel (UV254). All reactions were heated in temperature controlled silicone oil baths where the oil level reached at least ¾ of the reaction volume at any time. All yields are isolated yields of purified products. All metalation chemistry and handling of the resulting compounds was performed in a VAC-Atmospheres Nexus II nitrogen filled glovebox. All solvents in the glove box were taken from a Glass Contour Solvent Purification System utilizing alumina columns and solvents degassed/stored under argon gas. All vials and pipettes in the glovebox were heated to 120°C for a minimum of 24 h in an oven before being brought into the glovebox.

NMR spectra were recorded on a Varian Inova-500 (500 MHz) spectrometer at the MIT Department of Chemistry Instrumentation Facility and processed with a MestReNova software. $^1$H NMR chemical shifts are given in ppm with respect to solvent residual peak ($CDCl_3$, δ 7.26 ppm; $CD_2Cl_2$, δ 5.32 ppm; $C_6D_6$, δ 7.16 ppm), $^{13}C\{^1H\}$ NMR shifts are given in ppm with respect to ($CDCl_3$ δ 77.16 ppm, $CD_2Cl_2$ δ 53.84 ppm, $C_6D_6$ δ 128.06 ppm,).,[57] while $^{31}P\{^1H\}$ NMR spectra

were externally referenced to 85% $H_3PO_4$. Multiplicities are described as s = singlet, brs = broad singlet, d = doublet, t = triplet, q = quartet, dd = doublet of doublets, td = triplet of doublets, m = multiplet. Coupling constants are reported as J-values in Hz. High-resolution mass spectra were obtained at the Mass Spectrometry Laboratory in the Department of Chemistry Instrumentation Facility, MIT, using either Agilent QTOF 6545 with ESI ionization source or a JEOL AccuTOF-DART (JMST100LP, ionSense DART source).

X-ray structures of complexes **5.6**, **5.7′** and **5.10′** were collected using 0.24797 Å radiation at temperature of 15 K (Oxford Diffraction Helijet) on a vertical mounted Bruker D8 three-circle platform goniometer equipped with an Apex II CCD at ChemMatCARS located at Advances Photon Source (APS), Argonne National Laboratory (ANL). Structures were solved and refined as described above. X-ray structures of compounds **L2**, **5.8′** and **5.12** data were collected on a Bruker three-circle platform goniometer equipped with an Apex II CCD and an Oxford cryostream cooling device operating at 100 K. Radiation was from a graphite fine focus sealed tube Mo Kα (0.71073 Å) source. Crystals were mounted on a glass fiber pin using Paratone N oil. Data was collected as a series of φ and/or ω scans. Data was integrated using SAINT and scaled with multi-scan absorption correction using SADABS.[58] The structures were solved by intrinsic phasing using SHELXT (Apex3 program suite v2016.1.0) and refined against F2 on all data by full matrix least squares with SHELXL-97.[59] All non-hydrogen atoms were refined anisotropically. H atoms were placed at idealized positions and refined using a riding model. Olex 2[60] was used for the solution of structures.

*5-8-2. Synthetic Procedures*

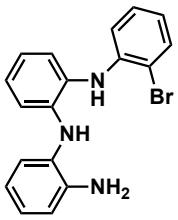

5.2

**Synthesis of N1-(2-aminophenyl)-N2-(2-bromophenyl)benzene-1,2-diamine (5.2).** Bis(2-aminophenyl)amine **5.1** (4.00g, 20.1 mmol, 1.00 eq), $Pd_2(dba)_3$ (405 mg, 0.44 mmol, 2.20 mol%), Xantphos (477 mg, 0.82 mmol, 4.1 mol%), NaO$^t$Bu (2.89 g, 30.2 mmol, 1.50 eq), and 80 mL of toluene were combined in a 200 mL Schlenk flask equipped with a stir bar. The Schlenk flask was sealed with a rubber septum and removed from the glovebox. Bromoiodobenzene (5.96 g, 21.1 mmol, 1.05 eq) was then injected using a syringe. The resulting reaction mixture was heated to 110 °C with vigorous stirring for 3 h. After it was cooled to room temperature, the mixture was filtered through a bed of silica, which was then washed with $CH_2Cl_2$ (40 mL). The compound was further purified using ethyl acetate/hexanes (20% EtOAc). The appropriate fractions ($R_f$ = 0.45 in 20% EtOAc) were collected and evaporated to dryness yielding (**5.2**) as a yellow gel (2.05 g, 28.0% yield). $^1$H NMR (500 MHz, $CD_3Cl$-$d_1$, 23 °C) δ (ppm): 7.52 (d, *J* = 7.5 Hz, 1H), 7.21 (d, *J* = 7.6 Hz, 1H), 7.15 (t, *J* = 7.7 Hz, 1H), 7.11 (t, *J* = 7.6 Hz, 1H), 7.04 (dd, *J* = 7.7, 12.1 Hz, 2H), 6.85 (t, *J* = 7.6 Hz, 1H), 6.80 (dd, *J* = 7.7, 14.4 Hz, 2H), 6.75 (dd, *J* = 4.6, 8.0 Hz, 2H), 6.71 (d, *J* = 7.5 Hz, 1H), 5.87 (s, 1H), 5.62 (br, 1H), 4.04 (br, 2H). $^{13}$C{$^1$H} NMR (126 MHz, $CD_3Cl$-$d_1$, 23 °C) δ (ppm): 143.1, 141.8, 141.6, 132.9, 128.5, 128.2, 128.0, 127.0, 126.4, 126.2, 125.6, 120.2, 119.7, 119.6, 116.5, 114.9, 114.7, 111.0. HRMS (DART) m/z calc for $C_{18}H_{17}BrN_3$ $[M+H]^+$: 354.0600, found 354.0591.

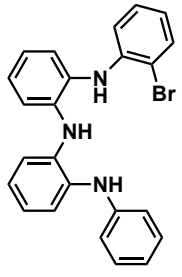

5.3

**Synthesis of N1-(2-bromophenyl)-N2-(2-(phenylamino)phenyl)benzene-1,2-diamine (5.3).** Copmound **5.2** (1.90g, 5.36 mmol, 1.00 eq), $Pd_2(dba)_3$ (110 mg, 0.12 mmol, 2.20 mol%), Xantphos (128 mg, 0.22 mmol, 4.1 mol%), NaO$^t$Bu (774 mg, 8.09 mmol, 1.50 eq), and 25 mL of toluene were combined in a 100 mL

Schlenk flask equipped with a stir bar. The Schlenk flask was sealed with a rubber septum and removed from the glovebox. Iodobenzene (1.09 g, 5.36 mmol, 1.00 eq) was then injected using a syringe. The resulting reaction mixture was heated to 110 °C with vigorous stirring for 3 h. After it was cooled to room temperature, the mixture was filtered through a bed of silica, which was then washed with $CH_2Cl_2$ (40 mL). The compound was further purified using ethyl acetate/hexanes (2% EtOAc). The appropriate fractions ($R_f$ = 0.30 in 2% EtOAc) were collected and evaporated to dryness yielding **5.3** as a yellow gel (1.41 g, 61.1% yield). $^1$H NMR (500 MHz, $CD_3Cl$-$d_1$, 23 °C) δ (ppm): 7.55 (d, *J* = 7.9 Hz, 1H), 7.34 (d, *J* = 7.5 Hz, 1H), 7.27 (t, *J* = 7.4 Hz, 3H), 7.16 (dt, *J* = 7.4, 15.2 Hz, 3H), 7.09 (d, *J* = 7.9 Hz, 1H), 7.04 (br, 2H), 6.98 (br, 4H), 6.84 (d, *J* = 8.1 Hz, 1H), 6.76 (t, *J* = 7.6 Hz, 1H), 5.95 (br, 3H). $^{13}$C{$^1$H} NMR (126 MHz, $CD_3Cl$-$d_1$, 23 °C) δ (ppm): 143.9, 142.7, 139.4, 135.6, 134.5, 132.9, 130.6, 129.5, 128.5, 126.1, 125.1, 123.8, 123.2, 121.5, 120.9, 120.6, 120.3, 117.8, 117.5, 115.1, 111.5. HRMS (DART) m/z calc for $C_{24}H_{21}BrN_3$ $[M+H]^+$: 430.0913, found 430.0903.

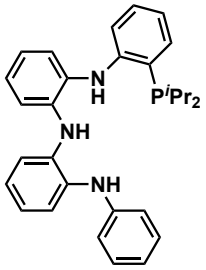


5.4

**Synthesis of N1-(2-diisopropylphosphinophenyl)-N2-(2-(phenylamino) phenyl)benzene-1,2-diamine (5.4).** A 100 mL round bottom flask equipped with a stir bar was charged with $Pd(OAc)_2$ (5.3 mg, 0.023 mmol, 4.0 mol%), DiPPF (11.6 mg, 0.028 mmol, 4.9 mol%), and toluene (4 mL). After the mixture was stirred for 5 min, NaO$^t$Bu (78.0 mg, 0.812 mmol, 1.40 eq) was added, followed by diisopropylphosphine (68.7 mg, 0.581 mmol, 1.00 eq). The round flask was sealed with a cap containing a PTFE septum and removed from the glovebox. Compound **5.3** (250.0 mg, 0.581 mmol, 1.00 eq) in toluene (2 mL) was added via syringe. The vial was then heated to 110 °C with vigorous stirring for 21 h, at which point complete conversion was confirmed by $^1$H and $^{31}$P

NMR of an aliquot of the reaction mixture. The cooled reaction mixture was then filtered through a bed of silica and washed with $CH_2Cl_2$ (20 mL). The solution was concentrated, and the resulting crude material was purified by flash chromatography (ethyl acetate/hexanes (2% EtOAc)), giving the product **5.4** as a yellow oil in 75.2% yield (204.3 mg, 0.437 mmol). $^1$H NMR (500 MHz, $CD_3Cl$-$d_1$, 23 °C) δ (ppm): 7.31 (d, *J* = 7.4 Hz, 2H), 7.22 (ddd, *J* = 25.4, 13.7, 8.6 Hz, 5H), 7.04 (t, *J* = 8.6 Hz, 3H), 6.94 (qd, *J* = 15.6, 7.4 Hz, 6H), 6.82 (m, 2H), 5.92 (s, 1H), 5.63 (s, 1H), 2.14 (m, 2H), 1.12 (dd, *J* = 15.8, 6.9 Hz, 6H), 0.93 (dd, *J* = 12.0, 6.9 Hz, 6H). $^{13}$C{$^1$H} NMR (126 MHz, $CD_3Cl$-$d_1$, 23 °C) δ (ppm): 150.8 (d, *J* = 18.5 Hz),143.8, 139.1, 135.9, 134.2, 133.3, 131.9, 130.0, 129.3, 125.1, 124.2, 123.3, 122.6, 121.2, 121.1, 120.7, 119.4, 119.3, 118.9, 117.7, 116.9, 114.0, 23.3 (d, *J* = 9.0 Hz), 20.2 (d, *J* = 17.9 Hz), 18.9 (d, *J* = 8.2 Hz). $^{31}$P{$^1$H} NMR (203 MHz, $CD_3Cl$-$d_1$) δ (ppm): –16.0 (s). HRMS (DART) m/z calc for $C_{30}H_{35}N_3P$ $[M+H]^+$: 468.2563, found 468.2573.

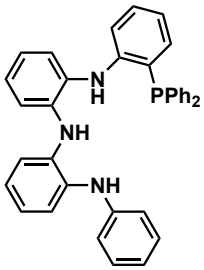


**5.5**

**Synthesis of N1-(2-diphenylphosphinophenyl)-N2-(2-(phenylamino)phenyl) benzene-1,2-diamine (5.5).** A 100 mL round bottom flask equipped with a stir bar was charged with $Pd(OAc)_2$ (5.5 mg, 0.024 mmol, 4.00 mol%), DiPPF (12.1 mg, 0.029 mmol, 4.78 mol%), and toluene (4 mL). After the mixture was stirred for 5 min, NaO$^t$Bu (81 mg, 0.843 mmol, 1.40 eq) was added, followed by diphenylphosphine (113 mg, 0.607 mmol, 1.00 eq). The round flask was sealed with a cap containing a PTFE septum and removed from the glovebox. Compound **5.3** (261.4 mg, 0.607 mmol, 1.00 eq) in toluene (2 mL) was added via syringe. The vial was then heated to 110 °C with vigorous stirring for 21 h, at which point complete conversion was confirmed by $^1$H and $^{31}$P NMR of an aliquot of the reaction mixture. The cooled reaction mixture was then filtered through a bed of

silica and washed with $CH_2Cl_2$ (20 mL). The solution was concentrated, and the resulting crude material was purified by flash chromatography (ethyl acetate/hexanes (2% EtOAc)), giving the product **5.5** as a yellow oil in 68.0% yield (221 mg, 0.413 mmol). $^1$H NMR (500 MHz, $CD_3Cl$-$d_1$, 23 °C) δ (ppm): 7.33 (m, 10H), 7.26 (dd, *J* = 15.7, 7.9 Hz, 4H), 7.13 (d, *J* = 7.7 Hz, 1H), 7.01 (t, *J* = 7.5 Hz, 2H), 6.94 (m, 5H), 6.86 (m, 5H), 6.13 (d, *J* = 5.8 Hz, 1H), 5.48 (s, 1H), 5.40 (s, 1H). $^{13}$C{$^1$H} NMR (126 MHz, $CD_3Cl$-$d_1$, 23 °C) δ (ppm): 147.7, 147.6, 143.6, 138.8, 135.2, 135.1, 134.3, 133.9, 133.7, 133.6, 131.3, 130.3, 129.4, 129.1, 128.8, 128.7, 125.2, 124.2, 123.6, 123.1, 122.2, 122.0, 121.3, 120.7, 120.4, 118.6, 117.7, 117.4, 114.7. $^{31}$P{$^1$H} NMR (203 MHz, $CD_3Cl$-$d_1$) δ (ppm): –18.5 (s). HRMS (DART) m/z calc for $C_{36}H_{31}N_3P$ $[M+H]^+$: 536.2250, found 536.2243.

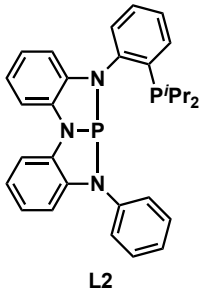

L2

**Synthesis of L2.** Triamine phosphine **5.4** (400 mg, 0.855 mmol, 1.00 eq) and triethylamine (259.5 mg, 2.565 mmol, 3.00 eq) was dissolved in THF/$Et_2O$ (1/2, 8 mL). To the solution was added phosphorus trichloride (0.075 mL, 0.855 mmol, 1.00 eq) dropwise via syringe. The reaction mixture was stirred at –78°C for 1 h and then warmed to room temperature. After 4 h of stirring at room temperature, the solvent was removed, and the resulting solid mixture was brought into a nitrogen-filled glovebox. The resulting thick white solid mixture was re-dissolved in $Et_2O$ (20 mL) and the suspension was pipette filtered through glass paper to remove triethylammonium salt. The filtrate was concentrated in vacuo to afford pure product of **L2** as off-white solids (288 mg, 0.581 mmol, 68.0%). $^1$H NMR (500 MHz, $C_6D_6$-$d_6$, 23 °C) δ (ppm): 7.41 (dd, *J* = 15.4, 7.4 Hz, 2H), 7.33 (d, *J* = 6.9 Hz, 1H), 7.07 (m, 5H), 6.93 (t, *J* = 7.2 Hz, 2H), 6.81 (m, 3H), 6.72 (m, 3H), 6.19 (d, *J* = 7.0 Hz, 1H), 1.77 (m, 1H), 1.60 (m, 1H), 0.93 (dd, *J* = 13.6, 6.4 Hz, 3H), 0.77 (m, 6H), 0.64 (dd, *J* = 11.5, 7.0 Hz, 3H). $^{13}$C{$^1$H}

NMR (126 MHz, $C_6D_6$-$d_6$, 23 °C) δ (ppm): 145.6 (dd, *J* = 24.4, 11.3 Hz), 142.0, 141.9, 141.6 (d, *J* = 8.0 Hz), 141.1, 141.0, 138.8, 138.6, 138.1, 134.4 (d, *J* = 2.2 Hz), 131.5, 130.3, 129.3, 127.4, 125.2, 125.0 (d, *J* = 5.7 Hz), 124.3, 124.0, 120.3, 119.8, 118.5 (d, *J* = 5.2 Hz), 117.9 (d, *J* = 5.3 Hz), 111.5, 111.3, 25.2 (d, *J* = 14.1 Hz), 21.0 (d, *J* = 8.0 Hz), 20.0 (dd, *J* = 38.3, 16.0 Hz). $^{31}P\{^1H\}$ NMR (203 MHz, $C_6D_6$-$d_6$) δ (ppm): 154.3 (d, *J* = 86.0 Hz), –7.93 (d, J = 86.0 Hz). HRMS (DART) m/z calc for $C_{30}H_{32}N_3P_2$ $[M+H]^+$: 496.2066, found 496.2062.

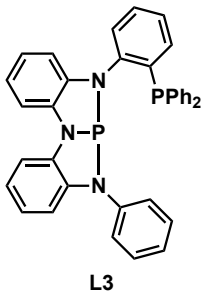

L3

**Synthesis of L3.** Triamine phosphine **5.5** (133 mg, 0.248 mmol, 1.00 eq) and triethylamine (75.3 mg, 0.744 mmol, 3.00 eq) was dissolved in THF/$Et_2O$ (1/2, 8 mL). To the solution was added phosphorus trichloride (0.022 mL, 0.249 mmol, 1.00 eq) dropwise via syringe. The reaction mixture was stirred at –78°C for 1 h and then warmed to room temperature. After 4 h of stirring at room temperature, the solvent was removed, and the resulting solid mixture was brought into a nitrogen-filled glovebox. The resulting thick white solid mixture was re-dissolved in $Et_2O$ (20 mL) and the suspension was pipette filtered through glass paper to remove triethylammonium salt. The filtrate was concentrated in vacuo to afford pure product of **L3** as off-white solids (116 mg, 0.206 mmol, 83.0%). Crystals suitable for single-crystal diffraction analysis were obtained from a slow diffusion of pentane into an $Et_2O$ solution at −35 °C. $^1H$ NMR (500 MHz, $C_6D_6$-$d_6$, 23 °C) δ (ppm): 7.43 (d, *J* = 6.7 Hz, 1H), 7.38 (d, *J* = 7.6 Hz, 1H), 7.33 (d, *J* = 7.9 Hz, 1H), 7.26 (br, 2H), 7.22 (d, *J* = 7.8 Hz, 2H), 7.09 (m, 1H), 7.02 (dt, *J* = 15.5, 7.4 Hz, 5H), 6.94 (br, 5H), 6.88 (m, 6H), 6.65 (t, *J* = 7.6 Hz, 1H), 6.57 (t, *J* = 7.6 Hz, 1H), 5.87 (d, *J* = 7.7 Hz, 1H). $^{13}C$ NMR (101 MHz, Chloroform-*d*) δ 143.8 (dd, *J* = 24.2, 11.7 Hz), 142.6 (d, *J* = 8.4 Hz), 141.1 (dd, *J* = 5.9, 2.3 Hz), 140.6 (d, *J* = 14.0 Hz), 140.2

(d, $J$ = 18.2 Hz), 139.5 (d, $J$ = 5.9 Hz), 137.4, 135.5, 134.3 (d, $J$ = 22.0 Hz), 133.4 (d, $J$ = 19.0 Hz), 130.7, 129.3, 128.5, 128.3 (d, $J$ = 5.9 Hz), 128.1, 128.0, 125.4, 125.0 (d, $J$ = 6.8 Hz), 124.7, 123.6, 120.6, 119.1, 118.8 (d, $J$ = 6.1 Hz), 116.8 (d, $J$ = 4.6 Hz), 111.89, 110.72. $^{31}P\{^{1}H\}$ NMR (203 MHz, $C_6D_6$-$d_6$) δ (ppm): 155.6 (d, $J$ = 48 Hz), –16.4 (d, J = 47 Hz). HRMS (DART) m/z calc for $C_{36}H_{28}N_3P_2$ $[M+H]^+$: 564.1753, found 564.1747.

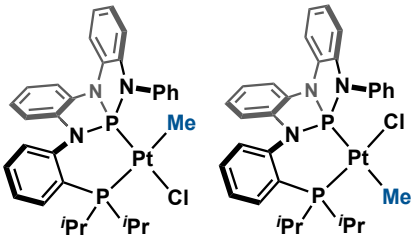


**5.6**-*cis* **5.6**-*trans*

**Synthesis of PtClMe$^{i}$Pr$_2$PNNNP (5.6).** A solution of **L1** (20 mg, 0.04 mmol, 1.00 eq) in 2 mL of $C_6H_6$ was added to a solution of (cod)Pt(Me)(Cl) (14.4 mg, 0.04 mmol, 1.00 eq) in 2 mL of $C_6H_6$ to prompt an immediate color change to light yellow/green. After stirring at ambient temperature for 0.5 h, the reaction mixture was concentrated to dryness and the residue was taken up in $Et_2O$ and solvent was decanted, and the residue was dried *in vacuo* to afford 27.2 mg of the title compound as an off-white solid (90.0% yield). The solid was re-dissolved in $CHCl_3$ and the resulting light-yellow solution was filtered through a tightly packed glass paper pipette filter and placed in a pentane diffusion chamber to grow colorless block shaped crystals. If upon complete diffusion of pentane into the solution the crystal yield is low, the vial was placed in a freezer at −35 °C for 24 h prior to crystal collection. The supernatant was removed and the crystals washed with additional pentane. The crystals were then dried under vacuum to yield a mixture of **5.6**-*cis* and **5.6**-*trans* as a white crystalline material. Crystals suitable for single-crystal diffraction analysis were obtained from a slow diffusion of pentane into an $CHCl_3$ solution at 25 °C. $^{1}H$ NMR (500 MHz, $CDCl_3$-$d_1$) δ 7.66 (tt, $J$ = 17.7, 8.0 Hz, 5H), 7.57 (d, $J$ = 7.4 Hz, 1H), 7.54 – 7.35 (m, 3H), 7.13 (d, $J$ = 7.2 Hz, 1H), 6.95 (q, $J$ = 7.1

Hz, 5H), 6.81 (d, $J$ = 7.5 Hz, 0H), 6.77 (d, $J$ = 7.6 Hz, 1H), 6.49 – 6.44 (m, 0H), 6.42 (d, $J$ = 7.3 Hz, 1H), 3.09 (dt, $J$ = 13.6, 6.9 Hz, 1H), 2.87 (d, $J$ = 39.9 Hz, 0H), 2.70 (dd, 1H), 2.59 (dt, $J$ = 13.3, 6.7 Hz, 0H), 1.37 (dd, $J$ = 15.4, 7.0 Hz, 3H), 1.16 (dd, $J$ = 16.0, 6.9 Hz, 1H), 0.58 (dd, $J$ = 16.9, 7.0 Hz, 4H), 0.53 (d, $J$ = 7.1 Hz, 1H). $^{31}P\{^{1}H\}$ NMR (203 MHz, $CDCl_3$-$d_1$) δ (ppm): **5.6**-*cis*: 100.2 (td, $^{1}J_{Pt-P}$ = 6700, $^{2}J_{P-P}$ = 28.0 Hz), 17.4 (td, $^{1}J_{Pt-P}$ = 1695, $^{2}J_{P-P}$ = 28.0 Hz). **5.6**-*trans*: 142.3 (td, $^{1}J_{Pt-P}$ = 2601, $^{2}J_{P-P}$ = 27.0 Hz), 15.9 (td, $^{1}J_{Pt-P}$ = 4048, $^{2}J_{P-P}$ = 27.0 Hz). $^{13}C$ NMR (126 MHz, $CDCl_3$-$d_1$) δ 143.15, 142.80 (d, $J$ = 8.5 Hz), 140.14 (d, $J$ = 6.7 Hz), 139.79, 139.69 (d, $J$ = 11.4 Hz), 139.25, 138.33, 137.16 (d, $J$ = 10.7 Hz), 136.77 (d, $J$ = 13.1 Hz), 136.56 (d, $J$ = 8.4 Hz), 136.03 (d, $J$ = 4.0 Hz), 135.94, 133.21, 132.69, 132.56, 132.13, 130.12, 129.91, 129.81, 129.60, 128.23, 128.17, 127.75, 127.68, 126.08 (d, $J$ = 5.0 Hz), 125.31, 124.58, 124.18, 124.12, 121.29 (d, $J$ = 11.4 Hz), 121.08 (d, $J$ = 5.5 Hz), 120.18 (d, $J$ = 33.4 Hz), 119.46 (d, $J$ = 10.2 Hz), 119.22 (d, $J$ = 8.9 Hz), 116.62 (d, $J$ = 8.9 Hz), 115.82 (d, $J$ = 10.0 Hz), 110.37, 110.28 (d, $J$ = 5.5 Hz), 109.17 (d, $J$ = 5.7 Hz), 108.52, 25.69 (d, $J$ = 38.6 Hz), 24.89, 24.67, 24.71 – 24.37 (m), 19.23 (d, $J$ = 4.4 Hz), 19.00 (d, $J$ = 94.1 Hz), 18.28 – 18.12 (m), 18.10, 16.83 (d, $J$ = 5.6 Hz), 16.53 (d, $J$ = 5.2 Hz), 5.96 (dd, $J$ = 149.7, 6.9 Hz), 3.76 (dd, $J$ = 85.8, 5.0 Hz). HRMS (DART) m/z calc for $C_{31}H_{34}N_3P_2Pt$ $[M\text{-}Cl]^+$: 705.1870, found 705.1868.

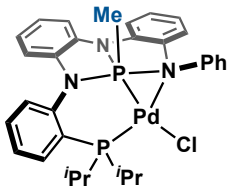

**5.7´**

**Synthesis of PdCliPr$_2$PNNNPMe (5.7´)** To a 20 mL scintillation vial was added **L2** (30 mg, 0.060 mmol, 1.00 eq), (cod)Pd(Me)(Cl) (16.2 mg, 0.060 mmol, 1.00 eq), and $C_6H_6$ (4.00g). The reaction immediately turned dark violet. The reaction was stirred using a small Teflon coated magnetic stir bar at ambient temperature for 1 h, during which time a light orange solution was observed. The mixture

was concentrated to dryness and the residue was washed with pentane twice and dried *in vacuo* to afford the title complex as a yellow solid (40 mg, 99% yield). The solid was re-dissolved in $PhCF_3$ and the resulting yellow solution was filtered through a tightly packed glass paper pipette filter and placed in a pentane diffusion chamber to grow yellow needle shaped crystals. The supernatant was removed and the crystals washed with additional pentane. If upon complete diffusion of pentane into the solution the crystal yield is low, the vial was placed in a freezer at −35 °C for 24 h prior to crystal collection. The crystals were then dried under vacuum to yield **5** as a yellow crystalline material. $^{1}$H NMR (500 MHz, $CD_2Cl_2$-$d_2$, 23 °C) δ (ppm): 7.90 (br, 1H), 7.74 (br, 1H), 7.64 (br, 2H), 7.57 (br, 1H), 7.52 (br, 2H), 7.28 (br, 3H), 7.18 (br, 1H), 7.12 (br, 1H), 7.05 (br, 2H), 6.89 (br, 2H), 6.78 (br, 1H), 2.81 (m, 1H), 2.20 (m, 1H), 1.60 (d, $J$ = 10.7 Hz, 3H),1.47 (m, 6H), 0.92 (d, $J$ = 15.9 Hz, 6H). $^{13}$C{$^{1}$H} NMR (126 MHz, $CD_2Cl_2$-$d_2$, 23 °C) δ (ppm):147.6, 144.7 (t, $J$ = 7,5 Hz), 138.2, 135.0 (d, $J$ = 2.8 Hz), 132.4, 132.1, 131.9, 129.8 (d, $J$ = 7.5 Hz), 129.2, 128.2 (d, $J$ = 4.0 Hz), 126.5, 125.1, 123.9, 122.4, 122.3 (d, $J$ = 5.3 Hz), 121.2, 118.4, 114.7 (d, $J$ = 7.8 Hz), 111.8 (d, $J$ = 7.0 Hz), 106.6, 26.1 (d, $J$ = 21.9 Hz), 22.7 (d, $J$ = 24.7 Hz), 19.8, 19.4 (d, $J$ = 5.4 Hz), 16.8 (dd, $J$ = 19.2, 4.5 Hz), 16.2 (d, $J$ = 7.8 Hz), 15.5 (d, $J$ = 8.2 Hz). $^{31}$P{$^{1}$H} NMR (203 MHz, $CD_2Cl_2$-$d_2$) δ (ppm): 31.0 (d, $^{2}J_{P-P}$ = 42.5 Hz), 0.50 (d, $^{2}J_{P-P}$ = 42.2 Hz). $^{31}$P NMR (203 MHz, $CD_2Cl_2$-$d_2$) δ (ppm): 30.9 (m), 0.50 (dq, $^{2}J_{P-P}$ = 42.2, $^{1}J_{P-C}$ = 10.5 Hz). Crystals suitable for single-crystal diffraction analysis were obtained from $PhCF_3$ solution layered with pentane at −35 °C. HRMS (DART) m/z calc for $C_{31}H_{35}ClN_3P_2Pd$ $[M+H]^+$: 652.1021 found 652.1025.

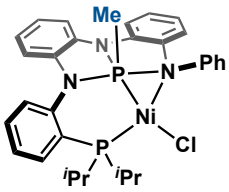

5.8´

**Synthesis of NiCliPr$_2$PNNNPMe (5.8´)** To a 20 mL scintillation vial was added **L2** (20 mg, 0.040 mmol, 1.00 eq), $(Me_3P)_2Ni(Me)(Cl)$ (11.6 mg, 0.040 mmol, 1.00 eq), and $C_6H_6$ (4 mL). The reaction immediately turned dark brown. The reaction was stirred using a small Teflon coated magnetic stir bar at ambient temperature for 1 h, during which time a light orange solution was observed. The mixture was concentrated to dryness and the residue was washed with pentane twice and dried *in vacuo* to afford the title complex as a yellow solid (8.8 mg, 37% yield). The solid was re-dissolved in toluene and the resulting yellow solution was filtered through a tightly packed glass paper pipette filter and placed in a pentane diffusion chamber to grow yellow needle shaped crystals. The supernatant was removed and the crystals washed with additional pentane. If upon complete diffusion of pentane into the solution the crystal yield is low, the vial was placed in a freezer at −35 °C for 24 h prior to crystal collection. The crystals were then dried under vacuum to yield **5.8´** as an orange crystalline material. Crystals suitable for single-crystal diffraction analysis were obtained from toluene solution layered with pentane at −35 °C. $^1$H NMR (500 MHz, $C_6D_6$) δ 7.84 (d, $J$ = 8.1 Hz, 1H), 7.57 (dd, $J$ = 5.9, 2.9 Hz, 1H), 7.52 (d, $J$ = 7.9 Hz, 1H), 7.10 (m, 4H), 7.01 (m, 4H), 6.87 (m, 2H), 6.76 (m, 4H), 2.11 (sepd, $J$ = 7.0, 4.0 Hz, 1H), 2.01 (sepd, $J$ = 7.1, 4.1 Hz, 1H), 1.56 (td, $J$ = 18.1, 16.9, 6.9 Hz, 6H), 1.11 (d, $J$ = 6.8 Hz, 3H), 0.96 (dd, $J$ = 17.1, 7.2 Hz, 1H), 0.47 (dd, $J$ = 13.5, 7.0 Hz, 3H). $^{13}$C NMR (101 MHz, $C_6D_6$) δ 148.77 (d, $J$ = 6.6 Hz), 145.60, 134.84, 132.45, 131.42, 129.67, 129.34, 129.18, 128.16 (d, $J$ = 2.4 Hz), 127.94, 126.49 (d, $J$ = 4.5 Hz), 125.70, 124.46, 124.11 (d, $J$ = 5.0 Hz), 123.24, 122.96, 122.27, 120.93, 119.32, 115.51 (d, $J$ = 7.1 Hz), 111.22 (d, $J$ = 6.9 Hz), 106.56, 25.23 (d, $J$ = 20.8 Hz), 22.31 (d, $J$ = 23.5 Hz), 20.05 (d, $J$ = 3.3 Hz), 19.50 (d, $J$ = 5.0 Hz), 17.70 (d, $J$ = 3.4 Hz), 16.70 (d, $J$ = 4.9 Hz), 14.28. $^{31}$P NMR (162

MHz, $CDCl_3$-$d_1$) δ 30.7 (d, *J* = 86 Hz), -14.9 (d, *J* = 87 Hz). HRMS (DART) *m/z* calc for $C_{31}H_{35}ClN_3P_2Ni$ $[M+H]^+$: 604.1343, found 604.1337.

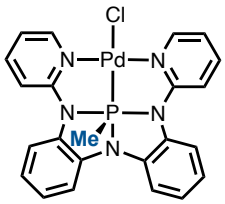

**5.10´**

**Synthesis of PdCl(L1$^{Me}$) (5.10´).** In a 20 mL scintillation vial (cod)PdClMe (10.0 mg, 0.038 mmol, 1.0 eq) was suspended in $C_6D_6$ (1 mL). To a vial was added a solution of **L1** (14.3 mg, 0.038 mmol, 1.0 eq) in $C_6D_6$ (1 mL) dropwise. The reaction mixture immediately turned orange. After stirred for 15 min, the mixture was concentrated to dryness and the residue was washed with pentane twice and dried *in vacuo* to afford the title complex as an orange solid (18 mg, 90%). Crystals suitable for single-crystal diffraction analysis were obtained from $CH_2Cl_2$ solution layered with pentane at –35 ºC. $^1$H NMR (400 MHz, $CDCl_3$) δ 9.43 (d, J = 6.1 Hz, 2H), 7.74 – 7.66 (m, 2H), 7.66 – 7.57 (m, 2H), 7.47 (d, J = 8.4 Hz, 2H), 7.31 (dd, J = 7.6, 1.5 Hz, 2H), 7.12 – 6.97 (m, 5H), 6.88 – 6.78 (m, 2H), 1.77 (d, J = 9.7 Hz, 3H). $^{13}$C NMR (101 MHz, $CDCl_3$) δ 152.5, 140.1, 131.3, 130.9 (d, *J* = 9.4 Hz), 122.5, 121.7, 116.2, 113.4, 112.8, 112.7, 109.9 (d, *J* = 4.4 Hz), 23.8 (d, *J* = 81 Hz). $^{31}$P NMR (162 MHz, $CDCl_3$) δ –17.2. HRMS (DART) *m/z* calc for $C_{23}H_{20}ClN_5PPd$ $[M+H]^+$: 538.0174, found 538.0192.

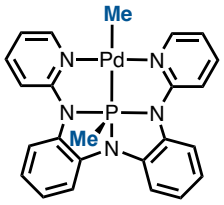

**5.11´**

**Synthesis of PdMe(L1$^{Me}$) (5.11´).** In a 20 mL scintillation vial (tmeda)$PdMe_2$ (11.9 mg, 0.047 mmol, 1.0 eq) was suspended in $C_6D_6$ (1 mL). To a vial was added a solution of **L1** (16.8 mg, 0.047 mmol, 1.0 eq) in $C_6D_6$ (1 mL) dropwise. The reaction mixture immediately turned orange. After stirred for 30 min, the mixture was concentrated to dryness and the residue was washed with pentane twice and dried *in*

*vacuo* to afford the title complex as an orange solid (18.6 mg, 77%). $^{1}$H NMR (400 MHz, $C_6D_6$) δ 8.67 (d, *J* = 5.9 Hz, 2H), 7.59 (dd, *J* = 7.4, 1.9 Hz, 2H), 7.06 (dd, *J* = 10.7, 8.2 Hz, 4H), 6.97 – 6.75 (m, 8H), 6.05 (t, *J* = 6.5 Hz, 2H), 1.44 (d, *J* = 3.4 Hz, 3H), 0.86 (d, *J* = 13.4 Hz, 3H). $^{31}$P NMR (162 MHz, $C_6D_6$) δ 20.7. HRMS (DART) *m/z* calc for $C_{24}H_{23}N_5PPd$ $[M+H]^+$: 518.0720, found 518.0410.

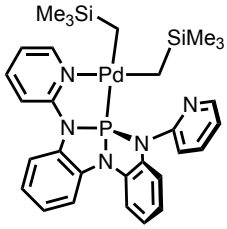

5.12

**Synthesis of Pd(CH$_2$TMS)$_2$(L1) (5.12).** In a 20 mL scintillation vial (cod)Pd(CH$_2$TMS)$_2$ (18.5 mg, 0.048 mmol, 1.0 eq) was suspended in toluene (1 mL). To a vial was added a solution of **L1** (18.7 mg, 0.049 mmol, 1.0 eq) in toluene (1 mL) dropwise. The reaction mixture immediately turned orange. After stirred for 15 min, the mixture was layered with pentane and left at –35 ºC overnight to afford colorless plate crystals (13.9 mg, 44%). Crystals suitable for single-crystal diffraction analysis were obtained from toluene solution layered with pentane at –35 ºC. $^{1}$H NMR (400 MHz, $C_6D_6$) δ 8.19 (s, 2H), 7.43 – 7.33 (m, 2H), 7.04 – 6.97 (m, 2H), 6.96 – 6.68 (m, 8H), 6.46 (dd, *J* = 7.4, 5.2 Hz, 2H), 0.91 (d, *J* = 14 Hz 2H), 0.70 (d, *J* = 14 Hz, 2H), 0.23 (s, 9H), 0.19 (s, 9H). $^{31}$P NMR (162 MHz, $C_6D_6$) δ 154.0. HRMS (DART) *m/z* calc for $C_{30}H_{39}N_5PPdSi_2$ $[M+H]^+$: 662.1511, found 662.1499.

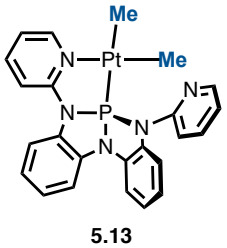

5.13

**Synthesis of PtMe$_2$(L1) (5.13).** In a 20 mL scintillation vial (cod)PdMe$_2$ (17.6 mg, 0.053 mmol, 1.0 eq) was suspended in toluene (1 mL). To a vial was added a solution of **L1** (20.2 mg, 0.053 mmol, 1.0 eq) in toluene (1 mL) dropwise. The colorless reaction mixture was stirred for 30 min and filtered. The filtrate

was layered with pentane and left at –35 ºC overnight to afford colorless plate crystals (14.2 mg, 44%). $^{1}$H NMR (400 MHz, $C_6D_6$) δ 8.98 (dd, *J* = 5.8, 1.8 Hz, 1H), 7.88 (dd, *J* = 4.9, 1.9 Hz, 1H), 7.36 (dd, *J* = 6.7, 2.3 Hz, 1H), 7.31 (dd, *J* = 7.6, 1.6 Hz, 1H), 7.12 (d, *J* = 8.1 Hz, 1H), 7.08 – 7.01 (m, 2H), 6.93 (td, *J* = 7.8, 2.0 Hz, 1H), 6.88 – 6.72 (m, 5H), 6.72 – 6.62 (m, 1H), 6.35 (dd, *J* = 7.3, 4.9 Hz, 1H), 6.30 (ddd, *J* = 7.2, 5.6, 1.3 Hz, 1H), 1.44 (d, *J* = 10 Hz, 3H), 1.34 (d, *J* = 11 Hz, 3H). $^{31}$P NMR (162 MHz, DMSO) δ 160.5 (d, Pt satellite $^{1}J_{Pt–P}$ = 3044 Hz). HRMS (DART) *m/z* calc for $C_{24}H_{23}N_5PPt$ $[M+H]^+$: 607.1336, found 607.1333.

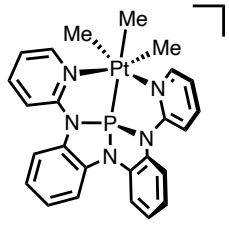

**5.15**

**Synthesis of [PtMe$_3$(L1)]OTf (5.15).** In a 20 mL scintillation vial (cod)PdMe$_2$ (43.7 mg, 0.131 mmol, 1.0 eq) was suspended in $C_6D_6$ (2 mL). To a vial was added a solution of **L1** (50.0 mg, 0.131 mmol, 1.0 eq) in $C_6D_6$ (2 mL) dropwise. The colorless reaction mixture was stirred for 30 min and filtered. To the resulting solution of **5.13** was added 3 drops of MeOTf and the immediately formed precipitate was collected by decantation and dried in vacuo. Recrystallization by slow diffusion of pentane into a dichloromethane solution at –35 ºC affords colorless crystals of **5.15**. $^{1}$H NMR (400 MHz, $CDCl_3$) δ 8.64 (d, *J* = 6.1 Hz, 2H), 8.23 (t, *J* = 8.1 Hz, 2H), 8.04 (d, *J* = 8.4 Hz, 2H), 7.80 (dd, *J* = 7.8, 1.5 Hz, 2H), 7.70 (d, *J* = 8.0 Hz, 2H), 7.45 – 7.25 (m, 8H), 1.36 (d, *J* = 10.3 Hz, 3H, $^{195}$Pt satellite $^{2}J_{Pt–H}$ = 63 Hz), 1.05 (d, *J* = 10.1 Hz, 6H, $^{195}$Pt satellite $^{2}J_{Pt–H}$ = 72 Hz). $^{31}$P NMR (162 MHz, $CDCl_3$) δ 160.5 (s, $^{195}$Pt satellite $^{1}J_{Pt–P}$ = 1818 Hz). HRMS (DART) *m/z* calc for $C_{25}H_{25}N_5PPt$ $[M–OTf]^+$: 621.1490, found 621.1543.

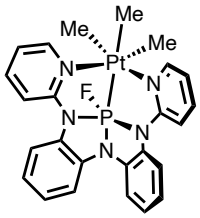


5.16

**Synthesis of $PtMe_3(L1^F)$ (5.16).** To a vial with a $CDCl_3$ solution (1 mL) of **5.15** (4.2 mg, 0.0054 mmol, 1 eq) was added tris(dimethylamino)sulfonium trimethyldifluorosilicate (TASF) (1.5 mg, 0.0054 mmol, 1 eq) at room temperature and stirred for 15 min. The product was not isolated due to a fast decomposition process. $^1$H NMR (500 MHz, $CDCl_3$) δ 8.51 (d, $J$ = 5.8 Hz, 2H), 7.84 (d, $J$ = 7.9 Hz, 2H), 7.76 – 7.68 (m, 2H), 7.61 (d, $J$ = 8.5 Hz, 2H), 7.00 (t, $J$ = 7.6 Hz, 2H), 6.94 (t, $J$ = 7.8 Hz, 2H), 6.83 (t, $J$ = 6.4 Hz, 2H), 0.66 (d, $J$ = 8.7 Hz, 6H), 0.56 (d, $J$ = 14.9 Hz, 3H).$^{19}$F NMR (471 MHz, $CDCl_3$) δ -51.7 (d, $J$ = 1055 Hz, $^{195}$Pt satellite $^2J_{Pt-H}$ = 72 Hz). $^{31}$P NMR (203 MHz, $CDCl_3$) δ 58.7 (d, $J$ = 1055 Hz).

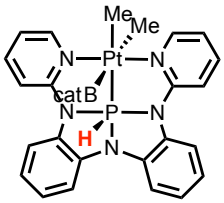


5.17

**Reaction of 5.13 and HBcat (5.17).** To a J-young tube filled with a $C_6D_6$ solution (1 mL) of **5.13** (5.0 mg, 0.0082 mmol, 1.0 eq) was added catecholborane (4.9 mg, 0.040 mmol, 5.0 eq) at room temperature and left for 15 min. The product **5.17** was not isolated due to a fast decomposition process. $^{31}$P NMR (203 MHz, $CDCl_3$) δ 104.9 ppm ($^1J_{Pt-P}$ = 2185 Hz).

## 5-9. References


1. Johansson Seechurn, C. C. C.; Kitching, M. O.; Colacot, T. J.; Snieckus, V. Palladium-Catalyzed Cross-Coupling: A Historical Contextual Perspective to the 2010 Nobel Prize. *Angew. Chem. Int. Ed.* **2012**, *51*, 5062–5085.
2. Nakazawa, H.; Yamaguchi, Y.; Mizuta, T.; Ichimura, S.; Miyoshi, K. Migratory Insertion of a Phosphorus Ligand into a Transition Metal-Alkyl Bond. *Organometallics* **1995**, *14*, 4635–4643.
3. Kawamura, K.; Nakazawa, H.; Miyoshi, K. Reaction of Ruthenium Complexes Having Both a Phosphite and a Group 14 Element Ligand with a Lewis Acid. *Organometallics* **1999**, *18*, 4785–4794.
4. Poitras, A. M.; Knight, S. E.; Bezpalko, M. W.; Foxman, B. M.; Thomas, C. M. Addition of $H_2$ Across a Cobalt-Phosphorus Bond. *Angew. Chem. Int. Ed.* **2018**, *57*, 1497–1500.
5. Hickey, A. K.; Muñoz, S. B.; Lutz, S. A.; Pink, M.; Chen, C.-H.; Smith, J. M. Arrested α-Hydride Migration Activates a Phosphido Ligand for C–H Insertion. *Chem. Commun.* **2017**, *53*, 412–415.
6. Kim, Y. E.; Oh, S.; Kim, S.; Kim, O.; Kim, J.; Han, S. W.; Lee, Y. Phosphinite-Ni(0) Mediated Formation of a Phosphide-Ni(II)-OCOOMe Species via Uncommon Metal-Ligand Cooperation. *J. Am. Chem. Soc.* **2015**, *137*, 4280–4283.
7. Svara, J.; Mathey, F. Electrophilic Insertion of Terminal Phosphinidene Complexes into the C-H Bonds of Ferrocene. *Organometallics* **1986**, *5*, 1159–1161.
8. Ng, Y. X.; Mathey, F. Mechanism of Phosphinidene Complex Arylation by Arylboronic Acids. *Organometallics* **2014**, *33*, 1322–1324.
9. Özbolat, A.; Khan, A. A.; Von Frantzius, G.; Nieger, M.; Streubel, R. Dehydroiodination of Iodo- and Diiodomethane by a Transient Phosphinidene Complex. *Angew. Chem. Int. Ed.* **2007**, *46*, 2104–2107.
10. Schulten, C.; von Frantzius, G.; Schnakenburg, G.; Espinosa, A.; Streubel, R. Deoxygenation of Carbon Dioxide by Electrophilic Terminal Phosphinidene Complexes. *Chem. Sci.* **2012**, *3*, 3526.
11. Xu, H.; Williard, P. G.; Bernskoetter, W. H. Intermolecular Methyl Group Exchange and Reversible P − Me Bond Cleavage at Cobalt(III) Dimethyl Halide Species. *Organometallics* **2013**, *32*, 798-806.
12. Green, M. L. H.; Smith, M. J.; Felkin, H.; Swierczewski, G. Substitution at Phosphorus in the Reaction between Dichlorobis(Triphenylphosphine)Nickel and Methylmagnesium Bromide. *J. Chem. Soc. D* **1971**, 158–159.
13. Macgregor, S. A. Transition Metal-Mediated P–C/X Exchange at Bound Phosphine Ligands (X = Aryl, Alkyl, $NR_2$, OR and F): Scope and Mechanisms. *Chem. Soc. Rev.* **2006**, *36*, 67–76.
14. For reactions of heavier tricoordinate pnictogen ligands, see: (a) Jones, J. S.; Wade, C. R.; Gabbaï, F. P. Redox and Anion Exchange Chemistry of a Stibine-Nickel Complex: Writing the L, X, Z Ligand Alphabet with a Single Element. *Angew. Chem. Int. Ed.* **2014**, *53*, 8876–8879. (b) Jones, J. S.; Gabbaï, F. P. Coordination- and Redox-Noninnocent Behavior of Ambiphilic Ligands Containing Antimony. *Acc. Chem. Res.* **2016**, *49*, 857–867.(c) Sen, S.; Ke, I. S.; Gabbaï, F. P. Anion-Controlled Positional Switching of a Phenyl Group about the Dinuclear Core of a AuSb Complex. *Inorg. Chem.* **2016**, *55*, 9162–9172. (d) You, D.; Yang, H.; Sen, S.; Gabbaï, F. P. Modulating the σ-Accepting Properties of an Antimony Z-Type Ligand via Anion Abstraction: Remote-Controlled Reactivity of the Coordinated Platinum Atom. *J. Am. Chem. Soc.* **2018**, *140*, 9644–9651.
15. Ren, P.; Vechorkin, O.; von Allmen, K.; Scopelliti, R.; Hu, X. A Structure–Activity Study of Ni-Catalyzed Alkyl–Alkyl Kumada Coupling. Improved Catalysts for Coupling of Secondary Alkyl Halides. *J. Am. Chem. Soc.* **2011**, *133*, 7084−7095.
16. Zhao, W.; McCarthy, S. M.; Lai, T. Y.; Yennawar, H. P.; Radosevich, A. T. Reversible Intermolecular E-H Oxidative Addition to a Geometrically Deformed and Structurally Dynamic Phosphorous Triamide. *J. Am. Chem. Soc.* **2014**, *136*, 17634–17644.

17. Kühl, O. *Phosphorus-31 NMR Spectroscopy: A Concise Introduction for the Synthetic Organic and Organometallic Chemist*; Springer-Verlag: Berlin, 2008.
18. (a) Contreras, R. H.; Peralta, J. E. Angular dependence of spin–spin coupling constants. *Prog. Nucl. Magn. Reson. Spectrosc*. **2000**, *37*, 321. (b) McFarlane, H. E. C.; McFarlane, W. Polyphosphorus ligands—V. The synthesis, phosphorus-31 NMR spectra and conformations of the polykis(diphenylphosphino) benzens $(Ph_2P)_nC_6H_{6-n}$ (n=1–4). *Polyhedron* **1988**, *7*, 1875. (c) McFarlane, H. E. C.; McFarlane, W. Synthesis and NMR spectra of derivatives of the polykis(diphenylphosphino)benzenes, $(Ph_2P)_nC_6H_{6-n}$ (n=2 to 4). *Polyhedron* **1999**, *18*, 2117.
19. Hierso, J.-C. Indirect Nonbonded Nuclear Spin−Spin Coupling: A Guide for the Recognition and Understanding of "Through-Space" NMR J Constants in Small Organic, Organometallic, and Coordination Compounds. *Chem. Rev*. **2014**, *114*, 4838−4867.
20. Yang, L.; Powell, D. R.; Houser, R. P. Structural variation in copper(I) complexes with pyridylmethylamide ligands: structural analysis with a new four-coordinate geometry index, τ4. *Dalton Trans*. **2007**, 955−964.
21. Waddell, P. G.; Slawin, A. M. Z.; Woollins, J. D. Correlating Pt-P Bond Lengths and Pt-P Coupling Constants. *Dalton. Trans.* **2010**, *39*, 8620–8625.
22. Addison, A. W.; Rao, T. N.; Reedijk, J.; van Rijn, J.; Verschoor, G. C. Synthesis, structure, and spectroscopic properties of copper(II) compounds containing nitrogen–sulphur donor ligands; the crystal and molecular structure of aqua[1,7-bis(N-methylbenzimidazol-2′-yl)-2,6-dithiaheptane]copper(II) perchlorate. *J. Chem. Soc., Dalton Trans*. **1984**, 1349−1356.
23. Vierling, P.; Riess, J. G.; Grand, A. Coordination chemistry of the bicycloaminophosphorane $Ph(H)P[(OCH_2CH_2)_2N]$, a potential P/N ligand. Access to iron and ruthenium phosphoranides. Reversible migration of a phenyl group between iron and phosphorus: crystal and molecular structure of $CpFe(CO)[P(OCH_2CH_2)_2N](C_6H_5)$. *Inorg. Chem.* **1986**, *25*, 4144−4152.
24. (a) Macgregor, S. A.; Neave, G. W.; Smith, C. Theoretical studies on C-heteroatom bond formation via reductive elimination from group 10 $M(PH_3)_2(CH_3)(X)$ species (X = $CH_3$, $NH_2$, OH, SH) and the determination of metal-X bond strengths using density functional theory. *Faraday Discuss*. **2003**, *124*, 111−127. (b) Ananikov, V. P.; Musaev, D. G.; Morokuma, K. Theoretical Insight into the C-C Coupling Reactions of the Vinyl, Phenyl, Ethynyl, and Methyl Complexes of Palladium and Platinum. *Organometallics* **2005**, *24*, 715−723.
25. The selectivity for migration of the methyl moiety instead of the chloride can similarly be rationalized on thermodynamic grounds.
26. Knizia, G. Intrinsic Atomic Orbitals: An Unbiased Bridge between Quantum Theory and Chemical Concepts. *J. Chem. Theory Comput.* **2013**, *9*, 4834–4843.
27. (a) Klein, J. E. M. N.; Havenith, R. W. A.; Knizia, G. The Pentagonal-Pyramidal Hexamethylbenzene Dication: Many Shades of Coordination Chemistry at Carbon. *Chem. Eur. J.* **2018**, *24*, 12340–12345. (b)Steen, J. S.; Knizia, G.; Klein, J. E. M. N. σ-Noninnocence: Masked Phenyl-Cation Transfer at Formal NiIV. *Angew. Chem. Int. Ed.* **2019**, *58*, 13133–13139.
28. Thom, A. J. W.; Sundstrom, E. J.; Head-Gordon, M. LOBA: A Localized Orbital Bonding Analysis to Calculate Oxidation States, with Application to a Model Water Oxidation Catalyst. *Phys. Chem. Chem. Phys.* **2009**, *11*, 11297–11304.
29. (a) Gimferrer, M.; Mynsbrugge, J. Van Der; Bell, A. T.; Salvador, P.; Head-Gordon, M. Facing the Challenges of Borderline Oxidation State Assignments Using State-of-the-Art Computational Methods. *Inorg. Chem.* **2020**, *59*, 15410–15420. (b) Sundstrom, E. J.; Yang, X.; Thoi, V. S.; Karunadasa, H. I.; Chang, C. J.; Long, J. R.; Head-Gordon, M. Computational and Experimental Study of the Mechanism of Hydrogen Generation from Water by a Molecular Molybdenum-Oxo Electrocatalyst. *J. Am. Chem. Soc.* **2012**, *134*, 5233–5242. (c) Nguyen, A. I.; Suess, D. L. M.; Darago, L. E.; Oyala, P. H.; Levine, D. S.; Ziegler, M. S.; Britt, R. D.; Tilley, T. D. Manganese-Cobalt Oxido

Cubanes Relevant to Manganese-Doped Water Oxidation Catalysts. *J. Am. Chem. Soc.* **2017**, *139*, 5579–5587. (d) Cook, A. W.; Hrobárik, P.; Damon, P. L.; Najera, D.; Horváth, B.; Wu, G.; Hayton, T. W. Synthesis and Characterization of a Linear, Two-Coordinate Pt(II) Ketimide Complex. *Inorg. Chem.* **2019**, *58*, 15927–15935. (e) Angersbach-Bludau, F.; Schulz, C.; Schöffel, J.; Burger, P. Syntheses and Electronic Structures of μ-Nitrido Bridged Pyridine, Diimine Iridium Complexes. *Chem. Commun.* **2014**, *50*, 8735–8738. (f) Liu, X.; Liu, X. R. Photosensitive Tin Sulfur Dioxide Complexes with Unexpected Bonding Modes. *Chem. Eur. J.* **2019**, *25*, 5698–5707. (g) Guo, J.; Lu, Y.; Zhao, R.; Liu, Z.; Menberu, W.; Wang, Z. X. Strong Preference of the Redox-Neutral Mechanism over the Redox Mechanism for the TiIV Catalysis Involved in the Carboamination of Alkyne with Alkene and Diazene. *Chem. Eur. J.* **2018**, *24*, 7010–7025. (h) Bezdek, M. J.; Chirik, P. J. Pyridine(Diimine) Chelate Hydrogenation in a Molybdenum Nitrido Ethylene Complex. *Organometallics* **2019**, *38*, 1682–1687.

30. Jiang, T.; Zhang, H.; Ding, Y.; Zou, S.; Chang, R.; Huang, H. Transition-Metal-Catalyzed Reactions Involving Reductive Elimination between Dative Ligands and Covalent Ligands. *Chem. Soc. Rev.* **2020**, *49*, 1487–1516.
31. Mason, M. R.; Verkade, J. G. Fluoride-Assisted Reduction of Palladium(II) Phosphine Complexes. *Organometallics* **1990**, *9*, 864–865.
32. Mason, M. R.; Verkade, J. G. Fluoride-Induced Reduction of Palladium(II) and Platinum(II) Phosphine Complexes. *Organometallics* **1992**, *11*, 2212–2220.
33. McLaughlin, P. A.; Verkade, J. G. Fluoride-Catalyzed Reduction of Palladium(II) to Palladium(0)−Phosphine Complexes. *Organometallics* **1998**, *17*, 5937–5940.
34. Wakioka, M.; Ozawa, F. Substituent Effects on P−C Reductive Elimination from Styrylpalladium(II) Phosphine Complexes †. *Organometallics* **2010**, *29* (21), 5570–5578.
35. Khusnutdinova, J. R.; Milstein, D. Metal-Ligand Cooperation. *Angew. Chem. Int. Ed.* **2015**, *54*, 12236–12273.
36. Calderazzo, F. Synthetic and Mechanistic Aspects of Inorganic Insertion Reactions. Insertion of Carbon Monoxide. *Angew. Chem Int. Ed.* **1977**, *16*, 299–311..
37. E. J.; Alexander, J. J. Carbon Monoxide Insertion into Transition Metal-Carbon Sigma-Bonds. *Coord. Chem. Rev.* **1980**, *33*, 195–225.
38. Anderson, G. K. Carbonyl-Insertion Reactions of Square-Planar Complexes. *Acc. Chem. Res*. **1984**, *17*, 67−74.
39. Berke, H.; Hoffmann, R. Organometallic Migration Reactions. *J. Am. Chem. Soc.* **1978**, *100*, 7224−7236.
40. Garrou, P. E.; Heck, R. F. The Mechanism of Carbonylation of Halo(bis ligand)organoplatinum(II), -palladium(II), and -nickel(II) Complexes. *J. Am. Chem. Soc*. **1976**, *98*, 4115−4127.
41. Feichtner, K. S.; Gessner, V. H. Cooperative Bond Activation Reactions with Carbene Complexes. *Chem. Commun.* **2018**, *54* (50), 6540–6553.
42. Blom, B.; Stoelzel, M.; Driess, M. New Vistas in N-Heterocyclic Silylene (NHSi) Transition-Metal Coordination Chemistry: Syntheses, Structures and Reactivity towards Activation of Small Molecules. *Chem. Eur. J.* **2013**, *19*, 40–62.
43. Noyori, R.; Ohkuma, T. *Angew. Chem., Int. Ed.*, **2001**, *40*, 40.
44. Schneider, S.; Meiners, J.; Askevold, B. Cooperative Aliphatic PNP Amido Pincer Ligands-Versatile Building Blocks for Coordination Chemistry and Catalysis. *Eur. J. Inorg. Chem.* **2012**, *3*, 412–429.
45. Alberico, E.; Sponholz, P.; Cordes, C.; Nielsen, M.; Drexler, H.-J.; Baumann, W.; Junge, H.; Beller, M.; *Angew. Chem. Int. Ed.* **2013**, *52*, 14162.
46. Bielinski, E. A.; Lagaditis, P. O.; Zhang, Y.; Mercado, B. Q.; Wurtele, C.; Bernskoetter, W. H.; Hazari N.; Schneider, S. *J. Am. Chem. Soc.* **2014**, *136*, 10234.
47. Noyori, R.; Yamakawa, M.; Hashiguchi, S. *J. Org. Chem.* **2001**, *66*, 7931.

48. For reactions of heavier tricoordinate pnictogen ligands, see: (a) Jones, J. S.; Wade, C. R.; Gabbaï, F. P. Redox and Anion Exchange Chemistry of a Stibine-Nickel Complex: Writing the L, X, Z Ligand Alphabet with a Single Element. *Angew. Chem. Int. Ed.* **2014**, *53*, 8876–8879. (b) Jones, J. S.; Gabbaï, F. P. Coordination- and Redox-Noninnocent Behavior of Ambiphilic Ligands Containing Antimony. *Acc. Chem. Res.* **2016**, *49*, 857–867. (c) Sen, S.; Ke, I. S.; Gabbaï, F. P. Anion-Controlled Positional Switching of a Phenyl Group about the Dinuclear Core of a AuSb Complex. *Inorg. Chem.* **2016**, *55*, 9162–9172. (d) You, D.; Yang, H.; Sen, S.; Gabbaï, F. P. Modulating the σ-Accepting Properties of an Antimony Z-Type Ligand via Anion Abstraction: Remote-Controlled Reactivity of the Coordinated Platinum Atom. *J. Am. Chem. Soc.* **2018**, *140*, 9644–9651.
49. Gelling, A.; Orrell, K. G.; Osborne, A. G.; Šik, V. The Energetics and Mechanism of Fluxionality of 2,2′:6′,2″-Terpyridine Derivatives When Acting as Bidentate Ligands in Transition-Metal Complexes. A Detailed Dynamic NMR Study. *J. Chem. Soc. Dalton Trans.* **1998**, *27*, 937–946.
50. Abel, E. W.; Gelling, A.; Orrell, K. G.; Osborne, A. G.; Šik, V. The Mechanism of 1,4-Metallotropic Shifts in Transition-Metal Complexes of Bidentate 2,2′: 6′,2″-Terpyridine Ligands. *Chem. Commun.* **1996**, *53*, 2329–2330.
51. Cleveland, G. T.; Radosevich, A. T. A Nontrigonal Tricoordinate Phosphorus Ligand Exhibiting Reversible "Nonspectator" L/X-Switching. *Angew. Chem. Int. Ed.* **2019**, *58*, 15005–15009.
52. Lin, Y. C.; Hatzakis, E.; McCarthy, S. M.; Reichl, K. D.; Lai, T. Y.; Yennawar, H. P.; Radosevich, A. T. P-N Cooperative Borane Activation and Catalytic Hydroboration by a Distorted Phosphorous Triamide Platform. *J. Am. Chem. Soc.* **2017**, *139*, 6008–6016.
53. Ren, P.; Vechorkin, O.; Allmen, K. von; Scopelliti, R.; Hu, X. A Structure–Activity Study of Ni-Catalyzed Alkyl–Alkyl Kumada Coupling. Improved Catalysts for Coupling of Secondary Alkyl Halides. *J. Am. Chem. Soc.* **2011**, *133*, 7084–7095.
54. Clark, H. C.; Manzer, L. E. *J. Organomet. Chem*. **1973**, *59*, 411−428.
55. Beck, R.; Klein, H.-F. The Crystal Structures of Trimethylphosphane Supported Nickel- and Cobalt-Methyl Complexes: Octahedral *mer-cis*-[$Co^{III}I(CH_3)_2(PMe_3)_3$] and Square Planar *trans*-[$Ni^{II}Cl(CH_3)(PMe_3)_2$]. *Z für Anorg*. *Allg*. *Chem*. **2008**, *634*, 1971–1974.
56. Tanushi, A.; Radosevich, A. T. Insertion of a Nontrigonal Phosphorus Ligand into a Transition Metal-Hydride: Direct Access to a Metallohydrophosphorane. *J. Am. Chem. Soc.* **2018**, *140*, 8114–8118.
57. Fulmer, G. R.; Miller, A. J. M.; Sherden, N. H.; Gottlieb, H. E.; Nudelman, A.; Stoltz, B. M.; Bercaw, J. E.; Goldberg, K. I. NMR Chemical Shifts of Trace Impurities: Common Laboratory Solvents, Organics, and Gases in Deuterated Solvents Relevant to the Organometallic Chemist. *Organometallics* **2010**, *29*, 2176–2179.
58. Bruker AXS (2009). Apex II. Bruker AXS, Madison, Wisconsin.
59. Sheldrick, G. M. *Acta Cryst.* **2010**, *D66*, 479–485.
60. Dolomanov, O.V., Bourhis, L.J., Gildea, R.J, Howard, J.A.K. & Puschmann, H. *J*. *Appl*. *Cryst*. 2009, *42*, 339-341.

# Appendix A . Supplementary Data for Chapter 2

## A.1. X-ray Diffraction Data

See the published article (*Angew. Chem. Int. Ed.* **2019**, *58*, 6993–6998.) or CCDC (https://www.ccdc.cam.ac.uk ) for cif files and detailed structural data of $P(NMePh)_3$ and **2.2**.

**Structural Data for $P(NMePh)_3$**

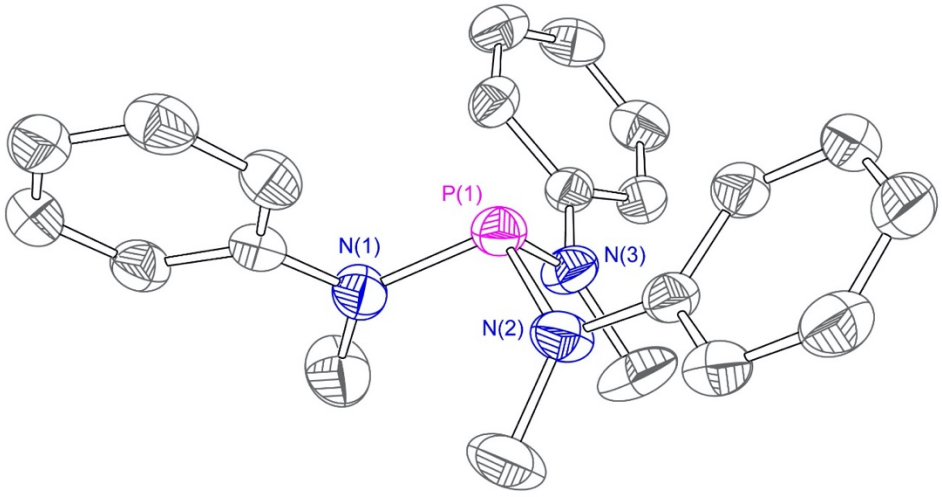

**Table A-1.** Crystal data and structure refinement for $P(NMePh)_3$.

| | | |
|---|---|---|
| Identification code | smm8r | |
| Empirical formula | C21 H24 N3 P | |
| Formula weight | 349.40 | |
| Temperature | 199(2) K | |
| Wavelength | 0.71073 Å | |
| Crystal system | Rhombohedral | |
| Space group | R3 | |
| Unit cell dimensions | a = 12.724(3) Å | α= 90°. |
| | b = 12.724(3) Å | β= 90°. |
| | c = 9.994(4) Å | γ = 120°. |
| Volume | 1401.3(7) $Å^3$ | |
| Z | 3 | |
| Density (calculated) | 1.242 $Mg/m^3$ | |
| Absorption coefficient | 0.155 $mm^{-1}$ | |
| F(000) | 558 | |
| Crystal size | 0.23 x 0.22 x 0.16 $mm^3$ | |
| Theta range for data collection | 2.75 to 28.25°. | |
| Index ranges | -15<=h<=16, -16<=k<=14, -8<=l<=13 | |
| Reflections collected | 2382 | |
| Independent reflections | 991 [R(int) = 0.0291] | |
| Completeness to theta = 28.25° | 99.1 % | |
| Absorption correction | Semi-empirical from equivalents | |
| Max. and min. transmission | 0.9756 and 0.9652 | |
| Refinement method | Full-matrix least-squares on $F^2$ | |
| Data / restraints / parameters | 991 / 1 / 77 | |
| Goodness-of-fit on $F^2$ | 1.145 | |
| Final R indices [I>2sigma(I)] | R1 = 0.0348, wR2 = 0.1010 | |
| R indices (all data) | R1 = 0.0352, wR2 = 0.1015 | |
| Absolute structure parameter | 0.40(14) | |
| Largest diff. peak and hole | 0.187 and -0.233 $e.Å^{-3}$ | |

**Structural Data for 2.2.**

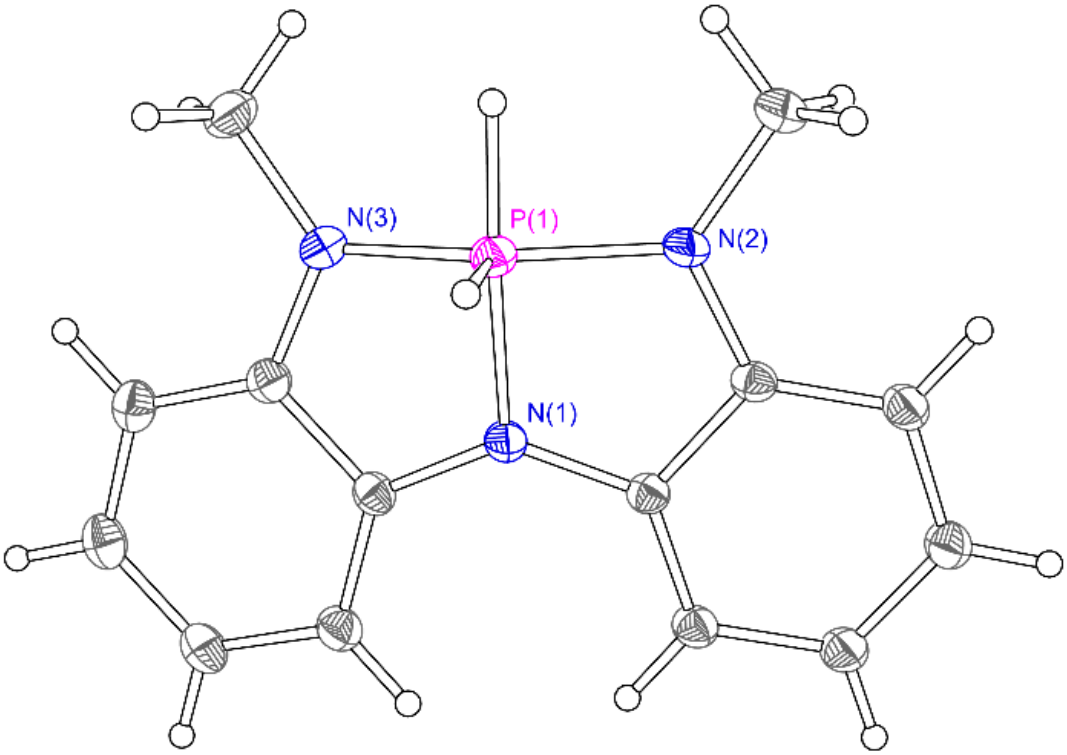

**Table A-2.** Crystal data and structure refinement for **2.2**.

| | | |
|---|---|---|
| Identification code | PH2-16 | |
| Empirical formula | C14 H16 N3 P | |
| Formula weight | 257.27 | |
| Temperature | 100(2) K | |
| Wavelength | 0.71073 Å | |
| Crystal system | Trigonal | |
| Space group | R-3 | |
| Unit cell dimensions | a = 29.7625(13) Å | α= 90°. |
| | b = 29.7625(13) Å | β= 90°. |
| | c = 7.5469(4) Å | γ = 120°. |
| Volume | 5789.5(6) $Å^3$ | |
| Z | 18 | |
| Density (calculated) | 1.328 $Mg/m^3$ | |
| Absorption coefficient | 0.199 $mm^{-1}$ | |
| F(000) | 2448 | |
| Crystal size | 0.429 x 0.064 x 0.062 $mm^3$ | |
| Theta range for data collection | 1.368 to 34.031°. | |
| Index ranges | -46<=h<=46, -46<=k<=46, -11<=l<=11 | |
| Reflections collected | 104083 | |
| Independent reflections | 5163 [R(int) = 0.0482] | |
| Completeness to theta = 25.242° | 99.9 % | |
| Absorption correction | Semi-empirical from equivalents | |
| Max. and min. transmission | 0.7467 and 0.7008 | |
| Refinement method | Full-matrix least-squares on $F^2$ | |
| Data / restraints / parameters | 5163 / 0 / 171 | |
| Goodness-of-fit on $F^2$ | 1.054 | |
| Final R indices [I>2sigma(I)] | R1 = 0.0373, wR2 = 0.0963 | |
| R indices (all data) | R1 = 0.0507, wR2 = 0.1037 | |
| Extinction coefficient | n/a | |
| Largest diff. peak and hole0.525 and -0.299 $e.Å^{-3}$ | | |

## A.2. DFT Calculation

**Table A-3.** Experimental and calculated (TDDFT) P K-edge XANES peak positions (eV). Peak positions were determined by analysis of the 2nd derivative trace of the experimental and simulated spectra.

| **$P(NMePh)_3$** | | **2.1.** | | **2.2.** | |
|---|---|---|---|---|---|
| **Expt** | **Calc** | **Expt** | **Calc** | **Expt** | **Calc** |
| 2147.0 | 2147.1 | 2145.9 | 2146.0 | 2148.4 | 2148.6 |
| 2147.4 | | 2147.5 | 2147.7 | 2149.7 | 2149.5 |
| 2148.6 | 2148.4 | 2148.4 | 2148.1 | 2150.7 | 2150.5 |
| 2149.4 | 2149.5 | 2148.6 | 2148.9 | | 2150.8 |
| | 2151.0 | 2149.6 | 2149.6 | | 2151.3 |
| | | | 2150.6 | | |

**Table A-4**.Calculated P 3p orbital composition and energy of selected MOs in $P(NMePh)_3$, $C_{2v}$-**2.1**, **2.1**, and **2.2**. The dashed line indicates the break between occupied and unoccupied MOs (HOMO/LUMO gap).

| **$P(NMePh)_3$** | | | **$C_{2v}$-2.1** | | | **2.1** | | | **2.2** | | | |
|---|---|---|---|---|---|---|---|---|---|---|---|---|
| **MO** | **E (eV)** | **P 3p** | **MO** | **E (eV)** | **P 3p** | **MO** | **E (eV)** | **P 3p** | **MO** | **E (eV)** | **P 3p** | **H 1s** |
| 104 | 2.70 | 2.6% | 78 | 3.71 | 20.3% | 78 | 3.40 | 30.8% | 79 | 3.39 | 2.0% | 0.3% |
| 103 | 2.58 | 10.7% | 77 | 3.16 | 5.1% | 77 | 3.25 | 1.3% | 78 | 3.29 | 19.5% | 21.4% |
| 102 | 2.02 | 2.2% | 76 | 3.05 | 12.2% | 76 | 2.86 | 3.0% | 77 | 2.97 | 20.9% | - |
| 101 | 1.49 | 53.2% | 75 | 2.75 | 6.7% | 75 | 2.74 | 5.2% | 76 | 2.65 | 2.5% | 7.4% |
| 100 | 1.40 | 47.4% | 74 | 2.55 | 6.4% | 74 | 2.34 | 4.0% | 75 | 2.51 | 45.6% | - |
| 99 | 0.49 | 2.3% | 73 | 1.64 | 55.8% | 73 | 1.95 | 64.1% | 74 | 2.24 | 11.4% | 15.3% |
| 98 | 0.29 | 7.7% | 72 | 0.92 | 2.6% | 72 | 0.55 | 7.2% | 73 | 1.41 | 27.5% | 5.6% |
| 97 | 0.19 | 1.4% | 71 | 0.63 | 4.5% | 71 | 0.45 | 9.1% | 72 | 1.04 | 1.4% | 0.4% |
| 96 | 0.13 | 2.2% | 70 | 0.58 | - | 70 | 0.40 | 5.5% | 71 | 0.65 | 2.9% | - |
| 95 | 0.03 | 7.7% | 69 | -0.19 | 0.2% | 69 | 0.13 | 3.8% | 70 | 0.23 | 9.9% | 1.8% |
| 94 | -0.06 | 5.6% | 68 | -1.69 | 43.8% | 68 | -0.41 | 56.6% | 69 | 0.07 | 1.2% | - |
| 93 | -5.07 | 4.6% | 67 | -5.14 | 0.4% | 67 | -4.96 | 6.3% | 68 | -4.73 | 1.4% | 5.0% |
| 92 | -5.58 | 1.7% | 66 | -5.77 | 23.8% | 66 | -5.36 | 1.5% | 67 | -5.46 | 1.0% | - |
| 91 | -5.83 | 2.0% | 65 | -5.89 | 18.7% | 65 | -6.15 | 0.6% | 66 | -5.94 | 0.6% | 1.5% |
| 90 | -6.53 | 6.3% | 64 | -6.13 | 10.2% | 64 | -6.58 | 0.1% | 65 | -6.60 | - | - |
| 89 | -6.62 | 0.5% | 63 | -6.90 | 0.1% | 63 | -7.20 | 25.4% | 64 | -7.72 | 1.4% | 17.6% |
| 88 | -6.72 | 2.1% | | | | | | | 43 | -12.86 | 9.0% | 5.6% |
| 87 | -6.96 | 18.4% | | | | | | | 42 | -13.17 | 20.9% | 11.4% |
| P 1s | -2098.88 | | P 1s | -2098.39 | | P 1s | -2099.00 | | P 1s | -2100.21 | | |

The calculation of the energies of $P(NH_2)_3$ of all $C_s$ symmetry was performed at the level of B3LYP/6-31G*. The 2D contour maps depicting the energies (Figure 7 and Figure S4) were plotted in Origin 2019 and smoothing effect was performed to each plot for clarity.

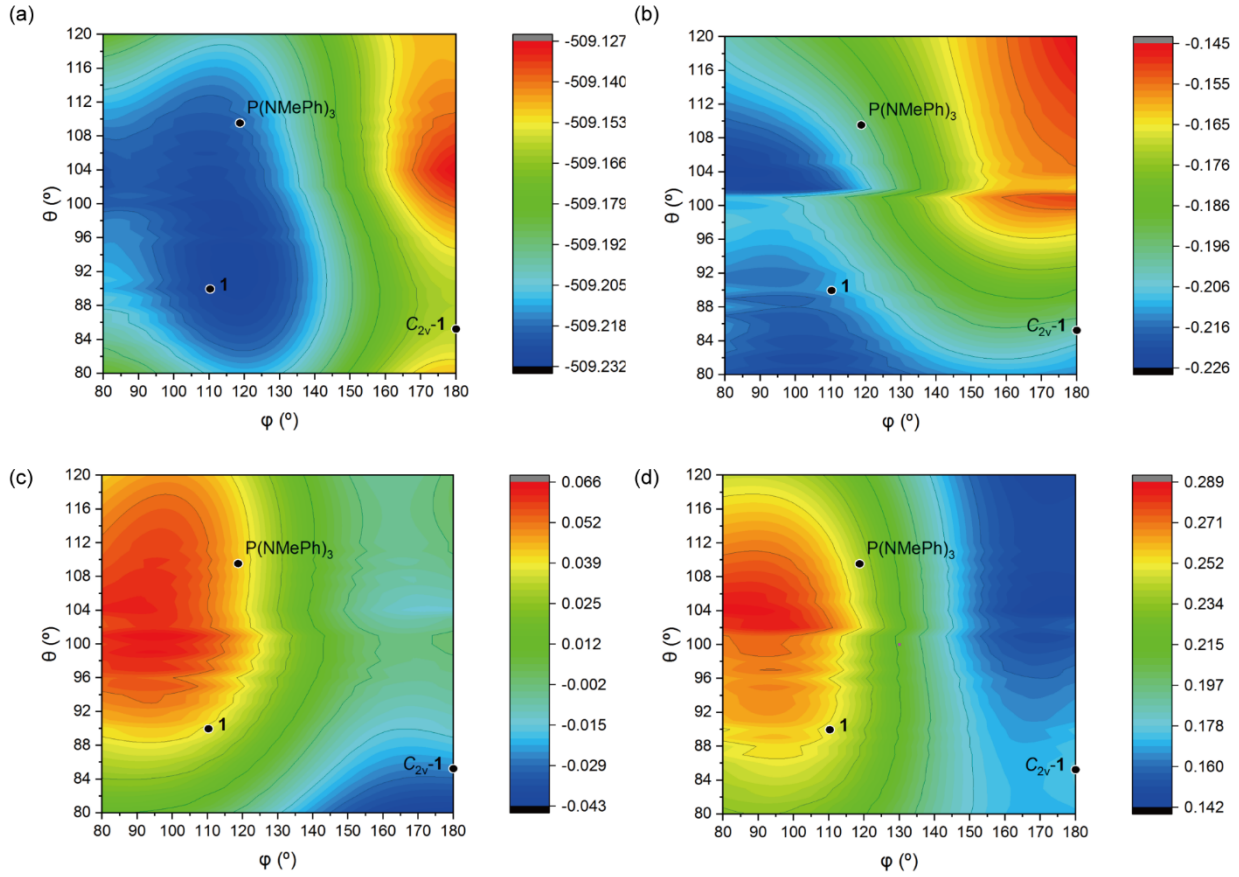


**Figure A-1.** Contour maps depicting the orbital of (a) Total electronic energy, (b) HOMO energies, (c) LUMO energies, (d) ΔHOMO–LUMO for all $P(NH_2)_3$ structures with $C_s$-symmetry. Energies are shown in a units of Hartrees. Points corresponding to the structures of $P(NMePh)_3$, **2.1** and $C_{2v}$-**2.1** are superimposed as black points. Although there is a discontinuity on the line of $\theta$=101° in Figure S3b, this is due to the conformational changes of the hydrogens and not essential factor of this calculation. Since the energy gap between HOMO and LUMO reflect the trend of LUMO rather than HOMO, this does not affect any conclusions.

## A.3. Multinuclear NMR spectra

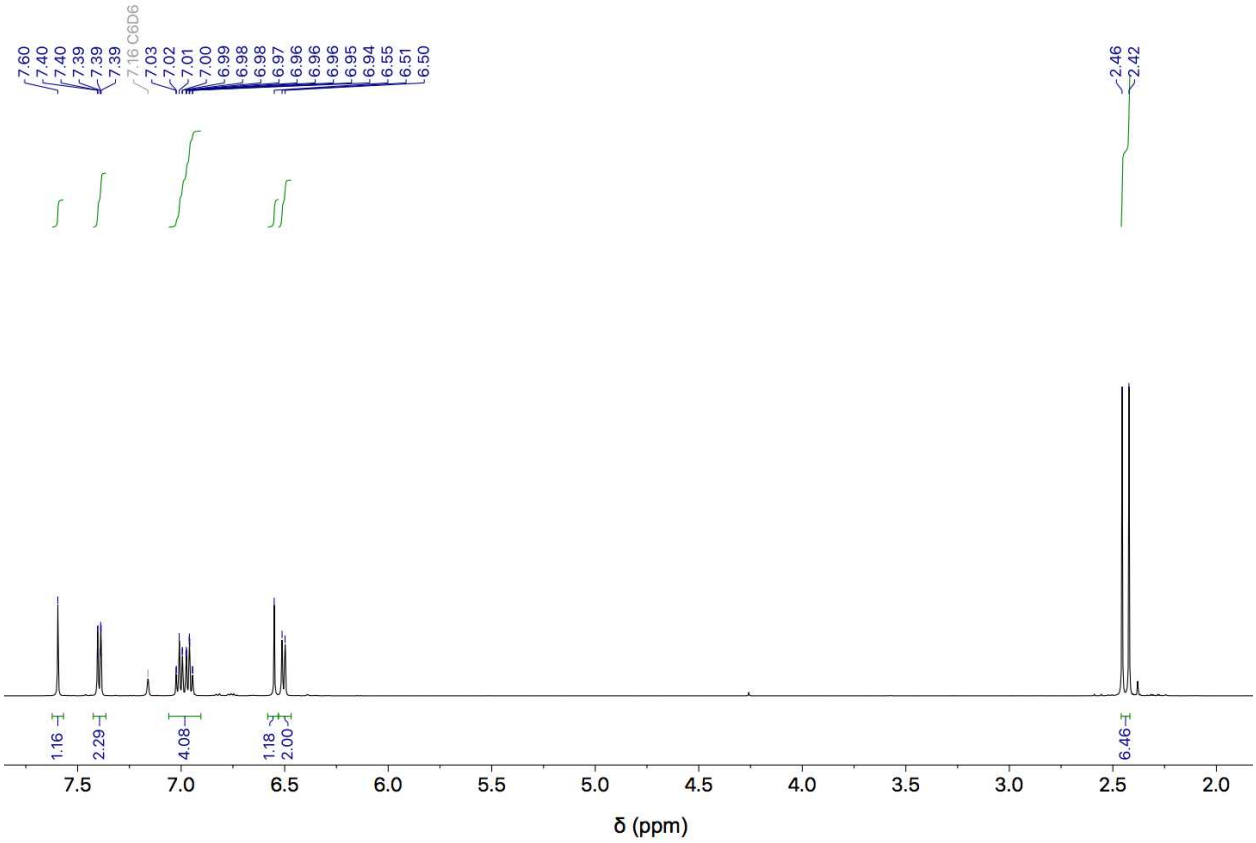


**Figure A-2.** $^{1}$H NMR spectrum ($C_6D_6$) of **2.2**.

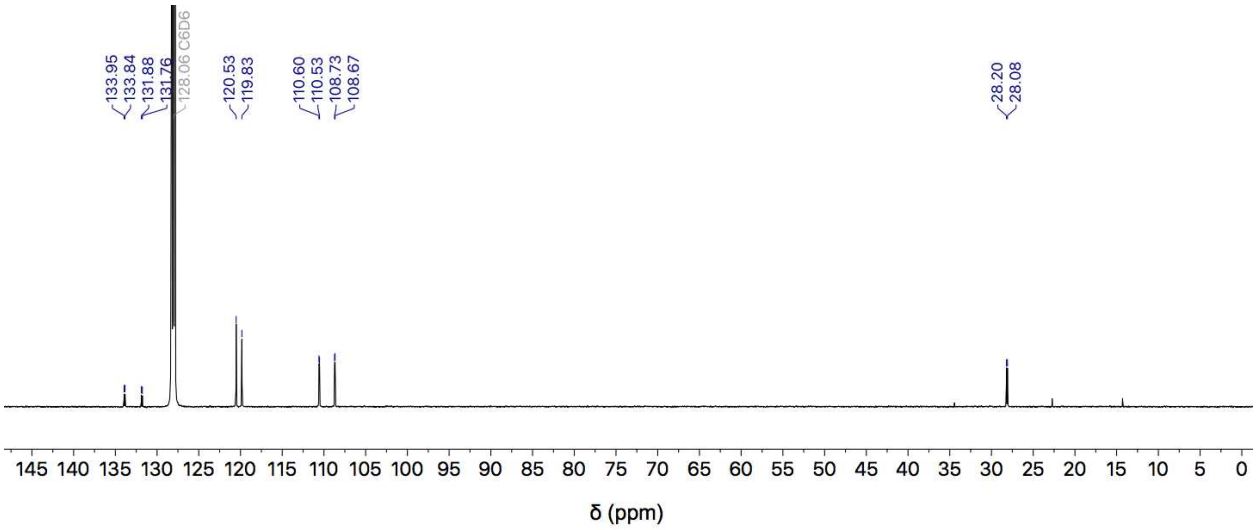


**Figure A-3.** $^{13}C$ NMR spectrum ($C_6D_6$) of **2.2**.

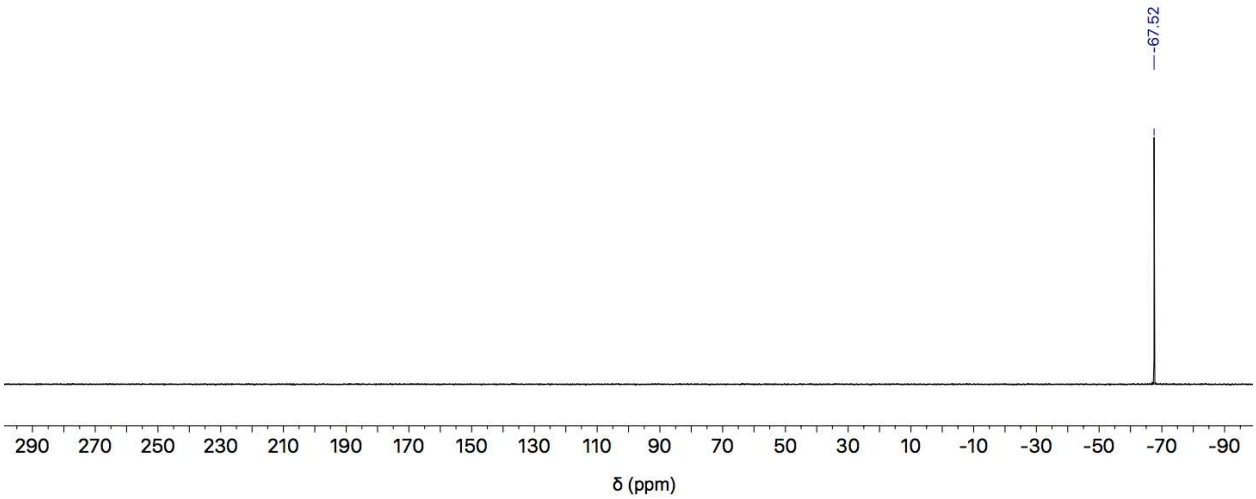


**Figure A-4.** $^{31}P\{^{1}H\}$ NMR spectrum ($C_6D_6$) of **2.2**.

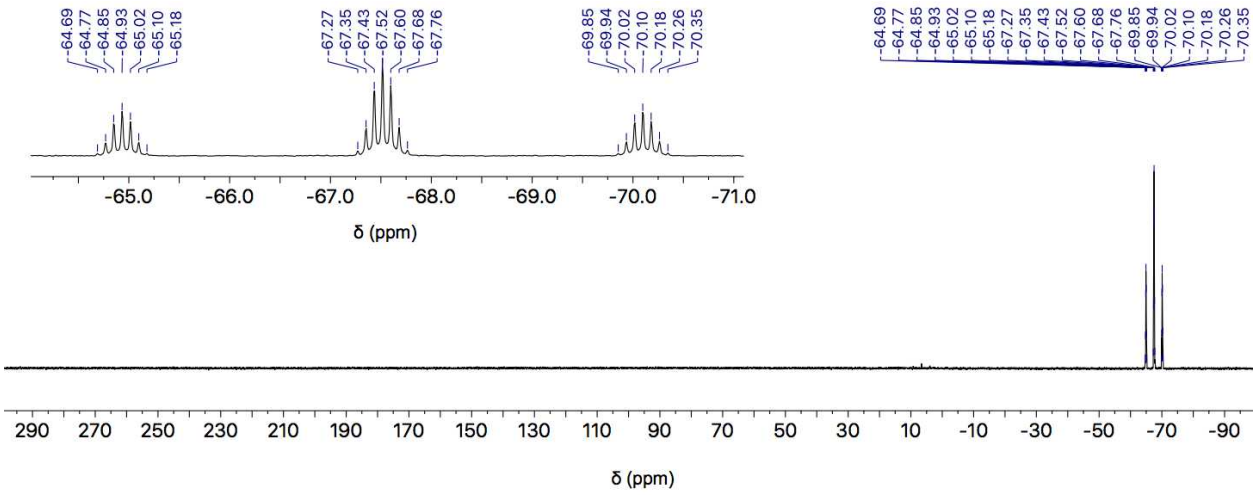


**Figure A-5**. $^{31}$P NMR spectrum of **2.2**.

# Appendix B . Supplementary Data for Chapter 3

## B.1. X-ray diffraction

See the published article (*J. Am. Chem. Soc.* **2018**, *140*, 8114–8118.) or CCDC (https://www.ccdc.cam.ac.uk ) for cif files and detailed structural data of **L1**, **3.3** and **3.4**.

**Structural Data for L1**

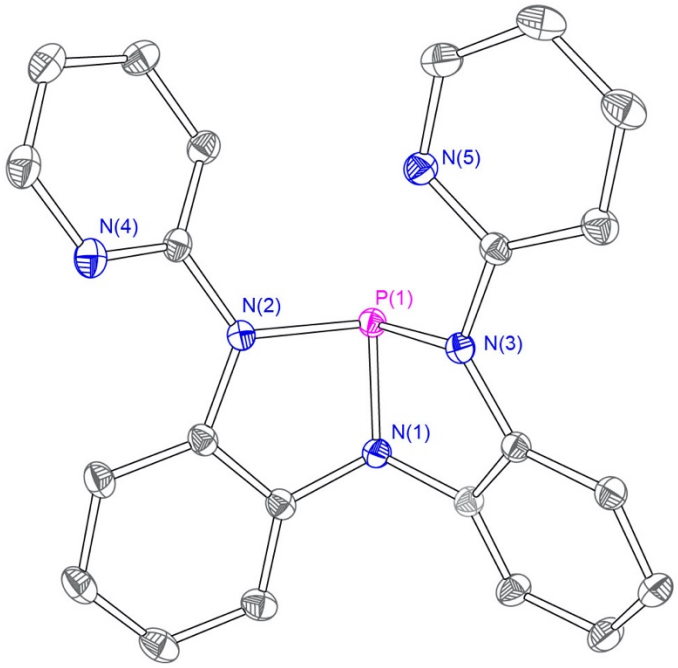

**Table B-1.** Crystal data and structure refinement for **L1**. (CCDC 1859480)

| | | |
|---|---|---|
| Identification code | X17164 | |
| Empirical formula | C22 H16 N5 P | |
| Formula weight | 381.37 | |
| Temperature | 100(2) K | |
| Wavelength | 0.71073 Å | |
| Crystal system | Monoclinic | |
| Space group | C2/c | |
| Unit cell dimensions | a = 23.2935(15) Å | α = 90°. |
| | b = 10.5714(7) Å | β = 116.124(2)°. |
| | c = 15.8503(10) Å | γ = 90°. |
| Volume | 3504.3(4) $Å^3$ | |
| Z | 8 | |
| Density (calculated) | 1.446 $Mg/m^3$ | |
| Absorption coefficient | 0.176 $mm^{-1}$ | |
| F(000) | 1584 | |
| Crystal size | 0.208 x 0.156 x 0.090 $mm^3$ | |
| Theta range for data collection | 1.947 to 35.630°. | |
| Index ranges | -38<=h<=38, -15<=k<=17, -25<=l<=25 | |
| Reflections collected | 71875 | |
| Independent reflections | 8079 [R(int) = 0.0556] | |
| Completeness to theta = 25.242° | 99.8 % | |
| Absorption correction | Semi-empirical from equivalents | |
| Refinement method | Full-matrix least-squares on $F^2$ | |
| Data / restraints / parameters | 8079 / 0 / 253 | |
| Goodness-of-fit on $F^2$ | 1.035 | |
| Final R indices [I>2sigma(I)] | R1 = 0.0397, wR2 = 0.1028 | |
| R indices (all data) | R1 = 0.0523, wR2 = 0.1100 | |
| Extinction coefficient | n/a | |
| Largest diff. peak and hole | 0.507 and -0.330 e.$Å^{-3}$ | |

**Structural Data for 3.3.**

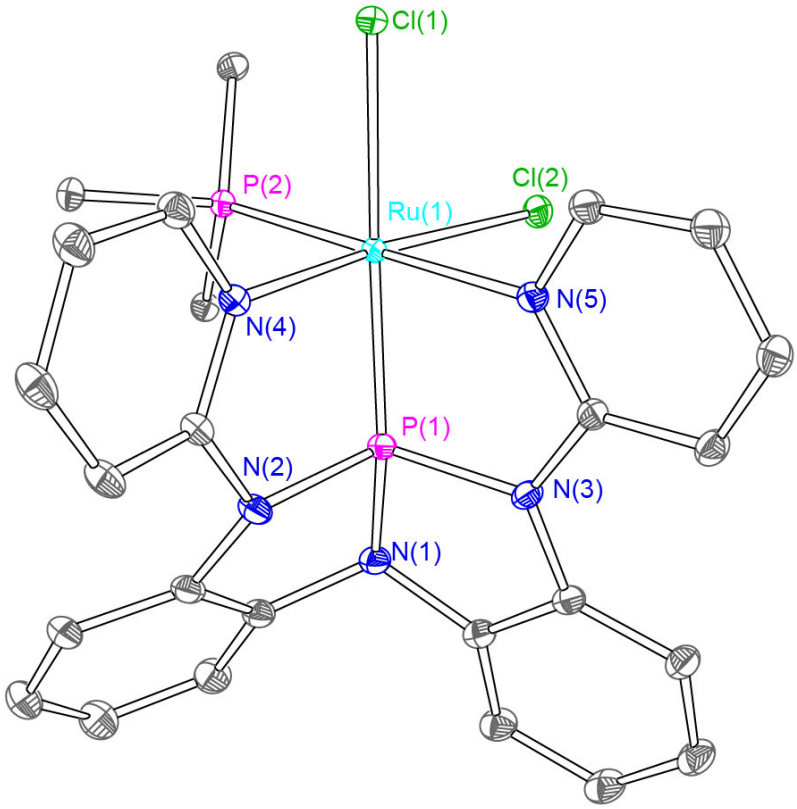

**Table B-2.** Crystal data and structure refinement for **3.3**. (CCDC 1859481)

| | | |
|---|---|---|
| Identification code | RuCl2_8 | |
| Empirical formula | C41 H33 Cl4 N5 P2 Ru | |
| Formula weight | 900.53 | |
| Temperature | 100(2) K | |
| Wavelength | 0.71073 Å | |
| Crystal system | Monoclinic | |
| Space group | $P2_1/n$ | |
| Unit cell dimensions | a = 11.4147(3) Å | □= 90°. |
| | b = 24.3387(8) Å | □= 92.1539(11)°. |
| | c = 13.5456(4) Å | □ = 90°. |
| Volume | 3760.57(19) $Å^3$ | |
| Z | 4 | |
| Density (calculated) | 1.591 $Mg/m^3$ | |
| Absorption coefficient | 0.826 $mm^{-1}$ | |
| F(000) | 1824 | |
| Crystal size | 0.230 x 0.160 x 0.060 $mm^3$ | |
| Theta range for data collection | 2.838 to 37.815°. | |
| Index ranges | -19<=h<=19, -41<=k<=41, -22<=l<=23 | |
| Reflections collected | 216705 | |
| Independent reflections | 20154 [R(int) = 0.0490] | |
| Completeness to theta = 25.242° | 99.8 % | |
| Absorption correction | Semi-empirical from equivalents | |
| Max. and min. transmission | 0.7474 and 0.6688 | |
| Refinement method | Full-matrix least-squares on $F^2$ | |
| Data / restraints / parameters | 20154 / 0 / 497 | |
| Goodness-of-fit on $F^2$ | 1.041 | |
| Final R indices [I>2sigma(I)] | R1 = 0.0278, wR2 = 0.0666 | |
| R indices (all data) | R1 = 0.0399, wR2 = 0.0722 | |
| Extinction coefficient | n/a | |
| Largest diff. peak and hole | 0.621 and -0.960 $e.Å^{-3}$ | |

**Structural Data of for 3.4.**

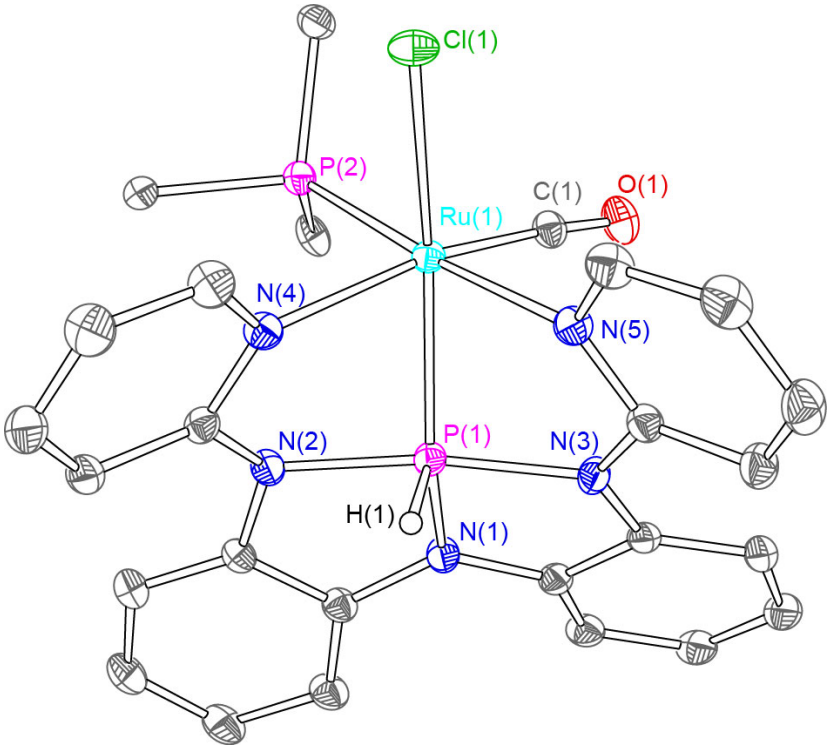

**Table B-3.** Crystal data and structure refinement for **3.4**. (CCDC 1859482)

| | | |
|---|---|---|
| Identification code | Ru8 | |
| Empirical formula | C41 H32 Cl N5 O P2 Ru | |
| Formula weight | 809.17 | |
| Temperature | 100(2) K | |
| Wavelength | 0.71073 Å | |
| Crystal system | Monoclinic | |
| Space group | $P2_1/c$ | |
| Unit cell dimensions | a = 11.6372(4) Å | □= 90°. |
| | b = 44.6425(16) Å | □= 96.7742(11)°. |
| | c = 20.0826(7) Å | □ = 90°. |
| Volume | 10360.3(6) $Å^3$ | |
| Z | 12 | |
| Density (calculated) | 1.556 $Mg/m^3$ | |
| Absorption coefficient | 0.667 $mm^{-1}$ | |
| F(000) | 4944 | |
| Crystal size | 0.220 x 0.100 x 0.060 $mm^3$ | |
| Theta range for data collection | 1.983 to 37.825°. | |
| Index ranges | -20<=h<=18, -76<=k<=77, -34<=l<=34 | |
| Reflections collected | 702712 | |
| Independent reflections | 55583 [R(int) = 0.0912] | |
| Completeness to theta = 25.242° | 99.9 % | |
| Absorption correction | None | |
| Refinement method | Full-matrix least-squares on $F^2$ | |
| Data / restraints / parameters | 55583 / 946 / 1505 | |
| Goodness-of-fit on $F^2$ | 1.014 | |
| Final R indices [I>2sigma(I)] | R1 = 0.0436, wR2 = 0.0960 | |
| R indices (all data) | R1 = 0.0806, wR2 = 0.1143 | |
| Extinction coefficient | n/a | |
| Largest diff. peak and hole | 1.860 and -1.863 e.$Å^{-3}$ | |

**Structural Data for 3.16.**

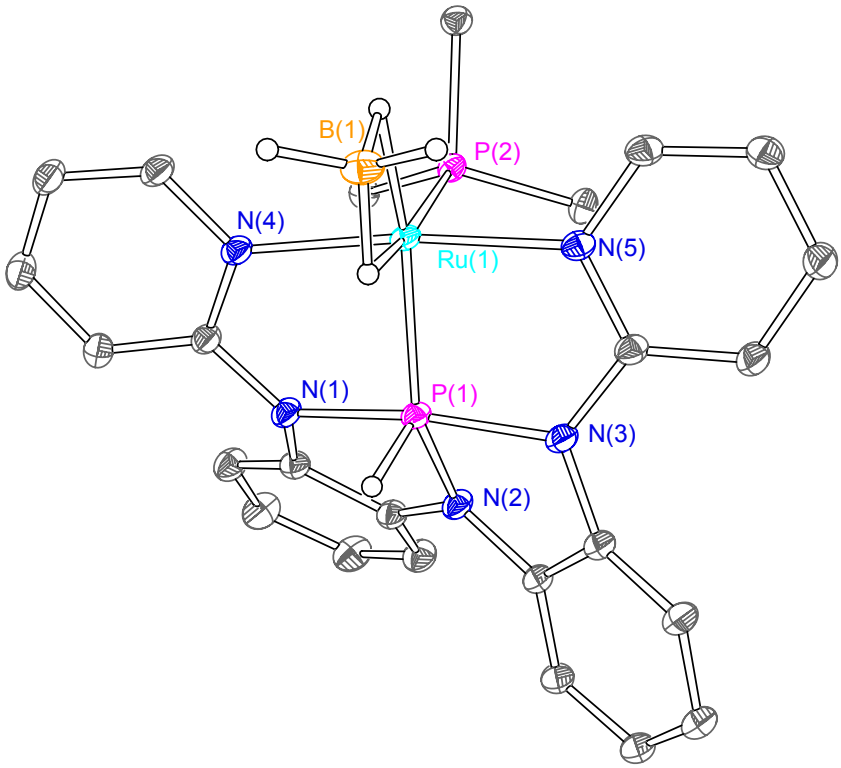

**Table B-4.** Crystal data and structure refinement for **3.16**.

| | | |
|---|---|---|
| Identification code | RuMPBH4-6 | |
| Empirical formula | C40 H36 B N5 P2 Ru | |
| Formula weight | 760.56 | |
| Temperature | 100(2) K | |
| Wavelength | 0.71073 Å | |
| Crystal system | Monoclinic | |
| Space group | $P2_1/n$ | |
| Unit cell dimensions | a = 12.9136(4) Å | a= 90°. |
| | b = 14.8041(4) Å | b= 91.6108(12)°. |
| | c = 17.9860(5) Å | g = 90°. |
| Volume | 3437.10(17) $Å^3$ | |
| Z | 4 | |
| Density (calculated) | 1.470 $Mg/m^3$ | |
| Absorption coefficient | 0.587 $mm^{-1}$ | |
| F(000) | 1560 | |
| Crystal size | 0.116 x 0.096 x 0.065 $mm^3$ | |
| Theta range for data collection | 2.359 to 36.375°. | |
| Index ranges | -21<=h<=21, -24<=k<=24, -29<=l<=29 | |
| Reflections collected | 273385 | |
| Independent reflections | 16694 [R(int) = 0.0641] | |
| Completeness to theta = 25.242° | 99.9 % | |
| Absorption correction | Semi-empirical from equivalents | |
| Max. and min. transmission | 0.7458 and 0.7155 | |
| Refinement method | Full-matrix least-squares on $F^2$ | |
| Data / restraints / parameters | 16694 / 1 / 457 | |
| Goodness-of-fit on $F^2$ | 1.033 | |
| Final R indices [I>2sigma(I)] | R1 = 0.0289, wR2 = 0.0647 | |
| R indices (all data) | R1 = 0.0401, wR2 = 0.0700 | |
| Extinction coefficient | n/a | |
| Largest diff. peak and hole | 0.625 and -0.750 $e.Å^{-3}$ | |

**Table B-5.** Atomic coordinates ( x $10^4$) and equivalent isotropic displacement parameters ($Å^2$x $10^3$) for **3.16**. U(eq) is defined as one third of the trace of the orthogonalized $U^{ij}$ tensor.

| | x | y | z | U(eq) |
|---|---|---|---|---|
| Ru(1) | 5875(1) | 3807(1) | 3224(1) | 11(1) |
| P(2) | 5553(1) | 3916(1) | 2011(1) | 13(1) |
| N(3) | 4794(1) | 3595(1) | 1240(1) | 15(1) |
| N(4) | 6385(1) | 2931(1) | 1746(1) | 15(1) |
| C(41) | 5028(1) | 2776(1) | 895(1) | 16(1) |
| C(42) | 5959(1) | 2392(1) | 1176(1) | 15(1) |
| C(43) | 6260(1) | 1549(1) | 915(1) | 20(1) |
| C(44) | 5642(1) | 1106(1) | 381(1) | 24(1) |
| C(45) | 4712(1) | 1474(1) | 124(1) | 24(1) |
| C(46) | 4391(1) | 2311(1) | 390(1) | 20(1) |
| N(5) | 4556(1) | 4820(1) | 2108(1) | 16(1) |
| C(51) | 4231(1) | 4311(1) | 911(1) | 16(1) |
| C(52) | 4108(1) | 5033(1) | 1409(1) | 16(1) |
| C(53) | 3688(1) | 5848(1) | 1162(1) | 21(1) |
| C(54) | 3331(1) | 5921(1) | 424(1) | 24(1) |
| C(55) | 3413(1) | 5196(1) | -57(1) | 23(1) |
| C(56) | 3882(1) | 4390(1) | 175(1) | 20(1) |
| N(6) | 4621(1) | 4656(1) | 3387(1) | 14(1) |
| C(61) | 7190(1) | 2689(1) | 2222(1) | 15(1) |
| C(62) | 8048(1) | 2177(1) | 2002(1) | 19(1) |
| C(63) | 8813(1) | 1942(1) | 2517(1) | 22(1) |
| C(64) | 8743(1) | 2245(1) | 3249(1) | 20(1) |
| C(65) | 7913(1) | 2781(1) | 3426(1) | 17(1) |
| N(7) | 7137(1) | 3003(1) | 2934(1) | 14(1) |
| C(71) | 4127(1) | 5016(1) | 2774(1) | 15(1) |
| C(72) | 3225(1) | 5541(1) | 2852(1) | 20(1) |
| C(73) | 2846(1) | 5695(1) | 3548(1) | 21(1) |
| C(74) | 3357(1) | 5336(1) | 4172(1) | 19(1) |
| C(75) | 4233(1) | 4830(1) | 4063(1) | 16(1) |

| | | | | |
|---|---|---|---|---|
| P(8) | 4845(1) | 2577(1) | 3428(1) | 12(1) |
| C(111) | 3471(1) | 2774(1) | 3206(1) | 16(1) |
| C(112) | 2764(1) | 2926(1) | 3765(1) | 20(1) |
| C(113) | 1738(1) | 3151(1) | 3581(1) | 27(1) |
| C(114) | 1411(1) | 3221(1) | 2844(1) | 29(1) |
| C(115) | 2114(1) | 3096(1) | 2284(1) | 26(1) |
| C(116) | 3138(1) | 2881(1) | 2463(1) | 20(1) |
| C(121) | 4826(1) | 2192(1) | 4401(1) | 16(1) |
| C(122) | 5235(1) | 2714(1) | 4984(1) | 18(1) |
| C(123) | 5197(1) | 2412(1) | 5718(1) | 24(1) |
| C(124) | 4759(1) | 1579(1) | 5873(1) | 26(1) |
| C(125) | 4347(1) | 1054(1) | 5296(1) | 25(1) |
| C(126) | 4377(1) | 1357(1) | 4566(1) | 21(1) |
| C(131) | 5189(1) | 1505(1) | 2989(1) | 15(1) |
| C(132) | 6120(1) | 1099(1) | 3228(1) | 20(1) |
| C(133) | 6438(1) | 289(1) | 2914(1) | 25(1) |
| C(134) | 5834(1) | -125(1) | 2366(1) | 26(1) |
| C(135) | 4908(1) | 267(1) | 2129(1) | 27(1) |
| C(136) | 4587(1) | 1078(1) | 2441(1) | 21(1) |
| B(9) | 6873(1) | 4762(1) | 3910(1) | 18(1) |

**Table B-6.** Bond lengths [Å] and angles [°] for **3.16**.

| | |
|---|---|
| Ru(1)-N(6) | 2.0780(10) |
| Ru(1)-N(7) | 2.0958(10) |
| Ru(1)-P(2) | 2.2161(3) |
| Ru(1)-B(9) | 2.2570(13) |
| Ru(1)-P(8) | 2.2900(3) |
| P(2)-N(3) | 1.7423(10) |
| P(2)-N(5) | 1.8691(10) |
| P(2)-N(4) | 1.8802(10) |
| N(3)-C(41) | 1.3987(15) |
| N(3)-C(51) | 1.4053(14) |
| N(4)-C(61) | 1.3763(14) |
| N(4)-C(42) | 1.3982(14) |
| C(41)-C(46) | 1.3918(16) |
| C(41)-C(42) | 1.4102(16) |
| C(42)-C(43) | 1.3931(16) |
| C(43)-C(44) | 1.3954(18) |
| C(44)-C(45) | 1.3858(19) |
| C(45)-C(46) | 1.3948(18) |
| N(5)-C(71) | 1.3656(14) |
| N(5)-C(52) | 1.4053(14) |
| C(51)-C(56) | 1.3919(16) |
| C(51)-C(52) | 1.4059(16) |
| C(52)-C(53) | 1.3901(16) |
| C(53)-C(54) | 1.3963(18) |
| C(54)-C(55) | 1.385(2) |
| C(55)-C(56) | 1.3960(18) |
| N(6)-C(75) | 1.3530(14) |
| N(6)-C(71) | 1.3653(14) |
| C(61)-N(7) | 1.3659(15) |
| C(61)-C(62) | 1.4075(16) |
| C(62)-C(63) | 1.3809(17) |
| C(63)-C(64) | 1.3963(19) |

| | |
|---|---|
| C(64)-C(65) | 1.3776(17) |
| C(65)-N(7) | 1.3589(14) |
| C(71)-C(72) | 1.4106(16) |
| C(72)-C(73) | 1.3772(17) |
| C(73)-C(74) | 1.3899(17) |
| C(74)-C(75) | 1.3758(17) |
| P(8)-C(111) | 1.8307(11) |
| P(8)-C(131) | 1.8325(11) |
| P(8)-C(121) | 1.8415(11) |
| C(111)-C(112) | 1.3941(17) |
| C(111)-C(116) | 1.4024(17) |
| C(112)-C(113) | 1.3976(18) |
| C(113)-C(114) | 1.383(2) |
| C(114)-C(115) | 1.388(2) |
| C(115)-C(116) | 1.3892(17) |
| C(121)-C(122) | 1.3942(16) |
| C(121)-C(126) | 1.4006(16) |
| C(122)-C(123) | 1.3950(17) |
| C(123)-C(124) | 1.3874(19) |
| C(124)-C(125) | 1.391(2) |
| C(125)-C(126) | 1.3893(18) |
| C(131)-C(136) | 1.3897(16) |
| C(131)-C(132) | 1.4017(16) |
| C(132)-C(133) | 1.3922(18) |
| C(133)-C(134) | 1.383(2) |
| C(134)-C(135) | 1.385(2) |
| C(135)-C(136) | 1.3933(18) |

| | |
|---|---|
| N(6)-Ru(1)-N(7) | 173.41(4) |
| N(6)-Ru(1)-P(2) | 88.24(3) |
| N(7)-Ru(1)-P(2) | 85.49(3) |
| N(6)-Ru(1)-B(9) | 88.81(4) |
| N(7)-Ru(1)-B(9) | 93.20(5) |
| P(2)-Ru(1)-B(9) | 125.51(3) |

| | |
|---|---|
| N(6)-Ru(1)-P(8) | 90.02(3) |
| N(7)-Ru(1)-P(8) | 92.74(3) |
| P(2)-Ru(1)-P(8) | 97.018(11) |
| B(9)-Ru(1)-P(8) | 137.39(3) |
| N(3)-P(2)-N(5) | 84.01(4) |
| N(3)-P(2)-N(4) | 84.22(4) |
| N(5)-P(2)-N(4) | 168.23(4) |
| N(3)-P(2)-Ru(1) | 148.19(4) |
| N(5)-P(2)-Ru(1) | 94.06(3) |
| N(4)-P(2)-Ru(1) | 95.77(3) |
| C(41)-N(3)-C(51) | 125.68(9) |
| C(41)-N(3)-P(2) | 117.71(8) |
| C(51)-N(3)-P(2) | 113.68(8) |
| C(61)-N(4)-C(42) | 125.59(10) |
| C(61)-N(4)-P(2) | 118.13(8) |
| C(42)-N(4)-P(2) | 114.36(7) |
| C(46)-C(41)-N(3) | 125.98(10) |
| C(46)-C(41)-C(42) | 121.13(11) |
| N(3)-C(41)-C(42) | 112.53(10) |
| C(43)-C(42)-N(4) | 130.55(10) |
| C(43)-C(42)-C(41) | 118.90(10) |
| N(4)-C(42)-C(41) | 110.28(10) |
| C(42)-C(43)-C(44) | 119.59(11) |
| C(45)-C(44)-C(43) | 121.19(12) |
| C(44)-C(45)-C(46) | 119.91(11) |
| C(41)-C(46)-C(45) | 119.15(11) |
| C(71)-N(5)-C(52) | 124.80(10) |
| C(71)-N(5)-P(2) | 122.10(7) |
| C(52)-N(5)-P(2) | 110.16(7) |
| C(56)-C(51)-N(3) | 127.79(11) |
| C(56)-C(51)-C(52) | 120.15(11) |
| N(3)-C(51)-C(52) | 111.87(9) |
| C(53)-C(52)-N(5) | 128.89(11) |
| C(53)-C(52)-C(51) | 120.42(10) |

| | |
|---|---|
| N(5)-C(52)-C(51) | 110.35(9) |
| C(52)-C(53)-C(54) | 119.13(12) |
| C(55)-C(54)-C(53) | 120.23(12) |
| C(54)-C(55)-C(56) | 121.10(11) |
| C(51)-C(56)-C(55) | 118.81(11) |
| C(75)-N(6)-C(71) | 118.38(10) |
| C(75)-N(6)-Ru(1) | 123.45(7) |
| C(71)-N(6)-Ru(1) | 118.06(7) |
| N(7)-C(61)-N(4) | 115.91(10) |
| N(7)-C(61)-C(62) | 120.51(10) |
| N(4)-C(61)-C(62) | 123.54(10) |
| C(63)-C(62)-C(61) | 120.04(11) |
| C(62)-C(63)-C(64) | 119.22(11) |
| C(65)-C(64)-C(63) | 118.28(11) |
| N(7)-C(65)-C(64) | 123.60(11) |
| C(65)-N(7)-C(61) | 118.21(10) |
| C(65)-N(7)-Ru(1) | 122.62(8) |
| C(61)-N(7)-Ru(1) | 119.17(7) |
| N(6)-C(71)-N(5) | 115.72(10) |
| N(6)-C(71)-C(72) | 120.23(10) |
| N(5)-C(71)-C(72) | 124.04(10) |
| C(73)-C(72)-C(71) | 119.77(11) |
| C(72)-C(73)-C(74) | 119.87(11) |
| C(75)-C(74)-C(73) | 117.86(11) |
| N(6)-C(75)-C(74) | 123.89(10) |
| C(111)-P(8)-C(131) | 106.83(5) |
| C(111)-P(8)-C(121) | 102.56(5) |
| C(131)-P(8)-C(121) | 98.75(5) |
| C(111)-P(8)-Ru(1) | 113.69(4) |
| C(131)-P(8)-Ru(1) | 118.04(4) |
| C(121)-P(8)-Ru(1) | 114.93(4) |
| C(112)-C(111)-C(116) | 118.66(11) |
| C(112)-C(111)-P(8) | 121.26(9) |
| C(116)-C(111)-P(8) | 119.67(9) |

| | |
|---|---|
| C(111)-C(112)-C(113) | 120.26(13) |
| C(114)-C(113)-C(112) | 120.43(13) |
| C(113)-C(114)-C(115) | 119.81(12) |
| C(116)-C(115)-C(114) | 120.03(13) |
| C(115)-C(116)-C(111) | 120.74(13) |
| C(122)-C(121)-C(126) | 118.63(11) |
| C(122)-C(121)-P(8) | 121.92(9) |
| C(126)-C(121)-P(8) | 119.44(9) |
| C(121)-C(122)-C(123) | 120.77(11) |
| C(124)-C(123)-C(122) | 120.01(12) |
| C(123)-C(124)-C(125) | 119.77(12) |
| C(126)-C(125)-C(124) | 120.23(12) |
| C(125)-C(126)-C(121) | 120.59(12) |
| C(136)-C(131)-C(132) | 118.68(11) |
| C(136)-C(131)-P(8) | 124.21(9) |
| C(132)-C(131)-P(8) | 117.12(9) |
| C(133)-C(132)-C(131) | 120.35(12) |
| C(134)-C(133)-C(132) | 120.32(12) |
| C(133)-C(134)-C(135) | 119.81(12) |
| C(134)-C(135)-C(136) | 120.13(13) |
| C(131)-C(136)-C(135) | 120.71(12) |

---

Symmetry transformations used to generate equivalent atoms:

**Table B-7.** Anisotropic displacement parameters ($Å^2 x\ 10^3$) for **3.16**. The anisotropic displacement factor exponent takes the form: $-2p^2[\ h^2\ a^{*2}U^{11} + ...\ + 2\ h\ k\ a^*\ b^*\ U^{12}\ ]$

| | $U^{11}$ | $U^{22}$ | $U^{33}$ | $U^{23}$ | $U^{13}$ | $U^{12}$ |
|---|---|---|---|---|---|---|
| Ru(1) | 12(1) | 12(1) | 10(1) | 1(1) | -2(1) | -2(1) |
| P(2) | 13(1) | 15(1) | 11(1) | 1(1) | -2(1) | 0(1) |
| N(3) | 16(1) | 17(1) | 12(1) | -2(1) | -4(1) | 4(1) |
| N(4) | 14(1) | 17(1) | 13(1) | -1(1) | -3(1) | 2(1) |
| C(41) | 16(1) | 18(1) | 13(1) | -1(1) | -1(1) | 1(1) |
| C(42) | 16(1) | 17(1) | 13(1) | 0(1) | -1(1) | 1(1) |
| C(43) | 23(1) | 18(1) | 19(1) | -2(1) | -3(1) | 4(1) |
| C(44) | 31(1) | 19(1) | 23(1) | -5(1) | -5(1) | 4(1) |
| C(45) | 28(1) | 21(1) | 21(1) | -5(1) | -7(1) | -1(1) |
| C(46) | 20(1) | 23(1) | 17(1) | -2(1) | -4(1) | 0(1) |
| N(5) | 18(1) | 17(1) | 12(1) | 1(1) | -2(1) | 4(1) |
| C(51) | 14(1) | 20(1) | 12(1) | 2(1) | -2(1) | 3(1) |
| C(52) | 17(1) | 20(1) | 13(1) | 2(1) | -1(1) | 4(1) |
| C(53) | 24(1) | 22(1) | 17(1) | 4(1) | -1(1) | 8(1) |
| C(54) | 25(1) | 30(1) | 18(1) | 7(1) | 0(1) | 10(1) |
| C(55) | 22(1) | 34(1) | 14(1) | 5(1) | -1(1) | 8(1) |
| C(56) | 19(1) | 28(1) | 12(1) | 0(1) | -2(1) | 4(1) |
| N(6) | 16(1) | 13(1) | 12(1) | 0(1) | -2(1) | -1(1) |
| C(61) | 13(1) | 16(1) | 15(1) | 2(1) | -2(1) | 0(1) |
| C(62) | 15(1) | 23(1) | 19(1) | 0(1) | 0(1) | 3(1) |
| C(63) | 14(1) | 25(1) | 25(1) | 4(1) | -1(1) | 4(1) |
| C(64) | 14(1) | 24(1) | 22(1) | 6(1) | -4(1) | 1(1) |
| C(65) | 14(1) | 20(1) | 16(1) | 4(1) | -4(1) | -1(1) |
| N(7) | 12(1) | 16(1) | 14(1) | 2(1) | -2(1) | -2(1) |
| C(71) | 17(1) | 14(1) | 12(1) | -1(1) | -2(1) | 1(1) |
| C(72) | 22(1) | 24(1) | 14(1) | -1(1) | -3(1) | 8(1) |
| C(73) | 22(1) | 25(1) | 16(1) | -3(1) | -1(1) | 8(1) |
| C(74) | 23(1) | 21(1) | 13(1) | -3(1) | -1(1) | 2(1) |
| C(75) | 21(1) | 16(1) | 12(1) | -1(1) | -2(1) | 0(1) |

| | | | | | | |
|---|---|---|---|---|---|---|
| P(8) | 11(1) | 12(1) | 13(1) | 0(1) | -2(1) | -1(1) |
| C(111) | 13(1) | 13(1) | 22(1) | -1(1) | -2(1) | -1(1) |
| C(112) | 15(1) | 18(1) | 28(1) | -4(1) | 1(1) | -1(1) |
| C(113) | 16(1) | 24(1) | 42(1) | -8(1) | 3(1) | 1(1) |
| C(114) | 16(1) | 21(1) | 49(1) | -4(1) | -9(1) | 2(1) |
| C(115) | 20(1) | 21(1) | 36(1) | 3(1) | -12(1) | -1(1) |
| C(116) | 16(1) | 20(1) | 24(1) | 3(1) | -5(1) | -2(1) |
| C(121) | 15(1) | 17(1) | 15(1) | 3(1) | 0(1) | -1(1) |
| C(122) | 20(1) | 20(1) | 15(1) | 2(1) | -1(1) | -3(1) |
| C(123) | 28(1) | 28(1) | 16(1) | 4(1) | -1(1) | -2(1) |
| C(124) | 28(1) | 30(1) | 19(1) | 9(1) | 3(1) | 0(1) |
| C(125) | 28(1) | 23(1) | 24(1) | 8(1) | 4(1) | -4(1) |
| C(126) | 23(1) | 18(1) | 21(1) | 3(1) | 2(1) | -4(1) |
| C(131) | 15(1) | 12(1) | 18(1) | 0(1) | 1(1) | -2(1) |
| C(132) | 15(1) | 17(1) | 28(1) | 0(1) | -1(1) | 0(1) |
| C(133) | 19(1) | 18(1) | 39(1) | 2(1) | 7(1) | 4(1) |
| C(134) | 31(1) | 16(1) | 33(1) | -2(1) | 12(1) | 0(1) |
| C(135) | 36(1) | 18(1) | 26(1) | -6(1) | 1(1) | -4(1) |
| C(136) | 22(1) | 17(1) | 22(1) | -2(1) | -2(1) | -2(1) |
| B(9) | 20(1) | 18(1) | 15(1) | 1(1) | -3(1) | -6(1) |

**Table B-8.** Hydrogen coordinates ( x $10^4$) and isotropic displacement parameters ($Å^2$x $10^3$) for **3.16**.

| | x | y | z | U(eq) |
|---|---|---|---|---|
| H(43) | 6883 | 1278 | 1099 | 24 |
| H(44) | 5863 | 542 | 189 | 29 |
| H(45) | 4295 | 1157 | -232 | 28 |
| H(46) | 3745 | 2559 | 228 | 24 |
| H(53) | 3644 | 6348 | 1490 | 25 |
| H(54) | 3030 | 6471 | 252 | 29 |
| H(55) | 3146 | 5247 | -552 | 28 |
| H(56) | 3961 | 3904 | -164 | 23 |
| H(62) | 8101 | 1994 | 1498 | 23 |
| H(63) | 9381 | 1578 | 2376 | 26 |
| H(64) | 9255 | 2086 | 3616 | 24 |
| H(65) | 7882 | 3008 | 3919 | 21 |
| H(72) | 2879 | 5787 | 2424 | 24 |
| H(73) | 2237 | 6046 | 3603 | 26 |
| H(74) | 3109 | 5438 | 4657 | 23 |
| H(75) | 4586 | 4587 | 4489 | 20 |
| H(1P) | 6212(11) | 4518(10) | 1713(8) | 15 |
| H(112) | 2981 | 2876 | 4272 | 25 |
| H(113) | 1261 | 3257 | 3964 | 33 |
| H(114) | 707 | 3354 | 2722 | 35 |
| H(115) | 1896 | 3158 | 1777 | 31 |
| H(116) | 3618 | 2804 | 2077 | 24 |
| H(122) | 5542 | 3281 | 4881 | 22 |
| H(123) | 5472 | 2776 | 6111 | 29 |
| H(124) | 4741 | 1369 | 6372 | 31 |
| H(125) | 4043 | 485 | 5402 | 30 |
| H(126) | 4090 | 995 | 4176 | 25 |
| H(132) | 6537 | 1377 | 3607 | 24 |

| | | | | |
|---|---|---|---|---|
| H(133) | 7072 | 19 | 3077 | 30 |
| H(134) | 6054 | -677 | 2151 | 32 |
| H(135) | 4491 | -18 | 1754 | 32 |
| H(136) | 3950 | 1342 | 2277 | 25 |
| H(1B) | 6454(13) | 4082(12) | 4142(10) | 21 |
| H(2B) | 6686(13) | 4776(12) | 3231(9) | 21 |
| H(3B) | 6529(13) | 5353(12) | 4160(9) | 21 |
| H(4B) | 7724(13) | 4685(12) | 3997(9) | 21 |

**Table B-9.** Torsion angles [°] for **3.16**.

| | |
|---|---|
| N(5)-P(2)-N(3)-C(41) | -170.77(9) |
| N(4)-P(2)-N(3)-C(41) | 8.91(9) |
| Ru(1)-P(2)-N(3)-C(41) | -82.72(11) |
| N(5)-P(2)-N(3)-C(51) | 27.45(8) |
| N(4)-P(2)-N(3)-C(51) | -152.86(9) |
| Ru(1)-P(2)-N(3)-C(51) | 115.50(8) |
| N(3)-P(2)-N(4)-C(61) | -172.84(9) |
| N(5)-P(2)-N(4)-C(61) | -171.3(2) |
| Ru(1)-P(2)-N(4)-C(61) | -24.82(9) |
| N(3)-P(2)-N(4)-C(42) | -7.76(8) |
| N(5)-P(2)-N(4)-C(42) | -6.2(3) |
| Ru(1)-P(2)-N(4)-C(42) | 140.27(8) |
| C(51)-N(3)-C(41)-C(46) | -35.86(18) |
| P(2)-N(3)-C(41)-C(46) | 164.78(10) |
| C(51)-N(3)-C(41)-C(42) | 151.00(11) |
| P(2)-N(3)-C(41)-C(42) | -8.35(13) |
| C(61)-N(4)-C(42)-C(43) | -5.2(2) |
| P(2)-N(4)-C(42)-C(43) | -168.96(11) |
| C(61)-N(4)-C(42)-C(41) | 168.76(11) |
| P(2)-N(4)-C(42)-C(41) | 4.97(12) |
| C(46)-C(41)-C(42)-C(43) | 2.87(18) |
| N(3)-C(41)-C(42)-C(43) | 176.39(11) |
| C(46)-C(41)-C(42)-N(4) | -171.86(11) |
| N(3)-C(41)-C(42)-N(4) | 1.65(14) |
| N(4)-C(42)-C(43)-C(44) | 173.80(13) |
| C(41)-C(42)-C(43)-C(44) | 0.31(18) |
| C(42)-C(43)-C(44)-C(45) | -2.4(2) |
| C(43)-C(44)-C(45)-C(46) | 1.3(2) |
| N(3)-C(41)-C(46)-C(45) | -176.55(12) |
| C(42)-C(41)-C(46)-C(45) | -3.96(18) |
| C(44)-C(45)-C(46)-C(41) | 1.9(2) |

| | |
|---|---|
| N(3)-P(2)-N(5)-C(71) | 133.39(10) |
| N(4)-P(2)-N(5)-C(71) | 131.9(2) |
| Ru(1)-P(2)-N(5)-C(71) | -14.74(9) |
| N(3)-P(2)-N(5)-C(52) | -28.04(8) |
| N(4)-P(2)-N(5)-C(52) | -29.6(3) |
| Ru(1)-P(2)-N(5)-C(52) | -176.16(7) |
| C(41)-N(3)-C(51)-C(56) | -6.39(19) |
| P(2)-N(3)-C(51)-C(56) | 153.69(11) |
| C(41)-N(3)-C(51)-C(52) | 178.69(11) |
| P(2)-N(3)-C(51)-C(52) | -21.24(12) |
| C(71)-N(5)-C(52)-C(53) | 48.23(19) |
| P(2)-N(5)-C(52)-C(53) | -150.95(11) |
| C(71)-N(5)-C(52)-C(51) | -138.58(11) |
| P(2)-N(5)-C(52)-C(51) | 22.24(12) |
| C(56)-C(51)-C(52)-C(53) | -3.48(18) |
| N(3)-C(51)-C(52)-C(53) | 171.88(11) |
| C(56)-C(51)-C(52)-N(5) | -177.34(11) |
| N(3)-C(51)-C(52)-N(5) | -1.98(14) |
| N(5)-C(52)-C(53)-C(54) | 176.54(12) |
| C(51)-C(52)-C(53)-C(54) | 3.95(19) |
| C(52)-C(53)-C(54)-C(55) | -1.2(2) |
| C(53)-C(54)-C(55)-C(56) | -2.1(2) |
| N(3)-C(51)-C(56)-C(55) | -174.35(12) |
| C(52)-C(51)-C(56)-C(55) | 0.20(18) |
| C(54)-C(55)-C(56)-C(51) | 2.6(2) |
| C(42)-N(4)-C(61)-N(7) | -144.72(11) |
| P(2)-N(4)-C(61)-N(7) | 18.53(13) |
| C(42)-N(4)-C(61)-C(62) | 37.52(17) |
| P(2)-N(4)-C(61)-C(62) | -159.23(9) |
| N(7)-C(61)-C(62)-C(63) | 3.99(18) |
| N(4)-C(61)-C(62)-C(63) | -178.35(11) |
| C(61)-C(62)-C(63)-C(64) | -2.35(19) |
| C(62)-C(63)-C(64)-C(65) | -0.83(19) |
| C(63)-C(64)-C(65)-N(7) | 2.62(18) |

| | |
|---|---|
| C(64)-C(65)-N(7)-C(61) | -1.05(17) |
| C(64)-C(65)-N(7)-Ru(1) | 179.21(9) |
| N(4)-C(61)-N(7)-C(65) | 179.89(10) |
| C(62)-C(61)-N(7)-C(65) | -2.27(16) |
| N(4)-C(61)-N(7)-Ru(1) | -0.36(13) |
| C(62)-C(61)-N(7)-Ru(1) | 177.47(8) |
| C(75)-N(6)-C(71)-N(5) | 179.79(10) |
| Ru(1)-N(6)-C(71)-N(5) | -3.97(13) |
| C(75)-N(6)-C(71)-C(72) | -1.10(16) |
| Ru(1)-N(6)-C(71)-C(72) | 175.14(9) |
| C(52)-N(5)-C(71)-N(6) | 172.30(10) |
| P(2)-N(5)-C(71)-N(6) | 13.65(14) |
| C(52)-N(5)-C(71)-C(72) | -6.77(18) |
| P(2)-N(5)-C(71)-C(72) | -165.42(10) |
| N(6)-C(71)-C(72)-C(73) | 0.44(19) |
| N(5)-C(71)-C(72)-C(73) | 179.47(12) |
| C(71)-C(72)-C(73)-C(74) | 0.3(2) |
| C(72)-C(73)-C(74)-C(75) | -0.29(19) |
| C(71)-N(6)-C(75)-C(74) | 1.11(17) |
| Ru(1)-N(6)-C(75)-C(74) | -174.92(9) |
| C(73)-C(74)-C(75)-N(6) | -0.41(19) |
| C(131)-P(8)-C(111)-C(112) | 125.17(10) |
| C(121)-P(8)-C(111)-C(112) | 21.86(11) |
| Ru(1)-P(8)-C(111)-C(112) | -102.84(9) |
| C(131)-P(8)-C(111)-C(116) | -62.34(10) |
| C(121)-P(8)-C(111)-C(116) | -165.64(9) |
| Ru(1)-P(8)-C(111)-C(116) | 69.66(10) |
| C(116)-C(111)-C(112)-C(113) | 1.97(18) |
| P(8)-C(111)-C(112)-C(113) | 174.54(10) |
| C(111)-C(112)-C(113)-C(114) | 0.4(2) |
| C(112)-C(113)-C(114)-C(115) | -2.2(2) |
| C(113)-C(114)-C(115)-C(116) | 1.5(2) |
| C(114)-C(115)-C(116)-C(111) | 0.85(19) |
| C(112)-C(111)-C(116)-C(115) | -2.59(18) |

| | |
|---|---|
| P(8)-C(111)-C(116)-C(115) | -175.28(10) |
| C(111)-P(8)-C(121)-C(122) | -111.59(10) |
| C(131)-P(8)-C(121)-C(122) | 138.87(10) |
| Ru(1)-P(8)-C(121)-C(122) | 12.29(11) |
| C(111)-P(8)-C(121)-C(126) | 67.60(11) |
| C(131)-P(8)-C(121)-C(126) | -41.94(11) |
| Ru(1)-P(8)-C(121)-C(126) | -168.52(9) |
| C(126)-C(121)-C(122)-C(123) | -0.08(18) |
| P(8)-C(121)-C(122)-C(123) | 179.11(10) |
| C(121)-C(122)-C(123)-C(124) | 0.7(2) |
| C(122)-C(123)-C(124)-C(125) | -0.8(2) |
| C(123)-C(124)-C(125)-C(126) | 0.3(2) |
| C(124)-C(125)-C(126)-C(121) | 0.3(2) |
| C(122)-C(121)-C(126)-C(125) | -0.42(19) |
| P(8)-C(121)-C(126)-C(125) | -179.64(10) |
| C(111)-P(8)-C(131)-C(136) | 15.29(12) |
| C(121)-P(8)-C(131)-C(136) | 121.33(11) |
| Ru(1)-P(8)-C(131)-C(136) | -114.26(10) |
| C(111)-P(8)-C(131)-C(132) | -164.54(9) |
| C(121)-P(8)-C(131)-C(132) | -58.50(10) |
| Ru(1)-P(8)-C(131)-C(132) | 65.91(10) |
| C(136)-C(131)-C(132)-C(133) | 0.84(18) |
| P(8)-C(131)-C(132)-C(133) | -179.32(10) |
| C(131)-C(132)-C(133)-C(134) | -0.4(2) |
| C(132)-C(133)-C(134)-C(135) | -0.2(2) |
| C(133)-C(134)-C(135)-C(136) | 0.3(2) |
| C(132)-C(131)-C(136)-C(135) | -0.73(19) |
| P(8)-C(131)-C(136)-C(135) | 179.44(10) |
| C(134)-C(135)-C(136)-C(131) | 0.2(2) |

Symmetry transformations used to generate equivalent atoms:

**Structural Data for 3.23**

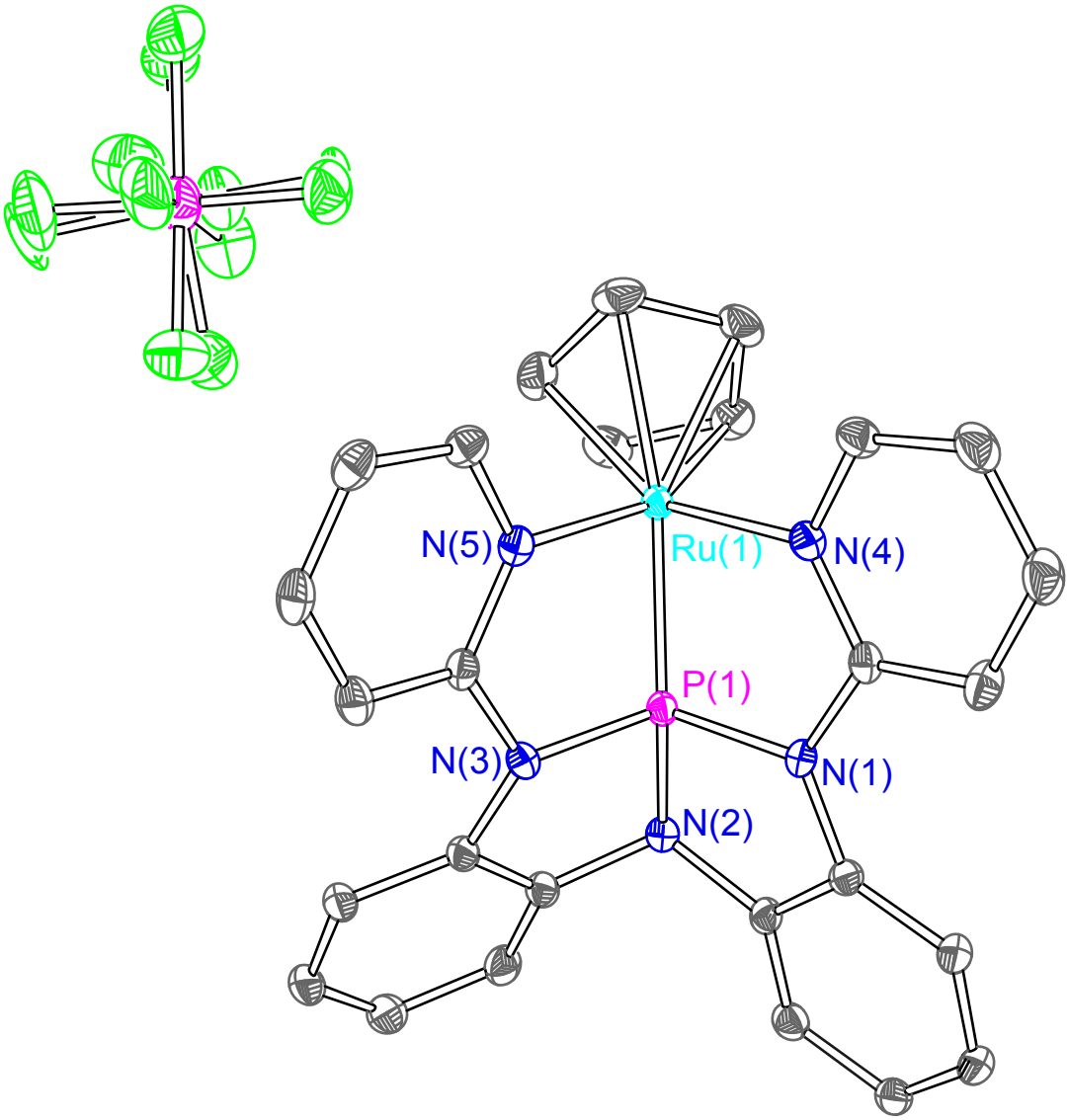

**Table B-10**. Crystal data and structure refinement for **3.23**.

| | | |
|---|---|---|
| Identification code | RuCp9 | |
| Empirical formula | C29 H23 Cl6 F6 N5 P2 Ru | |
| Formula weight | 931.23 | |
| Temperature | 100(2) K | |
| Wavelength | 0.71073 Å | |
| Crystal system | Monoclinic | |
| Space group | $P2_1/n$ | |
| Unit cell dimensions | a = 18.5071(8) Å | a= 90°. |
| | b = 8.3411(4) Å | b= 93.2110(19)°. |
| | c = 21.6315(10) Å | g = 90°. |
| Volume | 3334.0(3) $Å^3$ | |
| Z | 4 | |
| Density (calculated) | 1.855 $Mg/m^3$ | |
| Absorption coefficient | 1.114 $mm^{-1}$ | |
| F(000) | 1848 | |
| Crystal size | 0.235 x 0.095 x 0.035 $mm^3$ | |
| Theta range for data collection | 1.410 to 36.380°. | |
| Index ranges | -30<=h<=30, -13<=k<=13, -36<=l<=36 | |
| Reflections collected | 234290 | |
| Independent reflections | 16145 [R(int) = 0.0833] | |
| Completeness to theta = 25.242° | 100.0 % | |
| Absorption correction | Semi-empirical from equivalents | |
| Max. and min. transmission | 0.7471 and 0.6758 | |
| Refinement method | Full-matrix least-squares on $F^2$ | |
| Data / restraints / parameters | 16145 / 420 / 551 | |
| Goodness-of-fit on $F^2$ | 1.056 | |
| Final R indices [I>2sigma(I)] | R1 = 0.0405, wR2 = 0.0771 | |
| R indices (all data) | R1 = 0.0687, wR2 = 0.0886 | |
| Extinction coefficient | n/a | |
| Largest diff. peak and hole | 0.714 and -1.222 $e.Å^{-3}$ | |

**Table B-11**Atomic coordinates ( x $10^4$) and equivalent isotropic displacement parameters ($Å^2$x $10^3$) for **3.23**. U(eq) is defined as one third of the trace of the orthogonalized $U^{ij}$ tensor.

| | x | y | z | U(eq) |
|---|---|---|---|---|
| Ru(1) | 7598(1) | 8382(1) | 4593(1) | 13(1) |
| P(1) | 8062(1) | 6100(1) | 4344(1) | 12(1) |
| N(2) | 8655(1) | 5128(2) | 3896(1) | 15(1) |
| N(3) | 7338(1) | 4985(2) | 4042(1) | 14(1) |
| N(1) | 8446(1) | 5301(2) | 5018(1) | 14(1) |
| C(41) | 7514(1) | 4213(2) | 3484(1) | 15(1) |
| C(42) | 8257(1) | 4344(2) | 3391(1) | 15(1) |
| C(43) | 8548(1) | 3791(2) | 2856(1) | 20(1) |
| C(44) | 8092(1) | 3004(2) | 2419(1) | 23(1) |
| C(45) | 7362(1) | 2846(2) | 2514(1) | 22(1) |
| C(46) | 7059(1) | 3462(2) | 3039(1) | 18(1) |
| C(51) | 9025(1) | 4235(2) | 4908(1) | 14(1) |
| C(52) | 9145(1) | 4161(2) | 4273(1) | 15(1) |
| C(53) | 9687(1) | 3221(2) | 4053(1) | 18(1) |
| C(54) | 10112(1) | 2298(2) | 4471(1) | 19(1) |
| C(55) | 9994(1) | 2353(2) | 5094(1) | 20(1) |
| C(56) | 9452(1) | 3322(2) | 5322(1) | 18(1) |
| N(5) | 7822(1) | 7348(2) | 5474(1) | 15(1) |
| C(61) | 6656(1) | 5515(2) | 4200(1) | 15(1) |
| C(62) | 6022(1) | 4626(2) | 4096(1) | 19(1) |
| C(63) | 5376(1) | 5258(2) | 4276(1) | 21(1) |
| C(64) | 5376(1) | 6716(2) | 4582(1) | 21(1) |
| C(65) | 6022(1) | 7510(2) | 4695(1) | 18(1) |
| N(4) | 6657(1) | 6956(2) | 4494(1) | 15(1) |
| C(71) | 8251(1) | 6037(2) | 5563(1) | 15(1) |
| C(72) | 8451(1) | 5497(2) | 6160(1) | 20(1) |
| C(73) | 8207(1) | 6302(3) | 6664(1) | 24(1) |
| C(74) | 7742(1) | 7596(3) | 6574(1) | 23(1) |
| C(75) | 7557(1) | 8061(2) | 5977(1) | 18(1) |

| | | | | |
|---|---|---|---|---|
| C(101) | 7111(1) | 10838(2) | 4617(1) | 25(1) |
| C(102) | 7822(1) | 10913(2) | 4892(1) | 23(1) |
| C(103) | 8319(1) | 10445(2) | 4449(1) | 22(1) |
| C(104) | 7906(1) | 10100(2) | 3885(1) | 24(1) |
| C(105) | 7169(1) | 10313(2) | 3992(1) | 25(1) |
| P(2) | 4771(1) | 10647(1) | 3560(1) | 29(1) |
| F(81A) | 5288(10) | 10950(40) | 4196(13) | 25(2) |
| F(82A) | 5211(12) | 8990(30) | 3460(12) | 39(3) |
| F(83A) | 4270(30) | 10280(40) | 2899(18) | 53(4) |
| F(84A) | 4364(8) | 12348(15) | 3820(8) | 38(2) |
| F(85A) | 5290(9) | 11661(19) | 3238(7) | 32(2) |
| F(86A) | 4228(13) | 9710(30) | 3998(13) | 41(3) |
| F(81B) | 5279(5) | 10760(17) | 4170(5) | 39(2) |
| F(82B) | 5010(4) | 8855(9) | 3447(4) | 38(1) |
| F(83B) | 4251(9) | 10570(16) | 2962(7) | 57(2) |
| F(84B) | 4510(4) | 12427(5) | 3608(4) | 46(1) |
| F(85B) | 5442(4) | 11269(9) | 3147(3) | 43(1) |
| F(86B) | 4116(4) | 10016(11) | 3949(5) | 48(2) |
| C(1S) | 3412(1) | 6822(2) | 3555(1) | 22(1) |
| Cl(1A) | 3367(10) | 6110(40) | 4290(11) | 30(3) |
| Cl(2A) | 2609(7) | 7915(15) | 3382(5) | 36(2) |
| Cl(3A) | 3525(9) | 5440(20) | 2975(7) | 35(2) |
| Cl(1B) | 3385(3) | 5945(14) | 4305(3) | 25(1) |
| Cl(2B) | 2627(2) | 7982(5) | 3368(1) | 28(1) |
| Cl(3B) | 3490(3) | 5295(7) | 3005(3) | 35(1) |
| C(2S) | 10130(1) | 8814(2) | 2856(1) | 21(1) |
| Cl(4A) | 10873(8) | 9229(18) | 3350(6) | 31(2) |
| Cl(5A) | 9533(5) | 7721(19) | 3231(5) | 52(2) |
| Cl(6A) | 9758(8) | 10621(14) | 2538(7) | 46(2) |
| Cl(4B) | 10887(3) | 9337(6) | 3367(2) | 24(1) |
| Cl(5B) | 9537(2) | 7515(3) | 3248(1) | 23(1) |
| Cl(6B) | 9661(2) | 10533(3) | 2606(2) | 34(1) |

**Table B-12**. Bond lengths [Å] and angles [°] for **3.23**.

| | |
|---|---|
| Ru(1)-N(4) | 2.1101(14) |
| Ru(1)-N(5) | 2.1103(15) |
| Ru(1)-P(1) | 2.1678(5) |
| Ru(1)-C(105) | 2.1912(19) |
| Ru(1)-C(104) | 2.1968(19) |
| Ru(1)-C(103) | 2.2103(18) |
| Ru(1)-C(102) | 2.2403(19) |
| Ru(1)-C(101) | 2.2406(19) |
| P(1)-N(2) | 1.7091(15) |
| P(1)-N(1) | 1.7191(14) |
| P(1)-N(3) | 1.7297(15) |
| N(2)-C(52) | 1.434(2) |
| N(2)-C(42) | 1.439(2) |
| N(3)-C(61) | 1.398(2) |
| N(3)-C(41) | 1.421(2) |
| N(1)-C(71) | 1.395(2) |
| N(1)-C(51) | 1.422(2) |
| C(41)-C(46) | 1.393(2) |
| C(41)-C(42) | 1.406(2) |
| C(42)-C(43) | 1.383(2) |
| C(43)-C(44) | 1.395(3) |
| C(44)-C(45) | 1.384(3) |
| C(45)-C(46) | 1.392(3) |
| C(51)-C(56) | 1.388(2) |
| C(51)-C(52) | 1.404(2) |
| C(52)-C(53) | 1.380(2) |
| C(53)-C(54) | 1.396(3) |
| C(54)-C(55) | 1.379(3) |
| C(55)-C(56) | 1.399(3) |
| N(5)-C(75) | 1.356(2) |
| N(5)-C(71) | 1.359(2) |
| C(61)-N(4) | 1.360(2) |

| | |
|---|---|
| C(61)-C(62) | 1.395(2) |
| C(62)-C(63) | 1.382(3) |
| C(63)-C(64) | 1.385(3) |
| C(64)-C(65) | 1.377(3) |
| C(65)-N(4) | 1.357(2) |
| C(71)-C(72) | 1.398(2) |
| C(72)-C(73) | 1.378(3) |
| C(73)-C(74) | 1.388(3) |
| C(74)-C(75) | 1.373(3) |
| C(101)-C(102) | 1.415(3) |
| C(101)-C(105) | 1.430(3) |
| C(102)-C(103) | 1.421(3) |
| C(103)-C(104) | 1.432(3) |
| C(104)-C(105) | 1.408(3) |
| P(2)-F(85A) | 1.482(14) |
| P(2)-F(84B) | 1.567(4) |
| P(2)-F(83B) | 1.571(13) |
| P(2)-F(81B) | 1.578(11) |
| P(2)-F(82B) | 1.582(7) |
| P(2)-F(86B) | 1.602(9) |
| P(2)-F(86A) | 1.62(2) |
| P(2)-F(82A) | 1.63(2) |
| P(2)-F(81A) | 1.65(3) |
| P(2)-F(85B) | 1.653(6) |
| P(2)-F(83A) | 1.69(3) |
| P(2)-F(84A) | 1.716(14) |
| C(1S)-Cl(1A) | 1.70(2) |
| C(1S)-Cl(3A) | 1.725(15) |
| C(1S)-Cl(3B) | 1.754(6) |
| C(1S)-Cl(2A) | 1.766(12) |
| C(1S)-Cl(2B) | 1.773(4) |
| C(1S)-Cl(1B) | 1.782(9) |
| C(2S)-Cl(5A) | 1.677(12) |
| C(2S)-Cl(4A) | 1.727(16) |

| | |
|---|---|
| C(2S)-Cl(6B) | 1.746(4) |
| C(2S)-Cl(6A) | 1.780(12) |
| C(2S)-Cl(4B) | 1.789(6) |
| C(2S)-Cl(5B) | 1.789(3) |

| | |
|---|---|
| N(4)-Ru(1)-N(5) | 88.86(6) |
| N(4)-Ru(1)-P(1) | 79.41(4) |
| N(5)-Ru(1)-P(1) | 78.77(4) |
| N(4)-Ru(1)-C(105) | 94.83(7) |
| N(5)-Ru(1)-C(105) | 151.89(7) |
| P(1)-Ru(1)-C(105) | 129.32(6) |
| N(4)-Ru(1)-C(104) | 122.80(7) |
| N(5)-Ru(1)-C(104) | 148.32(7) |
| P(1)-Ru(1)-C(104) | 106.14(6) |
| C(105)-Ru(1)-C(104) | 37.42(8) |
| N(4)-Ru(1)-C(103) | 157.79(7) |
| N(5)-Ru(1)-C(103) | 110.88(7) |
| P(1)-Ru(1)-C(103) | 113.44(5) |
| C(105)-Ru(1)-C(103) | 62.96(7) |
| C(104)-Ru(1)-C(103) | 37.93(8) |
| N(4)-Ru(1)-C(102) | 134.30(7) |
| N(5)-Ru(1)-C(102) | 95.79(7) |
| P(1)-Ru(1)-C(102) | 146.09(6) |
| C(105)-Ru(1)-C(102) | 62.17(8) |
| C(104)-Ru(1)-C(102) | 62.32(7) |
| C(103)-Ru(1)-C(102) | 37.24(7) |
| N(4)-Ru(1)-C(101) | 100.74(7) |
| N(5)-Ru(1)-C(101) | 114.32(7) |
| P(1)-Ru(1)-C(101) | 166.90(6) |
| C(105)-Ru(1)-C(101) | 37.63(8) |
| C(104)-Ru(1)-C(101) | 62.58(8) |
| C(103)-Ru(1)-C(101) | 62.50(7) |
| C(102)-Ru(1)-C(101) | 36.81(8) |
| N(2)-P(1)-N(1) | 92.81(7) |

| | |
|---|---|
| N(2)-P(1)-N(3) | 92.17(7) |
| N(1)-P(1)-N(3) | 112.76(7) |
| N(2)-P(1)-Ru(1) | 146.42(6) |
| N(1)-P(1)-Ru(1) | 106.31(5) |
| N(3)-P(1)-Ru(1) | 104.89(5) |
| C(52)-N(2)-C(42) | 117.17(14) |
| C(52)-N(2)-P(1) | 110.40(11) |
| C(42)-N(2)-P(1) | 109.26(11) |
| C(61)-N(3)-C(41) | 127.20(14) |
| C(61)-N(3)-P(1) | 115.34(11) |
| C(41)-N(3)-P(1) | 110.81(11) |
| C(71)-N(1)-C(51) | 130.48(14) |
| C(71)-N(1)-P(1) | 115.54(12) |
| C(51)-N(1)-P(1) | 112.38(11) |
| C(46)-C(41)-C(42) | 119.64(16) |
| C(46)-C(41)-N(3) | 129.23(16) |
| C(42)-C(41)-N(3) | 111.06(14) |
| C(43)-C(42)-C(41) | 121.57(16) |
| C(43)-C(42)-N(2) | 125.52(16) |
| C(41)-C(42)-N(2) | 112.89(14) |
| C(42)-C(43)-C(44) | 118.40(18) |
| C(45)-C(44)-C(43) | 120.11(17) |
| C(44)-C(45)-C(46) | 121.87(17) |
| C(45)-C(46)-C(41) | 118.29(17) |
| C(56)-C(51)-C(52) | 119.45(15) |
| C(56)-C(51)-N(1) | 129.94(15) |
| C(52)-C(51)-N(1) | 110.61(14) |
| C(53)-C(52)-C(51) | 121.34(16) |
| C(53)-C(52)-N(2) | 124.89(15) |
| C(51)-C(52)-N(2) | 113.77(14) |
| C(52)-C(53)-C(54) | 118.98(17) |
| C(55)-C(54)-C(53) | 120.04(16) |
| C(54)-C(55)-C(56) | 121.26(17) |
| C(51)-C(56)-C(55) | 118.92(16) |

| | |
|---|---|
| C(75)-N(5)-C(71) | 118.27(15) |
| C(75)-N(5)-Ru(1) | 118.93(12) |
| C(71)-N(5)-Ru(1) | 122.72(11) |
| N(4)-C(61)-C(62) | 121.63(16) |
| N(4)-C(61)-N(3) | 114.61(14) |
| C(62)-C(61)-N(3) | 123.69(16) |
| C(63)-C(62)-C(61) | 119.00(17) |
| C(62)-C(63)-C(64) | 119.54(17) |
| C(65)-C(64)-C(63) | 118.88(17) |
| N(4)-C(65)-C(64) | 122.62(17) |
| C(65)-N(4)-C(61) | 118.17(15) |
| C(65)-N(4)-Ru(1) | 120.04(12) |
| C(61)-N(4)-Ru(1) | 121.68(11) |
| N(5)-C(71)-N(1) | 114.26(14) |
| N(5)-C(71)-C(72) | 120.85(16) |
| N(1)-C(71)-C(72) | 124.88(16) |
| C(73)-C(72)-C(71) | 119.55(18) |
| C(72)-C(73)-C(74) | 119.66(17) |
| C(75)-C(74)-C(73) | 118.22(17) |
| N(5)-C(75)-C(74) | 123.26(17) |
| C(102)-C(101)-C(105) | 107.10(18) |
| C(102)-C(101)-Ru(1) | 71.58(11) |
| C(105)-C(101)-Ru(1) | 69.31(11) |
| C(101)-C(102)-C(103) | 109.02(18) |
| C(101)-C(102)-Ru(1) | 71.60(11) |
| C(103)-C(102)-Ru(1) | 70.23(11) |
| C(102)-C(103)-C(104) | 107.15(17) |
| C(102)-C(103)-Ru(1) | 72.53(11) |
| C(104)-C(103)-Ru(1) | 70.52(11) |
| C(105)-C(104)-C(103) | 108.07(18) |
| C(105)-C(104)-Ru(1) | 71.07(11) |
| C(103)-C(104)-Ru(1) | 71.54(11) |
| C(104)-C(105)-C(101) | 108.64(18) |
| C(104)-C(105)-Ru(1) | 71.51(11) |

| | |
|---|---|
| C(101)-C(105)-Ru(1) | 73.06(11) |
| F(84B)-P(2)-F(83B) | 85.1(6) |
| F(84B)-P(2)-F(81B) | 93.4(6) |
| F(83B)-P(2)-F(81B) | 178.4(7) |
| F(84B)-P(2)-F(82B) | 174.7(5) |
| F(83B)-P(2)-F(82B) | 89.8(5) |
| F(81B)-P(2)-F(82B) | 91.6(6) |
| F(84B)-P(2)-F(86B) | 91.8(3) |
| F(83B)-P(2)-F(86B) | 88.4(8) |
| F(81B)-P(2)-F(86B) | 90.8(5) |
| F(82B)-P(2)-F(86B) | 89.9(3) |
| F(85A)-P(2)-F(86A) | 171.7(10) |
| F(85A)-P(2)-F(82A) | 94.7(8) |
| F(86A)-P(2)-F(82A) | 89.8(9) |
| F(85A)-P(2)-F(81A) | 86.7(10) |
| F(86A)-P(2)-F(81A) | 86.4(12) |
| F(82A)-P(2)-F(81A) | 88.4(14) |
| F(84B)-P(2)-F(85B) | 89.0(2) |
| F(83B)-P(2)-F(85B) | 90.6(7) |
| F(81B)-P(2)-F(85B) | 90.2(4) |
| F(82B)-P(2)-F(85B) | 89.3(3) |
| F(86B)-P(2)-F(85B) | 178.7(5) |
| F(85A)-P(2)-F(83A) | 92.5(18) |
| F(86A)-P(2)-F(83A) | 95(2) |
| F(82A)-P(2)-F(83A) | 89.3(15) |
| F(81A)-P(2)-F(83A) | 177.5(18) |
| F(85A)-P(2)-F(84A) | 89.4(5) |
| F(86A)-P(2)-F(84A) | 84.9(8) |
| F(82A)-P(2)-F(84A) | 168.4(10) |
| F(81A)-P(2)-F(84A) | 80.9(13) |
| F(83A)-P(2)-F(84A) | 101.4(15) |
| Cl(1A)-C(1S)-Cl(3A) | 117.3(13) |
| Cl(1A)-C(1S)-Cl(2A) | 107.1(9) |
| Cl(3A)-C(1S)-Cl(2A) | 109.0(6) |

| | |
|---|---|
| Cl(3B)-C(1S)-Cl(2B) | 109.8(2) |
| Cl(3B)-C(1S)-Cl(1B) | 109.1(4) |
| Cl(2B)-C(1S)-Cl(1B) | 111.5(3) |
| Cl(5A)-C(2S)-Cl(4A) | 109.5(6) |
| Cl(5A)-C(2S)-Cl(6A) | 113.3(5) |
| Cl(4A)-C(2S)-Cl(6A) | 110.3(6) |
| Cl(6B)-C(2S)-Cl(4B) | 110.4(2) |
| Cl(6B)-C(2S)-Cl(5B) | 109.65(19) |
| Cl(4B)-C(2S)-Cl(5B) | 109.5(2) |

---

Symmetry transformations used to generate equivalent atoms:

**Table B-13**. Anisotropic displacement parameters ($Å^2 x\ 10^3$) for **3.23**. The anisotropic displacement factor exponent takes the form: $-2p^2[\ h^2\ a^{*2}U^{11} + ... + 2\ h\ k\ a^*\ b^*\ U^{12}\ ]$

| | $U^{11}$ | $U^{22}$ | $U^{33}$ | $U^{23}$ | $U^{13}$ | $U^{12}$ |
|---|---|---|---|---|---|---|
| Ru(1) | 13(1) | 12(1) | 13(1) | 0(1) | -1(1) | -1(1) |
| P(1) | 12(1) | 12(1) | 13(1) | 0(1) | -1(1) | -1(1) |
| N(2) | 14(1) | 15(1) | 14(1) | 0(1) | 0(1) | 0(1) |
| N(3) | 14(1) | 14(1) | 15(1) | -2(1) | -1(1) | -2(1) |
| N(1) | 13(1) | 15(1) | 13(1) | 1(1) | -2(1) | 1(1) |
| C(41) | 18(1) | 13(1) | 14(1) | 1(1) | -3(1) | 0(1) |
| C(42) | 19(1) | 15(1) | 13(1) | 0(1) | -2(1) | 0(1) |
| C(43) | 22(1) | 23(1) | 15(1) | 0(1) | -1(1) | 4(1) |
| C(44) | 30(1) | 24(1) | 15(1) | -4(1) | -2(1) | 7(1) |
| C(45) | 30(1) | 21(1) | 16(1) | -3(1) | -7(1) | 2(1) |
| C(46) | 21(1) | 16(1) | 18(1) | -1(1) | -5(1) | 0(1) |
| C(51) | 11(1) | 13(1) | 18(1) | 0(1) | -1(1) | -1(1) |
| C(52) | 13(1) | 14(1) | 17(1) | 0(1) | -2(1) | -2(1) |
| C(53) | 15(1) | 18(1) | 20(1) | -4(1) | 0(1) | -1(1) |
| C(54) | 12(1) | 18(1) | 28(1) | -6(1) | -3(1) | 0(1) |
| C(55) | 17(1) | 18(1) | 25(1) | -1(1) | -6(1) | 3(1) |
| C(56) | 17(1) | 17(1) | 18(1) | 0(1) | -4(1) | 1(1) |
| N(5) | 15(1) | 15(1) | 15(1) | -1(1) | 0(1) | -2(1) |
| C(61) | 14(1) | 16(1) | 14(1) | 2(1) | -2(1) | -2(1) |
| C(62) | 17(1) | 20(1) | 18(1) | 1(1) | -1(1) | -5(1) |
| C(63) | 14(1) | 26(1) | 22(1) | 3(1) | -2(1) | -5(1) |
| C(64) | 14(1) | 24(1) | 26(1) | 4(1) | 2(1) | 0(1) |
| C(65) | 16(1) | 18(1) | 21(1) | 1(1) | 2(1) | 1(1) |
| N(4) | 14(1) | 16(1) | 15(1) | 2(1) | -1(1) | -1(1) |
| C(71) | 13(1) | 17(1) | 14(1) | 1(1) | -1(1) | -2(1) |
| C(72) | 18(1) | 26(1) | 16(1) | 4(1) | -1(1) | 3(1) |
| C(73) | 26(1) | 32(1) | 13(1) | 1(1) | -1(1) | 1(1) |
| C(74) | 29(1) | 26(1) | 14(1) | -4(1) | 1(1) | 0(1) |
| C(75) | 21(1) | 18(1) | 16(1) | -2(1) | 3(1) | 1(1) |

| | | | | | | |
|---|---|---|---|---|---|---|
| C(101) | 22(1) | 14(1) | 40(1) | 1(1) | 4(1) | 1(1) |
| C(102) | 32(1) | 13(1) | 24(1) | -2(1) | -2(1) | -6(1) |
| C(103) | 19(1) | 15(1) | 32(1) | 3(1) | 0(1) | -4(1) |
| C(104) | 35(1) | 15(1) | 22(1) | 3(1) | 5(1) | -4(1) |
| C(105) | 29(1) | 16(1) | 28(1) | 8(1) | -9(1) | -2(1) |
| P(2) | 31(1) | 20(1) | 36(1) | 5(1) | -11(1) | -6(1) |
| F(81A) | 20(5) | 32(7) | 23(4) | 1(4) | -7(3) | -7(3) |
| F(82A) | 53(8) | 30(4) | 34(4) | 2(3) | -5(6) | -1(5) |
| F(83A) | 70(7) | 38(10) | 45(5) | -18(6) | -37(4) | -6(7) |
| F(84A) | 42(5) | 26(3) | 45(6) | 5(4) | -8(4) | 4(3) |
| F(85A) | 36(5) | 37(5) | 24(4) | 8(3) | -1(3) | -9(3) |
| F(86A) | 37(7) | 33(6) | 50(5) | -1(5) | -8(5) | -18(5) |
| F(81B) | 46(3) | 35(3) | 34(2) | 5(2) | -15(2) | 1(2) |
| F(82B) | 45(3) | 28(2) | 43(2) | -1(1) | 6(2) | 5(2) |
| F(83B) | 62(3) | 42(4) | 60(5) | 0(3) | -38(3) | -15(3) |
| F(84B) | 53(2) | 22(1) | 60(3) | -1(2) | -18(2) | 7(1) |
| F(85B) | 45(2) | 51(3) | 35(2) | 9(2) | 5(1) | -14(2) |
| F(86B) | 35(2) | 42(3) | 68(4) | -15(2) | 13(2) | -8(2) |
| C(1S) | 21(1) | 22(1) | 22(1) | 2(1) | 2(1) | 1(1) |
| Cl(1A) | 30(4) | 36(5) | 23(3) | 7(2) | -1(2) | 3(2) |
| Cl(2A) | 36(4) | 19(3) | 50(4) | 8(2) | -11(3) | 9(2) |
| Cl(3A) | 37(4) | 49(5) | 19(2) | 2(2) | 4(2) | 23(4) |
| Cl(1B) | 19(1) | 35(2) | 20(1) | 6(1) | -2(1) | -2(1) |
| Cl(2B) | 31(1) | 26(1) | 27(1) | -2(1) | -1(1) | 9(1) |
| Cl(3B) | 40(1) | 34(1) | 32(2) | -9(1) | 8(1) | 9(1) |
| C(2S) | 20(1) | 24(1) | 18(1) | 0(1) | -1(1) | 0(1) |
| Cl(4A) | 20(3) | 43(4) | 28(4) | 17(3) | -7(2) | -12(2) |
| Cl(5A) | 34(3) | 97(6) | 26(2) | 4(3) | -2(2) | -33(3) |
| Cl(6A) | 47(4) | 56(4) | 34(2) | 2(2) | -9(2) | 31(3) |
| Cl(4B) | 18(1) | 32(1) | 21(1) | 0(1) | -2(1) | -3(1) |
| Cl(5B) | 20(1) | 30(1) | 21(1) | 2(1) | 0(1) | -7(1) |
| Cl(6B) | 35(1) | 22(1) | 42(1) | 1(1) | -14(1) | 4(1) |

Table 5. Hydrogen coordinates ( x $10^4$) and isotropic displacement parameters ($Å^2$x $10^3$) for 3.23.

| | x | y | z | U(eq) |
|---|---|---|---|---|
| H(43) | 9046 | 3943 | 2787 | 24 |
| H(44) | 8283 | 2576 | 2055 | 28 |
| H(45) | 7060 | 2302 | 2213 | 27 |
| H(46) | 6554 | 3372 | 3091 | 22 |
| H(53) | 9770 | 3203 | 3624 | 22 |
| H(54) | 10482 | 1630 | 4325 | 23 |
| H(55) | 10287 | 1722 | 5375 | 24 |
| H(56) | 9377 | 3353 | 5752 | 21 |
| H(62) | 6035 | 3602 | 3906 | 22 |
| H(63) | 4936 | 4696 | 4189 | 25 |
| H(64) | 4937 | 7161 | 4713 | 25 |
| H(65) | 6023 | 8485 | 4922 | 22 |
| H(72) | 8752 | 4581 | 6218 | 24 |
| H(73) | 8357 | 5972 | 7072 | 29 |
| H(74) | 7557 | 8145 | 6915 | 28 |
| H(75) | 7227 | 8926 | 5913 | 22 |
| H(101) | 6676 | 11089 | 4811 | 30 |
| H(102) | 7946 | 11227 | 5307 | 28 |
| H(103) | 8830 | 10373 | 4514 | 26 |
| H(104) | 8096 | 9784 | 3504 | 29 |
| H(105) | 6775 | 10137 | 3699 | 30 |
| H(1S) | 3826 | 7591 | 3554 | 26 |
| H(2S) | 10299 | 8151 | 2507 | 25 |

**Table B-14**. Torsion angles [°] for **3.23**.

| | |
|---|---|
| N(1)-P(1)-N(2)-C(52) | 0.86(12) |
| N(3)-P(1)-N(2)-C(52) | -112.06(12) |
| Ru(1)-P(1)-N(2)-C(52) | 126.48(11) |
| N(1)-P(1)-N(2)-C(42) | 131.10(12) |
| N(3)-P(1)-N(2)-C(42) | 18.18(12) |
| Ru(1)-P(1)-N(2)-C(42) | -103.29(13) |
| N(2)-P(1)-N(3)-C(61) | -170.14(12) |
| N(1)-P(1)-N(3)-C(61) | 95.90(13) |
| Ru(1)-P(1)-N(3)-C(61) | -19.36(13) |
| N(2)-P(1)-N(3)-C(41) | -16.56(12) |
| N(1)-P(1)-N(3)-C(41) | -110.53(12) |
| Ru(1)-P(1)-N(3)-C(41) | 134.21(10) |
| N(2)-P(1)-N(1)-C(71) | 165.49(12) |
| N(3)-P(1)-N(1)-C(71) | -100.97(13) |
| Ru(1)-P(1)-N(1)-C(71) | 13.43(13) |
| N(2)-P(1)-N(1)-C(51) | -1.63(12) |
| N(3)-P(1)-N(1)-C(51) | 91.91(12) |
| Ru(1)-P(1)-N(1)-C(51) | -153.69(10) |
| C(61)-N(3)-C(41)-C(46) | -17.1(3) |
| P(1)-N(3)-C(41)-C(46) | -166.80(16) |
| C(61)-N(3)-C(41)-C(42) | 159.77(16) |
| P(1)-N(3)-C(41)-C(42) | 10.09(18) |
| C(46)-C(41)-C(42)-C(43) | 2.2(3) |
| N(3)-C(41)-C(42)-C(43) | -175.03(16) |
| C(46)-C(41)-C(42)-N(2) | -179.16(15) |
| N(3)-C(41)-C(42)-N(2) | 3.6(2) |
| C(52)-N(2)-C(42)-C(43) | -70.7(2) |
| P(1)-N(2)-C(42)-C(43) | 162.81(15) |
| C(52)-N(2)-C(42)-C(41) | 110.70(17) |
| P(1)-N(2)-C(42)-C(41) | -15.76(18) |
| C(41)-C(42)-C(43)-C(44) | -3.8(3) |
| N(2)-C(42)-C(43)-C(44) | 177.78(17) |

| | |
|---|---|
| C(42)-C(43)-C(44)-C(45) | 2.5(3) |
| C(43)-C(44)-C(45)-C(46) | 0.3(3) |
| C(44)-C(45)-C(46)-C(41) | -1.9(3) |
| C(42)-C(41)-C(46)-C(45) | 0.7(3) |
| N(3)-C(41)-C(46)-C(45) | 177.33(17) |
| C(71)-N(1)-C(51)-C(56) | 17.6(3) |
| P(1)-N(1)-C(51)-C(56) | -177.70(15) |
| C(71)-N(1)-C(51)-C(52) | -162.73(16) |
| P(1)-N(1)-C(51)-C(52) | 1.94(17) |
| C(56)-C(51)-C(52)-C(53) | -1.3(3) |
| N(1)-C(51)-C(52)-C(53) | 179.07(15) |
| C(56)-C(51)-C(52)-N(2) | 178.38(15) |
| N(1)-C(51)-C(52)-N(2) | -1.3(2) |
| C(42)-N(2)-C(52)-C(53) | 53.8(2) |
| P(1)-N(2)-C(52)-C(53) | 179.73(14) |
| C(42)-N(2)-C(52)-C(51) | -125.79(16) |
| P(1)-N(2)-C(52)-C(51) | 0.11(18) |
| C(51)-C(52)-C(53)-C(54) | 1.6(3) |
| N(2)-C(52)-C(53)-C(54) | -177.96(16) |
| C(52)-C(53)-C(54)-C(55) | -1.1(3) |
| C(53)-C(54)-C(55)-C(56) | 0.2(3) |
| C(52)-C(51)-C(56)-C(55) | 0.3(3) |
| N(1)-C(51)-C(56)-C(55) | 179.92(17) |
| C(54)-C(55)-C(56)-C(51) | 0.2(3) |
| C(41)-N(3)-C(61)-N(4) | -139.59(17) |
| P(1)-N(3)-C(61)-N(4) | 8.93(19) |
| C(41)-N(3)-C(61)-C(62) | 43.4(3) |
| P(1)-N(3)-C(61)-C(62) | -168.13(14) |
| N(4)-C(61)-C(62)-C(63) | 2.6(3) |
| N(3)-C(61)-C(62)-C(63) | 179.49(16) |
| C(61)-C(62)-C(63)-C(64) | -3.3(3) |
| C(62)-C(63)-C(64)-C(65) | 0.7(3) |
| C(63)-C(64)-C(65)-N(4) | 2.9(3) |
| C(64)-C(65)-N(4)-C(61) | -3.6(3) |

| | |
|---|---|
| C(64)-C(65)-N(4)-Ru(1) | 172.63(14) |
| C(62)-C(61)-N(4)-C(65) | 0.8(2) |
| N(3)-C(61)-N(4)-C(65) | -176.30(15) |
| C(62)-C(61)-N(4)-Ru(1) | -175.39(13) |
| N(3)-C(61)-N(4)-Ru(1) | 7.5(2) |
| C(75)-N(5)-C(71)-N(1) | 174.65(15) |
| Ru(1)-N(5)-C(71)-N(1) | -8.7(2) |
| C(75)-N(5)-C(71)-C(72) | -3.8(2) |
| Ru(1)-N(5)-C(71)-C(72) | 172.83(13) |
| C(51)-N(1)-C(71)-N(5) | 160.14(16) |
| P(1)-N(1)-C(71)-N(5) | -4.14(19) |
| C(51)-N(1)-C(71)-C(72) | -21.4(3) |
| P(1)-N(1)-C(71)-C(72) | 174.29(14) |
| N(5)-C(71)-C(72)-C(73) | 0.2(3) |
| N(1)-C(71)-C(72)-C(73) | -178.15(17) |
| C(71)-C(72)-C(73)-C(74) | 2.8(3) |
| C(72)-C(73)-C(74)-C(75) | -2.0(3) |
| C(71)-N(5)-C(75)-C(74) | 4.8(3) |
| Ru(1)-N(5)-C(75)-C(74) | -172.02(15) |
| C(73)-C(74)-C(75)-N(5) | -1.9(3) |
| C(105)-C(101)-C(102)-C(103) | 0.0(2) |
| Ru(1)-C(101)-C(102)-C(103) | 60.55(13) |
| C(105)-C(101)-C(102)-Ru(1) | -60.53(13) |
| C(101)-C(102)-C(103)-C(104) | 1.0(2) |
| Ru(1)-C(102)-C(103)-C(104) | 62.42(13) |
| C(101)-C(102)-C(103)-Ru(1) | -61.41(14) |
| C(102)-C(103)-C(104)-C(105) | -1.7(2) |
| Ru(1)-C(103)-C(104)-C(105) | 62.06(13) |
| C(102)-C(103)-C(104)-Ru(1) | -63.74(13) |
| C(103)-C(104)-C(105)-C(101) | 1.7(2) |
| Ru(1)-C(104)-C(105)-C(101) | 64.08(14) |
| C(103)-C(104)-C(105)-Ru(1) | -62.36(13) |
| C(102)-C(101)-C(105)-C(104) | -1.1(2) |
| Ru(1)-C(101)-C(105)-C(104) | -63.08(14) |

| | |
|---|---|
| C(102)-C(101)-C(105)-Ru(1) | 62.00(14) |

Symmetry transformations used to generate equivalent atoms:

**Structural Data for 3.24.**

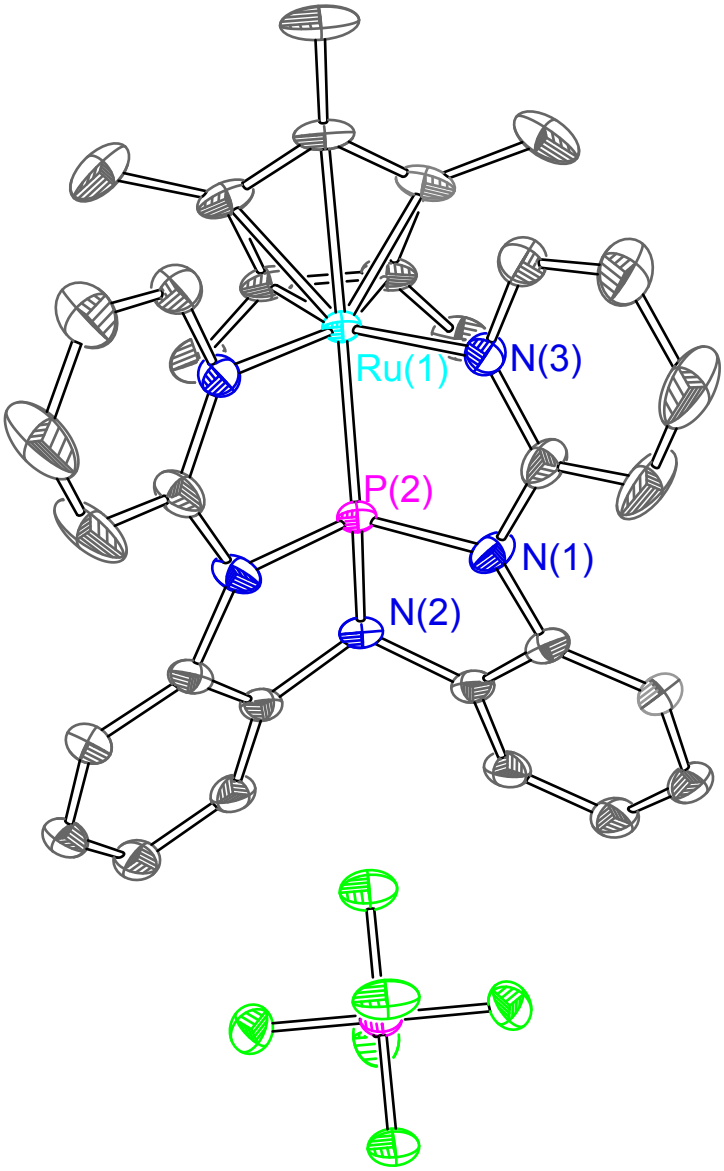

**Table B-15**. Crystal data and structure refinement for **3.24**.

| | | |
|---|---|---|
| Identification code | me5cpru-a | |
| Empirical formula | C32 H31 F6 N5 P2 Ru | |
| Formula weight | 762.63 | |
| Temperature | 99.99 K | |
| Wavelength | 0.71073 Å | |
| Crystal system | Orthorhombic | |
| Space group | Pnma | |
| Unit cell dimensions | a = 19.9724(4) Å | a= 90°. |
| | b = 11.5309(2) Å | b= 90°. |
| | c = 16.4044(4) Å | g = 90°. |
| Volume | 3777.93(14) $Å^3$ | |
| Z | 4 | |
| Density (calculated) | 1.341 $Mg/m^3$ | |
| Absorption coefficient | 0.556 $mm^{-1}$ | |
| F(000) | 1544 | |
| Crystal size | 0.245 x 0.155 x 0.124 $mm^3$ | |
| Theta range for data collection | 1.606 to 36.335°. | |
| Index ranges | -33<=h<=33, -19<=k<=19, -27<=l<=27 | |
| Reflections collected | 252341 | |
| Independent reflections | 9527 [R(int) = 0.0837] | |
| Completeness to theta = 25.242° | 99.9 % | |
| Absorption correction | None | |
| Refinement method | Full-matrix least-squares on $F^2$ | |
| Data / restraints / parameters | 9527 / 0 / 226 | |
| Goodness-of-fit on $F^2$ | 0.992 | |
| Final R indices [I>2sigma(I)] | R1 = 0.0361, wR2 = 0.0869 | |
| R indices (all data) | R1 = 0.0502, wR2 = 0.0943 | |
| Extinction coefficient | n/a | |
| Largest diff. peak and hole | 0.973 and -0.895 $e.Å^{-3}$ | |

**Table 2 Fractional Atomic Coordinates ($\times 10^4$) and Equivalent Isotropic Displacement Parameters ($Å^2 \times 10^3$) for Me5CpRu-a. $U_{eq}$ is defined as 1/3 of of the trace of the orthogonalised $U_{IJ}$ tensor.**

| Atom | *x* | *y* | *z* | U(eq) |
|---|---|---|---|---|
| Ru1 | 4268.8(2) | 7500 | 3066.4(2) | 15.97(4) |
| P1 | 5342.6(2) | 7500 | 3200.9(3) | 17.06(8) |
| P31 | 8372.4(3) | 7500 | 5667.0(4) | 26.37(11) |
| F34 | 7592.8(7) | 7500 | 5892.3(9) | 35.9(3) |
| F32 | 8562.8(9) | 7500 | 6617.5(10) | 42.8(4) |
| F36 | 8371.2(6) | 8894.4(9) | 5668.1(7) | 39.9(2) |
| F35 | 9153.6(7) | 7500 | 5447.8(13) | 44.4(4) |
| F33 | 8193.2(7) | 7500 | 4717.6(9) | 39.0(4) |
| N3 | 4543.1(6) | 6233.6(10) | 2186.6(7) | 21.8(2) |
| N2 | 5995.5(8) | 7500 | 3871.3(10) | 20.5(3) |
| N1 | 5617.2(6) | 6257.8(12) | 2724.5(8) | 24.7(2) |
| C2 | 6364.0(6) | 6430.3(13) | 3804.1(8) | 21.5(2) |
| C1 | 6164.5(7) | 5738.9(13) | 3139.2(8) | 22.4(2) |
| C6 | 6490.0(8) | 4698.3(14) | 2985.8(10) | 28.1(3) |
| C7 | 5166.9(8) | 5764.4(14) | 2171.0(10) | 28.2(3) |
| C3 | 6873.4(7) | 6087.3(14) | 4317.4(10) | 27.6(3) |
| C14 | 3898.1(7) | 8126.2(15) | 4236.4(8) | 26.4(3) |
| C12 | 3160.9(10) | 7500 | 3225.3(13) | 28.3(4) |
| C13 | 3442.0(7) | 8505.1(16) | 3616.9(9) | 29.3(3) |
| C4 | 7208.4(8) | 5054.1(15) | 4149.4(12) | 33.5(3) |
| C11 | 4100.6(9) | 5890.3(14) | 1610.8(10) | 29.2(3) |
| C5 | 7020.6(8) | 4376.8(15) | 3496.0(12) | 33.0(3) |
| C15 | 2608.4(11) | 7500 | 2596.4(16) | 42.2(7) |
| C17 | 4274.9(9) | 8879.4(18) | 4823.4(10) | 35.6(4) |
| C10 | 4244.4(11) | 5050.6(18) | 1039.5(13) | 45.8(5) |
| C16 | 3252.8(11) | 9729.6(19) | 3435.6(13) | 45.6(5) |
| C8 | 5343.2(12) | 4914(2) | 1608.0(13) | 53.1(6) |
| C9 | 4874.6(13) | 4554(2) | 1041.1(14) | 61.8(8) |

**Table B-16**. Bond lengths [Å] and angles [°] for **3.24**.

| Atom | Atom | Length/Å | Atom | Atom | Length/Å |
|---|---|---|---|---|---|
| Ru1 | P1 | 2.1560(5) | N2 | C2[1] | 1.4405(16) |
| Ru1 | N3[1] | 2.1250(12) | N1 | C1 | 1.4198(18) |
| Ru1 | N3 | 2.1250(12) | N1 | C7 | 1.3989(19) |
| Ru1 | C14 | 2.1803(14) | C2 | C1 | 1.409(2) |
| Ru1 | C14[1] | 2.1803(14) | C2 | C3 | 1.3787(19) |
| Ru1 | C12 | 2.228(2) | C1 | C6 | 1.388(2) |
| Ru1 | C13 | 2.2103(14) | C6 | C5 | 1.400(2) |
| Ru1 | C13[1] | 2.2103(14) | C7 | C8 | 1.393(2) |
| P1 | N2 | 1.7059(17) | C3 | C4 | 1.394(2) |
| P1 | N1[1] | 1.7214(12) | C14 | C14[1] | 1.444(3) |
| P1 | N1 | 1.7214(12) | C14 | C13 | 1.433(2) |
| P31 | F34 | 1.6002(16) | C14 | C17 | 1.499(2) |
| P31 | F32 | 1.6049(16) | C12 | C13 | 1.439(2) |
| P31 | F36[1] | 1.6078(11) | C12 | C13[1] | 1.439(2) |
| P31 | F36 | 1.6079(11) | C12 | C15 | 1.511(3) |
| P31 | F35 | 1.6012(17) | C13 | C16 | 1.492(3) |
| P31 | F33 | 1.5981(16) | C4 | C5 | 1.378(3) |
| N3 | C7 | 1.3585(19) | C11 | C10 | 1.378(2) |
| N3 | C11 | 1.3527(19) | C10 | C9 | 1.383(3) |
| N2 | C2 | 1.4405(16) | C8 | C9 | 1.383(3) |

[1]+X,3/2-Y,+Z

| Atom | Atom | Atom | Angle/° | Atom | Atom | Atom | Angle/° |
|---|---|---|---|---|---|---|---|
| P1 | Ru1 | C14 | 104.35(4) | F33 | P31 | F36 | 90.04(5) |
| P1 | Ru1 | C14[1] | 104.35(4) | F33 | P31 | F35 | 89.95(9) |
| P1 | Ru1 | C12 | 167.41(6) | C7 | N3 | Ru1 | 121.53(9) |
| P1 | Ru1 | C13[1] | 134.54(4) | C11 | N3 | Ru1 | 120.46(10) |
| P1 | Ru1 | C13 | 134.54(4) | C11 | N3 | C7 | 118.00(13) |
| N3[1] | Ru1 | P1 | 79.22(3) | C2 | N2 | P1 | 109.94(9) |
| N3 | Ru1 | P1 | 79.22(3) | C2[1] | N2 | P1 | 109.94(9) |
| N3 | Ru1 | N3[1] | 86.82(7) | C2[1] | N2 | C2 | 117.80(15) |
| N3 | Ru1 | C14[1] | 117.25(6) | C1 | N1 | P1 | 112.24(10) |

| | | | | | | | |
|---|---|---|---|---|---|---|---|
| N3 | Ru1 | C14 | 155.93(6) | C7 | N1 | P1 | 115.36(10) |
| N3[1] | Ru1 | C14[1] | 155.93(6) | C7 | N1 | C1 | 129.39(13) |
| N3[1] | Ru1 | C14 | 117.25(6) | C1 | C2 | N2 | 113.55(12) |
| N3 | Ru1 | C12 | 109.60(5) | C3 | C2 | N2 | 125.16(14) |
| N3[1] | Ru1 | C12 | 109.60(5) | C3 | C2 | C1 | 121.29(14) |
| N3[1] | Ru1 | C13[1] | 146.14(5) | C2 | C1 | N1 | 110.50(12) |
| N3 | Ru1 | C13 | 146.14(5) | C6 | C1 | N1 | 129.66(14) |
| N3[1] | Ru1 | C13 | 96.30(6) | C6 | C1 | C2 | 119.83(13) |
| N3 | Ru1 | C13[1] | 96.30(6) | C1 | C6 | C5 | 118.36(15) |
| C14 | Ru1 | C14[1] | 38.68(9) | N3 | C7 | N1 | 114.55(12) |
| C14 | Ru1 | C12 | 63.88(6) | N3 | C7 | C8 | 121.67(15) |
| C14[1] | Ru1 | C12 | 63.88(6) | C8 | C7 | N1 | 123.66(15) |
| C14[1] | Ru1 | C13[1] | 38.09(5) | C2 | C3 | C4 | 118.59(15) |
| C14 | Ru1 | C13[1] | 63.91(6) | C14[1] | C14 | Ru1 | 70.66(5) |
| C14 | Ru1 | C13 | 38.09(5) | C14[1] | C14 | C17 | 125.40(10) |
| C14[1] | Ru1 | C13 | 63.91(6) | C13 | C14 | Ru1 | 72.09(8) |
| C13 | Ru1 | C12 | 37.84(5) | C13 | C14 | C14[1] | 107.75(10) |
| C13[1] | Ru1 | C12 | 37.84(5) | C13 | C14 | C17 | 126.73(16) |
| C13[1] | Ru1 | C13 | 63.25(10) | C17 | C14 | Ru1 | 125.93(11) |
| N2 | P1 | Ru1 | 145.73(6) | C13[1] | C12 | Ru1 | 70.41(9) |
| N2 | P1 | N1[1] | 92.82(5) | C13 | C12 | Ru1 | 70.42(9) |
| N2 | P1 | N1 | 92.82(5) | C13 | C12 | C13[1] | 107.28(18) |
| N1[1] | P1 | Ru1 | 105.69(5) | C13 | C12 | C15 | 126.14(9) |
| N1 | P1 | Ru1 | 105.69(5) | C13[1] | C12 | C15 | 126.15(9) |
| N1[1] | P1 | N1 | 112.63(10) | C15 | C12 | Ru1 | 130.21(16) |
| F34 | P31 | F32 | 90.36(9) | C14 | C13 | Ru1 | 69.82(8) |
| F34 | P31 | F36 | 89.91(5) | C14 | C13 | C12 | 108.61(15) |
| F34 | P31 | F36[1] | 89.91(5) | C14 | C13 | C16 | 126.23(16) |
| F34 | P31 | F35 | 179.63(10) | C12 | C13 | Ru1 | 71.75(10) |
| F32 | P31 | F36[1] | 89.96(5) | C12 | C13 | C16 | 125.07(15) |
| F32 | P31 | F36 | 89.96(5) | C16 | C13 | Ru1 | 127.17(13) |
| F36[1] | P31 | F36 | 179.80(12) | C5 | C4 | C3 | 120.49(15) |
| F35 | P31 | F32 | 89.27(10) | N3 | C11 | C10 | 122.98(16) |
| F35 | P31 | F36[1] | 90.09(5) | C4 | C5 | C6 | 121.39(15) |
| F35 | P31 | F36 | 90.09(5) | C11 | C10 | C9 | 118.64(17) |
| F33 | P31 | F34 | 90.41(8) | C9 | C8 | C7 | 119.07(18) |

| | | | | | | | |
|---|---|---|---|---|---|---|---|
| F33 | P31 | F32 | 179.22(10) | C10 | C9 | C8 | 119.56(18) |
| F33 | P31 | F36[1] | 90.04(5) | | | | |

[1]+X,3/2-Y,+Z

**Table B-17.** Anisotropic displacement parameters ($Å^2 x\ 10^3$) for **3.24**. The anisotropic displacement factor exponent takes the form: $-2p^2[\ h^2\ a^{*2}U^{11} + ...\ + 2\ h\ k\ a^*\ b^*\ U^{12}\ ]$

| Atom | $U_{11}$ | $U_{22}$ | $U_{33}$ | $U_{23}$ | $U_{13}$ | $U_{12}$ |
|---|---|---|---|---|---|---|
| Ru1 | 12.50(6) | 19.96(6) | 15.44(6) | 0 | 0.72(4) | 0 |
| P1 | 12.84(17) | 20.7(2) | 17.59(19) | 0 | 1.97(14) | 0 |
| P31 | 20.8(2) | 29.2(3) | 29.1(3) | 0 | -8.89(19) | 0 |
| F34 | 27.0(7) | 54.6(9) | 26.0(6) | 0 | 2.1(5) | 0 |
| F32 | 58.8(10) | 35.8(8) | 33.8(7) | 0 | -24.9(7) | 0 |
| F36 | 36.5(5) | 30.2(5) | 52.9(7) | 6.8(5) | -10.9(5) | 4.2(4) |
| F35 | 18.6(6) | 42.1(9) | 72.5(12) | 0 | -10.0(7) | 0 |
| F33 | 22.8(6) | 67.9(11) | 26.3(6) | 0 | -0.9(5) | 0 |
| N3 | 22.6(5) | 21.6(5) | 21.2(5) | -2.4(4) | -3.1(4) | 1.7(4) |
| N2 | 13.2(6) | 27.1(8) | 21.2(7) | 0 | 0.0(5) | 0 |
| N1 | 20.6(5) | 29.1(6) | 24.3(5) | -7.0(5) | -2.6(4) | 9.0(4) |
| C2 | 14.5(5) | 25.8(6) | 24.2(6) | 4.7(5) | 1.9(4) | 0.1(5) |
| C1 | 15.6(5) | 26.9(6) | 24.8(6) | 2.0(5) | 2.1(4) | 4.1(5) |
| C6 | 22.1(6) | 27.2(7) | 35.0(7) | -0.3(6) | 1.2(5) | 5.2(5) |
| C7 | 29.5(7) | 29.8(7) | 25.2(6) | -8.9(5) | -6.7(5) | 10.2(6) |
| C3 | 19.4(6) | 30.6(7) | 32.7(7) | 7.9(6) | -5.3(5) | -3.5(5) |
| C14 | 16.6(5) | 43.4(8) | 19.2(5) | -5.3(5) | 1.3(4) | 4.9(5) |
| C12 | 12.0(7) | 51.3(13) | 21.6(8) | 0 | -0.7(6) | 0 |
| C13 | 18.7(6) | 46.5(9) | 22.5(6) | -5.3(6) | 0.7(5) | 11.6(6) |
| C4 | 22.1(6) | 31.4(8) | 47.0(9) | 11.1(7) | -8.1(6) | 1.2(6) |
| C11 | 30.6(7) | 30.2(7) | 26.9(7) | -6.1(6) | -8.8(6) | 2.0(6) |
| C5 | 21.8(6) | 27.2(7) | 49.9(10) | 8.0(7) | -1.0(6) | 6.5(5) |
| C15 | 16.6(9) | 82(2) | 27.9(11) | 0 | -5.6(8) | 0 |
| C17 | 31.5(8) | 49.4(10) | 26.0(7) | -14.8(7) | -3.4(6) | 8.0(7) |
| C10 | 55.4(12) | 41.9(10) | 40.2(9) | -20.5(8) | -24.6(9) | 12.3(9) |
| C16 | 44.2(10) | 52.2(11) | 40.3(9) | -12.1(8) | -7.7(8) | 27.0(9) |
| C8 | 56.2(12) | 57.1(12) | 46.0(10) | -30.9(10) | -22.5(10) | 36.8(11) |
| C9 | 77.6(17) | 57.0(13) | 50.9(12) | -34.8(11) | -31.7(12) | 37.2(12) |

**Table B-18.** Hydrogen coordinates ( x $10^4$) and isotropic displacement parameters ($Å^2$x $10^3$) for **3.24**.

| Atom | *x* | *y* | *z* | U(eq) |
|---|---|---|---|---|
| H6 | 6356.16 | 4215.96 | 2545.47 | 34 |
| H3 | 6993.58 | 6545.41 | 4776.01 | 33 |
| H4 | 7568.97 | 4815 | 4487.69 | 40 |
| H11 | 3671.2 | 6244.33 | 1599.92 | 35 |
| H5 | 7255.95 | 3677.05 | 3389.5 | 40 |
| H15A | 2744.61 | 7970.43 | 2127.31 | 63 |
| H15B | 2200.39 | 7826.53 | 2836.14 | 63 |
| H15C | 2521.63 | 6703.03 | 2417.73 | 63 |
| H17A | 4012.94 | 8971.46 | 5324.37 | 53 |
| H17B | 4352.17 | 9641.71 | 4576.59 | 53 |
| H17C | 4705.89 | 8517.31 | 4952.86 | 53 |
| H10 | 3917.24 | 4817.39 | 652.42 | 55 |
| H16A | 3614.98 | 10248.28 | 3607.38 | 68 |
| H16B | 2842.16 | 9927.22 | 3731.72 | 68 |
| H16C | 3176.84 | 9817.86 | 2848.68 | 68 |
| H8 | 5779.34 | 4584.84 | 1613.32 | 64 |
| H9 | 4985 | 3970.58 | 655.23 | 74 |

**Table B-19**. Torsion angles [°] for **3.24**..

| A | B | C | D | Angle/° | A | B | C | D | Angle/° |
|---|---|---|---|---|---|---|---|---|---|
| Ru1 | P1 | N2 | C2[1] | -114.37(10) | N1 | C7 | C8 | C9 | -174.5(2) |
| Ru1 | P1 | N2 | C2 | 114.37(10) | C2[1] | N2 | C2 | C1 | -118.23(15) |
| Ru1 | P1 | N1 | C1 | -143.09(9) | C2[1] | N2 | C2 | C3 | 60.8(2) |
| Ru1 | P1 | N1 | C7 | 19.16(13) | C2 | C1 | C6 | C5 | -1.1(2) |
| Ru1 | N3 | C7 | N1 | -5.5(2) | C2 | C3 | C4 | C5 | -1.7(2) |
| Ru1 | N3 | C7 | C8 | 178.40(17) | C1 | N1 | C7 | N3 | 148.79(15) |
| Ru1 | N3 | C11 | C10 | -178.18(16) | C1 | N1 | C7 | C8 | -35.2(3) |
| Ru1 | C14 | C13 | C12 | 61.59(12) | C1 | C2 | C3 | C4 | 2.3(2) |
| Ru1 | C14 | C13 | C16 | -121.92(18) | C1 | C6 | C5 | C4 | 1.7(3) |
| Ru1 | C12 | C13 | C14 | -60.38(10) | C7 | N3 | C11 | C10 | 3.3(3) |
| Ru1 | C12 | C13 | C16 | 123.08(17) | C7 | N1 | C1 | C2 | -163.02(15) |
| P1 | N2 | C2 | C1 | 8.75(15) | C7 | N1 | C1 | C6 | 15.6(3) |
| P1 | N2 | C2 | C3 | -172.25(12) | C7 | C8 | C9 | C10 | 0.5(4) |
| P1 | N1 | C1 | C2 | -3.91(15) | C3 | C2 | C1 | N1 | 177.84(13) |
| P1 | N1 | C1 | C6 | 174.69(13) | C3 | C2 | C1 | C6 | -0.9(2) |
| P1 | N1 | C7 | N3 | -9.80(19) | C3 | C4 | C5 | C6 | -0.3(3) |
| P1 | N1 | C7 | C8 | 166.20(18) | C14[1] | C14 | C13 | Ru1 | -62.04(4) |
| N3 | C7 | C8 | C9 | 1.2(4) | C14[1] | C14 | C13 | C12 | -0.45(14) |
| N3 | C11 | C10 | C9 | -1.6(3) | C14[1] | C14 | C13 | C16 | 176.04(15) |
| N2 | P1 | N1 | C1 | 7.75(11) | C13[1] | C12 | C13 | Ru1 | 61.10(14) |
| N2 | P1 | N1 | C7 | 170.00(12) | C13[1] | C12 | C13 | C14 | 0.7(2) |
| N2 | C2 | C1 | N1 | -3.11(17) | C13[1] | C12 | C13 | C16 | -175.82(13) |
| N2 | C2 | C1 | C6 | 178.13(13) | C11 | N3 | C7 | N1 | 173.02(14) |
| N2 | C2 | C3 | C4 | -176.60(14) | C11 | N3 | C7 | C8 | -3.1(3) |
| N1 | P1 | N2 | C2 | -9.21(11) | C11 | C10 | C9 | C8 | -0.4(4) |
| N1[1] | P1 | N2 | C2 | -122.05(11) | C15 | C12 | C13 | Ru1 | -126.1(2) |
| N1 | P1 | N2 | C2[1] | 122.05(11) | C15 | C12 | C13 | C14 | 173.56(19) |
| N1[1] | P1 | N2 | C2[1] | 9.21(11) | C15 | C12 | C13 | C16 | -3.0(3) |
| N1[1] | P1 | N1 | C1 | 101.98(11) | C17 | C14 | C13 | Ru1 | 121.88(15) |
| N1[1] | P1 | N1 | C7 | -95.77(13) | C17 | C14 | C13 | C12 | -176.53(16) |
| N1 | C1 | C6 | C5 | -179.59(15) | C17 | C14 | C13 | C16 | 0.0(3) |

## B.2. DFT Calculation

### *B.2.1. General computational information.*

Geometries were optimized in Orca 4.0.0[1] using the M06-2X[2] (for **L1**) or B3LYP[3] (for **3.3** and **3.4**) density functionals with the def2-TZVP basis set[4]. Calculations were carried out in the gas phase without symmetry constraint. Stationary points were characterized by frequency calculations to confirm their identity as local minima (zero imaginary frequencies). Natural Population Analysis for **3.4** was performed at B3LYP/def2-TZVP level with a NBO 6.0 package.[5]

For topological analysis of the electron density (QTAIM),[6] an all-electron single point calculation was conducted. A relativistic approximation was introduced by applying zeroth-order regular approximation (ZORA)[7] using the B3PW91[8] density functional with the relativistically recontracted version of def2-TZVP basis set. Coordinates obtained from the above geometry optimization is used as the input. Analysis and visualization of the QTAIM results were performed with the Multiwfn[9] program.

*B.2.2. Comparison of crystallographic and computed structures of **3.3** and **3.4***

**Table B-20.** Selected bond distances (Å) and angles (°) for **3.3** and **3.4**.

| metric | 2 | | 3 | |
|---|---|---|---|---|
| | *experimental* | *calculated* | *experimental* | *calculated* |
| $d(Ru_1–P_1)$ | 2.1262(3) | 2.138 | 2.2509(4) | 2.284 |
| $d(Ru_1–P_2)$ | 2.3329(3) | 2.365 | 2.3359(4) | 2.389 |
| $d(Ru_1–Cl_1)$ | 2.4836(3) | 2.496 | 2.4749(4) | 2.499 |
| $d(P_1–N_1)$ | 1.7085(9) | 1.727 | 1.7178(14) | 1.733 |
| $d(P_1–N_2)$ | 1.7280(9) | 1.737 | 1.8362(14) | 1.864 |
| $d(P_1–N_3)$ | 1.7135(9) | 1.745 | 1.8193(15) | 1.854 |
| $\angle Ru_1–P_1–N_1$ | 147.62(3) | 150.92 | 140.14(6) | 142.90 |
| $\angle P_1–Ru_1–Cl_1$ | 168.851(10) | 166.69 | 160.569(16) | 156.93 |
| $\angle N_2–P_1–N_3$ | 113.94(4) | 114.59 | 170.74(7) | 168.49 |
| $\angle N_1–P_1–N_2$ | 91.40(4) | 90.61 | 86.59(7) | 86.59 |
| $\angle N_1–P_1–N_3$ | 92.04(4) | 90.08 | 87.25(7) | 86.00 |

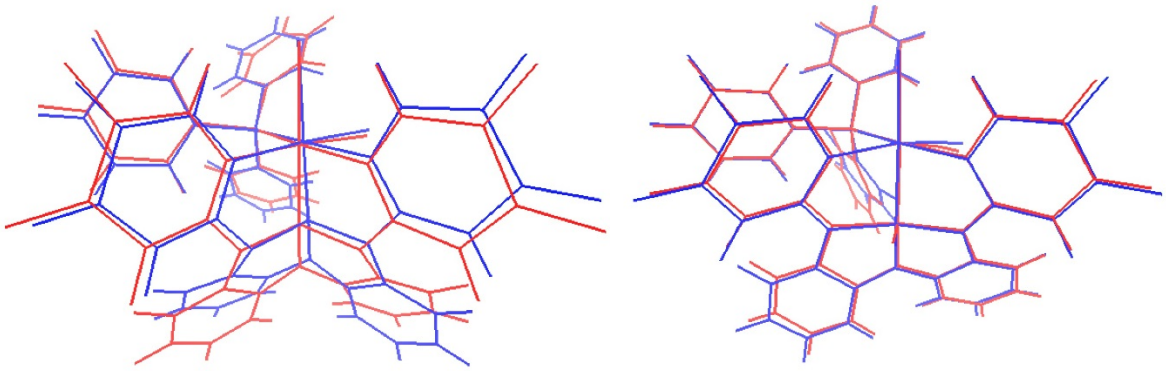

**Figure B-1**. Overlay of crystallographic (red line) and computational (blue line) structures for **2** (*left*) and **3** (*right*).

## B.3. Multinuclear NMR spectra

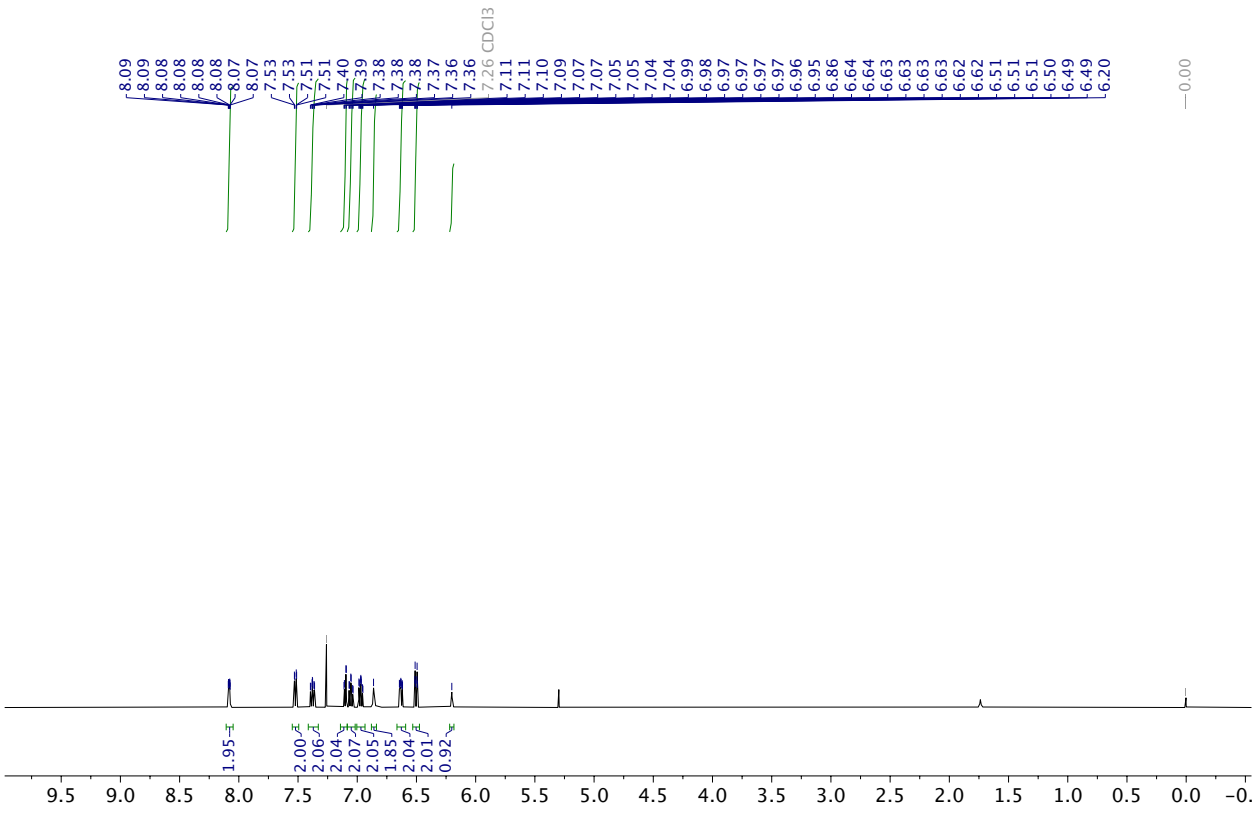


**Figure B-2**. $^{1}H$ NMR spectrum ($CDCl_3$) of **3.2**.

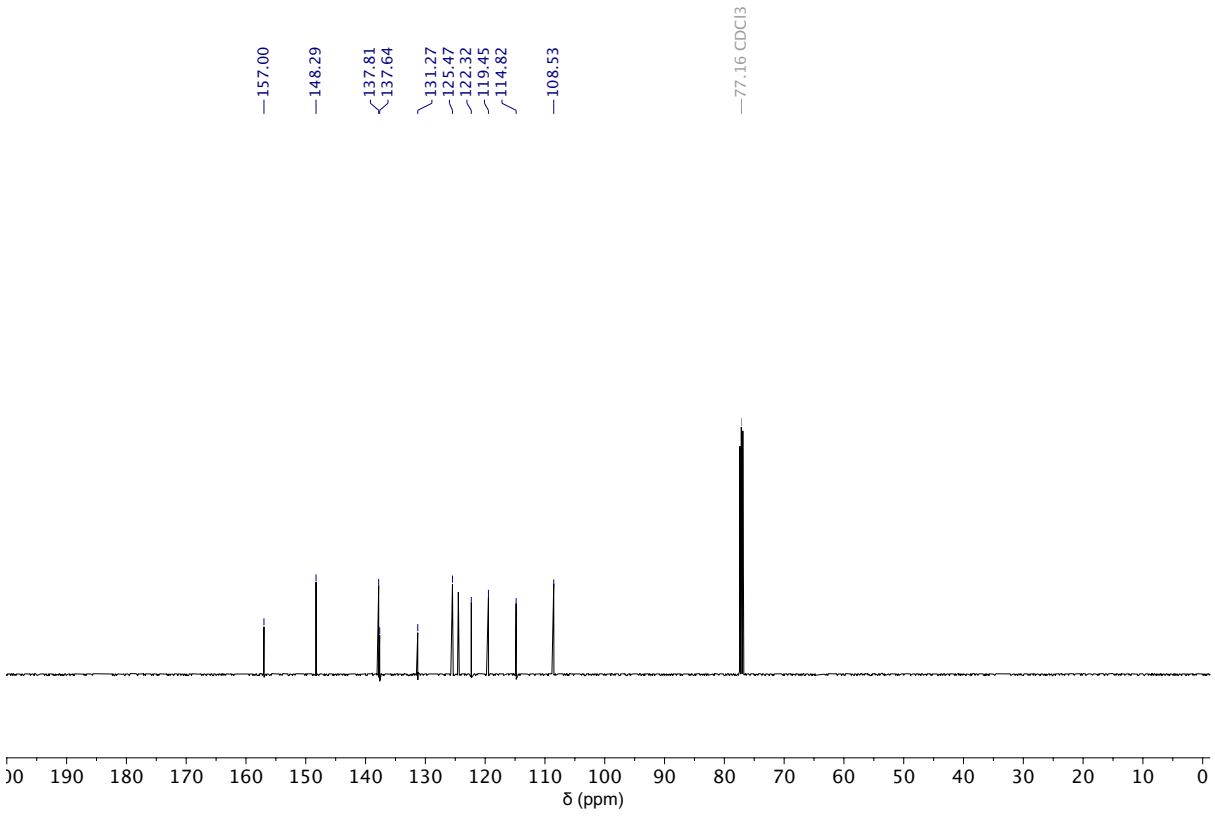


**Figure B-3**. $^{13}C$ NMR spectrum ($CDCl_3$) of **3.2**.

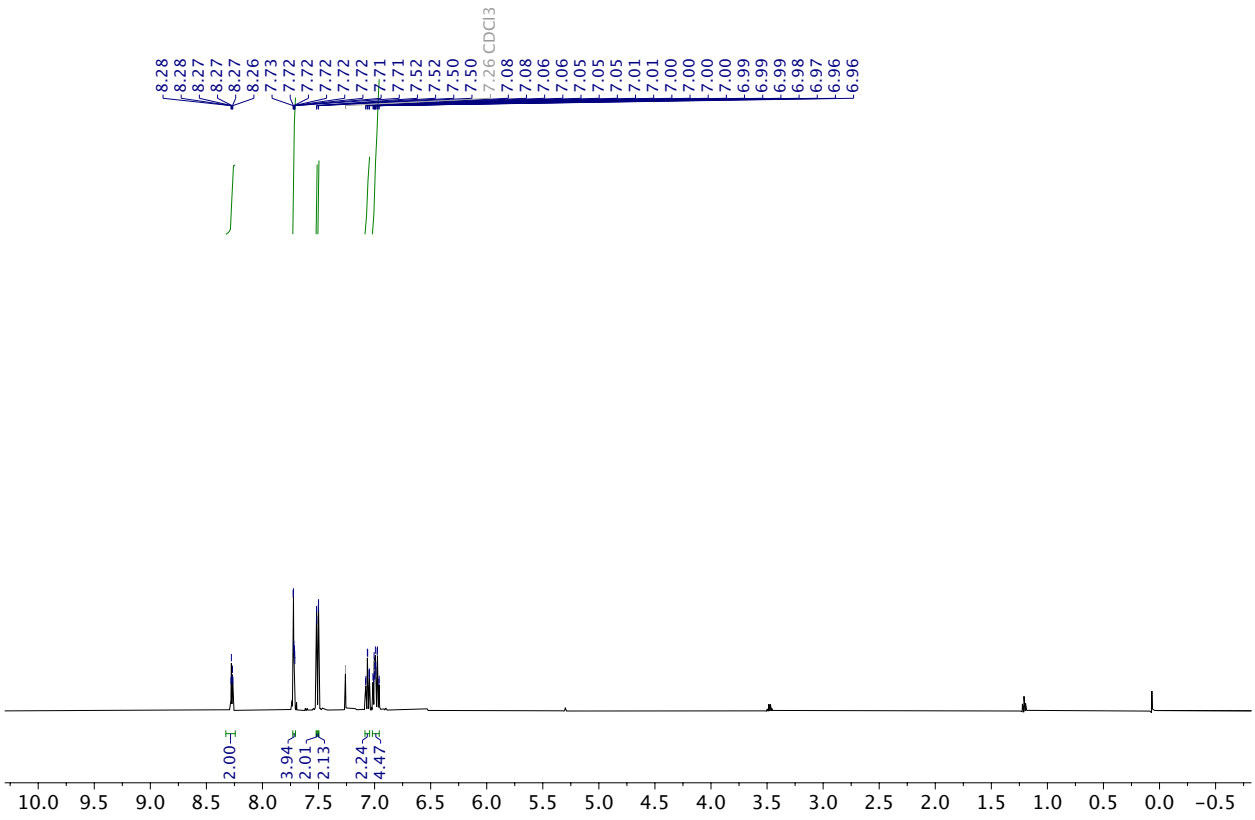


**Figure B-4**. $^{1}H$ NMR spectrum ($CDCl_3$) of **L1**

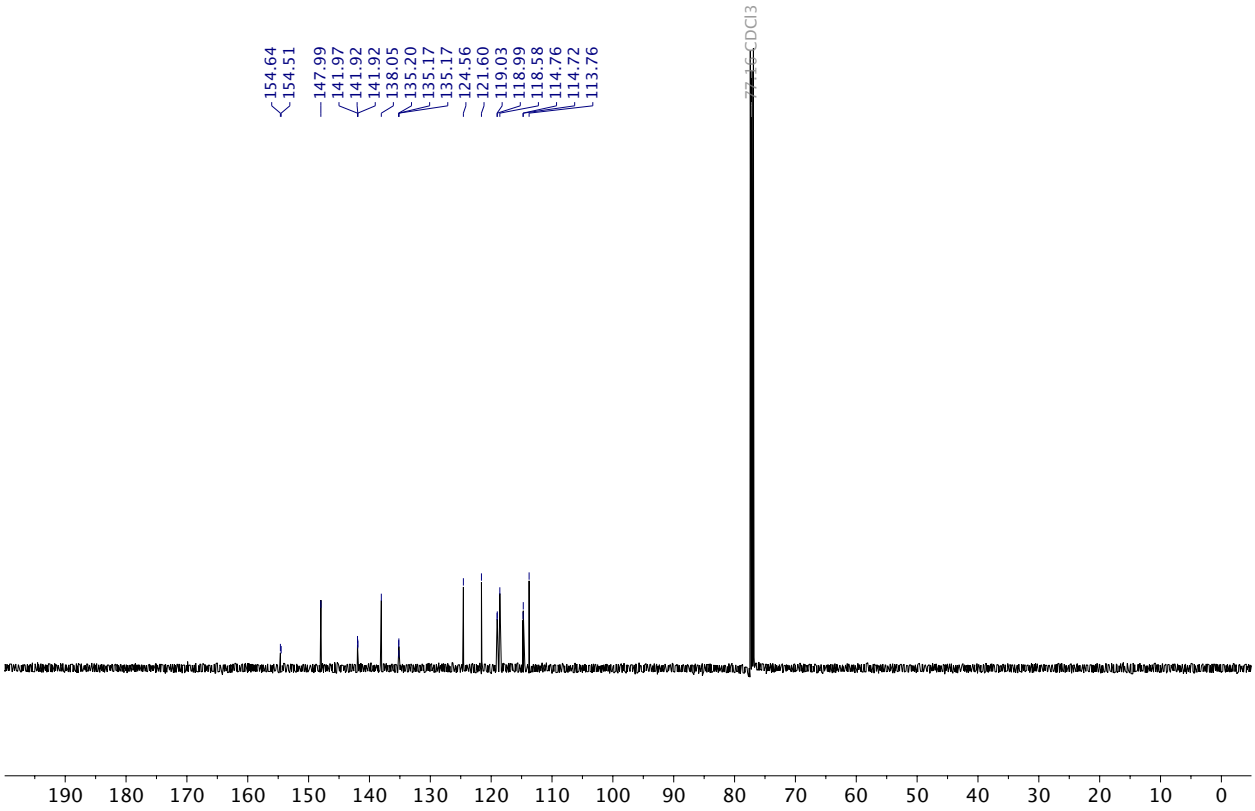


**Figure B-5**. $^{13}C$ NMR spectrum ($CDCl_3$) of **L1**.

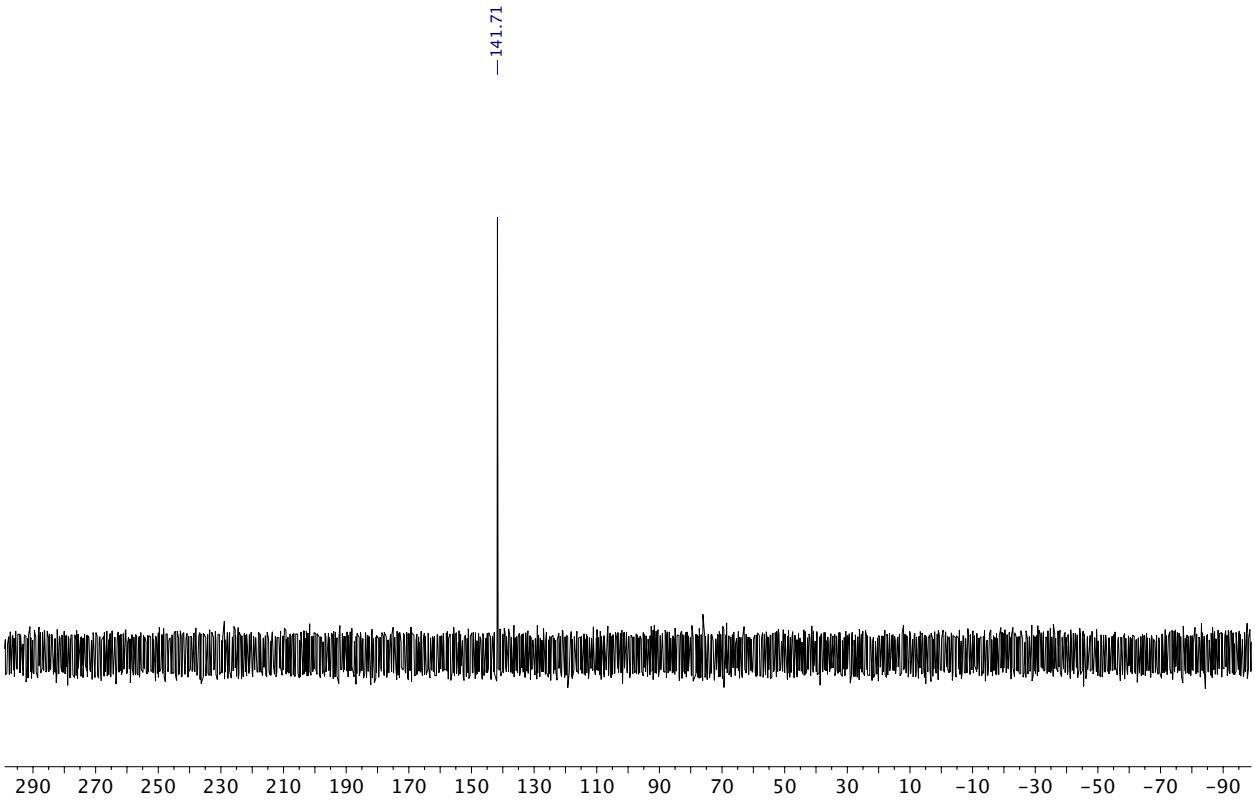


**Figure B-6**. $^{31}P\{^{1}H\}$ NMR spectrum ($CDCl_3$) of **L1**.

.

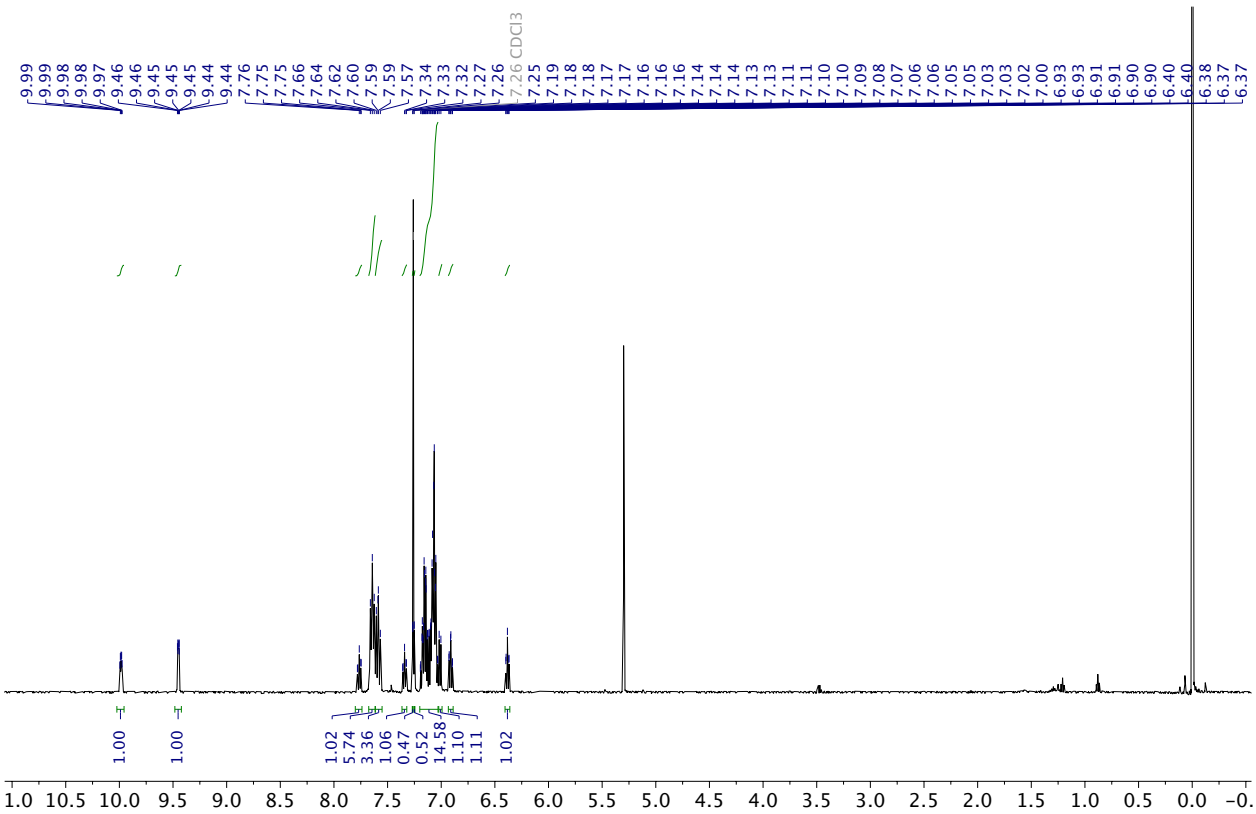

**Figure B-7**. $^{1}H$ NMR spectrum ($CDCl_3$) of **3.3**. Signals of recrystallization solvent $CH_2Cl_2$ and TMS is visible.

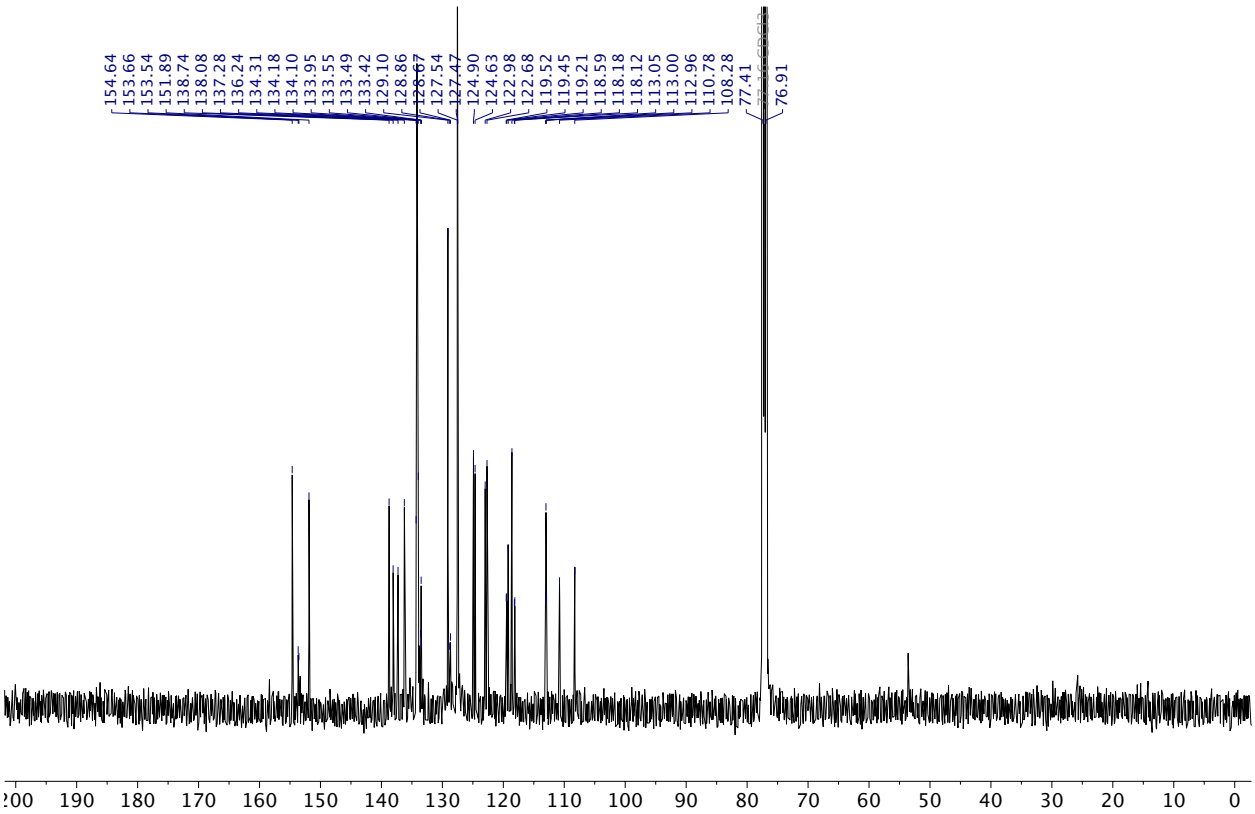


**Figure B-8**. $^{13}C$ NMR spectrum ($CDCl_3$) of **3.3**.

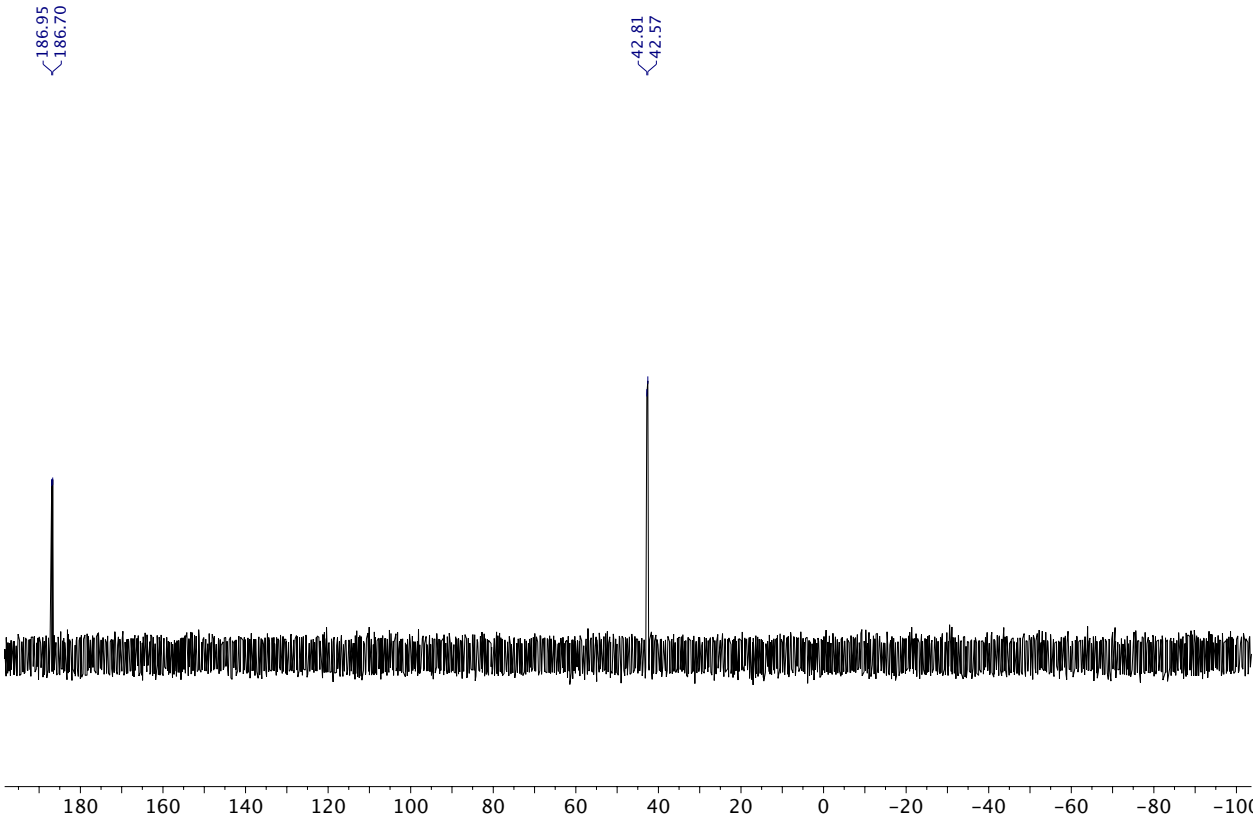


**Figure B-9**. $^{31}P\{^{1}H\}$ NMR spectrum ($CDCl_3$) of **3.3**.

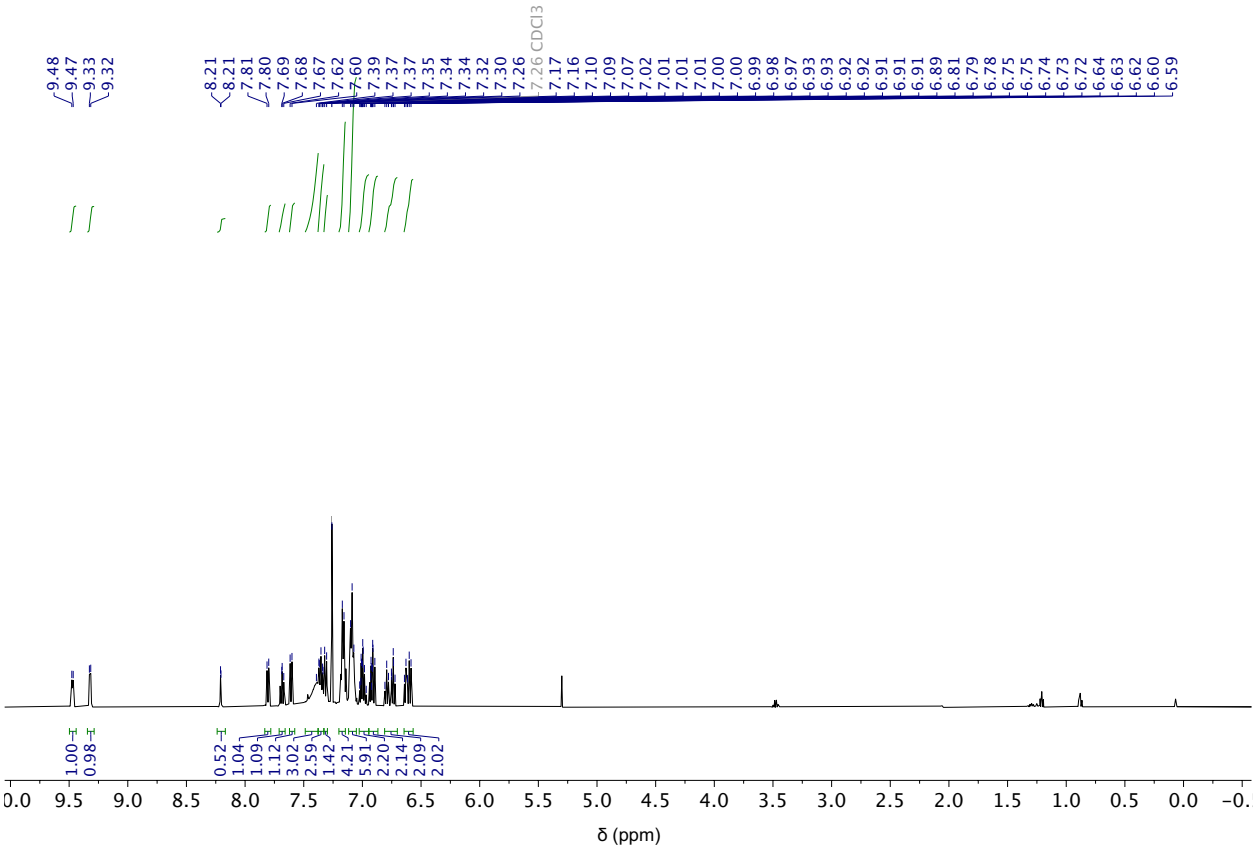


**Figure B-10**. $^{1}H$ NMR spectrum ($CDCl_3$) of **3.4**. A signal of recrystallization solvent ($CH_2Cl_2$) remains in the spectrum.

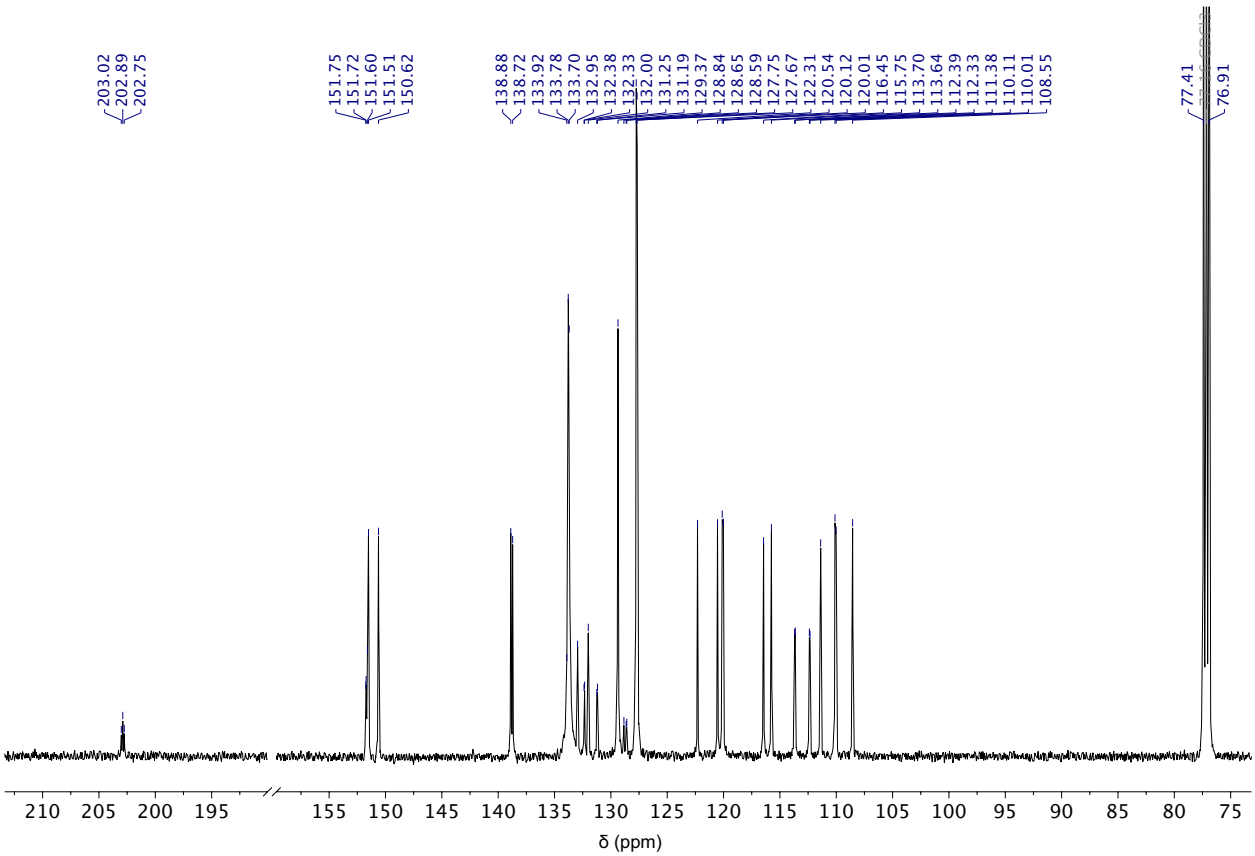


**Figure B-11**. $^{13}C$ NMR spectrum ($CDCl_3$) of **3.4**.

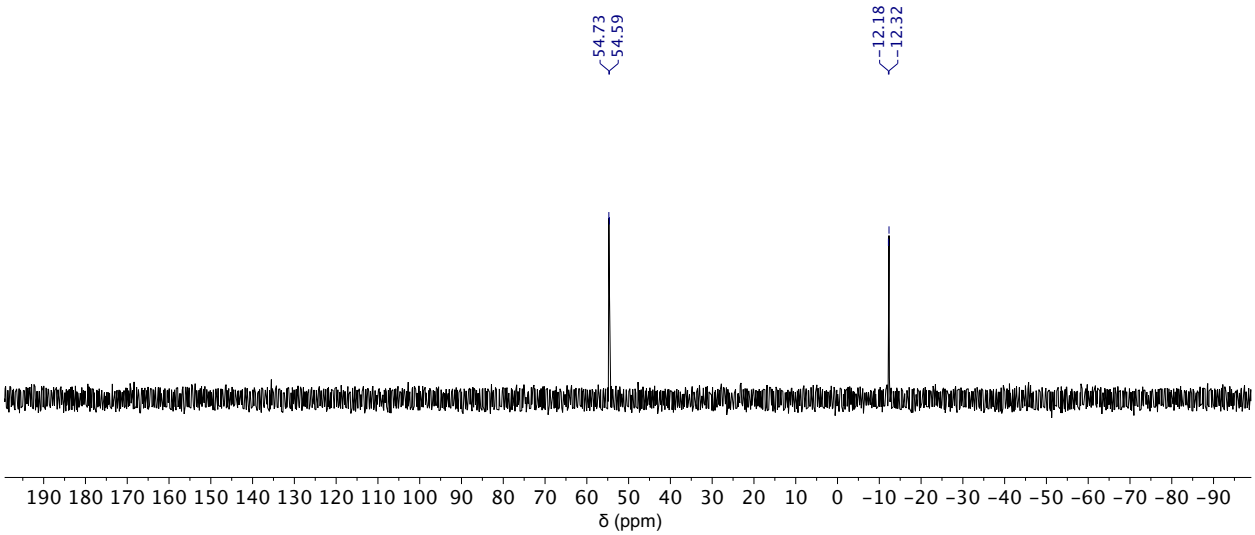


**Figure B-12**. $^{31}P\{^{1}H\}$ NMR spectrum ($CDCl_3$) of **3.4**.

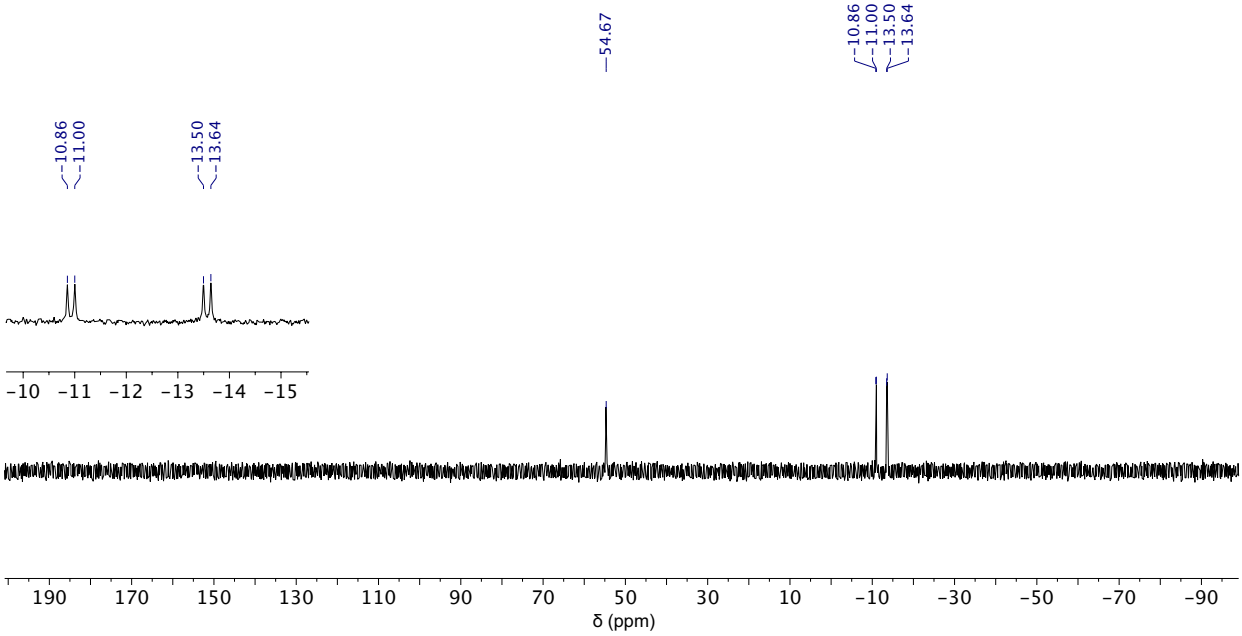


**Figure B-13**. $^{31}P$ NMR spectrum ($CDCl_3$) of **3.4.**

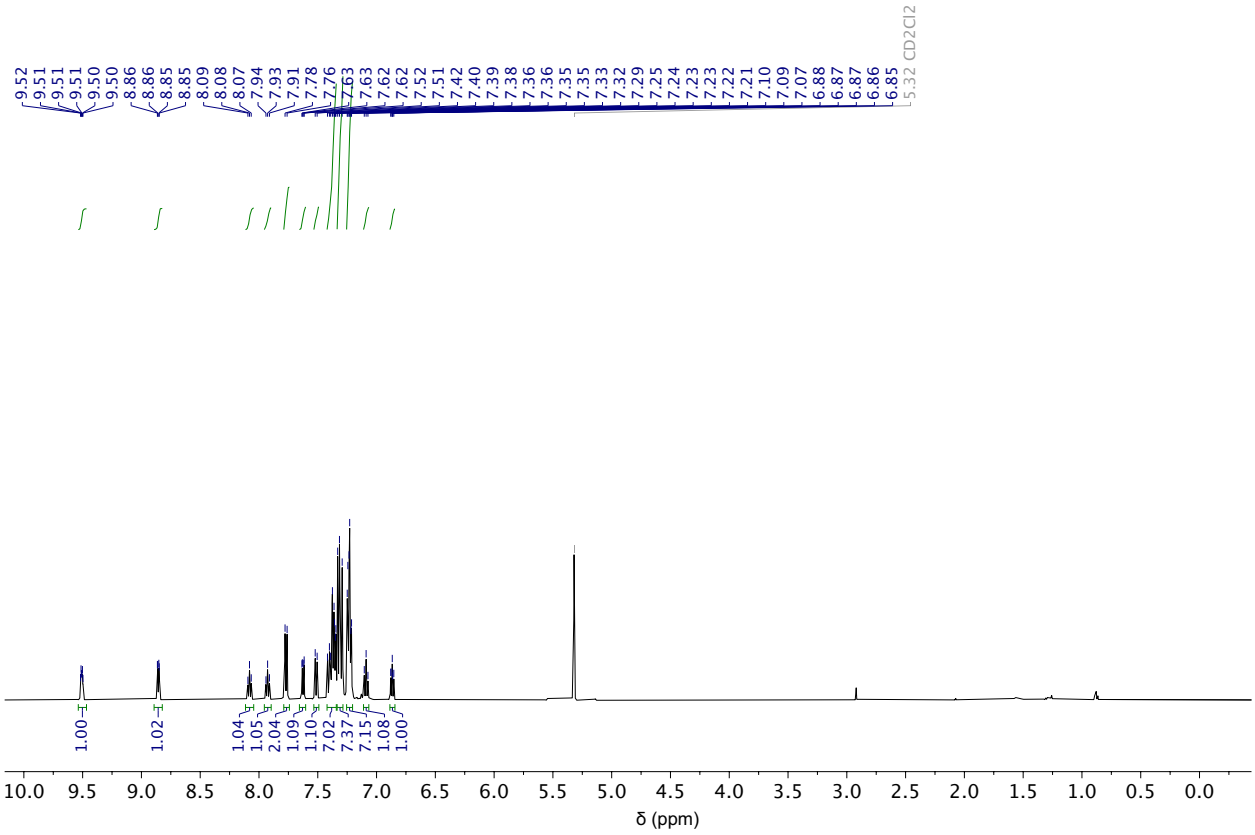


**Figure B-14**. $^{1}H$ NMR spectrum ($CD_2Cl_2$) of **3.5**.

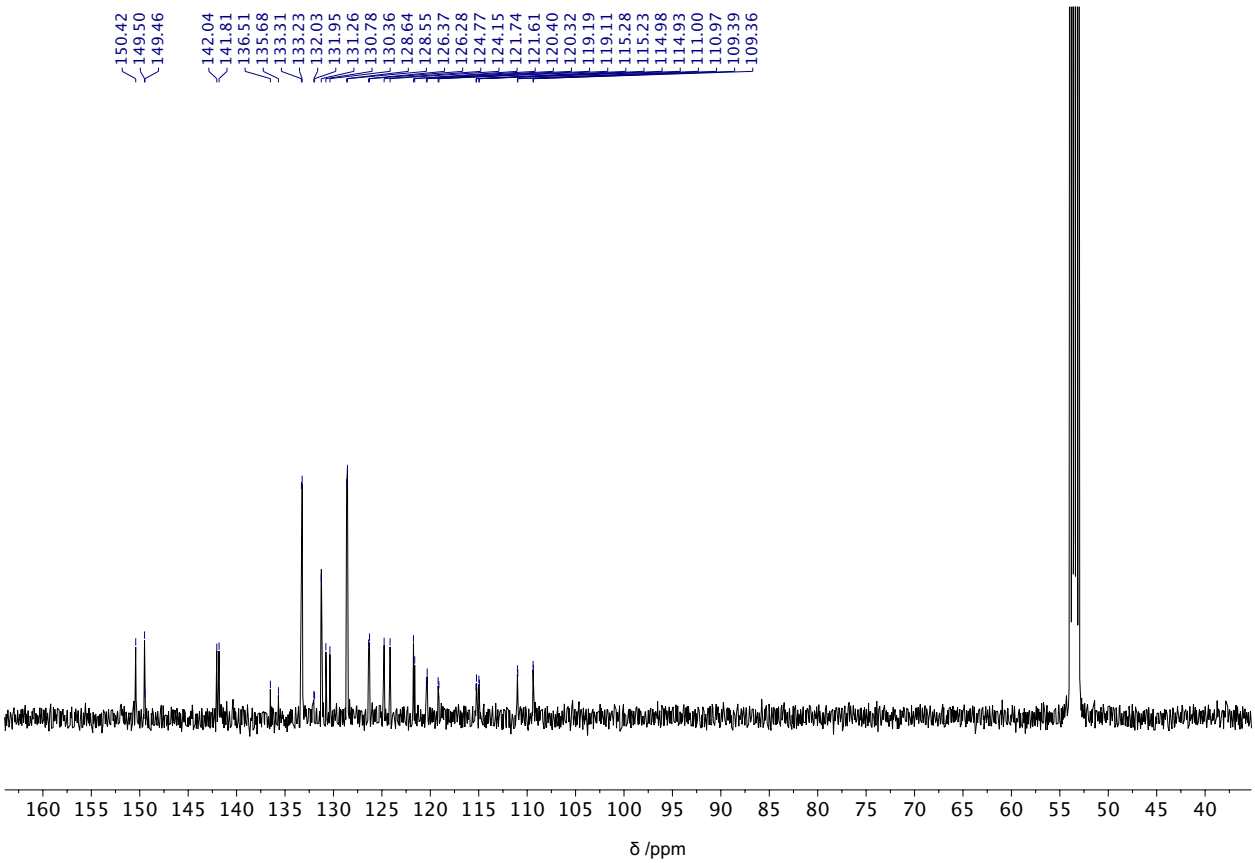


**Figure B-15**. $^{13}C$ NMR spectrum ($CD_2Cl_2$) of **3.5**.

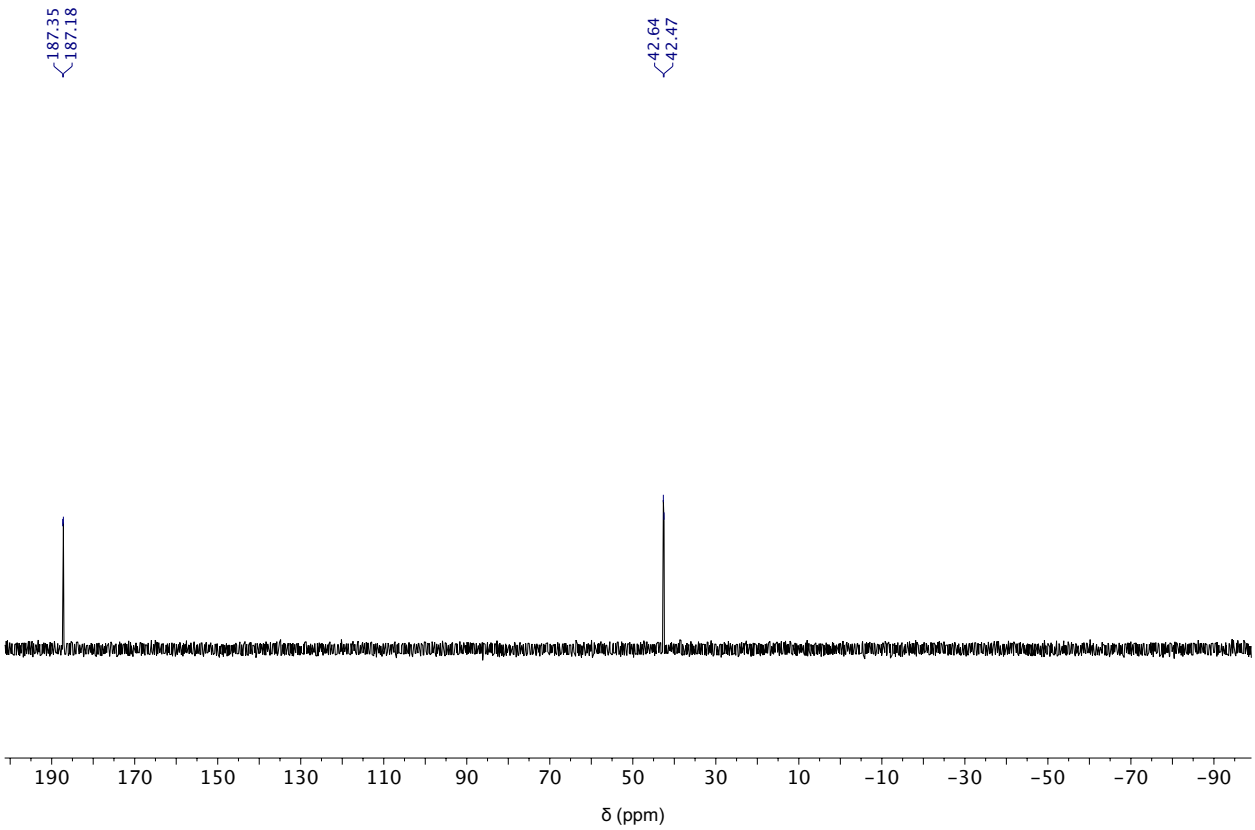


**Figure B-16**. $^{31}P\{^{1}H\}$ NMR spectrum ($CDCl_3$) of **3.5**.

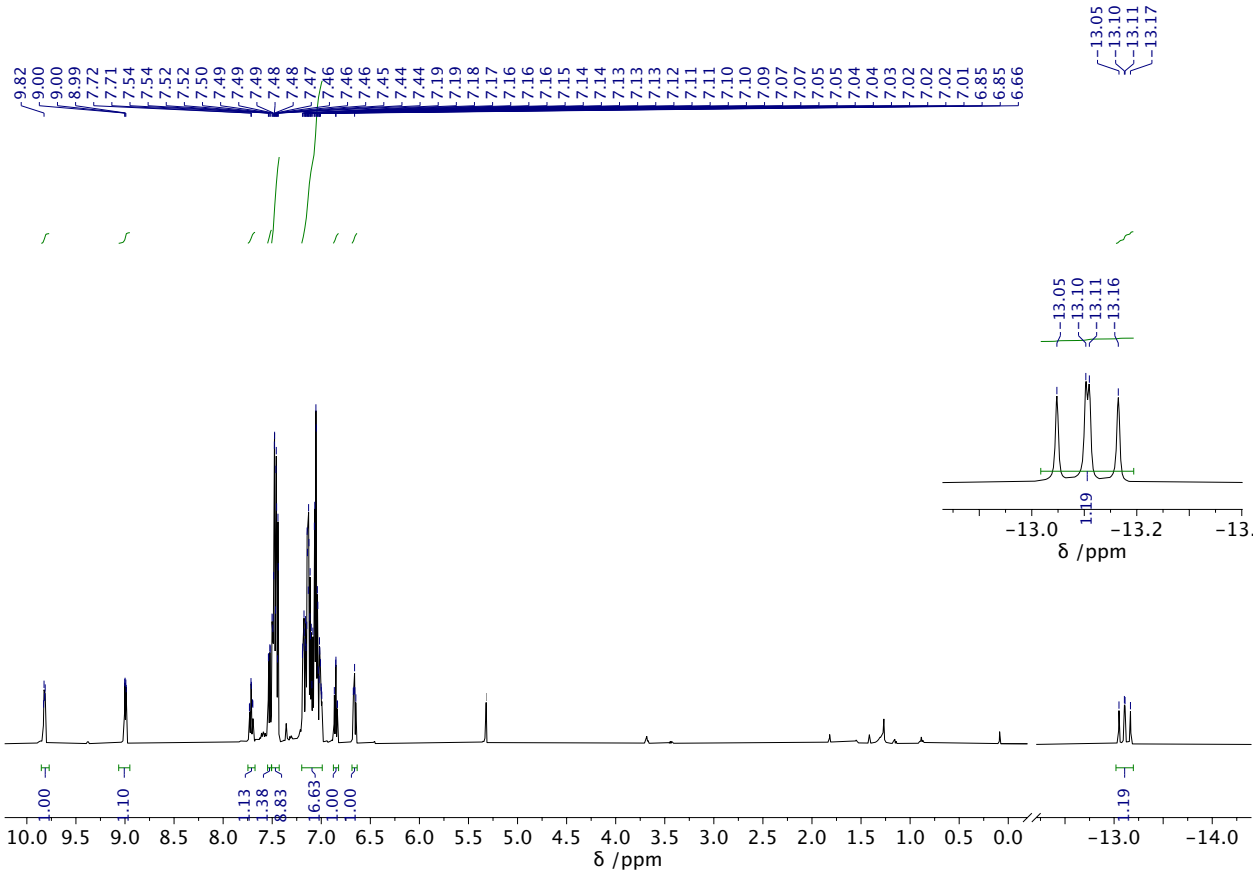


**Figure B-17**. $^{1}H$ NMR spectrum ($CD_2Cl_2$) of **3.6**.

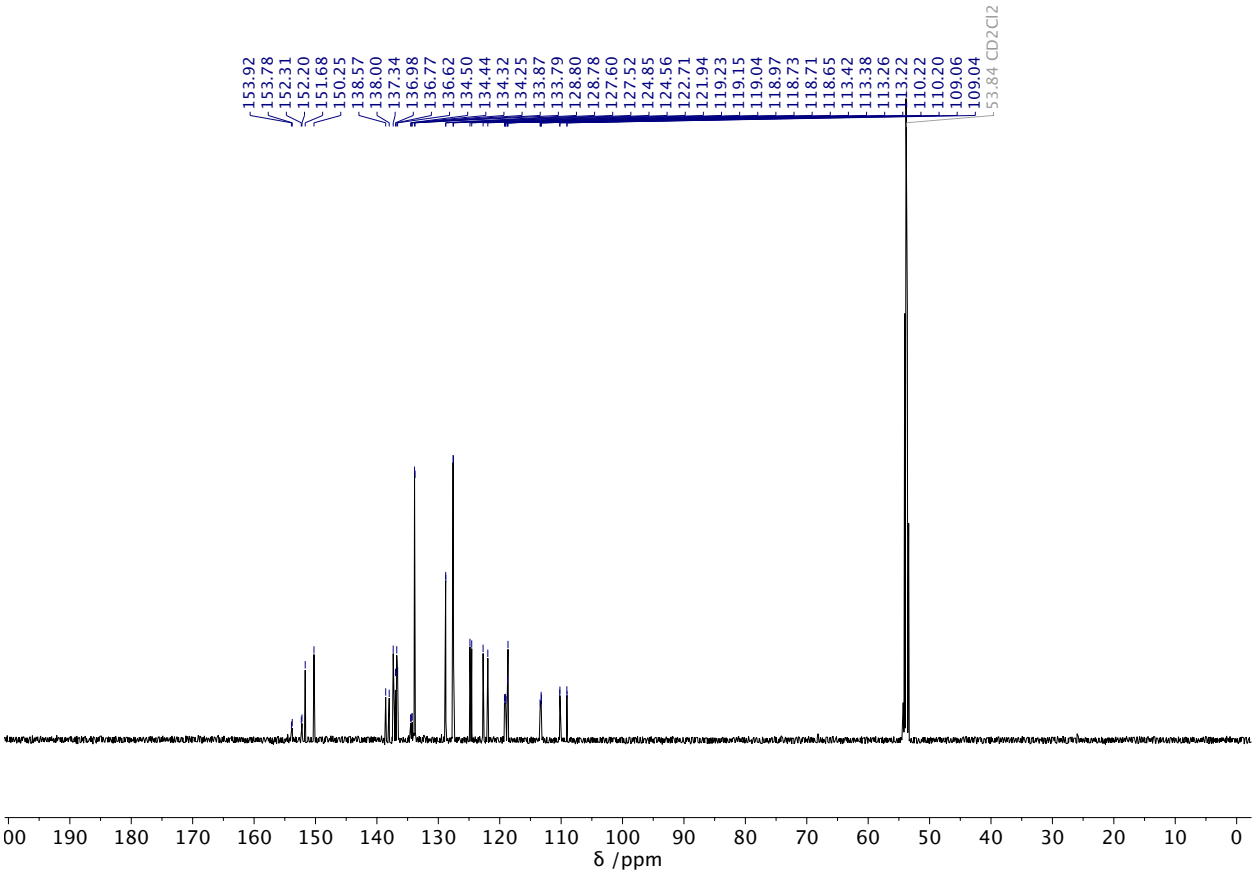


**Figure B-18**. $^{13}C$ NMR spectrum ($CD_2Cl_2$) of **3.6**.

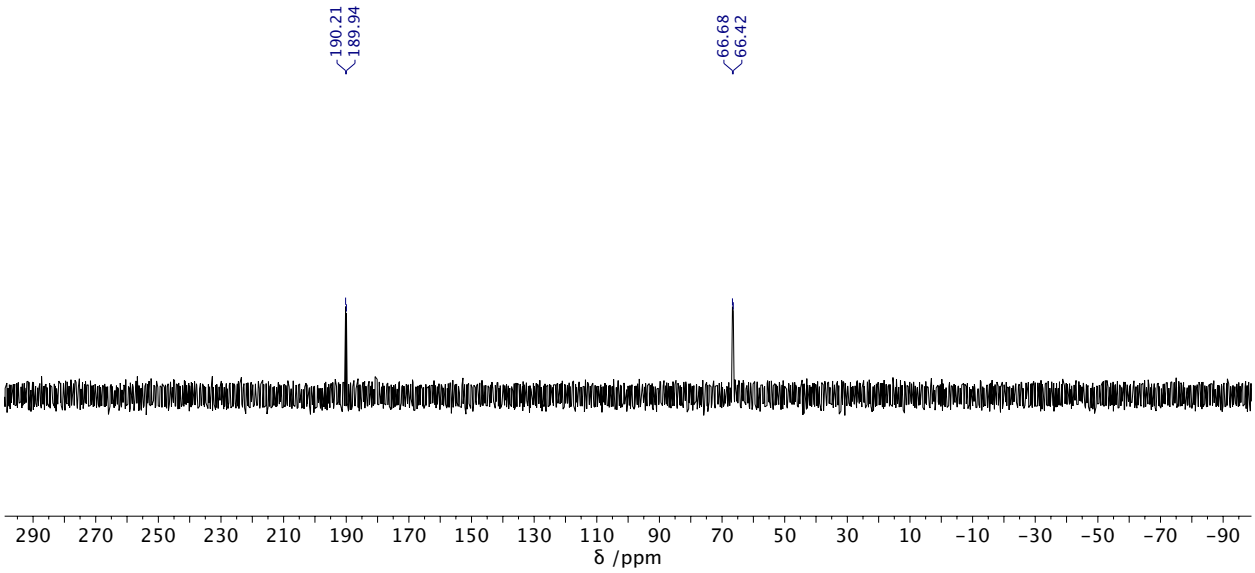


**Figure B-19**. $^{31}P\{^{1}H\}$ NMR spectrum ($C_6D_6$) of **3.6**.

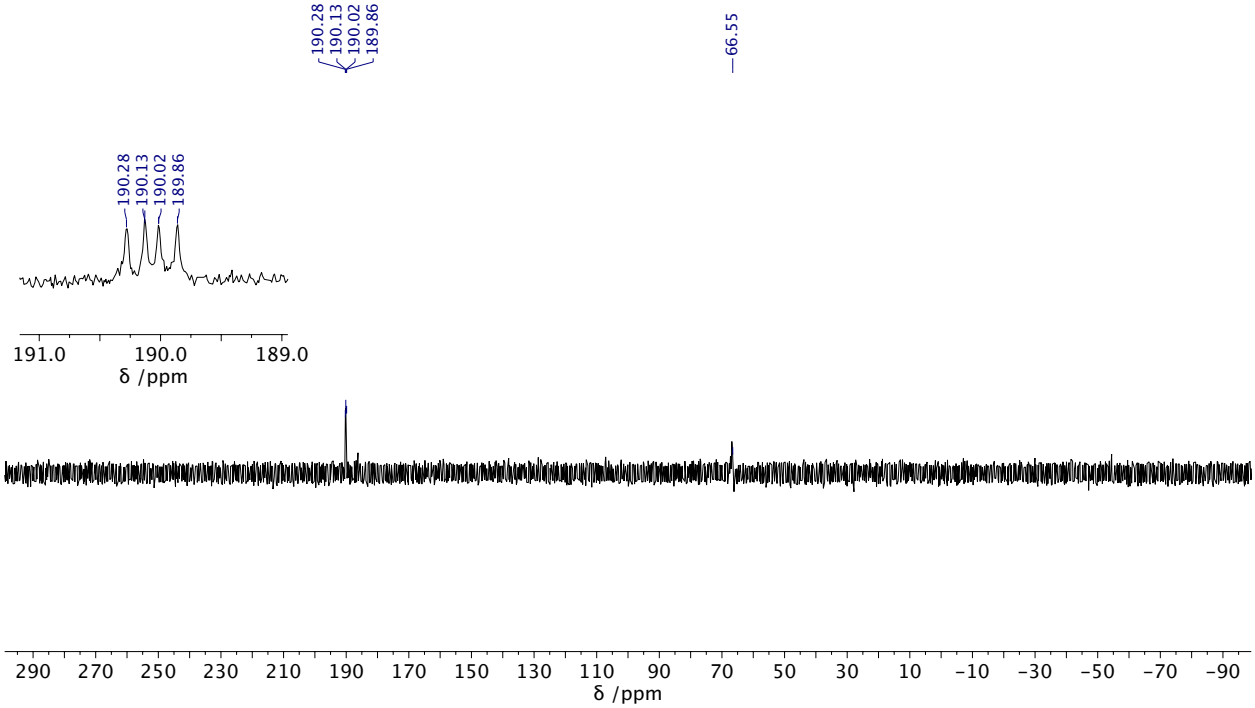


**Figure B-20**. $^{31}P$ NMR spectrum ($C_6D_6$) of **3.6**.

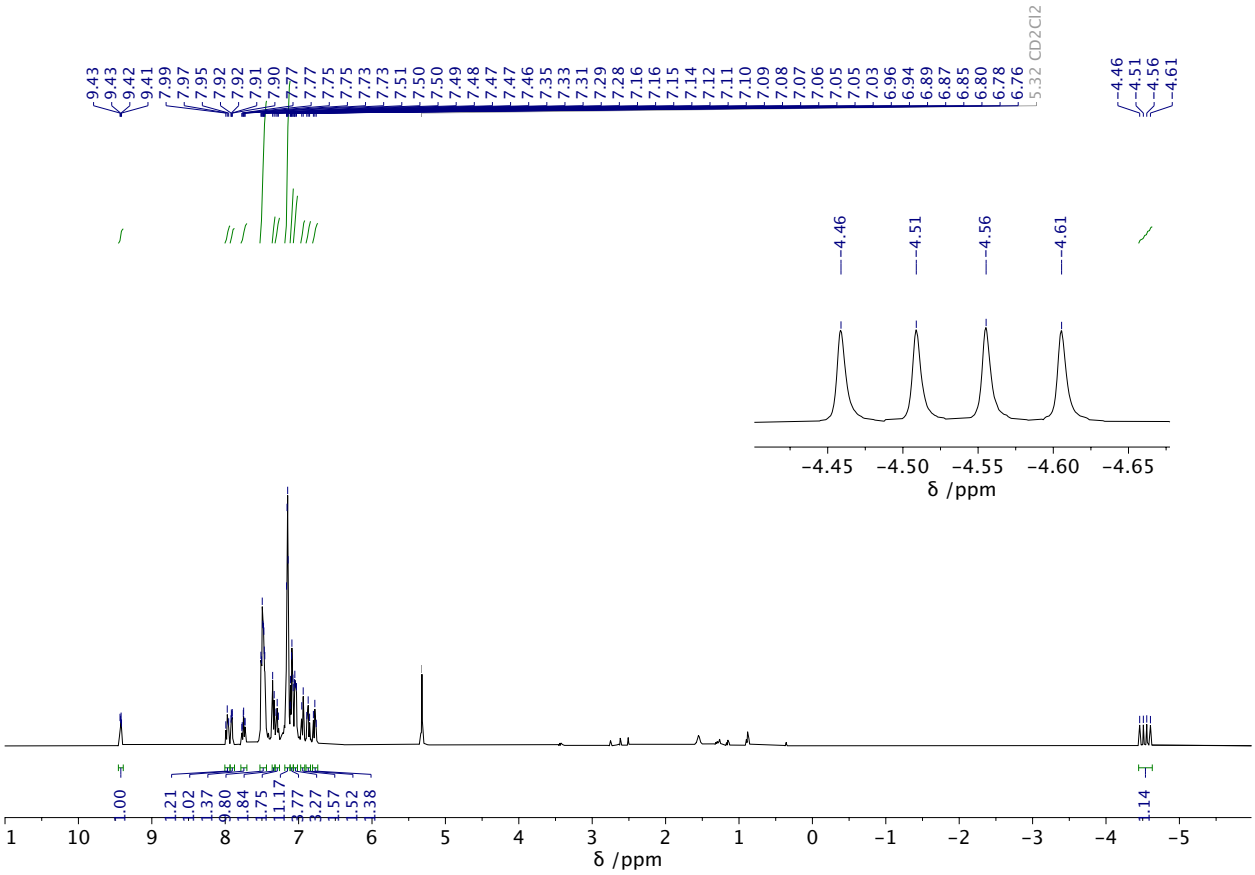


**Figure B-21**. $^{1}$H NMR spectrum ($CD_2Cl_2$) of **3.7**.

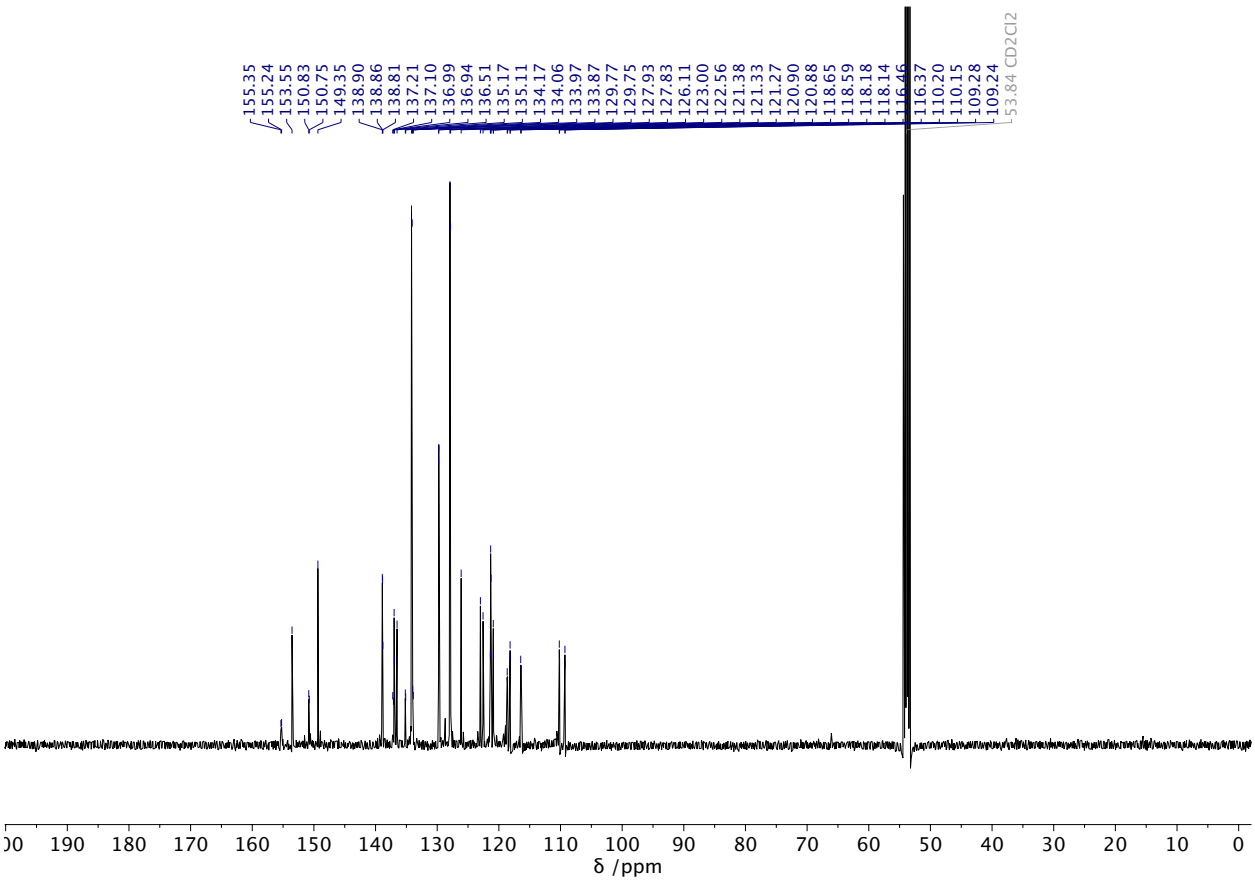


**Figure B-22**. $^{13}C$ NMR spectrum ($CD_2Cl_2$) of **3.7**.

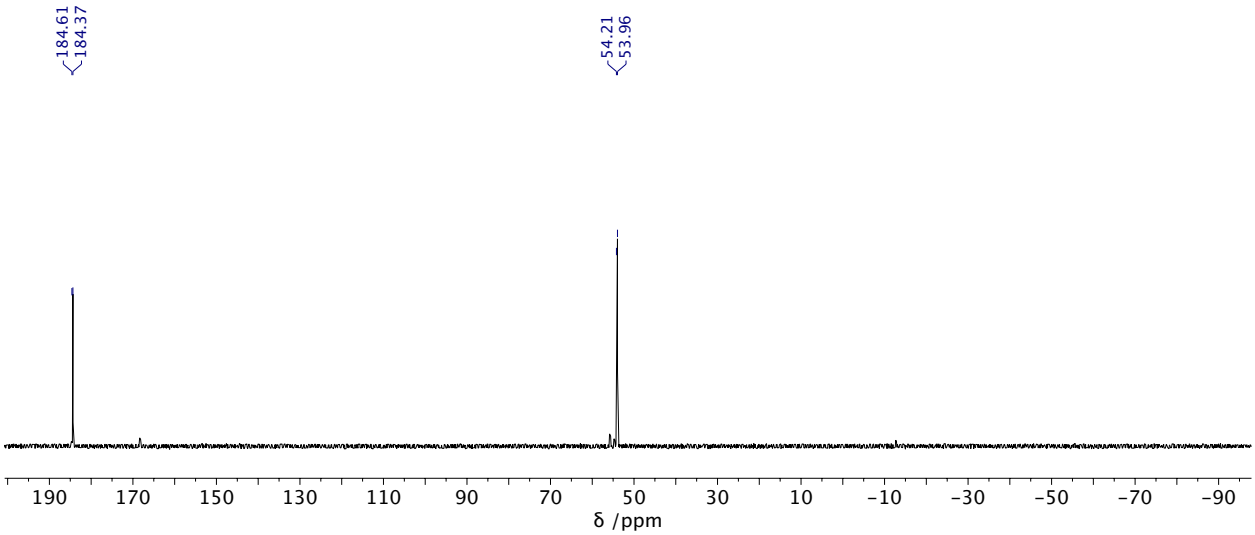


**Figure B-23**. $^{31}P\{^{1}H\}$ NMR spectrum ($CD_2Cl_2$) of **3.7**.

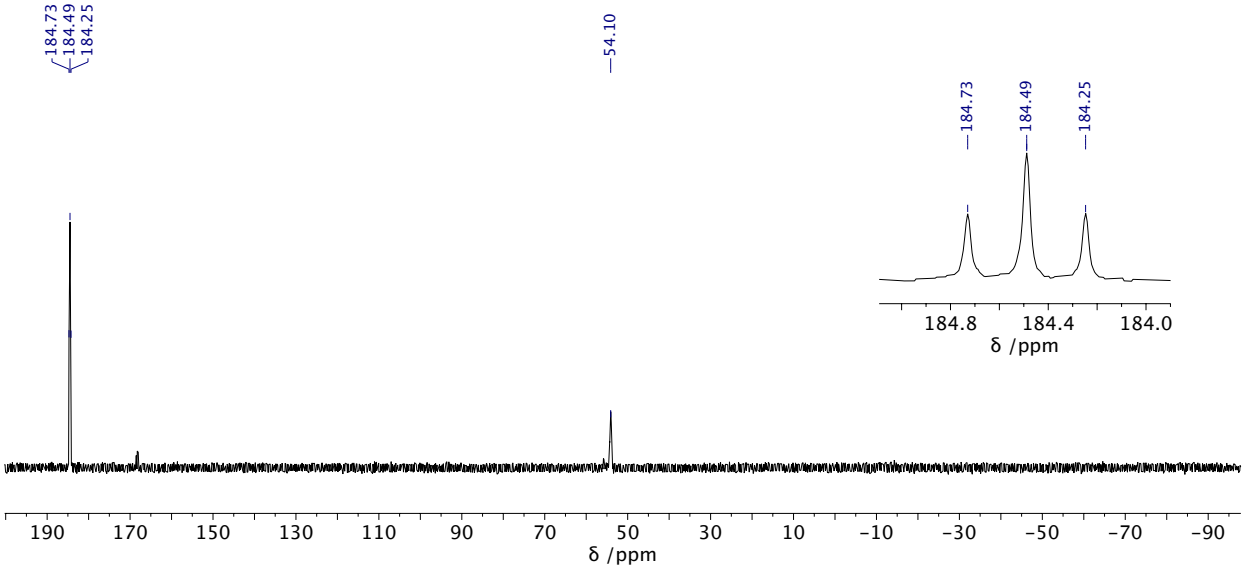


**Figure B-24**. $^{31}P$ NMR spectrum ($CD_2Cl_2$) of **3.7**.

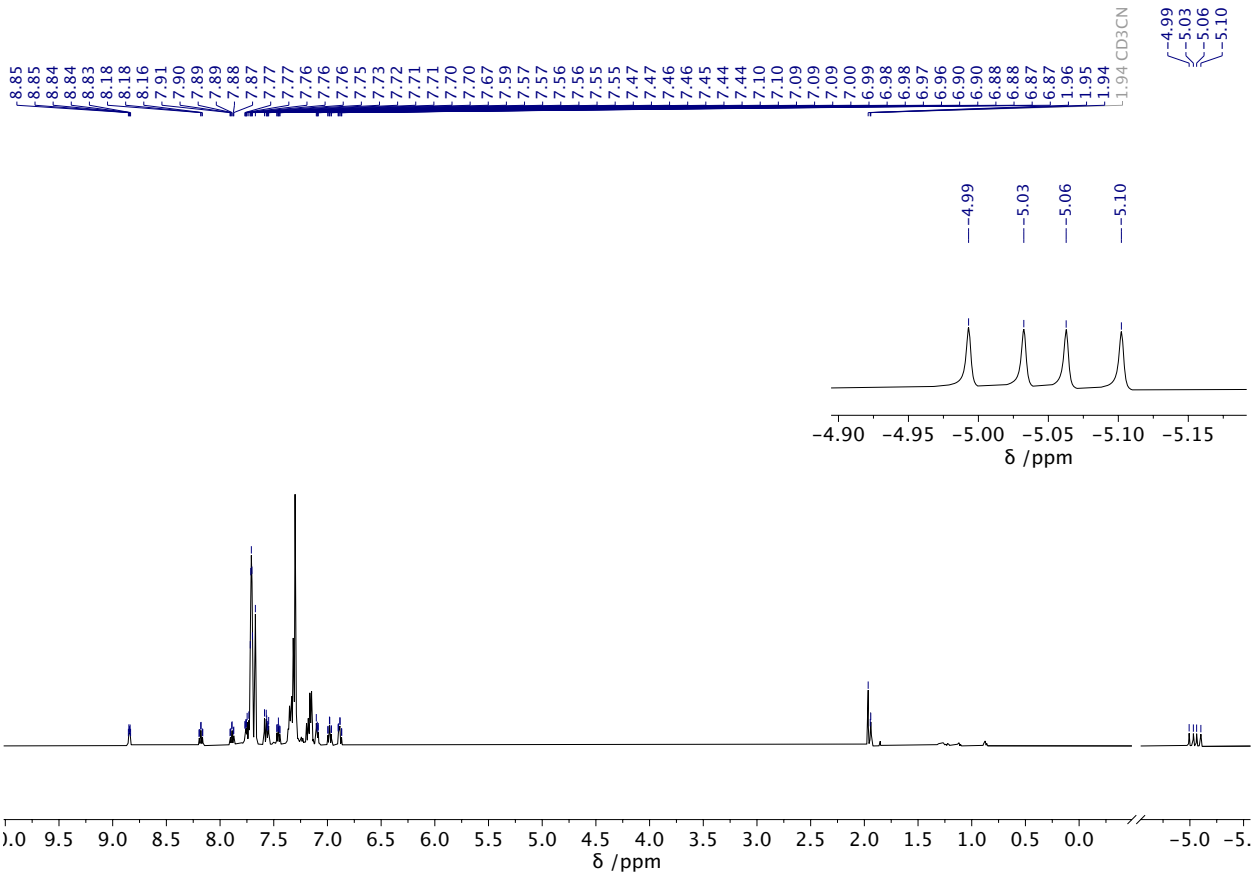


**Figure B-25**. $^{1}$H NMR spectrum ($CD_3CN$) of **3.8**.

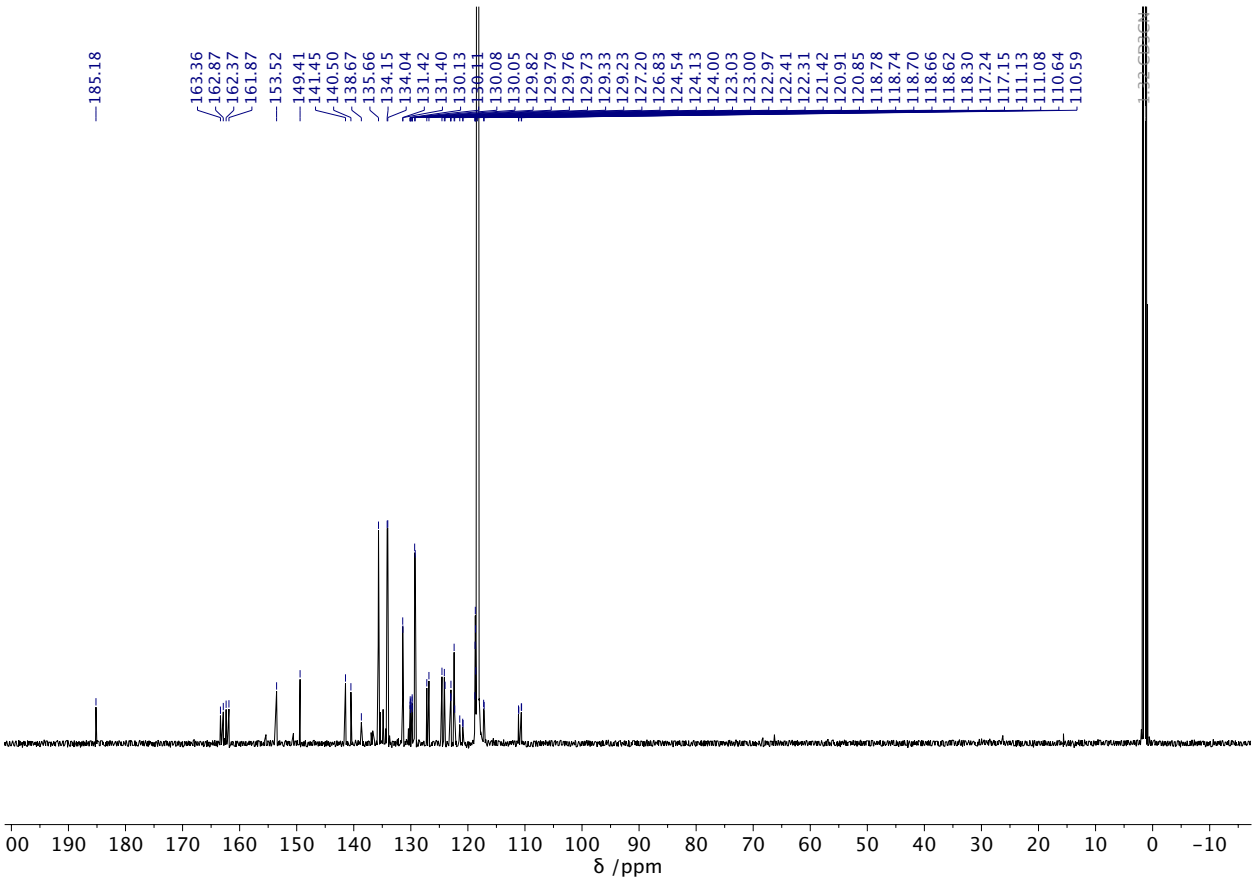


**Figure B-26**. $^{13}C$ NMR spectrum ($CD_3CN$) of **3.8**.

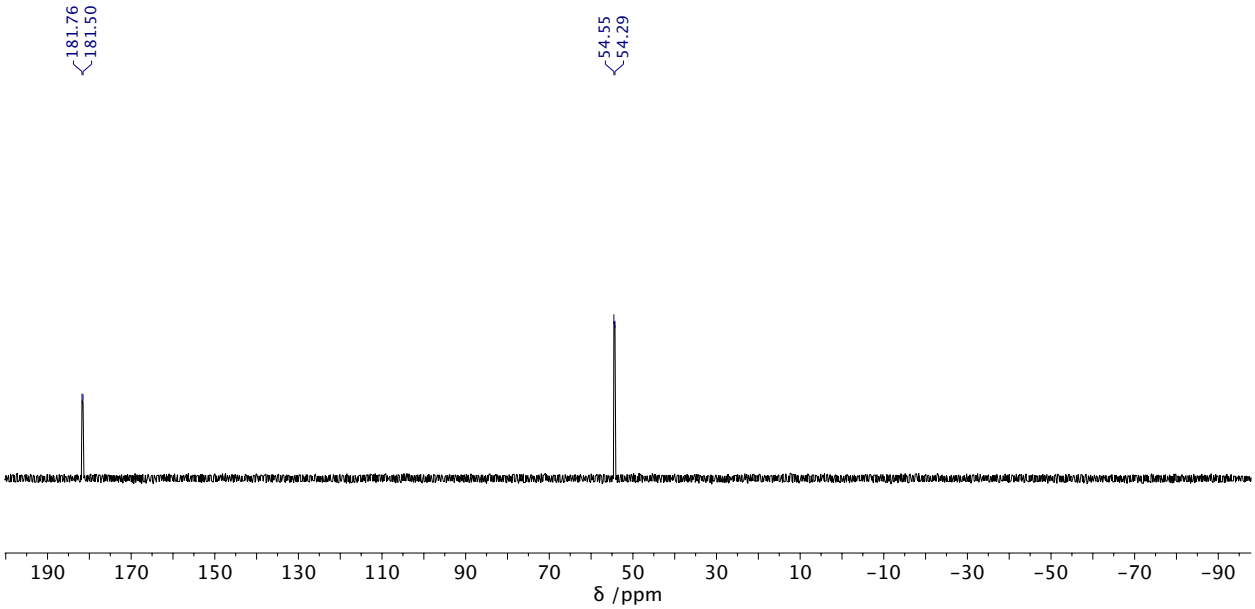


**Figure B-27**. $^{31}P\{^{1}H\}$ NMR spectrum ($CD_3CN$) of **3.8**.

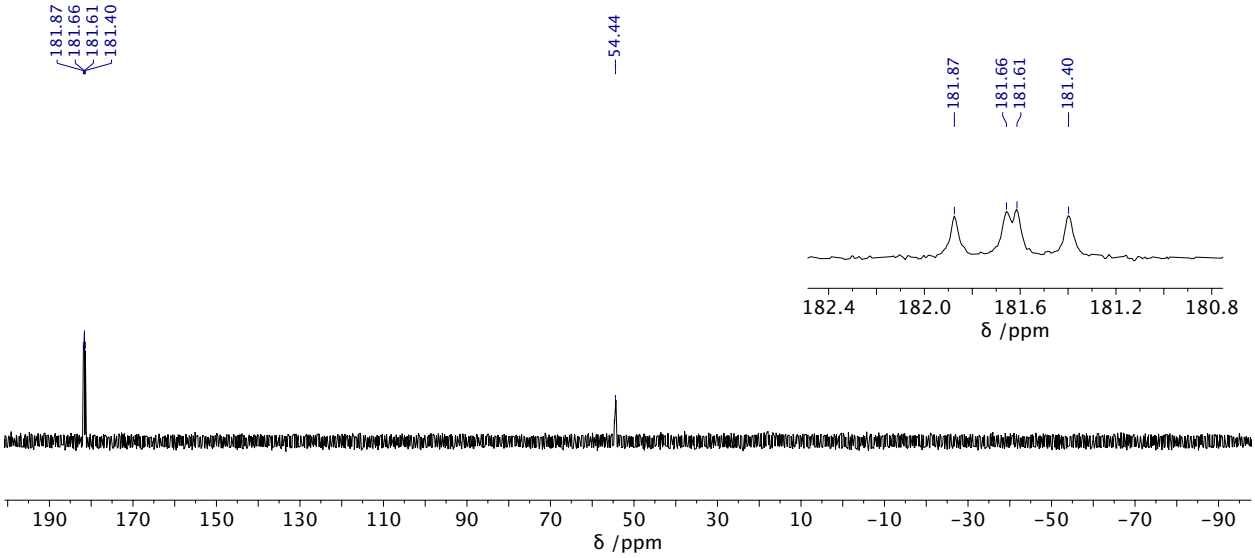


**Figure B-28**. $^{31}P$ NMR spectrum ($CD_3CN$) of **3.8**.

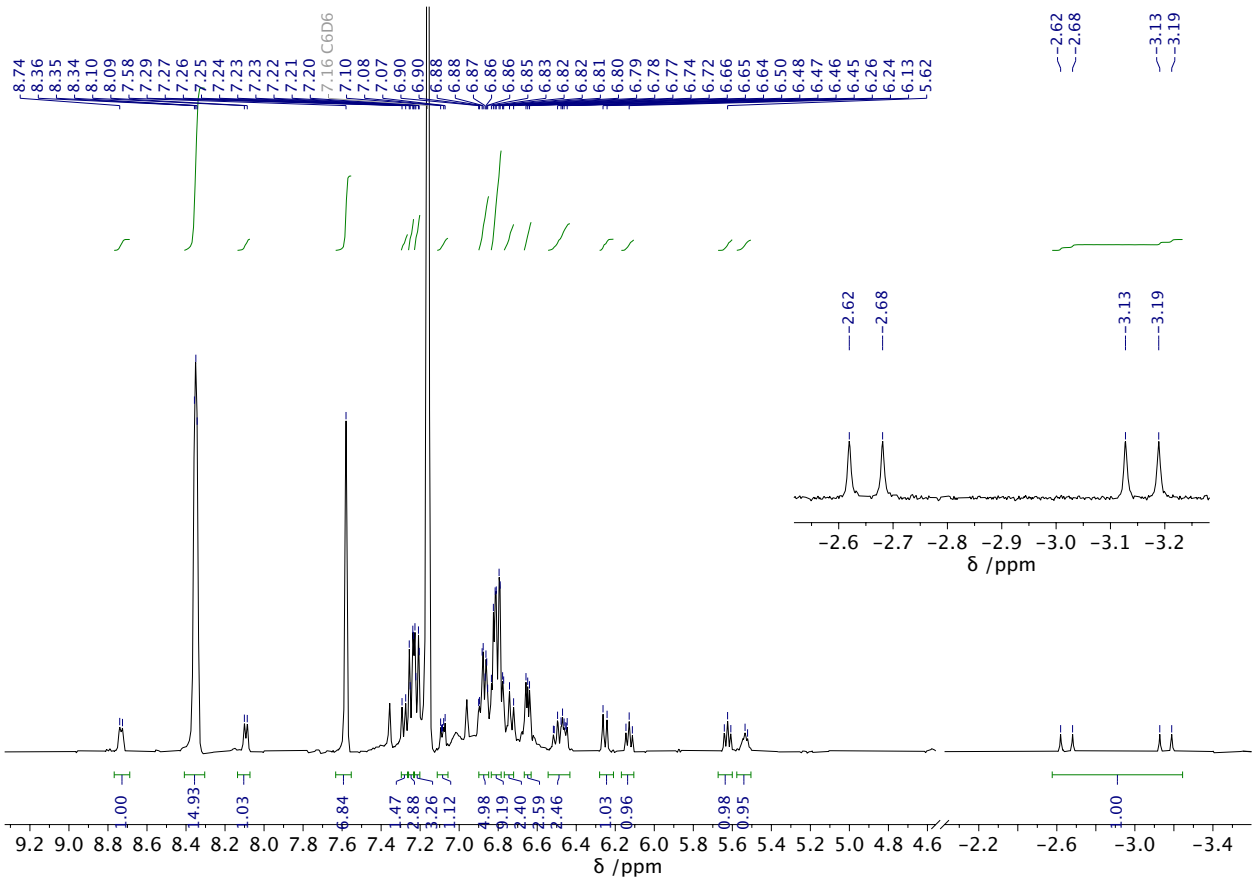


**Figure B-29**. $^{1}H$ NMR spectrum ($C_6D_6$) of **3.15**.

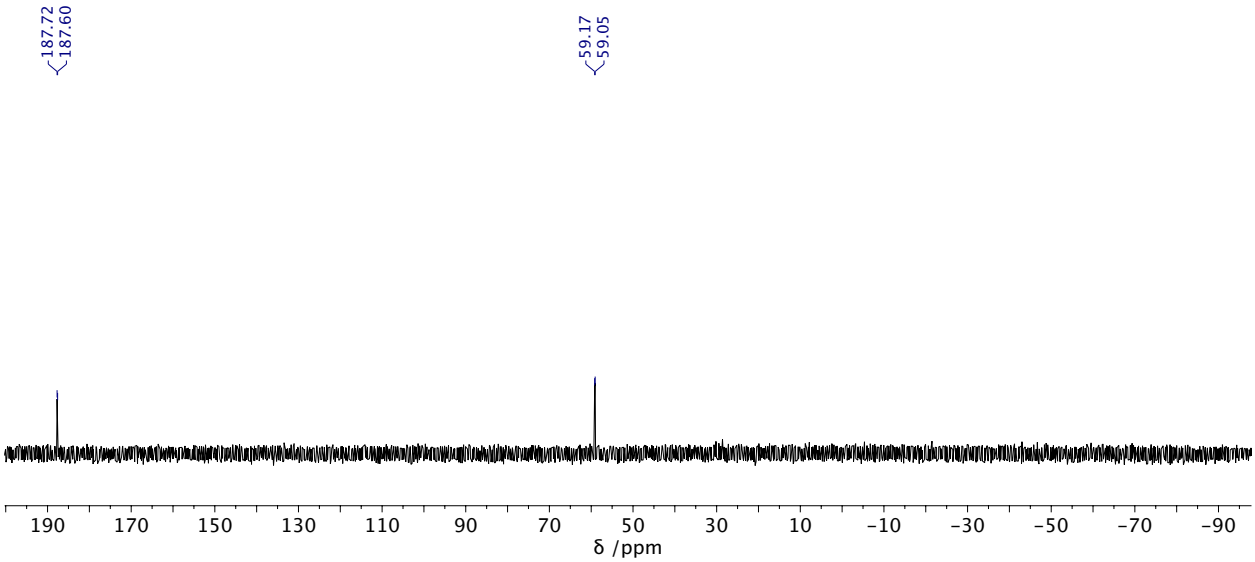


**Figure B-30**. $^{31}P\{^{1}H\}$ NMR spectrum ($C_6D_6$) of **3.15**.

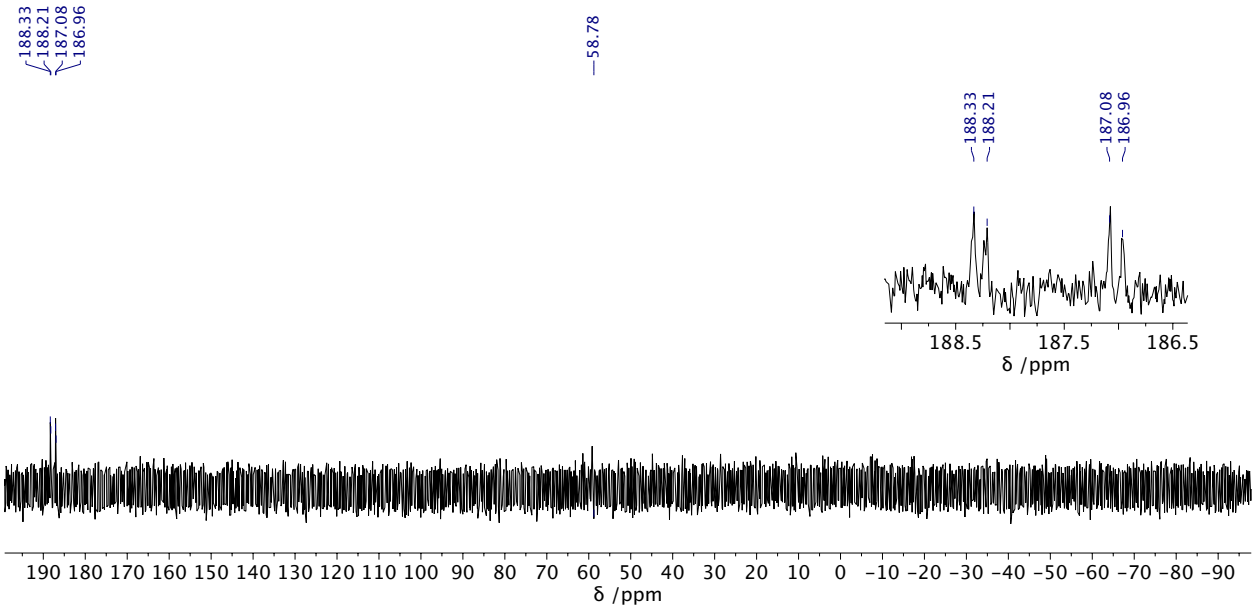


**Figure B-31**. $^{31}P$ NMR spectrum ($C_6D_6$) of **3.15**.

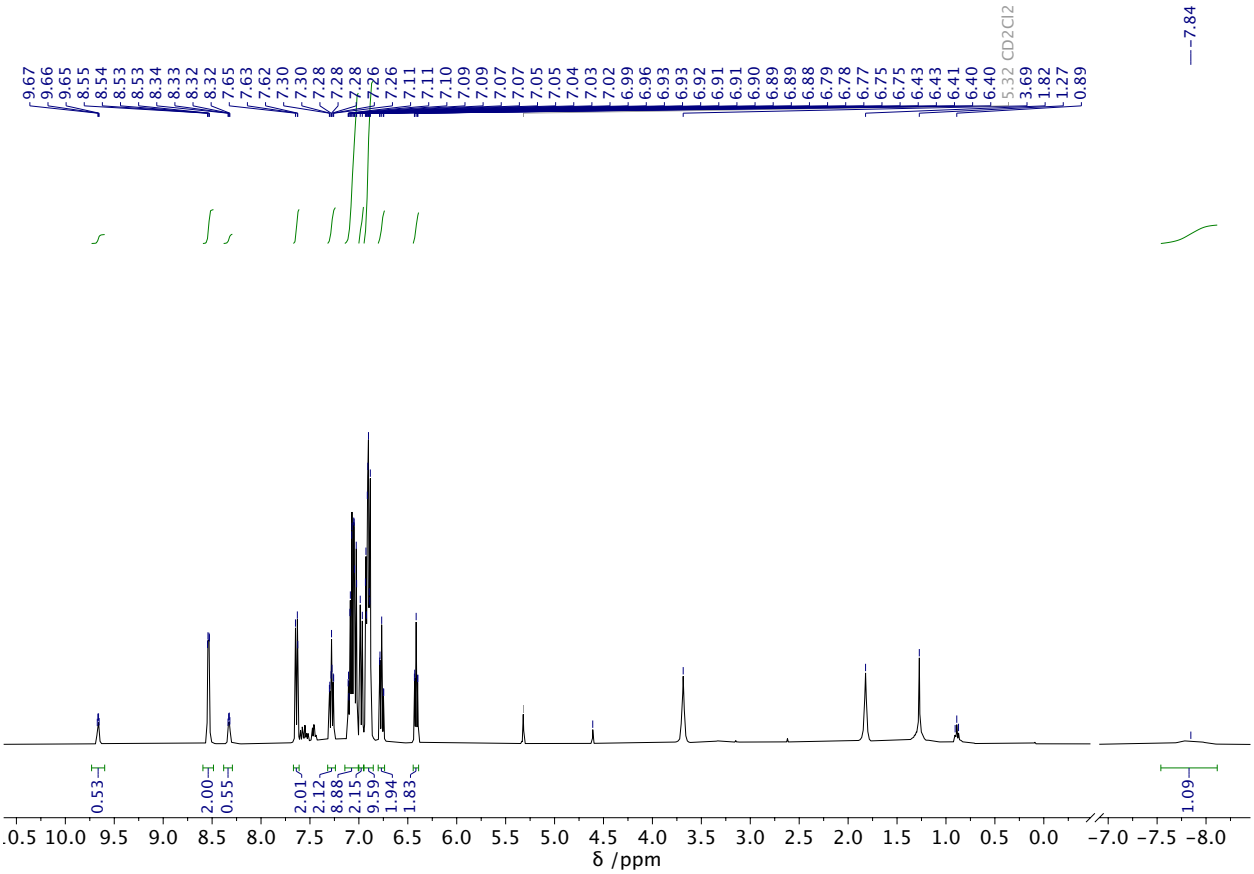


**Figure B-32.** $^{1}H$ NMR spectrum ($CD_2Cl_2$) of **3.16**. Signals of recrystallization solvents (THF, pentane) and $H_2$ (4.59 ppm) are visible too.

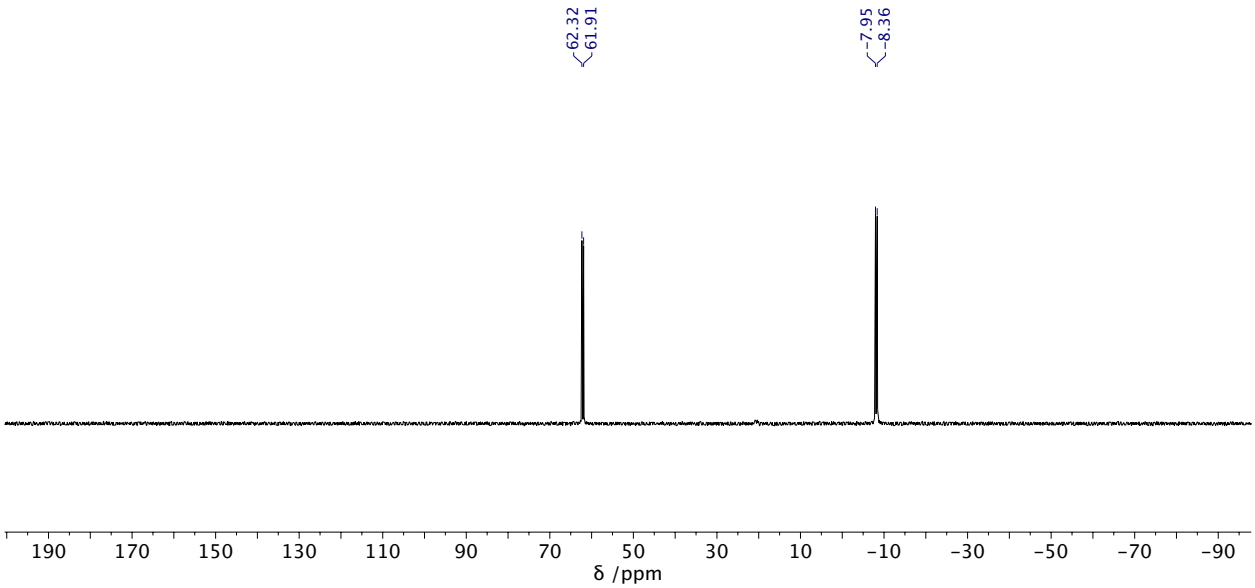


**Figure B-33.** $^{31}P\{^{1}H\}$ NMR spectrum ($CD_2Cl_2$) of **3.16**.

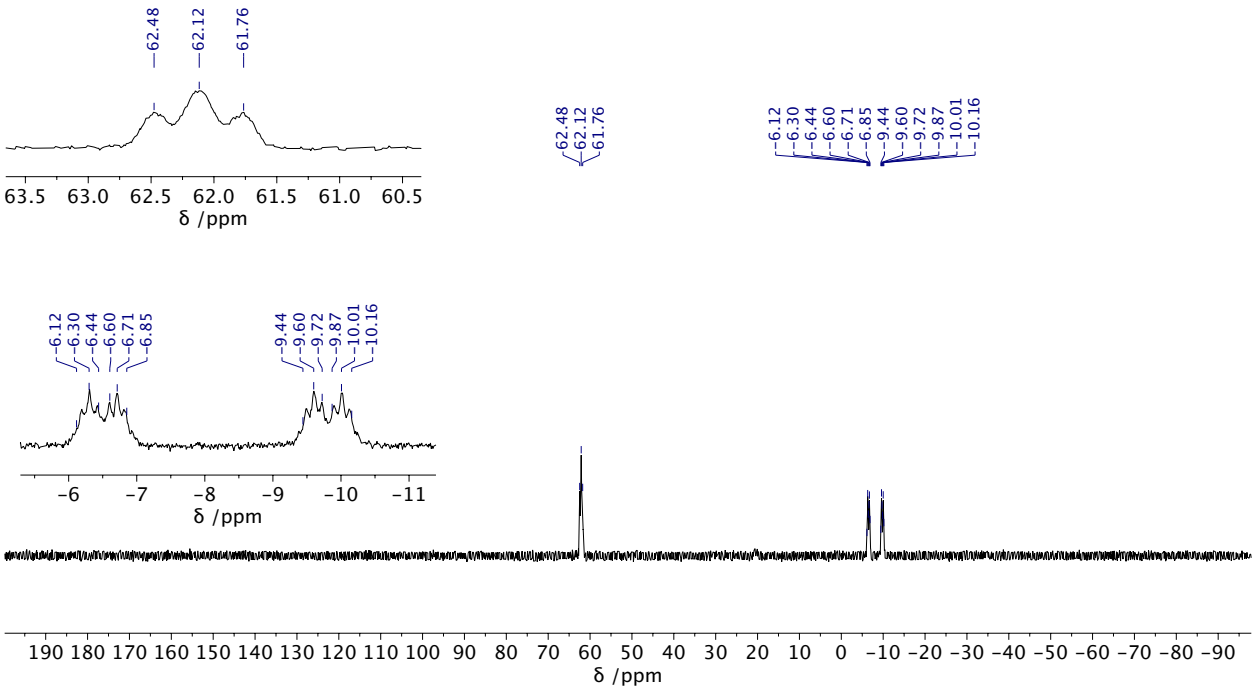


**Figure B-34.** $^{31}P$ NMR spectrum ($CD_2Cl_2$) of **3.16**.

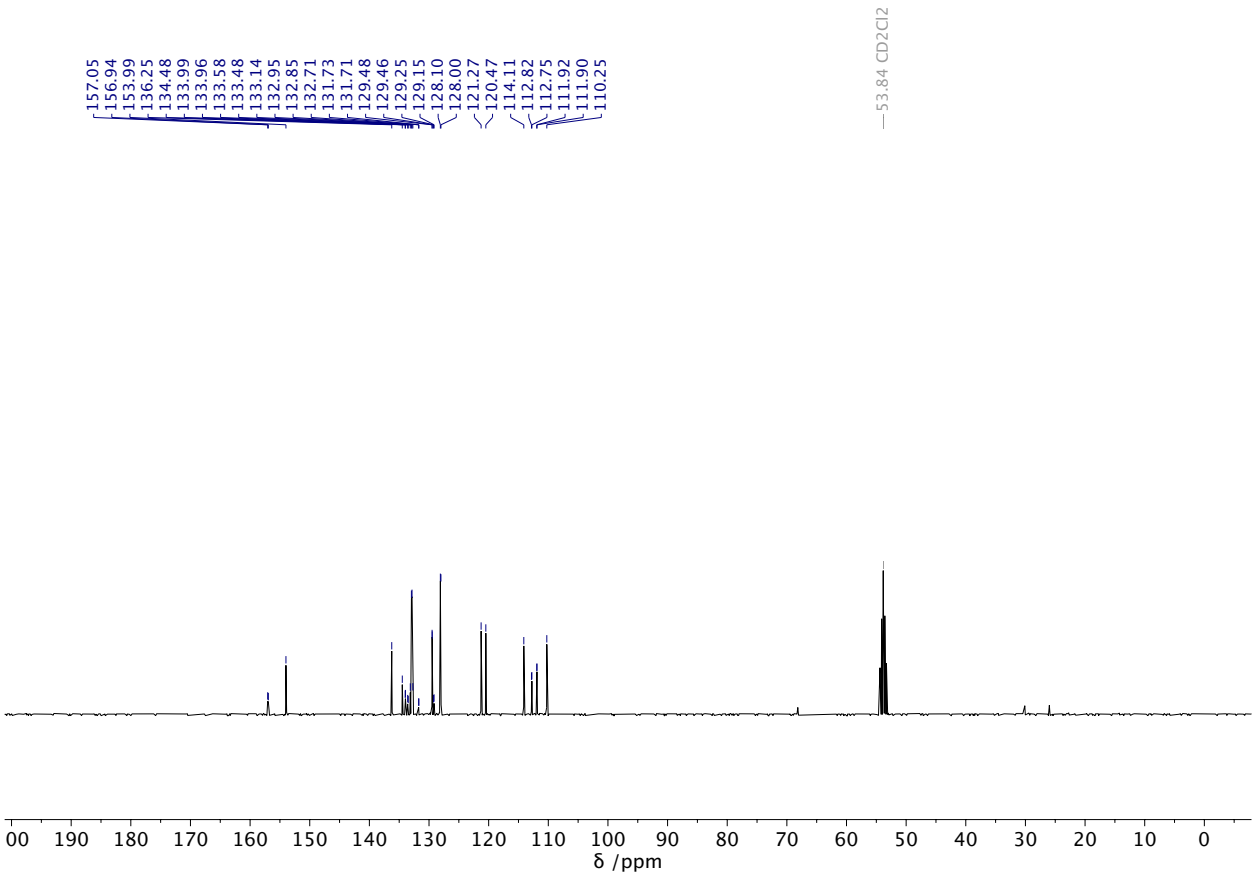


**Figure B-35.** $^{13}C$ NMR spectrum ($CD_2Cl_2$) of **3.16**.

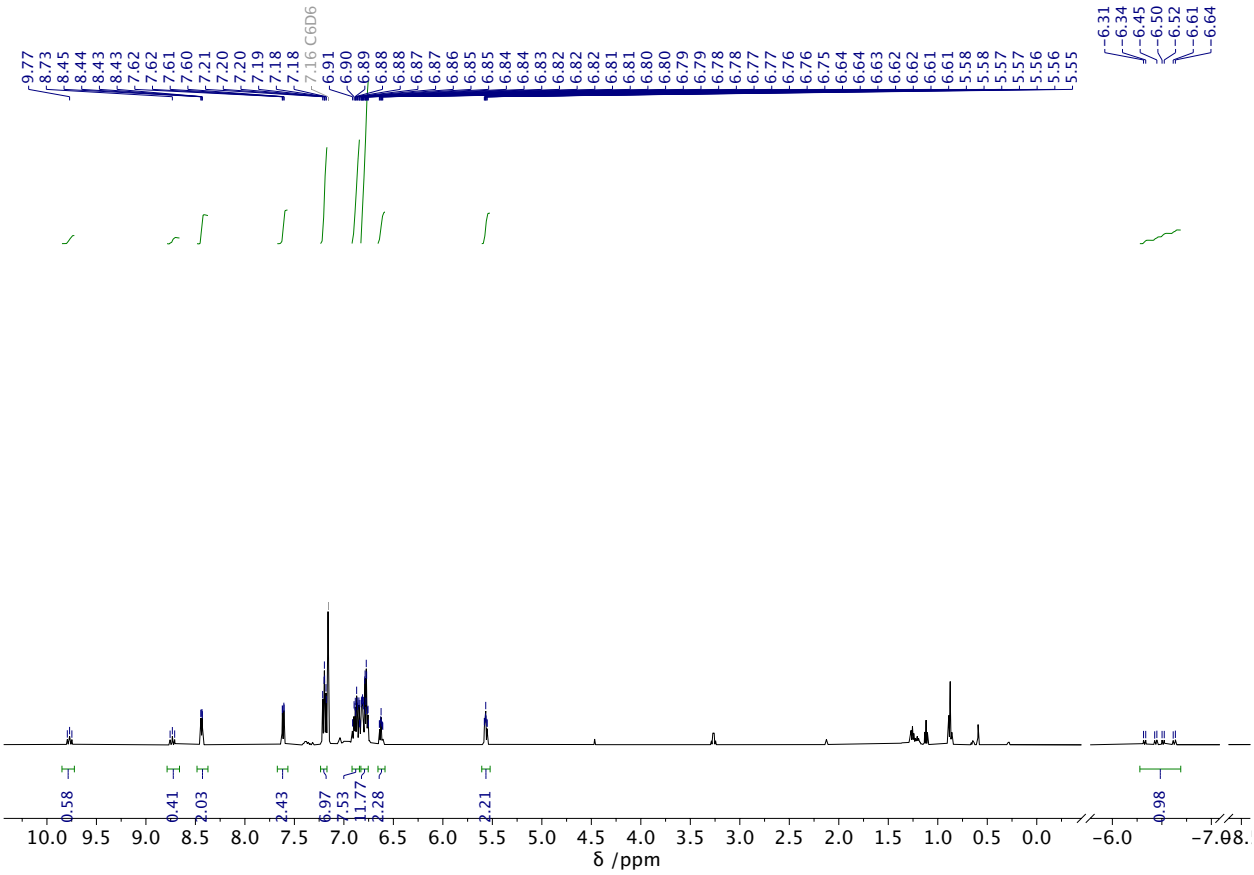


**Figure B-36**. $^{1}$H NMR spectrum ($C_6D_6$) of **3.17**. Signals of pentane are also obtained.

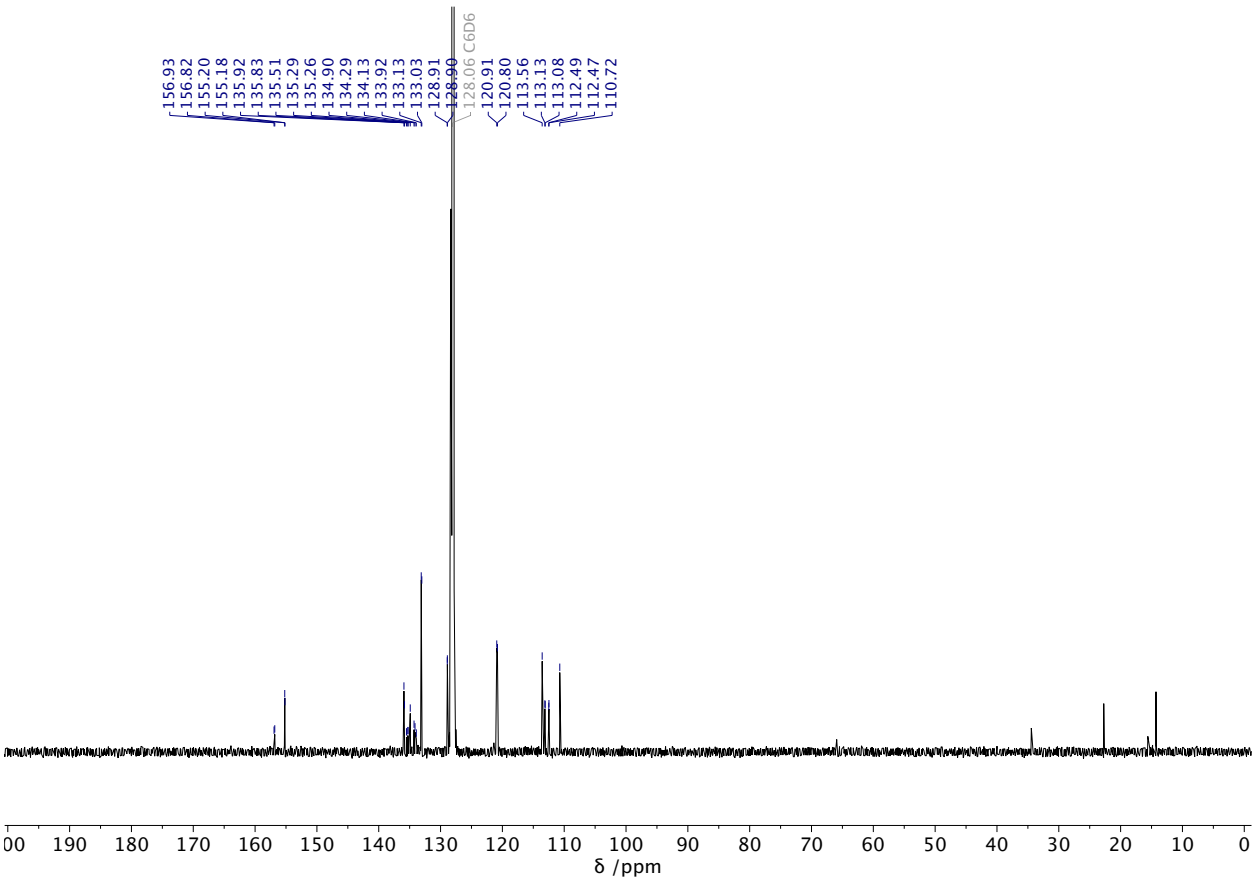


**Figure B-37**. $^{13}C$ NMR spectrum ($C_6D_6$) of **3.17**. Signals of pentane are also observed.

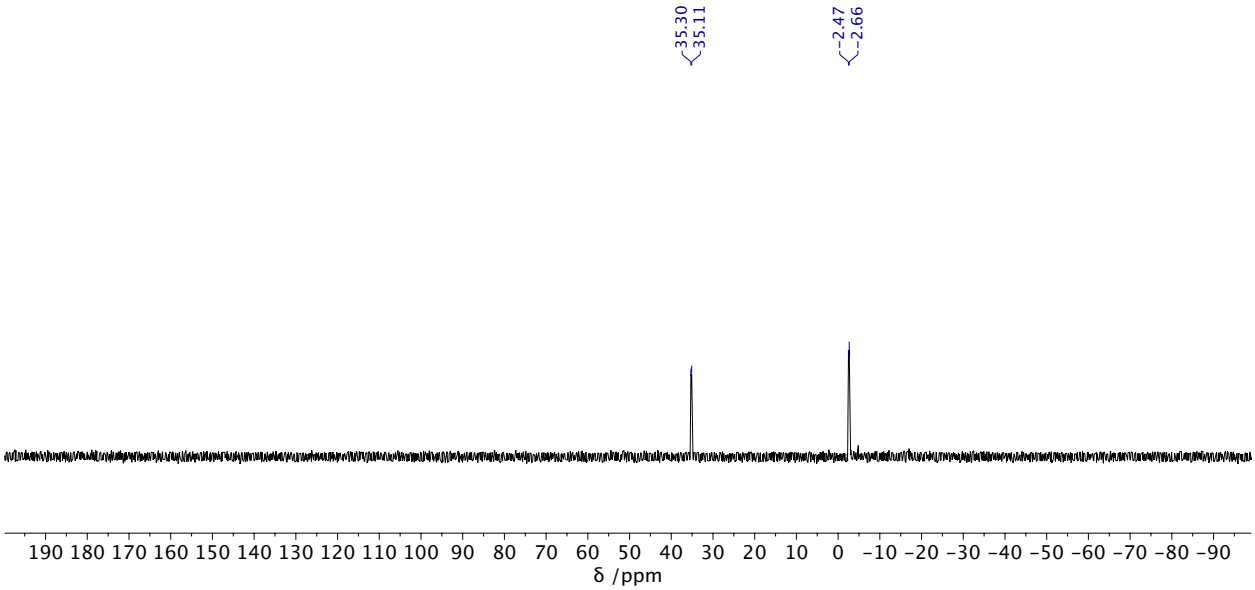


**Figure B-38**. $^{31}P\{^{1}H\}$ NMR spectrum (THF-$d_8$) of **3.17**.

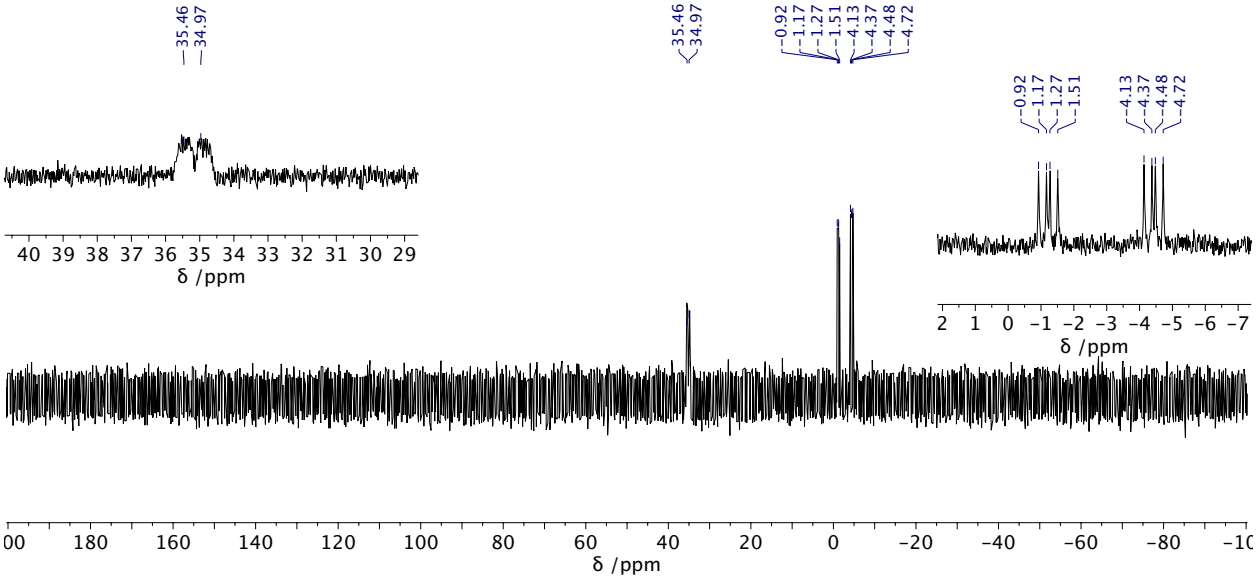


**Figure B-39**. $^{31}P$ NMR spectrum ($C_6D_6$) of **3.17**.

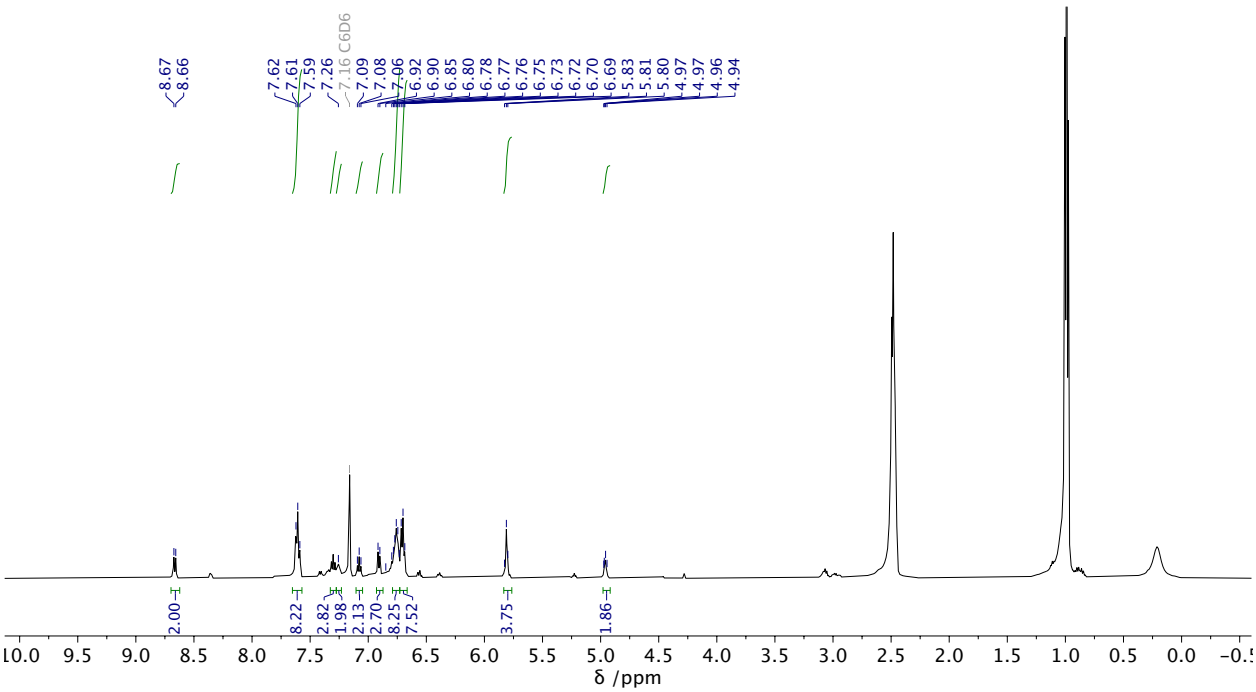


**Figure B-40**. $^{1}H$ NMR spectrum ($C_6D_6$) of **3.18**. Large signals are due to excess $Et_2NH$.

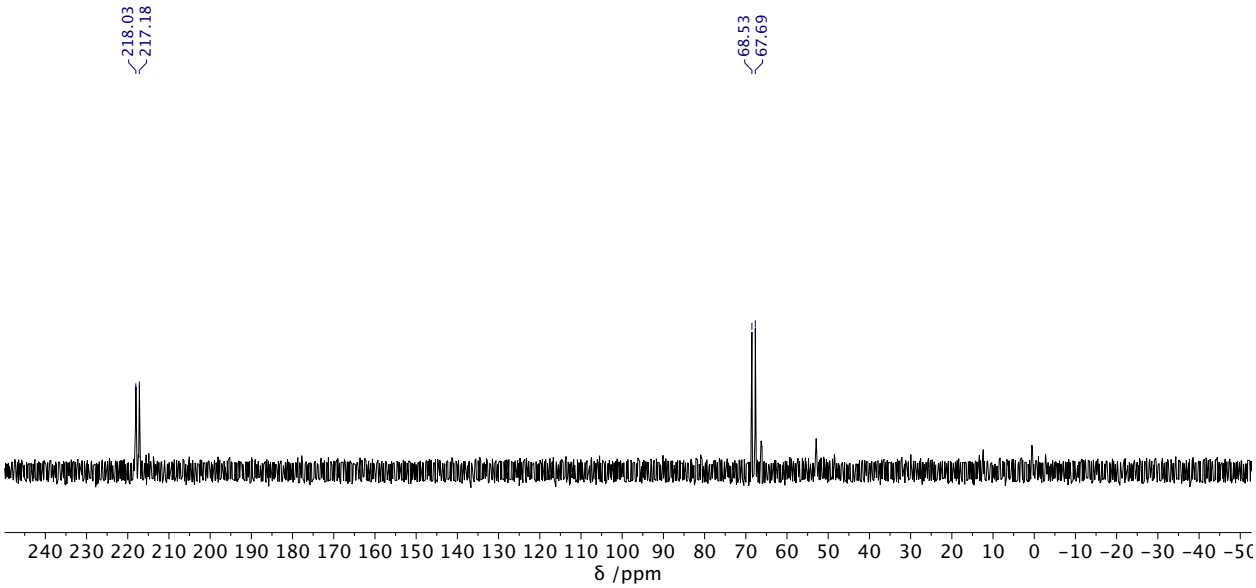


**Figure B-41**. $^{31}P\{^{1}H\}$ NMR spectrum ($C_6D_6$) of **3.18**.

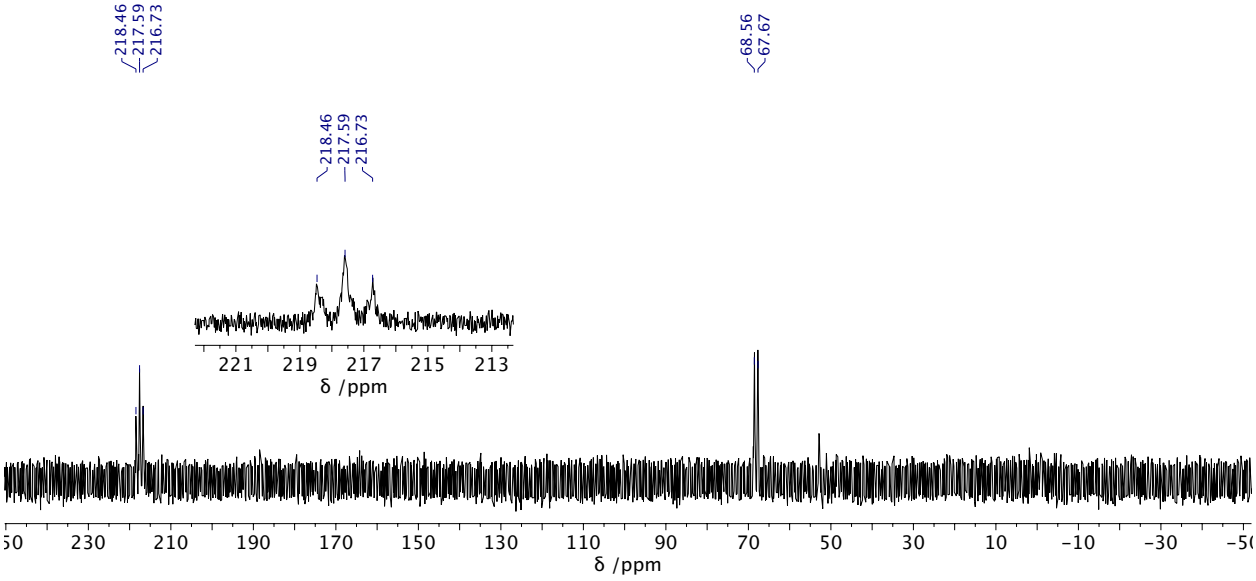


**Figure B-42**. $^{31}P$ NMR spectrum ($C_6D_6$) of **3.18**.

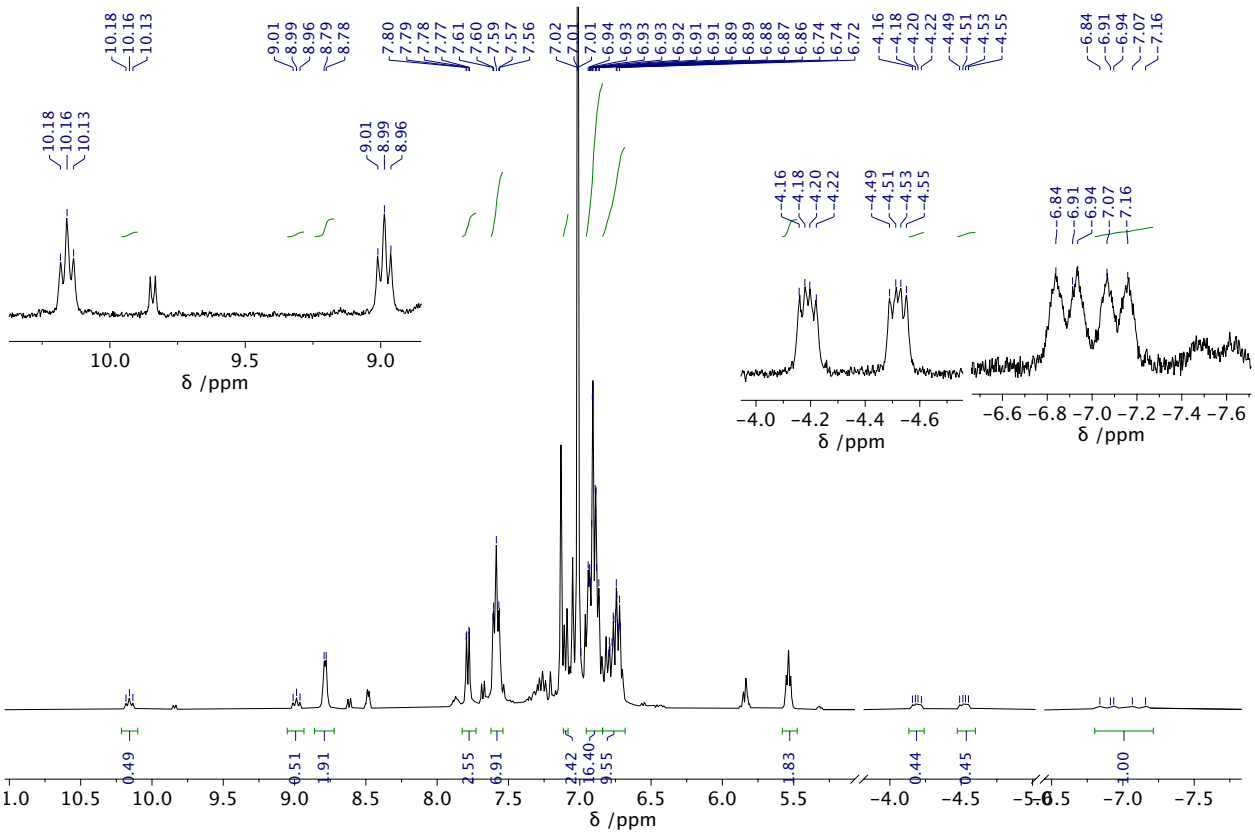


**Figure B-43**. $^{1}$H NMR spectrum (toluene-$d_8$) of **3.19**.

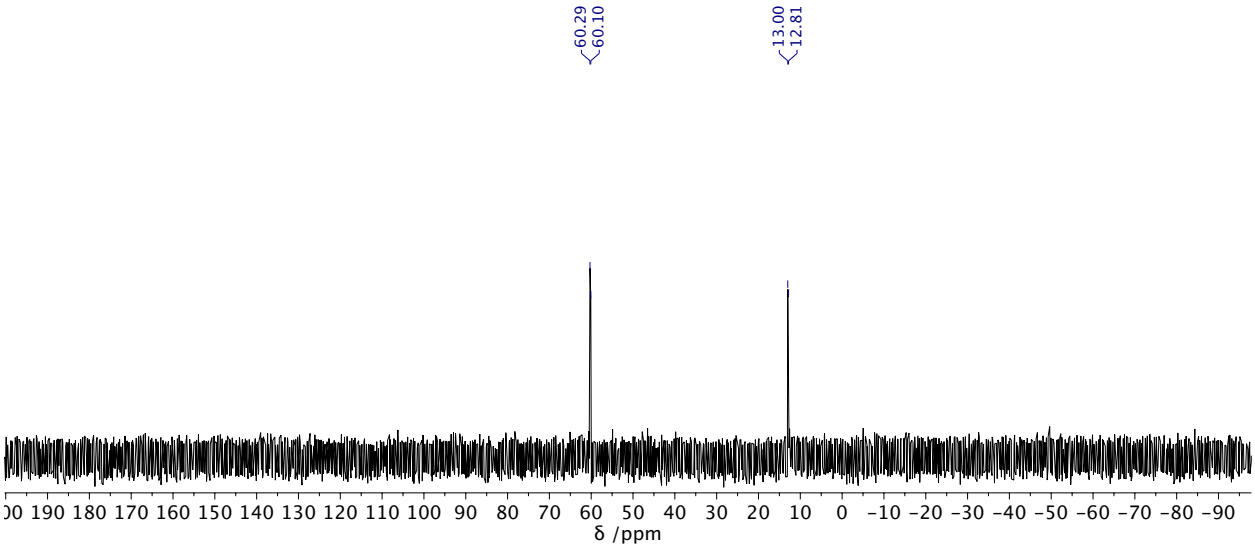


**Figure B-44**. $^{31}P\{^{1}H\}$ NMR spectrum (THF) of **3.19**.

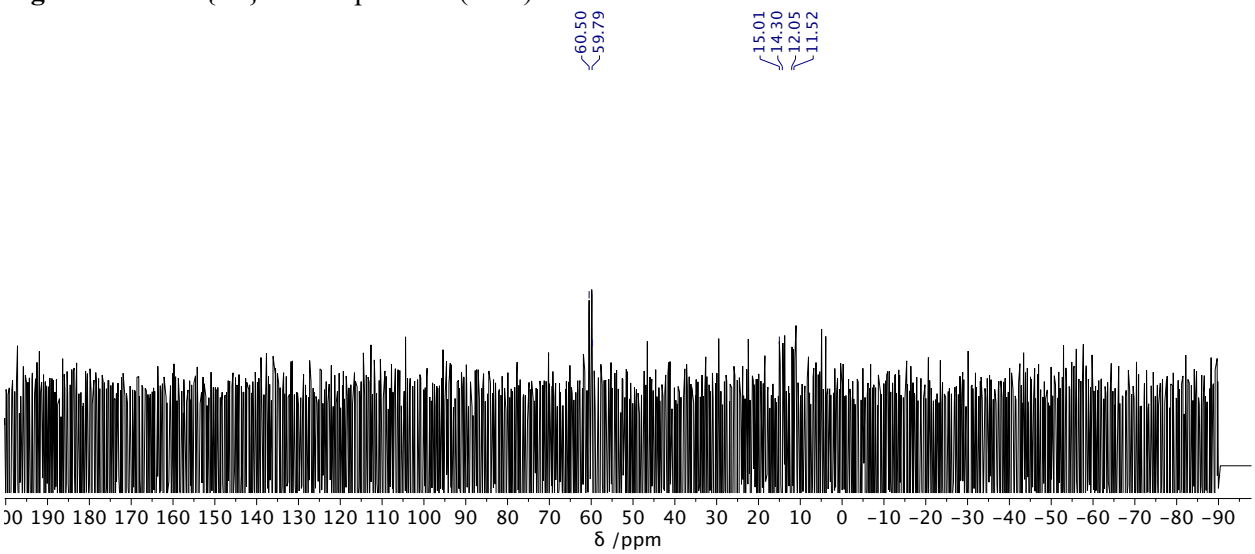


**Figure B-45**. $^{31}P$ NMR spectrum (THF) of **3.19**.

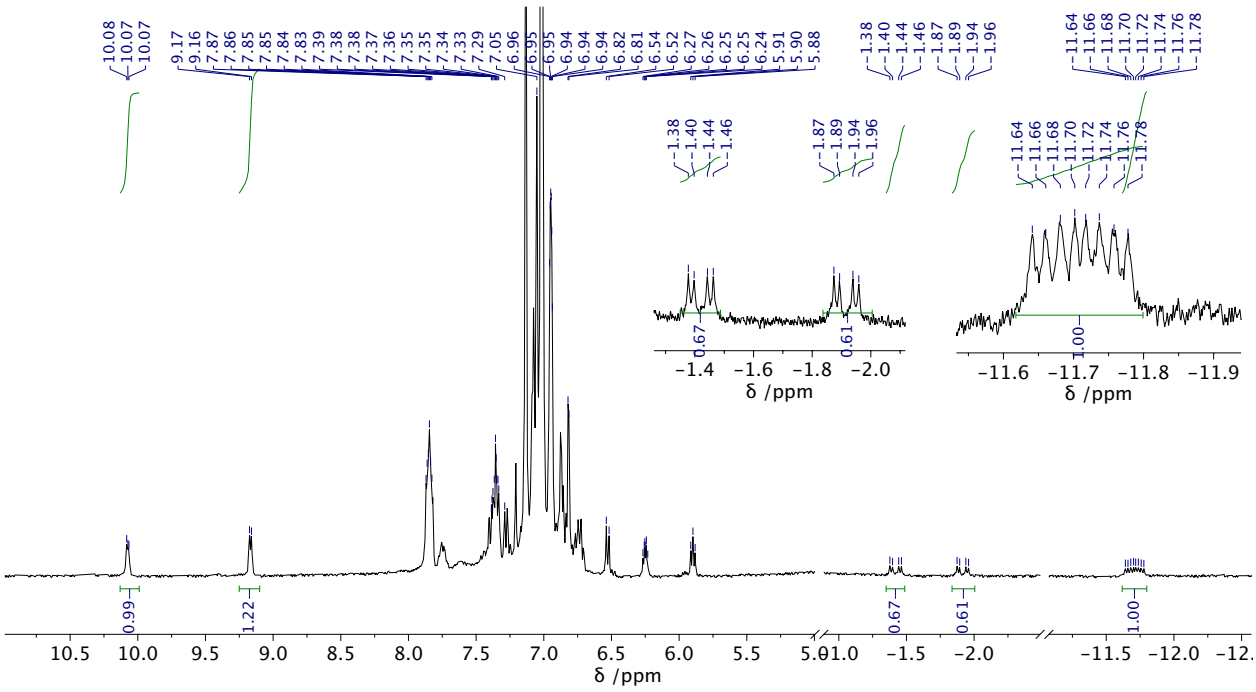


**Figure B-46**. $^{1}H$ NMR spectrum ($C_6D_6$) of **3.20**.

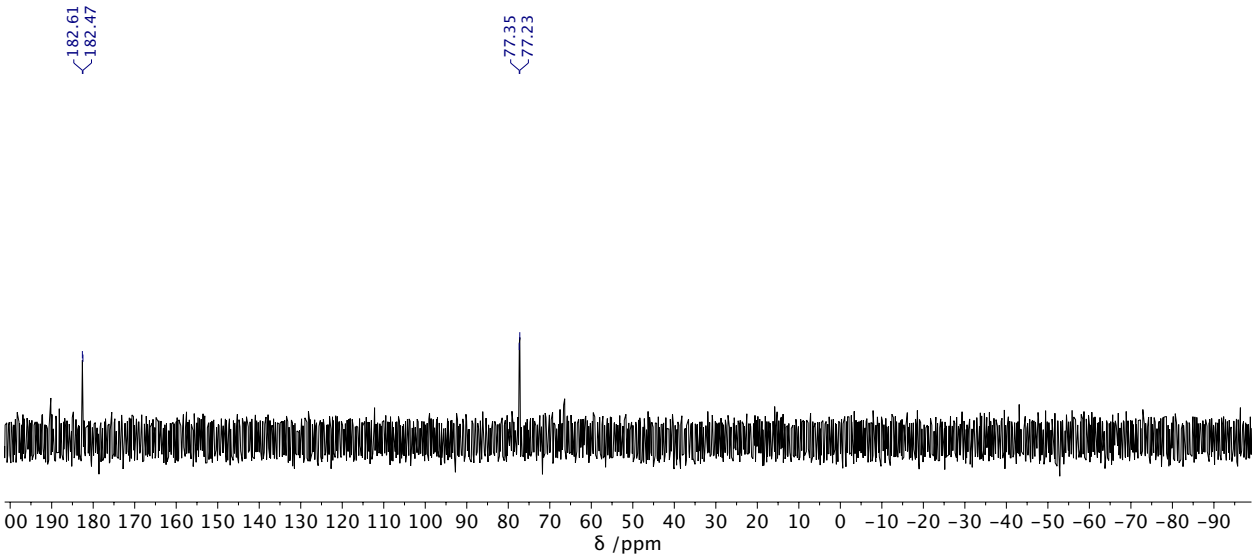


**Figure B-47**. $^{31}P\{^{1}H\}$ NMR spectrum ($C_6D_6$) of **3.20**.

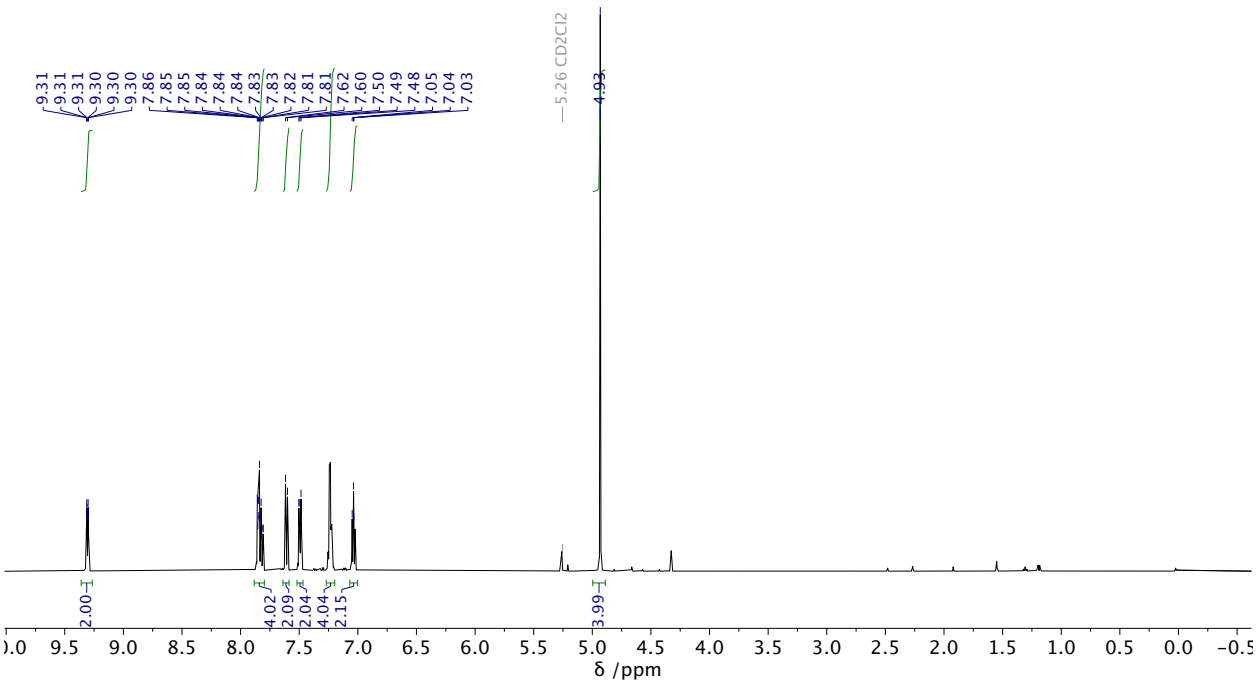


**Figure B-48**. $^{1}H$ NMR spectrum ($CD_2Cl_2$) of **3.23**.

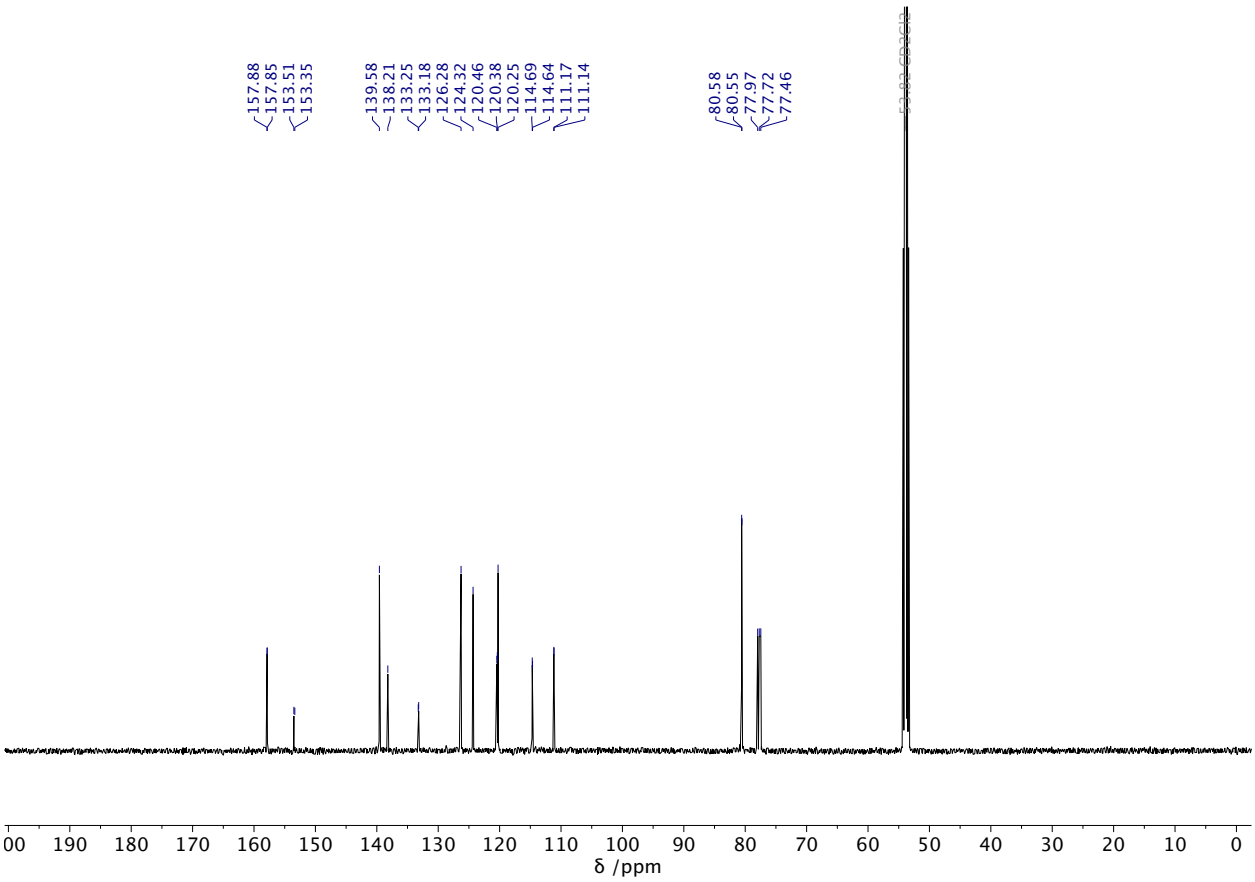


**Figure B-49**. $^{13}C\{^{1}H\}$ NMR spectrum ($CD_2Cl_2$) of **3.23**. Recrystallization solvent ($CDCl_3$) remains in the spectrum.

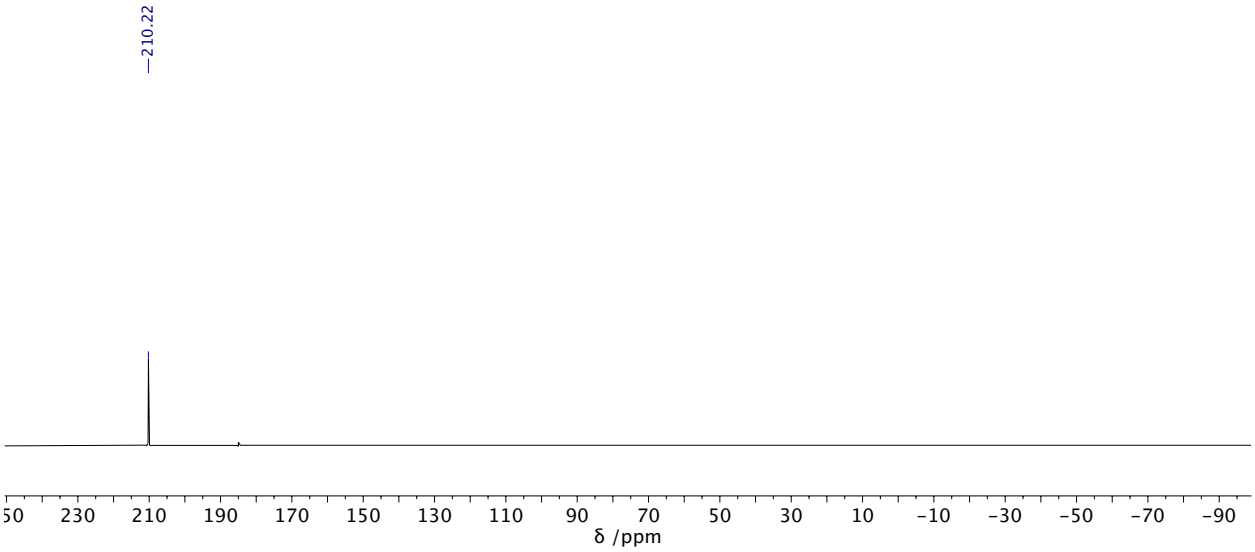


**Figure B-50**. $^{31}P\{^{1}H\}$ NMR spectrum ($CD_2Cl_2$) of **3.23**.

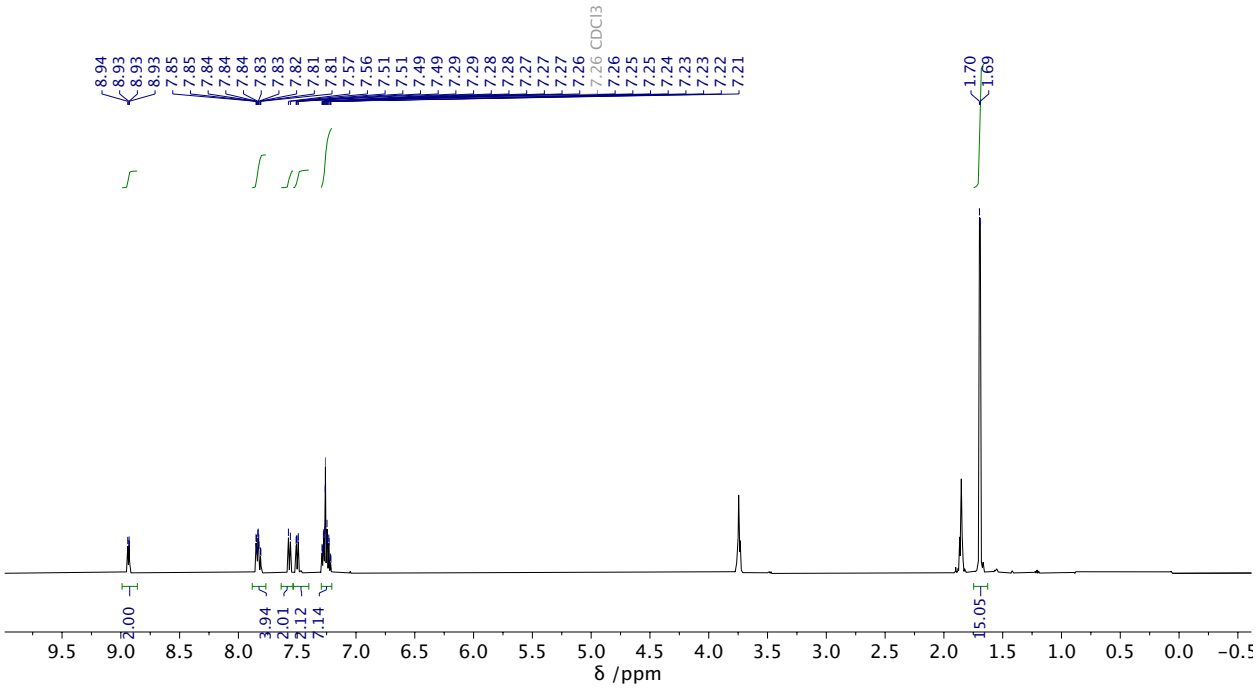


**Figure B-51**. $^{1}$H NMR spectrum ($CDCl_3$) of **3.24**. Signals of THF remain in the spectrum.

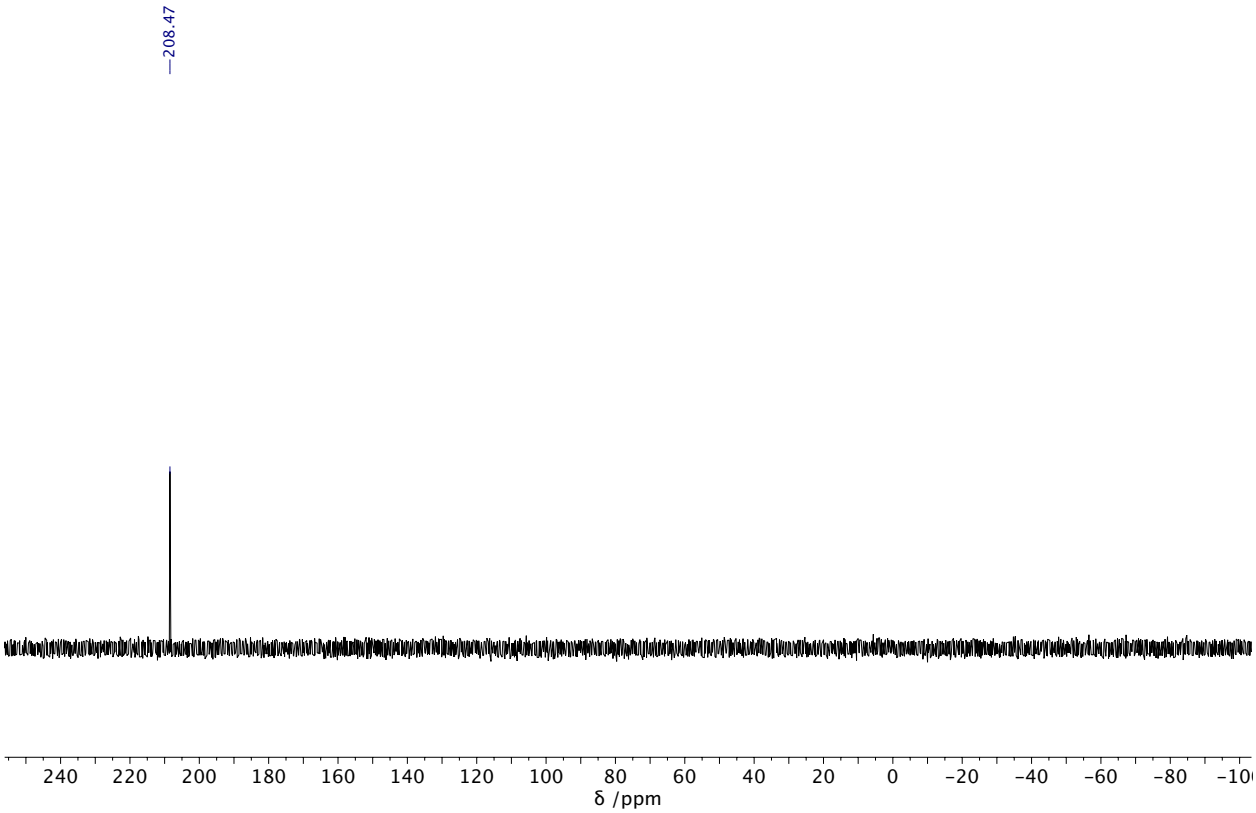


**Figure B-52**. $^{31}P\{^{1}H\}$ NMR spectrum ($CDCl_3$) of **3.24**.

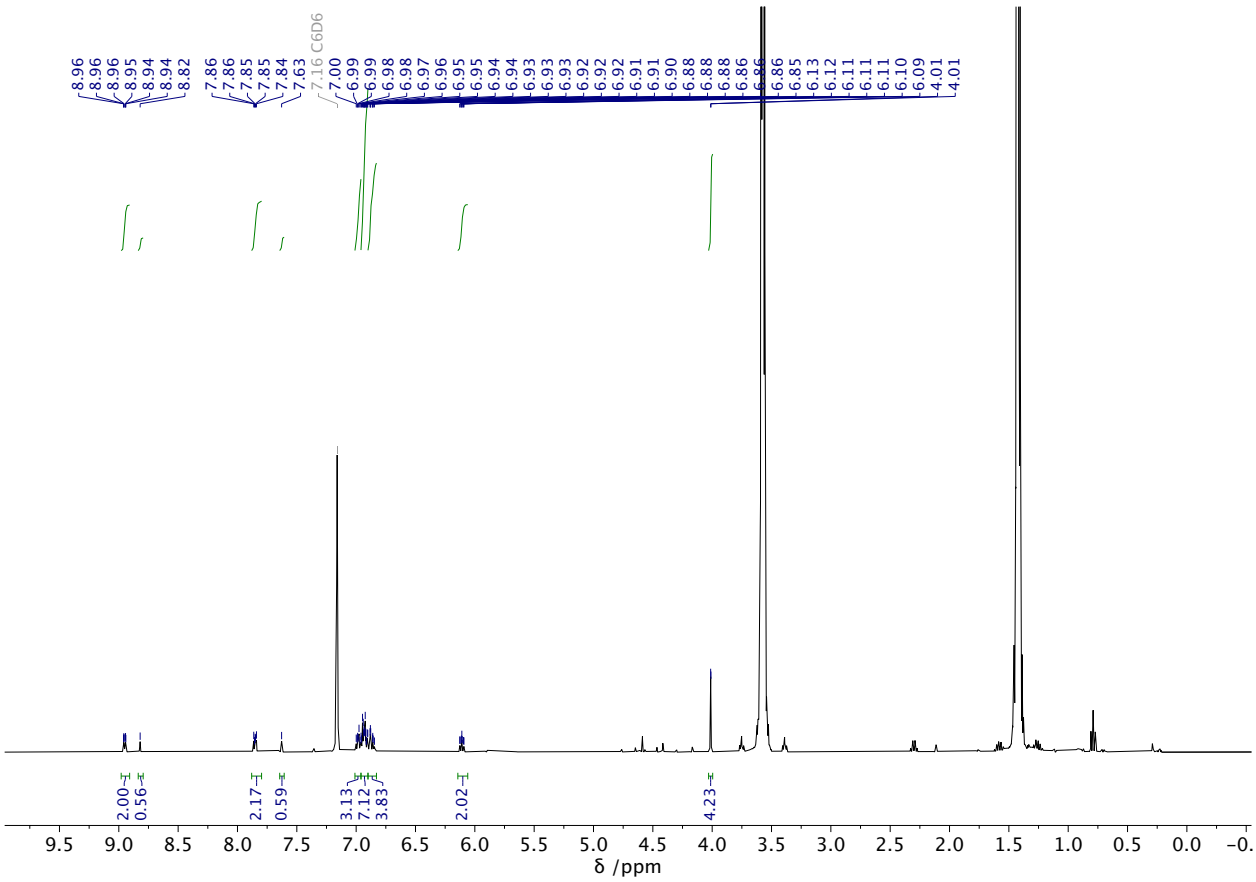


**Figure B-53**. $^{1}$H NMR spectrum ($C_6D_6$) of **3.25**.

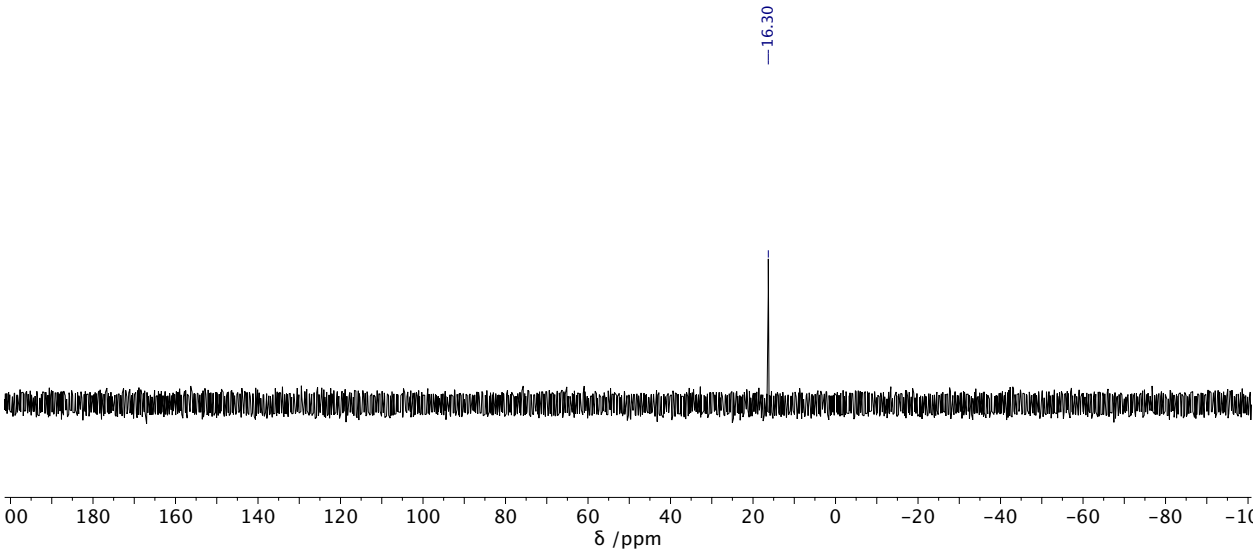


**Figure B-54**. $^{31}P\{^{1}H\}$ NMR spectrum ($C_6D_6$) of **3.25**.

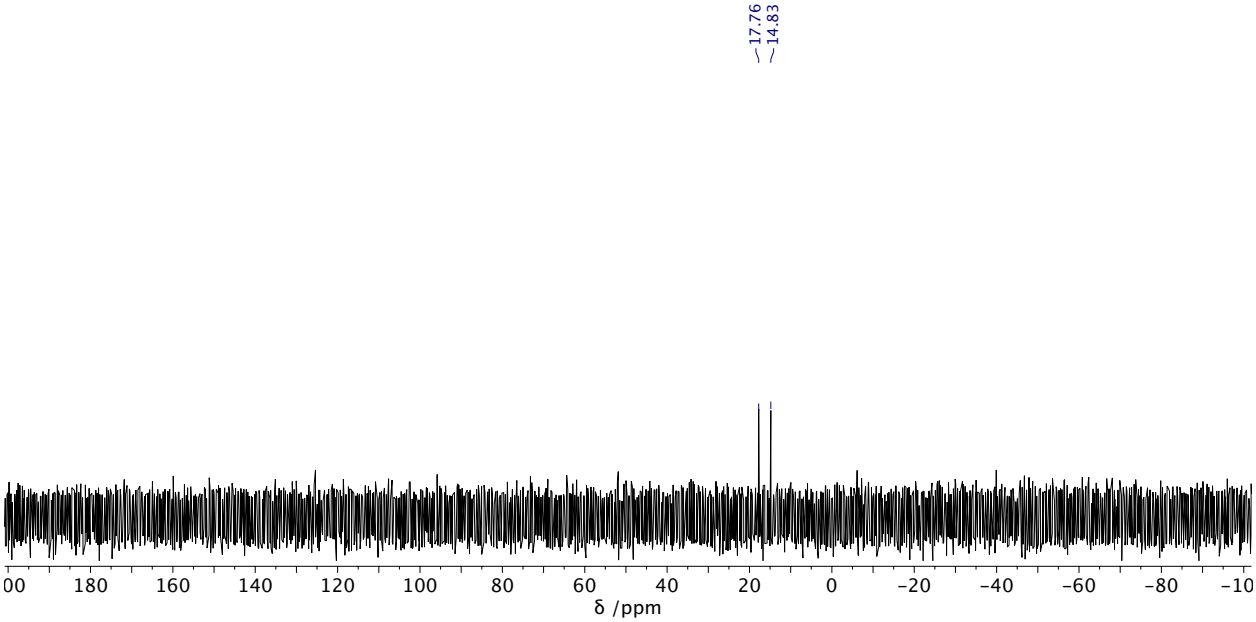


**Figure B-55**. $^{31}P$ NMR spectrum ($C_6D_6$) of **3.25**.

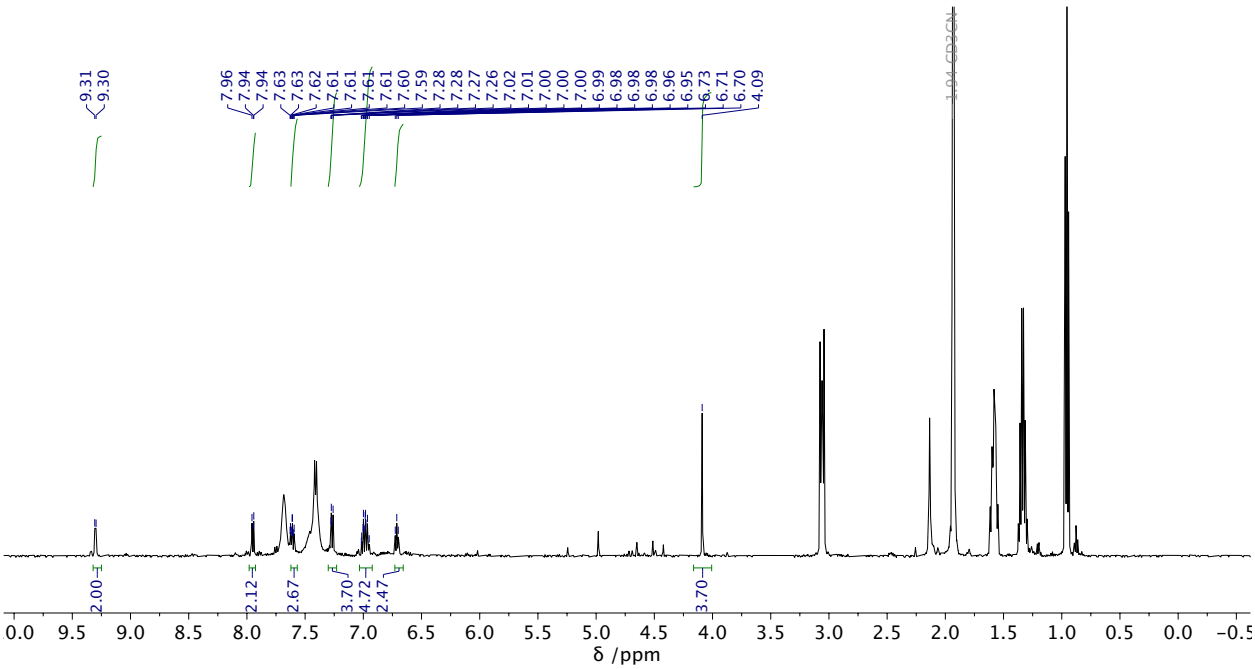


**Figure B-56**. $^{1}H$ NMR spectrum ($CD_3CN$) of **3.26**. Signals derived from TBAT remains in the spectrum.

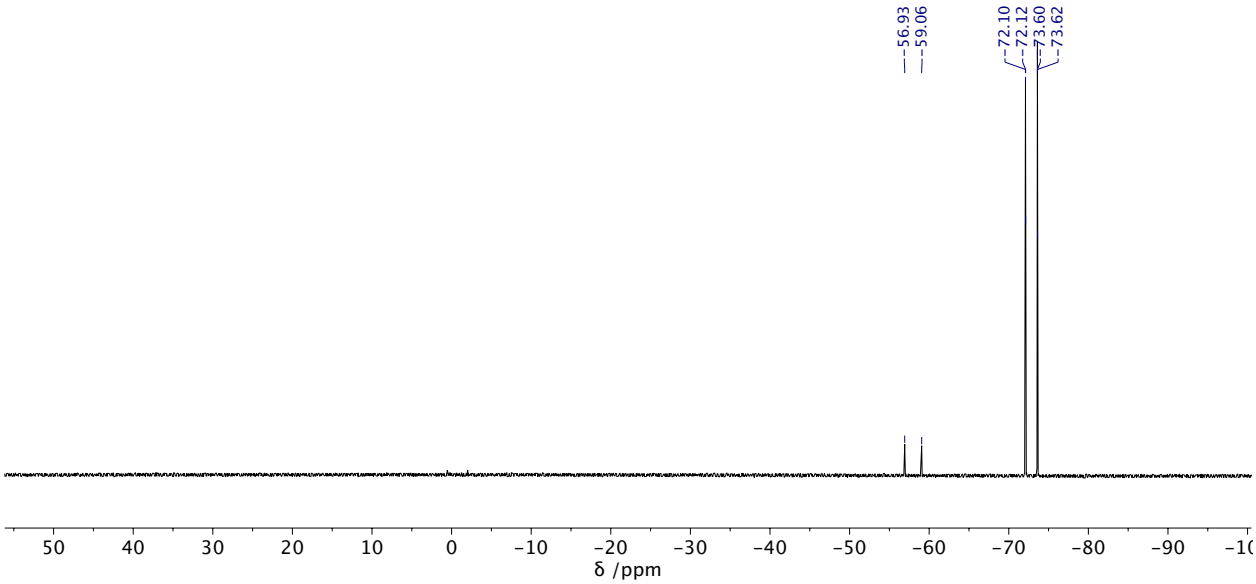


**Figure B-57**. $^{19}F$ NMR spectrum ($CDCl_3$) of **3.26**. The large signal around –76 ppm is due to $PF_6$ anion remains in the solution.

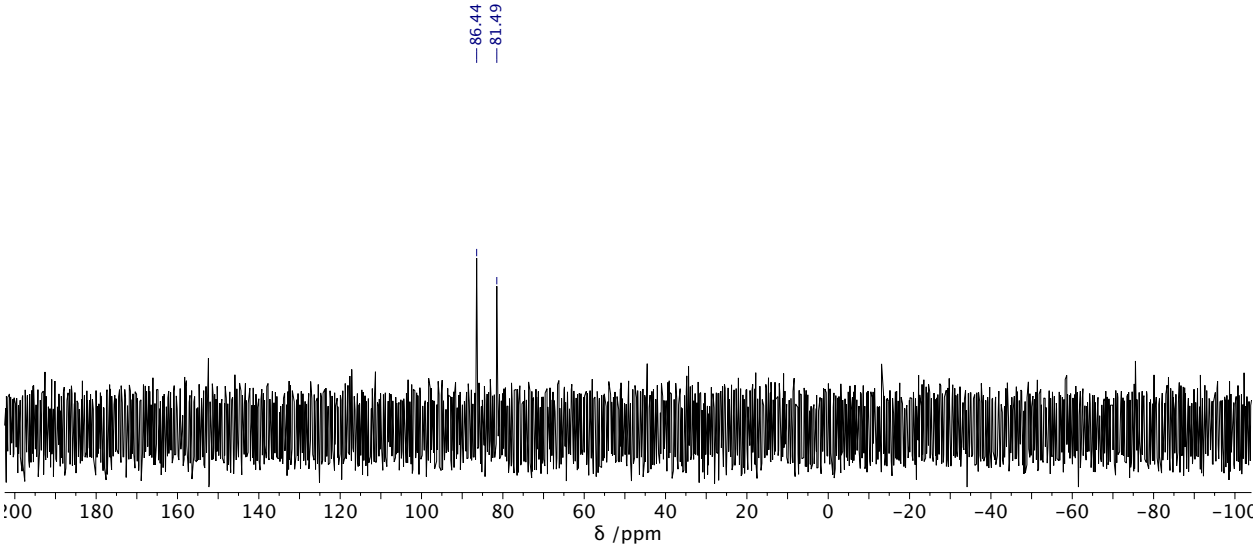


**Figure B-58**. $^{31}P\{^{1}H\}$ NMR spectrum ($CDCl_3$) of **3.26**.

## B.4. References


1. F. Neese, *WIREs Comput. Mol. Sci.*, **2012**, *2*, 73–78.
2. Y. Zhao and D. G. Truhlar, *Theor. Chem. Account*, **2008**, *120*, 215- 241.
3. (a) Becke, A. D.; *Phys. Rev. A.* **1988**, *38*, 3098. (b) Becke, A.D. *J.Chem.Phys*. **1993**, *98*, 5648. (c) Lee, C.; Yang, W.; Parr, R.G. *Phys. Rev. B.* **1988**, *37*, 785.
4. F. Weigend and R. Ahlrichs, *Phys. Chem. Chem. Phys.*, **2005**, *7*, 3297-3305.
5. E. Glendening, J. K. Badenhoop, A. E. Reed, J. E. Carpenter, J. A. Bohmann, C. M. Morales, C. R. Landis and F. Weinhold, *Natural Bond Orbital, version 6.0*, Theoretical Chemistry Institute, University of Wisconsin, Madison, 2013.
6. R. F. W. Bader, *Atoms in Molecules A Quantum Theory*, Oxford University Press, Oxford, 1990.
7. (a) van Lenthe, E.; Baerends, E. J.; Snijders, J. G. *J. Chem. Phys.* **1993**, *99*, 4597−4610. (b) van Lenthe, E.; Baerends, E. J.; Snijders, J. G. *J. Chem. Phys.* **1994**, *101*, 9783−9792.
8. Perdew, J. P.; Burke, K.; Wang, Y. *Phys. Rev. B* **1996**, *54*, 16533–16539.
9. Lu, T. Multiwfn: *A Multifunctional Wavefunction Analyzer*; Bejing Kein Research Center for Natural Sciences, Bejing, 2015.

# Appendix C . Supplementary Data for Chapter 4

## C.1. X-ray Diffraction

### Structural Data for 4.1

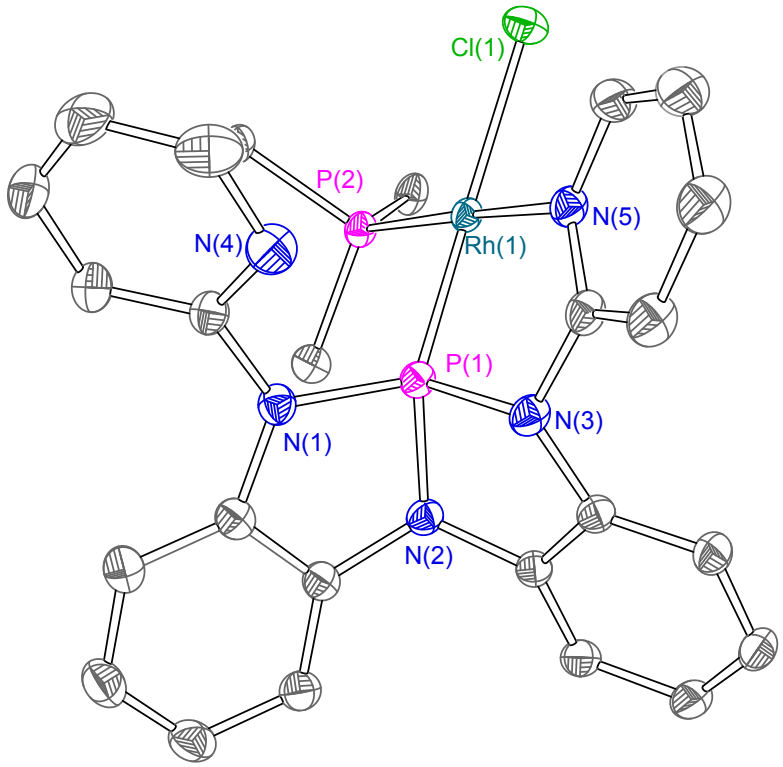

**Table C-1**. Crystal data and structure refinement for **4.1**

| | |
|---|---|
| Identification code | RhClPPh3L1-1 |
| Empirical formula | $C_{40}H_{31}ClN_5P_2Rh$ |
| Formula weight | 782.00 |
| Temperature/K | 100.0 |
| Crystal system | monoclinic |
| Space group | $P2_1/c$ |
| a/Å | 10.2353(2) |
| b/Å | 20.3324(5) |
| c/Å | 17.5562(4) |
| α/° | 90 |
| β/° | 102.0790(10) |
| γ/° | 90 |
| Volume/Å$^3$ | 3572.70(14) |
| Z | 4 |
| $\rho_{calc}$g/cm$^3$ | 1.454 |
| μ/mm$^{-1}$ | 0.679 |
| F(000) | 1592.0 |
| Crystal size/mm$^3$ | 0.13 × 0.12 × 0.1 |
| Radiation | MoKα (λ = 0.71073) |
| 2Θ range for data collection/° | 3.104 to 64.212 |
| Index ranges | $-15 \leq h \leq 15$, $-30 \leq k \leq 30$, $-26 \leq l \leq 26$ |
| Reflections collected | 153844 |
| Independent reflections | 12501 [$R_{int}$ = 0.0422, $R_{sigma}$ = 0.0201] |
| Data/restraints/parameters | 12501/0/442 |
| Goodness-of-fit on $F^2$ | 1.130 |
| Final R indexes [I>=2σ (I)] | $R_1$ = 0.0329, $wR_2$ = 0.0765 |
| Final R indexes [all data] | $R_1$ = 0.0378, $wR_2$ = 0.0784 |
| Largest diff. peak/hole / e Å$^{-3}$ | 0.68/-1.03 |

**Table C-2.** Fractional Atomic Coordinates ($\times 10^4$) and Equivalent Isotropic Displacement Parameters ($Å^2 \times 10^3$) for **4.1**. $U_{eq}$ is defined as 1/3 of of the trace of the orthogonalised $U_{IJ}$ tensor.

| Atom | *x* | *y* | *z* | U(eq) |
|---|---|---|---|---|
| Rh1 | 1933.6(2) | 7434.6(2) | 2495.1(2) | 15.45(3) |
| Cl1 | -350.9(4) | 7099.1(2) | 2063.2(3) | 26.37(9) |
| P1 | 3813.7(4) | 7884.1(2) | 2923.6(2) | 16.63(8) |
| P2 | 2655.6(4) | 6405.5(2) | 2816.5(2) | 17.41(8) |
| N1 | 4466.7(15) | 7907.6(7) | 3894.9(8) | 20.3(3) |
| N2 | 5388.4(14) | 7814.8(7) | 2730.0(8) | 18.9(3) |
| N3 | 3634.7(15) | 8660.9(7) | 2483.6(9) | 20.7(3) |
| N4 | 2651.8(17) | 8416.8(8) | 4226.1(10) | 29.2(3) |
| N5 | 1345.8(14) | 8445.5(7) | 2275.9(8) | 19.6(3) |
| C00B | 6400.5(17) | 7810.5(8) | 3422.8(10) | 19.6(3) |
| C1 | 5873.8(17) | 7869.2(8) | 4091.0(10) | 21.0(3) |
| C2 | 6707(2) | 7889.4(10) | 4822.5(11) | 26.9(4) |
| C3 | 8083(2) | 7837.8(10) | 4875.0(12) | 31.0(4) |
| C4 | 8599.6(19) | 7779.1(10) | 4211.4(12) | 29.6(4) |
| C5 | 7768.3(18) | 7763.8(9) | 3473.3(11) | 24.7(3) |
| C6 | 5508.3(16) | 8235.8(8) | 2100.4(9) | 18.9(3) |
| C7 | 6456.6(18) | 8187.1(9) | 1647.2(10) | 23.3(3) |
| C8 | 6418.6(19) | 8646.9(10) | 1048.3(11) | 27.9(4) |
| C9 | 5430(2) | 9125.1(10) | 909.7(11) | 27.3(4) |
| C10 | 4463.3(18) | 9168.1(9) | 1361.3(11) | 24.1(3) |
| C11 | 4514.8(17) | 8722.7(8) | 1965.8(10) | 19.7(3) |
| C12 | 3625.5(18) | 7974.5(8) | 4434.3(10) | 21.0(3) |
| C13 | 3792(2) | 7593.0(10) | 5102.2(11) | 29.7(4) |
| C14 | 2910(2) | 7691.2(13) | 5590.7(12) | 37.9(5) |
| C15 | 1901(2) | 8146.7(13) | 5397.0(13) | 39.5(5) |
| C16 | 1803(2) | 8492.4(12) | 4710.2(15) | 38.6(5) |
| C17 | 2320.0(18) | 8904.4(8) | 2313.6(10) | 21.2(3) |
| C18 | 2049(2) | 9576.3(9) | 2233.5(12) | 27.2(4) |
| C19 | 736(2) | 9784.0(9) | 2115.0(13) | 30.9(4) |
| C20 | -259(2) | 9321.6(10) | 2082.5(13) | 31.7(4) |
| C21 | 81.2(19) | 8664.8(9) | 2172.6(12) | 26.4(4) |
| C22 | 2202.4(19) | 5699.0(8) | 2146.8(10) | 23.2(3) |
| C23 | 3073(2) | 5163.9(9) | 2169.4(12) | 29.3(4) |
| C24 | 2734(3) | 4630.5(10) | 1669.5(13) | 37.0(5) |
| C25 | 1529(3) | 4625.5(11) | 1138.0(13) | 41.0(5) |
| C26 | 660(3) | 5139.8(11) | 1114.4(13) | 40.0(5) |
| C27 | 977(2) | 5679.0(10) | 1617.0(12) | 30.8(4) |
| C28 | 2095.3(17) | 6124.9(8) | 3687.2(10) | 20.1(3) |
| C29 | 2381(2) | 5495.4(9) | 3996.3(11) | 26.4(4) |
| C30 | 1902(2) | 5295.1(10) | 4642.8(12) | 30.7(4) |
| C31 | 1138(2) | 5713.1(10) | 4990.5(11) | 30.7(4) |
| C32 | 848(2) | 6340.9(11) | 4694.7(12) | 31.6(4) |
| C33 | 1330(2) | 6546.1(9) | 4044.2(11) | 27.1(4) |
| C34 | 4474.2(17) | 6305.3(8) | 3047.6(10) | 20.8(3) |

| | | | | |
|---|---|---|---|---|
| C35 | 5141.8(19) | 6328.9(9) | 2424.8(11) | 25.1(3) |
| C36 | 6520(2) | 6276.3(10) | 2558.5(13) | 30.9(4) |
| C37 | 7255(2) | 6205.0(10) | 3317.4(14) | 33.8(4) |
| C38 | 6618(2) | 6184.4(10) | 3927.6(13) | 31.2(4) |
| C39 | 5219.5(19) | 6235.1(9) | 3803.6(11) | 25.4(3) |

**Table C-3.** Anisotropic Displacement Parameters ($Å^2 \times 10^3$) for **4.1**. The Anisotropic displacement factor exponent takes the form: $-2\pi^2[h^2a^{*2}U_{11}+2hka^*b^*U_{12}+\ldots]$.

| **Atom** | **$U_{11}$** | **$U_{22}$** | **$U_{33}$** | **$U_{23}$** | **$U_{13}$** | **$U_{12}$** |
|---|---|---|---|---|---|---|
| Rh1 | 17.38(6) | 13.60(5) | 15.67(5) | 2.67(4) | 4.15(4) | 0.44(4) |
| Cl1 | 19.23(18) | 26.8(2) | 31.9(2) | -0.58(16) | 2.72(15) | -1.71(15) |
| P1 | 18.81(18) | 12.66(16) | 18.61(18) | 1.21(13) | 4.41(14) | 0.60(13) |
| P2 | 21.35(19) | 13.09(16) | 17.54(18) | 1.72(13) | 3.49(14) | -1.52(14) |
| N1 | 21.7(6) | 21.3(6) | 18.2(6) | -0.7(5) | 4.5(5) | 1.8(5) |
| N2 | 19.8(6) | 16.9(6) | 20.3(6) | 1.3(5) | 5.0(5) | -1.0(5) |
| N3 | 22.9(7) | 15.3(6) | 24.8(7) | 3.9(5) | 7.2(5) | 1.4(5) |
| N4 | 29.0(8) | 26.0(8) | 33.6(8) | 3.3(6) | 8.8(7) | 7.0(6) |
| N5 | 21.2(6) | 17.2(6) | 20.9(6) | 3.5(5) | 5.8(5) | 2.6(5) |
| C00B | 21.0(7) | 14.3(6) | 22.6(7) | 2.5(5) | 2.3(6) | 0.7(5) |
| C1 | 21.9(7) | 16.8(7) | 23.4(8) | 0.6(6) | 2.9(6) | 1.4(6) |
| C2 | 28.0(9) | 28.6(9) | 22.8(8) | 0.9(7) | 2.4(7) | 0.5(7) |
| C3 | 28.1(9) | 32.0(10) | 29.1(9) | 3.1(7) | -3.0(7) | 0.4(7) |
| C4 | 21.6(8) | 29.0(9) | 36.2(10) | 5.1(8) | 1.3(7) | 1.6(7) |
| C5 | 22.0(8) | 23.3(8) | 29.0(9) | 5.5(7) | 5.4(7) | 1.7(6) |
| C6 | 19.9(7) | 17.2(7) | 18.8(7) | 0.4(5) | 2.3(6) | -3.3(5) |
| C7 | 20.7(7) | 26.8(8) | 22.5(8) | -1.0(6) | 4.8(6) | -3.0(6) |
| C8 | 25.1(8) | 36.4(10) | 23.3(8) | 2.2(7) | 7.7(7) | -6.3(7) |
| C9 | 30.2(9) | 30.6(9) | 20.9(8) | 5.7(7) | 4.7(7) | -8.8(7) |
| C10 | 25.5(8) | 21.2(8) | 24.4(8) | 5.5(6) | 2.7(6) | -3.0(6) |
| C11 | 20.4(7) | 17.6(7) | 20.7(7) | 1.4(5) | 3.5(6) | -2.8(5) |
| C12 | 24.0(8) | 20.0(7) | 19.2(7) | -1.0(6) | 5.2(6) | 1.1(6) |
| C13 | 31.0(9) | 33.4(10) | 24.0(8) | 6.8(7) | 3.8(7) | 1.0(8) |
| C14 | 38.5(11) | 55.1(14) | 20.1(9) | 2.9(9) | 6.0(8) | -8.1(10) |
| C15 | 37.7(11) | 54.1(14) | 31.1(10) | -14.6(10) | 17.3(9) | -6.6(10) |
| C16 | 31.4(10) | 36.9(11) | 50.6(13) | -5.3(10) | 16.0(10) | 8.8(9) |
| C17 | 25.3(8) | 16.9(7) | 22.2(7) | 3.4(6) | 6.8(6) | 3.1(6) |
| C18 | 32.8(9) | 17.0(7) | 33.4(9) | 3.4(7) | 10.2(8) | 4.2(7) |
| C19 | 36.3(10) | 20.3(8) | 38.2(10) | 5.6(7) | 13.0(8) | 9.8(7) |
| C20 | 27.2(9) | 28.2(9) | 41.6(11) | 8.5(8) | 11.5(8) | 10.2(7) |
| C21 | 22.5(8) | 24.7(8) | 32.8(9) | 6.8(7) | 7.7(7) | 4.3(6) |
| C22 | 33.8(9) | 16.1(7) | 19.8(7) | 1.0(6) | 5.5(7) | -5.7(6) |
| C23 | 40.4(11) | 17.2(7) | 29.2(9) | -1.2(6) | 4.9(8) | -2.0(7) |
| C24 | 56.2(14) | 17.5(8) | 37.6(11) | -4.9(7) | 10.6(10) | -1.7(8) |
| C25 | 64.1(16) | 25.7(9) | 32.0(10) | -8.6(8) | 6.9(10) | -13.6(10) |
| C26 | 52.2(14) | 33.1(11) | 29.9(10) | -6.0(8) | -2.5(9) | -13.2(10) |
| C27 | 37.8(10) | 24.4(9) | 27.8(9) | -1.2(7) | 1.6(8) | -6.6(7) |

| | | | | | | |
|---|---|---|---|---|---|---|
| C28 | 24.3(8) | 16.9(7) | 18.4(7) | 3.2(5) | 2.8(6) | -3.9(6) |
| C29 | 34.6(10) | 18.1(7) | 26.0(8) | 5.0(6) | 4.9(7) | -3.2(7) |
| C30 | 39.7(11) | 23.5(8) | 27.2(9) | 9.3(7) | 3.6(8) | -6.5(7) |
| C31 | 34.0(10) | 34.3(10) | 23.7(8) | 9.1(7) | 5.6(7) | -9.5(8) |
| C32 | 37.8(11) | 34.2(10) | 25.3(9) | 6.7(7) | 12.7(8) | -0.7(8) |
| C33 | 35.2(10) | 23.1(8) | 24.9(8) | 5.9(6) | 11.1(7) | 0.8(7) |
| C34 | 23.8(8) | 11.4(6) | 26.8(8) | -0.2(5) | 4.3(6) | 1.0(5) |
| C35 | 27.8(9) | 19.7(7) | 28.8(9) | -0.7(6) | 7.9(7) | 1.4(6) |
| C36 | 29.8(9) | 22.7(8) | 42.8(11) | -5.6(8) | 13.8(8) | 1.2(7) |
| C37 | 25.5(9) | 21.8(8) | 52.6(13) | -9.2(8) | 4.8(8) | 5.3(7) |
| C38 | 31.1(10) | 23.0(8) | 35.1(10) | -2.7(7) | -2.7(8) | 5.4(7) |
| C39 | 28.5(9) | 18.6(7) | 27.5(8) | -0.1(6) | 2.0(7) | 2.4(6) |

**Table C-4.** Bond Lengths for **4.1**.

| **Atom** | **Atom** | **Length/Å** | **Atom** | **Atom** | **Length/Å** |
|---|---|---|---|---|---|
| Rh1 | Cl1 | 2.4012(4) | C8 | C9 | 1.388(3) |
| Rh1 | P1 | 2.1210(4) | C9 | C10 | 1.394(3) |
| Rh1 | P2 | 2.2513(4) | C10 | C11 | 1.388(2) |
| Rh1 | N5 | 2.1537(14) | C12 | C13 | 1.386(2) |
| P1 | N1 | 1.6970(15) | C13 | C14 | 1.384(3) |
| P1 | N2 | 1.7213(15) | C14 | C15 | 1.376(4) |
| P1 | N3 | 1.7509(14) | C15 | C16 | 1.381(4) |
| P2 | C22 | 1.8527(18) | C17 | C18 | 1.395(2) |
| P2 | C28 | 1.8325(17) | C18 | C19 | 1.382(3) |
| P2 | C34 | 1.8316(18) | C19 | C20 | 1.379(3) |
| N1 | C1 | 1.411(2) | C20 | C21 | 1.381(3) |
| N1 | C12 | 1.413(2) | C22 | C23 | 1.401(3) |
| N2 | C00B | 1.423(2) | C22 | C27 | 1.397(3) |
| N2 | C6 | 1.423(2) | C23 | C24 | 1.392(3) |
| N3 | C11 | 1.413(2) | C24 | C25 | 1.382(3) |
| N3 | C17 | 1.406(2) | C25 | C26 | 1.368(4) |
| N4 | C12 | 1.335(2) | C26 | C27 | 1.402(3) |
| N4 | C16 | 1.345(3) | C28 | C29 | 1.397(2) |
| N5 | C17 | 1.357(2) | C28 | C33 | 1.395(3) |
| N5 | C21 | 1.345(2) | C29 | C30 | 1.388(3) |
| C00B | C1 | 1.395(2) | C30 | C31 | 1.381(3) |
| C00B | C5 | 1.387(2) | C31 | C32 | 1.387(3) |
| C1 | C2 | 1.386(2) | C32 | C33 | 1.399(3) |
| C2 | C3 | 1.397(3) | C34 | C35 | 1.406(3) |
| C3 | C4 | 1.382(3) | C34 | C39 | 1.393(3) |
| C4 | C5 | 1.394(3) | C35 | C36 | 1.385(3) |
| C6 | C7 | 1.382(2) | C36 | C37 | 1.394(3) |
| C6 | C11 | 1.403(2) | C37 | C38 | 1.367(3) |
| C7 | C8 | 1.401(3) | C38 | C39 | 1.406(3) |

**Table C-5.** Bond Angles for **4.1**.

| Atom | Atom | Atom | Angle/° | Atom | Atom | Atom | Angle/° |
|---|---|---|---|---|---|---|---|
| P1 | Rh1 | Cl1 | 170.299(16) | C9 | C8 | C7 | 120.25(17) |
| P1 | Rh1 | P2 | 94.918(16) | C8 | C9 | C10 | 121.49(17) |
| P1 | Rh1 | N5 | 81.42(4) | C11 | C10 | C9 | 118.44(17) |
| P2 | Rh1 | Cl1 | 93.556(16) | C6 | C11 | N3 | 111.46(14) |
| N5 | Rh1 | Cl1 | 89.86(4) | C10 | C11 | N3 | 128.52(16) |
| N5 | Rh1 | P2 | 175.30(4) | C10 | C11 | C6 | 119.96(16) |
| N1 | P1 | Rh1 | 120.39(6) | N4 | C12 | N1 | 113.93(15) |
| N1 | P1 | N2 | 90.72(7) | N4 | C12 | C13 | 124.14(18) |
| N1 | P1 | N3 | 113.63(7) | C13 | C12 | N1 | 121.89(16) |
| N2 | P1 | Rh1 | 135.41(5) | C14 | C13 | C12 | 117.55(19) |
| N2 | P1 | N3 | 90.14(7) | C15 | C14 | C13 | 119.8(2) |
| N3 | P1 | Rh1 | 103.23(5) | C14 | C15 | C16 | 118.2(2) |
| C22 | P2 | Rh1 | 122.42(6) | N4 | C16 | C15 | 123.7(2) |
| C28 | P2 | Rh1 | 110.78(6) | N5 | C17 | N3 | 115.40(14) |
| C28 | P2 | C22 | 101.98(8) | N5 | C17 | C18 | 122.67(17) |
| C34 | P2 | Rh1 | 115.09(5) | C18 | C17 | N3 | 121.83(16) |
| C34 | P2 | C22 | 99.33(8) | C19 | C18 | C17 | 118.74(18) |
| C34 | P2 | C28 | 105.16(8) | C20 | C19 | C18 | 118.99(17) |
| C1 | N1 | P1 | 114.25(12) | C19 | C20 | C21 | 119.22(18) |
| C1 | N1 | C12 | 125.14(14) | N5 | C21 | C20 | 123.27(18) |
| C12 | N1 | P1 | 120.59(12) | C23 | C22 | P2 | 120.72(14) |
| C00B | N2 | P1 | 112.08(11) | C27 | C22 | P2 | 121.05(15) |
| C6 | N2 | P1 | 109.91(11) | C27 | C22 | C23 | 118.23(17) |
| C6 | N2 | C00B | 120.11(14) | C24 | C23 | C22 | 120.9(2) |
| C11 | N3 | P1 | 110.02(11) | C25 | C24 | C23 | 120.0(2) |
| C17 | N3 | P1 | 114.74(11) | C26 | C25 | C24 | 119.8(2) |
| C17 | N3 | C11 | 122.87(14) | C25 | C26 | C27 | 121.0(2) |
| C12 | N4 | C16 | 116.59(18) | C22 | C27 | C26 | 119.9(2) |
| C17 | N5 | Rh1 | 118.20(11) | C29 | C28 | P2 | 122.19(14) |
| C21 | N5 | Rh1 | 124.43(12) | C33 | C28 | P2 | 119.14(13) |
| C21 | N5 | C17 | 117.09(15) | C33 | C28 | C29 | 118.66(16) |
| C1 | C00B | N2 | 112.21(15) | C30 | C29 | C28 | 120.36(19) |
| C5 | C00B | N2 | 126.82(16) | C31 | C30 | C29 | 120.69(18) |
| C5 | C00B | C1 | 120.97(16) | C30 | C31 | C32 | 119.83(18) |
| C00B | C1 | N1 | 110.73(15) | C31 | C32 | C33 | 119.7(2) |
| C2 | C1 | N1 | 128.54(17) | C28 | C33 | C32 | 120.71(17) |
| C2 | C1 | C00B | 120.72(17) | C35 | C34 | P2 | 117.43(14) |
| C1 | C2 | C3 | 118.40(18) | C39 | C34 | P2 | 123.44(14) |
| C4 | C3 | C2 | 120.63(18) | C39 | C34 | C35 | 119.08(17) |
| C3 | C4 | C5 | 121.27(18) | C36 | C35 | C34 | 120.59(18) |
| C00B | C5 | C4 | 118.00(18) | C35 | C36 | C37 | 119.8(2) |
| C7 | C6 | N2 | 126.11(16) | C38 | C37 | C36 | 120.11(19) |
| C7 | C6 | C11 | 121.68(16) | C37 | C38 | C39 | 120.93(19) |
| C11 | C6 | N2 | 112.20(15) | C34 | C39 | C38 | 119.47(19) |
| C6 | C7 | C8 | 118.15(17) | | | | |

**Table C-6**. Torsion Angles for **4.1**.

| A | B | C | D | Angle/° | A | B | C | D | Angle/° |
|---|---|---|---|---|---|---|---|---|---|
| Rh1 | P1 | N1 | C1 | 146.90(10) | C2 | C3 | C4 | C5 | -0.6(3) |
| Rh1 | P1 | N1 | C12 | -34.36(15) | C3 | C4 | C5 | C00B | 0.1(3) |
| Rh1 | P1 | N2 | C00B | -137.16(9) | C5 | C00B | C1 | N1 | -179.90(15) |
| Rh1 | P1 | N2 | C6 | 86.56(12) | C5 | C00B | C1 | C2 | 0.7(3) |
| Rh1 | P1 | N3 | C11 | -114.90(11) | C6 | N2 | C00B | C1 | 130.79(16) |
| Rh1 | P1 | N3 | C17 | 28.60(13) | C6 | N2 | C00B | C5 | -48.4(2) |
| Rh1 | P2 | C22 | C23 | 149.95(13) | C6 | C7 | C8 | C9 | -1.5(3) |
| Rh1 | P2 | C22 | C27 | -31.26(18) | C7 | C6 | C11 | N3 | 177.95(15) |
| Rh1 | P2 | C28 | C29 | 178.28(13) | C7 | C6 | C11 | C10 | 0.4(3) |
| Rh1 | P2 | C28 | C33 | -0.09(16) | C7 | C8 | C9 | C10 | 0.7(3) |
| Rh1 | P2 | C34 | C35 | -73.04(14) | C8 | C9 | C10 | C11 | 0.7(3) |
| Rh1 | P2 | C34 | C39 | 104.25(14) | C9 | C10 | C11 | N3 | -178.29(17) |
| Rh1 | N5 | C17 | N3 | 1.0(2) | C9 | C10 | C11 | C6 | -1.2(3) |
| Rh1 | N5 | C17 | C18 | -175.55(14) | C11 | N3 | C17 | N5 | 118.14(17) |
| Rh1 | N5 | C21 | C20 | 175.70(16) | C11 | N3 | C17 | C18 | -65.3(2) |
| P1 | N1 | C1 | C00B | -0.85(18) | C11 | C6 | C7 | C8 | 1.0(3) |
| P1 | N1 | C1 | C2 | 178.49(16) | C12 | N1 | C1 | C00B | -179.53(15) |
| P1 | N1 | C12 | N4 | -42.8(2) | C12 | N1 | C1 | C2 | -0.2(3) |
| P1 | N1 | C12 | C13 | 135.16(16) | C12 | N4 | C16 | C15 | 0.6(3) |
| P1 | N2 | C00B | C1 | -0.52(17) | C12 | C13 | C14 | C15 | 1.1(3) |
| P1 | N2 | C00B | C5 | -179.71(15) | C13 | C14 | C15 | C16 | 0.2(4) |
| P1 | N2 | C6 | C7 | -161.14(14) | C14 | C15 | C16 | N4 | -1.1(4) |
| P1 | N2 | C6 | C11 | 17.84(17) | C16 | N4 | C12 | N1 | 178.73(18) |
| P1 | N3 | C11 | C6 | -15.87(17) | C16 | N4 | C12 | C13 | 0.8(3) |
| P1 | N3 | C11 | C10 | 161.38(16) | C17 | N3 | C11 | C6 | -155.84(15) |
| P1 | N3 | C17 | N5 | -20.1(2) | C17 | N3 | C11 | C10 | 21.4(3) |
| P1 | N3 | C17 | C18 | 156.42(15) | C17 | N5 | C21 | C20 | 1.9(3) |
| P2 | C22 | C23 | C24 | 179.74(16) | C17 | C18 | C19 | C20 | 0.2(3) |
| P2 | C22 | C27 | C26 | 179.76(16) | C18 | C19 | C20 | C21 | 0.3(3) |
| P2 | C28 | C29 | C30 | -177.99(15) | C19 | C20 | C21 | N5 | -1.4(3) |
| P2 | C28 | C33 | C32 | 177.91(16) | C21 | N5 | C17 | N3 | 175.15(16) |
| P2 | C34 | C35 | C36 | 178.08(14) | C21 | N5 | C17 | C18 | -1.4(3) |
| P2 | C34 | C39 | C38 | -177.73(14) | C22 | P2 | C28 | C29 | 46.47(17) |
| N1 | P1 | N2 | C00B | 0.03(12) | C22 | P2 | C28 | C33 | -131.90(15) |
| N1 | P1 | N2 | C6 | -136.25(12) | C22 | P2 | C34 | C35 | 59.55(14) |
| N1 | P1 | N3 | C11 | 113.03(12) | C22 | P2 | C34 | C39 | -123.16(15) |
| N1 | P1 | N3 | C17 | -103.47(13) | C22 | C23 | C24 | C25 | 0.4(3) |
| N1 | C1 | C2 | C3 | 179.59(18) | C23 | C22 | C27 | C26 | -1.4(3) |
| N1 | C12 | C13 | C14 | -179.42(18) | C23 | C24 | C25 | C26 | -1.2(4) |
| N2 | P1 | N1 | C1 | 0.47(13) | C24 | C25 | C26 | C27 | 0.7(4) |
| N2 | P1 | N1 | C12 | 179.21(13) | C25 | C26 | C27 | C22 | 0.6(3) |
| N2 | P1 | N3 | C11 | 22.17(12) | C27 | C22 | C23 | C24 | 0.9(3) |
| N2 | P1 | N3 | C17 | 165.67(13) | C28 | P2 | C22 | C23 | -85.69(16) |
| N2 | C00B | C1 | N1 | 0.85(19) | C28 | P2 | C22 | C27 | 93.10(16) |
| N2 | C00B | C1 | C2 | -178.55(16) | C28 | P2 | C34 | C35 | 164.77(13) |
| N2 | C00B | C5 | C4 | 178.96(17) | C28 | P2 | C34 | C39 | -17.95(16) |

| | | | | | | | | | |
|---|---|---|---|---|---|---|---|---|---|
| N2 | C6 | C7 | C8 | 179.84(16) | C28 | C29 | C30 | C31 | 0.0(3) |
| N2 | C6 | C11 | N3 | -1.1(2) | C29 | C28 | C33 | C32 | -0.5(3) |
| N2 | C6 | C11 | C10 | -178.60(15) | C29 | C30 | C31 | C32 | -0.3(3) |
| N3 | P1 | N1 | C1 | -90.00(13) | C30 | C31 | C32 | C33 | 0.2(3) |
| N3 | P1 | N1 | C12 | 88.74(14) | C31 | C32 | C33 | C28 | 0.2(3) |
| N3 | P1 | N2 | C00B | 113.66(12) | C33 | C28 | C29 | C30 | 0.4(3) |
| N3 | P1 | N2 | C6 | -22.62(12) | C34 | P2 | C22 | C23 | 22.12(17) |
| N3 | C17 | C18 | C19 | -175.96(18) | C34 | P2 | C22 | C27 | -159.10(16) |
| N4 | C12 | C13 | C14 | -1.7(3) | C34 | P2 | C28 | C29 | -56.78(16) |
| N5 | C17 | C18 | C19 | 0.3(3) | C34 | P2 | C28 | C33 | 124.84(15) |
| C00B | N2 | C6 | C7 | 66.6(2) | C34 | C35 | C36 | C37 | -0.5(3) |
| C00B | N2 | C6 | C11 | -114.40(17) | C35 | C34 | C39 | C38 | -0.5(3) |
| C00B | C1 | C2 | C3 | -1.1(3) | C35 | C36 | C37 | C38 | 0.3(3) |
| C1 | N1 | C12 | N4 | 135.77(17) | C36 | C37 | C38 | C39 | -0.1(3) |
| C1 | N1 | C12 | C13 | -46.2(3) | C37 | C38 | C39 | C34 | 0.2(3) |
| C1 | C00B | C5 | C4 | -0.2(3) | C39 | C34 | C35 | C36 | 0.7(3) |
| C1 | C2 | C3 | C4 | 1.1(3) | | | | | |

**Table C-7**. Hydrogen Atom Coordinates ($Å \times 10^4$) and Isotropic Displacement Parameters ($Å^2 \times 10^3$) for **4.1**.

| **Atom** | ***x*** | ***y*** | ***z*** | **U(eq)** |
|---|---|---|---|---|
| H2 | 6350.06 | 7937.28 | 5277.4 | 32 |
| H3 | 8670.24 | 7843.14 | 5371.85 | 37 |
| H4 | 9539.48 | 7748.64 | 4259.05 | 36 |
| H5 | 8127.42 | 7722.63 | 3018.49 | 30 |
| H7 | 7116.23 | 7851.3 | 1738.89 | 28 |
| H8 | 7072.26 | 8631.26 | 736.12 | 33 |
| H9 | 5411.13 | 9430.09 | 497.57 | 33 |
| H10 | 3785.36 | 9494.6 | 1257.75 | 29 |
| H13 | 4487 | 7275.92 | 5220.3 | 36 |
| H14 | 3000.63 | 7444.73 | 6058.57 | 46 |
| H15 | 1288.32 | 8221.28 | 5726.6 | 47 |
| H16 | 1096.09 | 8801.01 | 4571.72 | 46 |
| H18 | 2753.61 | 9885.17 | 2259.92 | 33 |
| H19 | 522.98 | 10238.45 | 2056.85 | 37 |
| H20 | -1168.64 | 9453.3 | 1999.16 | 38 |
| H21 | -612.54 | 8352.15 | 2160.97 | 32 |
| H23 | 3905.19 | 5165.06 | 2530.82 | 35 |
| H24 | 3331.98 | 4269.99 | 1693.76 | 44 |
| H25 | 1305.39 | 4265.74 | 789.87 | 49 |
| H26 | -170.88 | 5131.52 | 751.87 | 48 |
| H27 | 359.2 | 6030.41 | 1597.29 | 37 |
| H29 | 2905.15 | 5202.74 | 3762.69 | 32 |
| H30 | 2102.47 | 4865.97 | 4848.26 | 37 |
| H31 | 810.78 | 5570.86 | 5431.17 | 37 |
| H32 | 324.97 | 6630.65 | 4932.85 | 38 |
| H33 | 1133.91 | 6977 | 3843.41 | 32 |

| | | | | |
|---|---|---|---|---|
| H35 | 4642.85 | 6381.32 | 1907.6 | 30 |
| H36 | 6963.01 | 6288.87 | 2134.27 | 37 |
| H37 | 8201.03 | 6170.68 | 3410.65 | 41 |
| H38 | 7126.77 | 6135.19 | 4442.86 | 37 |
| H39 | 4786.32 | 6221.61 | 4232.01 | 30 |

**Structural Data for 4.3**

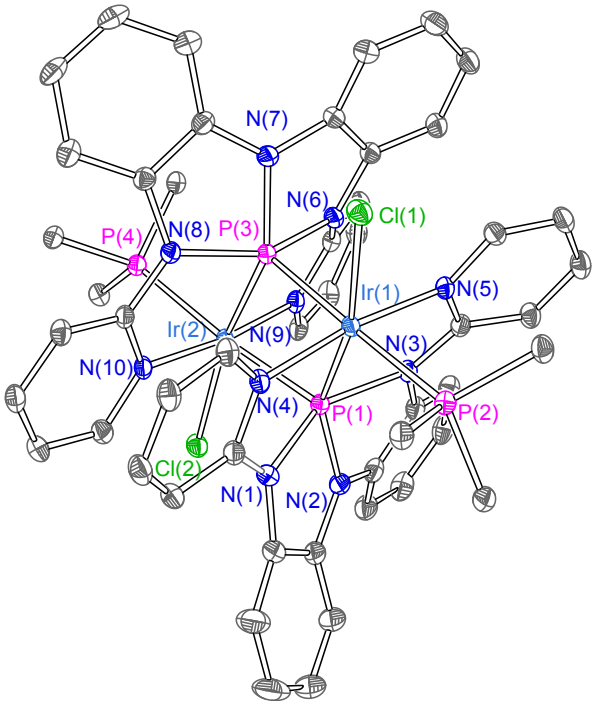


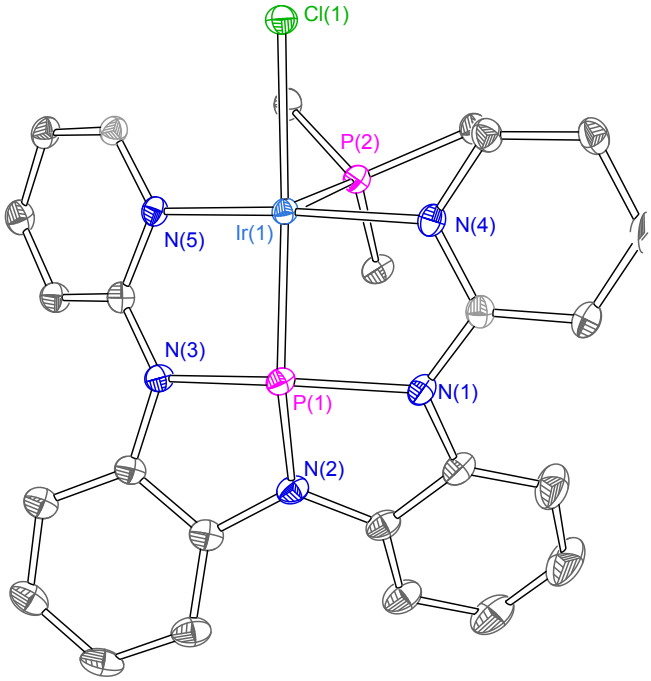

**Table C-8.** Crystal data and structure refinement for 4.3.

| | |
|---|---|
| Identification code | Irdimer-a |
| Empirical formula | $C_{40}H_{31}ClIrN_5P_2$ |
| Formula weight | 871.29 |
| Temperature/K | 100.0 |
| Crystal system | triclinic |
| Space group | P-1 |
| a/Å | 13.0950(5) |
| b/Å | 14.8808(6) |
| c/Å | 20.8072(8) |
| α/° | 71.7350(10) |
| β/° | 87.7050(10) |
| γ/° | 73.9020(10) |
| Volume/Å$^3$ | 3694.4(3) |
| Z | 4 |
| $\rho_{calc}$g/cm$^3$ | 1.566 |
| μ/mm$^{-1}$ | 3.808 |
| F(000) | 1720.0 |
| Crystal size/mm$^3$ | 0.225 × 0.07 × 0.015 |
| Radiation | MoKα (λ = 0.71073) |
| 2Θ range for data collection/° | 3.002 to 64.22 |
| Index ranges | $-19 \leq h \leq 18$, $-22 \leq k \leq 22$, $-31 \leq l \leq 31$ |
| Reflections collected | 290851 |
| Independent reflections | 25867 [$R_{int}$ = 0.0528, $R_{sigma}$ = 0.0274] |
| Data/restraints/parameters | 25867/0/883 |
| Goodness-of-fit on F$^2$ | 1.036 |
| Final R indexes [I>=2σ (I)] | $R_1$ = 0.0257, $wR_2$ = 0.0486 |
| Final R indexes [all data] | $R_1$ = 0.0361, $wR_2$ = 0.0517 |
| Largest diff. peak/hole / e Å$^{-3}$ | 2.02/-1.58 |

**Table C-9.** Fractional Atomic Coordinates (×10$^4$) and Equivalent Isotropic Displacement Parameters (Å$^2$×10$^3$) for **4.3**. $U_{eq}$ is defined as 1/3 of of the trace of the orthogonalised $U_{IJ}$ tensor.

| **Atom** | ***x*** | ***y*** | ***z*** | **U(eq)** |
|---|---|---|---|---|
| Ir1 | 7700.1(2) | 7227.5(2) | 7375.7(2) | 12.62(2) |
| Ir2 | 5167.9(2) | 7229.0(2) | 8199.4(2) | 13.13(2) |
| Cl2 | 4100.1(4) | 6031.7(4) | 8333.4(3) | 19.28(10) |
| Cl1 | 9022.4(4) | 8133.7(4) | 7514.0(3) | 18.58(9) |
| P3 | 6408.1(4) | 8090.9(4) | 7972.6(3) | 13.59(9) |
| P1 | 6310.4(4) | 6553.0(4) | 7443.0(3) | 14.02(10) |
| P4 | 4023.4(4) | 8068.3(4) | 8939.2(3) | 15.39(10) |
| P2 | 9064.8(4) | 6370.3(4) | 6754.3(3) | 15.46(10) |
| N5 | 7103.8(14) | 8234.5(13) | 6448.4(8) | 14.6(3) |
| N9 | 6146.3(14) | 6297.9(13) | 9040.6(8) | 15.1(3) |
| N8 | 5470.4(14) | 9103.6(13) | 7240.0(8) | 15.1(3) |
| N10 | 4174.1(14) | 8275.8(13) | 7415.2(8) | 15.7(3) |

| | | | | |
|---|---|---|---|---|
| N3 | 5755.2(14) | 7471.2(13) | 6550.1(8) | 15.1(3) |
| N7 | 6775.5(15) | 9126.8(13) | 8025.4(9) | 16.1(3) |
| N4 | 8345.8(14) | 6071.8(13) | 8238.8(8) | 15.5(3) |
| N6 | 6960.6(14) | 7547.4(13) | 8888.0(8) | 15.2(3) |
| N1 | 7137.8(15) | 5310.4(13) | 8006.6(9) | 16.8(3) |
| N2 | 5706.4(15) | 5813.8(13) | 7159.5(9) | 17.1(3) |
| C17 | 7586.0(17) | 8921.9(15) | 6093.9(10) | 16.4(4) |
| C69 | 4613.3(17) | 7886.3(16) | 9769.8(10) | 16.6(4) |
| C29 | 10232.7(17) | 5555.7(16) | 7303.6(11) | 18.2(4) |
| C58 | 4450.6(17) | 9127.5(16) | 7115.9(10) | 16.5(4) |
| C18 | 7979.9(17) | 5255.8(15) | 8403.7(10) | 16.2(4) |
| C56 | 6606.0(18) | 4819.0(17) | 9992.9(11) | 19.9(4) |
| C53 | 6874.0(17) | 6638.5(15) | 9272.7(10) | 15.0(4) |
| C63 | 3621.1(19) | 9408.2(16) | 8539.1(10) | 19.9(4) |
| C19 | 8450.6(18) | 4436.8(16) | 8970.5(11) | 19.4(4) |
| C55 | 7345.6(18) | 5157.6(17) | 10237.1(11) | 19.5(4) |
| C42 | 7165.9(17) | 9105.7(16) | 8645.5(11) | 17.0(4) |
| C54 | 7509.7(17) | 6047.7(16) | 9867.3(10) | 17.4(4) |
| C16 | 7326.5(18) | 9461.5(16) | 5425.0(11) | 19.4(4) |
| C30 | 10217.5(19) | 4583.9(17) | 7646.0(11) | 21.5(4) |
| C13 | 6267.9(17) | 8106.8(15) | 6152.1(10) | 15.8(4) |
| C34 | 11104.4(19) | 5853.2(18) | 7433.0(11) | 22.5(5) |
| C48 | 6645.6(18) | 9908.3(15) | 7419.6(10) | 17.4(4) |
| C2 | 4817.2(18) | 6327.6(17) | 6707.4(10) | 18.7(4) |
| C1 | 4865.6(17) | 7280.1(16) | 6327.4(10) | 16.8(4) |
| C41 | 7262.6(17) | 8195.7(16) | 9154.1(10) | 15.8(4) |
| C57 | 6052.5(18) | 5388.4(16) | 9389.8(11) | 18.5(4) |
| C6 | 4034.4(18) | 7902.9(18) | 5861.4(11) | 20.8(4) |
| C21 | 9710.2(18) | 5251.9(17) | 9132.0(11) | 19.9(4) |
| C5 | 3177.3(19) | 7561.2(19) | 5767.8(11) | 24.4(5) |
| C61 | 2429.5(18) | 9015.1(18) | 6860.0(11) | 22.7(5) |
| C59 | 3662.5(18) | 9973.5(17) | 6733.6(11) | 20.1(4) |
| C8 | 6071.8(19) | 4792.8(17) | 7426.4(11) | 19.7(4) |
| C70 | 4731(2) | 8652.9(17) | 9983.7(11) | 22.5(4) |
| C7 | 6916.8(19) | 4487.5(16) | 7909.3(11) | 20.3(4) |
| C46 | 7489.3(18) | 8107.0(18) | 9825.8(11) | 21.3(4) |
| C35 | 9530.5(17) | 7210.6(16) | 6022.4(11) | 19.0(4) |
| C62 | 3201.0(17) | 8223.1(17) | 7254.9(10) | 19.1(4) |
| C36 | 9235(2) | 7275.0(18) | 5369.5(11) | 25.2(5) |
| C77 | 1036.7(19) | 7654.5(18) | 8924.8(12) | 25.1(5) |
| C49 | 7228.8(19) | 10594.0(17) | 7225.8(11) | 21.6(4) |
| C20 | 9323.6(19) | 4430.6(17) | 9318.1(11) | 21.6(4) |
| C47 | 5878.0(17) | 9913.5(15) | 6970.0(10) | 16.5(4) |
| C43 | 7325(2) | 9896.6(18) | 8807.7(12) | 23.2(5) |
| C74 | 4858.0(18) | 6933.0(16) | 10231.9(11) | 19.3(4) |
| C22 | 9182.2(17) | 6058.1(16) | 8609.0(10) | 18.0(4) |
| C78 | 593.9(19) | 7914.0(18) | 9477.3(13) | 26.1(5) |
| C31 | 11057(2) | 3930.7(18) | 8094.2(12) | 25.8(5) |

| | | | | |
|---|---|---|---|---|
| C60 | 2660.2(19) | 9918.9(18) | 6617.7(11) | 23.2(5) |
| C75 | 2719.4(17) | 7867.3(16) | 9196.8(11) | 18.0(4) |
| C40 | 10086.9(18) | 7859.7(17) | 6095.2(12) | 22.1(4) |
| C9 | 5762(2) | 4109.8(18) | 7209.0(12) | 26.4(5) |
| C14 | 6017.1(18) | 8606.2(16) | 5452.1(10) | 18.8(4) |
| C64 | 4399(2) | 9910.1(17) | 8389.6(11) | 22.6(5) |
| C65 | 4130(2) | 10920.3(19) | 8049.5(12) | 29.9(6) |
| C12 | 7474(2) | 3492.7(18) | 8147.7(14) | 33.6(6) |
| C15 | 6544.9(18) | 9271.5(17) | 5095.7(11) | 21.2(4) |
| C80 | 2271.5(19) | 8095.9(18) | 9770.7(12) | 23.8(5) |
| C3 | 3930.7(19) | 6019.4(19) | 6641.6(12) | 23.3(5) |
| C23 | 8804.1(19) | 5516.7(17) | 6351.9(11) | 20.4(4) |
| C52 | 5688.1(19) | 10609.1(16) | 6327.6(11) | 20.3(4) |
| C4 | 3117.3(19) | 6636(2) | 6160.4(12) | 25.5(5) |
| C33 | 11944.5(19) | 5197(2) | 7880.1(12) | 27.3(5) |
| C50 | 7010(2) | 11304.3(17) | 6587.7(12) | 24.9(5) |
| C32 | 11919.9(19) | 4240(2) | 8209.0(12) | 28.4(5) |
| C44 | 7615(2) | 9772.1(18) | 9475.1(13) | 26.1(5) |
| C73 | 5207.5(19) | 6747.0(17) | 10895.5(11) | 21.9(4) |
| C51 | 6246(2) | 11315.1(17) | 6142.7(12) | 23.6(5) |
| C79 | 1215(2) | 8121.6(19) | 9903.8(13) | 28.0(5) |
| C39 | 10349(2) | 8533.1(18) | 5525.0(13) | 28.0(5) |
| C76 | 2089.5(18) | 7631.3(18) | 8784.5(11) | 22.2(4) |
| C68 | 2565(2) | 9945(2) | 8350.8(15) | 36.8(7) |
| C72 | 5330.5(19) | 7512.6(18) | 11100.5(11) | 23.7(5) |
| C24 | 7782(2) | 5492(2) | 6245.0(14) | 37.5(7) |
| C45 | 7684(2) | 8898.6(19) | 9978.3(12) | 25.0(5) |
| C66 | 3086(3) | 11442(2) | 7863.6(14) | 40.1(7) |
| C11 | 7136(3) | 2815(2) | 7934.7(16) | 41.5(7) |
| C38 | 10066(2) | 8576.9(19) | 4878.3(13) | 32.8(6) |
| C10 | 6290(3) | 3117(2) | 7474.4(14) | 34.1(6) |
| C71 | 5095(2) | 8458.3(19) | 10646.3(12) | 27.8(5) |
| C37 | 9502(2) | 7954.6(19) | 4804.0(12) | 31.7(6) |
| C28 | 9654(2) | 4910.3(19) | 6116.9(13) | 29.8(5) |
| C67 | 2308(3) | 10956(2) | 8014.5(18) | 50.9(9) |
| C27 | 9469(3) | 4284(2) | 5793.0(15) | 39.9(7) |
| C26 | 8447(3) | 4244(3) | 5704.3(17) | 50.8(9) |
| C25 | 7599(3) | 4846(3) | 5928.3(19) | 59.9(11) |

**Table C-10**. Anisotropic Displacement Parameters ($Å^2 \times 10^3$) for **4.3**. The Anisotropic displacement factor exponent takes the form: $-2\pi^2[h^2a^{*2}U_{11}+2hka^*b^*U_{12}+\ldots]$.

| **Atom** | $U_{11}$ | $U_{22}$ | $U_{33}$ | $U_{23}$ | $U_{13}$ | $U_{12}$ |
|---|---|---|---|---|---|---|
| Ir1 | 14.86(4) | 12.89(4) | 9.90(3) | -2.24(3) | 0.12(3) | -5.02(3) |
| Ir2 | 15.55(4) | 14.75(4) | 9.75(3) | -2.92(3) | 0.45(3) | -6.33(3) |
| Cl2 | 22.6(2) | 21.9(2) | 16.1(2) | -4.46(18) | 0.48(18) | -12.3(2) |
| Cl1 | 19.1(2) | 19.0(2) | 17.8(2) | -3.24(18) | -1.15(18) | -8.19(19) |

| | | | | | | |
|---|---|---|---|---|---|---|
| P3 | 16.8(2) | 13.5(2) | 11.1(2) | -3.52(18) | 0.97(18) | -5.76(19) |
| P1 | 17.6(2) | 14.6(2) | 11.1(2) | -3.91(18) | 1.05(18) | -6.62(19) |
| P4 | 17.5(2) | 16.4(2) | 13.0(2) | -4.56(19) | 1.17(19) | -6.0(2) |
| P2 | 17.3(2) | 15.8(2) | 13.3(2) | -4.59(19) | 2.36(19) | -4.9(2) |
| N5 | 17.4(8) | 14.6(8) | 10.5(7) | -2.6(6) | 0.2(6) | -3.9(6) |
| N9 | 18.2(8) | 17.3(8) | 9.9(7) | -2.9(6) | 1.3(6) | -6.7(7) |
| N8 | 17.9(8) | 14.0(8) | 12.3(7) | -2.2(6) | -0.6(6) | -5.0(7) |
| N10 | 17.7(8) | 17.6(8) | 10.6(7) | -3.4(6) | 0.4(6) | -4.3(7) |
| N3 | 17.8(8) | 17.2(8) | 11.2(7) | -3.5(6) | -0.3(6) | -7.1(7) |
| N7 | 20.2(9) | 15.0(8) | 14.1(8) | -3.9(6) | -0.8(6) | -7.1(7) |
| N4 | 18.5(8) | 15.2(8) | 11.3(7) | -2.4(6) | 1.4(6) | -4.4(7) |
| N6 | 19.4(8) | 16.5(8) | 11.6(7) | -4.1(6) | 0.2(6) | -8.1(7) |
| N1 | 21.1(9) | 13.0(8) | 15.7(8) | -3.0(6) | 0.5(7) | -5.5(7) |
| N2 | 22.7(9) | 17.9(9) | 14.0(8) | -5.8(7) | -0.1(7) | -9.7(7) |
| C17 | 16.8(9) | 15.4(9) | 16.1(9) | -3.6(7) | 2.2(7) | -4.8(8) |
| C69 | 17.3(10) | 19.6(10) | 14.1(9) | -6.4(8) | 1.4(7) | -5.9(8) |
| C29 | 18.4(10) | 19.6(10) | 15.4(9) | -4.5(8) | 1.9(7) | -4.5(8) |
| C58 | 19.9(10) | 18.7(10) | 11.9(8) | -5.8(7) | 1.8(7) | -5.9(8) |
| C18 | 17.0(9) | 16.4(9) | 13.5(9) | -4.0(7) | 1.6(7) | -3.2(8) |
| C56 | 22.7(11) | 18.8(10) | 16.2(9) | -1.3(8) | 2.5(8) | -7.6(8) |
| C53 | 17.8(9) | 17.1(9) | 10.7(8) | -4.0(7) | 1.9(7) | -6.4(8) |
| C63 | 28.5(12) | 18.5(10) | 12.7(9) | -3.7(8) | -1.1(8) | -7.5(9) |
| C19 | 23.8(11) | 15.8(10) | 16.0(9) | -1.8(8) | 1.6(8) | -5.2(8) |
| C55 | 22.1(10) | 21.1(10) | 12.2(9) | -2.2(8) | 1.2(8) | -4.7(8) |
| C42 | 17.7(10) | 19.2(10) | 16.3(9) | -7.9(8) | 1.3(7) | -6.3(8) |
| C54 | 18.4(10) | 20.1(10) | 12.7(9) | -3.7(7) | -0.8(7) | -5.6(8) |
| C16 | 21.6(10) | 17.7(10) | 15.8(9) | -0.9(8) | 3.7(8) | -5.9(8) |
| C30 | 22.9(11) | 20.8(11) | 20.1(10) | -5.7(8) | 0.5(8) | -5.6(9) |
| C13 | 17.5(9) | 16.2(9) | 12.9(9) | -4.9(7) | 1.5(7) | -3.0(8) |
| C34 | 21.8(11) | 25.6(12) | 18.8(10) | -3.6(9) | 0.5(8) | -8.3(9) |
| C48 | 22.6(10) | 13.8(9) | 15.5(9) | -4.0(7) | 2.9(8) | -5.7(8) |
| C2 | 20.7(10) | 24.5(11) | 13.8(9) | -8.5(8) | 1.7(7) | -7.9(9) |
| C1 | 17.2(10) | 21.3(10) | 13.1(9) | -5.8(8) | 1.0(7) | -6.9(8) |
| C41 | 15.6(9) | 17.5(10) | 15.5(9) | -5.8(7) | 1.1(7) | -5.7(8) |
| C57 | 21.1(10) | 19.3(10) | 16.1(9) | -4.4(8) | 2.9(8) | -8.6(8) |
| C6 | 20.8(11) | 26.3(11) | 16.9(10) | -8.1(8) | 0.9(8) | -7.6(9) |
| C21 | 17.8(10) | 23.9(11) | 14.6(9) | -2.7(8) | -1.3(7) | -3.9(8) |
| C5 | 19.8(11) | 38.1(14) | 16.8(10) | -10.2(9) | -1.1(8) | -8.3(10) |
| C61 | 16.5(10) | 31.5(12) | 18.1(10) | -5.8(9) | 0.1(8) | -5.6(9) |
| C59 | 20.3(10) | 21.2(11) | 15.0(9) | -1.9(8) | 0.6(8) | -4.2(8) |
| C8 | 26.3(11) | 20.2(10) | 16.2(9) | -6.7(8) | 4.4(8) | -11.3(9) |
| C70 | 30.5(12) | 18.4(10) | 19.3(10) | -6.4(8) | -0.8(9) | -6.9(9) |
| C7 | 27.7(11) | 17.0(10) | 17.6(10) | -4.9(8) | 2.4(8) | -9.3(9) |
| C46 | 23.1(11) | 25.1(11) | 16.9(10) | -8.1(8) | 0.9(8) | -7.0(9) |
| C35 | 18.3(10) | 19.5(10) | 16.0(9) | -3.5(8) | 4.6(8) | -3.1(8) |
| C62 | 18.5(10) | 26.5(11) | 14.3(9) | -7.7(8) | 3.8(7) | -8.6(9) |
| C36 | 33.3(13) | 21.8(11) | 17.5(10) | -4.6(9) | 4.3(9) | -5.2(10) |
| C77 | 22.8(11) | 27.9(12) | 24.9(11) | -3.4(9) | -0.2(9) | -13.1(10) |

| | | | | | | |
|---|---|---|---|---|---|---|
| C49 | 26.8(12) | 19.2(10) | 21.0(10) | -6.5(8) | 2.5(9) | -9.9(9) |
| C20 | 22.9(11) | 19.9(10) | 15.5(9) | 0.1(8) | -0.2(8) | -2.2(9) |
| C47 | 19.8(10) | 13.7(9) | 15.2(9) | -4.3(7) | 3.3(7) | -3.9(8) |
| C43 | 29.2(12) | 21.2(11) | 22.5(11) | -9.6(9) | 1.4(9) | -9.2(9) |
| C74 | 23.8(11) | 18.7(10) | 17.5(10) | -5.7(8) | 1.7(8) | -9.4(8) |
| C22 | 18.4(10) | 20.0(10) | 13.8(9) | -3.1(8) | -0.4(7) | -5.0(8) |
| C78 | 18.1(11) | 22.2(11) | 31.2(12) | 0.1(9) | 4.7(9) | -5.1(9) |
| C31 | 26.8(12) | 20.2(11) | 23.4(11) | -2.4(9) | -0.2(9) | -0.5(9) |
| C60 | 20.3(11) | 25.8(12) | 16.8(10) | -2.3(8) | -1.3(8) | -0.8(9) |
| C75 | 17.4(10) | 17.9(10) | 17.1(9) | -3.5(8) | 1.3(7) | -4.5(8) |
| C40 | 20.9(11) | 20.3(11) | 21.7(10) | -3.7(8) | 2.9(8) | -3.6(9) |
| C9 | 36.6(14) | 24.2(12) | 24.9(11) | -11.2(9) | 3.5(10) | -15.0(10) |
| C14 | 20.3(10) | 21.8(10) | 13.4(9) | -3.4(8) | -1.0(7) | -6.8(8) |
| C64 | 33.1(13) | 22.5(11) | 17.7(10) | -10.5(8) | 7.3(9) | -12.6(10) |
| C65 | 52.9(17) | 26.3(12) | 18.6(11) | -10.0(9) | 9.3(11) | -21.6(12) |
| C12 | 49.0(17) | 17.9(11) | 32.3(13) | -6.3(10) | -8.7(12) | -7.1(11) |
| C15 | 23.1(11) | 22.8(11) | 13.2(9) | -1.5(8) | 0.4(8) | -4.0(9) |
| C80 | 22.6(11) | 26.8(12) | 24.8(11) | -12.2(9) | 3.3(9) | -7.2(9) |
| C3 | 27.0(12) | 29.4(12) | 20.0(10) | -10.3(9) | 3.0(9) | -15.4(10) |
| C23 | 27.9(12) | 21.1(11) | 15.3(9) | -6.7(8) | 2.5(8) | -11.1(9) |
| C52 | 25.2(11) | 17.9(10) | 15.5(9) | -3.1(8) | 1.4(8) | -5.0(9) |
| C4 | 21.3(11) | 40.9(14) | 22.6(11) | -14.7(10) | 3.4(9) | -16.8(10) |
| C33 | 19.0(11) | 38.3(14) | 24.2(11) | -7.4(10) | 0.4(9) | -10.1(10) |
| C50 | 29.7(12) | 18.2(11) | 26.6(11) | -4.3(9) | 5.7(9) | -10.3(9) |
| C32 | 19.5(11) | 34.1(14) | 23.2(11) | -4.3(10) | -1.9(9) | 1.2(10) |
| C44 | 31.9(13) | 25.7(12) | 28.5(12) | -17.5(10) | 1.0(10) | -10.1(10) |
| C73 | 25.5(11) | 22.0(11) | 15.9(10) | -3.6(8) | 0.2(8) | -5.3(9) |
| C51 | 30.2(12) | 18.0(10) | 19.0(10) | -1.0(8) | 4.6(9) | -6.8(9) |
| C79 | 27.0(12) | 29.1(13) | 28.4(12) | -10.2(10) | 7.2(10) | -8.3(10) |
| C39 | 24.3(12) | 21.2(11) | 32.5(13) | -2.4(10) | 8.2(10) | -5.0(9) |
| C76 | 19.0(10) | 27.4(12) | 18.9(10) | -4.7(9) | -0.4(8) | -7.3(9) |
| C68 | 33.7(14) | 23.8(13) | 44.1(16) | 3.5(11) | -15.7(12) | -8.1(11) |
| C72 | 25.4(12) | 30.1(12) | 15.7(10) | -8.1(9) | -1.2(8) | -6.8(10) |
| C24 | 33.7(14) | 64(2) | 36.7(15) | -36.1(15) | 14.6(12) | -27.1(14) |
| C45 | 30.9(13) | 30.2(12) | 21.0(11) | -16.3(10) | 0.4(9) | -10.0(10) |
| C66 | 67(2) | 20.8(12) | 28.4(13) | 3.4(10) | -14.4(13) | -16.3(13) |
| C11 | 66(2) | 16.5(12) | 43.5(17) | -8.4(11) | -5.1(15) | -13.0(13) |
| C38 | 37.5(15) | 24.7(12) | 26.1(12) | 0.2(10) | 14.3(11) | -3.9(11) |
| C10 | 53.2(18) | 24.8(13) | 34.0(14) | -15.2(11) | 5.1(12) | -20.1(12) |
| C71 | 40.0(14) | 26.2(12) | 21.5(11) | -11.0(9) | -2.8(10) | -11.7(11) |
| C37 | 46.2(16) | 26.6(13) | 16.2(10) | -4.4(9) | 7.3(10) | -4.0(11) |
| C28 | 34.1(14) | 28.8(13) | 26.4(12) | -13.4(10) | -1.0(10) | -2.8(11) |
| C67 | 51(2) | 26.8(15) | 61(2) | 6.6(14) | -29.7(17) | -7.2(14) |
| C27 | 59(2) | 31.0(14) | 32.9(14) | -20.3(12) | 5.2(13) | -5.5(14) |
| C26 | 76(3) | 60(2) | 45.6(18) | -38.1(17) | 21.8(17) | -43(2) |
| C25 | 55(2) | 109(3) | 62(2) | -64(2) | 29.9(18) | -58(2) |

**Table C-11**. Bond Lengths for **4.3**.

| Atom | Atom | Length/Å | Atom | Atom | Length/Å |
|---|---|---|---|---|---|
| Ir1 | Cl1 | 2.5451(5) | C16 | C15 | 1.391(3) |
| Ir1 | P3 | 2.3838(5) | C30 | C31 | 1.394(3) |
| Ir1 | P1 | 2.2899(5) | C13 | C14 | 1.416(3) |
| Ir1 | P2 | 2.4652(6) | C34 | C33 | 1.395(3) |
| Ir1 | N5 | 2.0584(17) | C48 | C49 | 1.392(3) |
| Ir1 | N4 | 2.0681(17) | C48 | C47 | 1.397(3) |
| Ir2 | Cl2 | 2.4992(5) | C2 | C1 | 1.408(3) |
| Ir2 | P3 | 2.2846(5) | C2 | C3 | 1.387(3) |
| Ir2 | P1 | 2.3869(5) | C1 | C6 | 1.395(3) |
| Ir2 | P4 | 2.4815(6) | C41 | C46 | 1.398(3) |
| Ir2 | N9 | 2.0736(17) | C6 | C5 | 1.397(3) |
| Ir2 | N10 | 2.0580(17) | C21 | C20 | 1.390(3) |
| P3 | N8 | 1.9458(18) | C21 | C22 | 1.372(3) |
| P3 | N7 | 1.7724(18) | C5 | C4 | 1.386(4) |
| P3 | N6 | 1.9042(17) | C61 | C62 | 1.373(3) |
| P1 | N3 | 1.9527(18) | C61 | C60 | 1.394(3) |
| P1 | N1 | 1.8973(18) | C59 | C60 | 1.373(3) |
| P1 | N2 | 1.7635(18) | C8 | C7 | 1.402(3) |
| P4 | C69 | 1.831(2) | C8 | C9 | 1.390(3) |
| P4 | C63 | 1.833(2) | C70 | C71 | 1.392(3) |
| P4 | C75 | 1.845(2) | C7 | C12 | 1.393(3) |
| P2 | C29 | 1.833(2) | C46 | C45 | 1.400(3) |
| P2 | C35 | 1.846(2) | C35 | C36 | 1.394(3) |
| P2 | C23 | 1.833(2) | C35 | C40 | 1.406(3) |
| N5 | C17 | 1.355(3) | C36 | C37 | 1.396(3) |
| N5 | C13 | 1.363(3) | C77 | C78 | 1.381(4) |
| N9 | C53 | 1.362(3) | C77 | C76 | 1.391(3) |
| N9 | C57 | 1.358(3) | C49 | C50 | 1.395(3) |
| N8 | C58 | 1.359(3) | C47 | C52 | 1.392(3) |
| N8 | C47 | 1.400(3) | C43 | C44 | 1.396(3) |
| N10 | C58 | 1.366(3) | C74 | C73 | 1.390(3) |
| N10 | C62 | 1.359(3) | C78 | C79 | 1.384(4) |
| N3 | C13 | 1.359(3) | C31 | C32 | 1.388(4) |
| N3 | C1 | 1.401(3) | C75 | C80 | 1.405(3) |
| N7 | C42 | 1.395(3) | C75 | C76 | 1.395(3) |
| N7 | C48 | 1.400(3) | C40 | C39 | 1.394(3) |
| N4 | C18 | 1.367(3) | C9 | C10 | 1.385(4) |
| N4 | C22 | 1.356(3) | C14 | C15 | 1.373(3) |
| N6 | C53 | 1.372(3) | C64 | C65 | 1.394(3) |
| N6 | C41 | 1.399(3) | C65 | C66 | 1.374(4) |
| N1 | C18 | 1.373(3) | C12 | C11 | 1.397(4) |
| N1 | C7 | 1.407(3) | C80 | C79 | 1.392(3) |
| N2 | C2 | 1.403(3) | C3 | C4 | 1.395(3) |
| N2 | C8 | 1.391(3) | C23 | C24 | 1.378(4) |
| C17 | C16 | 1.372(3) | C23 | C28 | 1.403(3) |
| C69 | C70 | 1.395(3) | C52 | C51 | 1.392(3) |

| | | | | | |
|---|---|---|---|---|---|
| C69 | C74 | 1.399(3) | C33 | C32 | 1.382(4) |
| C29 | C30 | 1.403(3) | C50 | C51 | 1.383(4) |
| C29 | C34 | 1.397(3) | C44 | C45 | 1.372(4) |
| C58 | C59 | 1.414(3) | C73 | C72 | 1.385(3) |
| C18 | C19 | 1.413(3) | C39 | C38 | 1.387(4) |
| C56 | C55 | 1.386(3) | C68 | C67 | 1.394(4) |
| C56 | C57 | 1.373(3) | C72 | C71 | 1.385(3) |
| C53 | C54 | 1.411(3) | C24 | C25 | 1.398(4) |
| C63 | C64 | 1.394(3) | C66 | C67 | 1.378(5) |
| C63 | C68 | 1.392(4) | C11 | C10 | 1.373(4) |
| C19 | C20 | 1.373(3) | C38 | C37 | 1.380(4) |
| C55 | C54 | 1.378(3) | C28 | C27 | 1.383(4) |
| C42 | C41 | 1.410(3) | C27 | C26 | 1.378(5) |
| C42 | C43 | 1.390(3) | C26 | C25 | 1.387(5) |

**Table C-12**. Bond Angles for **4.3**.

| **Atom** | **Atom** | **Atom** | **Angle/°** | **Atom** | **Atom** | **Atom** | **Angle/°** |
|---|---|---|---|---|---|---|---|
| P3 | Ir1 | Cl1 | 91.398(18) | N1 | C18 | C19 | 124.3(2) |
| P3 | Ir1 | P2 | 178.343(19) | C57 | C56 | C55 | 118.7(2) |
| P1 | Ir1 | Cl1 | 166.608(18) | N9 | C53 | N6 | 116.35(18) |
| P1 | Ir1 | P3 | 75.666(19) | N9 | C53 | C54 | 119.84(19) |
| P1 | Ir1 | P2 | 105.952(19) | N6 | C53 | C54 | 123.78(19) |
| P2 | Ir1 | Cl1 | 87.008(18) | C64 | C63 | P4 | 119.26(18) |
| N5 | Ir1 | Cl1 | 93.09(5) | C68 | C63 | P4 | 122.41(19) |
| N5 | Ir1 | P3 | 92.72(5) | C68 | C63 | C64 | 118.3(2) |
| N5 | Ir1 | P1 | 91.01(5) | C20 | C19 | C18 | 120.1(2) |
| N5 | Ir1 | P2 | 86.91(5) | C54 | C55 | C56 | 119.3(2) |
| N5 | Ir1 | N4 | 172.10(7) | N7 | C42 | C41 | 112.42(18) |
| N4 | Ir1 | Cl1 | 91.20(5) | C43 | C42 | N7 | 126.7(2) |
| N4 | Ir1 | P3 | 93.81(5) | C43 | C42 | C41 | 120.3(2) |
| N4 | Ir1 | P1 | 86.31(5) | C55 | C54 | C53 | 120.1(2) |
| N4 | Ir1 | P2 | 86.68(5) | C17 | C16 | C15 | 117.8(2) |
| P3 | Ir2 | Cl2 | 167.156(19) | C31 | C30 | C29 | 120.9(2) |
| P3 | Ir2 | P1 | 75.702(19) | N5 | C13 | C14 | 118.57(19) |
| P3 | Ir2 | P4 | 99.819(19) | N3 | C13 | N5 | 116.98(18) |
| P1 | Ir2 | Cl2 | 91.840(18) | N3 | C13 | C14 | 124.40(19) |
| P1 | Ir2 | P4 | 174.970(19) | C33 | C34 | C29 | 120.9(2) |
| P4 | Ir2 | Cl2 | 92.749(18) | C49 | C48 | N7 | 127.2(2) |
| N9 | Ir2 | Cl2 | 91.25(5) | C49 | C48 | C47 | 120.2(2) |
| N9 | Ir2 | P3 | 86.28(5) | C47 | C48 | N7 | 112.49(18) |
| N9 | Ir2 | P1 | 92.56(5) | N2 | C2 | C1 | 111.90(19) |
| N9 | Ir2 | P4 | 89.40(5) | C3 | C2 | N2 | 127.5(2) |
| N10 | Ir2 | Cl2 | 92.76(5) | C3 | C2 | C1 | 120.5(2) |
| N10 | Ir2 | P3 | 90.91(5) | N3 | C1 | C2 | 109.96(18) |
| N10 | Ir2 | P1 | 92.41(5) | C6 | C1 | N3 | 130.1(2) |
| N10 | Ir2 | P4 | 85.32(5) | C6 | C1 | C2 | 119.6(2) |
| N10 | Ir2 | N9 | 173.52(7) | N6 | C41 | C42 | 110.19(17) |

| | | | | | | | |
|---|---|---|---|---|---|---|---|
| Ir2 | P3 | Ir1 | 103.67(2) | C46 | C41 | N6 | 130.0(2) |
| N8 | P3 | Ir1 | 102.33(6) | C46 | C41 | C42 | 119.2(2) |
| N8 | P3 | Ir2 | 89.85(6) | N9 | C57 | C56 | 123.0(2) |
| N7 | P3 | Ir1 | 109.52(6) | C1 | C6 | C5 | 119.3(2) |
| N7 | P3 | Ir2 | 146.74(7) | C22 | C21 | C20 | 118.1(2) |
| N7 | P3 | N8 | 81.30(8) | C4 | C5 | C6 | 120.6(2) |
| N7 | P3 | N6 | 82.44(8) | C62 | C61 | C60 | 117.9(2) |
| N6 | P3 | Ir1 | 104.01(6) | C60 | C59 | C58 | 120.5(2) |
| N6 | P3 | Ir2 | 91.67(6) | N2 | C8 | C7 | 112.23(19) |
| N6 | P3 | N8 | 152.45(8) | C9 | C8 | N2 | 126.7(2) |
| Ir1 | P1 | Ir2 | 103.41(2) | C9 | C8 | C7 | 120.7(2) |
| N3 | P1 | Ir1 | 89.74(6) | C71 | C70 | C69 | 119.8(2) |
| N3 | P1 | Ir2 | 103.37(6) | C8 | C7 | N1 | 110.29(19) |
| N1 | P1 | Ir1 | 91.98(6) | C12 | C7 | N1 | 130.2(2) |
| N1 | P1 | Ir2 | 104.19(6) | C12 | C7 | C8 | 119.0(2) |
| N1 | P1 | N3 | 151.17(8) | C41 | C46 | C45 | 119.8(2) |
| N2 | P1 | Ir1 | 147.66(7) | C36 | C35 | P2 | 118.96(18) |
| N2 | P1 | Ir2 | 108.84(7) | C36 | C35 | C40 | 118.3(2) |
| N2 | P1 | N3 | 80.75(8) | C40 | C35 | P2 | 122.49(17) |
| N2 | P1 | N1 | 82.53(8) | N10 | C62 | C61 | 123.4(2) |
| C69 | P4 | Ir2 | 116.59(7) | C35 | C36 | C37 | 120.7(2) |
| C69 | P4 | C63 | 104.33(10) | C78 | C77 | C76 | 120.4(2) |
| C69 | P4 | C75 | 99.49(10) | C48 | C49 | C50 | 119.1(2) |
| C63 | P4 | Ir2 | 111.15(7) | C19 | C20 | C21 | 119.8(2) |
| C63 | P4 | C75 | 99.96(10) | C48 | C47 | N8 | 110.60(18) |
| C75 | P4 | Ir2 | 122.68(7) | C52 | C47 | N8 | 129.0(2) |
| C29 | P2 | Ir1 | 112.06(7) | C52 | C47 | C48 | 120.1(2) |
| C29 | P2 | C35 | 107.85(10) | C42 | C43 | C44 | 119.4(2) |
| C29 | P2 | C23 | 99.72(11) | C73 | C74 | C69 | 121.0(2) |
| C35 | P2 | Ir1 | 113.70(7) | N4 | C22 | C21 | 123.4(2) |
| C23 | P2 | Ir1 | 121.95(8) | C77 | C78 | C79 | 119.5(2) |
| C23 | P2 | C35 | 99.79(10) | C32 | C31 | C30 | 120.0(2) |
| C17 | N5 | Ir1 | 122.84(14) | C59 | C60 | C61 | 119.6(2) |
| C17 | N5 | C13 | 119.57(17) | C80 | C75 | P4 | 119.56(17) |
| C13 | N5 | Ir1 | 117.03(14) | C76 | C75 | P4 | 121.67(17) |
| C53 | N9 | Ir2 | 118.26(14) | C76 | C75 | C80 | 118.1(2) |
| C57 | N9 | Ir2 | 122.84(15) | C39 | C40 | C35 | 120.3(2) |
| C57 | N9 | C53 | 118.80(18) | C10 | C9 | C8 | 119.7(2) |
| C58 | N8 | P3 | 123.82(14) | C15 | C14 | C13 | 120.5(2) |
| C58 | N8 | C47 | 123.31(18) | C63 | C64 | C65 | 120.9(2) |
| C47 | N8 | P3 | 111.16(14) | C66 | C65 | C64 | 120.3(3) |
| C58 | N10 | Ir2 | 116.96(14) | C7 | C12 | C11 | 119.4(3) |
| C62 | N10 | Ir2 | 123.32(15) | C14 | C15 | C16 | 119.8(2) |
| C62 | N10 | C58 | 118.96(18) | C79 | C80 | C75 | 120.4(2) |
| C13 | N3 | P1 | 123.76(14) | C2 | C3 | C4 | 119.4(2) |
| C13 | N3 | C1 | 123.95(17) | C24 | C23 | P2 | 121.24(19) |
| C1 | N3 | P1 | 111.50(13) | C24 | C23 | C28 | 119.1(2) |
| C42 | N7 | P3 | 119.11(14) | C28 | C23 | P2 | 119.61(19) |

| | | | | | | | |
|---|---|---|---|---|---|---|---|
| C42 | N7 | C48 | 125.57(18) | C51 | C52 | C47 | 119.6(2) |
| C48 | N7 | P3 | 115.32(14) | C5 | C4 | C3 | 120.3(2) |
| C18 | N4 | Ir1 | 118.56(14) | C32 | C33 | C34 | 120.2(2) |
| C22 | N4 | Ir1 | 122.23(14) | C51 | C50 | C49 | 120.8(2) |
| C22 | N4 | C18 | 118.93(18) | C33 | C32 | C31 | 119.9(2) |
| C53 | N6 | P3 | 119.71(14) | C45 | C44 | C43 | 120.8(2) |
| C53 | N6 | C41 | 123.80(17) | C72 | C73 | C74 | 119.6(2) |
| C41 | N6 | P3 | 115.50(14) | C50 | C51 | C52 | 120.1(2) |
| C18 | N1 | P1 | 120.00(14) | C78 | C79 | C80 | 120.6(2) |
| C18 | N1 | C7 | 124.16(18) | C38 | C39 | C40 | 120.8(3) |
| C7 | N1 | P1 | 115.24(14) | C77 | C76 | C75 | 120.9(2) |
| C2 | N2 | P1 | 115.43(15) | C63 | C68 | C67 | 120.1(3) |
| C8 | N2 | P1 | 119.63(15) | C73 | C72 | C71 | 119.9(2) |
| C8 | N2 | C2 | 124.74(18) | C23 | C24 | C25 | 120.4(3) |
| N5 | C17 | C16 | 123.3(2) | C44 | C45 | C46 | 120.3(2) |
| C70 | C69 | P4 | 123.69(17) | C65 | C66 | C67 | 119.3(3) |
| C70 | C69 | C74 | 118.89(19) | C10 | C11 | C12 | 121.2(3) |
| C74 | C69 | P4 | 117.11(16) | C37 | C38 | C39 | 119.1(2) |
| C30 | C29 | P2 | 117.43(17) | C11 | C10 | C9 | 119.9(2) |
| C34 | C29 | P2 | 124.39(17) | C72 | C71 | C70 | 120.8(2) |
| C34 | C29 | C30 | 118.1(2) | C38 | C37 | C36 | 120.8(2) |
| N8 | C58 | N10 | 116.33(19) | C27 | C28 | C23 | 120.4(3) |
| N8 | C58 | C59 | 124.7(2) | C66 | C67 | C68 | 121.1(3) |
| N10 | C58 | C59 | 118.9(2) | C26 | C27 | C28 | 120.2(3) |
| N4 | C18 | N1 | 116.25(18) | C27 | C26 | C25 | 120.0(3) |
| N4 | C18 | C19 | 119.43(19) | C26 | C25 | C24 | 119.9(3) |

**Table C-13.** Torsion Angles for **4.3**.

| **A** | **B** | **C** | **D** | **Angle/°** | **A** | **B** | **C** | **D** | **Angle/°** |
|---|---|---|---|---|---|---|---|---|---|
| Ir1 | P3 | N7 | C42 | -106.96(16) | C29 | C30 | C31 | C32 | 0.3(4) |
| Ir1 | P3 | N7 | C48 | 72.72(16) | C29 | C34 | C33 | C32 | -0.7(4) |
| Ir1 | P1 | N1 | C18 | 25.96(16) | C58 | N8 | C47 | C48 | 147.6(2) |
| Ir1 | P1 | N1 | C7 | -145.52(15) | C58 | N8 | C47 | C52 | -38.9(3) |
| Ir1 | P1 | N2 | C2 | -104.32(17) | C58 | N10 | C62 | C61 | -7.0(3) |
| Ir1 | P1 | N2 | C8 | 80.5(2) | C58 | C59 | C60 | C61 | -2.1(3) |
| Ir1 | P2 | C29 | C30 | 88.66(17) | C18 | N4 | C22 | C21 | 2.2(3) |
| Ir1 | P2 | C29 | C34 | -87.50(19) | C18 | N1 | C7 | C8 | -174.15(19) |
| Ir1 | P2 | C35 | C36 | -108.73(18) | C18 | N1 | C7 | C12 | -2.8(4) |
| Ir1 | P2 | C35 | C40 | 65.0(2) | C18 | C19 | C20 | C21 | 3.2(3) |
| Ir1 | P2 | C23 | C24 | 15.2(2) | C56 | C55 | C54 | C53 | 4.7(3) |
| Ir1 | P2 | C23 | C28 | -168.03(16) | C53 | N9 | C57 | C56 | 4.6(3) |
| Ir1 | N5 | C17 | C16 | 166.43(17) | C53 | N6 | C41 | C42 | -173.66(19) |
| Ir1 | N5 | C13 | N3 | 14.0(2) | C53 | N6 | C41 | C46 | -2.8(4) |
| Ir1 | N5 | C13 | C14 | -163.49(15) | C63 | P4 | C69 | C70 | -2.5(2) |
| Ir1 | N4 | C18 | N1 | -5.4(2) | C63 | P4 | C69 | C74 | 171.05(17) |
| Ir1 | N4 | C18 | C19 | 176.58(15) | C63 | P4 | C75 | C80 | -77.15(19) |
| Ir1 | N4 | C22 | C21 | -171.56(17) | C63 | P4 | C75 | C76 | 93.3(2) |

| | | | | | | | | | |
|---|---|---|---|---|---|---|---|---|---|
| Ir2 | P3 | N7 | C42 | 76.7(2) | C63 | C64 | C65 | C66 | 0.9(4) |
| Ir2 | P3 | N7 | C48 | -103.59(17) | C63 | C68 | C67 | C66 | -0.1(5) |
| Ir2 | P1 | N1 | C18 | -78.41(16) | C55 | C56 | C57 | N9 | -4.3(3) |
| Ir2 | P1 | N1 | C7 | 110.11(15) | C42 | N7 | C48 | C49 | 28.4(4) |
| Ir2 | P1 | N2 | C2 | 71.33(15) | C42 | N7 | C48 | C47 | -155.8(2) |
| Ir2 | P1 | N2 | C8 | -103.85(16) | C42 | C41 | C46 | C45 | -4.1(3) |
| Ir2 | P4 | C69 | C70 | 120.49(18) | C42 | C43 | C44 | C45 | -3.9(4) |
| Ir2 | P4 | C69 | C74 | -65.97(18) | C30 | C29 | C34 | C33 | 1.2(3) |
| Ir2 | P4 | C63 | C64 | -62.01(18) | C30 | C31 | C32 | C33 | 0.2(4) |
| Ir2 | P4 | C63 | C68 | 115.2(2) | C13 | N5 | C17 | C16 | -4.8(3) |
| Ir2 | P4 | C75 | C80 | 159.63(15) | C13 | N3 | C1 | C2 | 152.9(2) |
| Ir2 | P4 | C75 | C76 | -29.9(2) | C13 | N3 | C1 | C6 | -33.9(3) |
| Ir2 | N9 | C53 | N6 | -5.7(2) | C13 | C14 | C15 | C16 | -0.4(3) |
| Ir2 | N9 | C53 | C54 | 176.24(15) | C34 | C29 | C30 | C31 | -1.0(3) |
| Ir2 | N9 | C57 | C56 | -171.70(17) | C34 | C33 | C32 | C31 | 0.0(4) |
| Ir2 | N10 | C58 | N8 | 16.4(2) | C48 | N7 | C42 | C41 | -176.5(2) |
| Ir2 | N10 | C58 | C59 | -160.51(15) | C48 | N7 | C42 | C43 | 11.7(4) |
| Ir2 | N10 | C62 | C61 | 162.62(17) | C48 | C49 | C50 | C51 | -1.9(4) |
| P3 | N8 | C58 | N10 | -16.3(3) | C48 | C47 | C52 | C51 | -1.7(3) |
| P3 | N8 | C58 | C59 | 160.34(17) | C2 | N2 | C8 | C7 | -174.7(2) |
| P3 | N8 | C47 | C48 | -18.0(2) | C2 | N2 | C8 | C9 | 12.6(4) |
| P3 | N8 | C47 | C52 | 155.5(2) | C2 | C1 | C6 | C5 | -1.5(3) |
| P3 | N7 | C42 | C41 | 3.1(2) | C2 | C3 | C4 | C5 | -2.2(4) |
| P3 | N7 | C42 | C43 | -168.62(19) | C1 | N3 | C13 | N5 | 178.19(19) |
| P3 | N7 | C48 | C49 | -151.2(2) | C1 | N3 | C13 | C14 | -4.5(3) |
| P3 | N7 | C48 | C47 | 24.5(2) | C1 | C2 | C3 | C4 | 4.5(3) |
| P3 | N6 | C53 | N9 | -17.6(3) | C1 | C6 | C5 | C4 | 3.8(3) |
| P3 | N6 | C53 | C54 | 160.38(17) | C41 | N6 | C53 | N9 | 150.52(19) |
| P3 | N6 | C41 | C42 | -5.1(2) | C41 | N6 | C53 | C54 | -31.5(3) |
| P3 | N6 | C41 | C46 | 165.7(2) | C41 | C42 | C43 | C44 | 2.1(3) |
| P1 | N3 | C13 | N5 | -12.9(3) | C41 | C46 | C45 | C44 | 2.4(4) |
| P1 | N3 | C13 | C14 | 164.46(17) | C57 | N9 | C53 | N6 | 177.86(19) |
| P1 | N3 | C1 | C2 | -17.2(2) | C57 | N9 | C53 | C54 | -0.2(3) |
| P1 | N3 | C1 | C6 | 156.0(2) | C57 | C56 | C55 | C54 | -0.5(3) |
| P1 | N1 | C18 | N4 | -16.7(3) | C6 | C5 | C4 | C3 | -2.0(4) |
| P1 | N1 | C18 | C19 | 161.18(17) | C8 | N2 | C2 | C1 | -157.1(2) |
| P1 | N1 | C7 | C8 | -3.1(2) | C8 | N2 | C2 | C3 | 27.1(3) |
| P1 | N1 | C7 | C12 | 168.2(2) | C8 | C7 | C12 | C11 | -4.2(4) |
| P1 | N2 | C2 | C1 | 28.0(2) | C8 | C9 | C10 | C11 | -2.0(4) |
| P1 | N2 | C2 | C3 | -147.7(2) | C70 | C69 | C74 | C73 | 0.4(3) |
| P1 | N2 | C8 | C7 | 0.0(3) | C7 | N1 | C18 | N4 | 154.0(2) |
| P1 | N2 | C8 | C9 | -172.7(2) | C7 | N1 | C18 | C19 | -28.1(3) |
| P4 | C69 | C70 | C71 | 173.95(19) | C7 | C8 | C9 | C10 | 0.3(4) |
| P4 | C69 | C74 | C73 | -173.50(18) | C7 | C12 | C11 | C10 | 2.6(5) |
| P4 | C63 | C64 | C65 | 176.20(17) | C35 | P2 | C29 | C30 | -145.46(17) |
| P4 | C63 | C68 | C67 | -176.5(3) | C35 | P2 | C29 | C34 | 38.4(2) |
| P4 | C75 | C80 | C79 | 168.29(19) | C35 | P2 | C23 | C24 | -110.8(2) |
| P4 | C75 | C76 | C77 | -168.41(18) | C35 | P2 | C23 | C28 | 65.9(2) |

| | | | | | | | | | |
|---|---|---|---|---|---|---|---|---|---|
| P2 | C29 | C30 | C31 | -177.39(18) | C35 | C36 | C37 | C38 | 0.1(4) |
| P2 | C29 | C34 | C33 | 177.32(18) | C35 | C40 | C39 | C38 | 0.1(4) |
| P2 | C35 | C36 | C37 | 175.14(19) | C62 | N10 | C58 | N8 | -173.32(18) |
| P2 | C35 | C40 | C39 | -174.99(18) | C62 | N10 | C58 | C59 | 9.8(3) |
| P2 | C23 | C24 | C25 | 179.1(3) | C62 | C61 | C60 | C59 | 5.1(3) |
| P2 | C23 | C28 | C27 | -178.0(2) | C36 | C35 | C40 | C39 | -1.2(3) |
| N5 | C17 | C16 | C15 | -1.5(3) | C77 | C78 | C79 | C80 | 1.7(4) |
| N5 | C13 | C14 | C15 | -5.8(3) | C49 | C48 | C47 | N8 | 173.8(2) |
| N9 | C53 | C54 | C55 | -4.4(3) | C49 | C48 | C47 | C52 | -0.4(3) |
| N8 | P3 | N7 | C42 | 152.96(17) | C49 | C50 | C51 | C52 | -0.3(4) |
| N8 | P3 | N7 | C48 | -27.36(16) | C20 | C21 | C22 | N4 | -4.2(3) |
| N8 | C58 | C59 | C60 | 178.0(2) | C47 | N8 | C58 | N10 | 179.85(18) |
| N8 | C47 | C52 | C51 | -174.7(2) | C47 | N8 | C58 | C59 | -3.5(3) |
| N10 | C58 | C59 | C60 | -5.4(3) | C47 | C48 | C49 | C50 | 2.2(3) |
| N3 | P1 | N1 | C18 | 119.03(19) | C47 | C52 | C51 | C50 | 2.1(3) |
| N3 | P1 | N1 | C7 | -52.5(2) | C43 | C42 | C41 | N6 | 173.8(2) |
| N3 | P1 | N2 | C2 | -29.74(15) | C43 | C42 | C41 | C46 | 1.8(3) |
| N3 | P1 | N2 | C8 | 155.08(17) | C43 | C44 | C45 | C46 | 1.6(4) |
| N3 | C13 | C14 | C15 | 176.9(2) | C74 | C69 | C70 | C71 | 0.5(4) |
| N3 | C1 | C6 | C5 | -174.2(2) | C74 | C73 | C72 | C71 | 0.6(4) |
| N7 | C42 | C41 | N6 | 1.5(3) | C22 | N4 | C18 | N1 | -179.40(18) |
| N7 | C42 | C41 | C46 | -170.5(2) | C22 | N4 | C18 | C19 | 2.6(3) |
| N7 | C42 | C43 | C44 | 173.2(2) | C22 | C21 | C20 | C19 | 1.4(3) |
| N7 | C48 | C49 | C50 | 177.6(2) | C78 | C77 | C76 | C75 | 0.1(4) |
| N7 | C48 | C47 | N8 | -2.3(3) | C60 | C61 | C62 | N10 | -0.5(3) |
| N7 | C48 | C47 | C52 | -176.50(19) | C75 | P4 | C69 | C70 | -105.4(2) |
| N4 | C18 | C19 | C20 | -5.3(3) | C75 | P4 | C69 | C74 | 68.13(19) |
| N6 | P3 | N7 | C42 | -4.72(16) | C75 | P4 | C63 | C64 | 167.01(18) |
| N6 | P3 | N7 | C48 | 174.96(17) | C75 | P4 | C63 | C68 | -15.8(2) |
| N6 | C53 | C54 | C55 | 177.7(2) | C75 | C80 | C79 | C78 | 0.6(4) |
| N6 | C41 | C46 | C45 | -174.2(2) | C40 | C35 | C36 | C37 | 1.2(4) |
| N1 | P1 | N2 | C2 | 173.83(16) | C40 | C39 | C38 | C37 | 1.1(4) |
| N1 | P1 | N2 | C8 | -1.34(17) | C9 | C8 | C7 | N1 | 175.2(2) |
| N1 | C18 | C19 | C20 | 176.9(2) | C9 | C8 | C7 | C12 | 2.8(4) |
| N1 | C7 | C12 | C11 | -174.8(3) | C64 | C63 | C68 | C67 | 0.8(4) |
| N2 | P1 | N1 | C18 | 173.97(17) | C64 | C65 | C66 | C67 | -0.2(4) |
| N2 | P1 | N1 | C7 | 2.48(16) | C65 | C66 | C67 | C68 | -0.1(5) |
| N2 | C2 | C1 | N3 | -4.7(2) | C12 | C11 | C10 | C9 | 0.6(5) |
| N2 | C2 | C1 | C6 | -178.72(19) | C80 | C75 | C76 | C77 | 2.2(3) |
| N2 | C2 | C3 | C4 | 179.9(2) | C3 | C2 | C1 | N3 | 171.4(2) |
| N2 | C8 | C7 | N1 | 2.0(3) | C3 | C2 | C1 | C6 | -2.6(3) |
| N2 | C8 | C7 | C12 | -170.4(2) | C23 | P2 | C29 | C30 | -41.78(19) |
| N2 | C8 | C9 | C10 | 172.5(2) | C23 | P2 | C29 | C34 | 142.1(2) |
| C17 | N5 | C13 | N3 | -174.26(18) | C23 | P2 | C35 | C36 | 22.7(2) |
| C17 | N5 | C13 | C14 | 8.2(3) | C23 | P2 | C35 | C40 | -163.55(19) |
| C17 | C16 | C15 | C14 | 4.0(3) | C23 | C24 | C25 | C26 | -1.7(6) |
| C69 | P4 | C63 | C64 | 64.43(19) | C23 | C28 | C27 | C26 | -0.6(4) |
| C69 | P4 | C63 | C68 | -118.3(2) | C73 | C72 | C71 | C70 | 0.3(4) |

| | | | | | | | | | |
|---|---|---|---|---|---|---|---|---|---|
| C69 | P4 | C75 | C80 | 29.4(2) | C39 | C38 | C37 | C36 | -1.2(4) |
| C69 | P4 | C75 | C76 | -160.21(19) | C76 | C77 | C78 | C79 | -2.0(4) |
| C69 | C70 | C71 | C72 | -0.8(4) | C76 | C75 | C80 | C79 | -2.5(3) |
| C69 | C74 | C73 | C72 | -0.9(4) | C68 | C63 | C64 | C65 | -1.1(3) |
| C29 | P2 | C35 | C36 | 126.36(19) | C24 | C23 | C28 | C27 | -1.1(4) |
| C29 | P2 | C35 | C40 | -59.9(2) | C28 | C23 | C24 | C25 | 2.3(4) |
| C29 | P2 | C23 | C24 | 139.0(2) | C28 | C27 | C26 | C25 | 1.2(5) |
| C29 | P2 | C23 | C28 | -44.3(2) | C27 | C26 | C25 | C24 | -0.1(6) |

**Table C-14.** Hydrogen Atom Coordinates (Å×$10^4$) and Isotropic Displacement Parameters (Å$^2$×$10^3$) for **4.3**.

| **Atom** | ***x*** | ***y*** | ***z*** | **U(eq)** |
|---|---|---|---|---|
| H17 | 8130.82 | 9035.81 | 6319.75 | 20 |
| H56 | 6484.54 | 4204.89 | 10238.14 | 24 |
| H19 | 8162.8 | 3889.74 | 9111.31 | 23 |
| H55 | 7735.36 | 4780.1 | 10654.97 | 23 |
| H54 | 8051.24 | 6263.81 | 10012.67 | 21 |
| H16 | 7669.39 | 9948.71 | 5194.46 | 23 |
| H30 | 9627.59 | 4368.04 | 7571.44 | 26 |
| H34 | 11125.32 | 6511.55 | 7213.49 | 27 |
| H57 | 5581.98 | 5134.32 | 9208.26 | 22 |
| H6 | 4050.92 | 8552.71 | 5610.2 | 25 |
| H21 | 10322.39 | 5255.3 | 9360.25 | 24 |
| H5 | 2630.26 | 7967.43 | 5431.72 | 29 |
| H61 | 1759.83 | 8949.34 | 6755.15 | 27 |
| H59 | 3828.15 | 10584.46 | 6555.58 | 24 |
| H70 | 4563.19 | 9306.09 | 9678.21 | 27 |
| H46 | 7511.14 | 7511.66 | 10177.53 | 26 |
| H62 | 3046.71 | 7606.1 | 7425.01 | 23 |
| H36 | 8846.83 | 6851.83 | 5309.08 | 30 |
| H77 | 619.59 | 7490.9 | 8638.8 | 30 |
| H49 | 7768.61 | 10578.42 | 7524.07 | 26 |
| H20 | 9662.09 | 3866.44 | 9684.76 | 26 |
| H43 | 7236.57 | 10516.03 | 8467.58 | 28 |
| H74 | 4784.34 | 6405.16 | 10090.3 | 23 |
| H22 | 9414.73 | 6636.49 | 8500.79 | 22 |
| H78 | -131.76 | 7949.65 | 9563.8 | 31 |
| H31 | 11038.2 | 3273.66 | 8321.08 | 31 |
| H60 | 2126.75 | 10493.96 | 6373.75 | 28 |
| H40 | 10284.99 | 7839.07 | 6535.01 | 27 |
| H9 | 5191.2 | 4323.29 | 6879.68 | 32 |
| H14 | 5480.15 | 8480.02 | 5227.59 | 23 |
| H64 | 5122.65 | 9558.87 | 8521.22 | 27 |
| H65 | 4671.3 | 11249.33 | 7945.87 | 36 |
| H12 | 8078.07 | 3276.8 | 8452.25 | 40 |
| H15 | 6376.64 | 9601.07 | 4625.63 | 25 |

| | | | | |
|---|---|---|---|---|
| H80 | 2691.93 | 8233.72 | 10069.8 | 29 |
| H3 | 3877.95 | 5394.25 | 6921.75 | 28 |
| H52 | 5180.21 | 10602.04 | 6017.02 | 24 |
| H4 | 2519.6 | 6419.85 | 6101.62 | 31 |
| H33 | 12535.47 | 5409.05 | 7958.66 | 33 |
| H50 | 7389.94 | 11786.92 | 6457.05 | 30 |
| H32 | 12493.01 | 3795.24 | 8513.31 | 34 |
| H44 | 7767 | 10298.6 | 9582.17 | 31 |
| H73 | 5361.09 | 6098.18 | 11206.53 | 26 |
| H51 | 6103.07 | 11805.06 | 5710.38 | 28 |
| H79 | 918.64 | 8283.11 | 10291.06 | 34 |
| H39 | 10726.01 | 8967.5 | 5579.97 | 34 |
| H76 | 2383.72 | 7452.19 | 8402.54 | 27 |
| H68 | 2018.75 | 9622.09 | 8451.71 | 44 |
| H72 | 5575.64 | 7389.31 | 11551.94 | 28 |
| H24 | 7198.43 | 5916.98 | 6387.38 | 45 |
| H45 | 7864.94 | 8830.64 | 10432.06 | 30 |
| H66 | 2901.96 | 12130.66 | 7633.35 | 48 |
| H11 | 7498 | 2133.34 | 8111.42 | 50 |
| H38 | 10258.44 | 9029.35 | 4491.41 | 39 |
| H10 | 6066.76 | 2645.87 | 7338.32 | 41 |
| H71 | 5183.95 | 8980.68 | 10788.67 | 33 |
| H37 | 9293.76 | 7989.29 | 4362.85 | 38 |
| H28 | 10360.56 | 4929.86 | 6180.55 | 36 |
| H67 | 1585.71 | 11315.4 | 7887.21 | 61 |
| H27 | 10048.1 | 3880.64 | 5631.34 | 48 |
| H26 | 8324.13 | 3803.72 | 5489.56 | 61 |
| H25 | 6893.91 | 4819.45 | 5866.67 | 72 |

**Structural Data for 4.7**

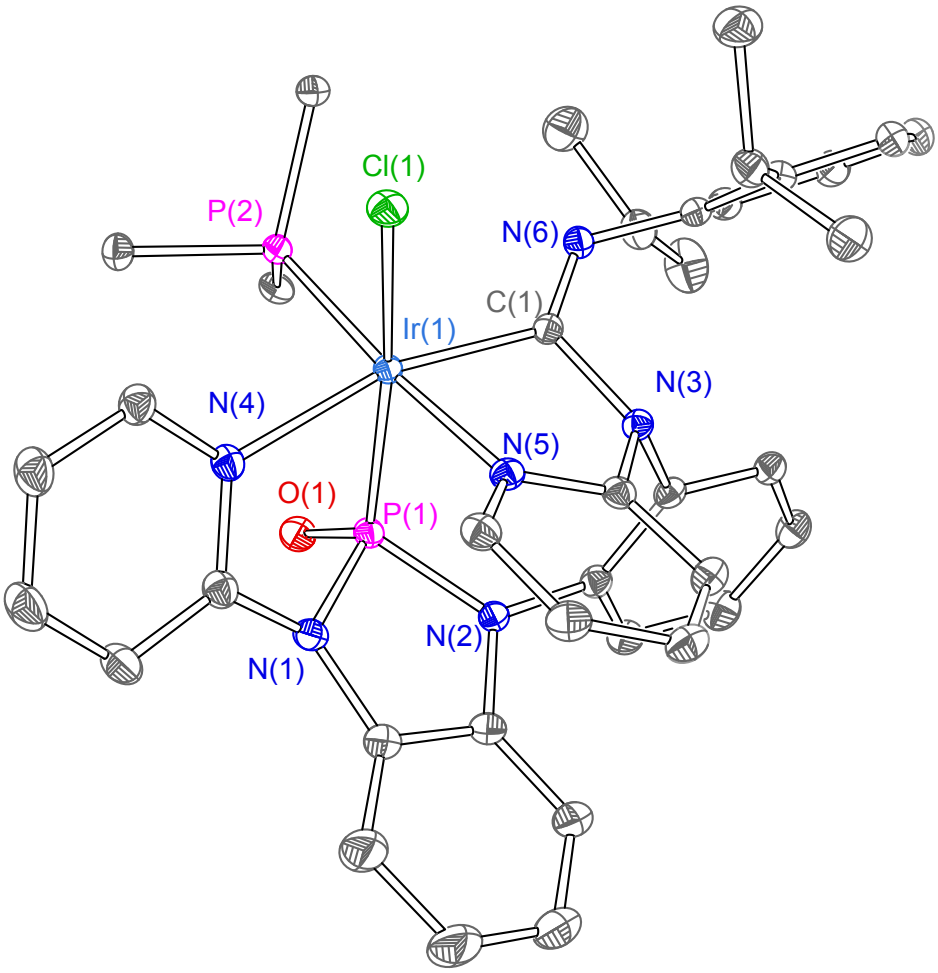

**Table C-15**. Crystal data and structure refinement for **4.7**.

| | |
|---|---|
| Identification code | IrNCO-a |
| Empirical formula | $C_{53}H_{48}ClIrN_6OP_2$ |
| Formula weight | 1074.56 |
| Temperature/K | 100.0 |
| Crystal system | triclinic |
| Space group | P-1 |
| a/Å | 13.0498(4) |
| b/Å | 13.9999(4) |
| c/Å | 16.8714(5) |
| α/° | 66.2370(10) |
| β/° | 76.6670(10) |
| γ/° | 82.7920(10) |
| Volume/Å$^3$ | 2743.15(14) |
| Z | 2 |
| $\varrho_{calc}$g/cm$^3$ | 1.301 |
| μ/mm$^{-1}$ | 2.580 |
| F(000) | 1080.0 |
| Crystal size/mm$^3$ | 0.3 × 0.27 × 0.14 |
| Radiation | MoKα (λ = 0.71073) |
| 2Θ range for data collection/° | 2.69 to 63.12 |
| Index ranges | -19 ≤ h ≤ 19, -20 ≤ k ≤ 20, -24 ≤ l ≤ 24 |
| Reflections collected | 168357 |
| Independent reflections | 18358 [$R_{int}$ = 0.0435, $R_{sigma}$ = 0.0240] |
| Data/restraints/parameters | 18358/0/581 |
| Goodness-of-fit on F$^2$ | 1.068 |
| Final R indexes [I>=2σ (I)] | $R_1$ = 0.0194, $wR_2$ = 0.0460 |
| Final R indexes [all data] | $R_1$ = 0.0221, $wR_2$ = 0.0467 |
| Largest diff. peak/hole / e Å$^{-3}$ | 1.01/-0.77 |

**Table C-16.** Fractional Atomic Coordinates (×10$^4$) and Equivalent Isotropic Displacement Parameters (Å$^2$×10$^3$) for **4.7**. $U_{eq}$ is defined as 1/3 of of the trace of the orthogonalised $U_{IJ}$ tensor**.**

| Atom | *x* | *y* | *z* | U(eq) |
|---|---|---|---|---|
| Ir1 | 6840.4(2) | 7814.2(2) | 5968.2(2) | 10.56(2) |
| Cl1 | 5182.8(3) | 8532.0(3) | 6577.6(2) | 16.52(6) |
| P1 | 8329.8(3) | 7537.2(3) | 5105.4(2) | 12.56(6) |
| P2 | 7616.8(3) | 7659.4(3) | 7113.1(2) | 12.27(6) |
| O1 | 9384.5(8) | 7407.2(9) | 5330.9(7) | 17.7(2) |
| N1 | 8257.7(10) | 8661.0(10) | 4166.2(8) | 15.6(2) |
| N2 | 8192.4(10) | 6790.5(10) | 4545.8(8) | 14.8(2) |

| | | | | |
|---|---|---|---|---|
| N3 | 6247.5(9) | 6073.4(9) | 5711.6(8) | 12.0(2) |
| N4 | 7293.6(10) | 9426.0(9) | 5110.1(8) | 14.2(2) |
| N5 | 6036.9(9) | 7874.2(9) | 5005.2(8) | 12.6(2) |
| N6 | 6319.3(9) | 5618.1(9) | 7224.0(8) | 13.8(2) |
| C1C | 6436.6(10) | 6320.2(11) | 6445.9(9) | 11.8(2) |
| C1 | 8268.7(13) | 8454.6(13) | 3413.0(10) | 20.7(3) |
| C2 | 8248.5(12) | 7371.7(12) | 3635.7(10) | 18.7(3) |
| C3 | 8225.5(15) | 6984.1(14) | 3002.1(11) | 26.4(3) |
| C4 | 8204(2) | 7691.4(17) | 2141.1(13) | 41.1(5) |
| C5 | 8203(2) | 8752.0(18) | 1922.9(13) | 49.9(7) |
| C6 | 8238.1(19) | 9149.4(15) | 2556.5(12) | 36.7(5) |
| C7 | 7989.7(11) | 5697.1(11) | 4931.8(9) | 14.5(3) |
| C8 | 7005.9(11) | 5341.4(11) | 5478.1(9) | 13.3(2) |
| C9 | 6785.8(12) | 4294.4(11) | 5789.8(9) | 15.1(3) |
| C10 | 7532.9(12) | 3595.0(12) | 5570.7(10) | 18.7(3) |
| C11 | 8512.2(13) | 3935.2(12) | 5047.0(11) | 20.9(3) |
| C12 | 8734.5(12) | 4984.6(12) | 4728.6(10) | 18.3(3) |
| C13 | 7914.7(11) | 9574.7(11) | 4304.2(10) | 15.8(3) |
| C14 | 8207.0(13) | 10569.4(12) | 3694.3(11) | 20.6(3) |
| C15 | 7831.3(14) | 11422.5(13) | 3907.1(11) | 24.1(3) |
| C16 | 7179.9(13) | 11276.2(12) | 4721.7(11) | 21.5(3) |
| C17 | 6945.2(12) | 10269.7(11) | 5304.2(10) | 16.9(3) |
| C18 | 5574.6(12) | 6812.4(12) | 4339.9(10) | 16.7(3) |
| C19 | 5956.7(11) | 6922.5(11) | 5005.5(9) | 13.0(2) |
| C20 | 5248.5(12) | 7698.4(12) | 3688.5(10) | 18.9(3) |
| C21 | 5290.9(12) | 8675.1(12) | 3716.7(10) | 18.2(3) |
| C22 | 5674.5(11) | 8731.4(11) | 4389.8(9) | 15.7(3) |
| C23 | 8024.2(12) | 8934.8(11) | 6950.0(10) | 15.5(3) |
| C24 | 8915.2(12) | 9359.8(12) | 6306.5(10) | 18.2(3) |
| C25 | 9202.4(13) | 10363.4(13) | 6115.6(11) | 23.0(3) |
| C26 | 8604.2(14) | 10950.7(13) | 6565.1(12) | 26.6(3) |
| C27 | 7711.7(14) | 10543.0(13) | 7195.0(13) | 27.2(4) |
| C28 | 7418.0(13) | 9535.1(12) | 7388.0(11) | 20.7(3) |
| C29 | 8816.4(11) | 6838.1(12) | 7280.1(10) | 15.8(3) |
| C30 | 9618.8(12) | 7080.1(13) | 7582.8(11) | 21.4(3) |
| C31 | 10475.0(13) | 6388.4(15) | 7769.7(12) | 27.3(4) |
| C32 | 10543.5(13) | 5453.6(14) | 7654.4(12) | 27.3(4) |
| C33 | 9754.3(13) | 5208.7(13) | 7350.4(11) | 22.3(3) |
| C34 | 8896.1(12) | 5902.2(12) | 7160.7(10) | 18.4(3) |
| C35 | 6823.3(11) | 7172.1(11) | 8238.3(9) | 15.2(3) |
| C36 | 7283.9(13) | 7107.1(14) | 8931.6(10) | 24.3(3) |
| C37 | 6734.8(15) | 6700.1(16) | 9802.0(11) | 29.2(4) |
| C38 | 5726.3(14) | 6348.2(15) | 9991.0(11) | 26.2(3) |
| C39 | 5265.7(13) | 6411.6(13) | 9308.7(10) | 21.6(3) |
| C40 | 5807.2(12) | 6826.8(12) | 8432.3(10) | 16.8(3) |
| C41 | 5780.2(11) | 4683.8(11) | 7507.4(9) | 14.3(3) |
| C42 | 6299.1(12) | 3714.2(12) | 7916.3(9) | 16.5(3) |
| C43 | 5745.3(13) | 2802.4(12) | 8243.7(10) | 20.5(3) |

| | | | | |
|---|---|---|---|---|
| C44 | 4693.0(14) | 2828.2(13) | 8191.9(10) | 22.1(3) |
| C45 | 4184.3(13) | 3782.9(12) | 7816.6(10) | 19.5(3) |
| C46 | 4700.8(11) | 4723.3(11) | 7475.4(9) | 15.3(3) |
| C47 | 7425.5(13) | 3689.0(12) | 8017.8(11) | 21.1(3) |
| C48 | 7433.3(15) | 3933.7(16) | 8828.2(12) | 31.1(4) |
| C49 | 8047.4(16) | 2665.5(14) | 8077.3(15) | 34.1(4) |
| C50 | 4066.5(12) | 5739.9(12) | 7140.6(10) | 18.0(3) |
| C51 | 3318.8(13) | 5919.5(14) | 7920.5(11) | 24.4(3) |
| C52 | 3468.0(13) | 5772.6(13) | 6448.8(11) | 22.8(3) |

**Table C-17.** Anisotropic Displacement Parameters ($Å^2×10^3$) for **4.7**. The Anisotropic displacement factor exponent takes the form: $-2\pi^2[h^2a^{*2}U_{11}+2hka^*b^*U_{12}+\ldots]$.

| **Atom** | $\mathbf{U_{11}}$ | $\mathbf{U_{22}}$ | $\mathbf{U_{33}}$ | $\mathbf{U_{23}}$ | $\mathbf{U_{13}}$ | $\mathbf{U_{12}}$ |
|---|---|---|---|---|---|---|
| Ir1 | 9.77(2) | 10.32(3) | 11.71(2) | -5.22(2) | -0.61(2) | -0.34(2) |
| Cl1 | 13.54(15) | 16.33(15) | 18.82(15) | -8.40(13) | 0.01(12) | 2.06(12) |
| P1 | 11.21(15) | 12.57(16) | 13.71(15) | -6.23(13) | 0.35(12) | -1.05(12) |
| P2 | 11.25(15) | 13.02(16) | 12.72(15) | -5.74(13) | -0.65(12) | -1.71(12) |
| O1 | 12.0(5) | 21.6(5) | 20.0(5) | -10.2(4) | -0.4(4) | -0.6(4) |
| N1 | 18.4(6) | 13.8(6) | 13.1(5) | -5.1(4) | 0.5(4) | -2.2(4) |
| N2 | 15.7(6) | 14.9(6) | 14.6(5) | -8.3(5) | 1.5(4) | -3.2(4) |
| N3 | 11.5(5) | 12.0(5) | 13.1(5) | -6.1(4) | -2.0(4) | 0.3(4) |
| N4 | 14.1(5) | 12.5(5) | 15.4(5) | -4.8(4) | -2.4(4) | -1.1(4) |
| N5 | 11.8(5) | 13.5(5) | 12.7(5) | -6.0(4) | -1.5(4) | 0.4(4) |
| N6 | 13.7(5) | 13.1(5) | 14.8(5) | -6.1(4) | -1.2(4) | -1.9(4) |
| C1C | 9.2(6) | 13.6(6) | 14.2(6) | -7.6(5) | -1.5(5) | 0.2(4) |
| C1 | 26.8(8) | 19.6(7) | 15.4(7) | -6.9(6) | -0.2(6) | -6.3(6) |
| C2 | 19.2(7) | 21.8(7) | 15.1(7) | -8.9(6) | 1.7(5) | -4.7(6) |
| C3 | 37.6(10) | 25.7(8) | 17.6(7) | -11.1(6) | 1.1(7) | -9.8(7) |
| C4 | 70.2(16) | 37.1(11) | 20.3(8) | -12.9(8) | -4.8(9) | -19.0(10) |
| C5 | 97(2) | 37.3(12) | 15.9(8) | -3.8(8) | -12.2(10) | -23.9(12) |
| C6 | 66.6(14) | 24.4(9) | 17.4(8) | -3.3(7) | -7.9(8) | -13.4(9) |
| C7 | 14.7(6) | 14.0(6) | 15.9(6) | -7.7(5) | -2.3(5) | 0.3(5) |
| C8 | 13.1(6) | 14.7(6) | 13.8(6) | -7.7(5) | -3.0(5) | 1.3(5) |
| C9 | 16.4(6) | 14.7(6) | 15.3(6) | -7.1(5) | -3.3(5) | -0.3(5) |
| C10 | 22.2(7) | 14.5(7) | 21.8(7) | -9.5(6) | -6.0(6) | 2.5(5) |
| C11 | 20.1(7) | 19.8(7) | 26.3(8) | -13.9(6) | -5.1(6) | 4.9(6) |
| C12 | 14.1(6) | 21.8(7) | 20.7(7) | -12.0(6) | -0.6(5) | 1.2(5) |
| C13 | 15.1(6) | 14.3(6) | 17.3(6) | -5.9(5) | -2.3(5) | -0.7(5) |
| C14 | 20.3(7) | 16.8(7) | 19.8(7) | -4.2(6) | 1.1(6) | -3.0(6) |
| C15 | 27.0(8) | 13.6(7) | 25.3(8) | -3.0(6) | -0.7(6) | -2.9(6) |
| C16 | 22.9(8) | 13.9(7) | 26.8(8) | -7.7(6) | -3.3(6) | -0.6(6) |
| C17 | 16.9(7) | 14.8(6) | 19.7(7) | -8.0(6) | -2.9(5) | 0.1(5) |
| C18 | 17.9(7) | 17.3(7) | 17.5(6) | -9.2(6) | -4.4(5) | 0.3(5) |
| C19 | 10.7(6) | 14.0(6) | 13.7(6) | -5.7(5) | -0.5(5) | -0.3(5) |
| C20 | 20.7(7) | 22.7(7) | 15.8(6) | -9.1(6) | -5.6(5) | 0.4(6) |
| C21 | 18.9(7) | 18.3(7) | 16.0(6) | -5.3(6) | -4.4(5) | 1.7(5) |

| | | | | | | |
|---|---|---|---|---|---|---|
| C22 | 14.7(6) | 14.8(6) | 15.9(6) | -5.6(5) | -1.3(5) | 0.7(5) |
| C23 | 15.8(6) | 14.8(6) | 17.0(6) | -6.2(5) | -4.4(5) | -2.1(5) |
| C24 | 16.6(7) | 18.0(7) | 19.4(7) | -6.0(6) | -3.6(5) | -2.4(5) |
| C25 | 19.1(7) | 18.2(7) | 27.9(8) | -2.6(6) | -6.5(6) | -6.3(6) |
| C26 | 29.3(9) | 15.9(7) | 37.6(9) | -9.6(7) | -12.8(7) | -3.0(6) |
| C27 | 29.1(9) | 20.2(8) | 37.3(10) | -17.0(7) | -5.7(7) | 0.4(6) |
| C28 | 20.2(7) | 19.2(7) | 24.6(8) | -11.6(6) | -1.8(6) | -2.0(6) |
| C29 | 12.5(6) | 17.2(7) | 15.5(6) | -4.9(5) | -1.0(5) | -0.7(5) |
| C30 | 17.1(7) | 23.3(8) | 24.4(8) | -8.9(6) | -5.8(6) | -0.9(6) |
| C31 | 15.9(7) | 31.9(9) | 34.9(9) | -11.6(8) | -10.2(7) | 0.8(6) |
| C32 | 16.0(7) | 29.3(9) | 31.9(9) | -8.4(7) | -5.5(6) | 5.5(6) |
| C33 | 19.1(7) | 20.2(7) | 24.7(8) | -8.5(6) | -1.2(6) | 3.1(6) |
| C34 | 16.2(7) | 18.3(7) | 20.5(7) | -7.8(6) | -3.0(5) | 0.1(5) |
| C35 | 16.0(6) | 15.5(6) | 13.8(6) | -6.6(5) | -0.2(5) | -1.8(5) |
| C36 | 21.7(8) | 35.8(9) | 16.1(7) | -9.0(7) | -2.4(6) | -8.7(7) |
| C37 | 29.1(9) | 43.6(11) | 15.0(7) | -10.5(7) | -3.0(6) | -7.3(8) |
| C38 | 28.2(9) | 33.4(9) | 13.9(7) | -8.1(6) | 2.9(6) | -7.5(7) |
| C39 | 20.8(7) | 25.5(8) | 17.9(7) | -9.6(6) | 3.3(6) | -7.6(6) |
| C40 | 17.5(7) | 18.1(7) | 15.6(6) | -8.0(5) | -0.7(5) | -2.9(5) |
| C41 | 17.2(7) | 15.1(6) | 11.5(6) | -6.2(5) | -0.9(5) | -3.0(5) |
| C42 | 19.7(7) | 15.0(6) | 13.9(6) | -4.8(5) | -2.9(5) | -1.2(5) |
| C43 | 29.3(8) | 14.9(7) | 16.0(7) | -3.8(5) | -4.4(6) | -3.5(6) |
| C44 | 29.6(8) | 18.1(7) | 17.3(7) | -5.3(6) | -0.3(6) | -10.1(6) |
| C45 | 19.9(7) | 22.7(7) | 16.4(7) | -7.9(6) | -0.1(5) | -8.2(6) |
| C46 | 16.3(7) | 16.8(7) | 12.7(6) | -6.0(5) | -0.3(5) | -3.5(5) |
| C47 | 21.7(7) | 17.5(7) | 22.6(7) | -5.4(6) | -6.3(6) | -0.1(6) |
| C48 | 30.9(9) | 38.1(10) | 27.0(9) | -12.2(8) | -11.6(7) | -1.3(8) |
| C49 | 29.4(9) | 22.5(9) | 48.4(12) | -10.8(8) | -12.6(8) | 4.8(7) |
| C50 | 14.5(6) | 20.2(7) | 19.9(7) | -9.0(6) | -2.1(5) | -1.4(5) |
| C51 | 16.6(7) | 33.9(9) | 25.7(8) | -16.7(7) | -2.1(6) | 2.2(6) |
| C52 | 22.3(8) | 24.7(8) | 22.1(7) | -8.4(6) | -6.7(6) | -0.5(6) |

**Table C-18** Bond Lengths for **4.7**.

| Atom | Atom | Length/Å | Atom | Atom | Length/Å |
|---|---|---|---|---|---|
| Ir1 | Cl1 | 2.4510(3) | C14 | C15 | 1.383(2) |
| Ir1 | P1 | 2.2378(4) | C15 | C16 | 1.390(2) |
| Ir1 | P2 | 2.3055(4) | C16 | C17 | 1.378(2) |
| Ir1 | N4 | 2.2010(12) | C18 | C19 | 1.3966(19) |
| Ir1 | N5 | 2.0976(12) | C18 | C20 | 1.383(2) |
| Ir1 | C1C | 2.0061(14) | C20 | C21 | 1.396(2) |
| P1 | O1 | 1.4816(11) | C21 | C22 | 1.375(2) |
| P1 | N1 | 1.7372(13) | C23 | C24 | 1.398(2) |
| P1 | N2 | 1.7136(12) | C23 | C28 | 1.394(2) |
| P2 | C23 | 1.8224(15) | C24 | C25 | 1.389(2) |
| P2 | C29 | 1.8283(15) | C25 | C26 | 1.389(3) |
| P2 | C35 | 1.8352(15) | C26 | C27 | 1.385(3) |
| N1 | C1 | 1.4089(19) | C27 | C28 | 1.397(2) |

| | | | | | |
|---|---|---|---|---|---|
| N1 | C13 | 1.3925(18) | C29 | C30 | 1.396(2) |
| N2 | C2 | 1.408(2) | C29 | C34 | 1.392(2) |
| N2 | C7 | 1.4339(18) | C30 | C31 | 1.389(2) |
| N3 | C1C | 1.4907(17) | C31 | C32 | 1.388(3) |
| N3 | C8 | 1.4407(17) | C32 | C33 | 1.384(2) |
| N3 | C19 | 1.3894(18) | C33 | C34 | 1.393(2) |
| N4 | C13 | 1.3620(19) | C35 | C36 | 1.401(2) |
| N4 | C17 | 1.3482(18) | C35 | C40 | 1.390(2) |
| N5 | C19 | 1.3492(18) | C36 | C37 | 1.392(2) |
| N5 | C22 | 1.3497(18) | C37 | C38 | 1.385(3) |
| N6 | C1C | 1.2721(18) | C38 | C39 | 1.385(2) |
| N6 | C41 | 1.4163(18) | C39 | C40 | 1.397(2) |
| C1 | C2 | 1.410(2) | C41 | C42 | 1.417(2) |
| C1 | C6 | 1.386(2) | C41 | C46 | 1.415(2) |
| C2 | C3 | 1.387(2) | C42 | C43 | 1.391(2) |
| C3 | C4 | 1.394(3) | C42 | C47 | 1.513(2) |
| C4 | C5 | 1.378(3) | C43 | C44 | 1.391(2) |
| C5 | C6 | 1.401(3) | C44 | C45 | 1.385(2) |
| C7 | C8 | 1.411(2) | C45 | C46 | 1.397(2) |
| C7 | C12 | 1.391(2) | C46 | C50 | 1.517(2) |
| C8 | C9 | 1.387(2) | C47 | C48 | 1.540(2) |
| C9 | C10 | 1.390(2) | C47 | C49 | 1.534(2) |
| C10 | C11 | 1.390(2) | C50 | C51 | 1.536(2) |
| C11 | C12 | 1.389(2) | C50 | C52 | 1.531(2) |
| C13 | C14 | 1.393(2) | | | |

**Table C-19** Bond Angles for **4.7**.

| **Atom** | **Atom** | **Atom** | **Angle/°** | **Atom** | **Atom** | **Atom** | **Angle/°** |
|---|---|---|---|---|---|---|---|
| P1 | Ir1 | Cl1 | 165.221(13) | C9 | C8 | C7 | 119.75(13) |
| P1 | Ir1 | P2 | 95.670(13) | C8 | C9 | C10 | 120.24(14) |
| P2 | Ir1 | Cl1 | 92.717(13) | C9 | C10 | C11 | 120.38(14) |
| N4 | Ir1 | Cl1 | 88.17(3) | C12 | C11 | C10 | 119.61(14) |
| N4 | Ir1 | P1 | 78.78(3) | C11 | C12 | C7 | 120.70(14) |
| N4 | Ir1 | P2 | 96.87(3) | N1 | C13 | C14 | 123.86(14) |
| N5 | Ir1 | Cl1 | 84.80(3) | N4 | C13 | N1 | 114.69(13) |
| N5 | Ir1 | P1 | 87.63(3) | N4 | C13 | C14 | 121.40(13) |
| N5 | Ir1 | P2 | 175.25(3) | C15 | C14 | C13 | 118.94(15) |
| N5 | Ir1 | N4 | 87.11(5) | C14 | C15 | C16 | 119.85(15) |
| C1C | Ir1 | Cl1 | 98.18(4) | C17 | C16 | C15 | 118.27(15) |
| C1C | Ir1 | P1 | 92.96(4) | N4 | C17 | C16 | 123.03(14) |
| C1C | Ir1 | P2 | 96.46(4) | C20 | C18 | C19 | 118.76(14) |
| C1C | Ir1 | N4 | 164.94(5) | N3 | C19 | C18 | 122.69(13) |
| C1C | Ir1 | N5 | 79.92(5) | N5 | C19 | N3 | 116.23(12) |
| O1 | P1 | Ir1 | 123.64(5) | N5 | C19 | C18 | 121.06(13) |
| O1 | P1 | N1 | 110.44(6) | C18 | C20 | C21 | 119.67(14) |
| O1 | P1 | N2 | 113.16(6) | C22 | C21 | C20 | 118.76(14) |
| N1 | P1 | Ir1 | 98.10(4) | N5 | C22 | C21 | 121.80(14) |

| | | | | | | | |
|---|---|---|---|---|---|---|---|
| N2 | P1 | Ir1 | 114.38(4) | C24 | C23 | P2 | 118.75(11) |
| N2 | P1 | N1 | 90.00(6) | C28 | C23 | P2 | 121.70(12) |
| C23 | P2 | Ir1 | 109.74(5) | C28 | C23 | C24 | 119.27(14) |
| C23 | P2 | C29 | 103.17(7) | C25 | C24 | C23 | 120.37(15) |
| C23 | P2 | C35 | 104.35(7) | C24 | C25 | C26 | 120.03(16) |
| C29 | P2 | Ir1 | 118.85(5) | C27 | C26 | C25 | 120.08(15) |
| C29 | P2 | C35 | 100.74(7) | C26 | C27 | C28 | 120.11(16) |
| C35 | P2 | Ir1 | 118.09(5) | C23 | C28 | C27 | 120.12(15) |
| C1 | N1 | P1 | 113.22(10) | C30 | C29 | P2 | 122.30(12) |
| C13 | N1 | P1 | 116.29(10) | C34 | C29 | P2 | 118.63(11) |
| C13 | N1 | C1 | 127.84(13) | C34 | C29 | C30 | 118.92(14) |
| C2 | N2 | P1 | 113.01(10) | C31 | C30 | C29 | 120.18(16) |
| C2 | N2 | C7 | 121.03(12) | C32 | C31 | C30 | 120.46(16) |
| C7 | N2 | P1 | 125.90(10) | C33 | C32 | C31 | 119.80(15) |
| C8 | N3 | C1C | 114.56(11) | C32 | C33 | C34 | 119.83(15) |
| C19 | N3 | C1C | 115.36(11) | C29 | C34 | C33 | 120.80(15) |
| C19 | N3 | C8 | 115.52(11) | C36 | C35 | P2 | 118.16(11) |
| C13 | N4 | Ir1 | 116.74(9) | C40 | C35 | P2 | 122.81(11) |
| C17 | N4 | Ir1 | 124.63(10) | C40 | C35 | C36 | 118.98(14) |
| C17 | N4 | C13 | 118.48(13) | C37 | C36 | C35 | 120.57(15) |
| C19 | N5 | Ir1 | 112.49(9) | C38 | C37 | C36 | 120.12(16) |
| C19 | N5 | C22 | 119.76(12) | C39 | C38 | C37 | 119.61(15) |
| C22 | N5 | Ir1 | 127.62(10) | C38 | C39 | C40 | 120.70(15) |
| C1C | N6 | C41 | 124.56(12) | C35 | C40 | C39 | 120.01(14) |
| N3 | C1C | Ir1 | 109.10(9) | N6 | C41 | C42 | 119.08(13) |
| N6 | C1C | Ir1 | 131.36(10) | C46 | C41 | N6 | 120.31(13) |
| N6 | C1C | N3 | 119.54(12) | C46 | C41 | C42 | 120.22(13) |
| N1 | C1 | C2 | 110.64(13) | C41 | C42 | C47 | 119.79(13) |
| C6 | C1 | N1 | 129.24(15) | C43 | C42 | C41 | 118.93(14) |
| C6 | C1 | C2 | 120.01(15) | C43 | C42 | C47 | 121.25(14) |
| N2 | C2 | C1 | 112.27(13) | C44 | C43 | C42 | 121.36(15) |
| C3 | C2 | N2 | 126.72(15) | C45 | C44 | C43 | 119.20(14) |
| C3 | C2 | C1 | 120.90(15) | C44 | C45 | C46 | 121.95(15) |
| C2 | C3 | C4 | 118.49(17) | C41 | C46 | C50 | 122.95(13) |
| C5 | C4 | C3 | 120.89(17) | C45 | C46 | C41 | 118.27(14) |
| C4 | C5 | C6 | 120.98(18) | C45 | C46 | C50 | 118.67(13) |
| C1 | C6 | C5 | 118.71(18) | C42 | C47 | C48 | 109.25(14) |
| C8 | C7 | N2 | 120.18(12) | C42 | C47 | C49 | 114.40(14) |
| C12 | C7 | N2 | 120.40(13) | C49 | C47 | C48 | 110.62(15) |
| C12 | C7 | C8 | 119.30(13) | C46 | C50 | C51 | 109.95(13) |
| C7 | C8 | N3 | 119.30(12) | C46 | C50 | C52 | 112.04(13) |
| C9 | C8 | N3 | 120.94(13) | C52 | C50 | C51 | 111.48(13) |

**Table C-20.** Torsion Angles for **4.7**.

| A | B | C | D | Angle/° | A | B | C | D | Angle/° |
|---|---|---|---|---|---|---|---|---|---|
| Ir1 | P1 | N1 | C1 | -122.40(10) | C8 | C7 | C12 | C11 | 1.0(2) |
| Ir1 | P1 | N1 | C13 | 40.67(11) | C8 | C9 | C10 | C11 | 0.8(2) |

| | | | | | | | | | |
|---|---|---|---|---|---|---|---|---|---|
| Ir1 | P1 | N2 | C2 | 107.59(10) | C9 | C10 | C11 | C12 | -1.2(2) |
| Ir1 | P1 | N2 | C7 | -69.52(12) | C10 | C11 | C12 | C7 | 0.3(2) |
| Ir1 | P2 | C23 | C24 | -74.63(12) | C12 | C7 | C8 | N3 | 178.03(12) |
| Ir1 | P2 | C23 | C28 | 99.21(13) | C12 | C7 | C8 | C9 | -1.3(2) |
| Ir1 | P2 | C29 | C30 | 145.55(11) | C13 | N1 | C1 | C2 | -155.84(15) |
| Ir1 | P2 | C29 | C34 | -39.12(14) | C13 | N1 | C1 | C6 | 20.3(3) |
| Ir1 | P2 | C35 | C36 | -178.13(11) | C13 | N4 | C17 | C16 | 0.7(2) |
| Ir1 | P2 | C35 | C40 | 4.62(15) | C13 | C14 | C15 | C16 | 0.5(3) |
| Ir1 | N4 | C13 | N1 | -5.56(16) | C14 | C15 | C16 | C17 | 1.3(3) |
| Ir1 | N4 | C13 | C14 | 177.03(11) | C15 | C16 | C17 | N4 | -1.9(2) |
| Ir1 | N4 | C17 | C16 | -174.74(12) | C17 | N4 | C13 | N1 | 178.67(13) |
| Ir1 | N5 | C19 | N3 | 10.23(15) | C17 | N4 | C13 | C14 | 1.3(2) |
| Ir1 | N5 | C19 | C18 | -171.40(11) | C18 | C20 | C21 | C22 | 1.0(2) |
| Ir1 | N5 | C22 | C21 | 170.68(11) | C19 | N3 | C1C | Ir1 | -25.29(13) |
| P1 | N1 | C1 | C2 | 4.86(17) | C19 | N3 | C1C | N6 | 154.04(13) |
| P1 | N1 | C1 | C6 | -179.00(18) | C19 | N3 | C8 | C7 | 57.39(17) |
| P1 | N1 | C13 | N4 | -25.50(17) | C19 | N3 | C8 | C9 | -123.26(14) |
| P1 | N1 | C13 | C14 | 151.84(13) | C19 | N5 | C22 | C21 | -4.8(2) |
| P1 | N2 | C2 | C1 | -7.65(17) | C19 | C18 | C20 | C21 | -1.0(2) |
| P1 | N2 | C2 | C3 | 176.08(14) | C20 | C18 | C19 | N3 | 176.43(13) |
| P1 | N2 | C7 | C8 | 68.88(17) | C20 | C18 | C19 | N5 | -1.8(2) |
| P1 | N2 | C7 | C12 | -115.08(14) | C20 | C21 | C22 | N5 | 1.9(2) |
| P2 | C23 | C24 | C25 | 174.99(12) | C22 | N5 | C19 | N3 | -173.62(12) |
| P2 | C23 | C28 | C27 | -174.95(13) | C22 | N5 | C19 | C18 | 4.7(2) |
| P2 | C29 | C30 | C31 | 174.63(13) | C23 | P2 | C29 | C30 | 23.89(15) |
| P2 | C29 | C34 | C33 | -174.65(12) | C23 | P2 | C29 | C34 | -160.78(12) |
| P2 | C35 | C36 | C37 | -177.16(15) | C23 | P2 | C35 | C36 | -56.01(14) |
| P2 | C35 | C40 | C39 | 176.51(12) | C23 | P2 | C35 | C40 | 126.74(13) |
| O1 | P1 | N1 | C1 | 107.05(11) | C23 | C24 | C25 | C26 | 0.0(2) |
| O1 | P1 | N1 | C13 | -89.88(12) | C24 | C23 | C28 | C27 | -1.1(2) |
| O1 | P1 | N2 | C2 | -103.62(11) | C24 | C25 | C26 | C27 | -1.0(3) |
| O1 | P1 | N2 | C7 | 79.26(13) | C25 | C26 | C27 | C28 | 0.8(3) |
| N1 | P1 | N2 | C2 | 8.69(11) | C26 | C27 | C28 | C23 | 0.3(3) |
| N1 | P1 | N2 | C7 | -168.42(12) | C28 | C23 | C24 | C25 | 1.0(2) |
| N1 | C1 | C2 | N2 | 1.70(19) | C29 | P2 | C23 | C24 | 53.00(13) |
| N1 | C1 | C2 | C3 | 178.22(15) | C29 | P2 | C23 | C28 | -133.16(13) |
| N1 | C1 | C6 | C5 | -176.7(2) | C29 | P2 | C35 | C36 | 50.72(14) |
| N1 | C13 | C14 | C15 | -178.99(15) | C29 | P2 | C35 | C40 | -126.53(13) |
| N2 | P1 | N1 | C1 | -7.76(12) | C29 | C30 | C31 | C32 | 0.2(3) |
| N2 | P1 | N1 | C13 | 155.31(11) | C30 | C29 | C34 | C33 | 0.8(2) |
| N2 | C2 | C3 | C4 | 174.86(18) | C30 | C31 | C32 | C33 | 0.1(3) |
| N2 | C7 | C8 | N3 | -5.9(2) | C31 | C32 | C33 | C34 | 0.1(3) |
| N2 | C7 | C8 | C9 | 174.76(13) | C32 | C33 | C34 | C29 | -0.5(2) |
| N2 | C7 | C12 | C11 | -175.13(14) | C34 | C29 | C30 | C31 | -0.7(2) |
| N3 | C8 | C9 | C10 | -178.90(13) | C35 | P2 | C23 | C24 | 157.91(12) |
| N4 | C13 | C14 | C15 | -1.8(2) | C35 | P2 | C23 | C28 | -28.25(14) |
| N6 | C41 | C42 | C43 | 176.01(13) | C35 | P2 | C29 | C30 | -83.77(14) |
| N6 | C41 | C42 | C47 | -1.9(2) | C35 | P2 | C29 | C34 | 91.56(13) |

| | | | | | | | | | |
|---|---|---|---|---|---|---|---|---|---|
| N6 | C41 | C46 | C45 | -175.78(13) | C35 | C36 | C37 | C38 | 0.4(3) |
| N6 | C41 | C46 | C50 | 0.3(2) | C36 | C35 | C40 | C39 | -0.7(2) |
| C1C | N3 | C8 | C7 | -80.33(16) | C36 | C37 | C38 | C39 | -0.5(3) |
| C1C | N3 | C8 | C9 | 99.02(15) | C37 | C38 | C39 | C40 | 0.0(3) |
| C1C | N3 | C19 | N5 | 9.77(17) | C38 | C39 | C40 | C35 | 0.6(2) |
| C1C | N3 | C19 | C18 | -168.56(13) | C40 | C35 | C36 | C37 | 0.2(3) |
| C1C | N6 | C41 | C42 | 126.48(15) | C41 | N6 | C1C | Ir1 | 163.20(11) |
| C1C | N6 | C41 | C46 | -60.72(19) | C41 | N6 | C1C | N3 | -16.0(2) |
| C1 | N1 | C13 | N4 | 134.69(15) | C41 | C42 | C43 | C44 | -1.2(2) |
| C1 | N1 | C13 | C14 | -48.0(2) | C41 | C42 | C47 | C48 | 80.91(18) |
| C1 | C2 | C3 | C4 | -1.1(3) | C41 | C42 | C47 | C49 | -154.48(15) |
| C2 | N2 | C7 | C8 | -108.02(16) | C41 | C46 | C50 | C51 | -105.94(16) |
| C2 | N2 | C7 | C12 | 68.03(19) | C41 | C46 | C50 | C52 | 129.51(15) |
| C2 | C1 | C6 | C5 | -0.9(3) | C42 | C41 | C46 | C45 | -3.1(2) |
| C2 | C3 | C4 | C5 | -0.1(3) | C42 | C41 | C46 | C50 | 173.02(13) |
| C3 | C4 | C5 | C6 | 0.9(4) | C42 | C43 | C44 | C45 | -0.8(2) |
| C4 | C5 | C6 | C1 | -0.3(4) | C43 | C42 | C47 | C48 | -96.95(17) |
| C6 | C1 | C2 | N2 | -174.84(17) | C43 | C42 | C47 | C49 | 27.7(2) |
| C6 | C1 | C2 | C3 | 1.7(3) | C43 | C44 | C45 | C46 | 1.0(2) |
| C7 | N2 | C2 | C1 | 169.62(13) | C44 | C45 | C46 | C41 | 1.0(2) |
| C7 | N2 | C2 | C3 | -6.7(2) | C44 | C45 | C46 | C50 | -175.28(14) |
| C7 | C8 | C9 | C10 | 0.4(2) | C45 | C46 | C50 | C51 | 70.13(17) |
| C8 | N3 | C1C | Ir1 | 112.49(11) | C45 | C46 | C50 | C52 | -54.42(18) |
| C8 | N3 | C1C | N6 | -68.18(16) | C46 | C41 | C42 | C43 | 3.2(2) |
| C8 | N3 | C19 | N5 | -127.61(13) | C46 | C41 | C42 | C47 | -174.70(13) |
| C8 | N3 | C19 | C18 | 54.06(18) | C47 | C42 | C43 | C44 | 176.64(14) |

**Table C-21** Hydrogen Atom Coordinates (Å×$10^4$) and Isotropic Displacement Parameters (Å$^2$×$10^3$) for **4.7.**

| **Atom** | ***x*** | ***y*** | ***z*** | **U(eq)** |
|---|---|---|---|---|
| H3 | 8224.51 | 6253.35 | 3151.5 | 32 |
| H4 | 8189.65 | 7438.87 | 1698.92 | 49 |
| H5 | 8177.95 | 9220.51 | 1334.16 | 60 |
| H6 | 8241.04 | 9881.11 | 2401.87 | 44 |
| H9 | 6121.99 | 4054.26 | 6154.31 | 18 |
| H10 | 7373.54 | 2880.37 | 5779.97 | 22 |
| H11 | 9026.17 | 3452.91 | 4907.77 | 25 |
| H12 | 9402.12 | 5218.16 | 4368.39 | 22 |
| H14 | 8657.24 | 10660.27 | 3141.15 | 25 |
| H15 | 8018.08 | 12106.97 | 3497.37 | 29 |
| H16 | 6903.55 | 11854.92 | 4872.96 | 26 |
| H17 | 6518.22 | 10165.55 | 5868.75 | 20 |
| H18 | 5539.36 | 6141.25 | 4334.81 | 20 |
| H20 | 4996.93 | 7642.55 | 3223.98 | 23 |
| H21 | 5059.09 | 9289.54 | 3279.11 | 22 |
| H22 | 5684.68 | 9391.72 | 4422.6 | 19 |

| | | | | |
|---|---|---|---|---|
| H24 | 9326.48 | 8960.05 | 5998.11 | 22 |
| H25 | 9808.31 | 10648 | 5677.49 | 28 |
| H26 | 8807.43 | 11632.83 | 6440.33 | 32 |
| H27 | 7298.62 | 10949.54 | 7496.22 | 33 |
| H28 | 6803.96 | 9258.48 | 7818.6 | 25 |
| H30 | 9579.54 | 7719.56 | 7661.4 | 26 |
| H31 | 11017.36 | 6556.52 | 7977.77 | 33 |
| H32 | 11130.36 | 4983.29 | 7783.85 | 33 |
| H33 | 9797.56 | 4569.33 | 7271.16 | 27 |
| H34 | 8358.82 | 5734.15 | 6947.4 | 22 |
| H36 | 7977.13 | 7342.8 | 8806.68 | 29 |
| H37 | 7052.08 | 6663.69 | 10267.23 | 35 |
| H38 | 5352.86 | 6065.01 | 10585.2 | 31 |
| H39 | 4574.16 | 6170.28 | 9437.95 | 26 |
| H40 | 5480.95 | 6873.02 | 7968.92 | 20 |
| H43 | 6092.99 | 2148.78 | 8508.1 | 25 |
| H44 | 4327.81 | 2198.44 | 8411.36 | 27 |
| H45 | 3462.59 | 3798.97 | 7790.34 | 23 |
| H47 | 7794.28 | 4261.99 | 7484.58 | 25 |
| H48A | 7063.94 | 3392.12 | 9362.57 | 47 |
| H48B | 7077.92 | 4614.29 | 8758.03 | 47 |
| H48C | 8163.02 | 3950.49 | 8879.79 | 47 |
| H49A | 8781.54 | 2732.16 | 8089.78 | 51 |
| H49B | 8023.19 | 2516.23 | 7562.25 | 51 |
| H49C | 7734.81 | 2094.11 | 8617.84 | 51 |
| H50 | 4571.88 | 6320.44 | 6851.75 | 22 |
| H51A | 2788.27 | 5382.9 | 8195.65 | 37 |
| H51B | 2968.17 | 6611.12 | 7706.88 | 37 |
| H51C | 3722.9 | 5879.07 | 8356.54 | 37 |
| H52A | 3970.92 | 5710.04 | 5940.46 | 34 |
| H52B | 3063.25 | 6436.02 | 6255.34 | 34 |
| H52C | 2986.72 | 5192.47 | 6707.72 | 34 |

**Structural Data for 4.9**

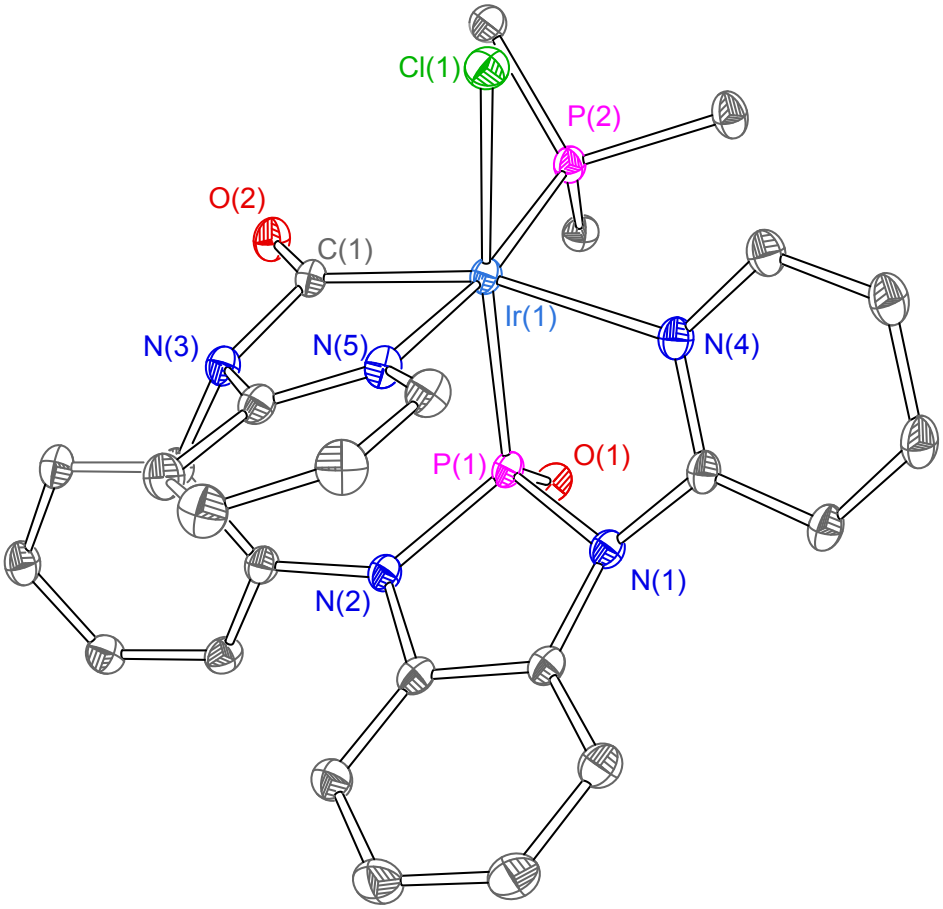

**Table C-22.** Crystal data and structure refinement for **4.9**.

| | |
|---|---|
| Identification code | IrCO2-a |
| Empirical formula | $C_{41}H_{31}N_5O_2P_2ClIr$ |
| Formula weight | 915.30 |
| Temperature/K | 100.0 |
| Crystal system | triclinic |
| Space group | P-1 |
| a/Å | 10.2362(3) |
| b/Å | 13.1450(4) |
| c/Å | 16.0024(5) |
| α/° | 99.2630(10) |
| β/° | 108.1240(10) |
| γ/° | 99.3850(10) |
| Volume/Å$^3$ | 1966.85(10) |
| Z | 2 |
| $\rho_{calc}$g/cm$^3$ | 1.546 |
| μ/mm$^{-1}$ | 3.585 |
| F(000) | 904.0 |
| Crystal size/mm$^3$ | 0.27 × 0.25 × 0.045 |
| Radiation | MoKα (λ = 0.71073) |
| 2Θ range for data collection/° | 2.748 to 64.204 |
| Index ranges | $-15 \leq h \leq 14$, $-19 \leq k \leq 19$, $-23 \leq l \leq 23$ |
| Reflections collected | 116259 |
| Independent reflections | 13747 [$R_{int}$ = 0.0351, $R_{sigma}$ = 0.0193] |
| Data/restraints/parameters | 13747/0/469 |
| Goodness-of-fit on $F^2$ | 1.056 |
| Final R indexes [I>=2σ (I)] | $R_1$ = 0.0176, $wR_2$ = 0.0429 |
| Final R indexes [all data] | $R_1$ = 0.0185, $wR_2$ = 0.0433 |
| Largest diff. peak/hole / e Å$^{-3}$ | 1.62/-1.05 |

**Table C-23.** Fractional Atomic Coordinates (×10$^4$) and Equivalent Isotropic Displacement Parameters (Å$^2$×10$^3$) for **4.9**. $U_{eq}$ is defined as 1/3 of of the trace of the orthogonalised $U_{IJ}$ tensor.

| Atom | *x* | *y* | *z* | U(eq) |
|---|---|---|---|---|
| Ir1 | 3357.6(2) | 2367.2(2) | 6370.2(2) | 12.07(2) |
| Cl1 | 4288.9(4) | 962.8(3) | 7035.7(2) | 18.53(6) |
| P1 | 2839.4(4) | 3635.8(3) | 5618.3(2) | 12.71(6) |
| P2 | 3768.2(4) | 3346.2(3) | 7795.7(2) | 14.45(6) |
| O1 | 2739.1(12) | 4691.4(8) | 6050.4(7) | 17.38(19) |
| O2 | 501.6(11) | 2091.9(9) | 6495.4(7) | 18.2(2) |
| N1 | 4140.0(12) | 3705.9(10) | 5129.8(8) | 14.4(2) |
| N2 | 1551.3(12) | 3156.0(10) | 4576.0(8) | 14.4(2) |
| N3 | 599.7(13) | 1364.5(9) | 5129.5(8) | 14.3(2) |
| N4 | 5425.2(13) | 2963.3(10) | 6268.0(8) | 15.0(2) |
| N5 | 2858.3(13) | 1313.5(9) | 5130.7(8) | 14.3(2) |
| C1 | 1288.7(14) | 1903.5(11) | 6086.3(9) | 13.6(2) |
| C2 | 2085.7(15) | 3112.0(11) | 3864.5(10) | 15.0(2) |

| | | | | |
|---|---|---|---|---|
| C3 | 3565.5(15) | 3434.6(11) | 4169.6(10) | 15.0(2) |
| C4 | 4270.5(16) | 3431.5(13) | 3556.3(10) | 19.9(3) |
| C5 | 3489.6(18) | 3054.0(15) | 2635.2(11) | 24.5(3) |
| C6 | 2031.7(18) | 2713.6(15) | 2335.9(11) | 24.3(3) |
| C7 | 1309.9(16) | 2750.4(13) | 2949.5(10) | 19.6(3) |
| C8 | 5446.0(14) | 3529.1(11) | 5629.8(9) | 14.6(2) |
| C9 | 6697.0(15) | 3904.4(12) | 5484.1(10) | 17.3(3) |
| C10 | 7916.8(15) | 3618.7(13) | 5955.8(11) | 19.5(3) |
| C11 | 7890.7(16) | 3016.8(13) | 6590.7(10) | 19.5(3) |
| C12 | 6640.0(15) | 2730.9(12) | 6745.5(10) | 17.4(3) |
| C13 | 71.4(15) | 2800.9(11) | 4394.4(9) | 14.8(2) |
| C14 | -885.8(16) | 3332.0(12) | 3929.6(10) | 17.2(3) |
| C15 | -2329.8(16) | 2908.2(12) | 3656.2(10) | 18.2(3) |
| C16 | -2825.5(16) | 1972.3(13) | 3873.6(11) | 19.8(3) |
| C17 | -1877.3(15) | 1458.6(12) | 4377.4(10) | 17.9(3) |
| C18 | -438.8(15) | 1862.7(11) | 4624.9(9) | 14.9(2) |
| C19 | 1458.4(15) | 1004.2(11) | 4681.2(10) | 14.5(2) |
| C20 | 903.1(16) | 330.0(12) | 3822.6(10) | 18.0(3) |
| C21 | 1822.4(18) | -43.5(12) | 3443.6(11) | 21.0(3) |
| C22 | 3276.3(17) | 253.4(13) | 3921.4(11) | 21.0(3) |
| C23 | 3752.5(16) | 926.4(12) | 4762.8(10) | 17.3(3) |
| C24 | 3036.7(16) | 2656.6(13) | 8519.8(10) | 18.4(3) |
| C25 | 2341.2(18) | 1592.4(14) | 8251.5(11) | 23.2(3) |
| C26 | 1729(2) | 1120.5(16) | 8802.1(13) | 31.4(4) |
| C27 | 1805(2) | 1713.6(18) | 9624.9(13) | 34.9(4) |
| C28 | 2501(2) | 2772.7(17) | 9899.9(12) | 32.1(4) |
| C29 | 3112.0(19) | 3246.5(15) | 9352.3(11) | 25.4(3) |
| C30 | 1687.1(16) | 4492.6(13) | 7607.4(10) | 19.1(3) |
| C31 | 3140.0(16) | 4561.8(12) | 7971.3(10) | 17.1(3) |
| C32 | 4014.1(18) | 5513.3(13) | 8532.8(11) | 21.9(3) |
| C33 | 3450(2) | 6384.4(14) | 8721.4(12) | 26.9(3) |
| C34 | 2007(2) | 6305.3(14) | 8361.8(11) | 25.3(3) |
| C35 | 1126.8(18) | 5354.1(14) | 7805.9(11) | 22.1(3) |
| C36 | 5668.5(16) | 3733.2(13) | 8386.1(10) | 20.0(3) |
| C37 | 6361.0(19) | 3153.4(18) | 8964.5(12) | 30.8(4) |
| C38 | 7834(2) | 3360(2) | 9294.9(14) | 44.3(6) |
| C39 | 8613(2) | 4165(2) | 9061.4(14) | 44.9(6) |
| C40 | 7932(2) | 4759.8(17) | 8503.6(14) | 36.8(5) |
| C41 | 6461.9(18) | 4541.6(14) | 8149.8(12) | 25.3(3) |

**Table C-24.** Anisotropic Displacement Parameters ($Å^2 \times 10^3$) for **4.9**. The Anisotropic displacement factor exponent takes the form: $-2\pi^2[h^2a^{*2}U_{11}+2hka^*b^*U_{12}+\ldots]$.

| **Atom** | **$U_{11}$** | **$U_{22}$** | **$U_{33}$** | **$U_{23}$** | **$U_{13}$** | **$U_{12}$** |
|---|---|---|---|---|---|---|
| Ir1 | 10.33(2) | 12.44(3) | 14.31(3) | 2.59(2) | 5.65(2) | 2.61(2) |
| Cl1 | 17.78(14) | 17.89(15) | 22.33(15) | 6.89(12) | 7.64(12) | 6.93(12) |
| P1 | 11.36(14) | 12.48(14) | 15.55(15) | 2.87(12) | 6.70(12) | 2.45(11) |

| | | | | | | |
|---|---|---|---|---|---|---|
| P2 | 12.09(14) | 16.46(16) | 14.60(15) | 2.38(12) | 5.55(12) | 1.97(12) |
| O1 | 19.4(5) | 14.6(5) | 20.7(5) | 3.4(4) | 10.3(4) | 4.5(4) |
| O2 | 14.4(5) | 21.2(5) | 20.6(5) | 2.4(4) | 9.6(4) | 3.4(4) |
| N1 | 12.0(5) | 16.9(5) | 16.2(5) | 3.9(4) | 7.3(4) | 3.5(4) |
| N2 | 11.3(5) | 17.2(5) | 15.6(5) | 3.8(4) | 6.1(4) | 2.5(4) |
| N3 | 12.2(5) | 13.8(5) | 17.3(5) | 2.9(4) | 5.9(4) | 3.1(4) |
| N4 | 12.4(5) | 15.6(5) | 17.1(5) | 2.1(4) | 6.4(4) | 2.9(4) |
| N5 | 13.3(5) | 12.6(5) | 17.5(5) | 2.0(4) | 6.5(4) | 3.5(4) |
| C1 | 11.5(5) | 12.8(5) | 16.0(6) | 2.6(4) | 5.0(5) | 1.2(4) |
| C2 | 15.1(6) | 14.6(6) | 17.6(6) | 5.0(5) | 8.3(5) | 3.6(5) |
| C3 | 14.4(6) | 14.8(6) | 17.4(6) | 4.4(5) | 7.4(5) | 3.2(5) |
| C4 | 16.6(6) | 26.2(7) | 20.2(7) | 5.9(6) | 10.4(5) | 5.5(5) |
| C5 | 24.2(7) | 33.0(9) | 20.4(7) | 6.0(6) | 13.7(6) | 5.9(6) |
| C6 | 24.2(7) | 32.3(8) | 16.3(6) | 3.2(6) | 8.8(6) | 5.1(6) |
| C7 | 16.9(6) | 23.6(7) | 17.7(6) | 4.4(5) | 6.0(5) | 2.9(5) |
| C8 | 11.8(5) | 14.6(6) | 17.0(6) | 1.0(5) | 6.3(5) | 1.8(5) |
| C9 | 13.9(6) | 18.0(6) | 20.4(6) | 2.4(5) | 8.7(5) | 1.0(5) |
| C10 | 12.8(6) | 23.4(7) | 21.9(7) | 1.0(5) | 8.3(5) | 2.0(5) |
| C11 | 12.9(6) | 23.8(7) | 21.2(7) | 1.5(5) | 6.3(5) | 5.2(5) |
| C12 | 13.5(6) | 19.3(6) | 18.9(6) | 2.2(5) | 5.5(5) | 4.4(5) |
| C13 | 12.9(5) | 15.7(6) | 16.6(6) | 3.2(5) | 6.6(5) | 3.0(5) |
| C14 | 16.1(6) | 18.1(6) | 20.0(6) | 6.6(5) | 8.1(5) | 5.3(5) |
| C15 | 15.2(6) | 22.2(7) | 18.7(6) | 4.8(5) | 6.7(5) | 6.8(5) |
| C16 | 13.0(6) | 22.7(7) | 22.3(7) | 3.0(5) | 5.7(5) | 3.1(5) |
| C17 | 14.3(6) | 15.5(6) | 22.8(7) | 3.0(5) | 6.5(5) | 1.5(5) |
| C18 | 13.3(6) | 15.1(6) | 16.3(6) | 2.5(5) | 5.5(5) | 3.4(5) |
| C19 | 14.5(6) | 12.7(6) | 17.5(6) | 3.6(5) | 6.7(5) | 3.4(5) |
| C20 | 18.6(6) | 15.3(6) | 18.0(6) | 0.8(5) | 5.6(5) | 2.6(5) |
| C21 | 23.8(7) | 18.3(7) | 20.6(7) | -0.4(5) | 9.4(6) | 5.3(6) |
| C22 | 22.0(7) | 20.4(7) | 22.5(7) | 1.0(5) | 10.8(6) | 7.7(6) |
| C23 | 16.4(6) | 17.9(6) | 20.8(6) | 3.7(5) | 9.7(5) | 6.6(5) |
| C24 | 15.6(6) | 23.4(7) | 17.5(6) | 6.5(5) | 7.1(5) | 3.6(5) |
| C25 | 23.2(7) | 24.4(7) | 23.2(7) | 6.2(6) | 11.2(6) | 2.0(6) |
| C26 | 32.8(9) | 31.1(9) | 32.0(9) | 10.4(7) | 16.1(8) | -1.0(7) |
| C27 | 36.6(10) | 43.0(11) | 27.7(9) | 11.5(8) | 18.3(8) | -1.5(8) |
| C28 | 36.7(10) | 39.6(10) | 21.3(7) | 6.0(7) | 15.8(7) | 1.6(8) |
| C29 | 27.2(8) | 29.1(8) | 18.9(7) | 3.6(6) | 10.0(6) | 1.0(6) |
| C30 | 16.6(6) | 22.1(7) | 19.3(6) | 3.8(5) | 7.8(5) | 4.0(5) |
| C31 | 17.9(6) | 19.0(6) | 15.5(6) | 2.8(5) | 8.3(5) | 3.4(5) |
| C32 | 20.9(7) | 21.9(7) | 20.0(7) | -1.4(5) | 6.8(6) | 3.6(6) |
| C33 | 30.1(8) | 22.2(7) | 24.0(7) | -3.5(6) | 8.1(7) | 5.2(6) |
| C34 | 31.4(8) | 24.2(8) | 22.2(7) | 1.8(6) | 10.9(6) | 12.1(7) |
| C35 | 22.3(7) | 26.6(8) | 20.6(7) | 5.5(6) | 9.7(6) | 9.8(6) |
| C36 | 14.5(6) | 26.3(7) | 16.3(6) | -1.1(5) | 5.6(5) | 2.0(5) |
| C37 | 19.4(7) | 52.4(12) | 21.5(7) | 10.8(7) | 6.2(6) | 9.8(7) |
| C38 | 21.6(8) | 82.5(18) | 26.3(9) | 10.0(10) | 2.7(7) | 18.9(10) |
| C39 | 14.4(7) | 74.9(17) | 29.9(9) | -14.6(10) | 3.9(7) | 1.1(9) |
| C40 | 21.5(8) | 38.5(10) | 40.1(10) | -17.1(8) | 16.9(8) | -7.8(7) |

| | | | | | | |
|---|---|---|---|---|---|---|
| C41 | 20.8(7) | 22.8(7) | 29.1(8) | -6.2(6) | 13.9(6) | -2.8(6) |

**Table C-25**. Bond Lengths for **4.9**.

| Atom | Atom | Length/Å | Atom | Atom | Length/Å |
|---|---|---|---|---|---|
| Ir1 | Cl1 | 2.4549(4) | C9 | C10 | 1.388(2) |
| Ir1 | P1 | 2.2466(4) | C10 | C11 | 1.388(2) |
| Ir1 | P2 | 2.3061(4) | C11 | C12 | 1.383(2) |
| Ir1 | N4 | 2.1991(12) | C13 | C14 | 1.392(2) |
| Ir1 | N5 | 2.0900(12) | C13 | C18 | 1.409(2) |
| Ir1 | C1 | 1.9885(14) | C14 | C15 | 1.392(2) |
| P1 | O1 | 1.4819(11) | C15 | C16 | 1.391(2) |
| P1 | N1 | 1.7385(12) | C16 | C17 | 1.397(2) |
| P1 | N2 | 1.7147(13) | C17 | C18 | 1.386(2) |
| P2 | C24 | 1.8388(15) | C19 | C20 | 1.398(2) |
| P2 | C31 | 1.8300(16) | C20 | C21 | 1.380(2) |
| P2 | C36 | 1.8206(16) | C21 | C22 | 1.399(2) |
| O2 | C1 | 1.2166(17) | C22 | C23 | 1.379(2) |
| N1 | C3 | 1.4237(18) | C24 | C25 | 1.393(2) |
| N1 | C8 | 1.4061(18) | C24 | C29 | 1.402(2) |
| N2 | C2 | 1.4055(18) | C25 | C26 | 1.395(2) |
| N2 | C13 | 1.4315(18) | C26 | C27 | 1.390(3) |
| N3 | C1 | 1.4695(18) | C27 | C28 | 1.387(3) |
| N3 | C18 | 1.4401(18) | C28 | C29 | 1.392(2) |
| N3 | C19 | 1.3894(18) | C30 | C31 | 1.400(2) |
| N4 | C8 | 1.3599(19) | C30 | C35 | 1.386(2) |
| N4 | C12 | 1.3533(19) | C31 | C32 | 1.395(2) |
| N5 | C19 | 1.3456(18) | C32 | C33 | 1.396(2) |
| N5 | C23 | 1.3542(18) | C33 | C34 | 1.388(3) |
| C2 | C3 | 1.406(2) | C34 | C35 | 1.394(2) |
| C2 | C7 | 1.389(2) | C36 | C37 | 1.391(3) |
| C3 | C4 | 1.387(2) | C36 | C41 | 1.404(2) |
| C4 | C5 | 1.400(2) | C37 | C38 | 1.397(3) |
| C5 | C6 | 1.387(2) | C38 | C39 | 1.390(4) |
| C6 | C7 | 1.400(2) | C39 | C40 | 1.382(4) |
| C8 | C9 | 1.3979(19) | C40 | C41 | 1.394(3) |

**Table C-26**. Bond Angles for **4.9**.

| Atom | Atom | Atom | Angle/° | Atom | Atom | Atom | Angle/° |
|---|---|---|---|---|---|---|---|
| P1 | Ir1 | Cl1 | 168.039(13) | C6 | C5 | C4 | 120.78(14) |
| P1 | Ir1 | P2 | 97.253(13) | C5 | C6 | C7 | 120.59(15) |
| P2 | Ir1 | Cl1 | 89.774(13) | C2 | C7 | C6 | 118.64(14) |
| N4 | Ir1 | Cl1 | 89.19(3) | N4 | C8 | N1 | 115.97(12) |
| N4 | Ir1 | P1 | 80.28(3) | N4 | C8 | C9 | 121.47(13) |
| N4 | Ir1 | P2 | 98.02(3) | C9 | C8 | N1 | 122.56(13) |
| N5 | Ir1 | Cl1 | 85.26(3) | C10 | C9 | C8 | 118.68(14) |

| | | | | | | | |
|---|---|---|---|---|---|---|---|
| N5 | Ir1 | P1 | 88.62(3) | C9 | C10 | C11 | 119.85(14) |
| N5 | Ir1 | P2 | 172.47(3) | C12 | C11 | C10 | 118.50(14) |
| N5 | Ir1 | N4 | 87.58(5) | N4 | C12 | C11 | 122.61(14) |
| C1 | Ir1 | Cl1 | 103.20(4) | C14 | C13 | N2 | 120.46(13) |
| C1 | Ir1 | P1 | 85.98(4) | C14 | C13 | C18 | 119.26(13) |
| C1 | Ir1 | P2 | 94.31(4) | C18 | C13 | N2 | 120.11(12) |
| C1 | Ir1 | N4 | 162.56(5) | C15 | C14 | C13 | 120.08(14) |
| C1 | Ir1 | N5 | 81.37(5) | C16 | C15 | C14 | 120.26(14) |
| O1 | P1 | Ir1 | 123.62(5) | C15 | C16 | C17 | 120.19(14) |
| O1 | P1 | N1 | 112.74(6) | C18 | C17 | C16 | 119.50(14) |
| O1 | P1 | N2 | 111.52(6) | C13 | C18 | N3 | 116.85(12) |
| N1 | P1 | Ir1 | 99.30(4) | C17 | C18 | N3 | 122.56(13) |
| N2 | P1 | Ir1 | 113.17(4) | C17 | C18 | C13 | 120.59(13) |
| N2 | P1 | N1 | 90.72(6) | N3 | C19 | C20 | 122.05(13) |
| C24 | P2 | Ir1 | 115.93(5) | N5 | C19 | N3 | 116.30(12) |
| C31 | P2 | Ir1 | 121.85(5) | N5 | C19 | C20 | 121.62(13) |
| C31 | P2 | C24 | 98.56(7) | C21 | C20 | C19 | 118.61(14) |
| C36 | P2 | Ir1 | 108.01(5) | C20 | C21 | C22 | 119.80(14) |
| C36 | P2 | C24 | 105.79(7) | C23 | C22 | C21 | 118.55(14) |
| C36 | P2 | C31 | 105.19(7) | N5 | C23 | C22 | 121.95(14) |
| C3 | N1 | P1 | 112.39(9) | C25 | C24 | P2 | 122.67(12) |
| C8 | N1 | P1 | 117.16(10) | C25 | C24 | C29 | 118.94(14) |
| C8 | N1 | C3 | 123.45(12) | C29 | C24 | P2 | 118.28(12) |
| C2 | N2 | P1 | 113.05(9) | C24 | C25 | C26 | 120.55(16) |
| C2 | N2 | C13 | 120.43(12) | C27 | C26 | C25 | 120.05(18) |
| C13 | N2 | P1 | 126.51(10) | C28 | C27 | C26 | 119.82(17) |
| C18 | N3 | C1 | 113.99(11) | C27 | C28 | C29 | 120.30(17) |
| C19 | N3 | C1 | 116.90(11) | C28 | C29 | C24 | 120.34(17) |
| C19 | N3 | C18 | 114.93(12) | C35 | C30 | C31 | 120.50(15) |
| C8 | N4 | Ir1 | 116.99(9) | C30 | C31 | P2 | 117.75(11) |
| C12 | N4 | Ir1 | 124.13(10) | C32 | C31 | P2 | 122.93(12) |
| C12 | N4 | C8 | 118.66(12) | C32 | C31 | C30 | 118.88(14) |
| C19 | N5 | Ir1 | 112.50(9) | C31 | C32 | C33 | 120.51(16) |
| C19 | N5 | C23 | 119.40(13) | C34 | C33 | C32 | 120.14(16) |
| C23 | N5 | Ir1 | 128.10(10) | C33 | C34 | C35 | 119.61(15) |
| O2 | C1 | Ir1 | 133.43(11) | C30 | C35 | C34 | 120.35(16) |
| O2 | C1 | N3 | 115.81(12) | C37 | C36 | P2 | 121.42(13) |
| N3 | C1 | Ir1 | 109.93(9) | C37 | C36 | C41 | 119.49(16) |
| N2 | C2 | C3 | 112.63(12) | C41 | C36 | P2 | 118.46(13) |
| C7 | C2 | N2 | 126.53(13) | C36 | C37 | C38 | 120.3(2) |
| C7 | C2 | C3 | 120.77(13) | C39 | C38 | C37 | 119.8(2) |
| C2 | C3 | N1 | 111.00(12) | C40 | C39 | C38 | 120.11(18) |
| C4 | C3 | N1 | 128.69(13) | C39 | C40 | C41 | 120.5(2) |
| C4 | C3 | C2 | 120.29(13) | C40 | C41 | C36 | 119.66(19) |
| C3 | C4 | C5 | 118.85(14) | | | | |

**Table C-27**. Torsion Angles for **4.9**.

| A | B | C | D | Angle/° | A | B | C | D | Angle/° |
|---|---|---|---|---|---|---|---|---|---|
| Ir1 | P1 | N1 | C3 | 117.95(9) | C8 | N1 | C3 | C2 | 145.91(13) |
| Ir1 | P1 | N1 | C8 | -33.85(11) | C8 | N1 | C3 | C4 | -32.4(2) |
| Ir1 | P1 | N2 | C2 | -104.18(10) | C8 | N4 | C12 | C11 | -2.1(2) |
| Ir1 | P1 | N2 | C13 | 74.53(12) | C8 | C9 | C10 | C11 | -3.3(2) |
| Ir1 | P2 | C24 | C25 | 3.36(16) | C9 | C10 | C11 | C12 | -1.0(2) |
| Ir1 | P2 | C24 | C29 | -172.74(11) | C10 | C11 | C12 | N4 | 3.8(2) |
| Ir1 | P2 | C31 | C30 | 58.72(13) | C12 | N4 | C8 | N1 | 177.34(13) |
| Ir1 | P2 | C31 | C32 | -128.94(12) | C12 | N4 | C8 | C9 | -2.4(2) |
| Ir1 | P2 | C36 | C37 | -96.15(14) | C13 | N2 | C2 | C3 | -176.55(12) |
| Ir1 | P2 | C36 | C41 | 74.72(13) | C13 | N2 | C2 | C7 | 0.4(2) |
| Ir1 | N4 | C8 | N1 | 2.53(16) | C13 | C14 | C15 | C16 | 2.3(2) |
| Ir1 | N4 | C8 | C9 | -177.24(11) | C14 | C13 | C18 | N3 | -178.15(13) |
| Ir1 | N4 | C12 | C11 | 172.32(11) | C14 | C13 | C18 | C17 | 1.3(2) |
| Ir1 | N5 | C19 | N3 | -4.37(15) | C14 | C15 | C16 | C17 | 0.8(2) |
| Ir1 | N5 | C19 | C20 | 177.63(11) | C15 | C16 | C17 | C18 | -2.8(2) |
| Ir1 | N5 | C23 | C22 | -178.18(11) | C16 | C17 | C18 | N3 | -178.83(14) |
| P1 | N1 | C3 | C2 | -3.83(15) | C16 | C17 | C18 | C13 | 1.8(2) |
| P1 | N1 | C3 | C4 | 177.91(13) | C18 | N3 | C1 | Ir1 | -119.98(11) |
| P1 | N1 | C8 | N4 | 22.83(16) | C18 | N3 | C1 | O2 | 51.03(17) |
| P1 | N1 | C8 | C9 | -157.39(11) | C18 | N3 | C19 | N5 | 128.64(13) |
| P1 | N2 | C2 | C3 | 2.25(15) | C18 | N3 | C19 | C20 | -53.36(18) |
| P1 | N2 | C2 | C7 | 179.22(13) | C18 | C13 | C14 | C15 | -3.3(2) |
| P1 | N2 | C13 | C14 | 115.82(14) | C19 | N3 | C1 | Ir1 | 18.03(14) |
| P1 | N2 | C13 | C18 | -69.00(17) | C19 | N3 | C1 | O2 | -170.97(13) |
| P2 | C24 | C25 | C26 | -176.06(14) | C19 | N3 | C18 | C13 | -63.47(17) |
| P2 | C24 | C29 | C28 | 176.31(15) | C19 | N3 | C18 | C17 | 117.12(15) |
| P2 | C31 | C32 | C33 | -172.85(13) | C19 | N5 | C23 | C22 | 2.6(2) |
| P2 | C36 | C37 | C38 | 169.60(16) | C19 | C20 | C21 | C22 | 0.2(2) |
| P2 | C36 | C41 | C40 | -171.65(13) | C20 | C21 | C22 | C23 | -0.6(2) |
| O1 | P1 | N1 | C3 | -109.45(10) | C21 | C22 | C23 | N5 | -0.8(2) |
| O1 | P1 | N1 | C8 | 98.75(11) | C23 | N5 | C19 | N3 | 174.96(13) |
| O1 | P1 | N2 | C2 | 111.12(10) | C23 | N5 | C19 | C20 | -3.0(2) |
| O1 | P1 | N2 | C13 | -70.16(13) | C24 | P2 | C31 | C30 | -69.16(13) |
| N1 | P1 | N2 | C2 | -3.74(11) | C24 | P2 | C31 | C32 | 103.18(14) |
| N1 | P1 | N2 | C13 | 174.97(12) | C24 | P2 | C36 | C37 | 28.58(16) |
| N1 | C3 | C4 | C5 | 175.04(15) | C24 | P2 | C36 | C41 | -160.55(12) |
| N1 | C8 | C9 | C10 | -174.69(13) | C24 | C25 | C26 | C27 | 0.2(3) |
| N2 | P1 | N1 | C3 | 4.32(10) | C25 | C24 | C29 | C28 | 0.1(3) |
| N2 | P1 | N1 | C8 | -147.48(11) | C25 | C26 | C27 | C28 | -0.6(3) |
| N2 | C2 | C3 | N1 | 1.03(17) | C26 | C27 | C28 | C29 | 0.6(3) |
| N2 | C2 | C3 | C4 | 179.46(13) | C27 | C28 | C29 | C24 | -0.4(3) |
| N2 | C2 | C7 | C6 | -176.75(15) | C29 | C24 | C25 | C26 | 0.0(3) |
| N2 | C13 | C14 | C15 | 171.90(13) | C30 | C31 | C32 | C33 | -0.6(2) |
| N2 | C13 | C18 | N3 | 6.62(19) | C31 | P2 | C24 | C25 | 135.16(14) |
| N2 | C13 | C18 | C17 | -173.97(13) | C31 | P2 | C24 | C29 | -40.93(14) |
| N3 | C19 | C20 | C21 | -176.24(14) | C31 | P2 | C36 | C37 | 132.30(14) |

| | | | | | | | | |
|---|---|---|---|---|---|---|---|---|
| N4 | C8 | C9 | C10 | 5.1(2) | C31 | P2 | C36 | C41 | -56.83(14) |
| N5 | C19 | C20 | C21 | 1.7(2) | C31 | C30 | C35 | C34 | 0.8(2) |
| C1 | N3 | C18 | C13 | 75.38(16) | C31 | C32 | C33 | C34 | 1.0(3) |
| C1 | N3 | C18 | C17 | -104.02(16) | C32 | C33 | C34 | C35 | -0.5(3) |
| C1 | N3 | C19 | N5 | -8.98(18) | C33 | C34 | C35 | C30 | -0.4(3) |
| C1 | N3 | C19 | C20 | 169.02(13) | C35 | C30 | C31 | P2 | 172.34(12) |
| C2 | N2 | C13 | C14 | -65.55(19) | C35 | C30 | C31 | C32 | -0.3(2) |
| C2 | N2 | C13 | C18 | 109.63(16) | C36 | P2 | C24 | C25 | -116.30(14) |
| C2 | C3 | C4 | C5 | -3.1(2) | C36 | P2 | C24 | C29 | 67.60(14) |
| C3 | N1 | C8 | N4 | -125.59(14) | C36 | P2 | C31 | C30 | -178.19(12) |
| C3 | N1 | C8 | C9 | 54.2(2) | C36 | P2 | C31 | C32 | -5.85(15) |
| C3 | C2 | C7 | C6 | 0.0(2) | C36 | C37 | C38 | C39 | 1.5(3) |
| C3 | C4 | C5 | C6 | 1.6(3) | C37 | C36 | C41 | C40 | -0.6(2) |
| C4 | C5 | C6 | C7 | 0.6(3) | C37 | C38 | C39 | C40 | 0.0(3) |
| C5 | C6 | C7 | C2 | -1.4(3) | C38 | C39 | C40 | C41 | -1.7(3) |
| C7 | C2 | C3 | N1 | -176.13(13) | C39 | C40 | C41 | C36 | 2.1(3) |
| C7 | C2 | C3 | C4 | 2.3(2) | C41 | C36 | C37 | C38 | -1.2(3) |

**Table C-28.** Hydrogen Atom Coordinates (Å×10$^4$) and Isotropic Displacement Parameters (Å$^2$×10$^3$) for **4.9.**

| Atom | *x* | *y* | *z* | U(eq) |
|---|---|---|---|---|
| H4 | 5265.95 | 3681.2 | 3757.91 | 24 |
| H5 | 3963.52 | 3030.6 | 2210.13 | 29 |
| H6 | 1518.74 | 2453.14 | 1708.94 | 29 |
| H7 | 309.96 | 2532.58 | 2744.34 | 24 |
| H9 | 6712.19 | 4346.21 | 5070.66 | 21 |
| H10 | 8767.23 | 3834.43 | 5844.32 | 23 |
| H11 | 8713.61 | 2806.24 | 6911.57 | 23 |
| H12 | 6633.17 | 2356.37 | 7205.29 | 21 |
| H14 | -553.11 | 3984.61 | 3798.81 | 21 |
| H15 | -2979.6 | 3259.31 | 3319.81 | 22 |
| H16 | -3811.9 | 1681.93 | 3678.76 | 24 |
| H17 | -2215.49 | 836.89 | 4549.19 | 21 |
| H20 | -86.57 | 132.97 | 3506.66 | 22 |
| H21 | 1469.38 | -500.71 | 2859.96 | 25 |
| H22 | 3920.93 | -3.15 | 3671.53 | 25 |
| H23 | 4737.2 | 1124.55 | 5094.42 | 21 |
| H25 | 2283.27 | 1184.36 | 7688.92 | 28 |
| H26 | 1259.36 | 393.37 | 8614.76 | 38 |
| H27 | 1380.53 | 1394.38 | 9997.59 | 42 |
| H28 | 2561.48 | 3176.37 | 10464.74 | 38 |
| H29 | 3582.36 | 3973.32 | 9543.41 | 31 |
| H30 | 1080.3 | 3850.27 | 7221.45 | 23 |
| H32 | 5000.97 | 5569.02 | 8788.8 | 26 |
| H33 | 4055.1 | 7032.82 | 9096.75 | 32 |
| H34 | 1621.22 | 6896 | 8493.83 | 30 |

| | | | | |
|---|---|---|---|---|
| H35 | 137.73 | 5295.82 | 7561.76 | 26 |
| H37 | 5829.41 | 2614.43 | 9135.71 | 37 |
| H38 | 8302.66 | 2950.77 | 9678.09 | 53 |
| H39 | 9614.67 | 4306.89 | 9285.88 | 54 |
| H40 | 8469.6 | 5321.82 | 8359.86 | 44 |
| H41 | 5999.53 | 4937.86 | 7750.79 | 30 |

**Structural Data for 4.11**

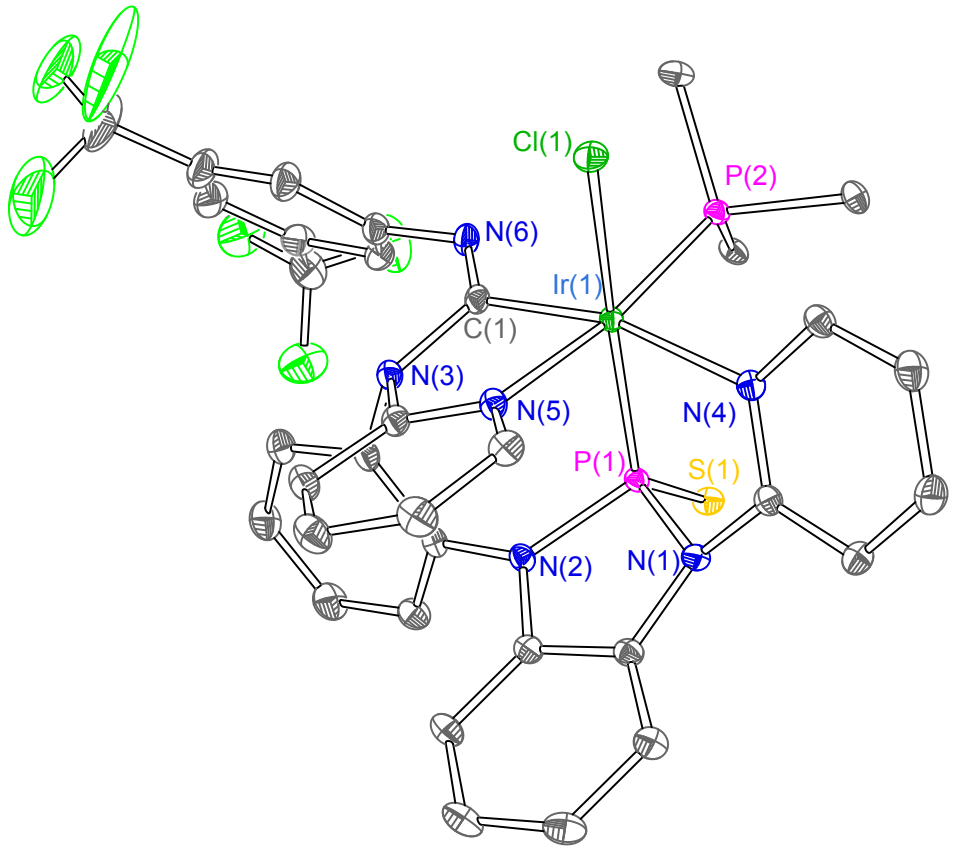

**Table C-29**. Crystal data and structure refinement for **4.11**.

| | |
|---|---|
| Identification code | IrNCS-a |
| Empirical formula | $C_{51}H_{38}Cl_5F_6IrN_6P_2S$ |
| Formula weight | 1312.32 |
| Temperature/K | 100.01 |
| Crystal system | monoclinic |
| Space group | C2/c |
| a/Å | 25.729(2) |
| b/Å | 10.4054(10) |
| c/Å | 40.467(4) |
| α/° | 90 |
| β/° | 91.937(2) |
| γ/° | 90 |
| Volume/Å$^3$ | 10827.4(18) |
| Z | 8 |
| $\rho_{calc}$g/cm$^3$ | 1.610 |
| μ/mm$^{-1}$ | 2.873 |
| F(000) | 5184.0 |
| Crystal size/mm$^3$ | 0.24 × 0.125 × 0.12 |
| Radiation | MoKα (λ = 0.71073) |
| 2Θ range for data collection/° | 3.696 to 64.176 |
| Index ranges | $-38 \le h \le 38$, $-15 \le k \le 15$, $-60 \le l \le 60$ |
| Reflections collected | 133466 |
| Independent reflections | 18816 [$R_{int}$ = 0.0457, $R_{sigma}$ = 0.0313] |
| Data/restraints/parameters | 18816/0/677 |
| Goodness-of-fit on $F^2$ | 1.083 |
| Final R indexes [I>=2σ (I)] | $R_1$ = 0.0300, $wR_2$ = 0.0577 |
| Final R indexes [all data] | $R_1$ = 0.0354, $wR_2$ = 0.0591 |
| Largest diff. peak/hole / e Å$^{-3}$ | 0.88/-1.82 |

**Table C-30.** Fractional Atomic Coordinates (×10$^4$) and Equivalent Isotropic Displacement Parameters (Å$^2$×10$^3$) for **4.11.** $U_{eq}$ is defined as 1/3 of of the trace of the orthogonalised $U_{IJ}$ tensor.

| **Atom** | ***x*** | ***y*** | ***z*** | **U(eq)** |
|---|---|---|---|---|
| Ir1 | 3777.9(2) | 4212.4(2) | 4228.3(2) | 8.95(2) |
| Cl1 | 4506.8(2) | 5690.4(5) | 4301.8(2) | 14.86(9) |
| S03 | 2942.0(2) | 1238.6(5) | 4194.6(2) | 13.36(9) |
| P1 | 3038.1(2) | 3077.9(5) | 4261.1(2) | 9.46(9) |
| P2 | 4362.4(2) | 2529.8(5) | 4161.3(2) | 10.68(9) |
| F1 | 2767.5(7) | 1993.4(18) | 2472.3(4) | 38.2(4) |
| F2 | 3324.3(7) | 2381.7(19) | 2104.0(4) | 40.1(4) |
| F3 | 3519.0(8) | 1110.0(17) | 2508.6(4) | 43.9(5) |
| N1 | 2860.3(6) | 3577.4(16) | 4654.0(4) | 11.1(3) |
| N2 | 2521.8(7) | 3903.8(16) | 4084.4(4) | 11.5(3) |
| N3 | 3181.9(7) | 5301.1(17) | 3681.1(4) | 12.3(3) |
| N4 | 3735.7(6) | 4104.2(16) | 4769.7(4) | 11.3(3) |
| N5 | 3306.4(7) | 5863.1(16) | 4239.1(4) | 11.8(3) |

| | | | | |
|---|---|---|---|---|
| N6 | 3851.0(7) | 3890.6(17) | 3505.8(4) | 14.4(3) |
| C1 | 2380.0(7) | 4252.0(19) | 4645.0(5) | 12.0(3) |
| C2 | 2192.9(8) | 4434.2(19) | 4317.6(5) | 12.2(4) |
| C3 | 1744.1(8) | 5141(2) | 4250.4(5) | 15.8(4) |
| C4 | 1478.0(8) | 5661(2) | 4512.3(6) | 19.3(4) |
| C5 | 1653.9(9) | 5454(2) | 4835.6(6) | 19.2(4) |
| C6 | 2104.8(8) | 4738(2) | 4905.6(5) | 15.4(4) |
| C7 | 2403.5(8) | 3970.3(19) | 3738.8(5) | 12.8(4) |
| C8 | 2720.2(8) | 4701(2) | 3533.3(5) | 14.0(4) |
| C9 | 2579.3(9) | 4856(2) | 3201.4(5) | 18.2(4) |
| C10 | 2130.6(9) | 4271(2) | 3071.8(6) | 22.0(5) |
| C11 | 1822.3(9) | 3539(2) | 3272.7(6) | 21.8(5) |
| C12 | 1957.3(8) | 3387(2) | 3605.0(5) | 16.8(4) |
| C13 | 3263.1(8) | 3816.8(19) | 4889.8(5) | 11.5(4) |
| C14 | 3185.0(8) | 3752(2) | 5227.7(5) | 14.1(4) |
| C15 | 3593.0(9) | 4049(2) | 5447.1(5) | 17.1(4) |
| C16 | 4075.6(9) | 4373(2) | 5325.7(5) | 16.7(4) |
| C17 | 4131.9(8) | 4372.5(19) | 4986.9(5) | 13.3(4) |
| C18 | 3064.7(8) | 6107.1(19) | 3945.2(5) | 12.6(4) |
| C19 | 2710.3(8) | 7122(2) | 3904.4(6) | 16.4(4) |
| C20 | 2602.7(9) | 7871(2) | 4173.9(6) | 18.8(4) |
| C21 | 2858.6(9) | 7622(2) | 4476.9(6) | 18.3(4) |
| C22 | 3212.4(8) | 6630(2) | 4499.4(5) | 14.7(4) |
| C23 | 3631.4(8) | 4442.6(19) | 3744.2(5) | 12.1(4) |
| C24 | 4327.8(8) | 1545(2) | 4802.9(5) | 14.8(4) |
| C25 | 4641.0(8) | 2103.0(19) | 4566.4(5) | 13.1(4) |
| C26 | 5147.9(8) | 2478(2) | 4661.0(5) | 16.0(4) |
| C27 | 5333.6(9) | 2282(2) | 4985.1(6) | 19.8(4) |
| C28 | 5020.8(9) | 1709(2) | 5215.4(6) | 20.6(5) |
| C29 | 4518.9(9) | 1332(2) | 5123.2(5) | 18.8(4) |
| C30 | 4935.5(8) | 2805(2) | 3912.9(5) | 15.2(4) |
| C31 | 5281.8(8) | 1769(2) | 3890.3(6) | 20.0(4) |
| C32 | 5706.4(9) | 1848(3) | 3688.8(6) | 27.3(5) |
| C33 | 5794.0(10) | 2953(3) | 3510.1(7) | 34.3(6) |
| C34 | 5456.2(11) | 3980(3) | 3531.2(7) | 31.2(6) |
| C35 | 5024.2(9) | 3912(2) | 3731.6(6) | 21.3(5) |
| C36 | 4155.1(8) | 1007.8(19) | 3966.6(5) | 13.4(4) |
| C37 | 4081.6(8) | -133(2) | 4139.7(5) | 15.0(4) |
| C38 | 3927.5(9) | -1251(2) | 3973.7(6) | 18.8(4) |
| C39 | 3847.1(9) | -1241(2) | 3634.0(6) | 20.5(5) |
| C40 | 3937.7(9) | -119(2) | 3456.9(6) | 20.3(4) |
| C41 | 4094.2(9) | 987(2) | 3621.9(6) | 17.4(4) |
| C42 | 3741.1(8) | 4125(2) | 3170.3(5) | 16.2(4) |
| C43 | 3561.3(8) | 3121(2) | 2968.9(5) | 17.3(4) |
| C44 | 3477.5(9) | 3313(2) | 2631.2(6) | 20.2(4) |
| C45 | 3570.6(10) | 4496(3) | 2487.9(6) | 25.2(5) |
| C46 | 3765.7(10) | 5487(3) | 2687.8(6) | 26.4(5) |
| C47 | 3855.2(9) | 5309(2) | 3025.8(6) | 21.5(5) |

| | | | | |
|---|---|---|---|---|
| C48 | 3275.7(10) | 2206(3) | 2429.5(6) | 27.5(5) |
| C49 | 3861.7(15) | 6783(4) | 2542.0(8) | 45.8(9) |
| F4A | 4043(3) | 6748(7) | 2242.4(16) | 63.7(19) |
| F5A | 3405(2) | 7466(6) | 2506.0(16) | 66.5(17) |
| F6A | 4164(5) | 7530(7) | 2730.9(16) | 83(4) |
| F4B | 4426(9) | 6970(30) | 2588(9) | 100(10) |
| F5B | 3710(20) | 7613(15) | 2631(13) | 170(20) |
| F6B | 3939(11) | 6630(20) | 2232(4) | 100(9) |
| Cl06 | 3085.7(3) | 4943.7(7) | 1499.6(2) | 34.50(15) |
| Cl08 | 2276.1(3) | 4308.3(8) | 1959.0(2) | 41.57(18) |
| C50 | 2483.7(12) | 5414(3) | 1663.2(8) | 38.4(7) |
| Cl07 | 4309.4(3) | 8249.4(8) | 1023.7(2) | 39.28(17) |
| Cl09 | 4762.6(5) | 7500.9(12) | 1665.9(2) | 67.4(3) |
| C51 | 4885.0(10) | 8009(3) | 1265.2(7) | 31.3(6) |

**Table C-31.** Anisotropic Displacement Parameters ($Å^2×10^3$) for **4.11**. The Anisotropic displacement factor exponent takes the form: $-2\pi^2[h^2a^{*2}U_{11}+2hka^*b^*U_{12}+\ldots]$.

| **Atom** | **$U_{11}$** | **$U_{22}$** | **$U_{33}$** | **$U_{23}$** | **$U_{13}$** | **$U_{12}$** |
|---|---|---|---|---|---|---|
| Ir1 | 8.94(3) | 8.37(3) | 9.45(3) | 0.48(3) | -1.04(2) | -0.83(3) |
| Cl1 | 13.4(2) | 13.9(2) | 17.2(2) | 0.07(18) | -1.09(16) | -4.78(18) |
| S03 | 13.4(2) | 10.1(2) | 16.7(2) | -1.99(18) | 1.41(18) | -2.02(18) |
| P1 | 8.3(2) | 9.3(2) | 10.7(2) | 0.23(17) | -0.69(17) | -0.45(17) |
| P2 | 9.3(2) | 10.4(2) | 12.3(2) | 0.38(18) | -0.76(17) | -0.56(18) |
| F1 | 34.6(9) | 48.0(11) | 31.8(9) | -7.5(8) | -2.8(7) | -14.0(8) |
| F2 | 50.2(10) | 55.3(11) | 14.7(7) | -8.8(7) | -0.4(7) | -6.3(9) |
| F3 | 59.3(12) | 32.7(9) | 38.3(10) | -12.9(8) | -18.5(9) | 8.2(8) |
| N1 | 10.0(7) | 12.1(8) | 11.1(8) | -1.0(6) | 0.5(6) | 0.2(6) |
| N2 | 11.0(7) | 12.9(8) | 10.4(7) | 0.1(6) | -1.7(6) | 1.0(6) |
| N3 | 12.8(8) | 11.9(8) | 11.9(8) | 1.2(6) | -1.8(6) | -0.1(6) |
| N4 | 11.8(7) | 10.3(8) | 11.8(7) | -0.5(6) | -0.9(6) | -0.7(6) |
| N5 | 12.8(7) | 8.7(7) | 13.9(8) | 0.7(6) | -1.7(6) | -1.2(6) |
| N6 | 17.1(8) | 15.0(8) | 11.1(8) | 2.3(6) | -0.3(6) | 1.2(7) |
| C1 | 10.5(8) | 10.7(8) | 14.8(9) | -0.3(7) | 0.2(7) | -0.8(7) |
| C2 | 11.4(8) | 9.5(9) | 15.8(9) | -0.3(7) | -0.1(7) | -1.0(7) |
| C3 | 12.0(9) | 16.4(10) | 18.8(10) | -1.3(8) | -3.3(7) | 1.8(8) |
| C4 | 13.3(9) | 19.4(11) | 25.1(11) | -4.4(9) | -1.6(8) | 4.9(8) |
| C5 | 15.7(10) | 20.8(11) | 21.4(11) | -5.4(8) | 3.7(8) | 1.3(8) |
| C6 | 14.3(9) | 15.8(10) | 16.2(10) | -1.2(8) | 0.2(7) | 0.6(8) |
| C7 | 13.9(9) | 12.0(9) | 12.2(9) | -0.1(7) | -2.2(7) | 2.3(7) |
| C8 | 13.9(9) | 12.4(9) | 15.3(9) | 1.1(7) | -4.2(7) | 0.7(7) |
| C9 | 18.8(10) | 20.6(11) | 14.9(10) | 2.4(8) | -2.6(8) | 1.3(8) |
| C10 | 23.6(11) | 27.1(12) | 14.7(10) | 0.7(9) | -7.8(8) | 0.1(10) |
| C11 | 19.6(10) | 25.4(12) | 19.9(11) | -2.3(9) | -7.7(8) | -2.0(9) |
| C12 | 14.7(9) | 17.6(10) | 18.0(10) | -2.1(8) | -2.5(8) | -1.0(8) |
| C13 | 12.2(8) | 9.7(8) | 12.5(9) | -0.3(7) | -0.1(7) | 0.7(7) |
| C14 | 15.5(9) | 14.4(9) | 12.5(9) | 0.6(7) | 0.9(7) | -1.2(8) |

| | | | | | | |
|---|---|---|---|---|---|---|
| C15 | 20.2(10) | 18.8(11) | 12.1(9) | 0.4(8) | -0.5(7) | 0.4(8) |
| C16 | 19.0(10) | 16.5(10) | 14.1(9) | -1.2(8) | -4.3(7) | -1.2(8) |
| C17 | 12.5(8) | 11.8(9) | 15.3(9) | -0.8(7) | -2.2(7) | 0.0(7) |
| C18 | 13.5(9) | 9.1(8) | 15.2(9) | 0.9(7) | -1.0(7) | -1.6(7) |
| C19 | 14.7(9) | 13.1(9) | 21.1(10) | 1.7(8) | -4.7(8) | -0.1(8) |
| C20 | 17.7(10) | 12.2(10) | 26.4(12) | -2.3(8) | -2.8(8) | 1.6(8) |
| C21 | 18.6(10) | 12.7(10) | 23.5(11) | -4.3(8) | -0.7(8) | -0.6(8) |
| C22 | 16.8(9) | 11.7(9) | 15.4(9) | -2.6(7) | 0.1(7) | -1.5(7) |
| C23 | 13.0(8) | 8.6(9) | 14.5(9) | 2.1(7) | -1.3(7) | -1.5(7) |
| C24 | 15.0(9) | 13.8(9) | 15.5(9) | -0.9(7) | -2.5(7) | 1.6(8) |
| C25 | 14.1(9) | 11.1(9) | 13.8(9) | -1.4(7) | -2.7(7) | 2.4(7) |
| C26 | 12.9(9) | 15.5(10) | 19.5(10) | -3.7(8) | -2.1(7) | 1.8(8) |
| C27 | 17.1(10) | 20.5(11) | 21.3(11) | -6.3(9) | -6.3(8) | 4.8(8) |
| C28 | 26.9(12) | 17.6(11) | 16.6(10) | -2.9(8) | -8.4(9) | 7.7(9) |
| C29 | 26.7(11) | 15.5(10) | 14.2(10) | 0.6(8) | -1.4(8) | 1.9(9) |
| C30 | 10.2(8) | 19.8(10) | 15.6(10) | -3.6(8) | 1.5(7) | -0.9(8) |
| C31 | 13.6(9) | 24.2(12) | 22.0(11) | -3.7(9) | -0.5(8) | 1.4(9) |
| C32 | 13.7(10) | 40.6(15) | 27.7(13) | -10.6(11) | 2.5(9) | 5.0(10) |
| C33 | 20.0(12) | 48.7(18) | 35.2(15) | -6.5(13) | 14.4(11) | -5.3(12) |
| C34 | 28.5(13) | 31.7(14) | 34.3(14) | 0.9(11) | 15.4(11) | -9.4(11) |
| C35 | 19.7(10) | 22.1(11) | 22.4(11) | -2.1(9) | 5.8(9) | -5.7(9) |
| C36 | 10.3(8) | 11.1(9) | 18.6(10) | -1.4(7) | -1.4(7) | 1.6(7) |
| C37 | 14.3(9) | 12.2(9) | 18.5(10) | -0.2(8) | 1.1(7) | -0.4(7) |
| C38 | 17.4(10) | 11.8(9) | 27.4(12) | -1.1(8) | 3.0(9) | -0.5(8) |
| C39 | 19.0(10) | 13.8(10) | 28.5(12) | -6.4(9) | -1.8(9) | -1.3(8) |
| C40 | 23.3(11) | 17.2(11) | 19.9(11) | -3.6(8) | -5.1(9) | 1.3(9) |
| C41 | 19.7(10) | 13.1(10) | 19.0(10) | 0.3(8) | -2.7(8) | 0.7(8) |
| C42 | 17.1(9) | 18.8(10) | 12.7(9) | 2.4(8) | 0.4(7) | 2.8(8) |
| C43 | 18.1(10) | 20.4(11) | 13.4(9) | 1.3(8) | 2.1(8) | 0.4(8) |
| C44 | 18.2(10) | 27.6(12) | 14.9(10) | -1.9(9) | -0.3(8) | -0.4(9) |
| C45 | 25.0(12) | 37.0(14) | 13.5(10) | 5.8(9) | -2.3(9) | -4.1(10) |
| C46 | 28.6(12) | 31.9(14) | 18.5(11) | 11.1(10) | -3.4(9) | -7.1(10) |
| C47 | 25.4(11) | 23.1(11) | 15.7(10) | 4.8(9) | -3.1(9) | -2.7(9) |
| C48 | 29.5(13) | 33.2(14) | 19.2(11) | -4.7(10) | -7.0(10) | 1.1(11) |
| C49 | 67(2) | 44(2) | 26.1(15) | 17.7(14) | -11.4(15) | -25.0(18) |
| F4A | 79(3) | 55(3) | 60(3) | 31(2) | 42(3) | 2(3) |
| F5A | 72(3) | 45(3) | 84(3) | 40(2) | 17(2) | 20(2) |
| F6A | 138(7) | 58(4) | 50(3) | 35(2) | -46(4) | -64(5) |
| F4B | 91(12) | 92(15) | 115(16) | 62(14) | -35(12) | -65(11) |
| F5B | 270(50) | 18(6) | 230(40) | 30(16) | 190(40) | 12(19) |
| F6B | 162(18) | 97(12) | 38(7) | 58(7) | -47(10) | -74(12) |
| Cl06 | 30.6(3) | 34.8(4) | 38.1(4) | 3.3(3) | 1.1(3) | 6.5(3) |
| Cl08 | 33.3(3) | 56.1(5) | 34.9(4) | 13.8(3) | -5.3(3) | 1.5(3) |
| C50 | 32.1(15) | 37.5(16) | 45.9(18) | 12.2(14) | 4.9(13) | 10.1(13) |
| Cl07 | 23.5(3) | 54.0(5) | 40.0(4) | -4.3(3) | -4.1(3) | -3.2(3) |
| Cl09 | 89.8(8) | 80.6(7) | 31.5(4) | 17.0(5) | 0.1(5) | -18.4(6) |
| C51 | 24.8(12) | 40.7(16) | 28.3(13) | 1.8(12) | 2.0(10) | 3.6(11) |

**Table C-32.** Bond Lengths for **4.11.**

| Atom | Atom | Length/Å | Atom | Atom | Length/Å |
|---|---|---|---|---|---|
| Ir1 | Cl1 | 2.4358(5) | C15 | C16 | 1.392(3) |
| Ir1 | P1 | 2.2476(5) | C16 | C17 | 1.384(3) |
| Ir1 | P2 | 2.3297(5) | C18 | C19 | 1.401(3) |
| Ir1 | N4 | 2.1999(17) | C19 | C20 | 1.376(3) |
| Ir1 | N5 | 2.1042(17) | C20 | C21 | 1.396(3) |
| Ir1 | C23 | 1.997(2) | C21 | C22 | 1.377(3) |
| S03 | P1 | 1.9473(7) | C24 | C25 | 1.398(3) |
| P1 | N1 | 1.7482(18) | C24 | C29 | 1.388(3) |
| P1 | N2 | 1.7175(17) | C25 | C26 | 1.402(3) |
| P2 | C25 | 1.822(2) | C26 | C27 | 1.395(3) |
| P2 | C30 | 1.835(2) | C27 | C28 | 1.386(3) |
| P2 | C36 | 1.840(2) | C28 | C29 | 1.389(3) |
| F1 | C48 | 1.343(3) | C30 | C31 | 1.404(3) |
| F2 | C48 | 1.340(3) | C30 | C35 | 1.389(3) |
| F3 | C48 | 1.335(3) | C31 | C32 | 1.387(3) |
| N1 | C1 | 1.420(3) | C32 | C33 | 1.381(4) |
| N1 | C13 | 1.407(3) | C33 | C34 | 1.382(4) |
| N2 | C2 | 1.402(3) | C34 | C35 | 1.400(3) |
| N2 | C7 | 1.423(3) | C36 | C37 | 1.394(3) |
| N3 | C8 | 1.453(3) | C36 | C41 | 1.399(3) |
| N3 | C18 | 1.399(3) | C37 | C38 | 1.395(3) |
| N3 | C23 | 1.477(3) | C38 | C39 | 1.383(3) |
| N4 | C13 | 1.358(3) | C39 | C40 | 1.394(3) |
| N4 | C17 | 1.352(2) | C40 | C41 | 1.384(3) |
| N5 | C18 | 1.347(3) | C42 | C43 | 1.394(3) |
| N5 | C22 | 1.350(3) | C42 | C47 | 1.399(3) |
| N6 | C23 | 1.271(3) | C43 | C44 | 1.390(3) |
| N6 | C42 | 1.399(3) | C44 | C45 | 1.385(4) |
| C1 | C2 | 1.407(3) | C44 | C48 | 1.495(3) |
| C1 | C6 | 1.386(3) | C45 | C46 | 1.393(4) |
| C2 | C3 | 1.388(3) | C46 | C47 | 1.392(3) |
| C3 | C4 | 1.391(3) | C46 | C49 | 1.496(4) |
| C4 | C5 | 1.386(3) | C49 | F4A | 1.314(6) |
| C5 | C6 | 1.400(3) | C49 | F5A | 1.375(7) |
| C7 | C8 | 1.407(3) | C49 | F6A | 1.324(5) |
| C7 | C12 | 1.392(3) | C49 | F4B | 1.470(18) |
| C8 | C9 | 1.389(3) | C49 | F5B | 1.022(18) |
| C9 | C10 | 1.392(3) | C49 | F6B | 1.28(2) |
| C10 | C11 | 1.384(3) | Cl06 | C50 | 1.774(3) |
| C11 | C12 | 1.386(3) | Cl08 | C50 | 1.756(3) |
| C13 | C14 | 1.391(3) | Cl07 | C51 | 1.764(3) |
| C14 | C15 | 1.386(3) | Cl09 | C51 | 1.744(3) |

**Table C-33**. Bond Angles for **4.11**.

| Atom | Atom | Atom | Angle/° | Atom | Atom | Atom | Angle/° |
|---|---|---|---|---|---|---|---|
| P1 | Ir1 | Cl1 | 167.041(18) | C17 | C16 | C15 | 118.30(19) |
| P1 | Ir1 | P2 | 99.41(2) | N4 | C17 | C16 | 122.84(19) |
| P2 | Ir1 | Cl1 | 89.505(19) | N3 | C18 | C19 | 121.18(19) |
| N4 | Ir1 | Cl1 | 88.54(5) | N5 | C18 | N3 | 117.15(18) |
| N4 | Ir1 | P1 | 81.02(5) | N5 | C18 | C19 | 121.67(19) |
| N4 | Ir1 | P2 | 97.55(5) | C20 | C19 | C18 | 118.7(2) |
| N5 | Ir1 | Cl1 | 85.65(5) | C19 | C20 | C21 | 119.3(2) |
| N5 | Ir1 | P1 | 86.41(5) | C22 | C21 | C20 | 119.2(2) |
| N5 | Ir1 | P2 | 172.19(5) | N5 | C22 | C21 | 121.8(2) |
| N5 | Ir1 | N4 | 88.47(6) | N3 | C23 | Ir1 | 111.28(14) |
| C23 | Ir1 | Cl1 | 99.39(6) | N6 | C23 | Ir1 | 128.04(15) |
| C23 | Ir1 | P1 | 89.35(6) | N6 | C23 | N3 | 120.51(18) |
| C23 | Ir1 | P2 | 94.42(6) | C29 | C24 | C25 | 120.8(2) |
| C23 | Ir1 | N4 | 165.70(7) | C24 | C25 | P2 | 119.93(15) |
| C23 | Ir1 | N5 | 80.36(7) | C24 | C25 | C26 | 118.75(19) |
| S03 | P1 | Ir1 | 127.72(3) | C26 | C25 | P2 | 120.78(17) |
| N1 | P1 | Ir1 | 98.38(6) | C27 | C26 | C25 | 120.1(2) |
| N1 | P1 | S03 | 112.46(6) | C28 | C27 | C26 | 120.4(2) |
| N2 | P1 | Ir1 | 110.94(6) | C27 | C28 | C29 | 119.8(2) |
| N2 | P1 | S03 | 109.97(6) | C24 | C29 | C28 | 120.2(2) |
| N2 | P1 | N1 | 90.42(8) | C31 | C30 | P2 | 116.07(17) |
| C25 | P2 | Ir1 | 108.32(7) | C35 | C30 | P2 | 124.65(17) |
| C25 | P2 | C30 | 103.42(10) | C35 | C30 | C31 | 119.1(2) |
| C25 | P2 | C36 | 105.96(10) | C32 | C31 | C30 | 120.5(2) |
| C30 | P2 | Ir1 | 118.70(7) | C33 | C32 | C31 | 120.2(2) |
| C30 | P2 | C36 | 97.27(10) | C32 | C33 | C34 | 119.8(2) |
| C36 | P2 | Ir1 | 121.19(7) | C33 | C34 | C35 | 120.7(3) |
| C1 | N1 | P1 | 112.19(13) | C30 | C35 | C34 | 119.7(2) |
| C13 | N1 | P1 | 117.39(13) | C37 | C36 | P2 | 124.05(16) |
| C13 | N1 | C1 | 123.37(17) | C37 | C36 | C41 | 118.40(19) |
| C2 | N2 | P1 | 113.13(13) | C41 | C36 | P2 | 117.47(16) |
| C2 | N2 | C7 | 121.91(17) | C36 | C37 | C38 | 120.6(2) |
| C7 | N2 | P1 | 124.76(14) | C39 | C38 | C37 | 120.2(2) |
| C8 | N3 | C23 | 115.84(16) | C38 | C39 | C40 | 119.7(2) |
| C18 | N3 | C8 | 112.19(17) | C41 | C40 | C39 | 120.0(2) |
| C18 | N3 | C23 | 114.73(16) | C40 | C41 | C36 | 121.0(2) |
| C13 | N4 | Ir1 | 116.28(13) | C43 | C42 | N6 | 119.3(2) |
| C17 | N4 | Ir1 | 125.11(14) | C43 | C42 | C47 | 119.0(2) |
| C17 | N4 | C13 | 118.50(17) | C47 | C42 | N6 | 121.4(2) |
| C18 | N5 | Ir1 | 112.63(13) | C44 | C43 | C42 | 120.3(2) |
| C18 | N5 | C22 | 119.20(18) | C43 | C44 | C48 | 117.8(2) |
| C22 | N5 | Ir1 | 128.13(14) | C45 | C44 | C43 | 121.0(2) |
| C23 | N6 | C42 | 125.25(19) | C45 | C44 | C48 | 121.2(2) |
| C2 | C1 | N1 | 111.12(17) | C44 | C45 | C46 | 118.6(2) |
| C6 | C1 | N1 | 128.85(18) | C45 | C46 | C49 | 119.9(2) |
| C6 | C1 | C2 | 120.00(19) | C47 | C46 | C45 | 121.1(2) |

| | | | | | | | |
|---|---|---|---|---|---|---|---|
| N2 | C2 | C1 | 112.68(17) | C47 | C46 | C49 | 118.9(3) |
| C3 | C2 | N2 | 126.44(19) | C46 | C47 | C42 | 119.9(2) |
| C3 | C2 | C1 | 120.77(19) | F1 | C48 | C44 | 112.2(2) |
| C2 | C3 | C4 | 119.0(2) | F2 | C48 | F1 | 105.8(2) |
| C5 | C4 | C3 | 120.4(2) | F2 | C48 | C44 | 112.9(2) |
| C4 | C5 | C6 | 121.0(2) | F3 | C48 | F1 | 106.2(2) |
| C1 | C6 | C5 | 118.8(2) | F3 | C48 | F2 | 107.1(2) |
| C8 | C7 | N2 | 119.89(18) | F3 | C48 | C44 | 112.1(2) |
| C12 | C7 | N2 | 120.49(19) | F4A | C49 | C46 | 114.0(4) |
| C12 | C7 | C8 | 119.49(19) | F4A | C49 | F5A | 104.2(4) |
| C7 | C8 | N3 | 118.09(18) | F4A | C49 | F6A | 109.2(6) |
| C9 | C8 | N3 | 122.10(19) | F5A | C49 | C46 | 110.8(4) |
| C9 | C8 | C7 | 119.80(19) | F6A | C49 | C46 | 113.7(3) |
| C8 | C9 | C10 | 120.0(2) | F6A | C49 | F5A | 104.0(7) |
| C11 | C10 | C9 | 120.3(2) | F4B | C49 | C46 | 104.0(8) |
| C10 | C11 | C12 | 120.2(2) | F5B | C49 | C46 | 123.5(10) |
| C11 | C12 | C7 | 120.3(2) | F5B | C49 | F4B | 104(2) |
| N4 | C13 | N1 | 116.37(17) | F5B | C49 | F6B | 121(3) |
| N4 | C13 | C14 | 121.57(18) | F6B | C49 | C46 | 108.0(11) |
| C14 | C13 | N1 | 122.05(18) | F6B | C49 | F4B | 87.4(15) |
| C15 | C14 | C13 | 119.2(2) | Cl08 | C50 | Cl06 | 111.31(16) |
| C14 | C15 | C16 | 119.6(2) | Cl09 | C51 | Cl07 | 112.54(16) |

**Table C-34.** Torsion Angles for **4.11**.

| **A** | **B** | **C** | **D** | **Angle/°** | **A** | **B** | **C** | **D** | **Angle/°** |
|---|---|---|---|---|---|---|---|---|---|
| Ir1 | P1 | N1 | C1 | 117.41(13) | C15 | C16 | C17 | N4 | 1.7(3) |
| Ir1 | P1 | N1 | C13 | -34.28(15) | C17 | N4 | C13 | N1 | 178.41(17) |
| Ir1 | P1 | N2 | C2 | -105.14(13) | C17 | N4 | C13 | C14 | -2.2(3) |
| Ir1 | P1 | N2 | C7 | 79.95(17) | C18 | N3 | C8 | C7 | -56.6(2) |
| Ir1 | P2 | C25 | C24 | 67.57(17) | C18 | N3 | C8 | C9 | 121.7(2) |
| Ir1 | P2 | C25 | C26 | -103.90(17) | C18 | N3 | C23 | Ir1 | 20.9(2) |
| Ir1 | P2 | C30 | C31 | 178.02(14) | C18 | N3 | C23 | N6 | -163.56(19) |
| Ir1 | P2 | C30 | C35 | -6.8(2) | C18 | N5 | C22 | C21 | 2.9(3) |
| Ir1 | P2 | C36 | C37 | -105.74(17) | C18 | C19 | C20 | C21 | 1.7(3) |
| Ir1 | P2 | C36 | C41 | 77.66(18) | C19 | C20 | C21 | C22 | -0.1(3) |
| Ir1 | N4 | C13 | N1 | 2.2(2) | C20 | C21 | C22 | N5 | -2.2(3) |
| Ir1 | N4 | C13 | C14 | -178.42(15) | C22 | N5 | C18 | N3 | 178.81(18) |
| Ir1 | N4 | C17 | C16 | 175.56(15) | C22 | N5 | C18 | C19 | -1.3(3) |
| Ir1 | N5 | C18 | N3 | -3.5(2) | C23 | N3 | C8 | C7 | 77.7(2) |
| Ir1 | N5 | C18 | C19 | 176.42(16) | C23 | N3 | C8 | C9 | -103.9(2) |
| Ir1 | N5 | C22 | C21 | -174.36(16) | C23 | N3 | C18 | N5 | -11.3(3) |
| S03 | P1 | N1 | C1 | -105.71(13) | C23 | N3 | C18 | C19 | 168.83(18) |
| S03 | P1 | N1 | C13 | 102.61(14) | C23 | N6 | C42 | C43 | -119.7(2) |
| S03 | P1 | N2 | C2 | 108.15(13) | C23 | N6 | C42 | C47 | 66.6(3) |
| S03 | P1 | N2 | C7 | -66.76(17) | C24 | C25 | C26 | C27 | 0.6(3) |
| P1 | N1 | C1 | C2 | -4.8(2) | C25 | P2 | C30 | C31 | 58.09(18) |

| | | | | | | | | | |
|---|---|---|---|---|---|---|---|---|---|
| P1 | N1 | C1 | C6 | 176.77(18) | C25 | P2 | C30 | C35 | -126.8(2) |
| P1 | N1 | C13 | N4 | 23.5(2) | C25 | P2 | C36 | C37 | 18.0(2) |
| P1 | N1 | C13 | C14 | -155.87(17) | C25 | P2 | C36 | C41 | -158.61(16) |
| P1 | N2 | C2 | C1 | 4.4(2) | C25 | C24 | C29 | C28 | 2.0(3) |
| P1 | N2 | C2 | C3 | -179.43(17) | C25 | C26 | C27 | C28 | 0.4(3) |
| P1 | N2 | C7 | C8 | -71.8(2) | C26 | C27 | C28 | C29 | -0.2(3) |
| P1 | N2 | C7 | C12 | 112.5(2) | C27 | C28 | C29 | C24 | -1.0(3) |
| P2 | C25 | C26 | C27 | 172.22(17) | C29 | C24 | C25 | P2 | -173.49(17) |
| P2 | C30 | C31 | C32 | 175.24(18) | C29 | C24 | C25 | C26 | -1.8(3) |
| P2 | C30 | C35 | C34 | -175.3(2) | C30 | P2 | C25 | C24 | -165.63(17) |
| P2 | C36 | C37 | C38 | -179.51(16) | C30 | P2 | C25 | C26 | 22.9(2) |
| P2 | C36 | C41 | C40 | -179.77(18) | C30 | P2 | C36 | C37 | 124.24(19) |
| N1 | P1 | N2 | C2 | -6.00(15) | C30 | P2 | C36 | C41 | -52.36(18) |
| N1 | P1 | N2 | C7 | 179.09(17) | C30 | C31 | C32 | C33 | 0.5(4) |
| N1 | C1 | C2 | N2 | 0.4(2) | C31 | C30 | C35 | C34 | -0.3(3) |
| N1 | C1 | C2 | C3 | -176.06(18) | C31 | C32 | C33 | C34 | -0.3(4) |
| N1 | C1 | C6 | C5 | 175.5(2) | C32 | C33 | C34 | C35 | -0.1(4) |
| N1 | C13 | C14 | C15 | -177.43(19) | C33 | C34 | C35 | C30 | 0.4(4) |
| N2 | P1 | N1 | C1 | 6.17(15) | C35 | C30 | C31 | C32 | -0.2(3) |
| N2 | P1 | N1 | C13 | -145.52(15) | C36 | P2 | C25 | C24 | -63.88(19) |
| N2 | C2 | C3 | C4 | -176.4(2) | C36 | P2 | C25 | C26 | 124.64(17) |
| N2 | C7 | C8 | N3 | 4.0(3) | C36 | P2 | C30 | C31 | -50.30(18) |
| N2 | C7 | C8 | C9 | -174.44(19) | C36 | P2 | C30 | C35 | 124.8(2) |
| N2 | C7 | C12 | C11 | 174.9(2) | C36 | C37 | C38 | C39 | 0.2(3) |
| N3 | C8 | C9 | C10 | -179.4(2) | C37 | C36 | C41 | C40 | 3.4(3) |
| N3 | C18 | C19 | C20 | 178.9(2) | C37 | C38 | C39 | C40 | 2.2(3) |
| N4 | C13 | C14 | C15 | 3.2(3) | C38 | C39 | C40 | C41 | -1.7(4) |
| N5 | C18 | C19 | C20 | -1.0(3) | C39 | C40 | C41 | C36 | -1.2(3) |
| N6 | C42 | C43 | C44 | -176.4(2) | C41 | C36 | C37 | C38 | -2.9(3) |
| N6 | C42 | C47 | C46 | 176.7(2) | C42 | N6 | C23 | Ir1 | -177.84(16) |
| C1 | N1 | C13 | N4 | -124.7(2) | C42 | N6 | C23 | N3 | 7.4(3) |
| C1 | N1 | C13 | C14 | 55.9(3) | C42 | C43 | C44 | C45 | 0.1(4) |
| C1 | C2 | C3 | C4 | -0.5(3) | C42 | C43 | C44 | C48 | -179.0(2) |
| C2 | N2 | C7 | C8 | 113.7(2) | C43 | C42 | C47 | C46 | 3.0(4) |
| C2 | N2 | C7 | C12 | -62.0(3) | C43 | C44 | C45 | C46 | 1.9(4) |
| C2 | C1 | C6 | C5 | -2.7(3) | C43 | C44 | C48 | F1 | 75.3(3) |
| C2 | C3 | C4 | C5 | -1.2(3) | C43 | C44 | C48 | F2 | -165.1(2) |
| C3 | C4 | C5 | C6 | 0.9(4) | C43 | C44 | C48 | F3 | -44.1(3) |
| C4 | C5 | C6 | C1 | 1.1(3) | C44 | C45 | C46 | C47 | -1.4(4) |
| C6 | C1 | C2 | N2 | 178.91(18) | C44 | C45 | C46 | C49 | -178.9(3) |
| C6 | C1 | C2 | C3 | 2.5(3) | C45 | C44 | C48 | F1 | -103.7(3) |
| C7 | N2 | C2 | C1 | 179.46(18) | C45 | C44 | C48 | F2 | 15.8(3) |
| C7 | N2 | C2 | C3 | -4.4(3) | C45 | C44 | C48 | F3 | 136.9(3) |
| C7 | C8 | C9 | C10 | -1.1(3) | C45 | C46 | C47 | C42 | -1.0(4) |
| C8 | N3 | C18 | N5 | 123.65(19) | C45 | C46 | C49 | F4A | -37.6(6) |
| C8 | N3 | C18 | C19 | -56.3(3) | C45 | C46 | C49 | F5A | 79.6(5) |
| C8 | N3 | C23 | Ir1 | -112.34(16) | C45 | C46 | C49 | F6A | -163.7(8) |
| C8 | N3 | C23 | N6 | 63.2(3) | C45 | C46 | C49 | F4B | -117.2(19) |

| | | | | | | | | | |
|---|---|---|---|---|---|---|---|---|---|
| C8 | C7 | C12 | C11 | -0.8(3) | C45 | C46 | C49 | F5B | 125(5) |
| C8 | C9 | C10 | C11 | 0.3(4) | C45 | C46 | C49 | F6B | -25.3(14) |
| C9 | C10 | C11 | C12 | 0.2(4) | C47 | C42 | C43 | C44 | -2.5(3) |
| C10 | C11 | C12 | C7 | 0.0(4) | C47 | C46 | C49 | F4A | 144.9(5) |
| C12 | C7 | C8 | N3 | 179.75(19) | C47 | C46 | C49 | F5A | -97.9(4) |
| C12 | C7 | C8 | C9 | 1.4(3) | C47 | C46 | C49 | F6A | 18.8(9) |
| C13 | N1 | C1 | C2 | 144.87(19) | C47 | C46 | C49 | F4B | 65(2) |
| C13 | N1 | C1 | C6 | -33.5(3) | C47 | C46 | C49 | F5B | -52(5) |
| C13 | N4 | C17 | C16 | -0.3(3) | C47 | C46 | C49 | F6B | 157.2(13) |
| C13 | C14 | C15 | C16 | -1.7(3) | C48 | C44 | C45 | C46 | -179.1(2) |
| C14 | C15 | C16 | C17 | -0.7(3) | C49 | C46 | C47 | C42 | 176.5(3) |

**Table C-35.** Hydrogen Atom Coordinates (Å×10$^4$) and Isotropic Displacement Parameters (Å$^2$×10$^3$) for **4.11.**

| Atom | *x* | *y* | *z* | U(eq) |
|---|---|---|---|---|
| H3 | 1620.64 | 5267.02 | 4028.93 | 19 |
| H4 | 1173.96 | 6159.64 | 4469.5 | 23 |
| H5 | 1465.54 | 5804.73 | 5012.34 | 23 |
| H6 | 2220.08 | 4588.28 | 5127.79 | 19 |
| H9 | 2789.07 | 5361.25 | 3062.87 | 22 |
| H10 | 2035.71 | 4374.85 | 2844.4 | 26 |
| H11 | 1517.25 | 3139.16 | 3182.72 | 26 |
| H12 | 1744.36 | 2882.92 | 3741.84 | 20 |
| H14 | 2856.25 | 3507.22 | 5307.33 | 17 |
| H15 | 3543.5 | 4032.25 | 5678.62 | 20 |
| H16 | 4359.06 | 4588.21 | 5471.8 | 20 |
| H17 | 4463.12 | 4569.19 | 4903.2 | 16 |
| H19 | 2547.43 | 7289.51 | 3694.63 | 20 |
| H20 | 2356.84 | 8549.86 | 4153.97 | 23 |
| H21 | 2789.49 | 8131.24 | 4665.33 | 22 |
| H22 | 3395.3 | 6481.9 | 4703.66 | 18 |
| H24 | 3980.19 | 1309.79 | 4743.81 | 18 |
| H26 | 5365.2 | 2867 | 4504.29 | 19 |
| H27 | 5676.55 | 2542.87 | 5048.36 | 24 |
| H28 | 5149.41 | 1574.83 | 5435.47 | 25 |
| H29 | 4305.72 | 927.09 | 5279.62 | 23 |
| H31 | 5225.07 | 1008.8 | 4013.84 | 24 |
| H32 | 5937.33 | 1139.45 | 3673.72 | 33 |
| H33 | 6085.84 | 3006.9 | 3373.09 | 41 |
| H34 | 5517.92 | 4739.6 | 3408.44 | 37 |
| H35 | 4792.6 | 4620.66 | 3743.44 | 26 |
| H37 | 4136.99 | -147.85 | 4372.96 | 18 |
| H38 | 3877.63 | -2022.25 | 4094.33 | 23 |
| H39 | 3730.71 | -1995.31 | 3521.94 | 25 |
| H40 | 3891.94 | -113.63 | 3222.99 | 24 |
| H41 | 4161.41 | 1744.11 | 3499.13 | 21 |
| H43 | 3495.65 | 2302.99 | 3062.78 | 21 |
| H45 | 3502.81 | 4629.32 | 2258.21 | 30 |
| H47 | 3993.5 | 5989.88 | 3158.09 | 26 |
| H50A | 2521.59 | 6272.61 | 1766.37 | 46 |
| H50B | 2217.69 | 5477.04 | 1481.37 | 46 |
| H51A | 5102.21 | 7358.79 | 1156.75 | 38 |
| H51B | 5083.97 | 8823.54 | 1276.26 | 38 |

**Structural Data for 4.20.**

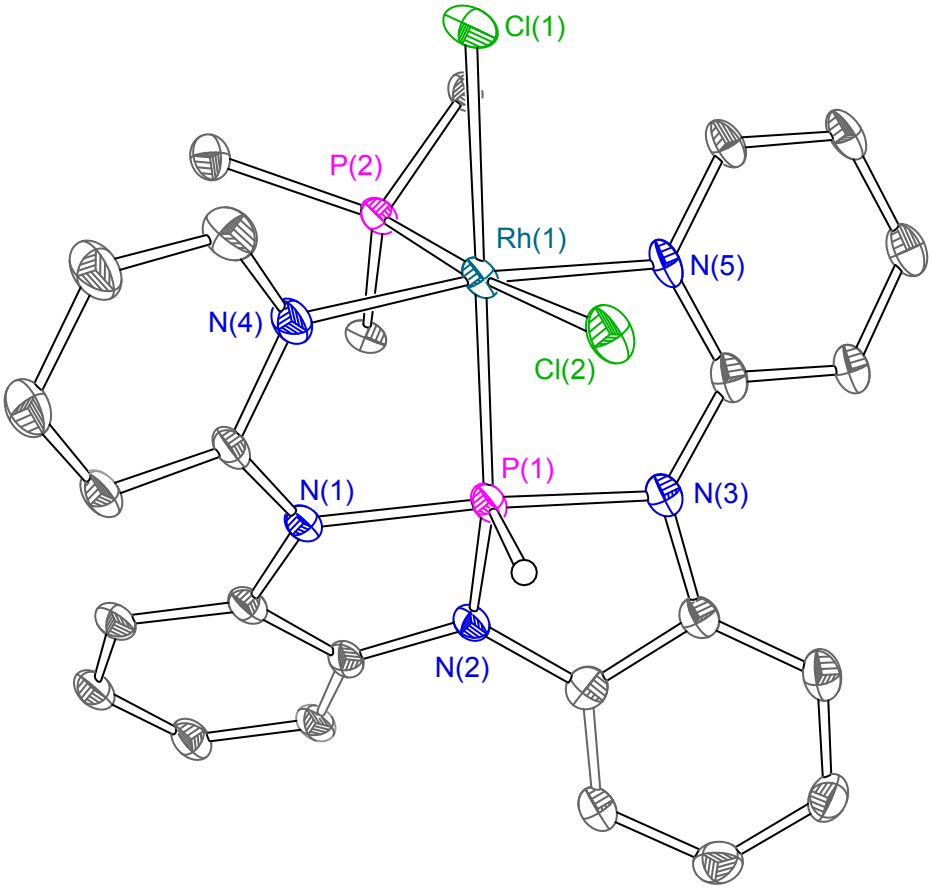

**Table C-36.** Crystal data and structure refinement for **4.20**.

| | |
|---|---|
| Identification code | RhHCl |
| Empirical formula | $C_{35.37}H_{28.63}Cl_{6.74}N_{4.21}P_{1.68}Rh_{0.84}$ |
| Formula weight | 890.27 |
| Temperature/K | 100.0 |
| Crystal system | monoclinic |
| Space group | $P2_1/c$ |
| a/Å | 16.4519(6) |
| b/Å | 18.5264(6) |
| c/Å | 57.365(2) |
| α/° | 90 |
| β/° | 97.0540(10) |
| γ/° | 90 |
| Volume/Å$^3$ | 17352.2(11) |
| Z | 19 |
| $\rho_{calc}$g/cm$^3$ | 1.619 |
| μ/mm$^{-1}$ | 0.999 |
| F(000) | 8512.0 |
| Crystal size/mm$^3$ | 0.05 × 0.045 × 0.035 |
| Radiation | MoKα (λ = 0.71073) |
| 2Θ range for data collection/° | 2.312 to 56.762 |
| Index ranges | $-21 \leq h \leq 21$, $-24 \leq k \leq 24$, $-76 \leq l \leq 76$ |
| Reflections collected | 554747 |
| Independent reflections | 43291 [$R_{int}$ = 0.1427, $R_{sigma}$ = 0.0671] |
| Data/restraints/parameters | 43291/0/2115 |
| Goodness-of-fit on $F^2$ | 1.046 |
| Final R indexes [I>=2σ (I)] | $R_1$ = 0.0607, $wR_2$ = 0.1314 |
| Final R indexes [all data] | $R_1$ = 0.1025, $wR_2$ = 0.1515 |
| Largest diff. peak/hole / e Å$^{-3}$ | 1.80/-1.64 |

**Table C-37.** Fractional Atomic Coordinates (×10$^4$) and Equivalent Isotropic Displacement Parameters (Å$^2$×10$^3$) for **4.20** $U_{eq}$ is defined as 1/3 of of the trace of the orthogonalised $U_{IJ}$ tensor**.**

| Atom | *x* | *y* | *z* | U(eq) |
|---|---|---|---|---|
| Rh1 | -4293.3(2) | 16343.1(2) | 1923.6(2) | 14.39(8) |
| Cl1 | -3750.9(8) | 16170.5(7) | 1544.0(2) | 22.4(3) |
| Cl2 | -4015.5(8) | 17607.3(7) | 1887.7(2) | 22.1(3) |
| P1 | -4844.2(8) | 16678.3(7) | 2245.1(2) | 14.6(2) |
| P2 | -4474.2(8) | 15094.0(7) | 1948.4(2) | 15.3(3) |
| N1 | -5885(2) | 16454(2) | 2111.7(7) | 16.4(9) |
| N2 | -5201(2) | 16423(2) | 2503.4(7) | 15.4(8) |
| N3 | -3839(3) | 16764(2) | 2426.5(7) | 16.3(9) |
| N4 | -5452(3) | 16544(2) | 1747.0(8) | 18.1(9) |
| N5 | -3179(2) | 16289(2) | 2125.4(8) | 16.5(9) |
| C1 | -6383(3) | 16129(3) | 2262.0(9) | 15.8(10) |
| C2 | -7140(3) | 15784(3) | 2206.9(10) | 19.8(11) |
| C3 | -7467(3) | 15424(3) | 2384.6(10) | 21.2(11) |

| | | | | |
|---|---|---|---|---|
| C4 | -7071(3) | 15396(3) | 2611.2(10) | 20.8(11) |
| C5 | -6309(3) | 15726(3) | 2665.3(10) | 18.7(10) |
| C6 | -5980(3) | 16102(3) | 2489.8(9) | 16.0(10) |
| C7 | -4743(3) | 16707(3) | 2704.6(9) | 17.7(10) |
| C8 | -5015(3) | 16851(3) | 2918.5(9) | 21.1(11) |
| C9 | -4500(4) | 17213(3) | 3090.8(10) | 25.9(12) |
| C10 | -3727(3) | 17426(3) | 3048.4(10) | 26.2(12) |
| C11 | -3448(3) | 17295(3) | 2832.0(10) | 22.5(11) |
| C12 | -3950(3) | 16916(3) | 2661.6(9) | 16.5(10) |
| C13 | -6085(3) | 16579(3) | 1877.2(9) | 16.7(10) |
| C14 | -6873(3) | 16761(3) | 1773.3(10) | 18.7(11) |
| C15 | -7011(3) | 16912(3) | 1538.0(10) | 24.9(12) |
| C16 | -6346(3) | 16891(3) | 1406.9(10) | 27.7(13) |
| C17 | -5583(3) | 16713(3) | 1516.9(10) | 23.8(12) |
| C18 | -3125(3) | 16535(3) | 2349.8(9) | 17.7(10) |
| C19 | -2354(3) | 16527(3) | 2491.0(10) | 20.2(11) |
| C20 | -1670(3) | 16280(3) | 2399.9(10) | 22.0(11) |
| C21 | -1732(3) | 16048(3) | 2167.6(10) | 21.9(11) |
| C22 | -2495(3) | 16062(3) | 2037.0(10) | 18.2(10) |
| C23 | -5246(3) | 14728(3) | 1721.3(9) | 19.3(11) |
| C24 | -6061(3) | 14930(3) | 1726.2(11) | 25.5(12) |
| C25 | -6685(3) | 14660(3) | 1562.4(11) | 30.3(13) |
| C26 | -6482(4) | 14159(4) | 1396.5(11) | 32.7(14) |
| C27 | -5686(4) | 13946(4) | 1394.9(11) | 34.9(15) |
| C28 | -5067(3) | 14224(3) | 1555.6(10) | 27.3(13) |
| C29 | -3533(3) | 14584(3) | 1927.9(9) | 17.4(10) |
| C30 | -3148(3) | 14201(3) | 2121.8(9) | 19.9(11) |
| C31 | -2422(3) | 13836(3) | 2107.8(10) | 22.2(11) |
| C32 | -2059(3) | 13839(3) | 1902.6(10) | 22.4(11) |
| C33 | -2428(3) | 14216(3) | 1709.5(10) | 22.2(11) |
| C34 | -3150(3) | 14579(3) | 1722.3(10) | 20.0(11) |
| C35 | -4806(3) | 14739(3) | 2218.2(9) | 17.0(10) |
| C36 | -5367(3) | 14165(3) | 2216.3(10) | 21.5(11) |
| C37 | -5560(3) | 13879(3) | 2423.0(10) | 21.1(11) |
| C38 | -5208(3) | 14143(3) | 2638.0(10) | 21.1(11) |
| C39 | -4637(3) | 14695(3) | 2645.1(9) | 19.7(11) |
| C40 | -4434(3) | 14990(3) | 2436.3(9) | 17.4(10) |
| Rh2 | 3468.5(2) | 8436.8(2) | 4251.5(2) | 14.95(8) |
| Cl3 | 3866.2(8) | 8657.6(7) | 3856.7(2) | 21.0(3) |
| Cl4 | 3495.5(8) | 7184.4(7) | 4143.7(2) | 21.6(3) |
| P3 | 3024.7(8) | 8034.8(7) | 4584.3(2) | 15.7(3) |
| P4 | 3464.8(8) | 9668.5(7) | 4325.0(2) | 15.8(3) |
| N6 | 4062(3) | 7803(2) | 4723.5(8) | 19.1(9) |
| N7 | 2831(3) | 8205(2) | 4868.7(7) | 16.8(9) |
| N8 | 1982(3) | 8361(2) | 4503.8(7) | 17.3(9) |
| N9 | 4646(3) | 8292(2) | 4411.8(8) | 18.1(9) |
| N10 | 2236(3) | 8472(2) | 4116.8(7) | 15.3(8) |
| C41 | 4029(3) | 7545(3) | 4954.0(9) | 21.4(11) |

| | | | | |
|---|---|---|---|---|
| C42 | 4537(4) | 7058(3) | 5084.4(10) | 26.2(12) |
| C43 | 4339(4) | 6844(3) | 5304.4(11) | 31.2(14) |
| C44 | 3649(4) | 7101(3) | 5388.8(10) | 28.9(13) |
| C45 | 3114(4) | 7568(3) | 5254.9(10) | 23.8(12) |
| C46 | 3307(3) | 7792(3) | 5037.9(9) | 19.3(11) |
| C47 | 2101(3) | 8574(3) | 4900.0(9) | 18.9(10) |
| C48 | 1883(3) | 8877(3) | 5103.8(10) | 23.0(11) |
| C49 | 1164(4) | 9271(3) | 5092.8(10) | 25.7(12) |
| C50 | 684(4) | 9371(3) | 4880.4(11) | 27.1(12) |
| C51 | 903(3) | 9081(3) | 4673.9(10) | 21.7(11) |
| C52 | 1611(3) | 8666(3) | 4685.4(9) | 17.8(10) |
| C53 | 4757(3) | 7991(3) | 4629.3(10) | 20.0(11) |
| C54 | 5553(3) | 7910(3) | 4746.9(10) | 23.5(12) |
| C55 | 6220(3) | 8093(3) | 4634.6(10) | 23.7(12) |
| C56 | 6100(3) | 8355(3) | 4407.2(11) | 24.4(12) |
| C57 | 5305(3) | 8459(3) | 4303.0(10) | 20.6(11) |
| C58 | 1675(3) | 8387(3) | 4269.6(9) | 17.1(10) |
| C59 | 838(3) | 8308(3) | 4190.1(9) | 19.3(11) |
| C60 | 573(3) | 8381(3) | 3953.0(10) | 23.8(12) |
| C61 | 1145(3) | 8510(3) | 3801.0(10) | 23.6(12) |
| C62 | 1961(3) | 8527(3) | 3886.6(9) | 20.1(11) |
| C63 | 4393(3) | 10197(3) | 4281.7(10) | 19.0(11) |
| C64 | 4684(3) | 10708(3) | 4448.2(10) | 24.2(12) |
| C65 | 5364(4) | 11129(3) | 4415.2(11) | 31.1(14) |
| C66 | 5754(3) | 11050(3) | 4220.1(12) | 31.6(14) |
| C67 | 5462(3) | 10541(3) | 4050.0(11) | 28.6(13) |
| C68 | 4790(3) | 10118(3) | 4081.0(10) | 22.6(11) |
| C69 | 3330(3) | 9909(3) | 4626.3(9) | 19.5(11) |
| C70 | 2778(4) | 10421(3) | 4688.9(10) | 25.3(12) |
| C71 | 2748(4) | 10599(3) | 4923.1(10) | 28.6(13) |
| C72 | 3288(4) | 10279(3) | 5096.3(10) | 30.2(13) |
| C73 | 3862(4) | 9785(3) | 5037.0(10) | 28.8(13) |
| C74 | 3877(4) | 9598(3) | 4802.9(10) | 24.3(12) |
| C75 | 2637(3) | 10099(3) | 4137.5(9) | 15.9(10) |
| C76 | 1831(3) | 10067(3) | 4193.1(9) | 18.7(10) |
| C77 | 1194(3) | 10365(3) | 4045.2(10) | 23.1(11) |
| C78 | 1339(3) | 10693(3) | 3837.8(10) | 23.9(12) |
| C79 | 2128(3) | 10713(3) | 3775.8(10) | 21.8(11) |
| C80 | 2780(3) | 10425(3) | 3925.1(9) | 18.7(10) |
| Rh3 | -704.2(2) | 13015.3(2) | 3180.5(2) | 15.12(8) |
| Cl5 | -994.8(8) | 11784.4(7) | 3262.7(3) | 25.2(3) |
| Cl6 | -1140.3(8) | 13306.6(7) | 3570.5(2) | 23.6(3) |
| P5 | -527.9(8) | 14247.7(7) | 3117.6(2) | 14.7(2) |
| P6 | -266.7(8) | 12574.5(7) | 2852.3(2) | 15.6(3) |
| N11 | -1320(3) | 12508(2) | 2697.0(8) | 16.9(9) |
| N12 | 12(2) | 12735(2) | 2575.1(8) | 16.9(9) |
| N13 | 810(2) | 12776(2) | 2954.5(8) | 17.4(9) |
| N14 | -1866(3) | 13073(2) | 3003.3(8) | 18.0(9) |

| | | | | |
|---|---|---|---|---|
| N15 | 485(3) | 12820(2) | 3334.9(8) | 17.8(9) |
| C81 | -1302(3) | 12285(3) | 2463.2(9) | 17.5(10) |
| C82 | -517(3) | 12427(3) | 2393.9(9) | 16.8(10) |
| C83 | -339(3) | 12209(3) | 2173.6(10) | 22.7(11) |
| C84 | -941(4) | 11864(3) | 2022.8(10) | 23.9(12) |
| C85 | -1707(3) | 11720(3) | 2091.4(10) | 23.9(12) |
| C86 | -1880(3) | 11913(3) | 2312.4(10) | 22.2(11) |
| C87 | 804(3) | 12998(3) | 2560.1(9) | 17.3(10) |
| C88 | 1112(3) | 13269(3) | 2363.9(10) | 20.4(11) |
| C89 | 1913(3) | 13537(3) | 2389.1(11) | 24.6(12) |
| C90 | 2372(3) | 13555(3) | 2606.6(11) | 25.8(12) |
| C91 | 2061(3) | 13306(3) | 2807.1(10) | 19.9(11) |
| C92 | 1269(3) | 13017(3) | 2780.5(9) | 18.0(10) |
| C93 | -2766(3) | 12859(3) | 2649.9(10) | 20.6(11) |
| C94 | -3403(3) | 13153(3) | 2750.7(11) | 25.4(12) |
| C95 | -3277(3) | 13399(3) | 2981.4(11) | 25.3(12) |
| C96 | -2506(3) | 13346(3) | 3101.5(10) | 21.8(11) |
| C97 | -1987(3) | 12801(3) | 2781.1(9) | 16.9(10) |
| C98 | 1876(3) | 12530(3) | 3280.9(10) | 21.8(11) |
| C99 | 2080(3) | 12486(3) | 3519.0(10) | 25.5(12) |
| C100 | 1477(4) | 12601(3) | 3666.6(11) | 28.4(13) |
| C101 | 688(4) | 12748(3) | 3568.6(10) | 25.0(12) |
| C102 | 1071(3) | 12711(3) | 3190.4(9) | 17.8(10) |
| C103 | -233(3) | 14531(3) | 2834.6(9) | 16.4(10) |
| C104 | 529(3) | 15315(3) | 2603.7(9) | 22.0(11) |
| C105 | 121(3) | 15031(3) | 2399.0(9) | 19.3(11) |
| C106 | -477(3) | 14499(3) | 2410.4(9) | 19.5(11) |
| C107 | -650(3) | 14255(3) | 2625.6(9) | 17.4(10) |
| C108 | 351(3) | 15065(3) | 2820.0(10) | 20.5(11) |
| C109 | 1042(3) | 14433(3) | 3354.9(10) | 24.1(12) |
| C110 | 236(3) | 14691(3) | 3327.3(9) | 17.5(10) |
| C111 | 1469(4) | 15387(3) | 3623.5(10) | 28.2(13) |
| C112 | 682(3) | 15664(3) | 3593.5(10) | 26.7(12) |
| C113 | 65(3) | 15320(3) | 3445.7(9) | 20.1(11) |
| C114 | 1649(3) | 14772(3) | 3502.8(11) | 27.0(13) |
| C115 | -1488(3) | 14752(3) | 3131.8(9) | 16.1(10) |
| C116 | -1797(3) | 14832(3) | 3346.7(9) | 18.7(10) |
| C117 | -2551(3) | 15164(3) | 3356.1(10) | 22.0(11) |
| C118 | -2998(3) | 15431(3) | 3153.4(10) | 22.1(11) |
| C119 | -2690(3) | 15357(3) | 2940.7(10) | 19.9(11) |
| C120 | -1936(3) | 15026(3) | 2929.1(10) | 18.5(10) |
| Rh4 | -1586.9(2) | 16441.8(2) | 4198.4(2) | 16.04(8) |
| Cl7 | -1235.9(9) | 16082.1(7) | 3810.2(2) | 25.5(3) |
| Cl8 | -1519.6(9) | 17671.9(7) | 4067.0(2) | 25.3(3) |
| P7 | -2005.7(8) | 16895.3(7) | 4526.4(2) | 15.1(3) |
| P8 | -1588.5(8) | 15226.1(7) | 4301.3(2) | 16.0(3) |
| N16 | -3046(2) | 16553(2) | 4454.7(7) | 17.2(9) |
| N17 | -2196(3) | 16767(2) | 4814.2(7) | 16.4(9) |

| | | | | |
|---|---|---|---|---|
| N18 | -955(3) | 17120(2) | 4659.3(8) | 18.9(9) |
| N19 | -2826(3) | 16466(2) | 4066.4(7) | 18.6(9) |
| N20 | -404(3) | 16573(2) | 4349.9(8) | 19.6(9) |
| C121 | -3413(3) | 16282(3) | 4640.6(9) | 18.0(10) |
| C122 | -2912(3) | 16405(3) | 4853.6(9) | 19.6(11) |
| C123 | -3121(3) | 16145(3) | 5061.7(10) | 22.5(11) |
| C124 | -3860(3) | 15765(3) | 5062.4(11) | 26.7(12) |
| C125 | -4351(4) | 15634(3) | 4853.2(11) | 26.6(12) |
| C126 | -4133(3) | 15887(3) | 4640.2(10) | 22.6(11) |
| C127 | -1679(3) | 17182(3) | 4977.1(9) | 18.9(10) |
| C128 | -962(3) | 17393(3) | 4888.2(9) | 20.0(11) |
| C129 | -423(4) | 17870(3) | 5016.0(11) | 27.4(13) |
| C130 | -592(4) | 18106(3) | 5234.8(10) | 30.5(13) |
| C131 | -1305(4) | 17890(3) | 5322.8(10) | 27.6(13) |
| C132 | -1855(3) | 17434(3) | 5193.3(10) | 23.1(11) |
| C133 | -3378(3) | 16552(3) | 4220.8(9) | 19.4(11) |
| C134 | -4213(3) | 16660(3) | 4148.0(10) | 25.2(12) |
| C135 | -4483(4) | 16664(4) | 3911.4(11) | 33.8(14) |
| C136 | -3924(4) | 16572(4) | 3752.9(11) | 36.6(15) |
| C137 | -3104(4) | 16495(3) | 3834.6(10) | 28.8(13) |
| C138 | -272(3) | 16896(3) | 4563.8(10) | 20.6(11) |
| C139 | 532(3) | 16953(3) | 4680.7(11) | 26.0(12) |
| C140 | 1178(3) | 16742(3) | 4567.0(12) | 29.9(14) |
| C141 | 1040(3) | 16475(3) | 4340.1(12) | 29.1(13) |
| C142 | 250(3) | 16387(3) | 4239.4(11) | 24.0(12) |
| C143 | -654(3) | 14691(3) | 4273.4(10) | 20.6(11) |
| C144 | -336(4) | 14249(3) | 4457.6(11) | 31.9(14) |
| C145 | 348(4) | 13809(4) | 4432.4(12) | 39.2(17) |
| C146 | 696(4) | 13810(3) | 4228.0(12) | 33.8(15) |
| C147 | 389(4) | 14250(3) | 4044.3(12) | 30.0(13) |
| C148 | -278(4) | 14691(3) | 4067.1(11) | 26.7(12) |
| C149 | -2409(3) | 14719(3) | 4130.3(9) | 17.5(10) |
| C150 | -3218(3) | 14828(3) | 4172.8(10) | 23.3(12) |
| C151 | -3849(3) | 14434(3) | 4050.6(11) | 29.1(13) |
| C152 | -3682(4) | 13932(3) | 3882.8(11) | 30.3(13) |
| C153 | -2884(4) | 13825(3) | 3839.4(11) | 28.7(13) |
| C154 | -2248(3) | 14212(3) | 3961.5(9) | 21.5(11) |
| C155 | -1717(3) | 15049(3) | 4607.6(9) | 19.1(11) |
| C156 | -1162(3) | 15375(3) | 4779.0(9) | 19.7(11) |
| C157 | -1171(4) | 15221(3) | 5015.2(10) | 25.8(12) |
| C158 | -1746(4) | 14748(3) | 5083.0(10) | 29.4(13) |
| C159 | -2288(4) | 14410(3) | 4914.8(11) | 32.9(14) |
| C160 | -2283(4) | 14547(3) | 4678.6(10) | 25.0(12) |
| Cl0L | -1501.3(9) | 8999.8(8) | 4596.0(3) | 30.0(3) |
| Cl0T | -2567.2(9) | 9859.2(9) | 4264.6(3) | 38.8(4) |
| Cl0Y | -827.0(10) | 9840.0(11) | 4242.9(4) | 51.6(5) |
| C1S | -1679(4) | 9329(3) | 4306.1(11) | 27.7(12) |
| Cl0M | 3462.0(10) | 15844.3(8) | 4596.9(3) | 32.8(3) |

| | | | | |
|---|---|---|---|---|
| Cl0V | 2428.3(10) | 14901.3(8) | 4284.1(3) | 39.9(4) |
| C163 | 3227(4) | 15538(3) | 4306.5(11) | 28.0(13) |
| Cl14 | 4073(7) | 15227(4) | 4185(3) | 33(2) |
| Cl18 | 4148(14) | 15050(40) | 4246(10) | 67(9) |
| Cl0N | 2182.3(9) | 17160.5(8) | 3517.4(3) | 32.8(3) |
| Cl0U | 3596.1(10) | 17569.2(9) | 3294.8(3) | 38.8(4) |
| Cl0X | 3565.6(11) | 16201.1(9) | 3537.6(4) | 51.0(5) |
| C167 | 3260(4) | 17113(3) | 3532.5(11) | 28.6(13) |
| Cl0O | 467.5(9) | 9802.3(9) | 3276.4(3) | 33.0(3) |
| Cl0Q | -670.8(9) | 9778.0(9) | 3625.8(3) | 32.9(3) |
| Cl0S | -1272.3(9) | 9727.6(9) | 3130.1(3) | 34.6(3) |
| C164 | -510(3) | 10068(3) | 3343.0(10) | 25.2(12) |
| Cl0P | -1541.7(10) | 16806.0(8) | 3196.6(3) | 36.5(4) |
| Cl10 | -1941.9(11) | 18145.8(9) | 3422.0(4) | 50.8(5) |
| Cl13 | -271.5(11) | 17803.1(13) | 3374.4(4) | 62.7(6) |
| C165 | -1222(4) | 17440(3) | 3417.9(11) | 28.9(13) |
| Cl0R | 3495.0(10) | 14544.9(8) | 3169.3(3) | 34.4(3) |
| Cl0W | 4085.5(10) | 14320.3(11) | 3657.9(3) | 44.3(4) |
| Cl11 | 5222.3(11) | 14673.5(11) | 3330.2(3) | 49.8(5) |
| C166 | 4306(4) | 14220(3) | 3367.6(10) | 26.9(12) |
| Cl0Z | -166.9(11) | 11877.0(11) | 4101.4(3) | 47.8(4) |
| Cl16 | -1864.5(15) | 11484.6(14) | 4002.6(5) | 83.2(9) |
| Cl17 | -1389.2(18) | 12621.2(16) | 4332.4(6) | 90.2(9) |
| C161 | -1178(4) | 12195(4) | 4069.5(14) | 46.8(19) |
| Cl01 | 3091(2) | 12054.0(15) | 4349.1(6) | 114.6(13) |
| Cl12 | 3989.0(12) | 12115.3(10) | 3953.5(3) | 47.8(4) |
| Cl15 | 3784.6(18) | 13405.5(11) | 4224.1(4) | 72.0(7) |
| C162 | 3920(6) | 12463(4) | 4232.2(13) | 51(2) |

**Table C-38.** Anisotropic Displacement Parameters ($Å^2 \times 10^3$) for **4.20**. The Anisotropic displacement factor exponent takes the form: $-2\pi^2[h^2a^{*2}U_{11}+2hka^*b^*U_{12}+\ldots]$.

| **Atom** | $\mathbf{U_{11}}$ | $\mathbf{U_{22}}$ | $\mathbf{U_{33}}$ | $\mathbf{U_{23}}$ | $\mathbf{U_{13}}$ | $\mathbf{U_{12}}$ |
|---|---|---|---|---|---|---|
| Rh1 | 10.22(17) | 13.86(18) | 19.3(2) | 2.47(15) | 2.84(14) | 0.56(14) |
| Cl1 | 19.1(6) | 28.1(7) | 21.4(6) | 4.0(5) | 7.9(5) | 5.3(5) |
| Cl2 | 17.4(6) | 15.7(6) | 33.4(7) | 4.9(5) | 3.7(5) | -0.7(5) |
| P1 | 10.6(6) | 13.2(6) | 20.1(7) | 0.5(5) | 2.5(5) | 0.5(5) |
| P2 | 12.3(6) | 14.3(6) | 19.8(7) | 0.1(5) | 4.4(5) | 0.0(5) |
| N1 | 11.0(19) | 22(2) | 16(2) | -1.9(17) | 2.2(16) | 2.2(16) |
| N2 | 12(2) | 17(2) | 18(2) | -0.3(17) | 1.9(16) | 2.2(16) |
| N3 | 13(2) | 16(2) | 20(2) | 2.0(17) | 2.0(16) | -0.5(16) |
| N4 | 12(2) | 21(2) | 21(2) | 0.8(18) | 0.5(17) | 3.2(17) |
| N5 | 9.2(19) | 14(2) | 26(2) | 4.7(17) | 1.7(17) | -2.0(16) |
| C1 | 13(2) | 14(2) | 22(3) | -0.1(19) | 5.8(19) | -0.4(18) |
| C2 | 13(2) | 20(3) | 27(3) | -4(2) | 4(2) | 4(2) |
| C3 | 13(2) | 18(3) | 33(3) | -3(2) | 6(2) | 1(2) |
| C4 | 15(3) | 19(3) | 30(3) | 1(2) | 7(2) | -1(2) |

| | | | | | | |
|---|---|---|---|---|---|---|
| C5 | 14(2) | 18(2) | 25(3) | -1(2) | 3(2) | 4.5(19) |
| C6 | 12(2) | 12(2) | 24(3) | -2.3(19) | 1.5(19) | 2.5(18) |
| C7 | 20(3) | 14(2) | 19(3) | 2.6(19) | -3(2) | 4.9(19) |
| C8 | 15(2) | 24(3) | 25(3) | 1(2) | 3(2) | -1(2) |
| C9 | 26(3) | 27(3) | 24(3) | -3(2) | 1(2) | 7(2) |
| C10 | 23(3) | 25(3) | 29(3) | -8(2) | -4(2) | -1(2) |
| C11 | 17(3) | 18(3) | 31(3) | 2(2) | 0(2) | -2(2) |
| C12 | 15(2) | 14(2) | 20(3) | 3.5(19) | 1.3(19) | 2.5(19) |
| C13 | 9(2) | 15(2) | 27(3) | -2(2) | 4.3(19) | -0.7(18) |
| C14 | 11(2) | 15(2) | 30(3) | -1(2) | 3(2) | 2.2(19) |
| C15 | 16(3) | 29(3) | 29(3) | 1(2) | -2(2) | 5(2) |
| C16 | 16(3) | 43(4) | 23(3) | 8(3) | 1(2) | 5(2) |
| C17 | 21(3) | 26(3) | 25(3) | 4(2) | 5(2) | 2(2) |
| C18 | 13(2) | 14(2) | 25(3) | 5(2) | -1(2) | 0.5(19) |
| C19 | 15(2) | 20(3) | 26(3) | 3(2) | 1(2) | -3(2) |
| C20 | 14(2) | 23(3) | 29(3) | 7(2) | -1(2) | 2(2) |
| C21 | 11(2) | 21(3) | 34(3) | 4(2) | 4(2) | 2(2) |
| C22 | 11(2) | 14(2) | 29(3) | 5(2) | 3(2) | 3.0(18) |
| C23 | 18(3) | 18(2) | 22(3) | 3(2) | 3(2) | -4(2) |
| C24 | 18(3) | 20(3) | 39(3) | -2(2) | 4(2) | 4(2) |
| C25 | 13(3) | 33(3) | 45(4) | 6(3) | 0(2) | 0(2) |
| C26 | 21(3) | 47(4) | 30(3) | -2(3) | -1(2) | -11(3) |
| C27 | 24(3) | 58(4) | 24(3) | -18(3) | 8(2) | -10(3) |
| C28 | 18(3) | 40(3) | 25(3) | -11(3) | 6(2) | -4(2) |
| C29 | 12(2) | 16(2) | 24(3) | -3(2) | 2(2) | 0.6(19) |
| C30 | 18(3) | 20(3) | 22(3) | 1(2) | 3(2) | 2(2) |
| C31 | 19(3) | 21(3) | 26(3) | 5(2) | 0(2) | 2(2) |
| C32 | 12(2) | 21(3) | 35(3) | -1(2) | 7(2) | 3(2) |
| C33 | 19(3) | 23(3) | 25(3) | -7(2) | 8(2) | -5(2) |
| C34 | 19(3) | 19(3) | 23(3) | -3(2) | 8(2) | -4(2) |
| C35 | 16(2) | 18(2) | 18(3) | 1(2) | 6.4(19) | 2.2(19) |
| C36 | 23(3) | 17(3) | 25(3) | -5(2) | 4(2) | -1(2) |
| C37 | 18(3) | 16(2) | 31(3) | -2(2) | 8(2) | -2(2) |
| C38 | 21(3) | 19(3) | 24(3) | 5(2) | 9(2) | 5(2) |
| C39 | 21(3) | 17(2) | 22(3) | -1(2) | 5(2) | 4(2) |
| C40 | 14(2) | 13(2) | 25(3) | 1(2) | 2(2) | -1.0(18) |
| Rh2 | 12.74(18) | 13.27(18) | 19.4(2) | 0.62(15) | 4.00(15) | -0.60(14) |
| Cl3 | 20.9(6) | 22.1(6) | 21.2(6) | 0.8(5) | 7.7(5) | -3.3(5) |
| Cl4 | 24.1(6) | 14.0(6) | 28.0(7) | -0.9(5) | 8.2(5) | 0.4(5) |
| P3 | 13.7(6) | 14.3(6) | 19.4(7) | 1.3(5) | 2.6(5) | 0.3(5) |
| P4 | 14.9(6) | 12.2(6) | 20.3(7) | 0.7(5) | 2.5(5) | 0.0(5) |
| N6 | 17(2) | 19(2) | 22(2) | 3.4(18) | 3.8(18) | 1.5(17) |
| N7 | 14(2) | 18(2) | 18(2) | 3.1(17) | 2.2(16) | -2.1(16) |
| N8 | 13(2) | 20(2) | 19(2) | 2.2(17) | 2.7(16) | 3.3(17) |
| N9 | 12(2) | 18(2) | 25(2) | 2.3(18) | 3.8(17) | 0.7(16) |
| N10 | 15(2) | 11.0(19) | 20(2) | 0.9(16) | 2.6(16) | 0.1(16) |
| C41 | 23(3) | 18(3) | 23(3) | 3(2) | 1(2) | 2(2) |
| C42 | 24(3) | 26(3) | 28(3) | 4(2) | 1(2) | 4(2) |

| | | | | | | |
|---|---|---|---|---|---|---|
| C43 | 32(3) | 28(3) | 31(3) | 8(3) | -9(3) | 0(3) |
| C44 | 38(3) | 28(3) | 19(3) | 4(2) | -3(2) | -6(3) |
| C45 | 29(3) | 20(3) | 21(3) | 1(2) | -1(2) | -5(2) |
| C46 | 18(3) | 19(3) | 19(3) | 1(2) | -3(2) | -3(2) |
| C47 | 20(3) | 16(2) | 22(3) | -2(2) | 8(2) | -2(2) |
| C48 | 24(3) | 17(3) | 29(3) | 1(2) | 5(2) | -4(2) |
| C49 | 27(3) | 23(3) | 29(3) | -7(2) | 12(2) | -1(2) |
| C50 | 24(3) | 23(3) | 36(3) | -5(2) | 9(2) | 3(2) |
| C51 | 16(3) | 23(3) | 26(3) | -3(2) | 3(2) | 4(2) |
| C52 | 15(2) | 17(2) | 22(3) | 0(2) | 5(2) | -2.0(19) |
| C53 | 15(2) | 17(2) | 27(3) | -3(2) | 4(2) | 2(2) |
| C54 | 21(3) | 22(3) | 26(3) | 0(2) | 0(2) | 3(2) |
| C55 | 15(3) | 18(3) | 37(3) | -3(2) | 0(2) | 2(2) |
| C56 | 16(3) | 20(3) | 38(3) | -1(2) | 4(2) | -2(2) |
| C57 | 15(2) | 16(2) | 32(3) | 2(2) | 7(2) | 1(2) |
| C58 | 15(2) | 9(2) | 28(3) | 3.5(19) | 3(2) | -0.1(18) |
| C59 | 17(3) | 16(2) | 26(3) | -2(2) | 5(2) | -3(2) |
| C60 | 18(3) | 20(3) | 32(3) | 0(2) | 1(2) | -1(2) |
| C61 | 21(3) | 28(3) | 20(3) | 0(2) | -1(2) | -2(2) |
| C62 | 14(2) | 24(3) | 23(3) | 2(2) | 4(2) | -4(2) |
| C63 | 13(2) | 11(2) | 32(3) | 6(2) | 0(2) | -3.5(19) |
| C64 | 23(3) | 26(3) | 23(3) | 4(2) | -2(2) | -5(2) |
| C65 | 31(3) | 26(3) | 33(3) | 7(2) | -10(3) | -10(2) |
| C66 | 16(3) | 24(3) | 53(4) | 15(3) | -4(3) | -3(2) |
| C67 | 19(3) | 25(3) | 44(4) | 8(3) | 12(3) | 1(2) |
| C68 | 16(3) | 20(3) | 31(3) | 5(2) | 4(2) | 2(2) |
| C69 | 21(3) | 15(2) | 24(3) | 1(2) | 4(2) | -5(2) |
| C70 | 26(3) | 21(3) | 29(3) | -3(2) | 4(2) | 0(2) |
| C71 | 35(3) | 26(3) | 26(3) | -3(2) | 8(3) | -1(3) |
| C72 | 45(4) | 26(3) | 19(3) | -5(2) | 3(3) | -8(3) |
| C73 | 36(3) | 24(3) | 25(3) | 2(2) | -2(3) | -6(3) |
| C74 | 27(3) | 21(3) | 24(3) | 3(2) | 2(2) | -1(2) |
| C75 | 14(2) | 14(2) | 19(3) | 1.4(19) | 0.1(19) | -1.0(18) |
| C76 | 19(3) | 18(2) | 19(3) | 2(2) | 5(2) | -1(2) |
| C77 | 16(3) | 22(3) | 32(3) | 1(2) | 2(2) | 0(2) |
| C78 | 16(3) | 24(3) | 30(3) | 3(2) | -4(2) | 0(2) |
| C79 | 18(3) | 24(3) | 23(3) | 3(2) | 4(2) | 0(2) |
| C80 | 17(3) | 17(2) | 21(3) | 2(2) | 0(2) | 0(2) |
| Rh3 | 11.67(18) | 12.39(17) | 22.1(2) | 2.22(15) | 5.15(15) | 1.42(14) |
| Cl5 | 19.9(6) | 14.1(6) | 43.1(8) | 7.7(5) | 9.3(6) | 0.8(5) |
| Cl6 | 24.0(7) | 24.7(6) | 24.0(7) | 4.2(5) | 10.1(5) | 6.5(5) |
| P5 | 13.0(6) | 13.5(6) | 18.0(6) | 0.5(5) | 3.9(5) | 0.2(5) |
| P6 | 10.9(6) | 12.8(6) | 23.2(7) | -0.5(5) | 3.0(5) | 0.6(5) |
| N11 | 14(2) | 14(2) | 22(2) | -2.3(17) | 2.9(17) | -2.0(16) |
| N12 | 11(2) | 14(2) | 26(2) | -0.5(17) | 2.9(17) | 0.1(16) |
| N13 | 8.9(19) | 19(2) | 25(2) | -1.5(18) | 4.0(17) | 0.5(16) |
| N14 | 13(2) | 12(2) | 30(2) | 1.0(17) | 4.5(18) | -1.6(16) |
| N15 | 13(2) | 16(2) | 25(2) | 1.2(17) | 4.2(17) | 0.7(16) |

| | | | | | | |
|---|---|---|---|---|---|---|
| C81 | 17(2) | 9(2) | 26(3) | 0.1(19) | 1(2) | 1.3(18) |
| C82 | 14(2) | 15(2) | 22(3) | 2.3(19) | 1.8(19) | 3.1(19) |
| C83 | 25(3) | 20(3) | 24(3) | 1(2) | 5(2) | 1(2) |
| C84 | 30(3) | 17(3) | 24(3) | 0(2) | 1(2) | 3(2) |
| C85 | 24(3) | 18(3) | 27(3) | 1(2) | -6(2) | -1(2) |
| C86 | 17(3) | 15(2) | 33(3) | 2(2) | -4(2) | -3(2) |
| C87 | 11(2) | 13(2) | 29(3) | -5(2) | 3(2) | 0.8(18) |
| C88 | 16(3) | 21(3) | 26(3) | 0(2) | 6(2) | 4(2) |
| C89 | 21(3) | 18(3) | 37(3) | 3(2) | 13(2) | 0(2) |
| C90 | 17(3) | 20(3) | 41(3) | -4(2) | 9(2) | -2(2) |
| C91 | 9(2) | 20(3) | 31(3) | -4(2) | 3(2) | -2.8(19) |
| C92 | 13(2) | 13(2) | 29(3) | -3(2) | 6(2) | 2.3(19) |
| C93 | 15(2) | 16(2) | 31(3) | 3(2) | 0(2) | 0.0(19) |
| C94 | 13(3) | 19(3) | 44(4) | 10(2) | 3(2) | 3(2) |
| C95 | 13(3) | 22(3) | 42(4) | 3(2) | 9(2) | 4(2) |
| C96 | 19(3) | 16(2) | 32(3) | 3(2) | 8(2) | -2(2) |
| C97 | 15(2) | 8(2) | 28(3) | 4.0(19) | 5(2) | 1.2(18) |
| C98 | 14(3) | 17(2) | 34(3) | -4(2) | 2(2) | 4(2) |
| C99 | 16(3) | 26(3) | 34(3) | 0(2) | -3(2) | 7(2) |
| C100 | 26(3) | 33(3) | 25(3) | 7(2) | -1(2) | 9(2) |
| C101 | 25(3) | 25(3) | 25(3) | 6(2) | 3(2) | 2(2) |
| C102 | 12(2) | 16(2) | 26(3) | -2(2) | 3(2) | 0.3(19) |
| C103 | 17(2) | 14(2) | 19(3) | -0.5(19) | 4(2) | 3.0(19) |
| C104 | 24(3) | 21(3) | 22(3) | 1(2) | 7(2) | -3(2) |
| C105 | 15(2) | 22(3) | 23(3) | 2(2) | 8(2) | -1(2) |
| C106 | 21(3) | 18(2) | 19(3) | -2(2) | 0(2) | 1(2) |
| C107 | 15(2) | 11(2) | 27(3) | -1(2) | 3(2) | 0.3(18) |
| C108 | 19(3) | 18(3) | 24(3) | -3(2) | 4(2) | -2(2) |
| C109 | 21(3) | 21(3) | 31(3) | 1(2) | 3(2) | -2(2) |
| C110 | 14(2) | 19(2) | 20(3) | 2(2) | 1.2(19) | -2.6(19) |
| C111 | 27(3) | 34(3) | 22(3) | 1(2) | 0(2) | -13(3) |
| C112 | 24(3) | 31(3) | 26(3) | -7(2) | 5(2) | -9(2) |
| C113 | 13(2) | 23(3) | 26(3) | -4(2) | 6(2) | -1(2) |
| C114 | 13(3) | 28(3) | 39(3) | 6(3) | -1(2) | -6(2) |
| C115 | 13(2) | 13(2) | 24(3) | 0.5(19) | 4.8(19) | -0.6(18) |
| C116 | 19(3) | 15(2) | 23(3) | 3(2) | 3(2) | 3(2) |
| C117 | 17(3) | 20(3) | 30(3) | -2(2) | 7(2) | -3(2) |
| C118 | 16(3) | 14(2) | 37(3) | -2(2) | 7(2) | 2.0(19) |
| C119 | 15(2) | 17(2) | 27(3) | 4(2) | -1(2) | 2.2(19) |
| C120 | 15(2) | 14(2) | 26(3) | 0(2) | 3(2) | -0.9(19) |
| Rh4 | 15.62(19) | 14.75(18) | 18.5(2) | 0.97(15) | 5.27(15) | 1.88(15) |
| Cl7 | 31.6(7) | 26.0(7) | 20.6(7) | 1.5(5) | 10.1(5) | 9.3(6) |
| Cl8 | 31.0(7) | 15.6(6) | 31.6(7) | 5.3(5) | 12.9(6) | 4.3(5) |
| P7 | 12.8(6) | 15.4(6) | 17.5(6) | -0.2(5) | 3.0(5) | 0.8(5) |
| P8 | 14.7(6) | 15.3(6) | 18.2(7) | -0.1(5) | 2.9(5) | 0.8(5) |
| N16 | 12(2) | 22(2) | 17(2) | 1.4(17) | 2.4(16) | 0.7(17) |
| N17 | 14(2) | 17(2) | 18(2) | -0.3(17) | 2.7(16) | 0.6(16) |
| N18 | 13(2) | 20(2) | 23(2) | -1.8(18) | 0.7(17) | -1.6(17) |

| | | | | | | |
|---|---|---|---|---|---|---|
| N19 | 22(2) | 18(2) | 16(2) | 1.0(17) | 2.7(17) | 2.7(18) |
| N20 | 15(2) | 14(2) | 31(3) | 2.9(18) | 6.7(18) | -3.3(16) |
| C121 | 16(2) | 17(2) | 21(3) | 1(2) | 3(2) | 1.3(19) |
| C122 | 16(2) | 18(2) | 26(3) | 1(2) | 4(2) | 6(2) |
| C123 | 21(3) | 23(3) | 24(3) | 7(2) | 3(2) | 2(2) |
| C124 | 25(3) | 25(3) | 33(3) | 7(2) | 12(2) | 4(2) |
| C125 | 22(3) | 24(3) | 35(3) | 4(2) | 11(2) | -2(2) |
| C126 | 17(3) | 21(3) | 30(3) | -2(2) | 4(2) | 0(2) |
| C127 | 20(3) | 14(2) | 23(3) | 1(2) | 1(2) | 1(2) |
| C128 | 20(3) | 17(2) | 23(3) | 1(2) | 1(2) | 2(2) |
| C129 | 22(3) | 25(3) | 35(3) | 2(2) | 0(2) | -3(2) |
| C130 | 37(3) | 27(3) | 26(3) | -5(2) | -5(3) | -6(3) |
| C131 | 39(3) | 21(3) | 21(3) | -4(2) | -3(2) | 2(2) |
| C132 | 20(3) | 24(3) | 25(3) | 1(2) | -1(2) | 0(2) |
| C133 | 20(3) | 15(2) | 24(3) | 1(2) | 3(2) | 1(2) |
| C134 | 21(3) | 28(3) | 27(3) | -4(2) | 1(2) | 0(2) |
| C135 | 22(3) | 44(4) | 33(3) | -1(3) | -5(3) | 6(3) |
| C136 | 36(4) | 50(4) | 22(3) | -3(3) | -7(3) | 17(3) |
| C137 | 28(3) | 37(3) | 22(3) | 3(2) | 5(2) | 7(3) |
| C138 | 12(2) | 18(3) | 33(3) | 5(2) | 5(2) | -0.1(19) |
| C139 | 18(3) | 21(3) | 38(3) | 5(2) | 0(2) | -3(2) |
| C140 | 16(3) | 22(3) | 53(4) | 14(3) | 5(3) | 1(2) |
| C141 | 21(3) | 20(3) | 49(4) | 4(3) | 15(3) | 2(2) |
| C142 | 19(3) | 18(3) | 38(3) | 4(2) | 13(2) | 0(2) |
| C143 | 18(3) | 16(2) | 26(3) | -6(2) | 0(2) | 0(2) |
| C144 | 33(3) | 33(3) | 30(3) | -4(3) | 2(3) | 10(3) |
| C145 | 43(4) | 35(4) | 37(4) | -7(3) | -6(3) | 25(3) |
| C146 | 25(3) | 27(3) | 47(4) | -13(3) | -3(3) | 8(2) |
| C147 | 25(3) | 21(3) | 47(4) | 0(3) | 14(3) | 0(2) |
| C148 | 25(3) | 21(3) | 36(3) | 3(2) | 10(2) | 5(2) |
| C149 | 15(2) | 16(2) | 21(3) | 2(2) | 2(2) | 1.7(19) |
| C150 | 17(3) | 19(3) | 33(3) | -3(2) | 3(2) | 3(2) |
| C151 | 16(3) | 34(3) | 37(3) | -7(3) | 4(2) | 1(2) |
| C152 | 22(3) | 26(3) | 41(4) | -12(3) | -3(3) | -5(2) |
| C153 | 27(3) | 29(3) | 30(3) | -9(2) | 4(2) | -3(2) |
| C154 | 20(3) | 22(3) | 24(3) | -5(2) | 6(2) | -3(2) |
| C155 | 20(3) | 15(2) | 22(3) | -1(2) | 1(2) | 2(2) |
| C156 | 20(3) | 16(2) | 23(3) | 2(2) | 4(2) | 2(2) |
| C157 | 32(3) | 18(3) | 28(3) | -3(2) | 2(2) | 3(2) |
| C158 | 41(4) | 27(3) | 21(3) | 3(2) | 8(3) | 9(3) |
| C159 | 36(4) | 34(3) | 31(3) | 5(3) | 12(3) | -6(3) |
| C160 | 26(3) | 27(3) | 23(3) | 1(2) | 6(2) | -9(2) |
| Cl0L | 36.8(8) | 23.8(7) | 29.7(8) | 1.8(6) | 4.8(6) | -5.0(6) |
| Cl0T | 23.2(7) | 31.2(8) | 62.8(11) | 14.1(7) | 9.3(7) | 3.5(6) |
| Cl0Y | 24.2(8) | 71.9(13) | 61.4(12) | 34.7(10) | 16.6(8) | 8.6(8) |
| C1S | 23(3) | 26(3) | 34(3) | 1(2) | 5(2) | 4(2) |
| Cl0M | 40.6(9) | 28.8(7) | 29.9(8) | 5.6(6) | 8.4(6) | 4.9(6) |
| Cl0V | 26.6(8) | 24.4(7) | 69.3(12) | -0.5(7) | 8.6(7) | -3.8(6) |

| | | | | | | |
|---|---|---|---|---|---|---|
| C163 | 30(3) | 24(3) | 31(3) | 2(2) | 10(3) | -10(2) |
| Cl14 | 30(2) | 24(5) | 46(4) | -8(2) | 15(2) | -2.9(15) |
| Cl18 | 32(4) | 101(17) | 70(13) | -48(14) | 22(6) | -18(7) |
| Cl0N | 25.4(7) | 36.2(8) | 36.5(8) | -6.7(6) | 3.1(6) | 0.0(6) |
| Cl0U | 35.9(9) | 42.5(9) | 40.6(9) | -6.4(7) | 15.2(7) | 2.7(7) |
| Cl0X | 41.0(10) | 21.7(8) | 85.6(15) | -10.5(8) | -10.5(9) | 6.7(7) |
| C167 | 28(3) | 20(3) | 35(3) | -7(2) | -5(3) | 4(2) |
| Cl0O | 23.3(7) | 41.8(9) | 34.3(8) | 4.3(7) | 4.8(6) | 7.0(6) |
| Cl0Q | 32.3(8) | 41.1(9) | 25.8(7) | -0.2(6) | 5.0(6) | -1.2(7) |
| Cl0S | 25.5(7) | 46.9(9) | 29.7(8) | 8.5(7) | -3.1(6) | -2.0(7) |
| C164 | 23(3) | 24(3) | 27(3) | 2(2) | -1(2) | 0(2) |
| Cl0P | 37.6(9) | 25.6(7) | 42.4(9) | 1.2(6) | -10.4(7) | -8.2(6) |
| Cl10 | 42.3(10) | 32.8(9) | 71.6(13) | -7.4(8) | -16.2(9) | 4.5(7) |
| Cl13 | 32.8(9) | 92.0(16) | 66.1(13) | -44.5(12) | 16.9(9) | -31.2(10) |
| C165 | 27(3) | 29(3) | 30(3) | 3(2) | -1(2) | -6(2) |
| Cl0R | 40.2(9) | 33.4(8) | 27.7(8) | -0.3(6) | -3.0(6) | -0.7(7) |
| Cl0W | 31.8(8) | 75.9(13) | 26.0(8) | 1.8(8) | 6.4(6) | 5.9(8) |
| Cl11 | 36.0(9) | 64.5(12) | 50.7(11) | -4.2(9) | 12.5(8) | -22.9(9) |
| C166 | 32(3) | 25(3) | 25(3) | -4(2) | 6(2) | -8(2) |
| Cl0Z | 36.1(9) | 54.9(11) | 52.3(11) | 11.1(9) | 5.6(8) | 3.9(8) |
| Cl16 | 56.5(14) | 75.9(16) | 106(2) | 38.1(15) | -35.6(13) | -25.5(12) |
| Cl17 | 75.3(18) | 88.1(19) | 115(2) | -8.8(17) | 43.9(16) | 9.5(15) |
| C161 | 40(4) | 45(4) | 55(5) | 24(4) | 6(3) | 0(3) |
| Cl01 | 159(3) | 62.4(16) | 147(3) | -1.1(17) | 117(3) | 2.9(18) |
| Cl12 | 47.6(11) | 50.8(11) | 44.5(10) | -4.2(8) | 3.7(8) | 9.0(8) |
| Cl15 | 114(2) | 34.7(10) | 62.9(14) | -3.3(9) | -6.9(13) | 16.9(12) |
| C162 | 77(6) | 38(4) | 40(4) | -5(3) | 8(4) | 4(4) |

**Table C-39.** Bond Lengths for **4.20**.

| **Atom** | **Atom** | **Length/Å** | **Atom** | **Atom** | **Length/Å** |
|---|---|---|---|---|---|
| Rh1 | Cl1 | 2.4730(13) | N11 | C97 | 1.365(6) |
| Rh1 | Cl2 | 2.4000(13) | N12 | C82 | 1.393(7) |
| Rh1 | P1 | 2.2404(14) | N12 | C87 | 1.403(6) |
| Rh1 | P2 | 2.3396(13) | N13 | C92 | 1.397(7) |
| Rh1 | N4 | 2.079(4) | N13 | C102 | 1.374(7) |
| Rh1 | N5 | 2.046(4) | N14 | C96 | 1.352(7) |
| P1 | N1 | 1.836(4) | N14 | C97 | 1.362(7) |
| P1 | N2 | 1.725(4) | N15 | C101 | 1.348(7) |
| P1 | N3 | 1.850(4) | N15 | C102 | 1.362(6) |
| P2 | C23 | 1.834(5) | C81 | C82 | 1.422(7) |
| P2 | C29 | 1.830(5) | C81 | C86 | 1.388(7) |
| P2 | C35 | 1.826(5) | C82 | C83 | 1.391(7) |
| N1 | C1 | 1.397(6) | C83 | C84 | 1.389(8) |
| N1 | C13 | 1.365(7) | C84 | C85 | 1.391(8) |
| N2 | C6 | 1.408(6) | C85 | C86 | 1.380(8) |
| N2 | C7 | 1.401(6) | C87 | C88 | 1.385(7) |
| N3 | C12 | 1.411(6) | C87 | C92 | 1.396(7) |

| | | | | | |
|---|---|---|---|---|---|
| N3 | C18 | 1.370(6) | C88 | C89 | 1.398(7) |
| N4 | C13 | 1.356(6) | C89 | C90 | 1.377(8) |
| N4 | C17 | 1.347(7) | C90 | C91 | 1.394(8) |
| N5 | C18 | 1.358(7) | C91 | C92 | 1.399(7) |
| N5 | C22 | 1.358(6) | C93 | C94 | 1.371(8) |
| C1 | C2 | 1.401(7) | C93 | C97 | 1.408(7) |
| C1 | C6 | 1.392(7) | C94 | C95 | 1.391(8) |
| C2 | C3 | 1.381(8) | C95 | C96 | 1.371(8) |
| C3 | C4 | 1.382(8) | C98 | C99 | 1.368(8) |
| C4 | C5 | 1.395(7) | C98 | C102 | 1.402(7) |
| C5 | C6 | 1.387(7) | C99 | C100 | 1.397(8) |
| C7 | C8 | 1.383(7) | C100 | C101 | 1.378(8) |
| C7 | C12 | 1.411(7) | C103 | C107 | 1.403(7) |
| C8 | C9 | 1.392(8) | C103 | C108 | 1.389(7) |
| C9 | C10 | 1.381(8) | C104 | C105 | 1.383(8) |
| C10 | C11 | 1.397(8) | C104 | C108 | 1.389(7) |
| C11 | C12 | 1.390(7) | C105 | C106 | 1.400(7) |
| C13 | C14 | 1.400(7) | C106 | C107 | 1.376(7) |
| C14 | C15 | 1.370(8) | C109 | C110 | 1.400(7) |
| C15 | C16 | 1.403(8) | C109 | C114 | 1.380(8) |
| C16 | C17 | 1.374(8) | C110 | C113 | 1.394(7) |
| C18 | C19 | 1.419(7) | C111 | C112 | 1.384(8) |
| C19 | C20 | 1.375(7) | C111 | C114 | 1.385(9) |
| C20 | C21 | 1.393(8) | C112 | C113 | 1.395(7) |
| C21 | C22 | 1.380(7) | C115 | C116 | 1.398(7) |
| C23 | C24 | 1.396(7) | C115 | C120 | 1.394(7) |
| C23 | C28 | 1.389(8) | C116 | C117 | 1.392(7) |
| C24 | C25 | 1.397(8) | C117 | C118 | 1.388(8) |
| C25 | C26 | 1.399(9) | C118 | C119 | 1.384(8) |
| C26 | C27 | 1.369(9) | C119 | C120 | 1.393(7) |
| C27 | C28 | 1.387(8) | Rh4 | Cl7 | 2.4602(13) |
| C29 | C30 | 1.403(7) | Rh4 | Cl8 | 2.4070(13) |
| C29 | C34 | 1.404(7) | Rh4 | P7 | 2.2449(13) |
| C30 | C31 | 1.383(7) | Rh4 | P8 | 2.3284(14) |
| C31 | C32 | 1.384(8) | Rh4 | N19 | 2.086(4) |
| C32 | C33 | 1.385(8) | Rh4 | N20 | 2.045(4) |
| C33 | C34 | 1.374(7) | P7 | N16 | 1.824(4) |
| C35 | C36 | 1.407(7) | P7 | N17 | 1.735(4) |
| C35 | C40 | 1.403(7) | P7 | N18 | 1.849(4) |
| C36 | C37 | 1.372(8) | P8 | C143 | 1.852(5) |
| C37 | C38 | 1.386(8) | P8 | C149 | 1.828(5) |
| C38 | C39 | 1.386(7) | P8 | C155 | 1.825(5) |
| C39 | C40 | 1.394(7) | N16 | C121 | 1.383(6) |
| Rh2 | Cl3 | 2.4677(13) | N16 | C133 | 1.385(7) |
| Rh2 | Cl4 | 2.4030(13) | N17 | C122 | 1.397(7) |
| Rh2 | P3 | 2.2527(14) | N17 | C127 | 1.413(7) |
| Rh2 | P4 | 2.3205(13) | N18 | C128 | 1.409(7) |
| Rh2 | N9 | 2.057(4) | N18 | C138 | 1.374(7) |

| | | | | | |
|---|---|---|---|---|---|
| Rh2 | N10 | 2.081(4) | N19 | C133 | 1.354(7) |
| P3 | N6 | 1.844(5) | N19 | C137 | 1.353(7) |
| P3 | N7 | 1.729(4) | N20 | C138 | 1.359(7) |
| P3 | N8 | 1.824(4) | N20 | C142 | 1.359(7) |
| P4 | C63 | 1.856(5) | C121 | C122 | 1.406(7) |
| P4 | C69 | 1.825(5) | C121 | C126 | 1.392(7) |
| P4 | C75 | 1.813(5) | C122 | C123 | 1.369(7) |
| N6 | C41 | 1.413(7) | C123 | C124 | 1.407(8) |
| N6 | C53 | 1.368(7) | C124 | C125 | 1.383(8) |
| N7 | C46 | 1.398(6) | C125 | C126 | 1.395(8) |
| N7 | C47 | 1.413(6) | C127 | C128 | 1.396(7) |
| N8 | C52 | 1.391(6) | C127 | C132 | 1.389(8) |
| N8 | C58 | 1.377(7) | C128 | C129 | 1.394(8) |
| N9 | C53 | 1.359(7) | C129 | C130 | 1.389(8) |
| N9 | C57 | 1.351(6) | C130 | C131 | 1.391(9) |
| N10 | C58 | 1.358(6) | C131 | C132 | 1.386(8) |
| N10 | C62 | 1.346(7) | C133 | C134 | 1.400(7) |
| C41 | C42 | 1.387(7) | C134 | C135 | 1.375(8) |
| C41 | C46 | 1.410(8) | C135 | C136 | 1.381(9) |
| C42 | C43 | 1.399(8) | C136 | C137 | 1.381(8) |
| C43 | C44 | 1.373(9) | C138 | C139 | 1.411(7) |
| C44 | C45 | 1.396(8) | C139 | C140 | 1.371(8) |
| C45 | C46 | 1.386(7) | C140 | C141 | 1.384(9) |
| C47 | C48 | 1.383(7) | C141 | C142 | 1.366(8) |
| C47 | C52 | 1.397(7) | C143 | C144 | 1.388(8) |
| C48 | C49 | 1.384(8) | C143 | C148 | 1.401(8) |
| C49 | C50 | 1.381(8) | C144 | C145 | 1.411(8) |
| C50 | C51 | 1.388(8) | C145 | C146 | 1.366(10) |
| C51 | C52 | 1.391(7) | C146 | C147 | 1.377(9) |
| C53 | C54 | 1.406(7) | C147 | C148 | 1.387(8) |
| C54 | C55 | 1.381(8) | C149 | C150 | 1.397(7) |
| C55 | C56 | 1.383(8) | C149 | C154 | 1.397(7) |
| C56 | C57 | 1.383(7) | C150 | C151 | 1.387(8) |
| C58 | C59 | 1.403(7) | C151 | C152 | 1.390(8) |
| C59 | C60 | 1.383(8) | C152 | C153 | 1.381(8) |
| C60 | C61 | 1.380(8) | C153 | C154 | 1.387(8) |
| C61 | C62 | 1.371(7) | C155 | C156 | 1.394(7) |
| C63 | C64 | 1.388(8) | C155 | C160 | 1.410(7) |
| C63 | C68 | 1.399(8) | C156 | C157 | 1.386(8) |
| C64 | C65 | 1.396(8) | C157 | C158 | 1.381(8) |
| C65 | C66 | 1.364(9) | C158 | C159 | 1.381(9) |
| C66 | C67 | 1.398(9) | C159 | C160 | 1.380(8) |
| C67 | C68 | 1.386(8) | Cl0L | C1S | 1.761(6) |
| C69 | C70 | 1.391(8) | Cl0T | C1S | 1.753(6) |
| C69 | C74 | 1.394(8) | Cl0Y | C1S | 1.766(6) |
| C70 | C71 | 1.390(8) | Cl0M | C163 | 1.758(6) |
| C71 | C72 | 1.382(9) | Cl0V | C163 | 1.758(6) |
| C72 | C73 | 1.387(9) | C163 | Cl14 | 1.729(11) |

| | | | | | |
|---|---|---|---|---|---|
| C73 | C74 | 1.390(8) | C163 | Cl18 | 1.83(4) |
| C75 | C76 | 1.403(7) | Cl0N | C167 | 1.766(6) |
| C75 | C80 | 1.406(7) | Cl0U | C167 | 1.751(7) |
| C76 | C77 | 1.379(7) | Cl0X | C167 | 1.763(6) |
| C77 | C78 | 1.382(8) | Cl0O | C164 | 1.768(6) |
| C78 | C79 | 1.388(7) | Cl0Q | C164 | 1.760(6) |
| C79 | C80 | 1.394(7) | Cl0S | C164 | 1.757(6) |
| Rh3 | Cl5 | 2.3889(13) | Cl0P | C165 | 1.762(6) |
| Rh3 | Cl6 | 2.4911(14) | Cl10 | C165 | 1.766(6) |
| Rh3 | P5 | 2.3351(13) | Cl13 | C165 | 1.748(6) |
| Rh3 | P6 | 2.2503(14) | Cl0R | C166 | 1.750(6) |
| Rh3 | N14 | 2.054(4) | Cl0W | C166 | 1.757(6) |
| Rh3 | N15 | 2.077(4) | Cl11 | C166 | 1.762(6) |
| P5 | C103 | 1.827(5) | Cl0Z | C161 | 1.753(8) |
| P5 | C110 | 1.825(5) | Cl16 | C161 | 1.746(8) |
| P5 | C115 | 1.845(5) | Cl17 | C161 | 1.774(9) |
| P6 | N11 | 1.852(4) | Cl01 | C162 | 1.763(9) |
| P6 | N12 | 1.734(5) | Cl12 | C162 | 1.740(7) |
| P6 | N13 | 1.834(4) | Cl15 | C162 | 1.760(8) |
| N11 | C81 | 1.407(7) | | | |

**Table C-40.** Bond Angles for **4.20**.

| **Atom** | **Atom** | **Atom** | **Angle/°** | **Atom** | **Atom** | **Atom** | **Angle/°** |
|---|---|---|---|---|---|---|---|
| Cl2 | Rh1 | Cl1 | 87.57(5) | N15 | Rh3 | P5 | 96.17(12) |
| P1 | Rh1 | Cl1 | 170.67(5) | N15 | Rh3 | P6 | 84.98(13) |
| P1 | Rh1 | Cl2 | 84.29(5) | C103 | P5 | Rh3 | 118.03(16) |
| P1 | Rh1 | P2 | 99.02(5) | C103 | P5 | C115 | 102.5(2) |
| P2 | Rh1 | Cl1 | 89.31(5) | C110 | P5 | Rh3 | 115.26(17) |
| P2 | Rh1 | Cl2 | 175.88(5) | C110 | P5 | C103 | 102.7(2) |
| N4 | Rh1 | Cl1 | 90.14(12) | C110 | P5 | C115 | 105.5(2) |
| N4 | Rh1 | Cl2 | 87.47(12) | C115 | P5 | Rh3 | 111.39(16) |
| N4 | Rh1 | P1 | 84.96(12) | N11 | P6 | Rh3 | 92.88(14) |
| N4 | Rh1 | P2 | 95.24(13) | N12 | P6 | Rh3 | 148.52(15) |
| N5 | Rh1 | Cl1 | 95.56(13) | N12 | P6 | N11 | 84.7(2) |
| N5 | Rh1 | Cl2 | 85.94(12) | N12 | P6 | N13 | 84.5(2) |
| N5 | Rh1 | P1 | 88.42(13) | N13 | P6 | Rh3 | 93.09(14) |
| N5 | Rh1 | P2 | 91.68(12) | N13 | P6 | N11 | 167.6(2) |
| N5 | Rh1 | N4 | 171.09(17) | C81 | N11 | P6 | 110.5(3) |
| N1 | P1 | Rh1 | 92.61(14) | C97 | N11 | P6 | 123.3(4) |
| N1 | P1 | N3 | 168.0(2) | C97 | N11 | C81 | 124.4(4) |
| N2 | P1 | Rh1 | 147.73(15) | C82 | N12 | P6 | 113.8(3) |
| N2 | P1 | N1 | 84.14(19) | C82 | N12 | C87 | 126.5(4) |
| N2 | P1 | N3 | 85.1(2) | C87 | N12 | P6 | 117.9(4) |
| N3 | P1 | Rh1 | 93.59(14) | C92 | N13 | P6 | 115.0(3) |
| C23 | P2 | Rh1 | 113.90(17) | C102 | N13 | P6 | 118.1(3) |
| C29 | P2 | Rh1 | 113.07(17) | C102 | N13 | C92 | 126.9(4) |
| C29 | P2 | C23 | 106.3(2) | C96 | N14 | Rh3 | 122.6(4) |

| | | | | | | | |
|---|---|---|---|---|---|---|---|
| C35 | P2 | Rh1 | 117.46(17) | C96 | N14 | C97 | 119.7(5) |
| C35 | P2 | C23 | 102.5(2) | C97 | N14 | Rh3 | 117.7(3) |
| C35 | P2 | C29 | 102.2(2) | C101 | N15 | Rh3 | 123.2(4) |
| C1 | N1 | P1 | 115.4(3) | C101 | N15 | C102 | 118.8(5) |
| C13 | N1 | P1 | 118.1(3) | C102 | N15 | Rh3 | 117.8(3) |
| C13 | N1 | C1 | 126.4(4) | N11 | C81 | C82 | 109.8(4) |
| C6 | N2 | P1 | 118.1(3) | C86 | C81 | N11 | 130.3(5) |
| C7 | N2 | P1 | 113.6(3) | C86 | C81 | C82 | 119.6(5) |
| C7 | N2 | C6 | 126.8(4) | N12 | C82 | C81 | 111.9(4) |
| C12 | N3 | P1 | 110.0(3) | C83 | C82 | N12 | 127.9(5) |
| C18 | N3 | P1 | 122.3(4) | C83 | C82 | C81 | 120.0(5) |
| C18 | N3 | C12 | 125.8(4) | C84 | C83 | C82 | 119.0(5) |
| C13 | N4 | Rh1 | 117.4(3) | C83 | C84 | C85 | 120.9(5) |
| C17 | N4 | Rh1 | 123.1(4) | C86 | C85 | C84 | 120.4(5) |
| C17 | N4 | C13 | 119.1(4) | C85 | C86 | C81 | 119.9(5) |
| C18 | N5 | Rh1 | 118.0(3) | C88 | C87 | N12 | 127.7(5) |
| C18 | N5 | C22 | 119.8(4) | C88 | C87 | C92 | 120.8(5) |
| C22 | N5 | Rh1 | 122.0(4) | C92 | C87 | N12 | 111.3(5) |
| N1 | C1 | C2 | 129.1(5) | C87 | C88 | C89 | 118.6(5) |
| C6 | C1 | N1 | 110.3(4) | C90 | C89 | C88 | 120.5(5) |
| C6 | C1 | C2 | 120.2(5) | C89 | C90 | C91 | 121.6(5) |
| C3 | C2 | C1 | 118.0(5) | C90 | C91 | C92 | 117.9(5) |
| C2 | C3 | C4 | 122.1(5) | N13 | C92 | C91 | 128.5(5) |
| C3 | C4 | C5 | 120.0(5) | C87 | C92 | N13 | 110.8(4) |
| C6 | C5 | C4 | 118.6(5) | C87 | C92 | C91 | 120.5(5) |
| C1 | C6 | N2 | 111.3(4) | C94 | C93 | C97 | 119.8(5) |
| C5 | C6 | N2 | 127.3(5) | C93 | C94 | C95 | 120.0(5) |
| C5 | C6 | C1 | 121.1(5) | C96 | C95 | C94 | 118.3(5) |
| N2 | C7 | C12 | 112.0(4) | N14 | C96 | C95 | 122.5(5) |
| C8 | C7 | N2 | 127.2(5) | N11 | C97 | C93 | 124.0(5) |
| C8 | C7 | C12 | 120.6(5) | N14 | C97 | N11 | 116.5(4) |
| C7 | C8 | C9 | 119.2(5) | N14 | C97 | C93 | 119.4(5) |
| C10 | C9 | C8 | 120.4(5) | C99 | C98 | C102 | 119.2(5) |
| C9 | C10 | C11 | 121.1(5) | C98 | C99 | C100 | 119.4(5) |
| C12 | C11 | C10 | 118.8(5) | C101 | C100 | C99 | 119.1(5) |
| C7 | C12 | N3 | 110.1(4) | N15 | C101 | C100 | 122.1(5) |
| C11 | C12 | N3 | 129.6(5) | N13 | C102 | C98 | 123.6(5) |
| C11 | C12 | C7 | 119.8(5) | N15 | C102 | N13 | 115.2(4) |
| N1 | C13 | C14 | 123.9(5) | N15 | C102 | C98 | 121.2(5) |
| N4 | C13 | N1 | 115.3(4) | C107 | C103 | P5 | 120.0(4) |
| N4 | C13 | C14 | 120.7(5) | C108 | C103 | P5 | 121.3(4) |
| C15 | C14 | C13 | 120.2(5) | C108 | C103 | C107 | 118.5(5) |
| C14 | C15 | C16 | 118.4(5) | C105 | C104 | C108 | 119.9(5) |
| C17 | C16 | C15 | 119.3(5) | C104 | C105 | C106 | 119.9(5) |
| N4 | C17 | C16 | 122.3(5) | C107 | C106 | C105 | 119.8(5) |
| N3 | C18 | C19 | 124.1(5) | C106 | C107 | C103 | 121.0(5) |
| N5 | C18 | N3 | 116.7(4) | C103 | C108 | C104 | 121.0(5) |
| N5 | C18 | C19 | 119.2(5) | C114 | C109 | C110 | 121.2(5) |

| | | | | | | | |
|---|---|---|---|---|---|---|---|
| C20 | C19 | C18 | 120.2(5) | C109 | C110 | P5 | 119.1(4) |
| C19 | C20 | C21 | 120.0(5) | C113 | C110 | P5 | 122.3(4) |
| C22 | C21 | C20 | 118.0(5) | C113 | C110 | C109 | 118.4(5) |
| N5 | C22 | C21 | 122.9(5) | C112 | C111 | C114 | 119.8(5) |
| C24 | C23 | P2 | 118.0(4) | C111 | C112 | C113 | 120.4(5) |
| C28 | C23 | P2 | 123.3(4) | C112 | C113 | C110 | 120.2(5) |
| C28 | C23 | C24 | 118.6(5) | C109 | C114 | C111 | 119.9(5) |
| C23 | C24 | C25 | 121.3(5) | C116 | C115 | P5 | 119.9(4) |
| C24 | C25 | C26 | 118.5(5) | C120 | C115 | P5 | 121.1(4) |
| C27 | C26 | C25 | 120.3(6) | C120 | C115 | C116 | 119.0(5) |
| C26 | C27 | C28 | 120.9(6) | C117 | C116 | C115 | 120.2(5) |
| C27 | C28 | C23 | 120.3(5) | C118 | C117 | C116 | 120.5(5) |
| C30 | C29 | P2 | 120.9(4) | C119 | C118 | C117 | 119.3(5) |
| C30 | C29 | C34 | 117.2(5) | C118 | C119 | C120 | 120.6(5) |
| C34 | C29 | P2 | 121.9(4) | C119 | C120 | C115 | 120.3(5) |
| C31 | C30 | C29 | 120.7(5) | Cl8 | Rh4 | Cl7 | 87.03(5) |
| C30 | C31 | C32 | 120.9(5) | P7 | Rh4 | Cl7 | 172.06(5) |
| C31 | C32 | C33 | 119.3(5) | P7 | Rh4 | Cl8 | 86.49(5) |
| C34 | C33 | C32 | 120.1(5) | P7 | Rh4 | P8 | 98.01(5) |
| C33 | C34 | C29 | 121.9(5) | P8 | Rh4 | Cl7 | 88.58(5) |
| C36 | C35 | P2 | 122.0(4) | P8 | Rh4 | Cl8 | 175.34(5) |
| C40 | C35 | P2 | 119.6(4) | N19 | Rh4 | Cl7 | 90.26(12) |
| C40 | C35 | C36 | 118.1(5) | N19 | Rh4 | Cl8 | 86.95(12) |
| C37 | C36 | C35 | 120.4(5) | N19 | Rh4 | P7 | 84.81(12) |
| C36 | C37 | C38 | 121.2(5) | N19 | Rh4 | P8 | 94.65(12) |
| C37 | C38 | C39 | 119.6(5) | N20 | Rh4 | Cl7 | 95.74(13) |
| C38 | C39 | C40 | 119.8(5) | N20 | Rh4 | Cl8 | 86.71(12) |
| C39 | C40 | C35 | 120.8(5) | N20 | Rh4 | P7 | 88.47(13) |
| Cl4 | Rh2 | Cl3 | 84.75(4) | N20 | Rh4 | P8 | 92.16(12) |
| P3 | Rh2 | Cl3 | 169.33(5) | N20 | Rh4 | N19 | 171.03(17) |
| P3 | Rh2 | Cl4 | 85.24(5) | N16 | P7 | Rh4 | 93.26(14) |
| P3 | Rh2 | P4 | 99.37(5) | N16 | P7 | N18 | 167.2(2) |
| P4 | Rh2 | Cl3 | 90.60(5) | N17 | P7 | Rh4 | 148.92(15) |
| P4 | Rh2 | Cl4 | 175.34(5) | N17 | P7 | N16 | 83.8(2) |
| N9 | Rh2 | Cl3 | 95.19(13) | N17 | P7 | N18 | 84.7(2) |
| N9 | Rh2 | Cl4 | 86.74(12) | N18 | P7 | Rh4 | 93.56(15) |
| N9 | Rh2 | P3 | 87.92(13) | C143 | P8 | Rh4 | 117.95(18) |
| N9 | Rh2 | P4 | 94.02(13) | C149 | P8 | Rh4 | 112.62(17) |
| N9 | Rh2 | N10 | 172.48(17) | C149 | P8 | C143 | 104.2(2) |
| N10 | Rh2 | Cl3 | 90.58(12) | C155 | P8 | Rh4 | 114.97(17) |
| N10 | Rh2 | Cl4 | 89.01(12) | C155 | P8 | C143 | 100.5(2) |
| N10 | Rh2 | P3 | 85.56(12) | C155 | P8 | C149 | 105.0(2) |
| N10 | Rh2 | P4 | 90.71(11) | C121 | N16 | P7 | 116.0(3) |
| N6 | P3 | Rh2 | 93.72(14) | C121 | N16 | C133 | 126.0(4) |
| N7 | P3 | Rh2 | 148.81(16) | C133 | N16 | P7 | 117.8(3) |
| N7 | P3 | N6 | 84.4(2) | C122 | N17 | P7 | 118.3(4) |
| N7 | P3 | N8 | 84.4(2) | C122 | N17 | C127 | 127.3(4) |
| N8 | P3 | Rh2 | 93.92(14) | C127 | N17 | P7 | 112.9(3) |

| | | | | | | | |
|---|---|---|---|---|---|---|---|
| N8 | P3 | N6 | 168.1(2) | C128 | N18 | P7 | 110.5(3) |
| C63 | P4 | Rh2 | 118.30(17) | C138 | N18 | P7 | 122.5(4) |
| C69 | P4 | Rh2 | 114.55(17) | C138 | N18 | C128 | 125.5(5) |
| C69 | P4 | C63 | 101.3(2) | C133 | N19 | Rh4 | 118.0(3) |
| C75 | P4 | Rh2 | 110.08(17) | C137 | N19 | Rh4 | 123.7(4) |
| C75 | P4 | C63 | 105.0(2) | C137 | N19 | C133 | 117.7(5) |
| C75 | P4 | C69 | 106.5(2) | C138 | N20 | Rh4 | 118.4(3) |
| C41 | N6 | P3 | 110.1(3) | C138 | N20 | C142 | 118.9(5) |
| C53 | N6 | P3 | 122.9(4) | C142 | N20 | Rh4 | 122.6(4) |
| C53 | N6 | C41 | 125.9(5) | N16 | C121 | C122 | 110.3(4) |
| C46 | N7 | P3 | 113.7(4) | N16 | C121 | C126 | 129.9(5) |
| C46 | N7 | C47 | 126.1(4) | C126 | C121 | C122 | 119.7(5) |
| C47 | N7 | P3 | 117.8(3) | N17 | C122 | C121 | 110.7(5) |
| C52 | N8 | P3 | 115.5(3) | C123 | C122 | N17 | 128.0(5) |
| C58 | N8 | P3 | 118.7(3) | C123 | C122 | C121 | 121.2(5) |
| C58 | N8 | C52 | 125.0(4) | C122 | C123 | C124 | 119.2(5) |
| C53 | N9 | Rh2 | 118.5(3) | C125 | C124 | C123 | 119.8(5) |
| C57 | N9 | Rh2 | 121.9(4) | C124 | C125 | C126 | 121.1(5) |
| C57 | N9 | C53 | 119.5(4) | C121 | C126 | C125 | 119.0(5) |
| C58 | N10 | Rh2 | 117.7(3) | C128 | C127 | N17 | 112.2(5) |
| C62 | N10 | Rh2 | 124.2(3) | C132 | C127 | N17 | 126.7(5) |
| C62 | N10 | C58 | 118.0(4) | C132 | C127 | C128 | 120.7(5) |
| C42 | C41 | N6 | 129.4(5) | C127 | C128 | N18 | 110.1(5) |
| C42 | C41 | C46 | 120.3(5) | C129 | C128 | N18 | 129.8(5) |
| C46 | C41 | N6 | 109.9(4) | C129 | C128 | C127 | 119.8(5) |
| C41 | C42 | C43 | 118.6(6) | C130 | C129 | C128 | 119.3(6) |
| C44 | C43 | C42 | 121.0(5) | C129 | C130 | C131 | 120.5(5) |
| C43 | C44 | C45 | 120.9(6) | C132 | C131 | C130 | 120.4(5) |
| C46 | C45 | C44 | 118.8(6) | C131 | C132 | C127 | 119.2(5) |
| N7 | C46 | C41 | 111.3(5) | N16 | C133 | C134 | 123.0(5) |
| C45 | C46 | N7 | 128.1(5) | N19 | C133 | N16 | 114.6(5) |
| C45 | C46 | C41 | 120.3(5) | N19 | C133 | C134 | 122.3(5) |
| C48 | C47 | N7 | 128.1(5) | C135 | C134 | C133 | 118.7(5) |
| C48 | C47 | C52 | 120.9(5) | C134 | C135 | C136 | 119.3(6) |
| C52 | C47 | N7 | 110.8(4) | C137 | C136 | C135 | 119.4(6) |
| C47 | C48 | C49 | 119.0(5) | N19 | C137 | C136 | 122.4(5) |
| C50 | C49 | C48 | 120.2(5) | N18 | C138 | C139 | 123.6(5) |
| C49 | C50 | C51 | 121.4(5) | N20 | C138 | N18 | 116.4(5) |
| C50 | C51 | C52 | 118.5(5) | N20 | C138 | C139 | 120.0(5) |
| N8 | C52 | C47 | 110.6(4) | C140 | C139 | C138 | 119.2(6) |
| N8 | C52 | C51 | 129.2(5) | C139 | C140 | C141 | 120.2(6) |
| C51 | C52 | C47 | 119.9(5) | C142 | C141 | C140 | 118.5(5) |
| N6 | C53 | C54 | 123.9(5) | N20 | C142 | C141 | 122.7(6) |
| N9 | C53 | N6 | 116.3(5) | C144 | C143 | P8 | 119.3(4) |
| N9 | C53 | C54 | 119.8(5) | C144 | C143 | C148 | 118.5(5) |
| C55 | C54 | C53 | 119.8(5) | C148 | C143 | P8 | 122.1(4) |
| C54 | C55 | C56 | 119.8(5) | C143 | C144 | C145 | 119.6(6) |
| C57 | C56 | C55 | 118.3(5) | C146 | C145 | C144 | 120.7(6) |

| | | | | | | | |
|---|---|---|---|---|---|---|---|
| N9 | C57 | C56 | 122.6(5) | C145 | C146 | C147 | 120.4(6) |
| N8 | C58 | C59 | 122.8(5) | C146 | C147 | C148 | 119.7(6) |
| N10 | C58 | N8 | 115.9(4) | C147 | C148 | C143 | 121.2(6) |
| N10 | C58 | C59 | 121.3(5) | C150 | C149 | P8 | 119.3(4) |
| C60 | C59 | C58 | 119.2(5) | C150 | C149 | C154 | 119.0(5) |
| C61 | C60 | C59 | 118.7(5) | C154 | C149 | P8 | 121.8(4) |
| C62 | C61 | C60 | 119.4(5) | C151 | C150 | C149 | 120.4(5) |
| N10 | C62 | C61 | 123.1(5) | C150 | C151 | C152 | 120.2(5) |
| C64 | C63 | P4 | 119.2(4) | C153 | C152 | C151 | 119.7(5) |
| C64 | C63 | C68 | 118.8(5) | C152 | C153 | C154 | 120.6(5) |
| C68 | C63 | P4 | 122.0(4) | C153 | C154 | C149 | 120.2(5) |
| C63 | C64 | C65 | 120.2(6) | C156 | C155 | P8 | 117.2(4) |
| C66 | C65 | C64 | 121.1(6) | C156 | C155 | C160 | 118.7(5) |
| C65 | C66 | C67 | 119.3(5) | C160 | C155 | P8 | 123.7(4) |
| C68 | C67 | C66 | 120.2(6) | C157 | C156 | C155 | 121.0(5) |
| C67 | C68 | C63 | 120.5(5) | C158 | C157 | C156 | 119.7(5) |
| C70 | C69 | P4 | 124.8(4) | C157 | C158 | C159 | 119.8(6) |
| C70 | C69 | C74 | 118.5(5) | C160 | C159 | C158 | 121.4(6) |
| C74 | C69 | P4 | 116.4(4) | C159 | C160 | C155 | 119.3(5) |
| C71 | C70 | C69 | 120.9(6) | Cl0L | C1S | Cl0Y | 109.6(3) |
| C72 | C71 | C70 | 119.8(6) | Cl0T | C1S | Cl0L | 111.2(3) |
| C71 | C72 | C73 | 120.2(6) | Cl0T | C1S | Cl0Y | 109.9(3) |
| C72 | C73 | C74 | 119.7(6) | Cl0M | C163 | Cl0V | 111.2(3) |
| C73 | C74 | C69 | 120.8(5) | Cl0M | C163 | Cl18 | 104.4(13) |
| C76 | C75 | P4 | 120.6(4) | Cl0V | C163 | Cl18 | 106.5(14) |
| C76 | C75 | C80 | 118.6(5) | Cl14 | C163 | Cl0M | 113.2(6) |
| C80 | C75 | P4 | 120.6(4) | Cl14 | C163 | Cl0V | 112.3(4) |
| C77 | C76 | C75 | 120.7(5) | Cl0U | C167 | Cl0N | 110.5(3) |
| C76 | C77 | C78 | 120.5(5) | Cl0U | C167 | Cl0X | 111.0(3) |
| C77 | C78 | C79 | 119.8(5) | Cl0X | C167 | Cl0N | 109.3(3) |
| C78 | C79 | C80 | 120.4(5) | Cl0Q | C164 | Cl0O | 111.0(3) |
| C79 | C80 | C75 | 119.9(5) | Cl0S | C164 | Cl0O | 109.9(3) |
| Cl5 | Rh3 | Cl6 | 86.73(5) | Cl0S | C164 | Cl0Q | 110.8(3) |
| P5 | Rh3 | Cl5 | 174.59(5) | Cl0P | C165 | Cl10 | 111.2(3) |
| P5 | Rh3 | Cl6 | 88.97(5) | Cl13 | C165 | Cl0P | 110.3(3) |
| P6 | Rh3 | Cl5 | 84.89(5) | Cl13 | C165 | Cl10 | 109.3(3) |
| P6 | Rh3 | Cl6 | 170.81(5) | Cl0R | C166 | Cl0W | 110.5(3) |
| P6 | Rh3 | P5 | 99.60(5) | Cl0R | C166 | Cl11 | 110.6(3) |
| N14 | Rh3 | Cl5 | 87.19(12) | Cl0W | C166 | Cl11 | 110.2(3) |
| N14 | Rh3 | Cl6 | 94.60(13) | Cl0Z | C161 | Cl17 | 110.1(4) |
| N14 | Rh3 | P5 | 89.88(12) | Cl16 | C161 | Cl0Z | 110.5(4) |
| N14 | Rh3 | P6 | 88.77(13) | Cl16 | C161 | Cl17 | 109.5(4) |
| N14 | Rh3 | N15 | 171.93(17) | Cl12 | C162 | Cl01 | 109.3(5) |
| N15 | Rh3 | Cl5 | 87.18(12) | Cl12 | C162 | Cl15 | 111.4(4) |
| N15 | Rh3 | Cl6 | 90.85(13) | Cl15 | C162 | Cl01 | 109.6(5) |

**Table C-41**. Torsion Angles for **4.20**.

| A | B | C | D | Angle/° | A | B | C | D | Angle/° |
|---|---|---|---|---|---|---|---|---|---|
| Rh1 | P1 | N1 | C1 | 140.4(3) | Rh3 | P5 | C103 | C107 | 47.6(4) |
| Rh1 | P1 | N1 | C13 | -35.9(4) | Rh3 | P5 | C103 | C108 | -138.1(4) |
| Rh1 | P1 | N2 | C6 | -77.3(4) | Rh3 | P5 | C110 | C109 | 57.5(5) |
| Rh1 | P1 | N2 | C7 | 115.9(4) | Rh3 | P5 | C110 | C113 | -128.7(4) |
| Rh1 | P1 | N3 | C12 | -174.6(3) | Rh3 | P5 | C115 | C116 | 69.7(4) |
| Rh1 | P1 | N3 | C18 | -9.0(4) | Rh3 | P5 | C115 | C120 | -107.1(4) |
| Rh1 | P2 | C23 | C24 | -66.3(5) | Rh3 | P6 | N11 | C81 | 175.6(3) |
| Rh1 | P2 | C23 | C28 | 118.2(5) | Rh3 | P6 | N11 | C97 | 10.3(4) |
| Rh1 | P2 | C29 | C30 | 112.3(4) | Rh3 | P6 | N12 | C82 | -114.1(4) |
| Rh1 | P2 | C29 | C34 | -65.4(5) | Rh3 | P6 | N12 | C87 | 80.2(5) |
| Rh1 | P2 | C35 | C36 | 141.8(4) | Rh3 | P6 | N13 | C92 | -142.3(3) |
| Rh1 | P2 | C35 | C40 | -45.0(5) | Rh3 | P6 | N13 | C102 | 34.8(4) |
| Rh1 | N4 | C13 | N1 | -1.9(6) | Rh3 | N14 | C96 | C95 | 178.5(4) |
| Rh1 | N4 | C13 | C14 | 175.7(4) | Rh3 | N14 | C97 | N11 | 0.5(6) |
| Rh1 | N4 | C17 | C16 | -175.6(4) | Rh3 | N14 | C97 | C93 | -177.3(4) |
| Rh1 | N5 | C18 | N3 | 3.5(6) | Rh3 | N15 | C101 | C100 | 178.3(4) |
| Rh1 | N5 | C18 | C19 | -177.9(4) | Rh3 | N15 | C102 | N13 | 2.9(6) |
| Rh1 | N5 | C22 | C21 | 177.5(4) | Rh3 | N15 | C102 | C98 | -175.7(4) |
| P1 | N1 | C1 | C2 | -167.6(4) | P5 | C103 | C107 | C106 | 175.4(4) |
| P1 | N1 | C1 | C6 | 4.8(5) | P5 | C103 | C108 | C104 | -175.2(4) |
| P1 | N1 | C13 | N4 | 28.4(6) | P5 | C110 | C113 | C112 | -176.1(4) |
| P1 | N1 | C13 | C14 | -149.1(4) | P5 | C115 | C116 | C117 | -175.2(4) |
| P1 | N2 | C6 | C1 | -7.6(5) | P5 | C115 | C120 | C119 | 175.1(4) |
| P1 | N2 | C6 | C5 | 165.4(4) | P6 | N11 | C81 | C82 | -20.7(5) |
| P1 | N2 | C7 | C8 | 152.7(4) | P6 | N11 | C81 | C86 | 152.8(5) |
| P1 | N2 | C7 | C12 | -21.0(5) | P6 | N11 | C97 | N14 | -8.3(6) |
| P1 | N3 | C12 | C7 | 20.8(5) | P6 | N11 | C97 | C93 | 169.3(4) |
| P1 | N3 | C12 | C11 | -151.0(5) | P6 | N12 | C82 | C81 | 21.6(5) |
| P1 | N3 | C18 | N5 | 4.8(6) | P6 | N12 | C82 | C83 | -153.1(5) |
| P1 | N3 | C18 | C19 | -173.7(4) | P6 | N12 | C87 | C88 | -168.9(4) |
| P2 | C23 | C24 | C25 | -178.5(5) | P6 | N12 | C87 | C92 | 6.0(5) |
| P2 | C23 | C28 | C27 | 177.2(5) | P6 | N13 | C92 | C87 | -4.3(5) |
| P2 | C29 | C30 | C31 | -177.8(4) | P6 | N13 | C92 | C91 | 170.2(4) |
| P2 | C29 | C34 | C33 | 177.7(4) | P6 | N13 | C102 | N15 | -28.1(6) |
| P2 | C35 | C36 | C37 | 175.5(4) | P6 | N13 | C102 | C98 | 150.5(4) |
| P2 | C35 | C40 | C39 | -175.9(4) | N11 | P6 | N12 | C82 | -27.3(3) |
| N1 | P1 | N2 | C6 | 8.3(4) | N11 | P6 | N12 | C87 | 167.0(4) |
| N1 | P1 | N2 | C7 | -158.5(4) | N11 | P6 | N13 | C92 | -23.7(11) |
| N1 | P1 | N3 | C12 | -53.8(11) | N11 | P6 | N13 | C102 | 153.4(8) |
| N1 | P1 | N3 | C18 | 111.8(10) | N11 | C81 | C82 | N12 | 0.7(6) |
| N1 | C1 | C2 | C3 | 172.1(5) | N11 | C81 | C82 | C83 | 175.9(4) |
| N1 | C1 | C6 | N2 | 1.4(6) | N11 | C81 | C86 | C85 | -176.7(5) |
| N1 | C1 | C6 | C5 | -172.2(4) | N12 | P6 | N11 | C81 | 27.1(3) |
| N1 | C13 | C14 | C15 | 176.8(5) | N12 | P6 | N11 | C97 | -138.2(4) |
| N2 | P1 | N1 | C1 | -7.4(4) | N12 | P6 | N13 | C92 | 6.2(4) |
| N2 | P1 | N1 | C13 | 176.3(4) | N12 | P6 | N13 | C102 | -176.7(4) |

| | | | | | | | | | |
|---|---|---|---|---|---|---|---|---|---|
| N2 | P1 | N3 | C12 | -26.9(3) | N12 | C82 | C83 | C84 | 175.4(5) |
| N2 | P1 | N3 | C18 | 138.6(4) | N12 | C87 | C88 | C89 | 177.0(5) |
| N2 | C7 | C8 | C9 | -172.5(5) | N12 | C87 | C92 | N13 | -0.8(6) |
| N2 | C7 | C12 | N3 | -1.1(6) | N12 | C87 | C92 | C91 | -175.8(4) |
| N2 | C7 | C12 | C11 | 171.6(4) | N13 | P6 | N11 | C81 | 57.0(11) |
| N3 | P1 | N1 | C1 | 19.5(11) | N13 | P6 | N11 | C97 | -108.3(10) |
| N3 | P1 | N1 | C13 | -156.9(9) | N13 | P6 | N12 | C82 | 158.9(4) |
| N3 | P1 | N2 | C6 | -166.3(4) | N13 | P6 | N12 | C87 | -6.8(4) |
| N3 | P1 | N2 | C7 | 26.9(3) | C81 | N11 | C97 | N14 | -171.6(4) |
| N3 | C18 | C19 | C20 | 179.2(5) | C81 | N11 | C97 | C93 | 6.1(8) |
| N4 | C13 | C14 | C15 | -0.6(8) | C81 | C82 | C83 | C84 | 1.0(8) |
| N5 | C18 | C19 | C20 | 0.8(7) | C82 | N12 | C87 | C88 | 27.4(8) |
| C1 | N1 | C13 | N4 | -147.6(5) | C82 | N12 | C87 | C92 | -157.7(5) |
| C1 | N1 | C13 | C14 | 34.9(8) | C82 | C81 | C86 | C85 | -3.8(7) |
| C1 | C2 | C3 | C4 | -0.2(8) | C82 | C83 | C84 | C85 | -1.5(8) |
| C2 | C1 | C6 | N2 | 174.6(4) | C83 | C84 | C85 | C86 | -0.6(8) |
| C2 | C1 | C6 | C5 | 1.0(7) | C84 | C85 | C86 | C81 | 3.3(8) |
| C2 | C3 | C4 | C5 | -1.2(8) | C86 | C81 | C82 | N12 | -173.6(4) |
| C3 | C4 | C5 | C6 | 2.5(8) | C86 | C81 | C82 | C83 | 1.6(7) |
| C4 | C5 | C6 | N2 | -174.8(5) | C87 | N12 | C82 | C81 | -174.1(4) |
| C4 | C5 | C6 | C1 | -2.4(7) | C87 | N12 | C82 | C83 | 11.1(8) |
| C6 | N2 | C7 | C8 | -12.8(8) | C87 | C88 | C89 | C90 | -2.6(8) |
| C6 | N2 | C7 | C12 | 173.5(4) | C88 | C87 | C92 | N13 | 174.5(4) |
| C6 | C1 | C2 | C3 | 0.3(7) | C88 | C87 | C92 | C91 | -0.5(7) |
| C7 | N2 | C6 | C1 | 157.3(5) | C88 | C89 | C90 | C91 | 0.5(8) |
| C7 | N2 | C6 | C5 | -29.7(8) | C89 | C90 | C91 | C92 | 1.6(8) |
| C7 | C8 | C9 | C10 | 0.0(8) | C90 | C91 | C92 | N13 | -175.6(5) |
| C8 | C7 | C12 | N3 | -175.3(4) | C90 | C91 | C92 | C87 | -1.6(7) |
| C8 | C7 | C12 | C11 | -2.6(7) | C92 | N13 | C102 | N15 | 148.6(5) |
| C8 | C9 | C10 | C11 | 1.0(9) | C92 | N13 | C102 | C98 | -32.8(8) |
| C9 | C10 | C11 | C12 | -2.8(8) | C92 | C87 | C88 | C89 | 2.5(7) |
| C10 | C11 | C12 | N3 | 174.7(5) | C93 | C94 | C95 | C96 | 0.7(8) |
| C10 | C11 | C12 | C7 | 3.6(8) | C94 | C93 | C97 | N11 | 179.1(5) |
| C12 | N3 | C18 | N5 | 168.0(4) | C94 | C93 | C97 | N14 | -3.3(7) |
| C12 | N3 | C18 | C19 | -10.5(8) | C94 | C95 | C96 | N14 | 1.0(8) |
| C12 | C7 | C8 | C9 | 0.7(8) | C96 | N14 | C97 | N11 | -177.3(4) |
| C13 | N1 | C1 | C2 | 8.4(8) | C96 | N14 | C97 | C93 | 4.9(7) |
| C13 | N1 | C1 | C6 | -179.1(5) | C97 | N11 | C81 | C82 | 144.4(5) |
| C13 | N4 | C17 | C16 | -2.8(8) | C97 | N11 | C81 | C86 | -42.1(8) |
| C13 | C14 | C15 | C16 | -1.0(8) | C97 | N14 | C96 | C95 | -3.8(8) |
| C14 | C15 | C16 | C17 | 0.7(9) | C97 | C93 | C94 | C95 | 0.5(8) |
| C15 | C16 | C17 | N4 | 1.2(9) | C98 | C99 | C100 | C101 | 0.7(9) |
| C17 | N4 | C13 | N1 | -175.1(5) | C99 | C98 | C102 | N13 | 179.2(5) |
| C17 | N4 | C13 | C14 | 2.5(7) | C99 | C98 | C102 | N15 | -2.3(8) |
| C18 | N3 | C12 | C7 | -144.2(5) | C99 | C100 | C101 | N15 | -3.4(9) |
| C18 | N3 | C12 | C11 | 44.0(8) | C101 | N15 | C102 | N13 | 178.3(5) |
| C18 | N5 | C22 | C21 | 1.8(7) | C101 | N15 | C102 | C98 | -0.3(7) |
| C18 | C19 | C20 | C21 | 0.9(8) | C102 | N13 | C92 | C87 | 178.9(5) |

| | | | | | | | | | |
|---|---|---|---|---|---|---|---|---|---|
| C19 | C20 | C21 | C22 | -1.2(8) | C102 | N13 | C92 | C91 | -6.6(8) |
| C20 | C21 | C22 | N5 | -0.2(8) | C102 | N15 | C101 | C100 | 3.1(8) |
| C22 | N5 | C18 | N3 | 179.3(4) | C102 | C98 | C99 | C100 | 2.0(8) |
| C22 | N5 | C18 | C19 | -2.1(7) | C103 | P5 | C110 | C109 | -72.3(5) |
| C23 | P2 | C29 | C30 | -122.1(4) | C103 | P5 | C110 | C113 | 101.6(5) |
| C23 | P2 | C29 | C34 | 60.2(5) | C103 | P5 | C115 | C116 | -163.2(4) |
| C23 | P2 | C35 | C36 | 16.1(5) | C103 | P5 | C115 | C120 | 20.0(5) |
| C23 | P2 | C35 | C40 | -170.7(4) | C104 | C105 | C106 | C107 | -0.7(8) |
| C23 | C24 | C25 | C26 | 2.2(9) | C105 | C104 | C108 | C103 | 0.0(8) |
| C24 | C23 | C28 | C27 | 1.7(9) | C105 | C106 | C107 | C103 | -0.2(8) |
| C24 | C25 | C26 | C27 | -0.5(10) | C107 | C103 | C108 | C104 | -0.9(8) |
| C25 | C26 | C27 | C28 | -0.5(10) | C108 | C103 | C107 | C106 | 0.9(7) |
| C26 | C27 | C28 | C23 | -0.1(10) | C108 | C104 | C105 | C106 | 0.8(8) |
| C28 | C23 | C24 | C25 | -2.8(9) | C109 | C110 | C113 | C112 | -2.2(8) |
| C29 | P2 | C23 | C24 | 168.6(4) | C110 | P5 | C103 | C107 | 175.6(4) |
| C29 | P2 | C23 | C28 | -7.0(5) | C110 | P5 | C103 | C108 | -10.1(5) |
| C29 | P2 | C35 | C36 | -93.9(5) | C110 | P5 | C115 | C116 | -56.0(5) |
| C29 | P2 | C35 | C40 | 79.3(4) | C110 | P5 | C115 | C120 | 127.2(4) |
| C29 | C30 | C31 | C32 | -0.1(8) | C110 | C109 | C114 | C111 | -1.3(9) |
| C30 | C29 | C34 | C33 | -0.1(8) | C111 | C112 | C113 | C110 | 0.3(9) |
| C30 | C31 | C32 | C33 | 0.2(8) | C112 | C111 | C114 | C109 | -0.6(9) |
| C31 | C32 | C33 | C34 | -0.3(8) | C114 | C109 | C110 | P5 | 176.8(4) |
| C32 | C33 | C34 | C29 | 0.2(8) | C114 | C109 | C110 | C113 | 2.7(8) |
| C34 | C29 | C30 | C31 | 0.0(8) | C114 | C111 | C112 | C113 | 1.1(9) |
| C35 | P2 | C23 | C24 | 61.6(5) | C115 | P5 | C103 | C107 | -75.1(4) |
| C35 | P2 | C23 | C28 | -113.9(5) | C115 | P5 | C103 | C108 | 99.2(4) |
| C35 | P2 | C29 | C30 | -15.0(5) | C115 | P5 | C110 | C109 | -179.2(4) |
| C35 | P2 | C29 | C34 | 167.3(4) | C115 | P5 | C110 | C113 | -5.4(5) |
| C35 | C36 | C37 | C38 | -0.3(8) | C115 | C116 | C117 | C118 | -1.2(8) |
| C36 | C35 | C40 | C39 | -2.4(7) | C116 | C115 | C120 | C119 | -1.7(7) |
| C36 | C37 | C38 | C39 | -1.5(8) | C116 | C117 | C118 | C119 | 0.7(8) |
| C37 | C38 | C39 | C40 | 1.2(8) | C117 | C118 | C119 | C120 | -0.7(8) |
| C38 | C39 | C40 | C35 | 0.7(8) | C118 | C119 | C120 | C115 | 1.2(8) |
| C40 | C35 | C36 | C37 | 2.2(8) | C120 | C115 | C116 | C117 | 1.7(7) |
| Rh2 | P3 | N6 | C41 | 177.4(3) | Rh4 | P7 | N16 | C121 | 140.7(3) |
| Rh2 | P3 | N6 | C53 | 8.9(4) | Rh4 | P7 | N16 | C133 | -36.0(4) |
| Rh2 | P3 | N7 | C46 | -116.6(4) | Rh4 | P7 | N17 | C122 | -77.4(5) |
| Rh2 | P3 | N7 | C47 | 79.7(5) | Rh4 | P7 | N17 | C127 | 115.2(4) |
| Rh2 | P3 | N8 | C52 | -140.0(3) | Rh4 | P7 | N18 | C128 | -176.2(3) |
| Rh2 | P3 | N8 | C58 | 30.7(4) | Rh4 | P7 | N18 | C138 | -9.2(4) |
| Rh2 | P4 | C63 | C64 | -136.3(4) | Rh4 | P8 | C143 | C144 | 132.8(4) |
| Rh2 | P4 | C63 | C68 | 46.3(5) | Rh4 | P8 | C143 | C148 | -50.5(5) |
| Rh2 | P4 | C69 | C70 | -131.7(4) | Rh4 | P8 | C149 | C150 | -71.7(4) |
| Rh2 | P4 | C69 | C74 | 54.3(4) | Rh4 | P8 | C149 | C154 | 109.8(4) |
| Rh2 | P4 | C75 | C76 | 79.3(4) | Rh4 | P8 | C155 | C156 | -55.7(4) |
| Rh2 | P4 | C75 | C80 | -96.1(4) | Rh4 | P8 | C155 | C160 | 131.3(4) |
| Rh2 | N9 | C53 | N6 | 0.4(6) | Rh4 | N19 | C133 | N16 | -5.2(6) |
| Rh2 | N9 | C53 | C54 | -177.7(4) | Rh4 | N19 | C133 | C134 | 172.3(4) |

| | | | | | | | | | |
|---|---|---|---|---|---|---|---|---|---|
| Rh2 | N9 | C57 | C56 | -179.1(4) | Rh4 | N19 | C137 | C136 | -174.4(5) |
| Rh2 | N10 | C58 | N8 | 6.5(6) | Rh4 | N20 | C138 | N18 | -1.0(6) |
| Rh2 | N10 | C58 | C59 | -171.4(4) | Rh4 | N20 | C138 | C139 | 175.8(4) |
| Rh2 | N10 | C62 | C61 | 176.4(4) | Rh4 | N20 | C142 | C141 | 179.9(4) |
| P3 | N6 | C41 | C42 | 150.7(5) | P7 | N16 | C121 | C122 | 6.2(5) |
| P3 | N6 | C41 | C46 | -22.2(5) | P7 | N16 | C121 | C126 | -168.8(5) |
| P3 | N6 | C53 | N9 | -7.1(7) | P7 | N16 | C133 | N19 | 30.5(6) |
| P3 | N6 | C53 | C54 | 170.8(4) | P7 | N16 | C133 | C134 | -147.0(4) |
| P3 | N7 | C46 | C41 | 22.5(5) | P7 | N17 | C122 | C121 | -7.2(6) |
| P3 | N7 | C46 | C45 | -151.5(5) | P7 | N17 | C122 | C123 | 168.7(4) |
| P3 | N7 | C47 | C48 | -167.8(4) | P7 | N17 | C127 | C128 | -21.5(5) |
| P3 | N7 | C47 | C52 | 6.7(6) | P7 | N17 | C127 | C132 | 152.2(5) |
| P3 | N8 | C52 | C47 | -7.0(6) | P7 | N18 | C128 | C127 | 21.0(5) |
| P3 | N8 | C52 | C51 | 166.1(5) | P7 | N18 | C128 | C129 | -152.3(5) |
| P3 | N8 | C58 | N10 | -27.4(6) | P7 | N18 | C138 | N20 | 7.8(6) |
| P3 | N8 | C58 | C59 | 150.5(4) | P7 | N18 | C138 | C139 | -169.0(4) |
| P4 | C63 | C64 | C65 | -177.8(4) | P8 | C143 | C144 | C145 | 176.4(5) |
| P4 | C63 | C68 | C67 | 177.4(4) | P8 | C143 | C148 | C147 | -175.7(5) |
| P4 | C69 | C70 | C71 | -176.5(4) | P8 | C149 | C150 | C151 | -178.0(5) |
| P4 | C69 | C74 | C73 | 175.6(4) | P8 | C149 | C154 | C153 | 178.4(4) |
| P4 | C75 | C76 | C77 | -176.9(4) | P8 | C155 | C156 | C157 | -174.5(4) |
| P4 | C75 | C80 | C79 | 175.9(4) | P8 | C155 | C160 | C159 | 174.8(5) |
| N6 | P3 | N7 | C46 | -28.8(4) | N16 | P7 | N17 | C122 | 8.6(4) |
| N6 | P3 | N7 | C47 | 167.6(4) | N16 | P7 | N17 | C127 | -158.7(4) |
| N6 | P3 | N8 | C52 | -10.0(12) | N16 | P7 | N18 | C128 | -54.2(11) |
| N6 | P3 | N8 | C58 | 160.7(9) | N16 | P7 | N18 | C138 | 112.8(9) |
| N6 | C41 | C42 | C43 | -175.1(6) | N16 | C121 | C122 | N17 | 0.4(6) |
| N6 | C41 | C46 | N7 | 1.1(6) | N16 | C121 | C122 | C123 | -175.9(5) |
| N6 | C41 | C46 | C45 | 175.7(5) | N16 | C121 | C126 | C125 | 176.0(5) |
| N6 | C53 | C54 | C55 | 177.9(5) | N16 | C133 | C134 | C135 | 178.7(5) |
| N7 | P3 | N6 | C41 | 28.6(4) | N17 | P7 | N16 | C121 | -8.3(4) |
| N7 | P3 | N6 | C53 | -139.9(4) | N17 | P7 | N16 | C133 | 175.0(4) |
| N7 | P3 | N8 | C52 | 8.8(4) | N17 | P7 | N18 | C128 | -27.3(4) |
| N7 | P3 | N8 | C58 | 179.4(4) | N17 | P7 | N18 | C138 | 139.7(4) |
| N7 | C47 | C48 | C49 | 174.5(5) | N17 | C122 | C123 | C124 | -177.1(5) |
| N7 | C47 | C52 | N8 | 0.5(6) | N17 | C127 | C128 | N18 | -0.8(6) |
| N7 | C47 | C52 | C51 | -173.4(5) | N17 | C127 | C128 | C129 | 173.3(5) |
| N8 | P3 | N6 | C41 | 47.4(11) | N17 | C127 | C132 | C131 | -174.3(5) |
| N8 | P3 | N6 | C53 | -121.1(10) | N18 | P7 | N16 | C121 | 18.7(11) |
| N8 | P3 | N7 | C46 | 155.1(4) | N18 | P7 | N16 | C133 | -158.0(8) |
| N8 | P3 | N7 | C47 | -8.6(4) | N18 | P7 | N17 | C122 | -165.6(4) |
| N8 | C58 | C59 | C60 | 176.4(5) | N18 | P7 | N17 | C127 | 27.1(4) |
| N9 | C53 | C54 | C55 | -4.2(8) | N18 | C128 | C129 | C130 | 175.2(5) |
| N10 | C58 | C59 | C60 | -5.8(7) | N18 | C138 | C139 | C140 | -177.3(5) |
| C41 | N6 | C53 | N9 | -173.8(5) | N19 | C133 | C134 | C135 | 1.4(8) |
| C41 | N6 | C53 | C54 | 4.2(8) | N20 | C138 | C139 | C140 | 6.0(8) |
| C41 | C42 | C43 | C44 | 1.0(9) | C121 | N16 | C133 | N19 | -145.9(5) |
| C42 | C41 | C46 | N7 | -172.5(5) | C121 | N16 | C133 | C134 | 36.7(8) |

| | | | | | | | | | |
|---|---|---|---|---|---|---|---|---|---|
| C42 | C41 | C46 | C45 | 2.1(8) | C121 | C122 | C123 | C124 | -1.5(8) |
| C42 | C43 | C44 | C45 | 1.7(9) | C122 | N17 | C127 | C128 | 172.5(5) |
| C43 | C44 | C45 | C46 | -2.5(9) | C122 | N17 | C127 | C132 | -13.7(8) |
| C44 | C45 | C46 | N7 | 174.2(5) | C122 | C121 | C126 | C125 | 1.4(8) |
| C44 | C45 | C46 | C41 | 0.6(8) | C122 | C123 | C124 | C125 | 2.3(8) |
| C46 | N7 | C47 | C48 | 30.8(8) | C123 | C124 | C125 | C126 | -1.3(9) |
| C46 | N7 | C47 | C52 | -154.7(5) | C124 | C125 | C126 | C121 | -0.6(8) |
| C46 | C41 | C42 | C43 | -2.9(8) | C126 | C121 | C122 | N17 | 175.9(5) |
| C47 | N7 | C46 | C41 | -175.5(5) | C126 | C121 | C122 | C123 | -0.3(8) |
| C47 | N7 | C46 | C45 | 10.5(8) | C127 | N17 | C122 | C121 | 158.1(5) |
| C47 | C48 | C49 | C50 | -1.5(8) | C127 | N17 | C122 | C123 | -26.0(8) |
| C48 | C47 | C52 | N8 | 175.5(5) | C127 | C128 | C129 | C130 | 2.4(8) |
| C48 | C47 | C52 | C51 | 1.6(8) | C128 | N18 | C138 | N20 | 172.7(5) |
| C48 | C49 | C50 | C51 | 0.4(9) | C128 | N18 | C138 | C139 | -4.0(8) |
| C49 | C50 | C51 | C52 | 1.7(8) | C128 | C127 | C132 | C131 | -1.1(8) |
| C50 | C51 | C52 | N8 | -175.3(5) | C128 | C129 | C130 | C131 | -2.1(9) |
| C50 | C51 | C52 | C47 | -2.6(8) | C129 | C130 | C131 | C132 | 0.1(9) |
| C52 | N8 | C58 | N10 | 142.2(5) | C130 | C131 | C132 | C127 | 1.4(8) |
| C52 | N8 | C58 | C59 | -39.9(7) | C132 | C127 | C128 | N18 | -174.9(5) |
| C52 | C47 | C48 | C49 | 0.5(8) | C132 | C127 | C128 | C129 | -0.9(8) |
| C53 | N6 | C41 | C42 | -41.2(9) | C133 | N16 | C121 | C122 | -177.4(5) |
| C53 | N6 | C41 | C46 | 145.9(5) | C133 | N16 | C121 | C126 | 7.6(9) |
| C53 | N9 | C57 | C56 | -2.0(8) | C133 | N19 | C137 | C136 | -3.4(9) |
| C53 | C54 | C55 | C56 | 0.0(8) | C133 | C134 | C135 | C136 | -0.9(9) |
| C54 | C55 | C56 | C57 | 3.2(8) | C134 | C135 | C136 | C137 | -1.5(10) |
| C55 | C56 | C57 | N9 | -2.2(8) | C135 | C136 | C137 | N19 | 3.8(10) |
| C57 | N9 | C53 | N6 | -176.7(5) | C137 | N19 | C133 | N16 | -176.8(5) |
| C57 | N9 | C53 | C54 | 5.2(7) | C137 | N19 | C133 | C134 | 0.7(8) |
| C58 | N8 | C52 | C47 | -177.0(5) | C138 | N18 | C128 | C127 | -145.5(5) |
| C58 | N8 | C52 | C51 | -3.8(9) | C138 | N18 | C128 | C129 | 41.2(9) |
| C58 | N10 | C62 | C61 | 0.8(8) | C138 | N20 | C142 | C141 | 3.8(8) |
| C58 | C59 | C60 | C61 | 1.9(8) | C138 | C139 | C140 | C141 | 0.0(8) |
| C59 | C60 | C61 | C62 | 3.1(8) | C139 | C140 | C141 | C142 | -4.0(8) |
| C60 | C61 | C62 | N10 | -4.6(8) | C140 | C141 | C142 | N20 | 2.2(8) |
| C62 | N10 | C58 | N8 | -177.6(4) | C142 | N20 | C138 | N18 | 175.3(5) |
| C62 | N10 | C58 | C59 | 4.4(7) | C142 | N20 | C138 | C139 | -7.8(7) |
| C63 | P4 | C69 | C70 | 99.8(5) | C143 | P8 | C149 | C150 | 159.3(4) |
| C63 | P4 | C69 | C74 | -74.2(4) | C143 | P8 | C149 | C154 | -19.2(5) |
| C63 | P4 | C75 | C76 | -152.4(4) | C143 | P8 | C155 | C156 | 72.0(4) |
| C63 | P4 | C75 | C80 | 32.3(5) | C143 | P8 | C155 | C160 | -101.0(5) |
| C63 | C64 | C65 | C66 | 0.1(9) | C143 | C144 | C145 | C146 | -0.5(10) |
| C64 | C63 | C68 | C67 | 0.1(8) | C144 | C143 | C148 | C147 | 1.1(9) |
| C64 | C65 | C66 | C67 | 0.4(9) | C144 | C145 | C146 | C147 | 0.9(10) |
| C65 | C66 | C67 | C68 | -0.7(9) | C145 | C146 | C147 | C148 | -0.3(9) |
| C66 | C67 | C68 | C63 | 0.4(8) | C146 | C147 | C148 | C143 | -0.7(9) |
| C68 | C63 | C64 | C65 | -0.4(8) | C148 | C143 | C144 | C145 | -0.5(9) |
| C69 | P4 | C63 | C64 | -10.3(5) | C149 | P8 | C143 | C144 | -101.6(5) |
| C69 | P4 | C63 | C68 | 172.4(4) | C149 | P8 | C143 | C148 | 75.2(5) |

| | | | | | | | | | |
|---|---|---|---|---|---|---|---|---|---|
| C69 | P4 | C75 | C76 | -45.5(5) | C149 | P8 | C155 | C156 | 179.9(4) |
| C69 | P4 | C75 | C80 | 139.1(4) | C149 | P8 | C155 | C160 | 6.9(5) |
| C69 | C70 | C71 | C72 | 1.8(9) | C149 | C150 | C151 | C152 | -0.7(9) |
| C70 | C69 | C74 | C73 | 1.2(8) | C150 | C149 | C154 | C153 | -0.2(8) |
| C70 | C71 | C72 | C73 | 0.3(9) | C150 | C151 | C152 | C153 | 0.4(10) |
| C71 | C72 | C73 | C74 | -1.7(9) | C151 | C152 | C153 | C154 | 0.0(10) |
| C72 | C73 | C74 | C69 | 0.9(9) | C152 | C153 | C154 | C149 | -0.1(9) |
| C74 | C69 | C70 | C71 | -2.6(8) | C154 | C149 | C150 | C151 | 0.6(8) |
| C75 | P4 | C63 | C64 | 100.4(5) | C155 | P8 | C143 | C144 | 7.0(5) |
| C75 | P4 | C63 | C68 | -76.9(5) | C155 | P8 | C143 | C148 | -176.2(5) |
| C75 | P4 | C69 | C70 | -9.7(5) | C155 | P8 | C149 | C150 | 54.1(5) |
| C75 | P4 | C69 | C74 | 176.3(4) | C155 | P8 | C149 | C154 | -124.4(5) |
| C75 | C76 | C77 | C78 | 0.7(8) | C155 | C156 | C157 | C158 | -1.1(8) |
| C76 | C75 | C80 | C79 | 0.5(8) | C156 | C155 | C160 | C159 | 1.9(8) |
| C76 | C77 | C78 | C79 | 1.1(8) | C156 | C157 | C158 | C159 | 2.5(9) |
| C77 | C78 | C79 | C80 | -2.1(8) | C157 | C158 | C159 | C160 | -1.8(10) |
| C78 | C79 | C80 | C75 | 1.3(8) | C158 | C159 | C160 | C155 | -0.5(9) |
| C80 | C75 | C76 | C77 | -1.5(8) | C160 | C155 | C156 | C157 | -1.1(8) |

**Table C-42.** Hydrogen Atom Coordinates (Å×10$^4$) and Isotropic Displacement Parameters (Å$^2$×10$^3$) for **4.20**.

| **Atom** | ***x*** | ***y*** | ***z*** | **U(eq)** |
|---|---|---|---|---|
| H1 | -4960(30) | 17450(30) | 2222(9) | 10(13) |
| H2 | -7419.89 | 15796.41 | 2051.92 | 24 |
| H3 | -7980.8 | 15188.51 | 2349.93 | 25 |
| H4 | -7317.03 | 15151.51 | 2730.17 | 25 |
| H5 | -6020.85 | 15693.69 | 2818.95 | 22 |
| H8 | -5546.49 | 16705.16 | 2947.53 | 25 |
| H9 | -4681.27 | 17314.11 | 3238.37 | 31 |
| H10 | -3379.04 | 17665.49 | 3168.56 | 31 |
| H11 | -2925.15 | 17461.81 | 2801.77 | 27 |
| H14 | -7312.27 | 16779.14 | 1866.11 | 22 |
| H15 | -7545.54 | 17028.83 | 1465.32 | 30 |
| H16 | -6421.82 | 16999.36 | 1243.75 | 33 |
| H17 | -5133.41 | 16708.93 | 1427.82 | 29 |
| H19 | -2309.8 | 16692.35 | 2648.83 | 24 |
| H20 | -1156.2 | 16268.71 | 2495.43 | 26 |
| H21 | -1264.38 | 15884.16 | 2101.08 | 26 |
| H22 | -2542.47 | 15904.96 | 1878.24 | 22 |
| H24 | -6193.15 | 15257.67 | 1843.24 | 31 |
| H25 | -7235.48 | 14813.94 | 1563.53 | 36 |
| H26 | -6898.44 | 13966.28 | 1284.41 | 39 |
| H27 | -5556.54 | 13602.04 | 1282.26 | 42 |
| H28 | -4517.69 | 14069.24 | 1552.27 | 33 |
| H30 | -3388.66 | 14191.77 | 2264.04 | 24 |
| H31 | -2169.57 | 13579.85 | 2240.87 | 27 |

| | | | | |
|---|---|---|---|---|
| H32 | -1561 | 13585.97 | 1894.29 | 27 |
| H33 | -2182.61 | 14223.65 | 1568.09 | 27 |
| H34 | -3396.86 | 14832.96 | 1588.11 | 24 |
| H36 | -5613.39 | 13974.47 | 2070.78 | 26 |
| H37 | -5941.48 | 13492.93 | 2418.74 | 25 |
| H38 | -5357.76 | 13946.64 | 2779.75 | 25 |
| H39 | -4385.56 | 14872.8 | 2791.86 | 24 |
| H40 | -4037.53 | 15364.19 | 2441.73 | 21 |
| H3A | 2790(30) | 7330(20) | 4560(8) | 2(11) |
| H42 | 5010.63 | 6872.48 | 5025.64 | 31 |
| H43 | 4686.5 | 6516.22 | 5396.8 | 37 |
| H44 | 3533.64 | 6958.67 | 5540.5 | 35 |
| H45 | 2625.79 | 7729.28 | 5311.4 | 29 |
| H48 | 2221.01 | 8816.4 | 5249.03 | 28 |
| H49 | 999.99 | 9473.01 | 5231.92 | 31 |
| H50 | 194.4 | 9645.23 | 4875.4 | 33 |
| H51 | 576.23 | 9164.17 | 4528 | 26 |
| H54 | 5632.67 | 7729.34 | 4903.04 | 28 |
| H55 | 6759.32 | 8039.27 | 4713.27 | 28 |
| H56 | 6551.82 | 8460.86 | 4324.64 | 29 |
| H57 | 5218.68 | 8654.58 | 4148.93 | 25 |
| H59 | 458.8 | 8204.51 | 4297.77 | 23 |
| H60 | 7.41 | 8343.62 | 3895.89 | 29 |
| H61 | 975.41 | 8585.98 | 3638.55 | 28 |
| H62 | 2349.7 | 8579.97 | 3778.36 | 24 |
| H64 | 4420.28 | 10771.64 | 4585.09 | 29 |
| H65 | 5559.62 | 11476.12 | 4530.52 | 37 |
| H66 | 6218.13 | 11337.14 | 4200.02 | 38 |
| H67 | 5725.92 | 10486.15 | 3912.69 | 34 |
| H68 | 4597.04 | 9770.68 | 3965.31 | 27 |
| H70 | 2416.36 | 10652.37 | 4570.03 | 30 |
| H71 | 2356.93 | 10938.86 | 4963.99 | 34 |
| H72 | 3265.74 | 10398.03 | 5256.47 | 36 |
| H73 | 4242.19 | 9575.37 | 5155.74 | 35 |
| H74 | 4265.17 | 9254.66 | 4762.76 | 29 |
| H76 | 1722.08 | 9838.8 | 4334.27 | 22 |
| H77 | 652.52 | 10344.18 | 4086.1 | 28 |
| H78 | 899.24 | 10903.8 | 3737.89 | 29 |
| H79 | 2224.4 | 10924.38 | 3630.87 | 26 |
| H80 | 3320.83 | 10448.82 | 3883.32 | 22 |
| H6 | -180(30) | 11690(30) | 2897(9) | 10(13) |
| H83 | 187.47 | 12294.94 | 2127.03 | 27 |
| H84 | -828.8 | 11723.74 | 1870.7 | 29 |
| H85 | -2113.83 | 11487.69 | 1985.36 | 29 |
| H86 | -2393.71 | 11790.45 | 2361.27 | 27 |
| H88 | 786.25 | 13273.82 | 2215.18 | 24 |
| H89 | 2141.63 | 13706.89 | 2255.15 | 30 |
| H90 | 2913.19 | 13742.52 | 2620.21 | 31 |

| | | | | |
|---|---|---|---|---|
| H91 | 2376.44 | 13332.16 | 2957.14 | 24 |
| H93 | -2849.98 | 12693.56 | 2491.96 | 25 |
| H94 | -3930.03 | 13188.81 | 2663.05 | 31 |
| H95 | -3715.03 | 13599.68 | 3053.92 | 30 |
| H96 | -2418.13 | 13506.03 | 3259.93 | 26 |
| H98 | 2274.77 | 12437.73 | 3178.02 | 26 |
| H99 | 2626.63 | 12379.17 | 3583.29 | 31 |
| H100 | 1610.24 | 12578 | 3832.39 | 34 |
| H101 | 273.3 | 12800.01 | 3668.93 | 30 |
| H104 | 929.91 | 15680.3 | 2596.42 | 26 |
| H105 | 245.81 | 15197.11 | 2250.78 | 23 |
| H106 | -762.84 | 14306.84 | 2270.16 | 23 |
| H107 | -1057.02 | 13895.17 | 2632.58 | 21 |
| H108 | 633.1 | 15261.91 | 2960.03 | 25 |
| H109 | 1172.63 | 14016.68 | 3270.15 | 29 |
| H111 | 1885.42 | 15619.09 | 3726.56 | 34 |
| H112 | 561.36 | 16091.67 | 3674.16 | 32 |
| H113 | -472.96 | 15515 | 3425.47 | 24 |
| H114 | 2190.17 | 14582.69 | 3521.8 | 32 |
| H116 | -1490.47 | 14659.02 | 3486.79 | 22 |
| H117 | -2761.69 | 15207.59 | 3502.35 | 26 |
| H118 | -3509.72 | 15661.5 | 3160.69 | 26 |
| H119 | -2996.02 | 15534.76 | 2801.22 | 24 |
| H120 | -1726.22 | 14987.46 | 2782.53 | 22 |
| H7 | -2240(30) | 17580(20) | 4478(8) | 1(11) |
| H123 | -2770.2 | 16221.74 | 5203.94 | 27 |
| H124 | -4022.43 | 15597.31 | 5206.32 | 32 |
| H125 | -4843.66 | 15368.26 | 4854.41 | 32 |
| H126 | -4471.54 | 15791.23 | 4497.11 | 27 |
| H129 | 55.24 | 18030.92 | 4954.08 | 33 |
| H130 | -217.43 | 18417.95 | 5325.07 | 37 |
| H131 | -1414.29 | 18055.6 | 5472.46 | 33 |
| H132 | -2348.01 | 17295.14 | 5251.8 | 28 |
| H134 | -4586.4 | 16729.26 | 4259.95 | 30 |
| H135 | -5047.8 | 16729.09 | 3857.67 | 41 |
| H136 | -4102.66 | 16561.53 | 3588.98 | 44 |
| H137 | -2720.32 | 16462.09 | 3724.04 | 35 |
| H139 | 624.03 | 17136.24 | 4836.39 | 31 |
| H140 | 1721.14 | 16778.27 | 4644.04 | 36 |
| H141 | 1485.76 | 16355.62 | 4256.43 | 35 |
| H142 | 154.5 | 16188.83 | 4085.82 | 29 |
| H144 | -576.9 | 14241.91 | 4599.75 | 38 |
| H145 | 568.82 | 13508.64 | 4558.75 | 47 |
| H146 | 1151.01 | 13506.61 | 4212.46 | 41 |
| H147 | 633.84 | 14251.47 | 3902.66 | 36 |
| H148 | -483.23 | 14997.08 | 3940.73 | 32 |
| H150 | -3336.76 | 15174.36 | 4286.07 | 28 |
| H151 | -4396.86 | 14507.47 | 4081.71 | 35 |

| | | | | |
|---|---|---|---|---|
| H152 | -4114.78 | 13664.88 | 3798.39 | 36 |
| H153 | -2769.52 | 13481.7 | 3724.67 | 34 |
| H154 | -1700.67 | 14133.27 | 3930.43 | 26 |
| H156 | -771.22 | 15706.62 | 4733.08 | 24 |
| H157 | -783.07 | 15441.13 | 5129.86 | 31 |
| H158 | -1769.8 | 14656.19 | 5244.98 | 35 |
| H159 | -2671.72 | 14074.42 | 4962.7 | 39 |
| H160 | -2656.55 | 14307.18 | 4564.96 | 30 |
| H1S | -1748.92 | 8908.68 | 4195.9 | 33 |
| H163 | 3016.55 | 15964.61 | 4210.93 | 34 |
| H16A | 3099.07 | 15947.92 | 4194.79 | 34 |
| H167 | 3506.5 | 17349.61 | 3681.34 | 34 |
| H164 | -538.88 | 10607.52 | 3338.92 | 30 |
| H165 | -1166.46 | 17189.78 | 3573.4 | 35 |
| H166 | 4379.95 | 13694.91 | 3336.22 | 32 |
| H161 | -1248.97 | 12554.81 | 3938.58 | 56 |
| H162 | 4437.26 | 12348.11 | 4336.18 | 62 |

## C.2. DFT Calculation

*C.2.1. General computational information.*

Geometries were optimized in Orca 4.0.0[1] using the B3LYP[2] density functionals with the def2-TZVP basis set[3]. Calculations were carried out in the gas phase without symmetry constraint. Stationary points were characterized by frequency calculations to confirm their identity as local minima (zero imaginary frequencies). For the final electronic energies, an all-electron single point calculation was conducted for the coordinates obtained in the calculations above. A relativistic approximation was introduced by applying zeroth-order regular approximation (ZORA)[4] using the B3LYP density functional with the relativistically recontracted version of def2-TZVP basis set.

Before the optimization of **4.12**, **4.15**, **4.16**, the geometries of six stereoisomers of **4.12** shown below were optimized under B3LYP/6-31G*/LANL2DZ level. Among the optimized structures, isomer A had the lowest total electronic energy and was used as the model of metal-centered oxidative addition product of **4.12**, **4.15** and **4.16**.

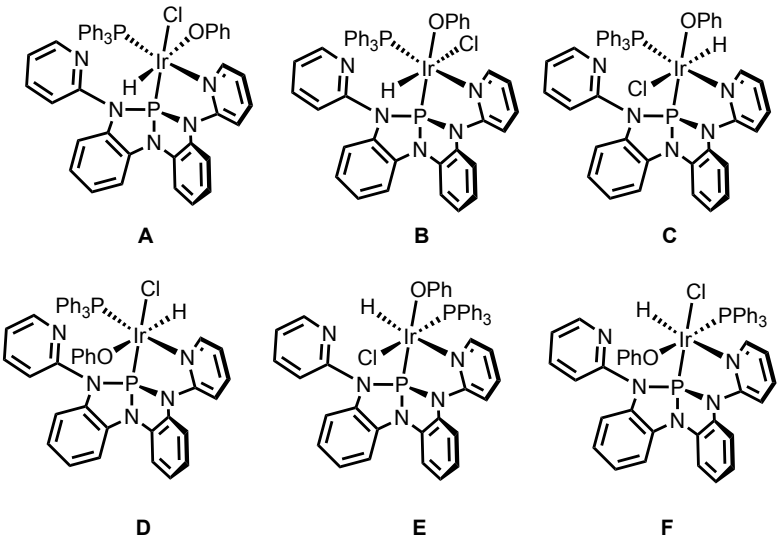

## C.3. Multinuclear NMR spectra

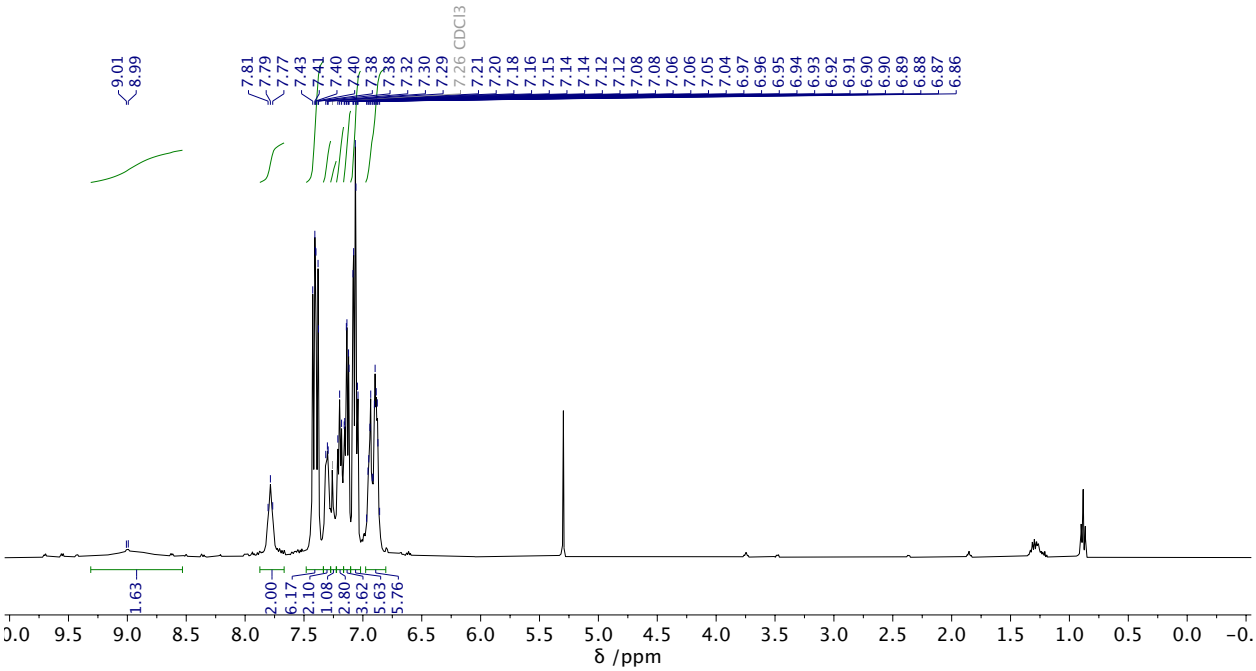


**Figure C-1.** $^{1}$H NMR spectrum ($CD_2Cl_2$) of **4.1**. Signals of recrystallization solvent (dichloromethane, pentane) are also observed.

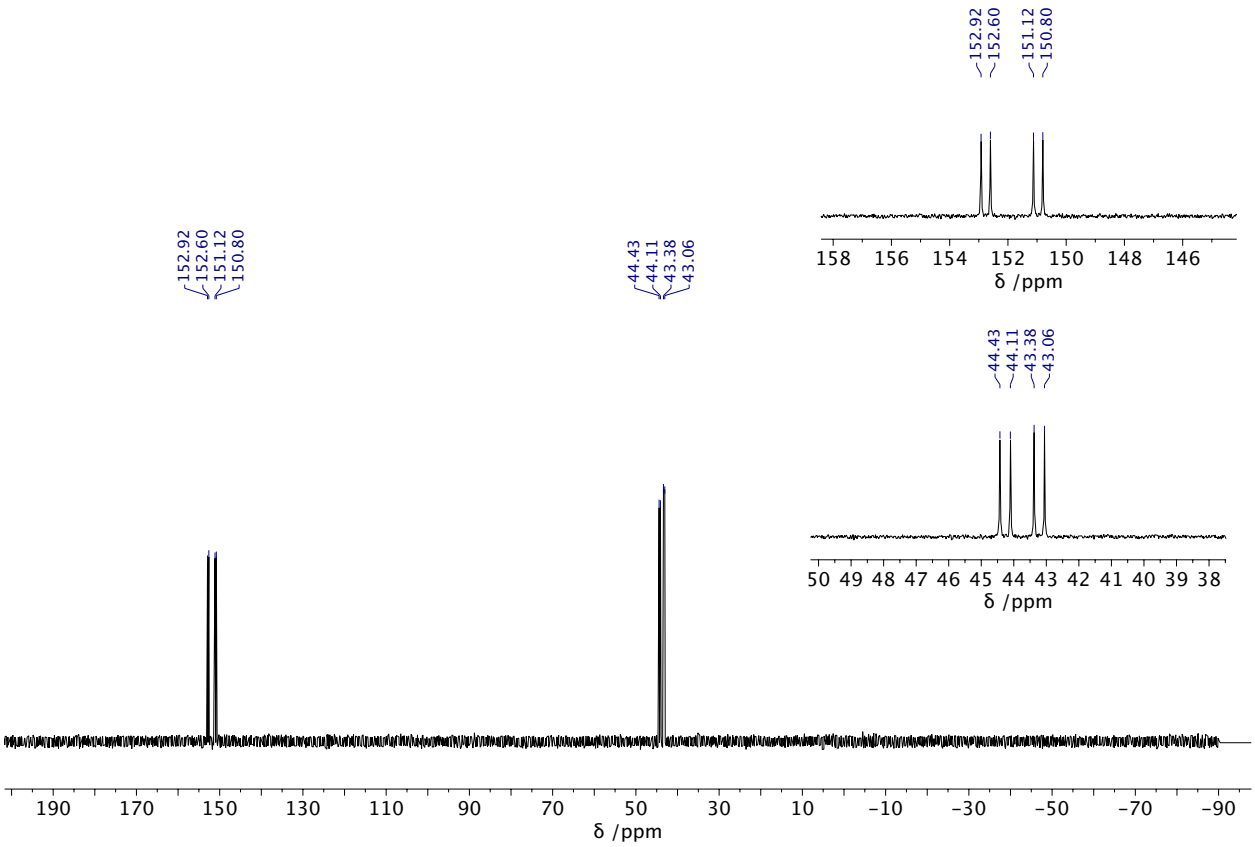


**Figure C-2.** $^{31}P\{^{1}H\}$ NMR spectrum ($CD_2Cl_2$) of **4.1**.

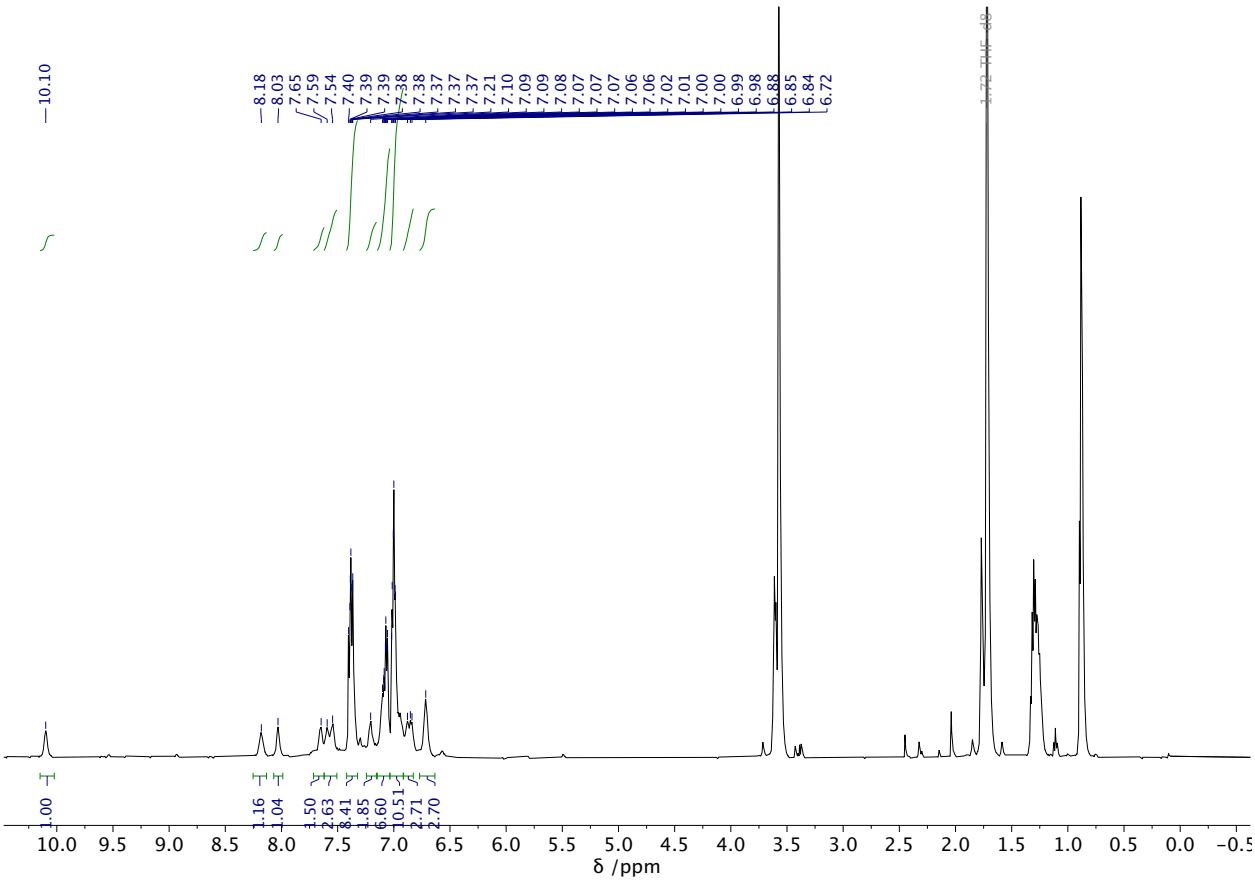


**Figure C-3.** $^{1}$H NMR spectrum of **4.2**. (THF–$d_8$). Signals of pentane used for recrystallization are also observed

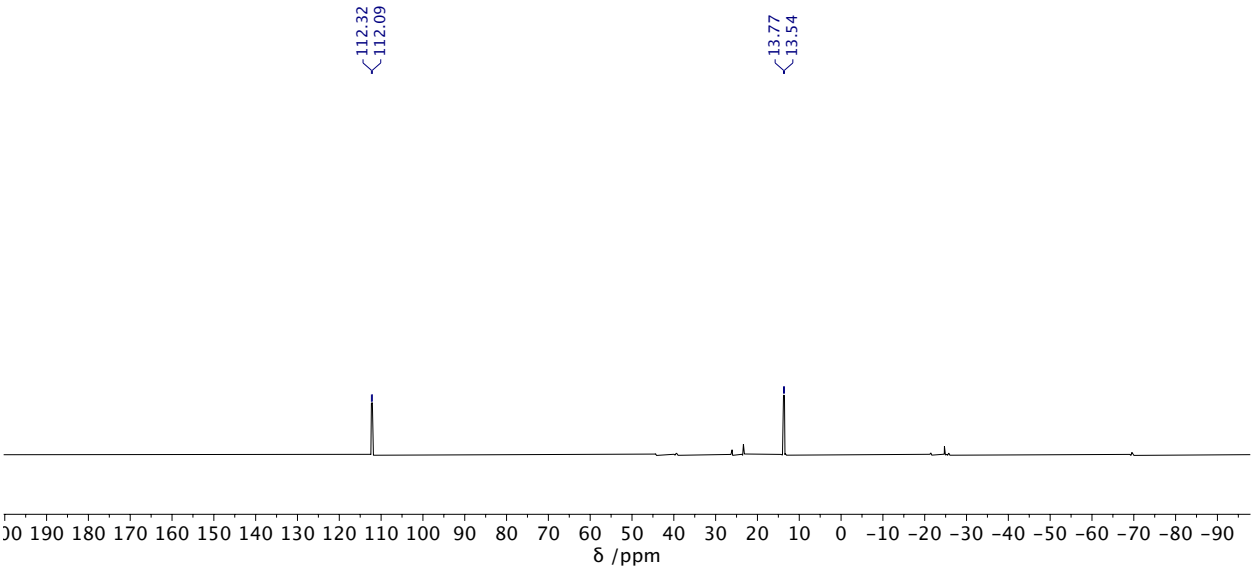


**Figure C-4.** $^{31}P\{^{1}H\}$ NMR spectrum (THF–$d_8$) of **4.2**.

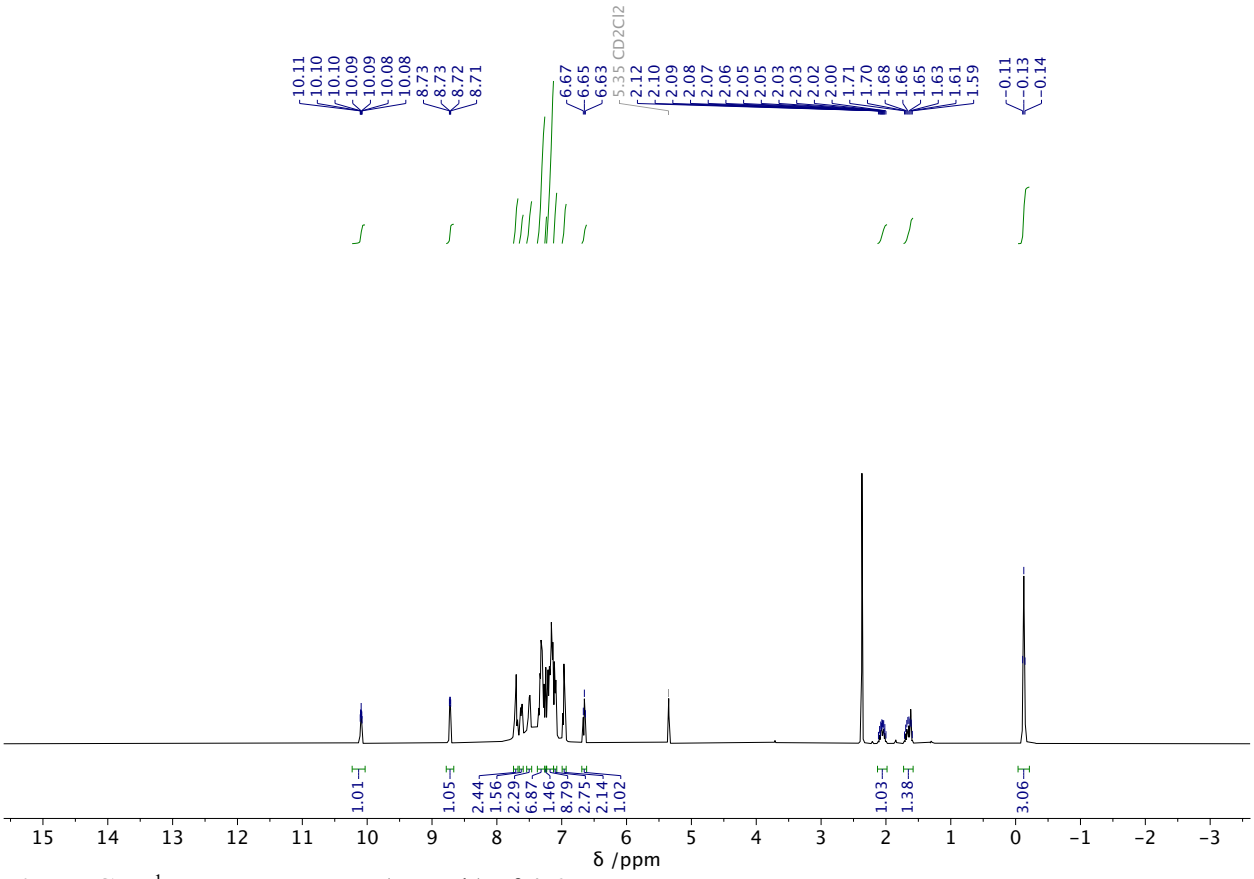


**Figure C-5.** $^{1}H$ NMR spectrum ($CD_2Cl_2$) of **4.6**.

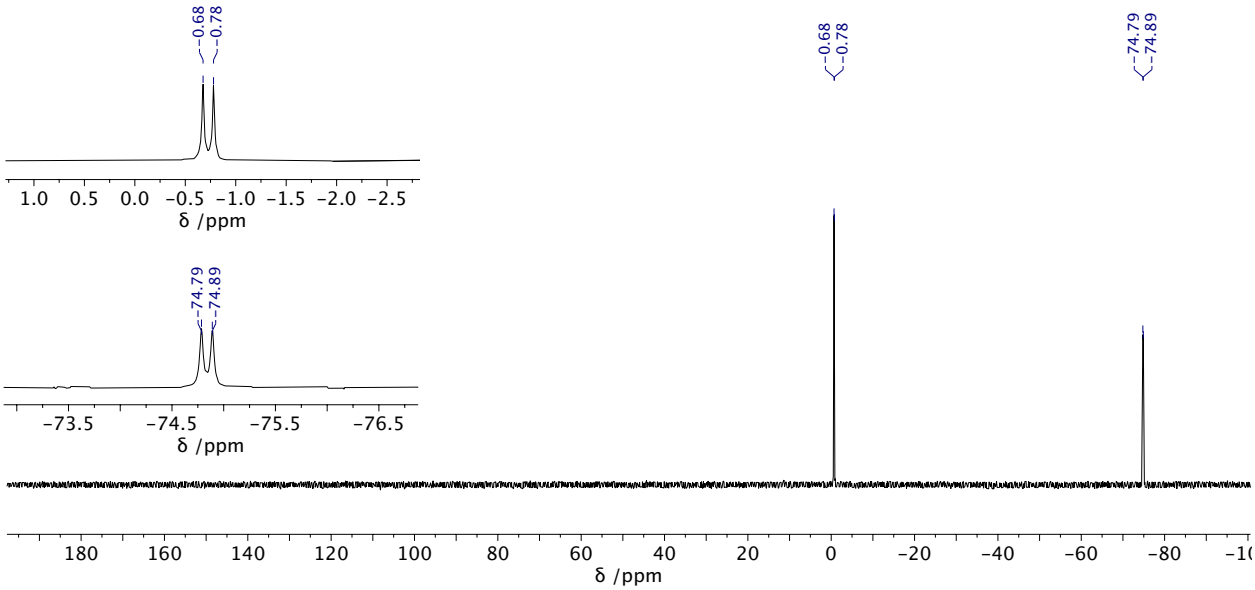


**Figure C-6.** $^{31}P\{^{1}H\}$ NMR spectrum ($CD_2Cl_2$) of **4.6**.

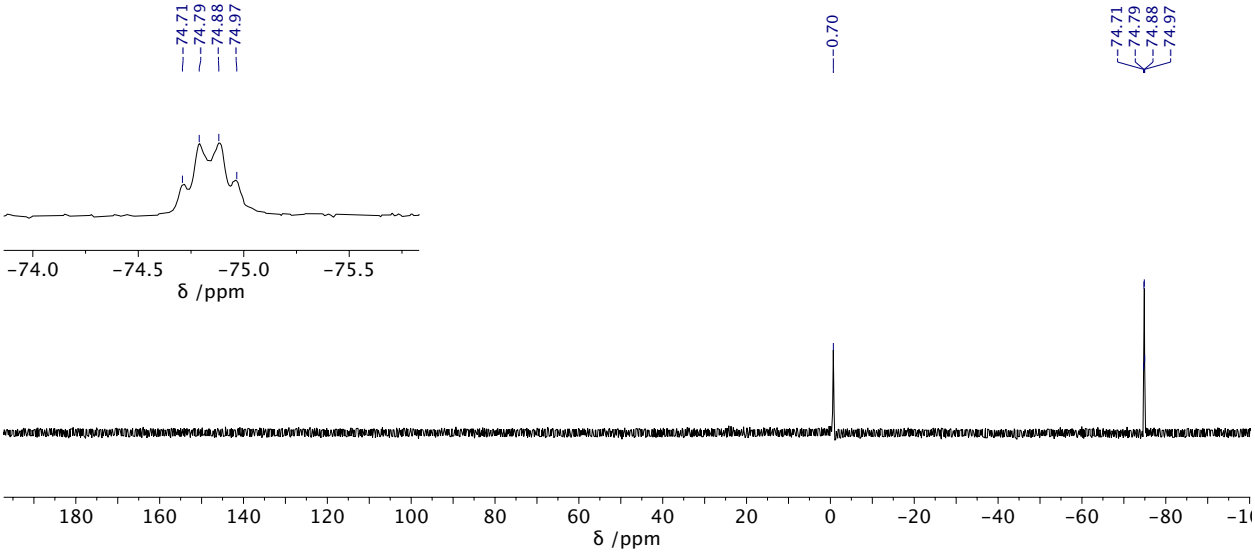


**Figure C-7.** $^{31}P$ NMR spectrum ($CD_2Cl_2$) of **4.6**.

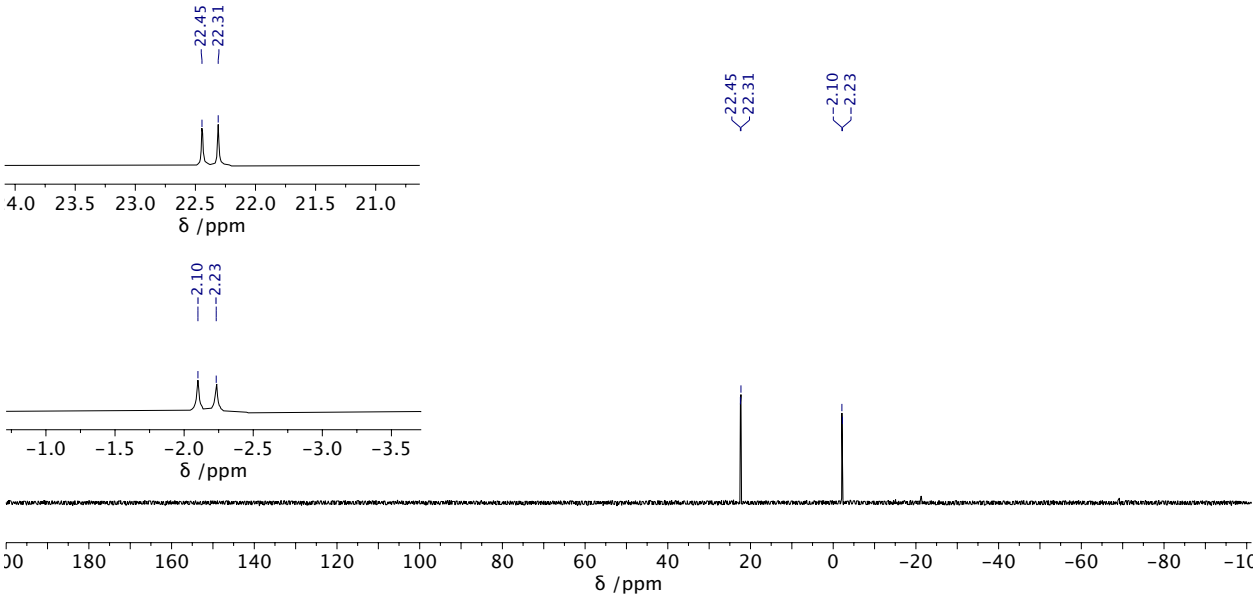


**Figure C-8.** $^{31}P\{^{1}H\}$ NMR spectrum (THF) of **4.7**.

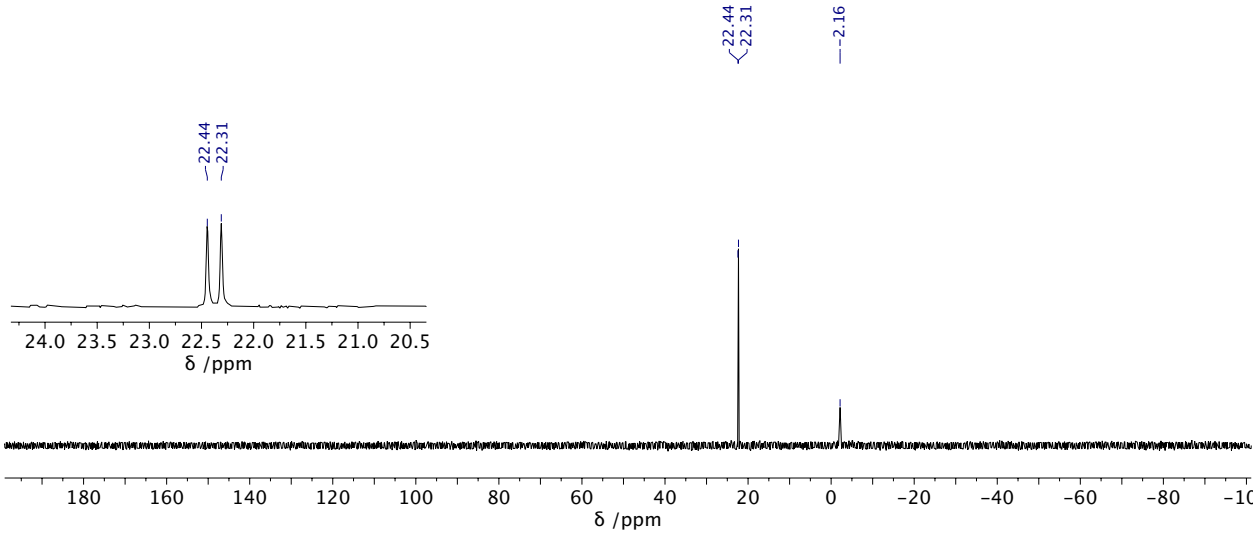


**Figure C-9.** $^{31}P$ NMR spectrum (THF) of **4.7**.

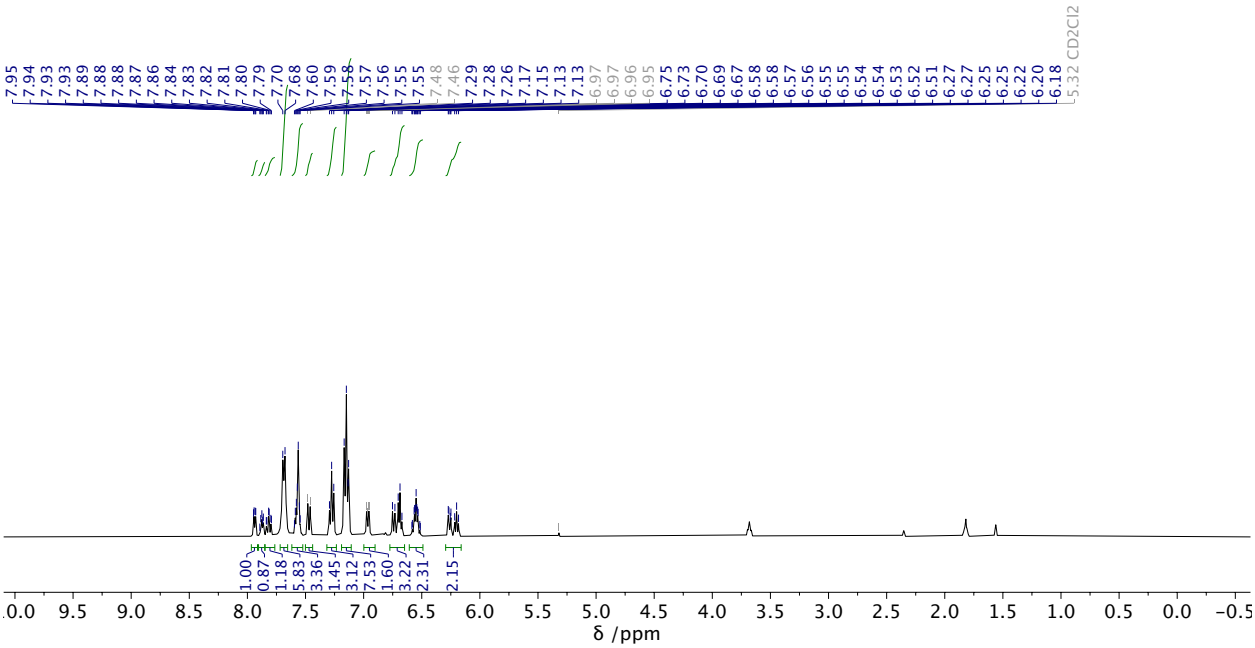


**Figure C-10.** $^{1}$H NMR spectrum ($CD_2Cl_2$) of **4.9**.

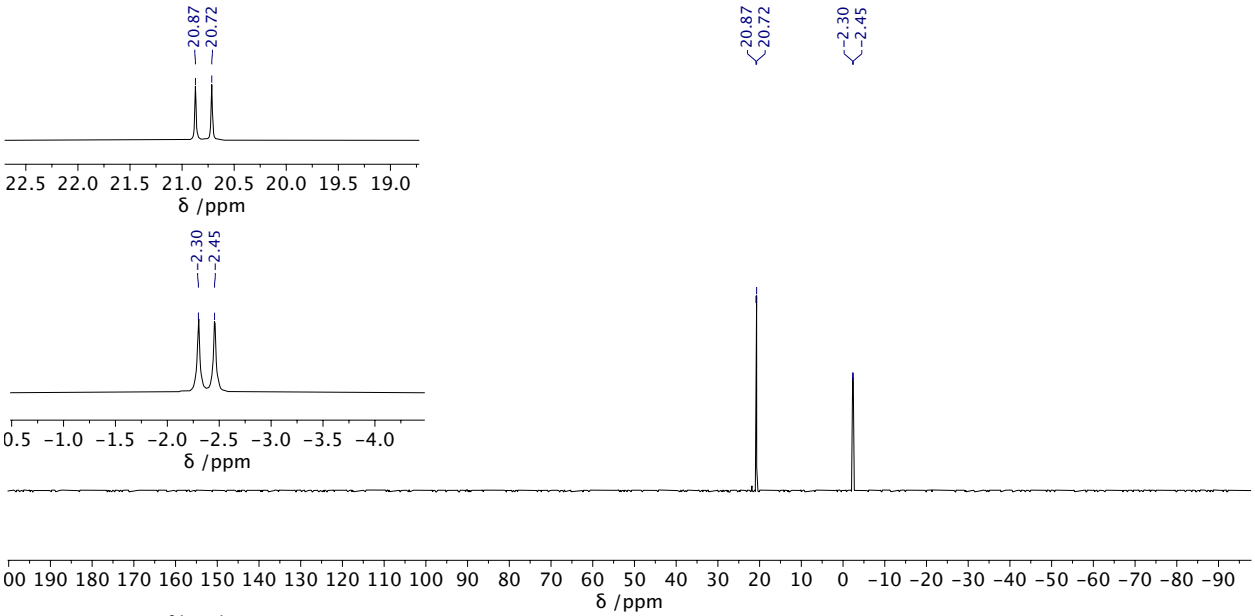


**Figure C-11.** $^{31}P\{^{1}H\}$ NMR spectrum ($CD_2Cl_2$) of **4.9**.

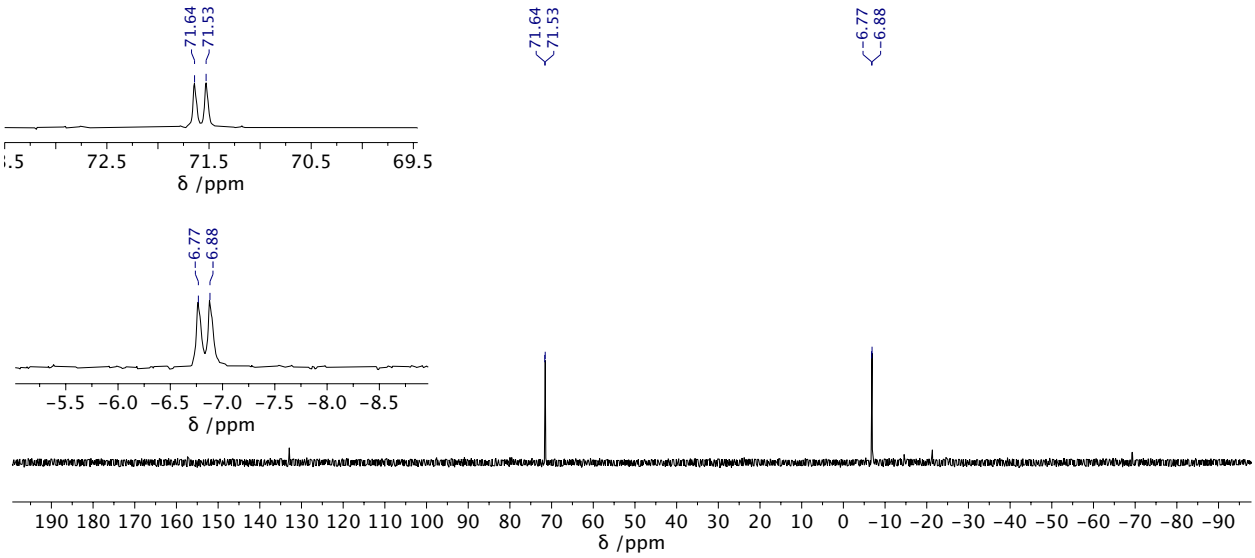


**Figure C-12.** $^{31}P\{^{1}H\}$ NMR spectrum of **4.10**.

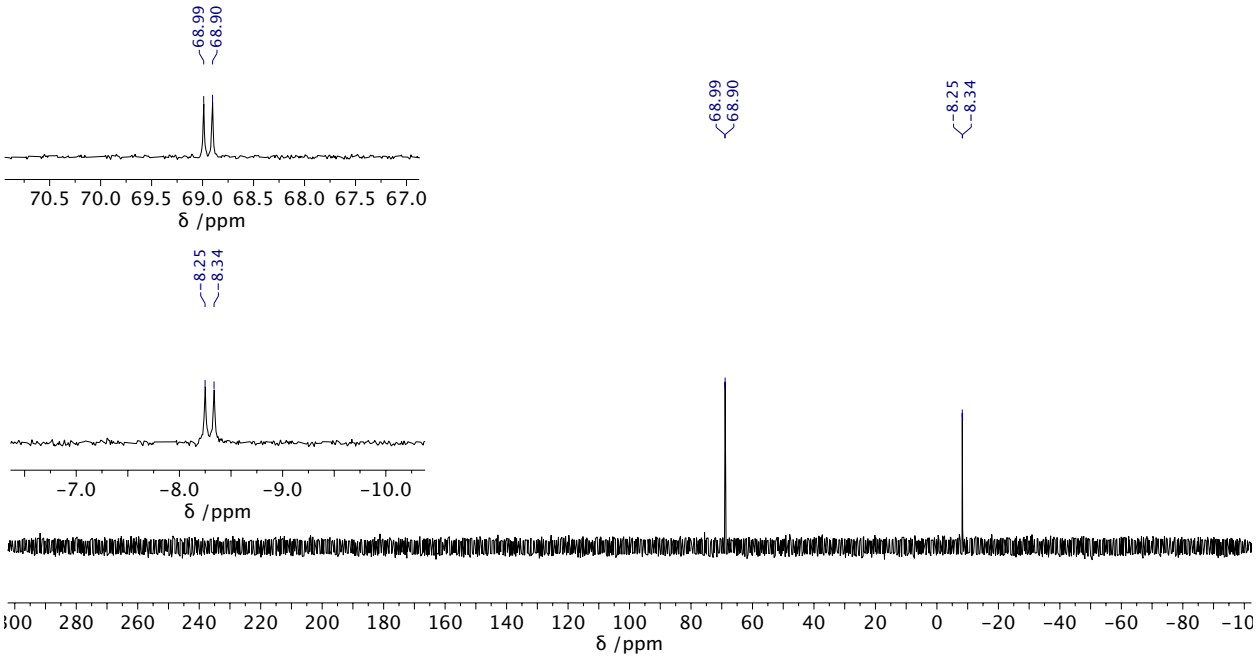


**Figure C-13.** $^{31}P\{^{1}H\}$ NMR spectrum ($CD_2Cl_2$) of **4.11**.

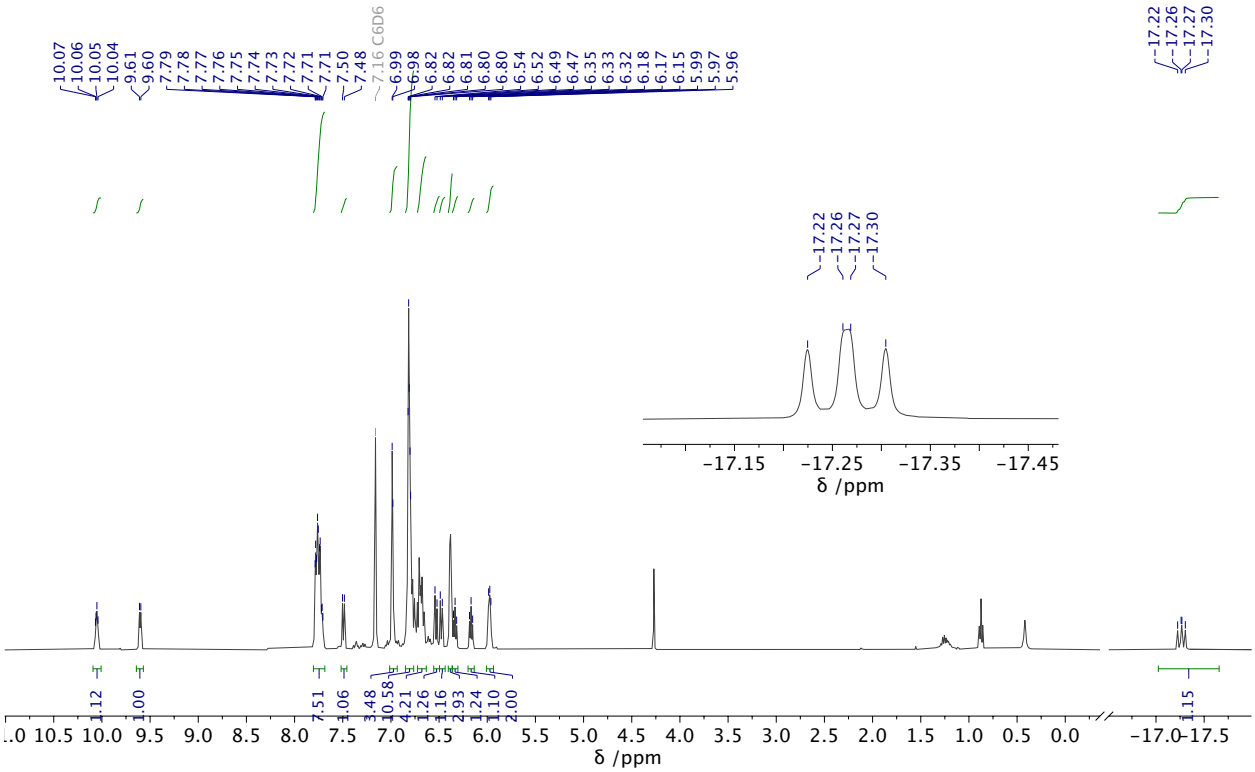


**Figure C-14.** $^{1}$H NMR ($C_6D_6$) spectrum of **4.12**.

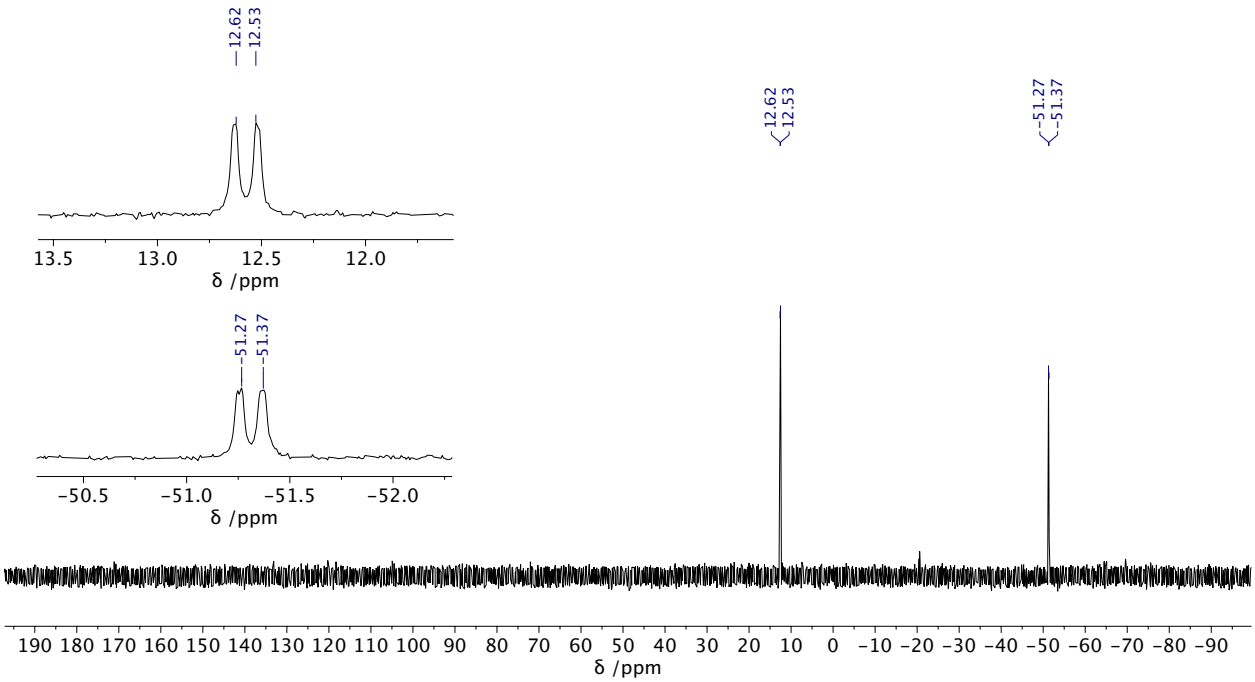


**Figure C-15.** $^{31}P\{^{1}H\}$ NMR spectrum ($C_6D_6$) of **4.12**.

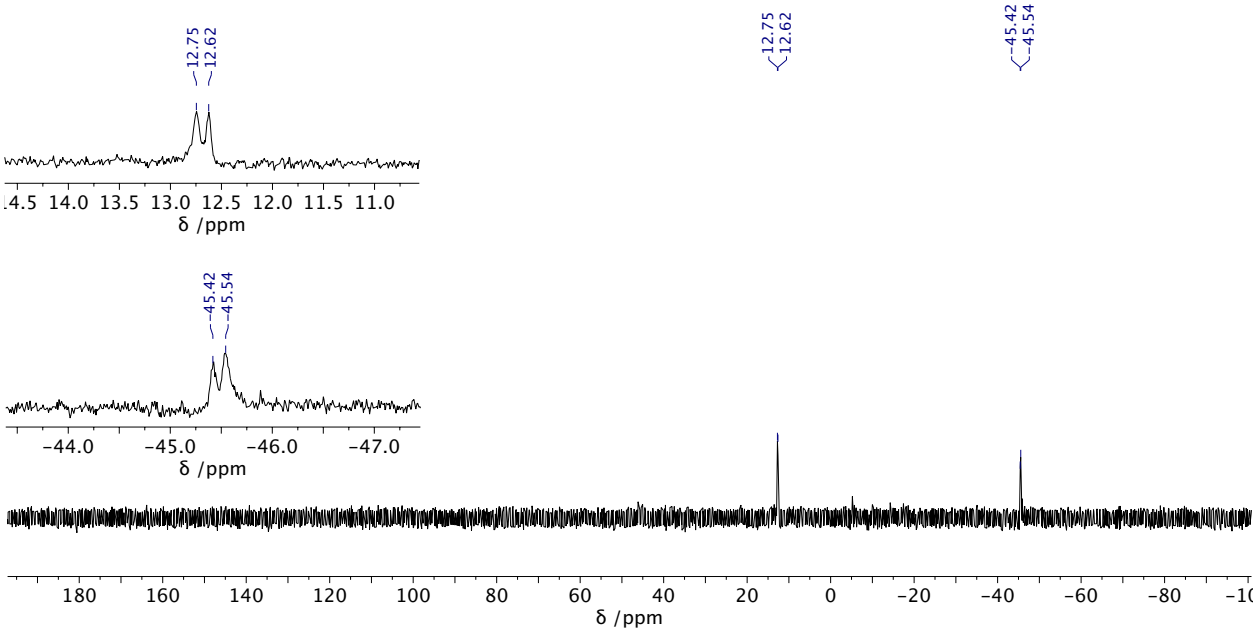


**Figure C-16.** $^{31}P\{^{1}H\}$ NMR spectrum of **4.13**.

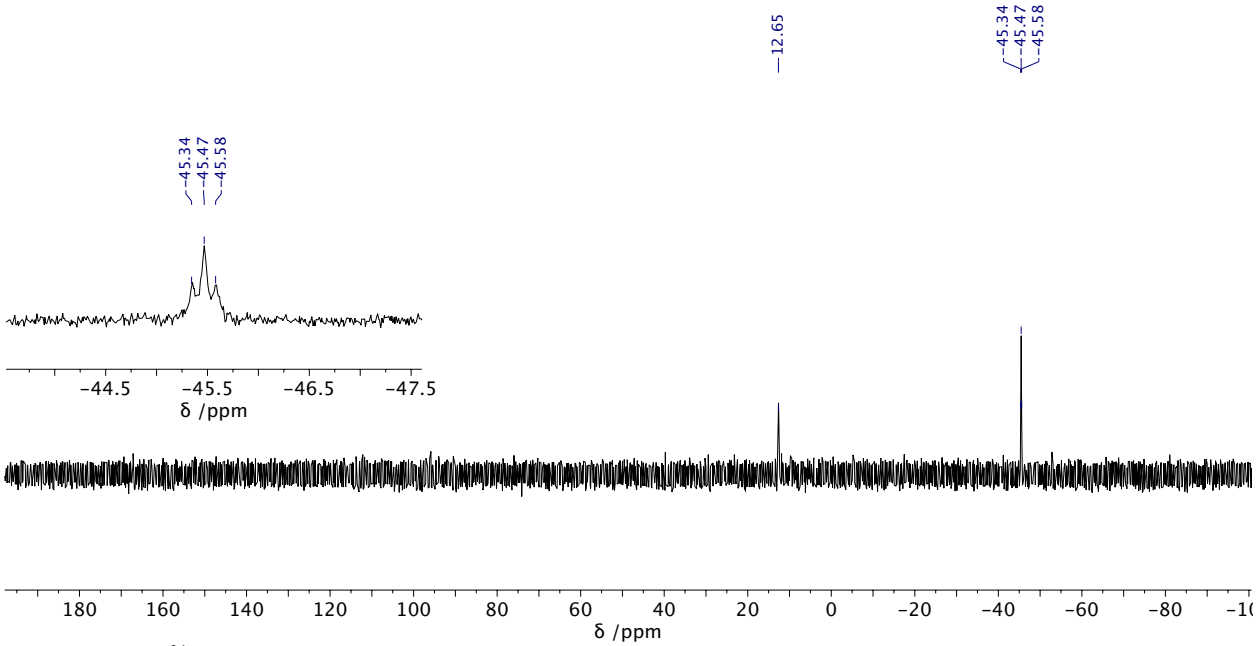


**Figure C-17.** $^{31}P$ NMR spectrum of **4.13**.

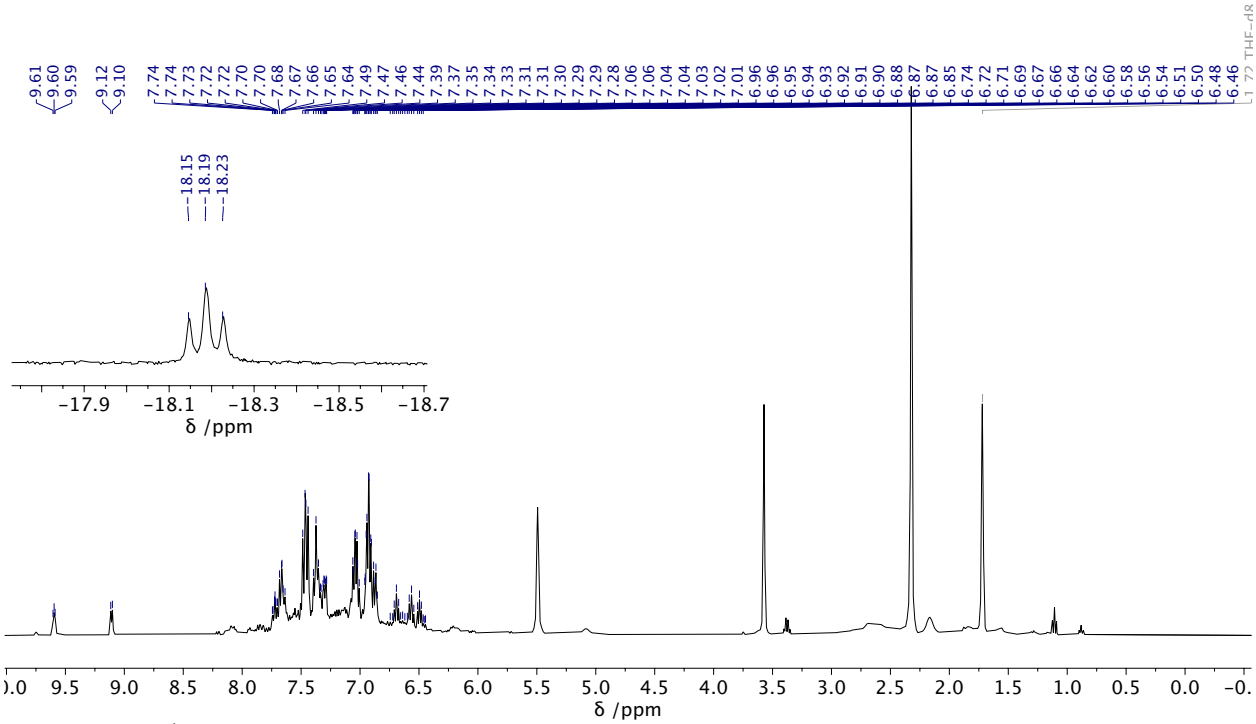


**Figure C-18.** $^{1}$H NMR spectrum of **4.14**.

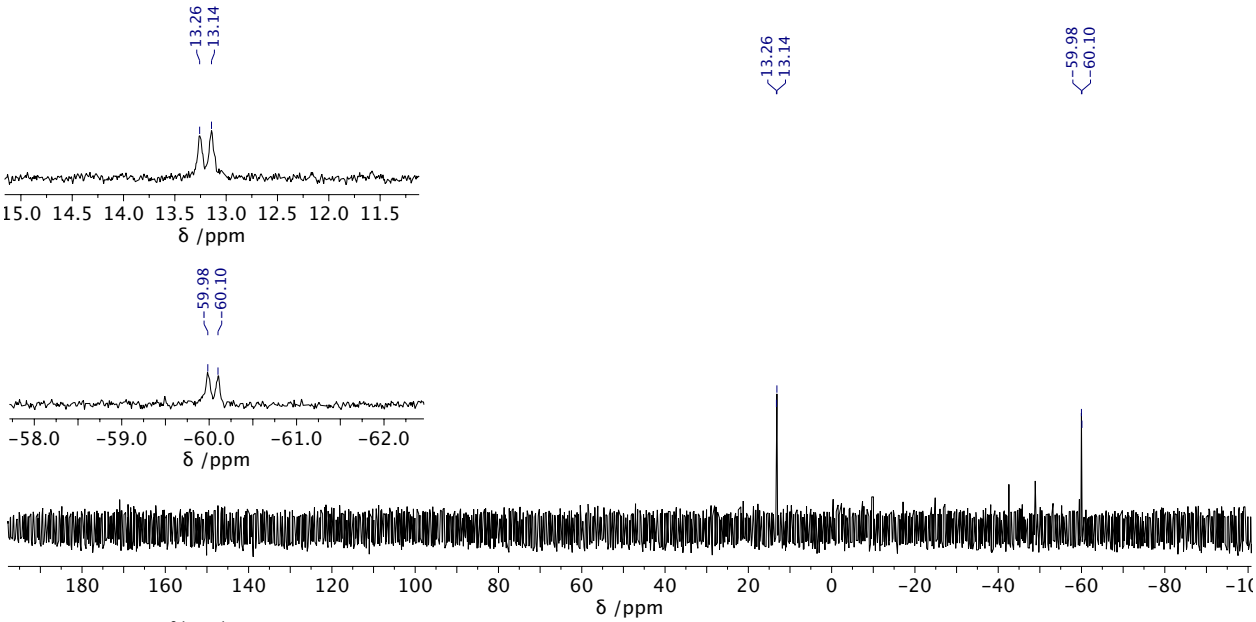


**Figure C-19.** $^{31}P\{^{1}H\}$ NMR spectrum (THF-d8) of **4.14**.

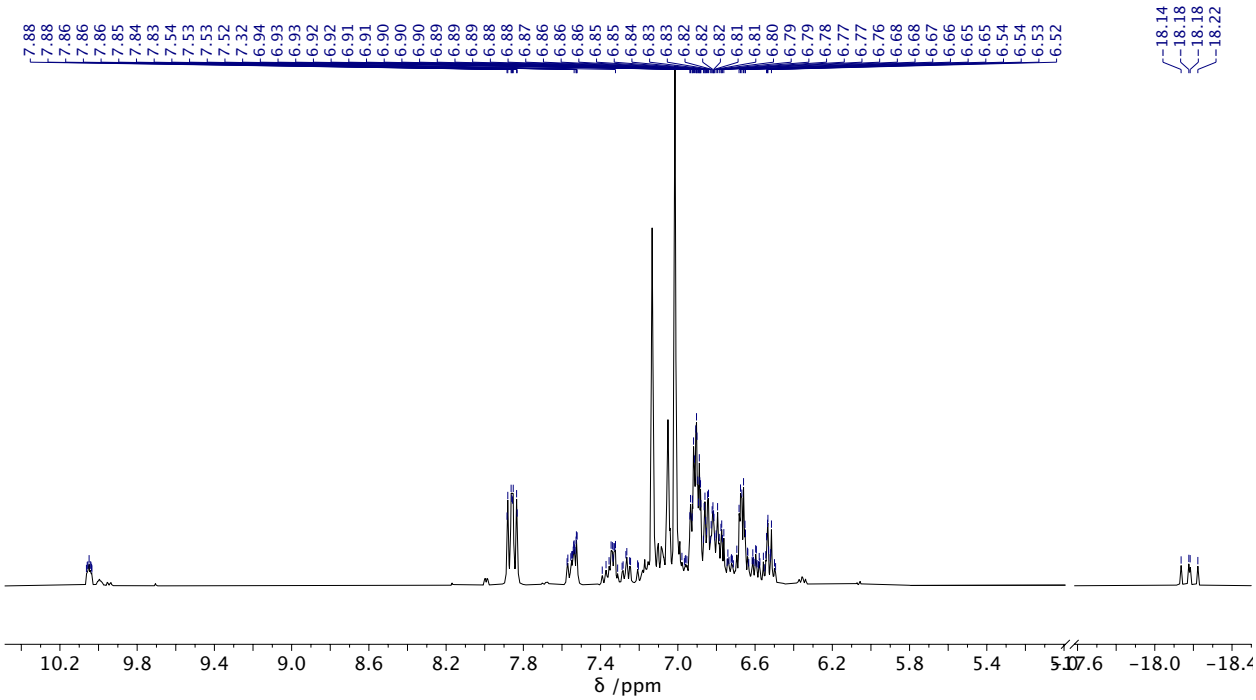


**Figure C-20.** $^{1}$H NMR spectrum (crude) of **4.15**.

**Figure C-21.** $^{13}C$ NMR spectrum of **4.15**.

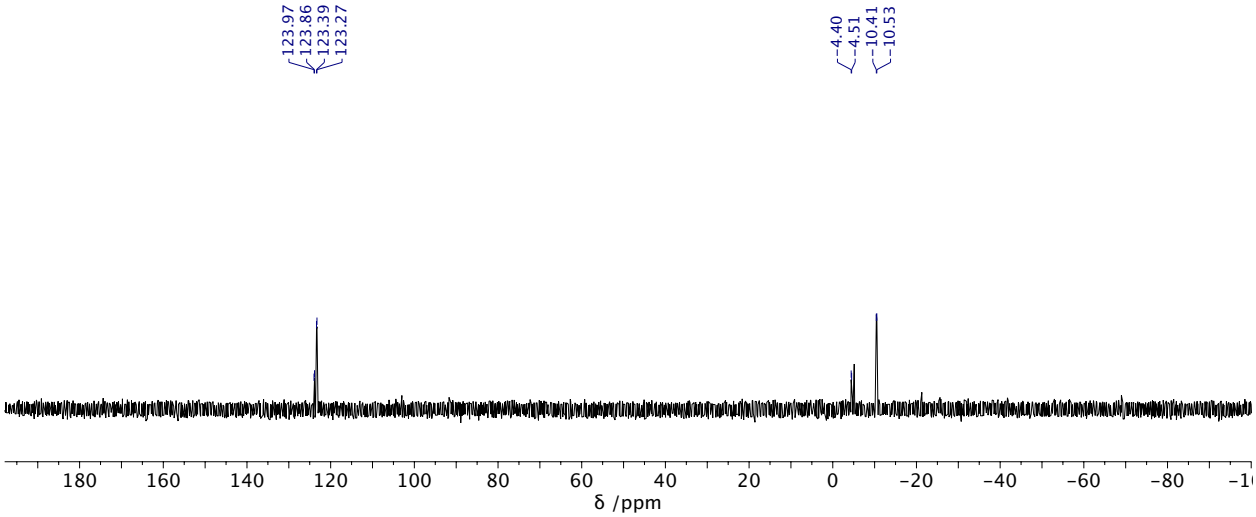


**Figure C-22.** $^{31}P\{^{1}H\}$ NMR spectrum of **4.15**.

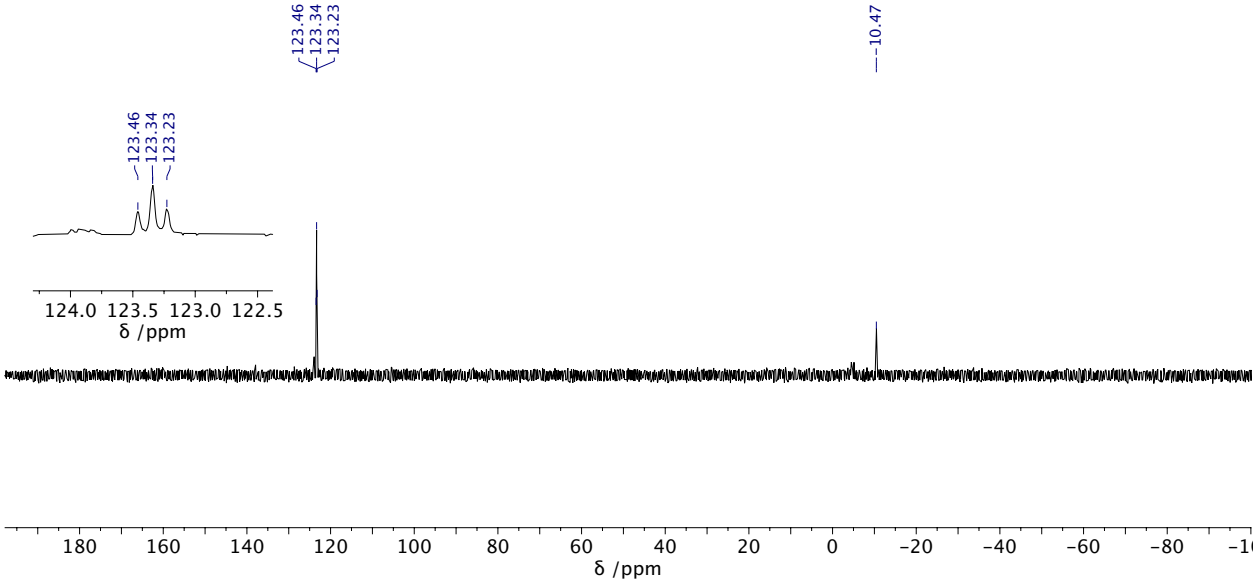


**Figure C-23.** $^{31}P$ NMR spectrum of **4.15**.

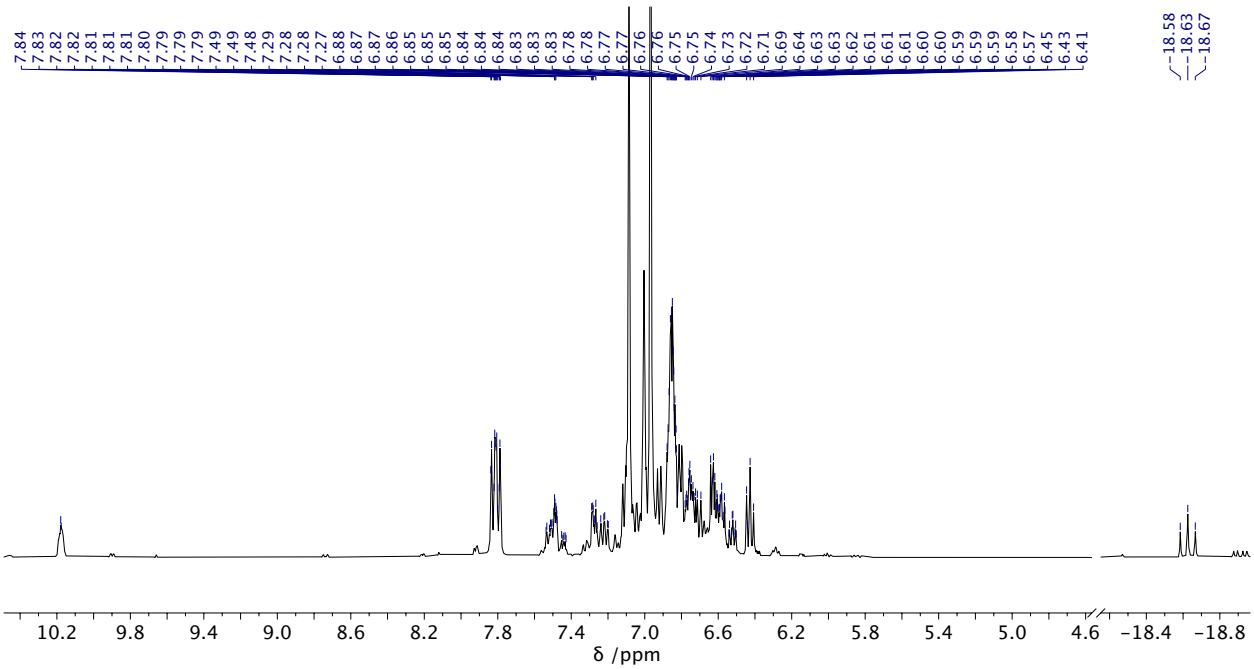


**Figure C-24.** $^{1}$H NMR spectrum (crude) of **4.16**.

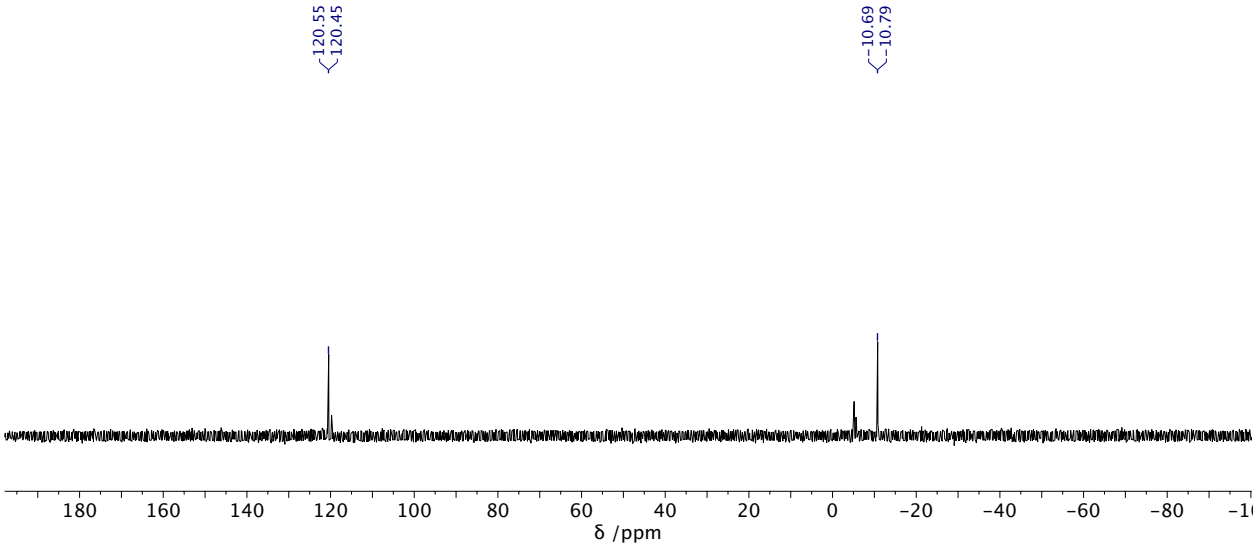


**Figure C-25.** $^{31}P\{^{1}H\}$ NMR spectrum of **4.16**.

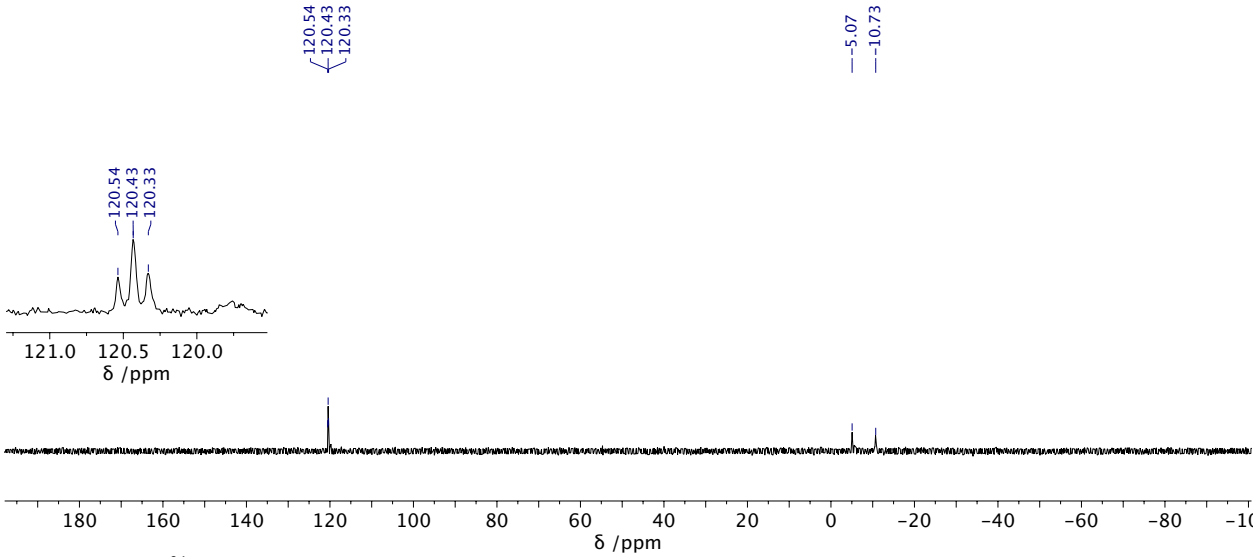


**Figure C-26.** $^{31}P$ NMR spectrum of **4.16**.

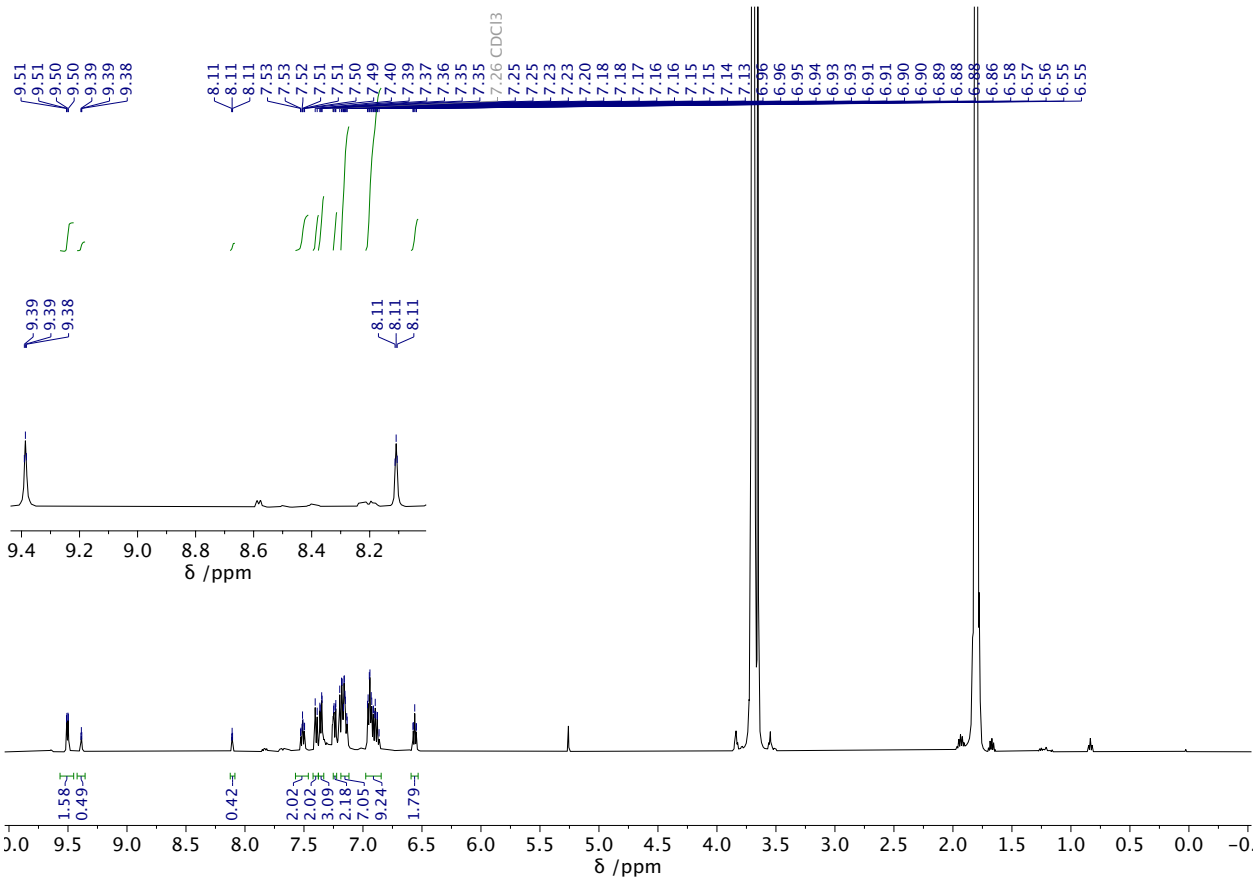


**Figure C-27.** $^{1}$H NMR spectrum ($CDCl_3$) of **4.20**. Signals of solvents (dichloromethane, pentane) remains.

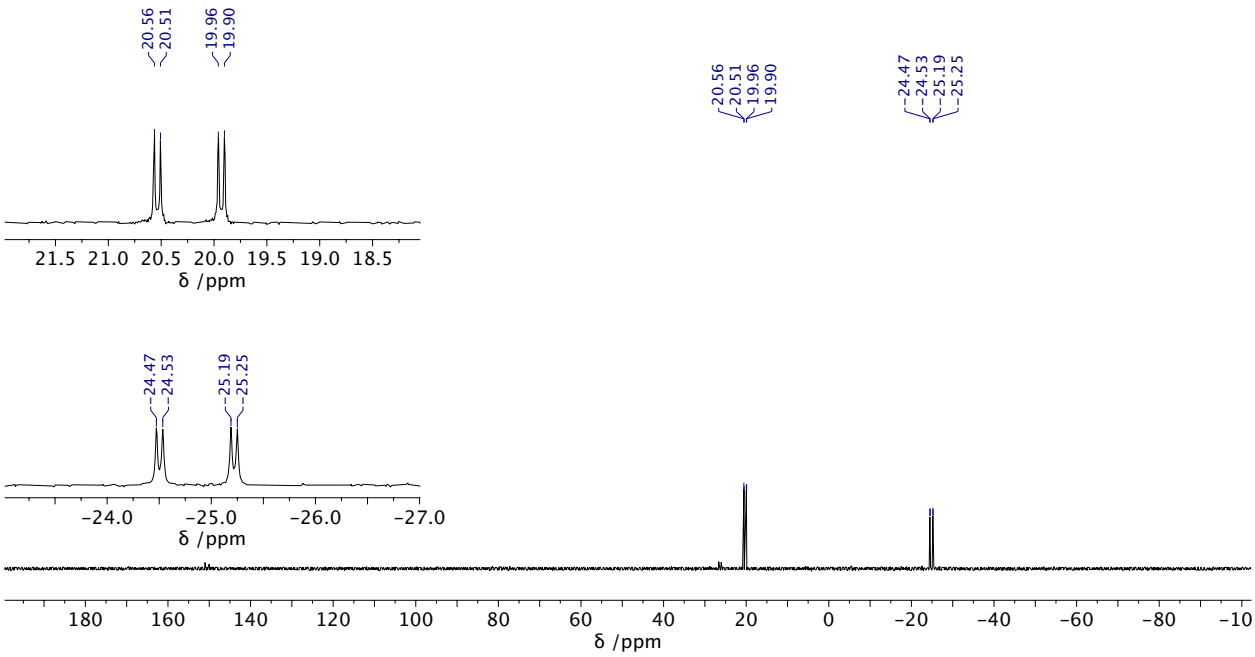


**Figure C-28.** $^{31}P\{^{1}H\}$ NMR spectrum ($CDCl_3$) of **4.20**.

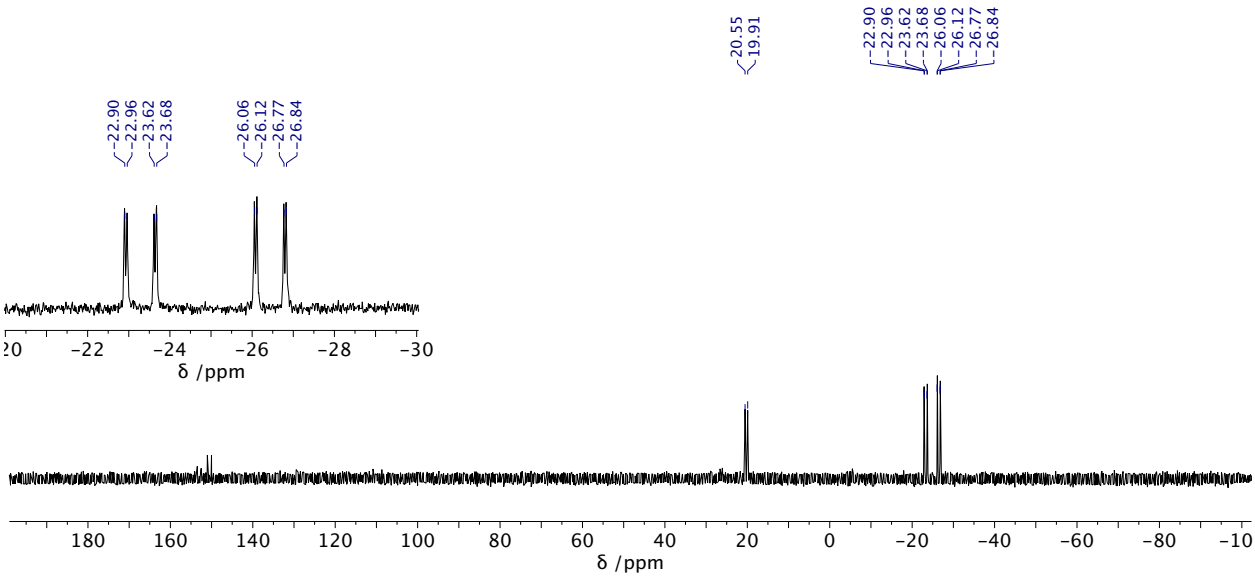


**Figure C-29.** $^{31}P$ NMR spectrum ($CDCl_3$) of **4.20**.

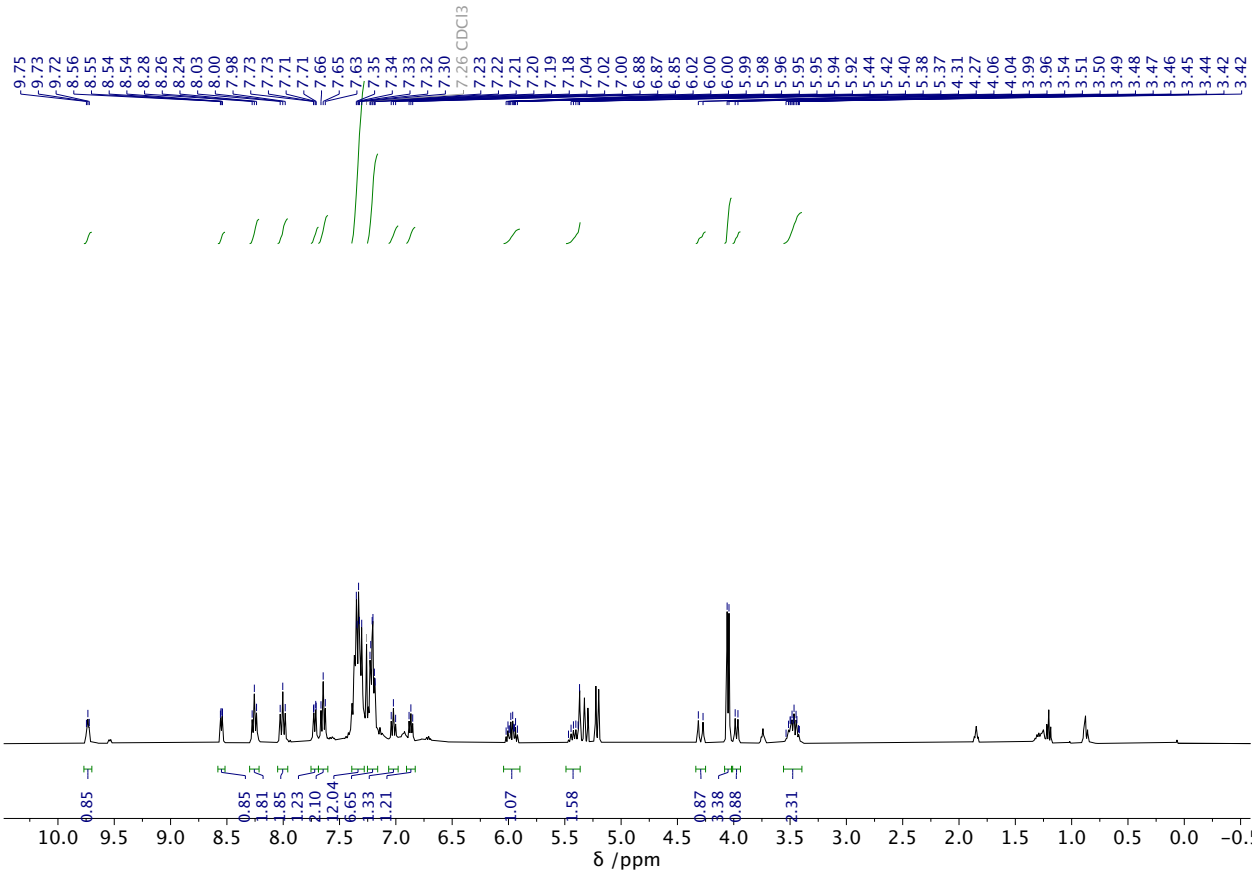


**Figure C-30.** $^{1}$H NMR spectrum of **4.22.**

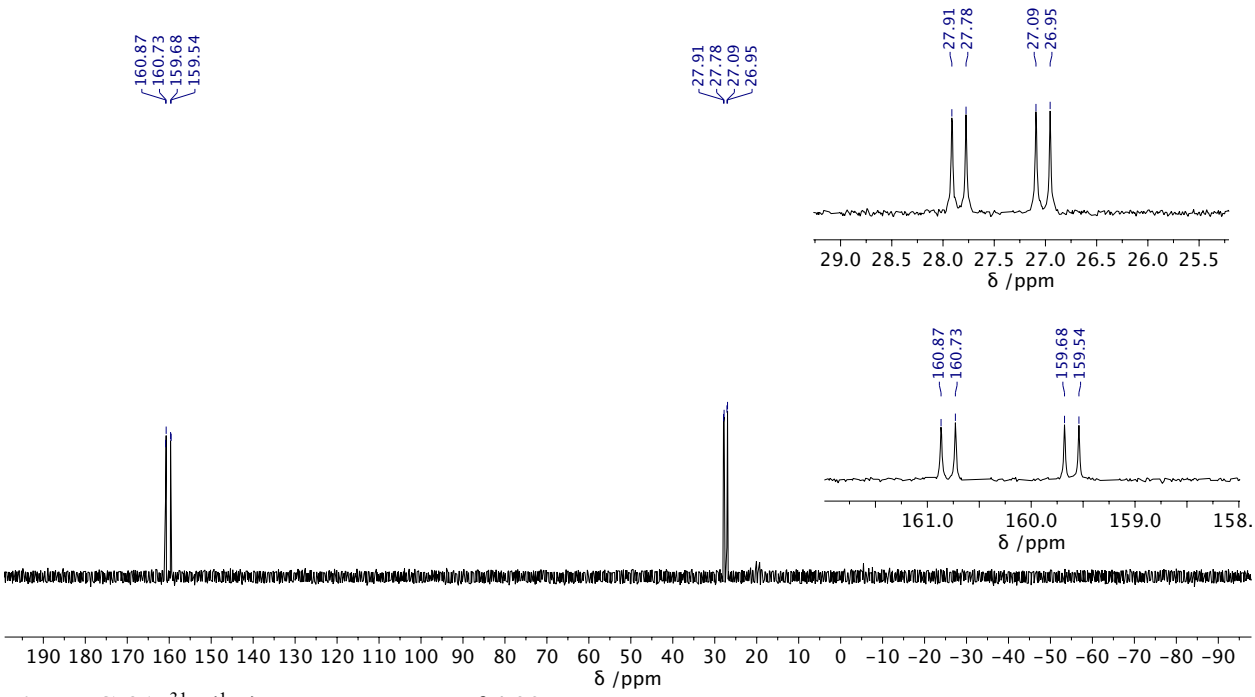


**Figure C-31.** $^{31}P\{^{1}H\}$ NMR spectrum of **4.22**.

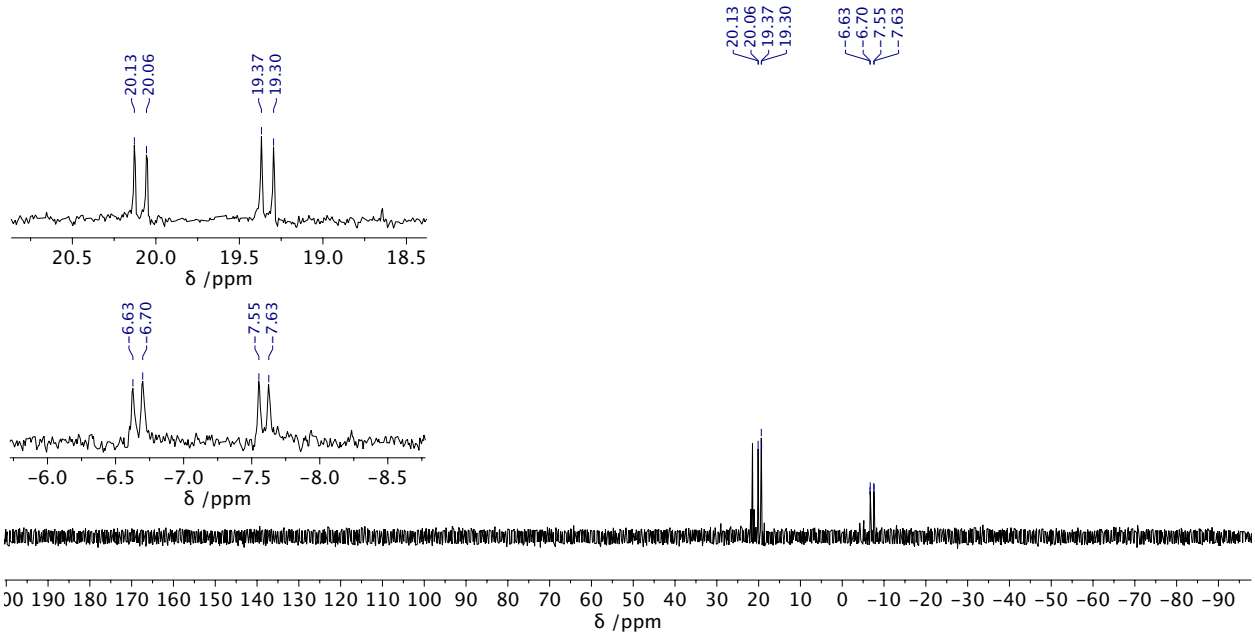


**Figure C-32.** $^{31}P\{^{1}H\}$ NMR spectrum of **4.23**.

## C.4. References


1. F. Neese, *WIREs Comput. Mol. Sci.*, **2012**, *2*, 73–78.
2. (a) Becke, A. D.; *Phys. Rev. A.* **1988**, *38*, 3098. (b) Becke, A.D. *J.Chem.Phys*. **1993**, *98*, 5648. (c) Lee, C.; Yang, W.; Parr, R.G. *Phys. Rev. B.* **1988**, *37*, 785.
3. F. Weigend and R. Ahlrichs, *Phys. Chem. Chem. Phys.*, **2005**, *7*, 3297-3305.
4. (a) van Lenthe, E.; Baerends, E. J.; Snijders, J. G. *J. Chem. Phys.* **1993**, *99*, 4597−4610. (b) van Lenthe, E.; Baerends, E. J.; Snijders, J. G. *J. Chem. Phys.* **1994**, *101*, 9783−9792.

# Appendix D . Supplementary Data for Chapter 5

## D.1. X-ray Diffraction

See the published article (*J. Am. Chem. Soc.* **2020**, *142*, 21285–21291.) or CCDC (https://www.ccdc.cam.ac.uk ) for cif files and detailed structural data of **L3**, **5.6**, **5.7′** and **5.8′**.

**Structural Data for L3**

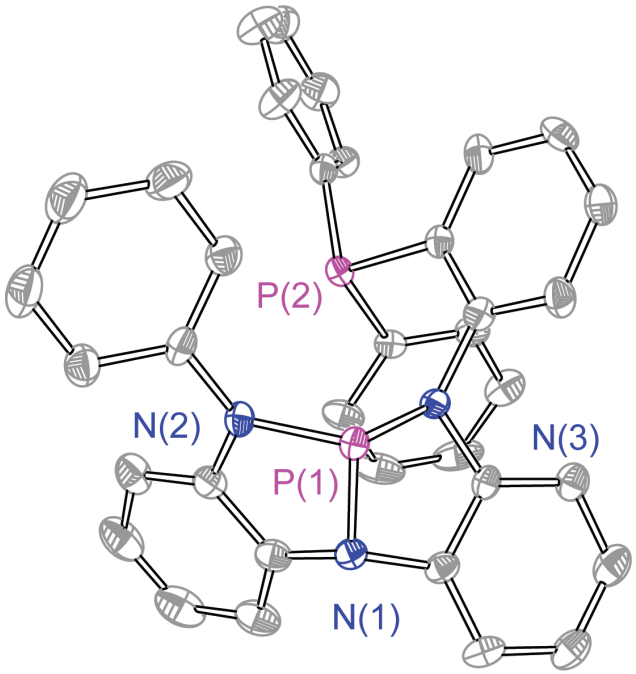


**Figure D-1.** Thermal ellipsoid plots of $\kappa^2$-chelating ligand **(L3)** drawn at the 50% probability level. H-atoms and solvent are omitted for clarity.

**Table D-1.** X-ray experimental details for complex **L3** (CCDC 2033415)

| | |
|---|---|
| *Crystal Data* | |
| Chemical formula | $C_{40}H_{37}N_3OP_2$ |
| Fw, g/mol | 637.66 |
| Crystal system, space group | monoclinic, $P2_1$ |
| Temperature (K) | 100(2) |
| $a$, $b$, $c$ (Å) | 18.9534(9), 8.4688(4), 21.9113(11) |
| α, β, γ (°) | 90, 107.1402(18), 90 |
| $V$ (Å$^3$) | 3360.8(3) |
| $Z$ | 4 |
| Radiation type | Mo $K\alpha$ |
| μ (mm$^{-1}$) | 0.166 |
| Crystal size (mm) | 0.350 × 0.105 × 0.040 |
| *Data collection* | |
| Diffractometer | Bruker Photon2 CPAD |
| Absorption correction | Multi-scan, *SADABS* |
| $T_{min}$, $T_{max}$ | 0.6610, 0.7214 |
| No. of measured, independent and observed [$I > 2\sigma(I)$] reflections | 245534, 19638, 14985 |
| $R_{int}$ | 0.1159 |
| $(\sin \theta/\lambda)_{max}$ (Å$^{-1}$) | 0.600 |
| *Refinement* | |
| $R[F^2 > 2\sigma(F^2)]$, $wR(F^2)$, $S$ | 0.0942, 0.2307, 1.071 |
| No. of reflections | 19638 |
| No. of parameters | 1339 |
| No. of restraints | 0 |
| H-atom treatment | H atoms treated by a mixture of independent and constrained refinement |
| $Dr_{max}$, $Dr_{min}$ (e Å$^{-3}$) | 1.029, –2.297 |

**Structural Data for PtClMeiPr$_2$PNNNP (5.6)**

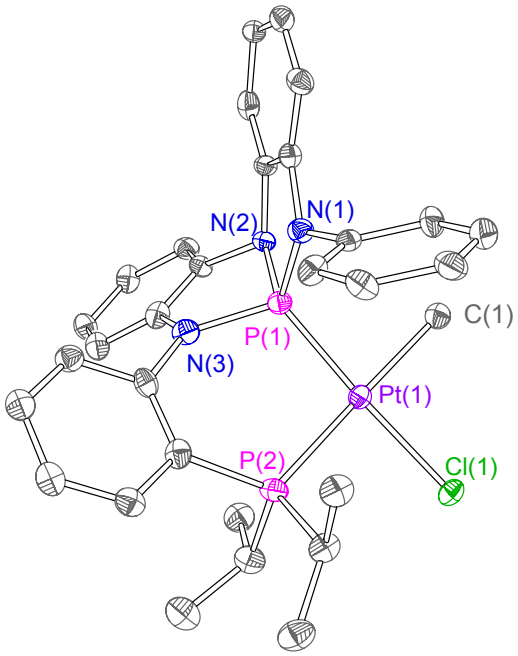


**Figure D-2.** Thermal ellipsoid plots of PtClMeiPr$_2$PNNNP **(5.6)** drawn at the 50% probability level. H-atoms are omitted for clarity.

**Table D-2.** X-ray experimental details for complex **5.6** (CCDC 2036533)

| | |
|---|---|
| *Crystal Data* | |
| Chemical formula | $C_{62}H_{68}Cl_2N_6P_4Pt_2$ |
| Fw, g/mol | 1482.18 |
| Crystal system, space group | Monoclinic, *P2(1)/c* |
| Temperature (K) | 15(2) |
| *a*, *b*, *c* (Å) | 21.249(3), 18.319(2), 14.6841(18) |
| α, β, γ (°) | 90, 101.7720(10), 90 |
| *V* (Å$^3$) | 5595.7(12) |
| *Z* | 4 |
| Radiation type | synchrotron |
| μ (mm$^{-1}$) | 0.297 |
| Crystal size (mm) | 0.01 × 0.01 × 0.01 |
| *Data collection* | |
| Diffractometer | Bruker *APEX*-II CCD |
| Absorption correction | Multi-scan, *SADABS* |
| $T_{min}$, $T_{max}$ | 0.9970, 0.9970 |
| No. of measured, independent and observed [$I > 2\sigma(I)$] reflections | 97120, 10021, 9299 |
| $R_{int}$ | 0.0475 |
| $(\sin \theta/\lambda)_{max}$ (Å$^{-1}$) | 0.597 |
| *Refinement* | |
| $R[F^2 > 2\sigma(F^2)]$, $wR(F^2)$, $S$ | 0.0463, 0.1258, 0.969 |
| No. of reflections | 10021 |
| No. of parameters | 718 |
| No. of restraints | 12 |
| H-atom treatment | H atoms treated by a mixture of independent and constrained refinement |
| $Dr_{max}$, $Dr_{min}$ (e Å$^{-3}$) | 0.328, – 0.270 |

**Structural Data for PdCliPr$_2$PNNNPMe (5.7′)**

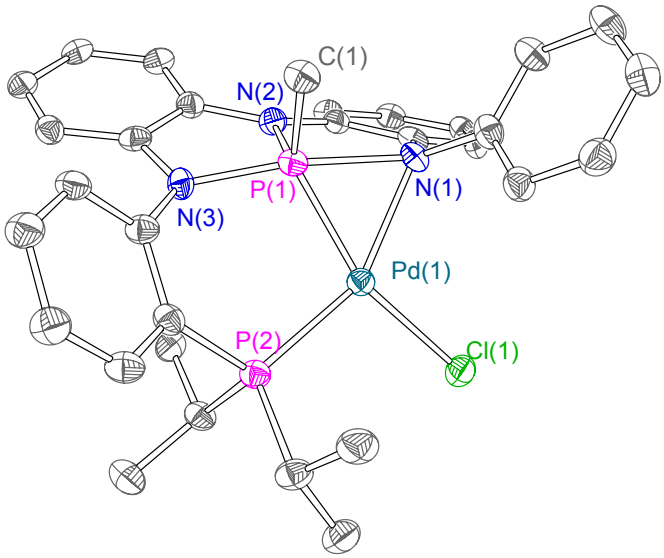


**Figure D-3.** Thermal ellipsoid plots of PdCliPr$_2$PNNNPMe **(5.7′)** drawn at the 50% probability level. H-atoms and solvent are omitted for clarity.

**Table D-3.** X-ray experimental details for complex **5.7′** (CCDC 2033417)

| | |
|---|---|
| *Crystal Data* | |
| Chemical formula | $C_{131}H_{141}Cl_4F_3N_{12}P_8Pd_4$ |
| Fw, g/mol | 2755.71 |
| Crystal system, space group | tetragonal, *P-42(1)/c* |
| Temperature (K) | 15(2) |
| *a*, *b*, *c* (Å) | 15.426(3), 15.426(3), 26.835(6) |
| α, β, γ (°) | 90, 90, 90 |
| *V* (Å$^3$) | 6386(3) |
| *Z* | 2 |
| Radiation type | synchrotron |
| μ (mm$^{-1}$) | 0.227 |
| Crystal size (mm) | 0.20 × 0.07 × 0.07 |
| *Data collection* | |
| Diffractometer | Bruker *APEX*-II CCD |
| Absorption correction | Multi-scan, *SADABS* |
| $T_{min}$, $T_{max}$ | 0.956, 0.984 |
| No. of measured, independent and observed [$I > 2\sigma(I)$] reflections | 131592, 5631, 5168 |
| $R_{int}$ | 0.0425 |
| $(\sin \theta/\lambda)_{max}$ (Å$^{-1}$) | 0.534 |
| *Refinement* | |
| $R[F^2 > 2\sigma(F^2)]$, $wR(F^2)$, $S$ | 0.0370, 0.0969, 1.087 |
| No. of reflections | 5631 |
| No. of parameters | 396 |
| No. of restraints | 0 |
| H-atom treatment | H atoms treated by a mixture of independent and constrained refinement |
| $Dr_{max}$, $Dr_{min}$ (e Å$^{-3}$) | 1.090, –0.998 |

**Structural Data for NiCliPr$_2$PNNNPMe (5.8′)**

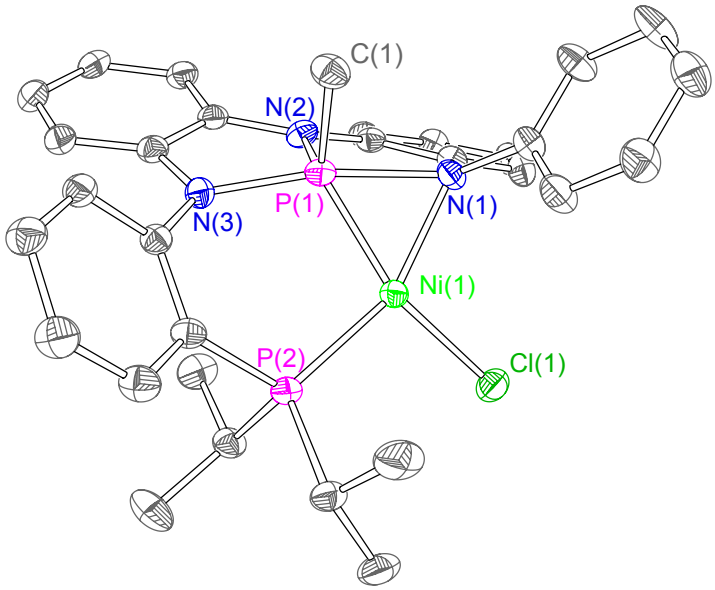


**Figure D-4.** Thermal ellipsoid plots of NiCliPr$_2$PNNNPMe **(5.8′)** drawn at the 50% probability level. H-atoms and solvent are omitted for clarity.

**Table D-4.** X-ray experimental details for complex **5.8´** (CCDC 2033418)

| | |
|---|---|
| *Crystal Data* | |
| Chemical formula | C33.75 H36 Cl N2 Ni P2 |
| Fw, g/mol | 625.74 |
| Crystal system, space group | Tetragonal, *P-42(1)/c* |
| Temperature (K) | 99.99 |
| *a*, *b*, *c* (Å) | 15.4791(13), 15.4791(13), 26.403(2) |
| α, β, γ (°) | 90, 90, 90 |
| *V* (Å$^3$) | 6326.3(12) |
| *Z* | 8 |
| Radiation type | Mo *Kα* |
| μ (mm$^{-1}$) | 0.824 |
| Crystal size (mm) | 0.285 x 0.22 x 0.015 |
| *Data collection* | |
| Diffractometer | Bruker APEX-II CCD |
| Absorption correction | Multi-scan, *SADABS* |
| $T_{min}$, $T_{max}$ | 0.6820, 0.7462 |
| No. of measured, independent and observed [$I > 2\sigma(I)$] reflections | 10098 |
| $R_{int}$ | 0.0601 |
| $(\sin \theta/\lambda)_{max}$ (Å$^{-1}$) | 0.710 |
| *Refinement* | |
| $R[F^2 > 2\sigma(F^2)]$, $wR(F^2)$, $S$ | 0.0523, 0.1476, 1.131 |
| No. of reflections | 10098 |
| No. of parameters | 409 |
| No. of restraints | 277 |
| H-atom treatment | H atoms treated by a mixture of independent and constrained refinement |
| $Dr_{max}$, $Dr_{min}$ (e Å$^{-3}$) | 2.207, -0.607 |

**Table D-5.** Selected metrical parameters for complexes **5.6**, **5.7′** and **5.8′**

| | **5.6** (M = Pt) | **5.7′** (M = Pd) | **5.8′** (M = Ni) |
|---|---|---|---|
| P(1)–N(1) | 1.730(5) | 1.716(5) | 1.761(4) |
| P(1)–N(2) | 1.670(5) | 2.002(5) | 1.990(4) |
| P(1)–N(3) | 1.717(5) | 1.766(5) | 1.720(13) |
| P(1)–C(1) | - | 1.815(6) | 1.834(4) |
| M(1)–C(1) | 2.126(7) | - | - |
| M(1)–N(2) | - | 2.002(5) | 1.993(3) |
| M(1)–Cl(1) | 2.3559(16) | 2.3752(17) | 2.2004(12) |
| M(1)–P(1) | 2.1642(14) | 2.1434(18) | 2.0511(12) |
| M(1)–P(2) | 2.3409(15) | 2.2567(17) | 2.1748(12) |
| N(2)−P(1)−M(1) | 115.87(18) | 63.34(16) | 61.99(11) |
| N(2)−P(1)−N(3) | 115.5(2) | 166.7(2) | 165.76(17) |
| N(2)−P(1)−N(1) | 93.2(2) | 85.5(2) | 85.74(16) |
| N(3)−P(1)−N(1) | 91.5(2) | 88.0(2) | 88.67(17) |
| C(1)−P(1)−N(1) | - | 112.6(3) | 110.6(2) |
| C(1)−P(1)−M(1) | - | 126.8(2) | 127.39(16) |
| P(1)−M(1)−P(2) | 94.45(5) | 98.76(6) | 98.82(5) |
| P(1)−M(1)−C(1) | 86.46(19) | - | - |
| P(1)−M(1)−Cl(1) | 173.81(6) | 154.29(6) | 154.09(5) |
| C(1)−M(1)−Cl(1) | 88.61(19) | - | - |
| P(2)−M(1)−Cl(1) | 90.65(5) | 103.84(6) | 102.56(4) |
| $\tau_4$ for metal center | 0.06 | 0.37 | 0.34 |
| $\tau_5$ for P center | N/A | 0.67 | 0.64 |

[a] $\tau_4$ is a metric for four coordinate complexes. $\tau_4 = 0$ for a perfect square planar and $\tau_4 = 1$ for a perfect tetrahedral. $\tau_5$ is a metric for five coordinate complexes. $\tau_5 = 0$ for a perfect square pyramid and $\tau_5 = 1$ for a perfect trigonal bipyramid.

**Structural Data for PdCl(L1$^{Me}$) (5.10′)**

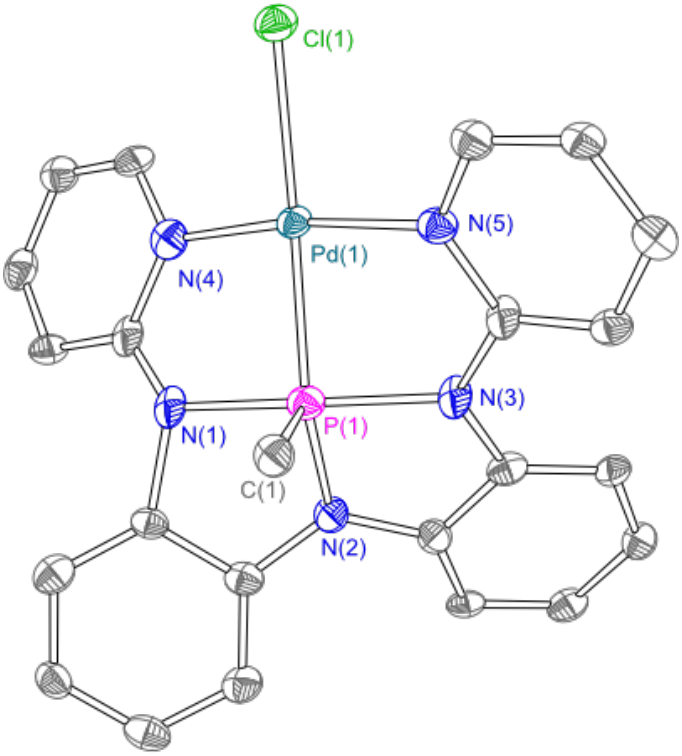


**Figure D-5.** Thermal ellipsoids rendered at the 50% level for **5.10′**. Hydrogen atoms are omitted for clarity.

**Table D-6**. Crystal data and structure refinement for **5.10´**.

| | |
|---|---|
| Identification code | sj5_0m |
| Empirical formula | $C_{23}H_{19}ClN_5PPd$ |
| Formula weight | 538.25 |
| Temperature/K | 15 |
| Crystal system | monoclinic |
| Space group | $P2_1/n$ |
| a/Å | 7.327(2) |
| b/Å | 16.062(5) |
| c/Å | 17.389(5) |
| α/° | 90 |
| β/° | 98.904(4) |
| γ/° | 90 |
| Volume/Å$^3$ | 2021.9(10) |
| Z | 4 |
| $\varrho_{calc}$g/cm$^3$ | 1.768 |
| μ/mm$^{-1}$ | 1.152 |
| F(000) | 1080.0 |
| Crystal size/mm$^3$ | ? × ? × ? |
| Radiation | MoKα (λ = 0.71073) |
| 2Θ range for data collection/° | 5.072 to 50.134 |
| Index ranges | $-8 \le h \le 8$, $-19 \le k \le 19$, $-20 \le l \le 20$ |
| Reflections collected | 43618 |
| Independent reflections | 3558 [$R_{int}$ = 0.1683, $R_{sigma}$ = 0.0783] |
| Data/restraints/parameters | 3558/6/264 |
| Goodness-of-fit on $F^2$ | 1.036 |
| Final R indexes [I>=2σ (I)] | $R_1$ = 0.0554, $wR_2$ = 0.1348 |
| Final R indexes [all data] | $R_1$ = 0.0726, $wR_2$ = 0.1461 |
| Largest diff. peak/hole / e Å$^{-3}$ | 2.30/-0.89 |

**Table D-7.** Fractional Atomic Coordinates ($\times 10^4$) and Equivalent Isotropic Displacement Parameters ($Å^2 \times 10^3$) for **5.10′**. $U_{eq}$ is defined as 1/3 of of the trace of the orthogonalised $U_{IJ}$ tensor.

| Atom | *x* | *y* | *z* | U(eq) |
|---|---|---|---|---|
| Pd1 | 3188.3(6) | 8686.8(3) | 6270.6(3) | 17.9(2) |
| Cl1 | 4632(2) | 9623.2(10) | 7285.6(9) | 25.6(4) |
| P1 | 2105(2) | 7741.5(10) | 5372.4(10) | 20.7(4) |
| N1 | 595(7) | 7329(4) | 6055(3) | 22.2(6) |
| N2 | 328(7) | 7460(3) | 4631(3) | 21.7(12) |
| N3 | 2925(7) | 8355(4) | 4601(3) | 22.2(6) |
| N4 | 1066(7) | 8400(4) | 6842(3) | 23.5(12) |
| N5 | 5132(7) | 8904(3) | 5554(3) | 21.5(11) |
| C1 | 3789(9) | 6898(4) | 5428(4) | 23.3(14) |
| C2 | -523(8) | 6634(4) | 5608(4) | 18.7(13) |
| C3 | -669(8) | 6756(4) | 4800(4) | 20.8(13) |
| C4 | -1586(9) | 6178(4) | 4286(4) | 24.5(14) |
| C5 | -2389(9) | 5495(4) | 4587(4) | 26.6(15) |
| C6 | -2242(9) | 5367(4) | 5383(4) | 23.6(14) |
| C7 | -1245(9) | 5930(4) | 5903(4) | 25.5(14) |
| C8 | 221(9) | 7861(4) | 3909(4) | 20.7(13) |
| C9 | 1729(8) | 8397(4) | 3895(4) | 20.0(13) |
| C10 | 1790(9) | 8924(4) | 3257(3) | 20.7(13) |
| C11 | 361(8) | 8888(4) | 2636(4) | 21.4(13) |
| C12 | -1137(9) | 8354(4) | 2646(4) | 23.4(14) |
| C13 | -1218(8) | 7830(4) | 3289(4) | 19.0(13) |
| C14 | 49(8) | 7708(4) | 6609(4) | 22.2(6) |
| C15 | -1478(9) | 7493(4) | 6978(4) | 22.5(14) |
| C16 | -1983(9) | 8021(4) | 7537(4) | 27.3(15) |
| C17 | -920(9) | 8721(4) | 7782(4) | 25.4(14) |
| C18 | 576(9) | 8893(4) | 7413(4) | 23.5(14) |
| C19 | 4629(8) | 8738(4) | 4784(4) | 22.2(6) |
| C20 | 5820(9) | 8902(4) | 4251(4) | 21.6(13) |
| C21 | 7529(8) | 9242(4) | 4513(4) | 22.5(14) |
| C22 | 8070(8) | 9377(4) | 5302(4) | 20.1(13) |
| C23 | 6845(9) | 9193(4) | 5806(4) | 23.3(14) |

**Table D-8**. Anisotropic Displacement Parameters ($Å^2 \times 10^3$) for **5.10′**. The Anisotropic displacement factor exponent takes the form: $-2\pi^2[h^2a^{*2}U_{11}+2hka^*b^*U_{12}+\ldots]$.

| Atom | $U_{11}$ | $U_{22}$ | $U_{33}$ | $U_{23}$ | $U_{13}$ | $U_{12}$ |
|---|---|---|---|---|---|---|
| Pd1 | 15.6(3) | 21.7(3) | 15.2(3) | -0.25(19) | -1.46(18) | -0.48(18) |
| Cl1 | 22.9(8) | 30.3(9) | 22.7(8) | -2.8(7) | 0.1(6) | -2.6(6) |
| P1 | 19.9(8) | 21.6(9) | 19.3(8) | -0.6(7) | -1.6(6) | -0.8(6) |
| N1 | 14.7(14) | 33.2(17) | 16.4(14) | 9.2(12) | -5.6(11) | -2.9(12) |
| N2 | 23(3) | 23(3) | 17(3) | 4(2) | -4(2) | -2(2) |
| N3 | 14.7(14) | 33.2(17) | 16.4(14) | 9.2(12) | -5.6(11) | -2.9(12) |
| N4 | 22(3) | 24(3) | 23(3) | 5(2) | -2(2) | 5(2) |
| N5 | 21(3) | 21(3) | 21(3) | 0(2) | -1(2) | 0(2) |
| C1 | 22(3) | 23(4) | 23(3) | 3(3) | -1(3) | 1(3) |
| C2 | 15(3) | 18(3) | 22(3) | -2(3) | -1(2) | -1(2) |
| C3 | 17(3) | 20(3) | 23(3) | -1(3) | -4(2) | 1(2) |
| C4 | 25(3) | 26(4) | 20(3) | 1(3) | -6(3) | 3(3) |
| C5 | 20(3) | 22(4) | 36(4) | -5(3) | -1(3) | -1(3) |
| C6 | 26(3) | 18(3) | 26(4) | 3(3) | 0(3) | 0(3) |
| C7 | 20(3) | 33(4) | 22(3) | -2(3) | 1(3) | 2(3) |
| C8 | 26(3) | 16(3) | 21(3) | 1(2) | 3(3) | 3(2) |
| C9 | 15(3) | 24(3) | 19(3) | -4(3) | -1(2) | 3(2) |
| C10 | 21(3) | 25(3) | 15(3) | -2(3) | -1(2) | -3(3) |
| C11 | 20(3) | 25(4) | 19(3) | 2(3) | 1(3) | 3(3) |
| C12 | 18(3) | 31(4) | 18(3) | -4(3) | -5(2) | 1(3) |
| C13 | 15(3) | 22(3) | 19(3) | -6(3) | -2(2) | -1(2) |
| C14 | 14.7(14) | 33.2(17) | 16.4(14) | 9.2(12) | -5.6(11) | -2.9(12) |
| C15 | 20(3) | 25(4) | 21(3) | -5(3) | -1(3) | -3(3) |
| C16 | 26(3) | 34(4) | 20(3) | 7(3) | -1(3) | 2(3) |
| C17 | 26(3) | 24(4) | 24(3) | 1(3) | -4(3) | 4(3) |
| C18 | 20(3) | 29(4) | 19(3) | -4(3) | -5(3) | -2(3) |
| C19 | 14.7(14) | 33.2(17) | 16.4(14) | 9.2(12) | -5.6(11) | -2.9(12) |
| C20 | 24(3) | 19(3) | 21(3) | -3(3) | 1(3) | 2(3) |
| C21 | 17(3) | 19(3) | 31(4) | 0(3) | 4(3) | 4(2) |
| C22 | 14(3) | 22(3) | 21(3) | 1(3) | -7(2) | 0(2) |
| C23 | 22(3) | 22(4) | 23(3) | 3(3) | -4(3) | 0(3) |

**Table D-9**. Bond Lengths for **5.10´**

| Atom | Atom | Length/Å | Atom | Atom | Length/Å |
|---|---|---|---|---|---|
| Pd1 | Cl1 | 2.4328(17) | C2 | C7 | 1.380(10) |
| Pd1 | P1 | 2.2342(18) | C3 | C4 | 1.388(9) |
| Pd1 | N4 | 2.023(6) | C4 | C5 | 1.384(10) |
| Pd1 | N5 | 2.062(5) | C5 | C6 | 1.388(10) |
| P1 | N1 | 1.865(5) | C6 | C7 | 1.401(10) |
| P1 | N2 | 1.744(5) | C8 | C9 | 1.404(9) |
| P1 | N3 | 1.839(5) | C8 | C13 | 1.388(9) |
| P1 | C1 | 1.825(7) | C9 | C10 | 1.402(9) |
| N1 | C2 | 1.525(8) | C10 | C11 | 1.384(9) |
| N1 | C14 | 1.256(9) | C11 | C12 | 1.396(9) |
| N2 | C3 | 1.402(8) | C12 | C13 | 1.408(9) |
| N2 | C8 | 1.402(8) | C14 | C15 | 1.416(9) |
| N3 | C9 | 1.396(8) | C15 | C16 | 1.382(10) |
| N3 | C19 | 1.384(8) | C16 | C17 | 1.397(10) |
| N4 | C14 | 1.364(9) | C17 | C18 | 1.381(10) |
| N4 | C18 | 1.361(9) | C19 | C20 | 1.393(9) |
| N5 | C19 | 1.359(8) | C20 | C21 | 1.378(9) |
| N5 | C23 | 1.346(8) | C21 | C22 | 1.385(9) |
| C2 | C3 | 1.406(9) | C22 | C23 | 1.380(9) |

**Table D-10.** Bond Angles for **5.10´.**

| Atom | Atom | Atom | Angle/° | Atom | Atom | Atom | Angle/° |
|---|---|---|---|---|---|---|---|
| P1 | Pd1 | Cl1 | 174.23(6) | C7 | C2 | C3 | 120.7(6) |
| N4 | Pd1 | Cl1 | 93.77(17) | N2 | C3 | C2 | 111.1(5) |
| N4 | Pd1 | P1 | 88.36(17) | C4 | C3 | N2 | 128.4(6) |
| N4 | Pd1 | N5 | 172.0(2) | C4 | C3 | C2 | 120.3(6) |
| N5 | Pd1 | Cl1 | 94.04(15) | C5 | C4 | C3 | 118.6(6) |
| N5 | Pd1 | P1 | 84.05(16) | C4 | C5 | C6 | 121.5(6) |
| N1 | P1 | Pd1 | 88.74(19) | C5 | C6 | C7 | 120.0(6) |
| N2 | P1 | Pd1 | 146.8(2) | C2 | C7 | C6 | 118.7(6) |
| N2 | P1 | N1 | 86.0(2) | N2 | C8 | C9 | 111.3(6) |
| N2 | P1 | N3 | 83.7(2) | C13 | C8 | N2 | 127.6(6) |
| N2 | P1 | C1 | 105.5(3) | C13 | C8 | C9 | 120.8(6) |

| | | | | | | | |
|---|---|---|---|---|---|---|---|
| N3 | P1 | Pd1 | 91.43(19) | N3 | C9 | C8 | 110.1(6) |
| N3 | P1 | N1 | 161.4(3) | N3 | C9 | C10 | 129.2(6) |
| C1 | P1 | Pd1 | 107.7(2) | C10 | C9 | C8 | 120.5(6) |
| C1 | P1 | N1 | 99.5(3) | C11 | C10 | C9 | 118.6(6) |
| C1 | P1 | N3 | 98.2(3) | C10 | C11 | C12 | 121.2(6) |
| C2 | N1 | P1 | 105.1(4) | C11 | C12 | C13 | 120.4(6) |
| C14 | N1 | P1 | 127.3(5) | C8 | C13 | C12 | 118.5(6) |
| C14 | N1 | C2 | 122.4(5) | N1 | C14 | N4 | 113.5(6) |
| C3 | N2 | P1 | 114.1(4) | N1 | C14 | C15 | 126.7(6) |
| C3 | N2 | C8 | 126.8(5) | N4 | C14 | C15 | 119.8(6) |
| C8 | N2 | P1 | 118.3(4) | C16 | C15 | C14 | 119.1(6) |
| C9 | N3 | P1 | 115.8(4) | C15 | C16 | C17 | 120.7(7) |
| C19 | N3 | P1 | 117.1(4) | C18 | C17 | C16 | 117.7(6) |
| C19 | N3 | C9 | 127.1(5) | N4 | C18 | C17 | 122.7(6) |
| C14 | N4 | Pd1 | 117.8(4) | N3 | C19 | C20 | 124.5(6) |
| C18 | N4 | Pd1 | 122.4(5) | N5 | C19 | N3 | 114.3(5) |
| C18 | N4 | C14 | 119.8(6) | N5 | C19 | C20 | 121.0(5) |
| C19 | N5 | Pd1 | 117.1(4) | C21 | C20 | C19 | 119.1(6) |
| C23 | N5 | Pd1 | 123.9(4) | C20 | C21 | C22 | 119.7(6) |
| C23 | N5 | C19 | 119.1(5) | C23 | C22 | C21 | 118.7(6) |
| C3 | C2 | N1 | 111.1(5) | N5 | C23 | C22 | 122.2(6) |
| C7 | C2 | N1 | 128.1(6) | | | | |

**Table D-11.** Torsion angles for **5.10′.**

| **A** | **B** | **C** | **D** | **Angle/°** | **A** | **B** | **C** | **D** | **Angle/°** |
|---|---|---|---|---|---|---|---|---|---|
| Pd1 | P1 | N1 | C2 | 177.8(3) | N4 | C14 | C15 | C16 | 4.1(9) |
| Pd1 | P1 | N1 | C14 | 23.1(5) | N5 | C19 | C20 | C21 | -0.2(10) |
| Pd1 | P1 | N2 | C3 | -113.6(5) | C1 | P1 | N1 | C2 | -74.5(4) |
| Pd1 | P1 | N2 | C8 | 75.7(6) | C1 | P1 | N1 | C14 | 130.8(6) |
| Pd1 | P1 | N3 | C9 | -139.0(5) | C1 | P1 | N2 | C3 | 66.6(5) |
| Pd1 | P1 | N3 | C19 | 39.8(5) | C1 | P1 | N2 | C8 | -104.0(5) |
| Pd1 | N4 | C14 | N1 | 0.4(7) | C1 | P1 | N3 | C9 | 113.0(5) |
| Pd1 | N4 | C14 | C15 | -178.5(5) | C1 | P1 | N3 | C19 | -68.3(5) |
| Pd1 | N4 | C18 | C17 | 177.1(5) | C2 | N1 | C14 | N4 | -169.0(5) |
| Pd1 | N5 | C19 | N3 | -6.7(7) | C2 | N1 | C14 | C15 | 9.8(10) |

| | | | | | | | | | |
|---|---|---|---|---|---|---|---|---|---|
| Pd1 | N5 | C19 | C20 | 176.9(5) | C2 | C3 | C4 | C5 | 1.7(9) |
| Pd1 | N5 | C23 | C22 | -176.1(5) | C3 | N2 | C8 | C9 | -164.3(6) |
| P1 | N1 | C2 | C3 | -24.8(6) | C3 | N2 | C8 | C13 | 21.7(10) |
| P1 | N1 | C2 | C7 | 151.2(6) | C3 | C2 | C7 | C6 | -4.5(9) |
| P1 | N1 | C14 | N4 | -18.3(8) | C3 | C4 | C5 | C6 | -2.1(10) |
| P1 | N1 | C14 | C15 | 160.4(5) | C4 | C5 | C6 | C7 | -0.8(10) |
| P1 | N2 | C3 | C2 | 23.3(7) | C5 | C6 | C7 | C2 | 4.1(10) |
| P1 | N2 | C3 | C4 | -151.3(6) | C7 | C2 | C3 | N2 | -173.5(6) |
| P1 | N2 | C8 | C9 | 5.0(7) | C7 | C2 | C3 | C4 | 1.6(9) |
| P1 | N2 | C8 | C13 | -169.0(5) | C8 | N2 | C3 | C2 | -167.0(6) |
| P1 | N3 | C9 | C8 | -7.2(7) | C8 | N2 | C3 | C4 | 18.4(10) |
| P1 | N3 | C9 | C10 | 167.1(6) | C8 | C9 | C10 | C11 | -1.7(9) |
| P1 | N3 | C19 | N5 | -25.8(8) | C9 | N3 | C19 | N5 | 152.8(6) |
| P1 | N3 | C19 | C20 | 150.5(5) | C9 | N3 | C19 | C20 | -30.9(11) |
| N1 | P1 | N2 | C3 | -32.1(5) | C9 | C8 | C13 | C12 | -0.4(9) |
| N1 | P1 | N2 | C8 | 157.3(5) | C9 | C10 | C11 | C12 | 1.4(10) |
| N1 | P1 | N3 | C9 | -48.7(11) | C10 | C11 | C12 | C13 | -0.6(10) |
| N1 | P1 | N3 | C19 | 130.0(8) | C11 | C12 | C13 | C8 | 0.1(9) |
| N1 | C2 | C3 | N2 | 2.9(7) | C13 | C8 | C9 | N3 | 176.1(6) |
| N1 | C2 | C3 | C4 | 178.0(5) | C13 | C8 | C9 | C10 | 1.2(9) |
| N1 | C2 | C7 | C6 | 179.8(6) | C14 | N1 | C2 | C3 | 131.4(6) |
| N1 | C14 | C15 | C16 | -174.6(6) | C14 | N1 | C2 | C7 | -52.6(9) |
| N2 | P1 | N1 | C2 | 30.5(4) | C14 | N4 | C18 | C17 | 0.6(9) |
| N2 | P1 | N1 | C14 | -124.1(6) | C14 | C15 | C16 | C17 | -5.2(10) |
| N2 | P1 | N3 | C9 | 8.1(5) | C15 | C16 | C17 | C18 | 3.9(10) |
| N2 | P1 | N3 | C19 | -173.1(5) | C16 | C17 | C18 | N4 | -1.6(10) |
| N2 | C3 | C4 | C5 | 175.9(6) | C18 | N4 | C14 | N1 | 177.0(6) |
| N2 | C8 | C9 | N3 | 1.6(7) | C18 | N4 | C14 | C15 | -1.8(9) |
| N2 | C8 | C9 | C10 | -173.2(6) | C19 | N3 | C9 | C8 | 174.2(6) |
| N2 | C8 | C13 | C12 | 173.1(6) | C19 | N3 | C9 | C10 | -11.5(11) |
| N3 | P1 | N1 | C2 | 87.0(9) | C19 | N5 | C23 | C22 | 4.3(9) |
| N3 | P1 | N1 | C14 | -67.6(10) | C19 | C20 | C21 | C22 | 3.0(9) |
| N3 | P1 | N2 | C3 | 163.4(5) | C20 | C21 | C22 | C23 | -2.2(9) |
| N3 | P1 | N2 | C8 | -7.2(5) | C21 | C22 | C23 | N5 | -1.5(10) |
| N3 | C9 | C10 | C11 | -175.5(6) | C23 | N5 | C19 | N3 | 173.0(6) |

| | | | | | | | | | |
|---|---|---|---|---|---|---|---|---|---|
| N3 | C19 | C20 | C21 | -176.2(6) | C23 | N5 | C19 | C20 | -3.4(9) |

**Table D-12.** Hydrogen Atom Coordinates (Å×10$^4$) and Isotropic Displacement Parameters (Å$^2$×10$^3$) for **5.10´**.

| **Atom** | ***x*** | ***y*** | ***z*** | **U(eq)** |
|---|---|---|---|---|
| H1A | 4688.82 | 7023.93 | 5098.1 | 35 |
| H1B | 3169.5 | 6388.11 | 5259.44 | 35 |
| H1C | 4394.58 | 6838.45 | 5955.47 | 35 |
| H4 | -1659.37 | 6247.09 | 3751.34 | 29 |
| H5 | -3042.02 | 5114.06 | 4247.25 | 32 |
| H6 | -2805.21 | 4907.59 | 5572.05 | 28 |
| H7 | -1072.8 | 5830.89 | 6435.85 | 31 |
| H10 | 2771.09 | 9290.52 | 3250.93 | 25 |
| H11 | 399.97 | 9225.79 | 2204.31 | 26 |
| H12 | -2089.05 | 8343.12 | 2224.38 | 28 |
| H13 | -2211.98 | 7472.28 | 3297.64 | 23 |
| H15 | -2131.75 | 7004.21 | 6846.08 | 27 |
| H16 | -3042.46 | 7907.88 | 7752 | 33 |
| H17 | -1209.23 | 9059.42 | 8179.63 | 30 |
| H18 | 1277.93 | 9364.84 | 7561.29 | 28 |
| H20 | 5465.08 | 8784.94 | 3725.48 | 26 |
| H21 | 8317.42 | 9379.82 | 4161.64 | 27 |
| H22 | 9236.61 | 9588.63 | 5488.64 | 24 |
| H23 | 7214.96 | 9271.17 | 6337.19 | 28 |

**Structural Data for $Pd(CH_2TMS)_2(L1)$ (5.12)**

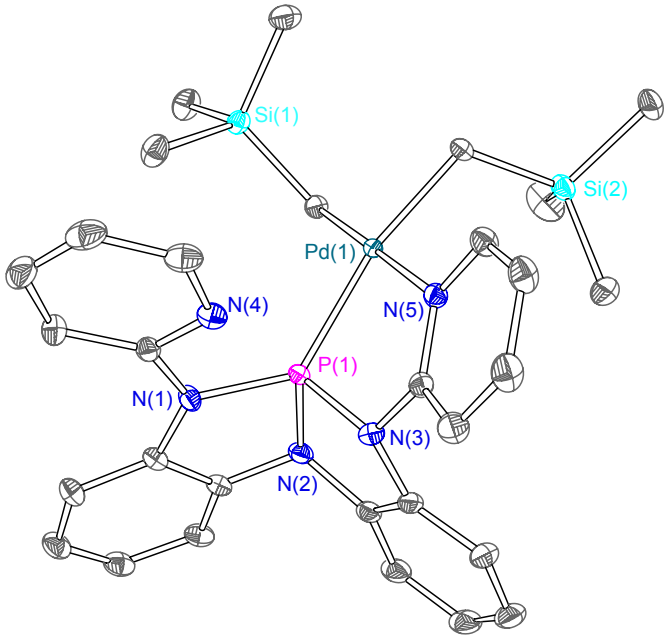


**Figure D-6** Thermal ellipsoids rendered at the 50% level for **5.12**. Hydrogen atoms are omitted for clarity.

**Table D-13**. Crystal Data and structure refinement for **5.12**.

| | |
|---|---|
| Identification code | PdCH2TMS |
| Empirical formula | $C_{30}H_{38}N_5Si_2PPd$ |
| Formula weight | 662.20 |
| Temperature/K | 100.0 |
| Crystal system | triclinic |
| Space group | P-1 |
| a/Å | 10.1876(16) |
| b/Å | 10.9351(17) |
| c/Å | 15.171(2) |
| α/° | 81.797(3) |
| β/° | 72.799(3) |
| γ/° | 74.096(3) |
| Volume/Å$^3$ | 1549.2(4) |
| Z | 2 |
| $\rho_{calc}$g/cm$^3$ | 1.420 |
| μ/mm$^{-1}$ | 0.756 |
| F(000) | 684.0 |
| Crystal size/mm$^3$ | 0.315 × 0.25 × 0.15 |
| Radiation | MoKα (λ = 0.71073) |
| 2Θ range for data collection/° | 2.816 to 71.384 |
| Index ranges | $-16 \leq h \leq 16$, $-17 \leq k \leq 17$, $-24 \leq l \leq 24$ |
| Reflections collected | 119168 |
| Independent reflections | 13976 [$R_{int}$ = 0.0307, $R_{sigma}$ = 0.0180] |
| Data/restraints/parameters | 13976/0/358 |
| Goodness-of-fit on $F^2$ | 1.041 |
| Final R indexes [I>=2σ (I)] | $R_1$ = 0.0196, $wR_2$ = 0.0482 |
| Final R indexes [all data] | $R_1$ = 0.0219, $wR_2$ = 0.0492 |
| Largest diff. peak/hole / e Å$^{-3}$ | 0.72/-0.59 |

**Table D-14.** Fractional Atomic Coordinates ($\times 10^4$) and Equivalent Isotropic Displacement Parameters ($Å^2 \times 10^3$) for **5.12**. $U_{eq}$ is defined as 1/3 of of the trace of the orthogonalised $U_{IJ}$ tensor.

| Atom | *x* | *y* | *z* | U(eq) |
|---|---|---|---|---|
| Pd1 | 3126.9(2) | 6457.9(2) | 2121.4(2) | 9.62(2) |
| P1 | 3067.0(2) | 6892.3(2) | 3552.1(2) | 11.97(4) |
| Si1 | 2113.8(3) | 9233.5(2) | 1096.9(2) | 14.12(4) |
| Si2 | 2277.2(3) | 4337.4(3) | 1183.6(2) | 17.05(5) |
| N1 | 3471.1(8) | 8125.7(7) | 3942.6(5) | 14.95(12) |
| N2 | 1639.0(8) | 6909.1(8) | 4524.4(5) | 15.33(13) |
| N3 | 3983.0(9) | 5416.7(7) | 3912.5(5) | 15.72(13) |
| N4 | 5566.8(8) | 7520.4(8) | 2879.4(5) | 16.37(13) |
| N5 | 4944.1(8) | 4943.6(7) | 2355.5(5) | 13.27(12) |
| C1 | 1465.2(9) | 7924.7(8) | 1891.9(6) | 13.98(13) |
| C2 | 3114.8(9) | 5704.8(8) | 938.2(6) | 13.39(13) |
| C3 | 2462.7(9) | 8633.8(8) | 4747.5(6) | 13.97(13) |
| C4 | 1380.7(9) | 7973.8(8) | 5049.9(6) | 14.50(14) |
| C5 | 212.6(10) | 8365.3(10) | 5791.0(6) | 18.47(16) |
| C6 | 161.6(11) | 9394.1(10) | 6265.6(7) | 20.86(17) |
| C7 | 1267.1(11) | 9995.2(9) | 6006.0(7) | 21.10(17) |
| C8 | 2435.6(10) | 9625.0(9) | 5243.6(6) | 18.26(15) |
| C9 | 1756.0(10) | 5657.0(9) | 4991.1(6) | 17.33(15) |
| C10 | 3074.2(11) | 4818.9(9) | 4641.2(6) | 17.24(15) |
| C11 | 3367.0(13) | 3550.5(10) | 4987.0(7) | 23.38(18) |
| C12 | 2312.1(14) | 3143.1(11) | 5703.0(8) | 28.7(2) |
| C13 | 1016.8(14) | 3973.3(12) | 6062.8(7) | 28.6(2) |
| C14 | 720.7(12) | 5246.8(11) | 5705.8(7) | 23.70(19) |
| C15 | 4701.9(9) | 8478.0(8) | 3396.9(6) | 14.14(13) |
| C16 | 4992.1(11) | 9671.4(9) | 3341.8(7) | 20.72(17) |
| C17 | 6266.1(12) | 9839.7(11) | 2726.6(8) | 25.3(2) |
| C18 | 7174.0(11) | 8851.8(12) | 2193.9(7) | 25.5(2) |
| C19 | 6769.7(10) | 7717.2(10) | 2280.5(7) | 21.38(17) |
| C20 | 5083.7(10) | 4713.6(8) | 3228.5(6) | 14.85(14) |
| C21 | 6257.0(11) | 3863.1(9) | 3450.5(7) | 21.23(17) |
| C22 | 7318.5(11) | 3201.7(10) | 2751.4(8) | 23.12(18) |
| C23 | 7182.9(10) | 3422.2(9) | 1853.6(7) | 20.63(17) |

| | | | | |
|---|---|---|---|---|
| C24 | 5995.8(10) | 4301.7(9) | 1685.3(6) | 16.86(15) |
| C25 | 3428.4(11) | 9775.8(10) | 1494.5(8) | 22.77(18) |
| C26 | 541.6(11) | 10633.4(9) | 1059.1(8) | 23.32(18) |
| C27 | 2998.8(11) | 8790.6(10) | -129.5(7) | 22.88(18) |
| C28 | 2823.1(12) | 3391.3(10) | 127.8(7) | 24.45(19) |
| C29 | 2736.5(14) | 3205.5(11) | 2171.0(8) | 28.4(2) |
| C30 | 295.1(12) | 4946.2(15) | 1457.1(10) | 35.7(3) |

**Table D-15.** Anisotropic Displacement Parameters ($Å^2 \times 10^3$) for **5.12**. The Anisotropic displacement factor exponent takes the form: $-2\pi^2[h^2a^{*2}U_{11}+2hka^*b^*U_{12}+\ldots]$.

| **Atom** | $\mathbf{U_{11}}$ | $\mathbf{U_{22}}$ | $\mathbf{U_{33}}$ | $\mathbf{U_{23}}$ | $\mathbf{U_{13}}$ | $\mathbf{U_{12}}$ |
|---|---|---|---|---|---|---|
| Pd1 | 11.08(3) | 9.35(3) | 8.51(2) | -0.89(2) | -2.66(2) | -2.46(2) |
| P1 | 14.53(9) | 12.85(8) | 9.57(8) | -1.22(6) | -3.38(7) | -4.65(7) |
| Si1 | 14.23(10) | 12.33(9) | 15.74(10) | 1.23(8) | -6.26(8) | -1.86(8) |
| Si2 | 18.01(11) | 19.29(11) | 15.84(11) | -4.55(9) | -2.54(9) | -8.29(9) |
| N1 | 15.4(3) | 16.7(3) | 13.7(3) | -5.3(2) | -0.8(2) | -6.5(2) |
| N2 | 17.4(3) | 19.8(3) | 10.2(3) | -1.8(2) | -2.1(2) | -8.2(3) |
| N3 | 20.1(3) | 14.8(3) | 12.0(3) | 1.3(2) | -4.7(2) | -4.4(3) |
| N4 | 14.9(3) | 19.2(3) | 14.5(3) | -1.6(2) | -3.8(2) | -3.3(3) |
| N5 | 14.4(3) | 12.7(3) | 13.8(3) | -0.9(2) | -5.5(2) | -3.3(2) |
| C1 | 12.9(3) | 13.0(3) | 14.0(3) | -1.5(3) | -2.5(3) | -0.9(3) |
| C2 | 14.3(3) | 14.6(3) | 11.5(3) | -3.0(2) | -3.8(3) | -2.4(3) |
| C3 | 13.5(3) | 16.2(3) | 12.2(3) | -3.3(3) | -3.9(3) | -2.0(3) |
| C4 | 14.6(3) | 18.2(3) | 10.9(3) | -2.2(3) | -4.1(3) | -3.2(3) |
| C5 | 15.3(4) | 24.3(4) | 13.5(3) | -2.0(3) | -2.2(3) | -2.7(3) |
| C6 | 19.5(4) | 23.3(4) | 14.9(4) | -4.4(3) | -2.7(3) | 2.1(3) |
| C7 | 24.1(4) | 19.9(4) | 17.2(4) | -7.1(3) | -5.2(3) | 0.6(3) |
| C8 | 19.6(4) | 18.4(4) | 17.5(4) | -6.6(3) | -5.0(3) | -3.2(3) |
| C9 | 23.4(4) | 21.8(4) | 11.6(3) | 0.2(3) | -5.8(3) | -12.8(3) |
| C10 | 25.4(4) | 18.7(4) | 12.2(3) | 2.5(3) | -8.2(3) | -11.2(3) |
| C11 | 36.0(5) | 19.9(4) | 18.9(4) | 5.2(3) | -12.5(4) | -12.1(4) |
| C12 | 47.3(7) | 27.4(5) | 20.9(4) | 9.9(4) | -15.9(4) | -23.3(5) |
| C13 | 42.6(6) | 36.2(6) | 16.3(4) | 7.0(4) | -9.1(4) | -28.0(5) |
| C14 | 29.7(5) | 33.0(5) | 14.0(4) | 0.4(3) | -3.7(3) | -20.1(4) |
| C15 | 14.9(3) | 15.9(3) | 13.3(3) | -0.7(3) | -4.4(3) | -5.9(3) |

| | | | | | | |
|---|---|---|---|---|---|---|
| C16 | 25.9(4) | 17.9(4) | 21.9(4) | -1.1(3) | -7.8(3) | -9.9(3) |
| C17 | 30.5(5) | 27.2(5) | 25.6(5) | 6.4(4) | -12.2(4) | -18.3(4) |
| C18 | 20.4(4) | 37.0(6) | 20.6(4) | 6.9(4) | -5.3(3) | -14.0(4) |
| C19 | 16.3(4) | 29.1(5) | 16.5(4) | 0.1(3) | -2.7(3) | -4.6(3) |
| C20 | 18.2(4) | 12.6(3) | 15.3(3) | -0.2(3) | -7.5(3) | -3.3(3) |
| C21 | 24.4(4) | 18.4(4) | 23.0(4) | -0.4(3) | -14.5(4) | -0.3(3) |
| C22 | 21.8(4) | 18.1(4) | 31.1(5) | -3.4(3) | -15.0(4) | 1.8(3) |
| C23 | 17.3(4) | 17.8(4) | 26.4(4) | -6.4(3) | -8.1(3) | 1.2(3) |
| C24 | 15.7(4) | 16.5(4) | 17.5(4) | -3.7(3) | -5.2(3) | -0.4(3) |
| C25 | 23.8(4) | 19.9(4) | 29.3(5) | 4.1(3) | -13.9(4) | -8.5(3) |
| C26 | 21.4(4) | 16.4(4) | 30.3(5) | 2.1(3) | -11.1(4) | 1.0(3) |
| C27 | 25.4(5) | 24.0(4) | 16.7(4) | 2.4(3) | -4.7(3) | -4.9(4) |
| C28 | 32.7(5) | 22.6(4) | 22.1(4) | -7.4(3) | -6.1(4) | -11.7(4) |
| C29 | 43.8(6) | 23.8(5) | 21.3(4) | 2.7(4) | -7.2(4) | -18.3(5) |
| C30 | 18.6(5) | 52.9(8) | 38.5(6) | -16.4(6) | -1.4(4) | -13.9(5) |

**Table D-16.** Bond Lengths for **5.12**.

| **Atom** | **Atom** | **Length/Å** | **Atom** | **Atom** | **Length/Å** |
|---|---|---|---|---|---|
| Pd1 | P1 | 2.2674(4) | N5 | C20 | 1.3543(11) |
| Pd1 | N5 | 2.1992(8) | N5 | C24 | 1.3497(11) |
| Pd1 | C1 | 2.0642(9) | C3 | C4 | 1.4103(12) |
| Pd1 | C2 | 2.0834(8) | C3 | C8 | 1.3950(12) |
| P1 | N1 | 1.7366(8) | C4 | C5 | 1.3894(12) |
| P1 | N2 | 1.7368(8) | C5 | C6 | 1.4014(14) |
| P1 | N3 | 1.7316(8) | C6 | C7 | 1.3873(15) |
| Si1 | C1 | 1.8693(9) | C7 | C8 | 1.4050(13) |
| Si1 | C25 | 1.8772(10) | C9 | C10 | 1.4028(14) |
| Si1 | C26 | 1.8968(10) | C9 | C14 | 1.3904(13) |
| Si1 | C27 | 1.8801(11) | C10 | C11 | 1.3951(13) |
| Si2 | C2 | 1.8589(9) | C11 | C12 | 1.4026(16) |
| Si2 | C28 | 1.8909(10) | C12 | C13 | 1.3864(19) |
| Si2 | C29 | 1.8876(12) | C13 | C14 | 1.4053(16) |
| Si2 | C30 | 1.8813(12) | C15 | C16 | 1.4010(13) |
| N1 | C3 | 1.4121(11) | C16 | C17 | 1.3982(15) |
| N1 | C15 | 1.4021(11) | C17 | C18 | 1.3910(17) |

| | | | | | |
|---|---|---|---|---|---|
| N2 | C4 | 1.4259(12) | C18 | C19 | 1.3885(16) |
| N2 | C9 | 1.4401(12) | C20 | C21 | 1.3952(13) |
| N3 | C10 | 1.4236(12) | C21 | C22 | 1.3891(15) |
| N3 | C20 | 1.4116(12) | C22 | C23 | 1.3899(15) |
| N4 | C15 | 1.3450(12) | C23 | C24 | 1.3885(13) |
| N4 | C19 | 1.3431(12) | | | |

**Table D-17.** Bond Angles for **5.12**.

| **Atom** | **Atom** | **Atom** | **Angle/°** | **Atom** | **Atom** | **Atom** | **Angle/°** |
|---|---|---|---|---|---|---|---|
| N5 | Pd1 | P1 | 80.38(2) | Si1 | C1 | Pd1 | 111.47(4) |
| C1 | Pd1 | P1 | 99.16(3) | Si2 | C2 | Pd1 | 113.79(4) |
| C1 | Pd1 | N5 | 177.98(3) | C4 | C3 | N1 | 110.59(7) |
| C1 | Pd1 | C2 | 86.92(3) | C8 | C3 | N1 | 129.39(8) |
| C2 | Pd1 | P1 | 168.36(2) | C8 | C3 | C4 | 120.01(8) |
| C2 | Pd1 | N5 | 93.89(3) | C3 | C4 | N2 | 113.00(7) |
| N1 | P1 | Pd1 | 132.18(3) | C5 | C4 | N2 | 126.01(8) |
| N1 | P1 | N2 | 90.49(4) | C5 | C4 | C3 | 120.99(8) |
| N2 | P1 | Pd1 | 124.93(3) | C4 | C5 | C6 | 118.66(9) |
| N3 | P1 | Pd1 | 99.36(3) | C7 | C6 | C5 | 120.46(9) |
| N3 | P1 | N1 | 111.59(4) | C6 | C7 | C8 | 121.21(9) |
| N3 | P1 | N2 | 91.89(4) | C3 | C8 | C7 | 118.44(9) |
| C1 | Si1 | C25 | 111.75(4) | C10 | C9 | N2 | 112.67(8) |
| C1 | Si1 | C26 | 108.68(4) | C14 | C9 | N2 | 126.73(10) |
| C1 | Si1 | C27 | 114.02(4) | C14 | C9 | C10 | 120.60(9) |
| C25 | Si1 | C26 | 108.88(5) | C9 | C10 | N3 | 112.06(8) |
| C25 | Si1 | C27 | 106.60(5) | C11 | C10 | N3 | 126.99(9) |
| C27 | Si1 | C26 | 106.70(5) | C11 | C10 | C9 | 120.93(9) |
| C2 | Si2 | C28 | 110.70(4) | C10 | C11 | C12 | 118.05(11) |
| C2 | Si2 | C29 | 113.43(5) | C13 | C12 | C11 | 121.26(10) |
| C2 | Si2 | C30 | 109.61(5) | C12 | C13 | C14 | 120.50(10) |
| C29 | Si2 | C28 | 107.84(5) | C9 | C14 | C13 | 118.65(11) |
| C30 | Si2 | C28 | 106.18(5) | N4 | C15 | N1 | 110.43(7) |
| C30 | Si2 | C29 | 108.81(6) | N4 | C15 | C16 | 123.29(8) |
| C3 | N1 | P1 | 113.64(6) | C16 | C15 | N1 | 126.20(8) |
| C15 | N1 | P1 | 115.40(6) | C17 | C16 | C15 | 117.07(9) |

| | | | | | | | |
|---|---|---|---|---|---|---|---|
| C15 | N1 | C3 | 130.92(7) | C18 | C17 | C16 | 120.10(9) |
| C4 | N2 | P1 | 111.41(6) | C19 | C18 | C17 | 118.38(9) |
| C4 | N2 | C9 | 118.80(7) | N4 | C19 | C18 | 122.75(10) |
| C9 | N2 | P1 | 109.95(6) | N5 | C20 | N3 | 116.11(7) |
| C10 | N3 | P1 | 111.09(6) | N5 | C20 | C21 | 122.89(8) |
| C20 | N3 | P1 | 116.77(6) | C21 | C20 | N3 | 120.98(8) |
| C20 | N3 | C10 | 121.92(8) | C22 | C21 | C20 | 118.82(9) |
| C19 | N4 | C15 | 118.37(8) | C21 | C22 | C23 | 118.85(9) |
| C20 | N5 | Pd1 | 117.44(6) | C24 | C23 | C22 | 118.89(9) |
| C24 | N5 | Pd1 | 125.01(6) | N5 | C24 | C23 | 123.25(9) |
| C24 | N5 | C20 | 117.29(8) | | | | |

**Table D-18.** Torsion Angles for **5.12**.

| **A** | **B** | **C** | **D** | **Angle/˚** | **A** | **B** | **C** | **D** | **Angle/˚** |
|---|---|---|---|---|---|---|---|---|---|
| Pd1 | P1 | N1 | C3 | 135.32(5) | C3 | N1 | C15 | N4 | 160.85(9) |
| Pd1 | P1 | N1 | C15 | -42.62(8) | C3 | N1 | C15 | C16 | -22.45(15) |
| Pd1 | P1 | N2 | C4 | -136.89(5) | C3 | C4 | C5 | C6 | -3.20(13) |
| Pd1 | P1 | N2 | C9 | 89.26(6) | C4 | N2 | C9 | C10 | -120.14(9) |
| Pd1 | P1 | N3 | C10 | -111.83(6) | C4 | N2 | C9 | C14 | 60.64(12) |
| Pd1 | P1 | N3 | C20 | 34.20(7) | C4 | C3 | C8 | C7 | -4.11(13) |
| Pd1 | N5 | C20 | N3 | 4.30(10) | C4 | C5 | C6 | C7 | -0.88(14) |
| Pd1 | N5 | C20 | C21 | -173.91(7) | C5 | C6 | C7 | C8 | 2.46(15) |
| Pd1 | N5 | C24 | C23 | 174.74(7) | C6 | C7 | C8 | C3 | 0.08(14) |
| P1 | N1 | C3 | C4 | 1.59(9) | C8 | C3 | C4 | N2 | -173.96(8) |
| P1 | N1 | C3 | C8 | -179.44(8) | C8 | C3 | C4 | C5 | 5.76(13) |
| P1 | N1 | C15 | N4 | -21.66(9) | C9 | N2 | C4 | C3 | 119.72(9) |
| P1 | N1 | C15 | C16 | 155.05(8) | C9 | N2 | C4 | C5 | -59.98(12) |
| P1 | N2 | C4 | C3 | -9.61(9) | C9 | C10 | C11 | C12 | -0.85(14) |
| P1 | N2 | C4 | C5 | 170.68(7) | C10 | N3 | C20 | N5 | 114.40(9) |
| P1 | N2 | C9 | C10 | 9.85(9) | C10 | N3 | C20 | C21 | -67.36(12) |
| P1 | N2 | C9 | C14 | -169.37(8) | C10 | C9 | C14 | C13 | -0.67(14) |
| P1 | N3 | C10 | C9 | -10.80(9) | C10 | C11 | C12 | C13 | -0.33(15) |
| P1 | N3 | C10 | C11 | 167.53(8) | C11 | C12 | C13 | C14 | 1.01(16) |
| P1 | N3 | C20 | N5 | -27.71(10) | C12 | C13 | C14 | C9 | -0.50(15) |

| | | | | | | | | | |
|---|---|---|---|---|---|---|---|---|---|
| P1 | N3 | C20 | C21 | 150.53(8) | C14 | C9 | C10 | N3 | 179.81(8) |
| N1 | P1 | N2 | C4 | 8.70(6) | C14 | C9 | C10 | C11 | 1.36(13) |
| N1 | P1 | N2 | C9 | -125.16(6) | C15 | N1 | C3 | C4 | 179.12(9) |
| N1 | P1 | N3 | C10 | 105.32(6) | C15 | N1 | C3 | C8 | -1.92(16) |
| N1 | P1 | N3 | C20 | -108.65(7) | C15 | N4 | C19 | C18 | 1.91(14) |
| N1 | C3 | C4 | N2 | 5.12(10) | C15 | C16 | C17 | C18 | 0.79(15) |
| N1 | C3 | C4 | C5 | -175.16(8) | C16 | C17 | C18 | C19 | 1.02(16) |
| N1 | C3 | C8 | C7 | 177.01(9) | C17 | C18 | C19 | N4 | -2.45(15) |
| N1 | C15 | C16 | C17 | -177.70(9) | C19 | N4 | C15 | N1 | 176.90(8) |
| N2 | P1 | N1 | C3 | -5.98(7) | C19 | N4 | C15 | C16 | 0.08(13) |
| N2 | P1 | N1 | C15 | 176.08(7) | C20 | N3 | C10 | C9 | -154.80(8) |
| N2 | P1 | N3 | C10 | 14.04(6) | C20 | N3 | C10 | C11 | 23.52(14) |
| N2 | P1 | N3 | C20 | 160.08(7) | C20 | N5 | C24 | C23 | 0.75(13) |
| N2 | C4 | C5 | C6 | 176.49(9) | C20 | C21 | C22 | C23 | 0.79(15) |
| N2 | C9 | C10 | N3 | 0.53(10) | C21 | C22 | C23 | C24 | 0.40(15) |
| N2 | C9 | C10 | C11 | -177.91(8) | C22 | C23 | C24 | N5 | -1.23(15) |
| N2 | C9 | C14 | C13 | 178.49(9) | C24 | N5 | C20 | N3 | 178.75(8) |
| N3 | P1 | N1 | C3 | -98.21(7) | C24 | N5 | C20 | C21 | 0.54(13) |
| N3 | P1 | N1 | C15 | 83.86(7) | C25 | Si1 | C1 | Pd1 | -51.85(6) |
| N3 | P1 | N2 | C4 | 120.32(6) | C26 | Si1 | C1 | Pd1 | -172.02(5) |
| N3 | P1 | N2 | C9 | -13.53(6) | C27 | Si1 | C1 | Pd1 | 69.12(6) |
| N3 | C10 | C11 | C12 | -179.04(9) | C28 | Si2 | C2 | Pd1 | -161.62(5) |
| N3 | C20 | C21 | C22 | -179.44(9) | C29 | Si2 | C2 | Pd1 | -40.24(6) |
| N4 | C15 | C16 | C17 | -1.39(14) | C30 | Si2 | C2 | Pd1 | 81.59(6) |
| N5 | C20 | C21 | C22 | -1.32(15) | | | | | |

**Table D-19.** Hydrogen Atom Coordinates (Å×$10^4$) and Isotropic Displacement Parameters (Å$^2$×$10^3$) for **5.12**.

| **Atom** | ***x*** | ***y*** | ***z*** | **U(eq)** |
|---|---|---|---|---|
| H1A | 872.88 | 7590.72 | 1619.29 | 17 |
| H1B | 866.52 | 8269.52 | 2489.31 | 17 |
| H2A | 2601.51 | 6385.88 | 570.37 | 16 |
| H2B | 4103.94 | 5423.96 | 557.45 | 16 |
| H5 | -536.43 | 7943.99 | 5972.42 | 22 |

| Atom | *x* | *y* | *z* | U(eq) |
|---|---|---|---|---|
| H6 | -635.32 | 9682.02 | 6768.5 | 25 |
| H7 | 1233.27 | 10669.39 | 6350.11 | 25 |
| H8 | 3189.56 | 10039.9 | 5070.03 | 22 |
| H11 | 4254.85 | 2979.44 | 4744.69 | 28 |
| H12 | 2488.42 | 2281.86 | 5946 | 34 |
| H13 | 324.19 | 3678.98 | 6554.5 | 34 |
| H14 | -168.71 | 5815.85 | 5947.75 | 28 |
| H16 | 4351.53 | 10336.83 | 3706.43 | 25 |
| H17 | 6512.06 | 10630.01 | 2672.28 | 30 |
| H18 | 8049.2 | 8951.04 | 1781.01 | 31 |
| H19 | 7369.09 | 7052.2 | 1900.25 | 26 |
| H21 | 6328.56 | 3738.55 | 4068.91 | 25 |
| H22 | 8123.21 | 2608.86 | 2884.58 | 28 |
| H23 | 7890.62 | 2978.67 | 1363.27 | 25 |
| H24 | 5920.07 | 4459.53 | 1067.86 | 20 |
| H25A | 3012.81 | 10012.11 | 2135.67 | 34 |
| H25B | 3672.88 | 10515.43 | 1098.46 | 34 |
| H25C | 4285.78 | 9082.95 | 1456.95 | 34 |
| H26A | -163.87 | 10353.31 | 869.95 | 35 |
| H26B | 859.08 | 11305.54 | 613.96 | 35 |
| H26C | 117.08 | 10964.72 | 1674.02 | 35 |
| H27A | 3825.55 | 8070.79 | -143.09 | 34 |
| H27B | 3303.61 | 9520.91 | -505.16 | 34 |
| H27C | 2328.48 | 8549.16 | -379.47 | 34 |
| H28A | 2455.46 | 3921.8 | -365.75 | 37 |
| H28B | 2437.1 | 2635.77 | 285.46 | 37 |
| H28C | 3859.6 | 3125.94 | -83.32 | 37 |
| H29A | 3753.98 | 2799.42 | 2002.26 | 43 |
| H29B | 2200.42 | 2550.56 | 2300.76 | 43 |
| H29C | 2493.53 | 3678.73 | 2722.66 | 43 |
| H30A | -51.33 | 5398.33 | 2026.18 | 53 |
| H30B | -140.49 | 4227.25 | 1541.41 | 53 |
| H30C | 44.71 | 5530.32 | 946.06 | 53 |

## D.2. DFT calculation

**Computational Details.** DFT calculations at the B3LYP level of theory were performed using the Orca 4.0.0.[1] Gas-phase geometry optimizations and frequency calculations for thermochemistry were carried out using the def2-TZVP basis set all atoms without symmetry constraint. B3LYP geometries well reproduced experimental metrical parameters, obtained by X-ray crystallography (tabulated in Table S7). Effective oxidation analysis (EOS) was conducted based on the Kohn-Sham wave functions computed at B3LYP/def2-TZVP level.[2] The analysis of intrinsic bond orbitals (IBOs) and the visualization of orbitals were conducted by IBOview.[3] The localized orbital bonding analysis (LOBA) was performed by Multiwfn.[4] All occupied orbitals were localized with Pipek-Mezey localization procedure[5] and used in the LOBA analysis. For topological analysis of the electron density (QTAIM),[6] an all-electron single point calculation was conducted. A relativistic approximation was introduced by applying zeroth-order regular approximation (ZORA)[7] using the B3LYP density functional with the relativistically recontracted version of def2-TZVP basis set. Coordinates obtained from the above geometry optimization is used as the input. Analysis and visualization of the QTAIM results were performed with the Multiwfn program.

**Table D-20.** Energy of 8-P-4 and 10-P-5, and their differences in energies (Hartree/Particle) for group 10 metal complexes (Pt, Pd, and Ni).

| | PtClMeiPr$_2$PNNNP (**5.6**, 8-P-4) | PtCliPr$_2$PNNNPMe (**5.6′,** 10-P-5) | Energy Difference |
|---|---|---|---|
| Thermal Energy, E | –2627.935335 | –2627.940321 | –0.004986 |
| Thermal Enthalpy, H | –2627.317284 | –2627.321633 | –0.004349 |
| Thermal Free Energy, G | –2627.418196 | –2627.421284 | –0.003088 |
| | PdClMeiPr$_2$PNNNP (**5.7**, 8-P-4) | PdCliPr$_2$PNNNPMe (**5.7′**, 10-P-5) | Energy Difference |
| Thermal Energy, E | –2636.465437 | –2636.481724 | –0.016286 |
| Thermal Enthalpy, H | –2635.847719 | –2635.863005 | –0.015286 |
| Thermal Free Energy, G | –2635.948877 | –2635.962377 | –0.013500 |
| | NiClMeiPr$_2$PNNNP (**5.8**, 8-P-4) | NiCliPr$_2$PNNNPMe (**5.8′**, 10-P-5) | Energy Difference |
| Thermal Energy, E | –4016.834067 | –4016.860843 | –0.026777 |
| Thermal Enthalpy, H | –4016.216102 | –4016.242079 | –0.025977 |
| Thermal Free Energy, G | –4016.315554 | –4016.340775 | –0.025221 |

**Table D-21**. IBO partial charge distributions for all metal–ligand bonds and oxidation state (OS) assignments based on LOBA for compounds **5.6-5.8** and **5.6′-5.8′**.

| **Compounds** | **P$^{NNN}$** | **P$^{iPr2Ar}$** | **Cl** | **Me** | **N** | **OS of M (LOBA)** |
|---|---|---|---|---|---|---|
| **5.6** | Pt (0.415)<br>P (1.516) | Pt (0.233)<br>P (1.636) | Pt (0.237)<br>Cl (1.694) | Pt (0.747)<br>C (1.212) | - | +II |
| **5.7** | Pd (0.378)<br>P (1.533) | Pd (0.203)<br>P (1.636) | Pd (0.233)<br>Cl (1.694) | Pd (0.903)<br>C (1.066) | - | +II |
| **5.8** | Ni (0.381)<br>P (1.545) | Ni (0.230)<br>P (1.634) | Ni (0.252)<br>Cl (1.689) | Ni (0.075)<br>C (1.156) | - | +II |
| **5.6′** | Pt (0.656)<br>P (1.299) | Pt (0.452)<br>P (1.479) | Pt (0.186)<br>Cl (1.741) | - | Pt (0.271)<br>N (1.544) | +II |
| **5.7′** | Pd (0.815)<br>P (1.154) | Pd (0.453)<br>P (1.463) | Pd (0.168)<br>Cl (1.748) | - | Pd (0.150)<br>N (1.620) | +II |
| **5.8′** | Ni (0.595)<br>P (1.357) | Ni (0.394)<br>P (1.546) | Ni (0.221)<br>Cl (1.720) | - | Ni (0.279)<br>N (1.554) | +II |

**Table D-22.** IBO partial charge distributions of the M–P1–N1 cycle for compounds **5.7′** and **5.8′**.

| Compounds | M–P1 | M–N1 | P1–N1 | P1–N3 |
|---|---|---|---|---|
| **5.7′** | Pd (0.815)<br>P (1.154) | Pd (0.150)<br>N (1.620) | P (0.347)<br>N (1.487) | P (0.494)<br>N (1.416) |
| **5.8′** | Ni (0.595)<br>P (1.357) | Ni (0.279)<br>N (1.554) | P (0.257)<br>N (1.560) | P (0.634)<br>N (1.331) |

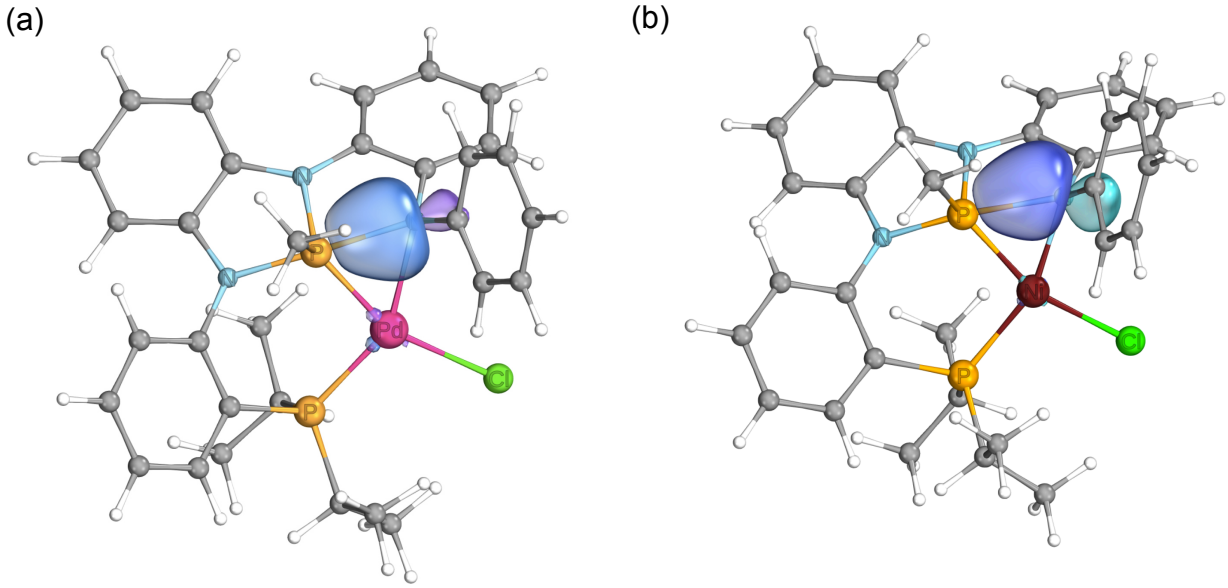


**Figure D-7.** IBO depictions of P1–N1 bond for compounds (a) **5.7′** and (b) **5.8′**. Numbers in parentheses correspond to the partial charge distributions of IBO. Orbital isosurface contains 80% of the integrated electron density of the orbital.

**Table D-23.** Energy of 8-P-4 and 10-P-5, and their differences in energies (Hartree/Particle) for group 10 metal complexes (Pt, Pd, and Ni).

| | $PdMe_2$(**L1**)<br>(**5.11**, 8-P-4) | Pd(Me)(**L1**$^{Me}$)<br>(**5.11′**, 10-P-5) | Energy Difference |
|---|---|---|---|
| Thermal Energy, E | –1670.228661 | –1670.265906 | –0.037245 |
| Thermal Enthalpy, H | –1670.227717 | –1670.264962 | –0.037245 |
| Thermal Free Energy, G | –1670.308012 | –1670.342083 | –0.034071 |
| | $Pd(CH_2TMS)_2$(**L1**)<br>(**5.12**, 8-P-4) | Pd($CH_2$TMS)(**L1**$^{CH2TMS}$)<br>(**5.12′**, 10-P-5) | Energy Difference |
| Thermal Energy, E | –2487.290072 | –2487.321707 | –0.031635 |
| Thermal Enthalpy, H | –2487.289128 | –2487.320763 | –0.031635 |

| | | | |
|---|---|---|---|
| Thermal Free Energy, G | –2487.394718 | –2487.425862 | –0.031144 |

**QTAIM analysis**

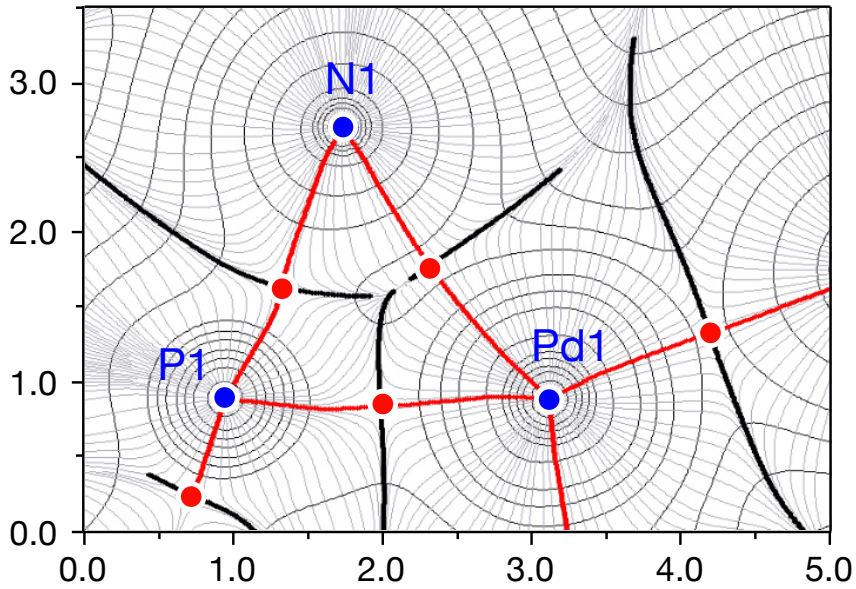


**Figure D-8.** Calculated electron density for **5′** in the plane defined by Pd–P–N coordinates. Electron density contours (–), gradient vector field (gray –), bond paths (red –), bond critical points (red •), and atomic basins (bold –) are depicted. Units are Å.

## D.3. Multinuclear NMR spectra

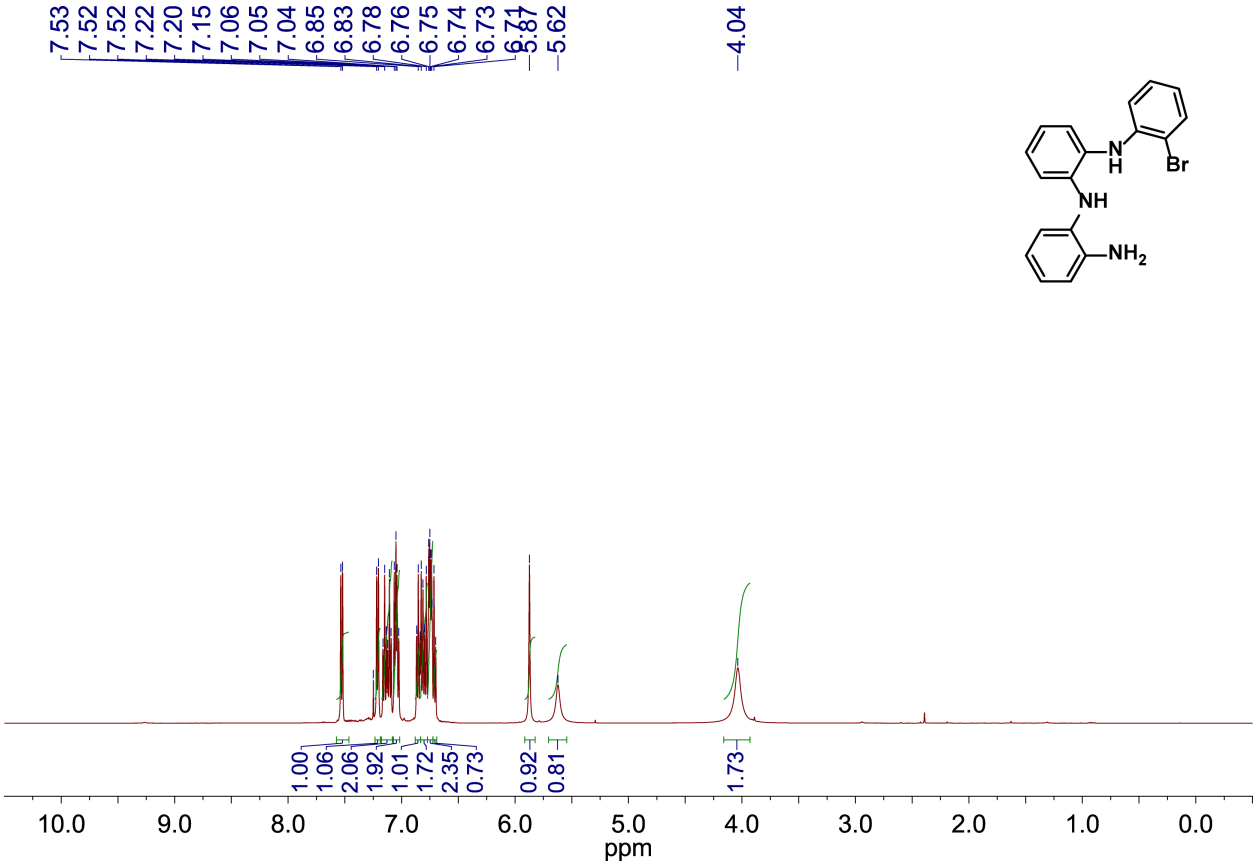


**Figure D-9.** $^{1}$H NMR spectrum of N1-(2-aminophenyl)-N2-(2-bromophenyl)benzene-1,2-diamine **(5.2)**

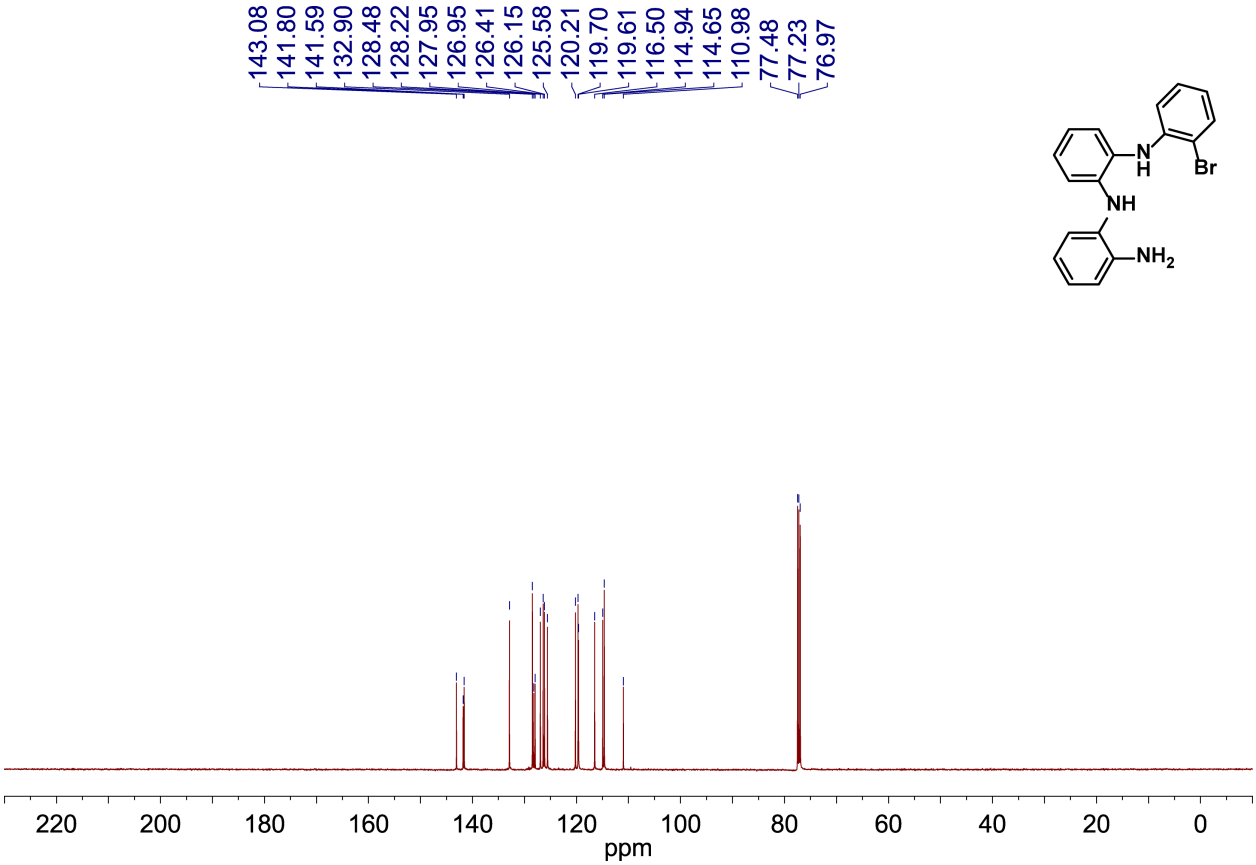


**Figure D-10.** $^{13}$C NMR spectrum of N1-(2-aminophenyl)-N2-(2-bromophenyl)benzene-1,2-diamine **(5.2)**.

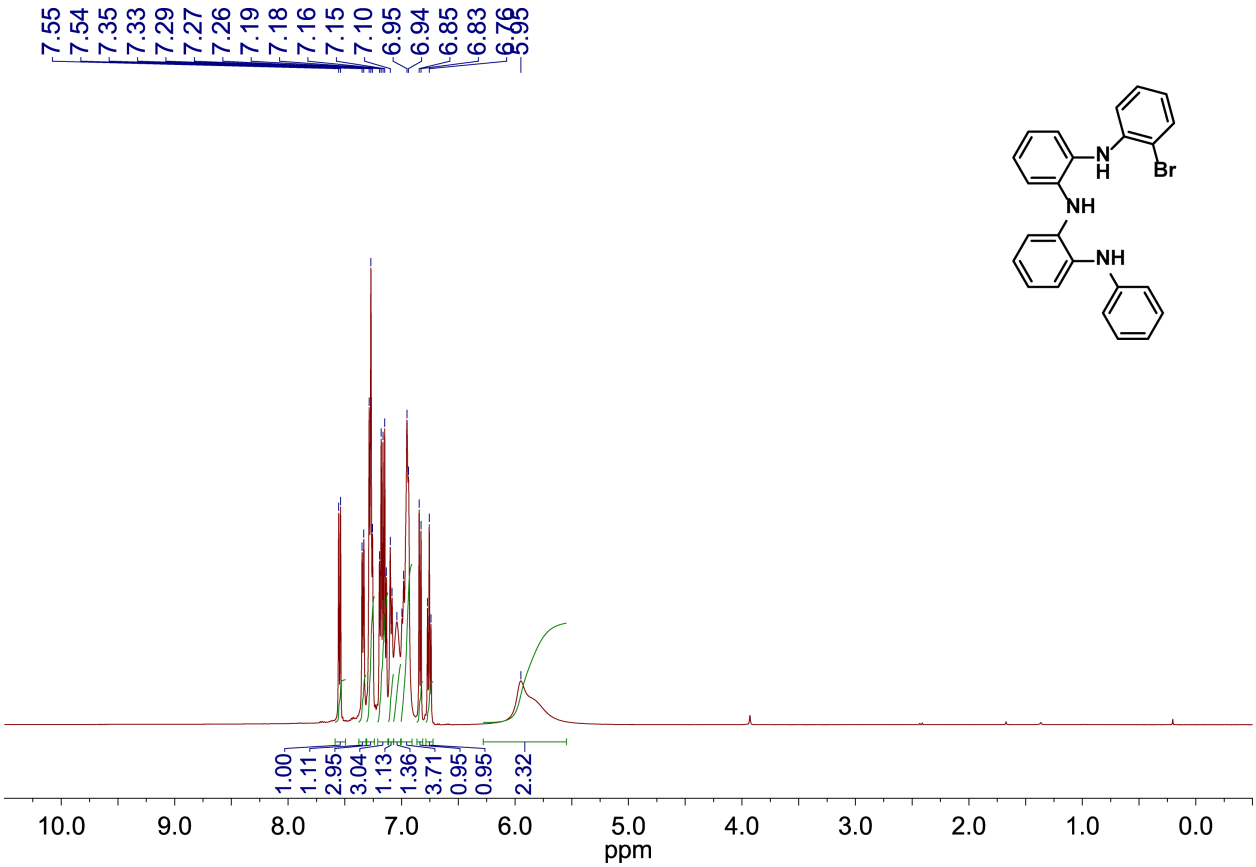


**Figure D-11.** $^{1}$H NMR spectrum of N1-(2-bromophenyl)-N2-(2-(phenylamino)phenyl)benzene-1,2-diamine **(5.3)**.

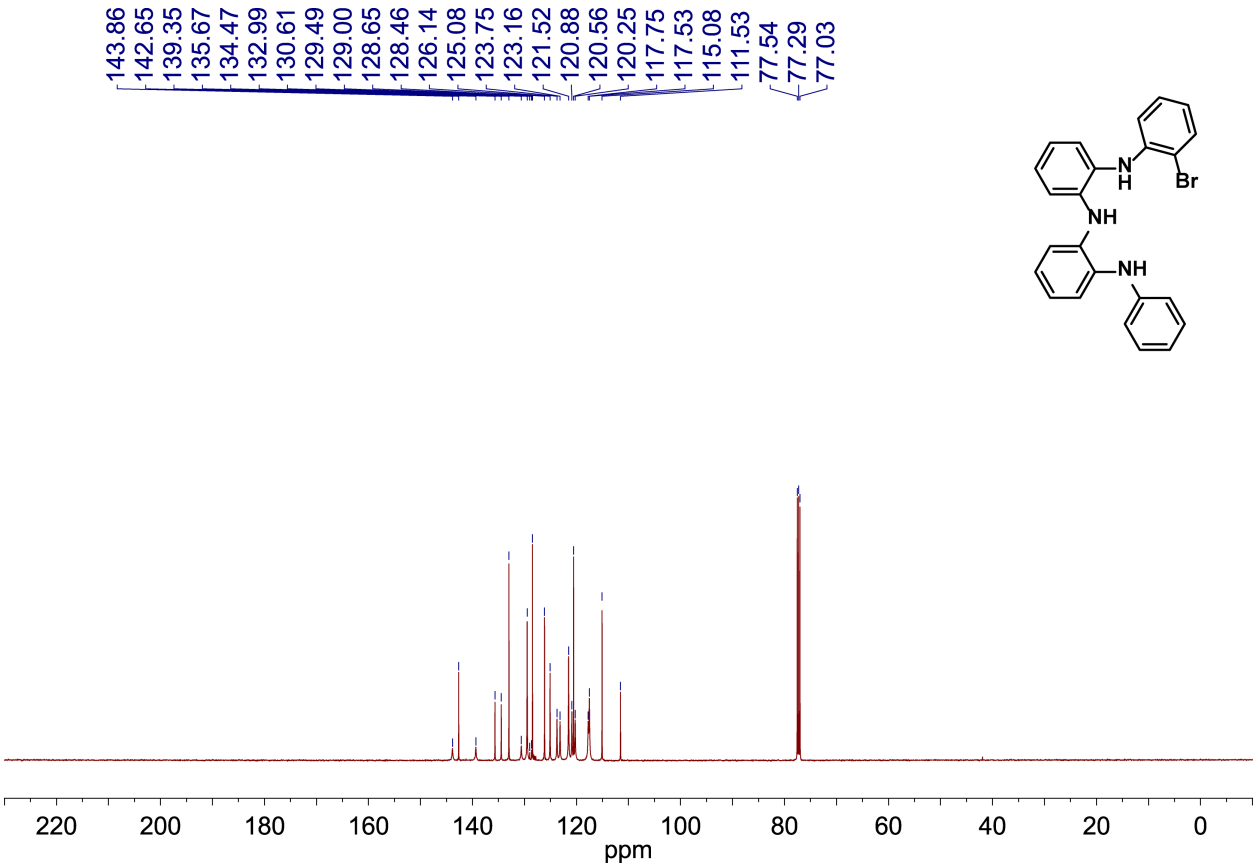


**Figure D-12**. $^{13}C$ NMR spectrum of N1-(2-bromophenyl)-N2-(2-(phenylamino)phenyl)benzene-1,2-diamine **(5.3)**.

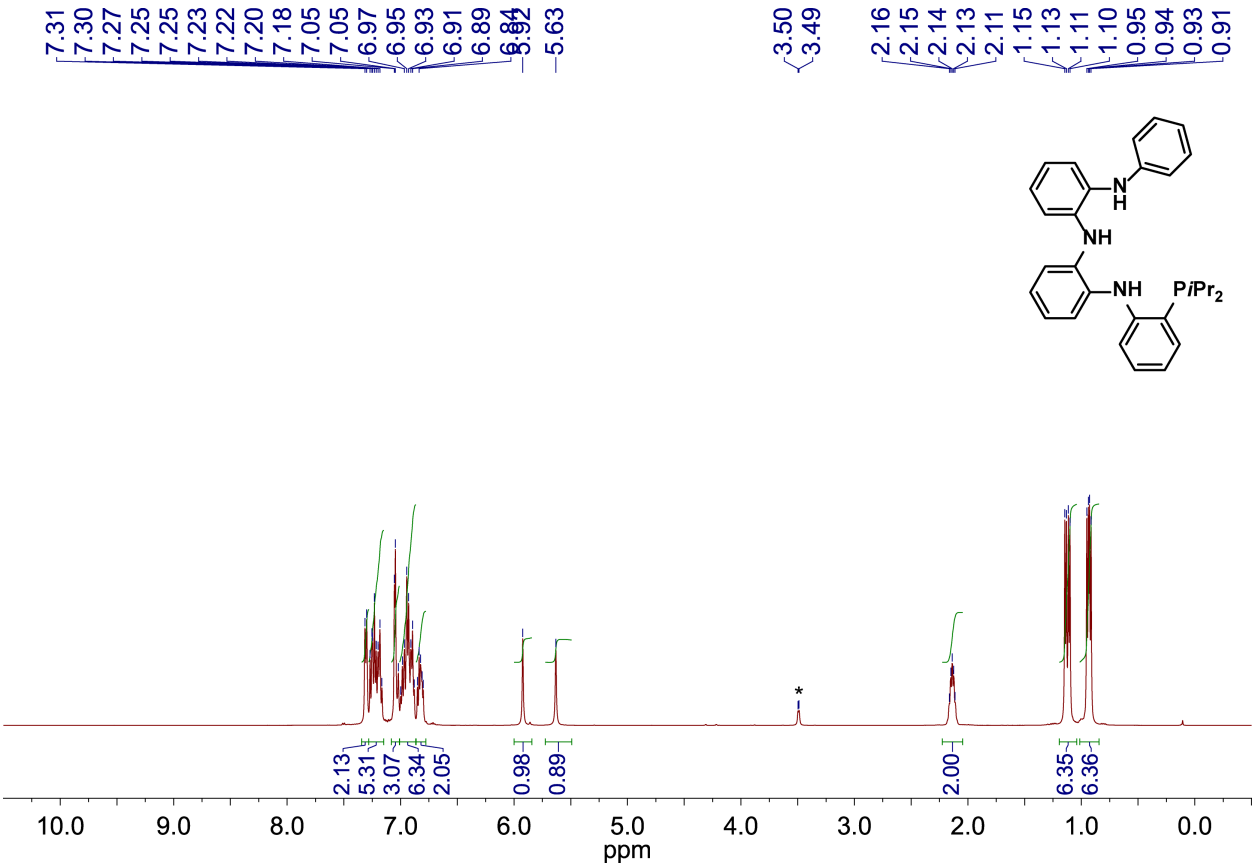


**Figure D-13.** $^{1}$H NMR spectrum of N1-(2-diisopropylphosphinophenyl)-N2-(2-(phenylamino)phenyl)benzene-1,2-diamine **(5.4)**. Asterisk symbol (*) denotes residual $^{1}$H peak of small amounts of MeOH from crystallization.

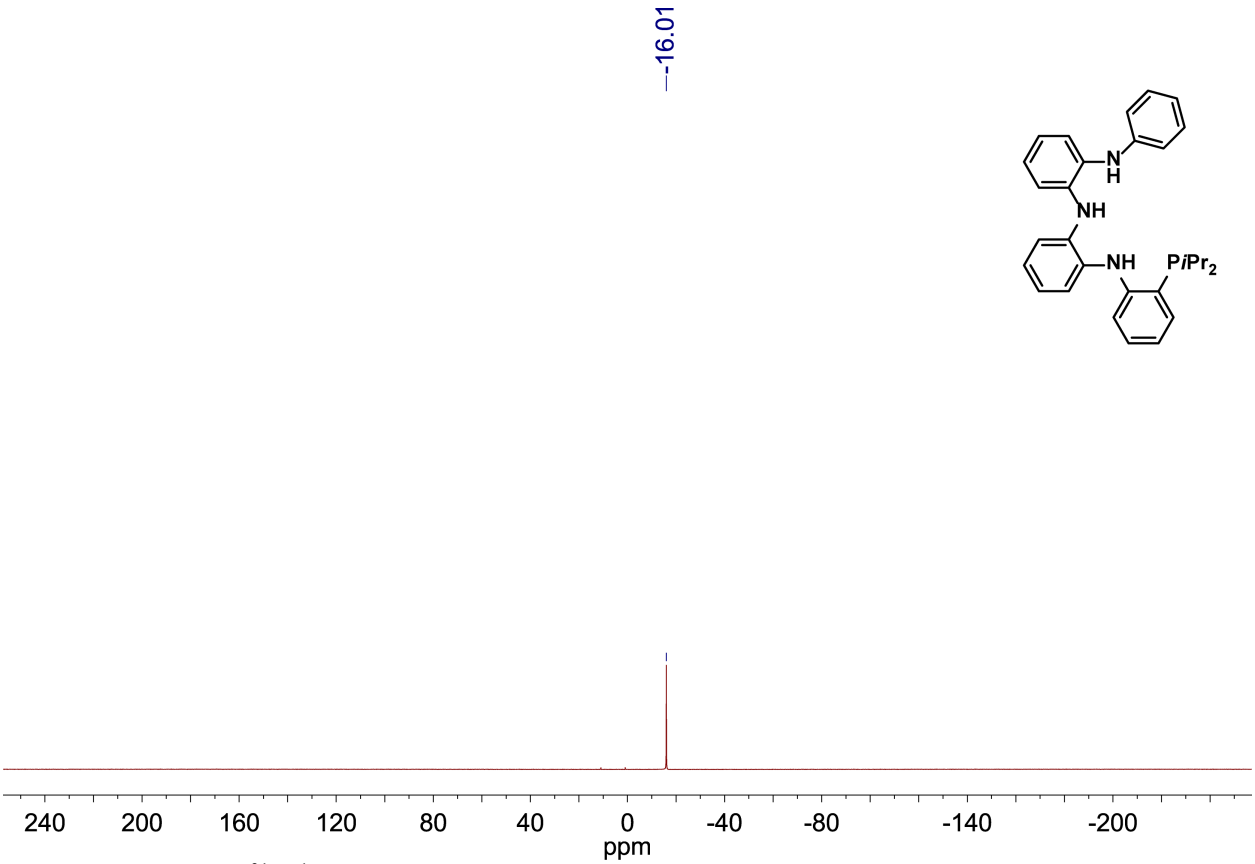


**Figure D-14.** $^{31}P\{^{1}H\}$ NMR spectrum of N1-(2-diisopropylphosphinophenyl)-N2-(2-(phenylamino)phenyl)benzene-1,2-diamine **(5.4)**.

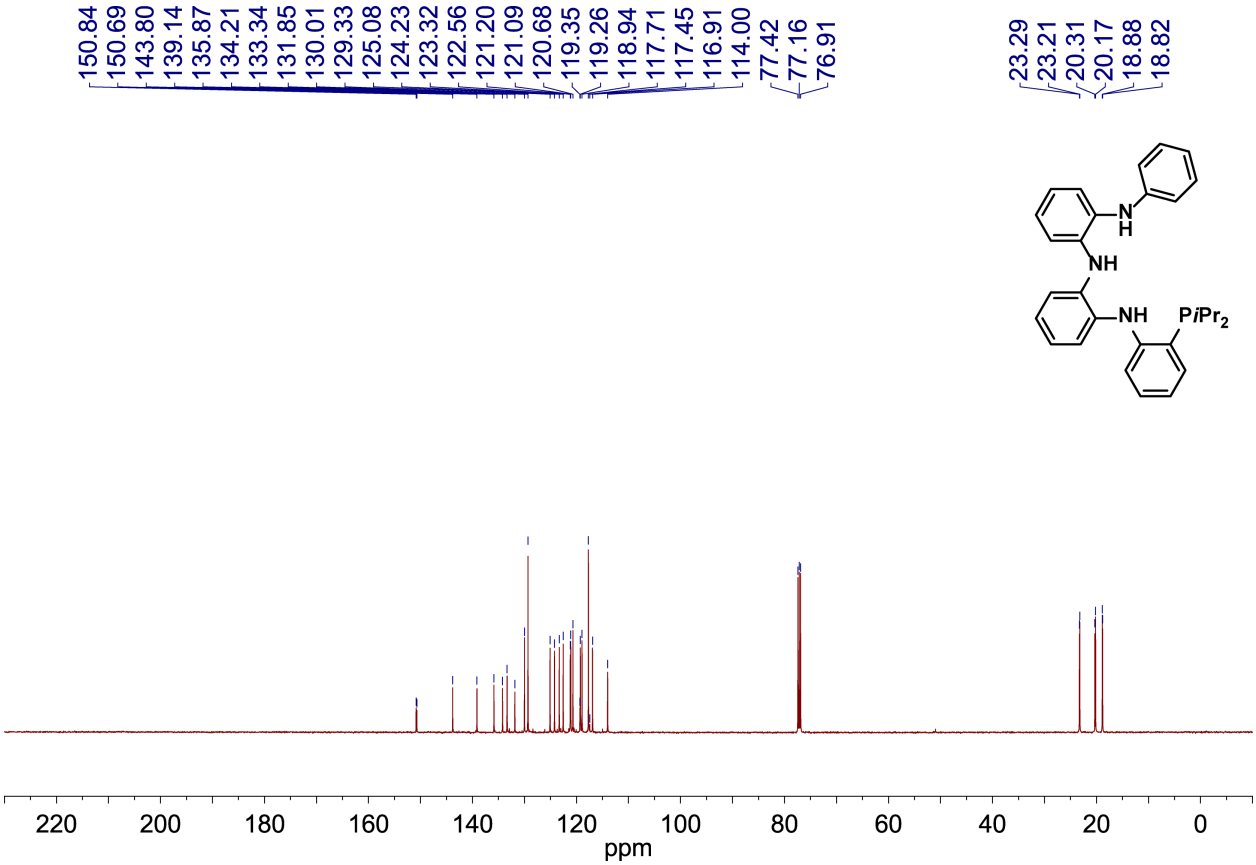


**Figure D-15.** $^{13}C$ NMR spectrum of N1-(2-diisopropylphosphinophenyl)-N2-(2-(phenylamino)phenyl)benzene-1,2-diamine **(5.4)**.

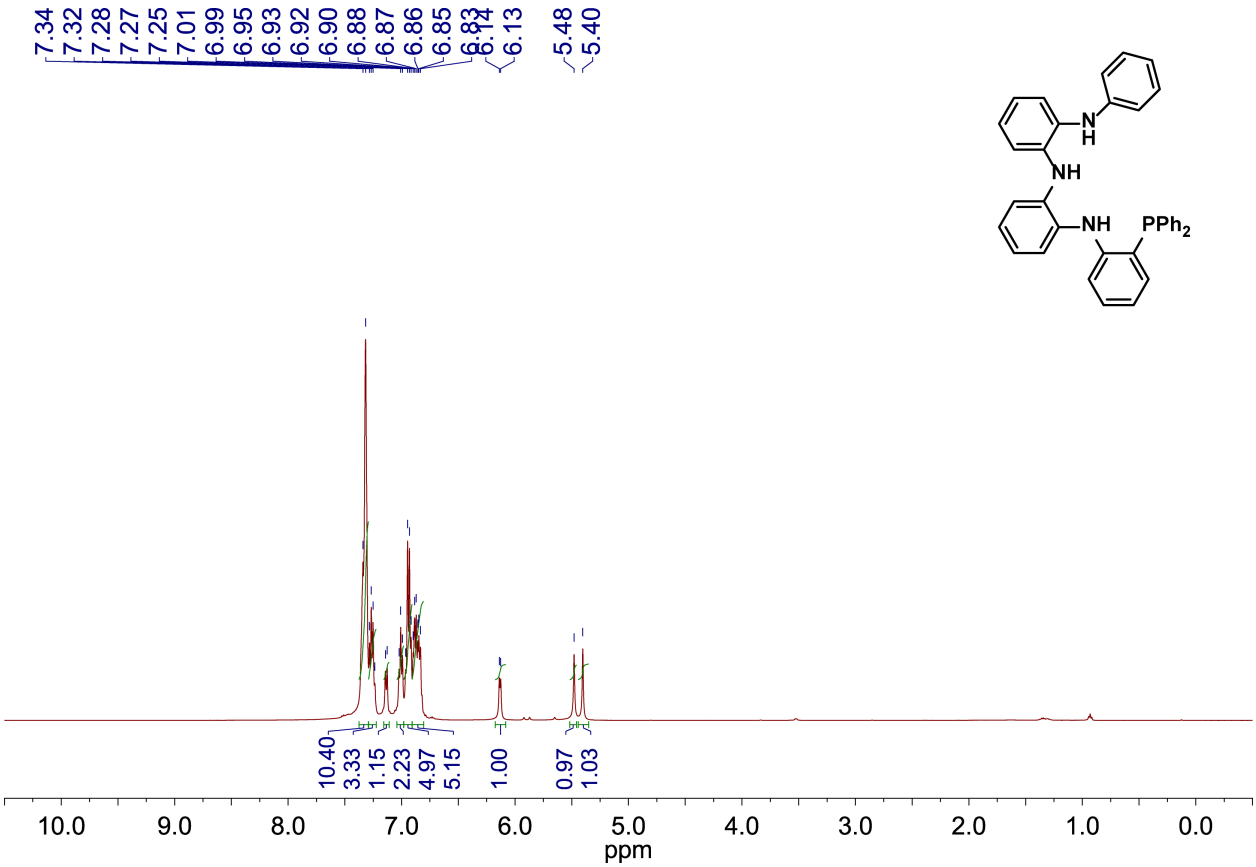


**Figure D-16.** $^{1}$H NMR spectrum of N1-(2-diphenylphosphinophenyl)-N2-(2-(phenylamino)phenyl)benzene-1,2-diamine **(5.5)**.

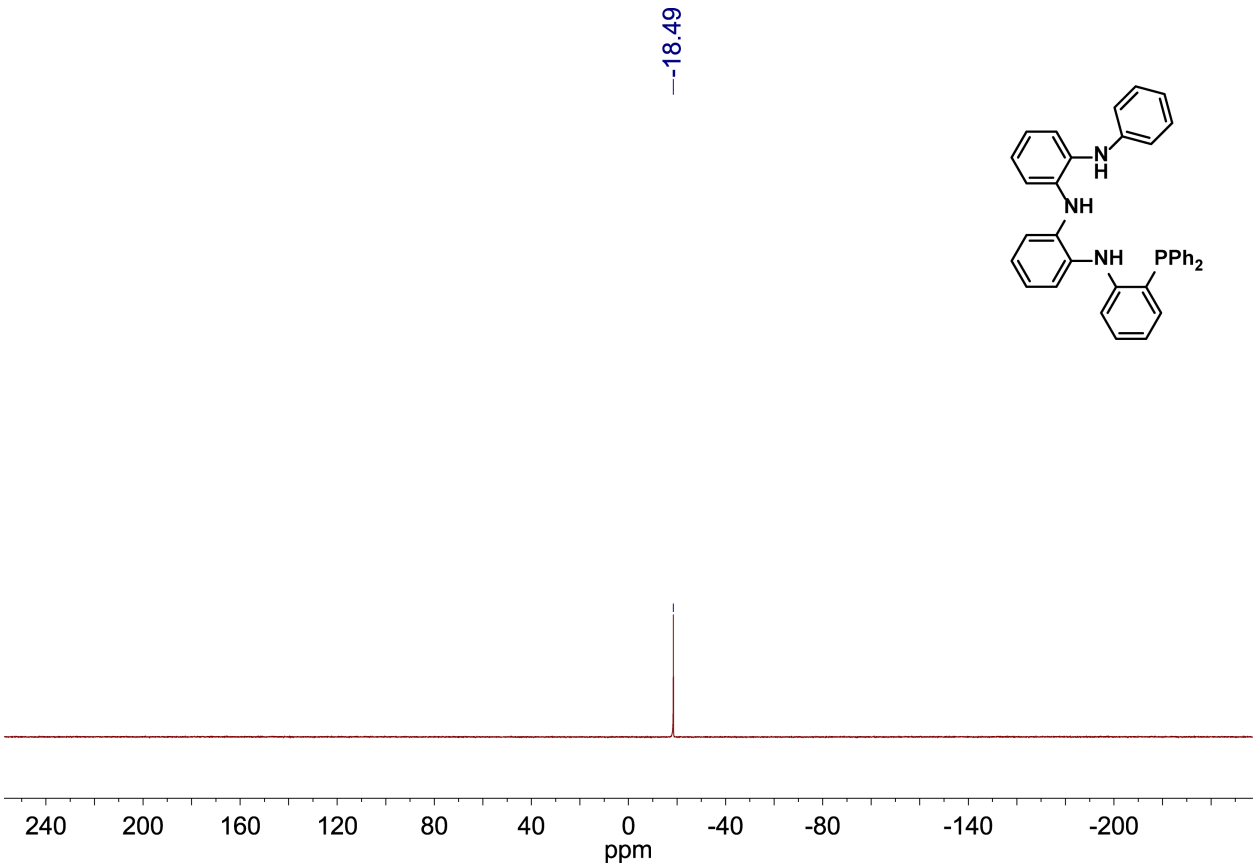


**Figure D-17.** $^{31}P\{^{1}H\}$ NMR spectrum of N1-(2-diphenylphosphinophenyl)-N2-(2-(phenylamino)phenyl)benzene-1,2-diamine **(5.5)**.

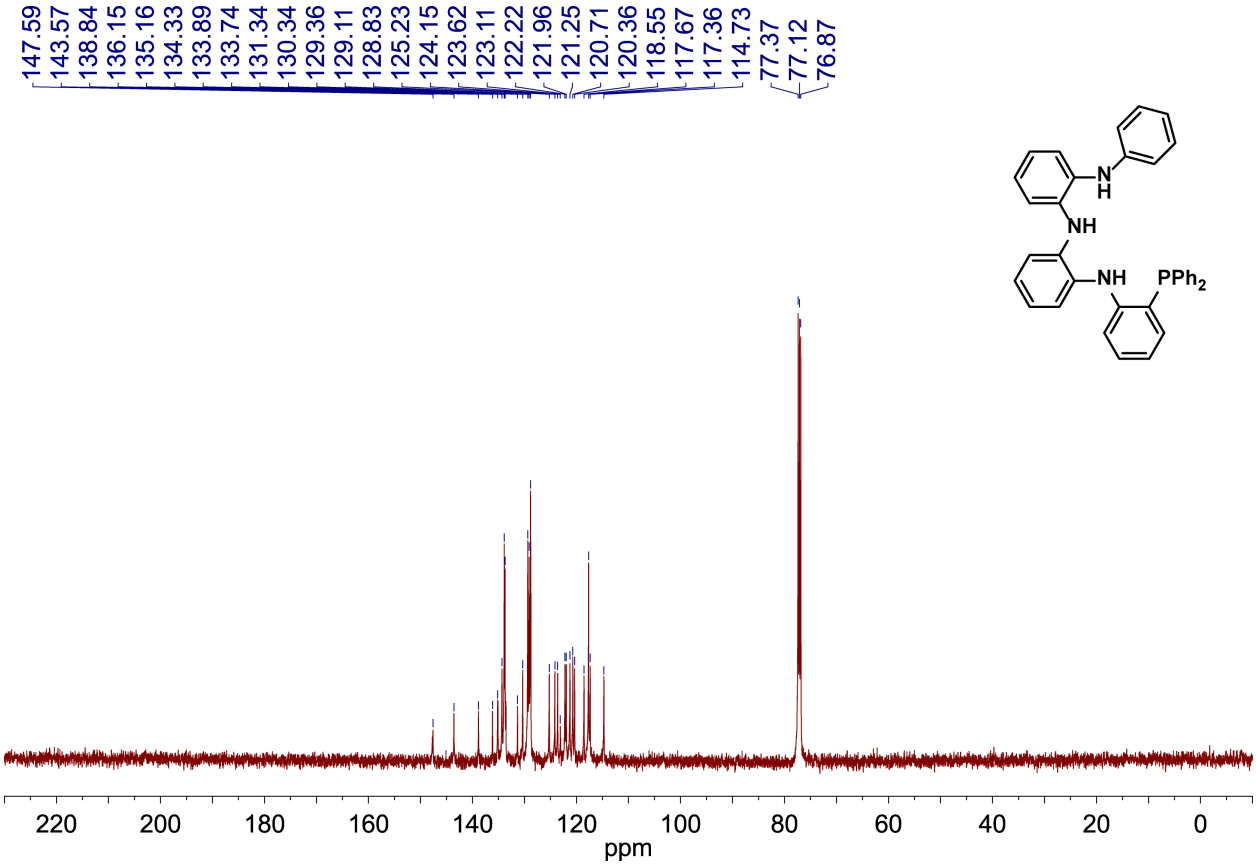


**Figure D-18.** $^{13}C$ NMR spectrum of N1-(2-diphenylphosphinophenyl)-N2-(2-(phenylamino)phenyl)benzene-1,2-diamine **(5.5)**.

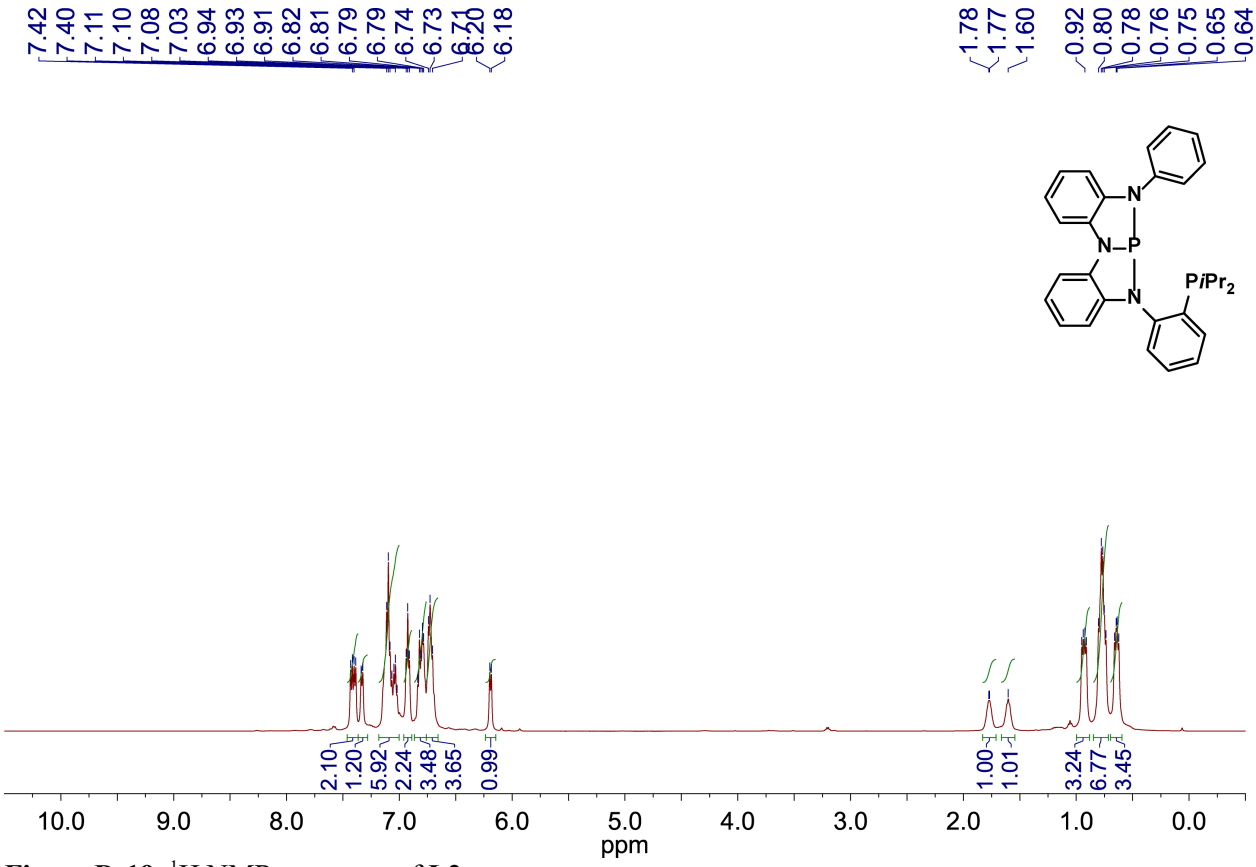


**Figure D-19.** $^{1}$H NMR spectrum of **L2**.

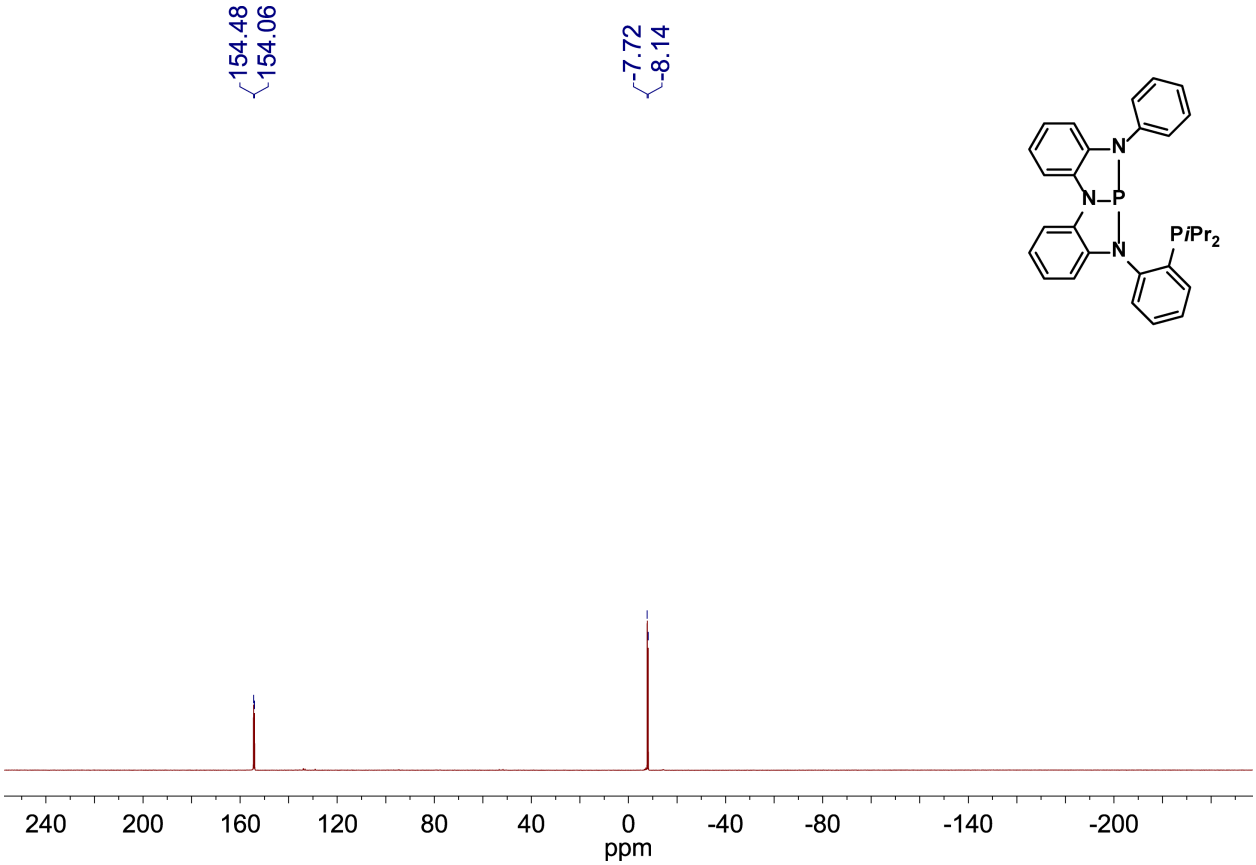


**Figure D-20.** $^{31}P\{^{1}H\}$ NMR spectrum of **L2**.

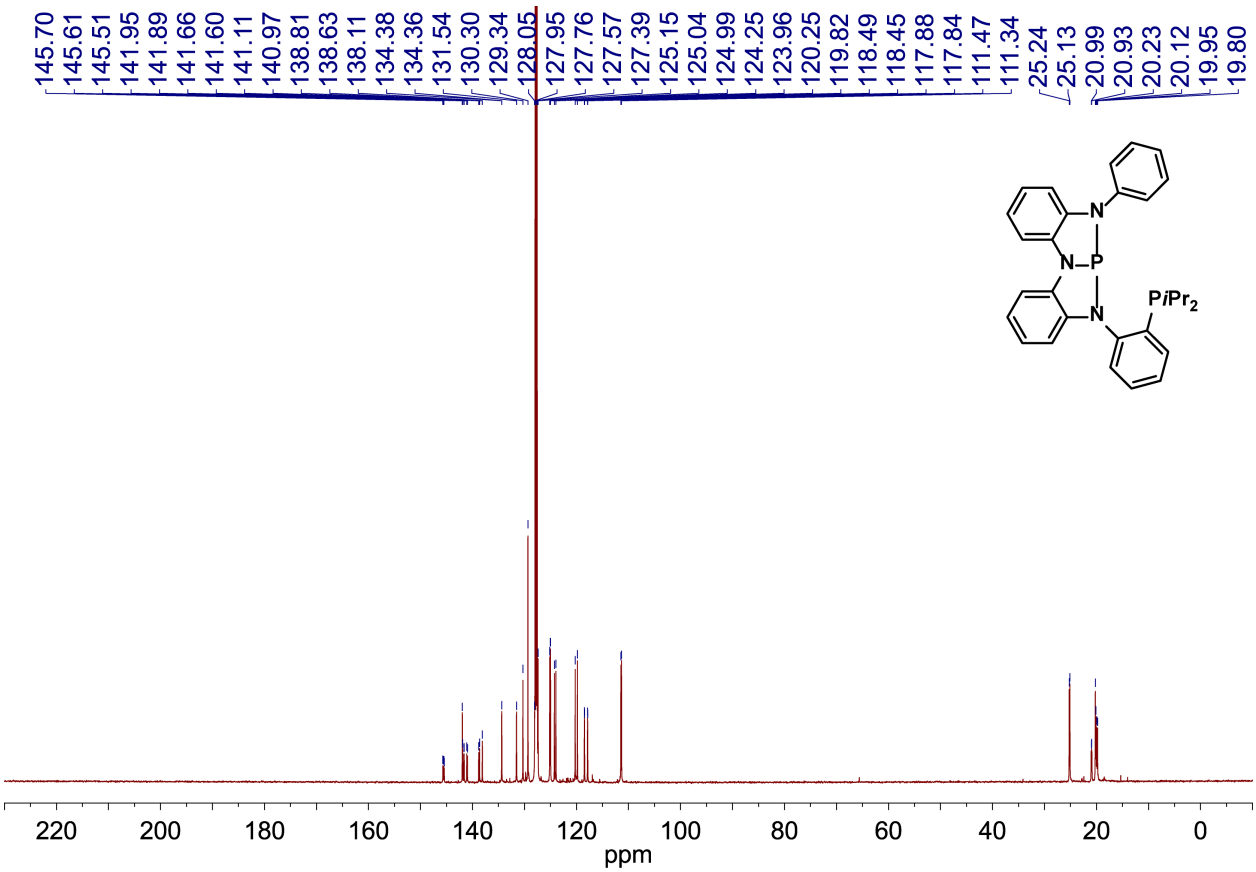


**Figure D-21.** $^{13}$C NMR spectrum of **L2**.

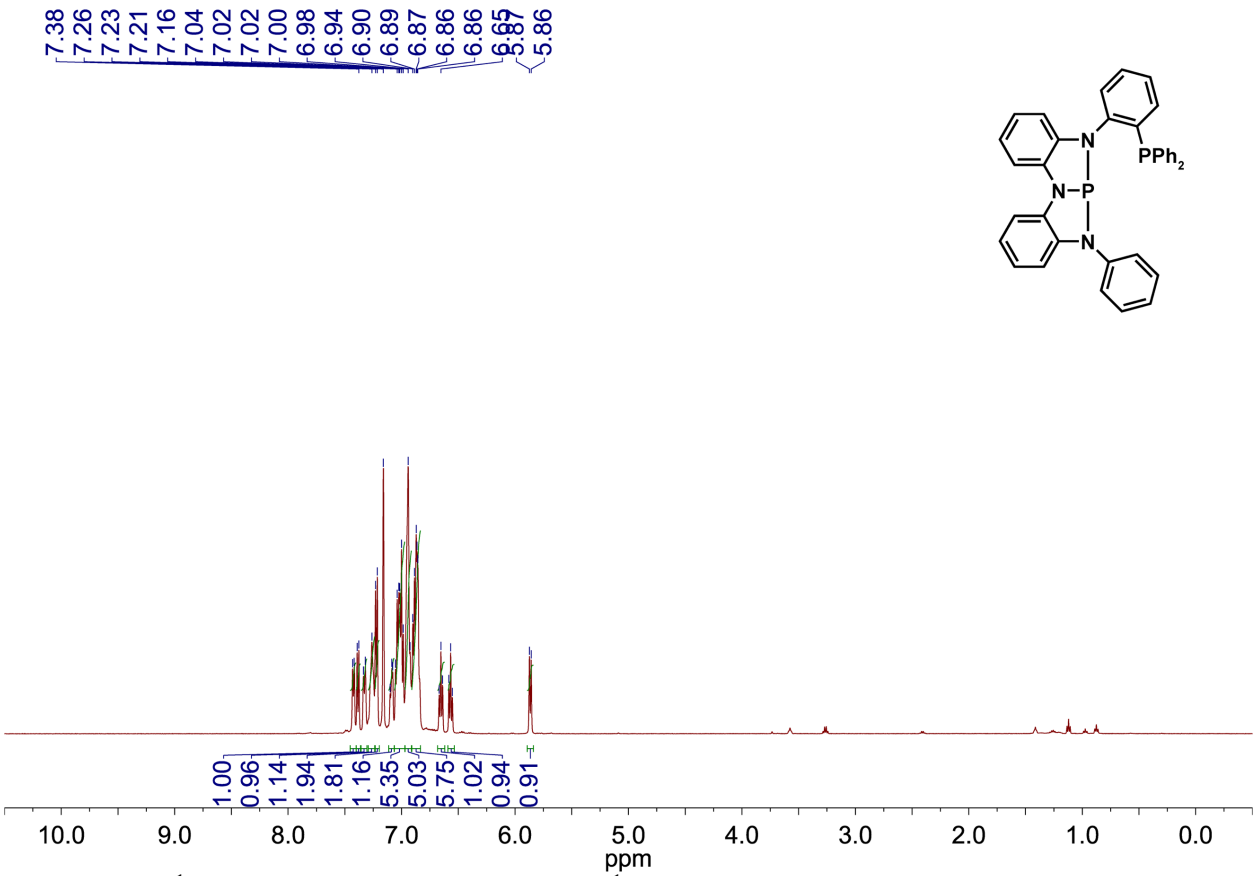


**Figure D-22.** $^{1}$H NMR spectrum of **L3**. Residual $^{1}$H peak of small amounts of $Et_2O$ and pentane from crystallization remain in the spectrum.

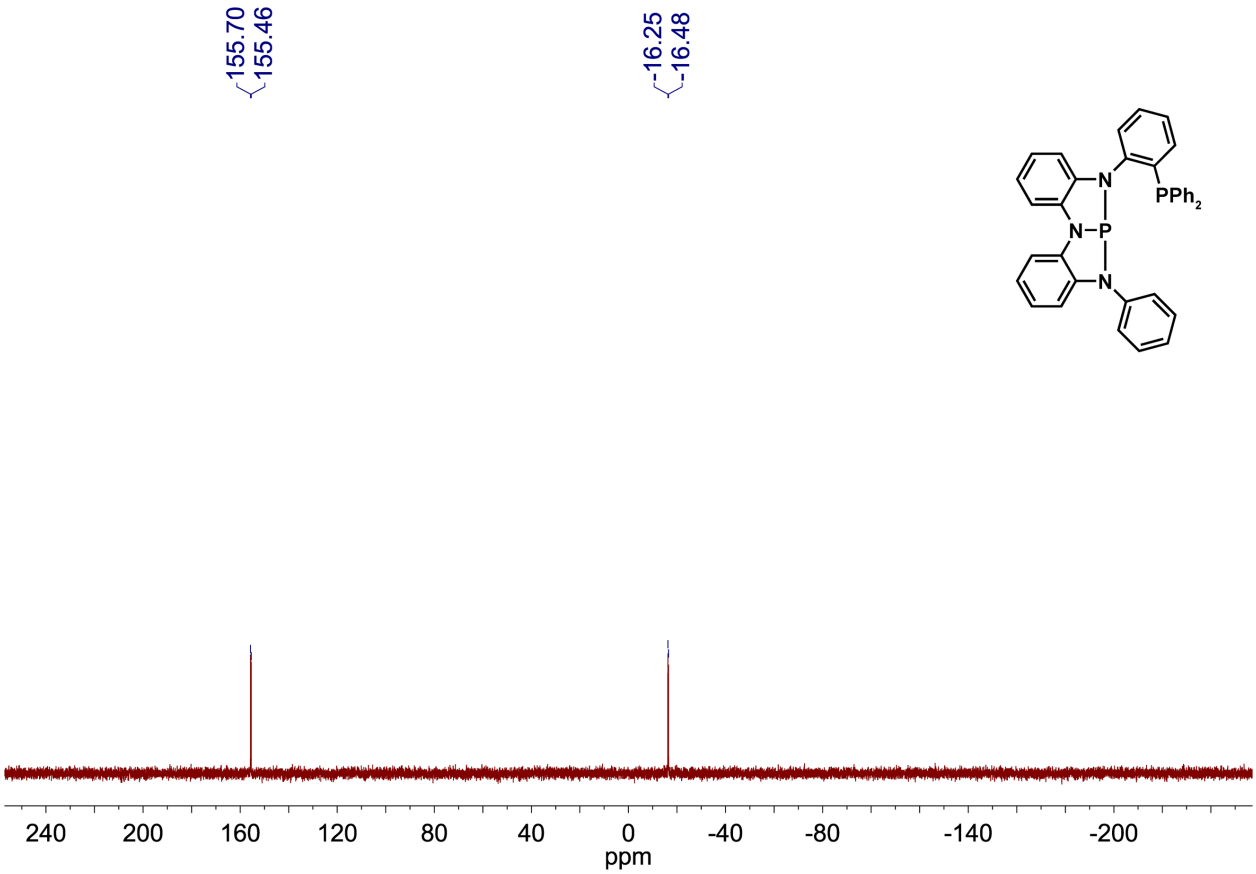


**Figure D-23.** $^{1}P\{^{1}H\}$ NMR spectrum of **L3** recorded in $C_6D_6$-$d_6$ at 23 °C.

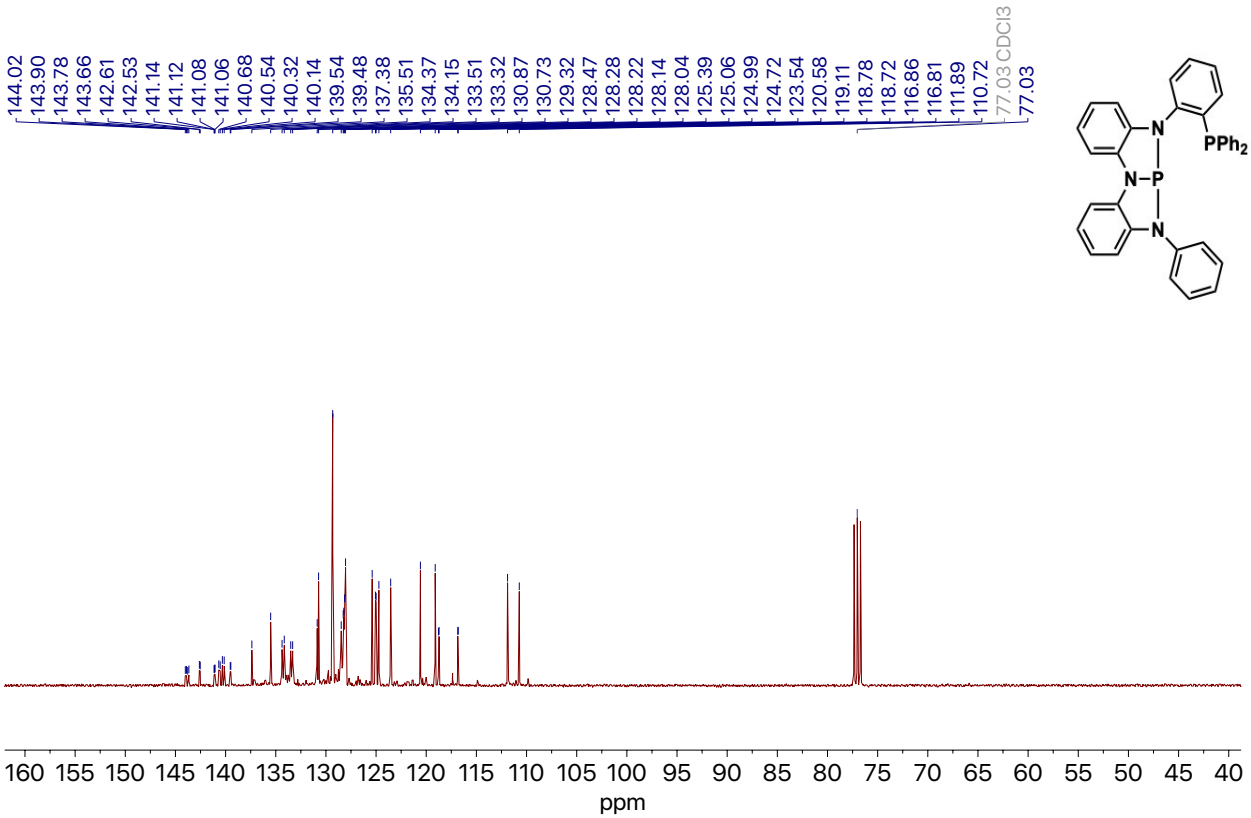


**Figure D-24.** $^{13}$C NMR spectrum of **L3**.

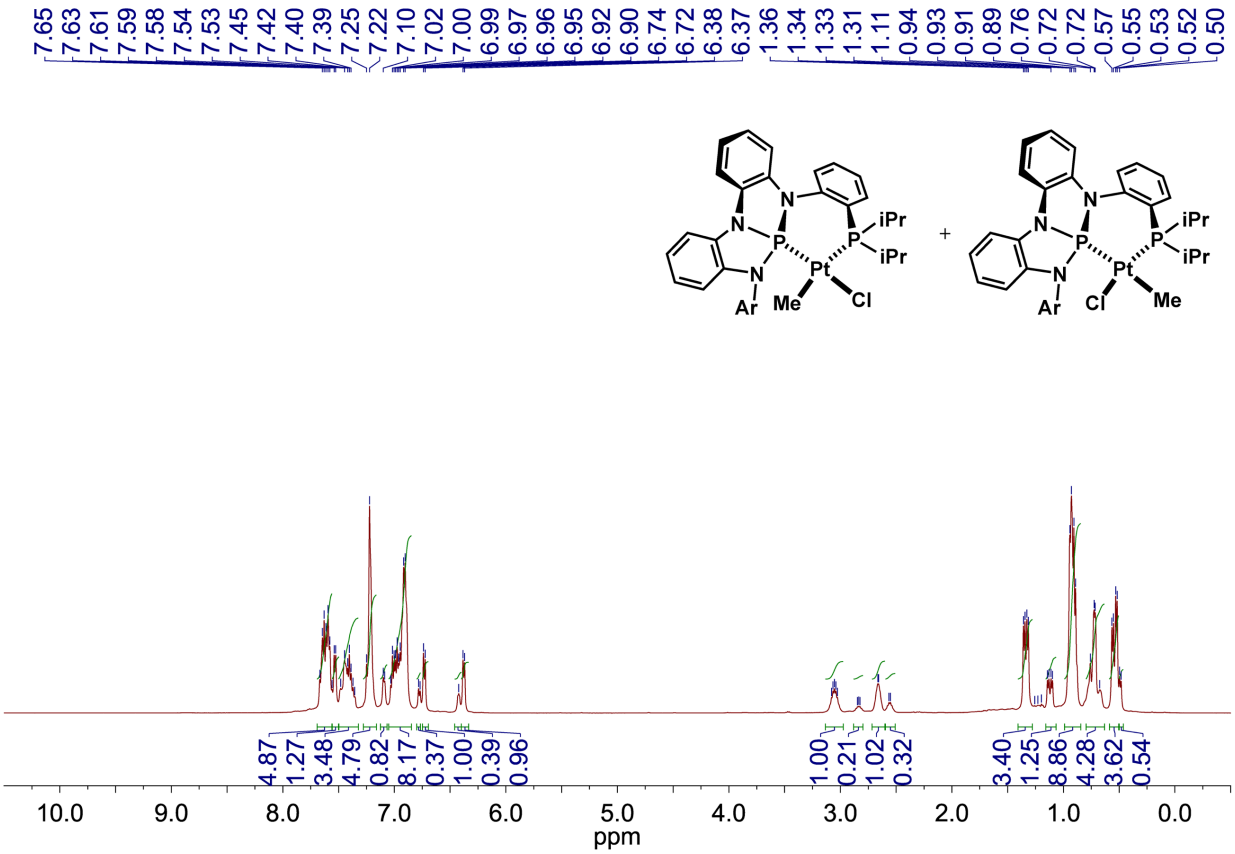


**Figure D-25.** $^{1}$H NMR spectrum of PtClMeiPr$_2$PNNNP **(5.6)**.

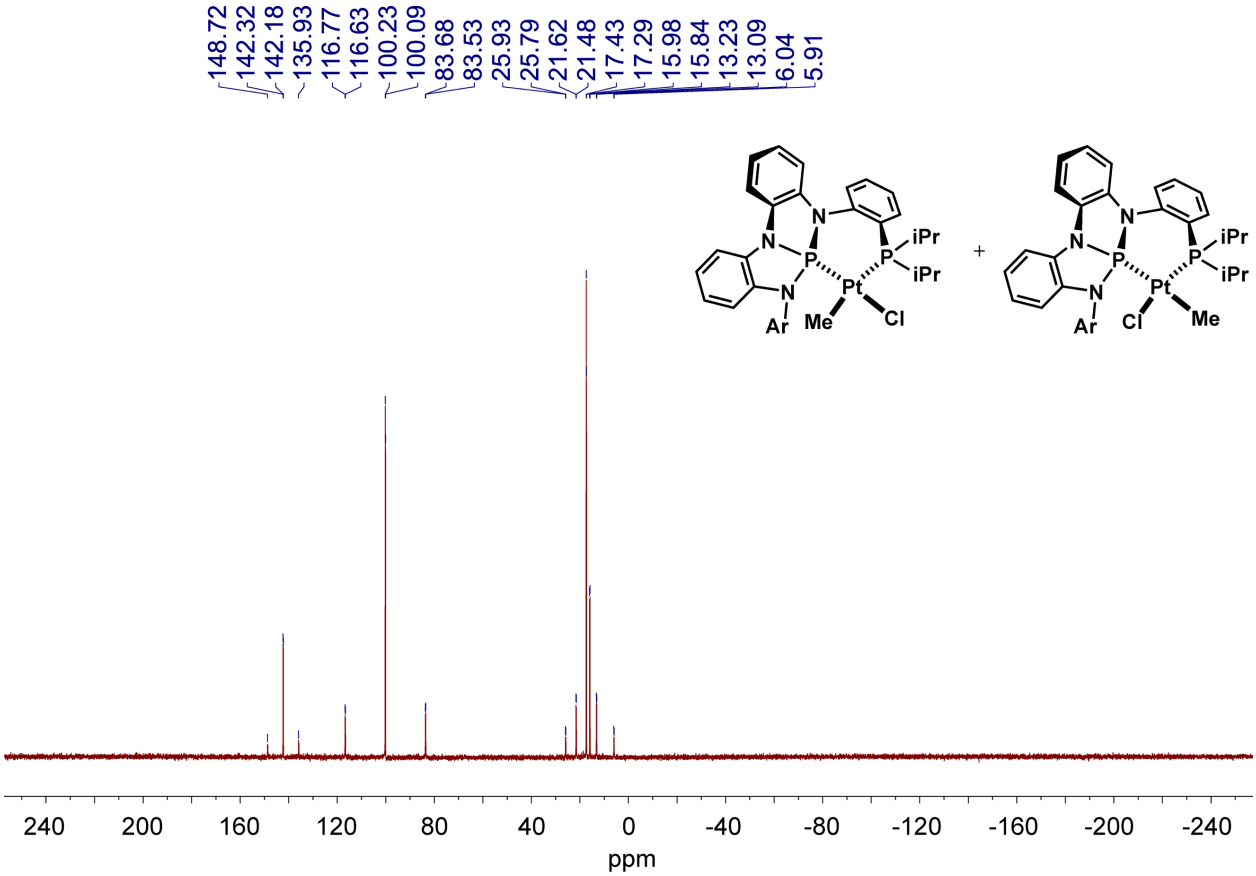


**Figure D-26.** $^{31}P\{^{1}H\}$ NMR spectrum of PtClMeiPr$_2$PNNNP **(5.6)**.

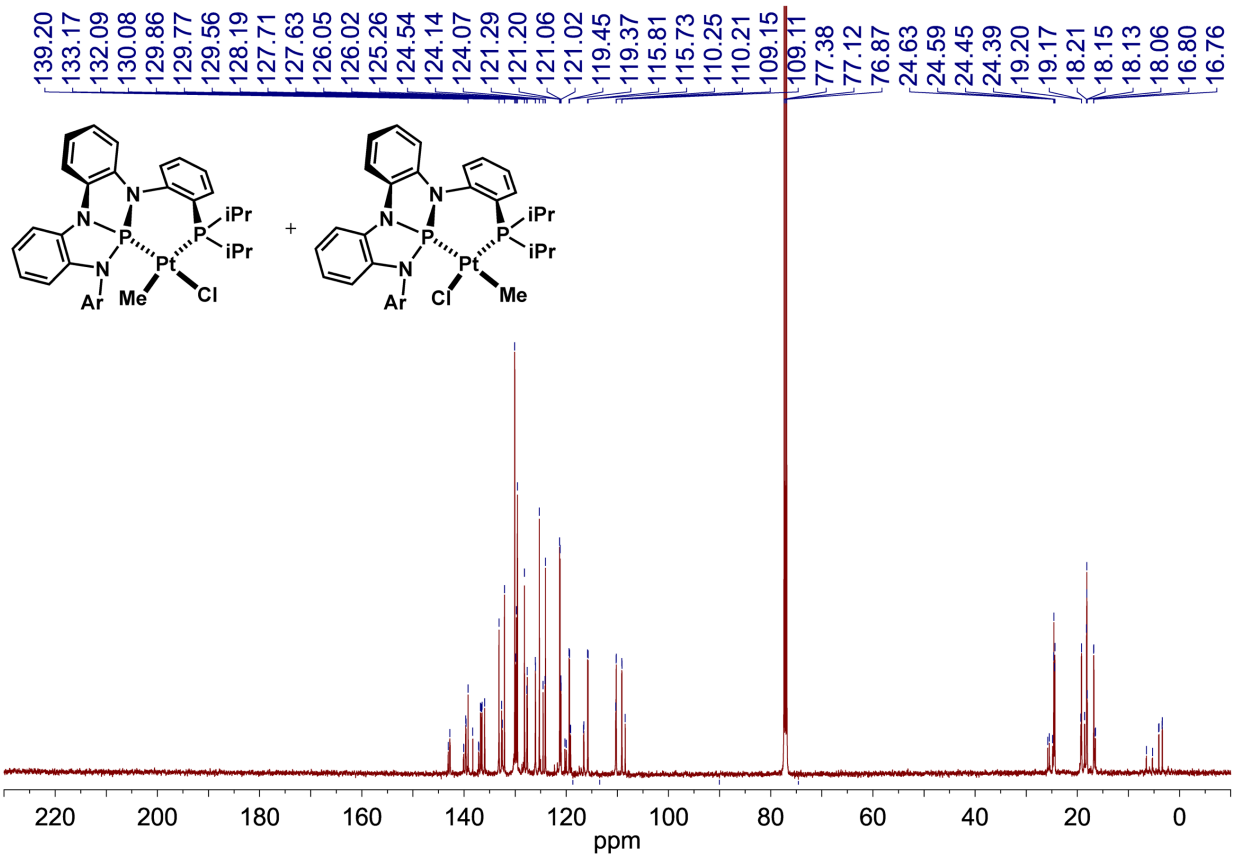


**Figure D-27.** $^{13}$C NMR spectrum of PtClMeiPr$_2$PNNNP **(5.6)**.

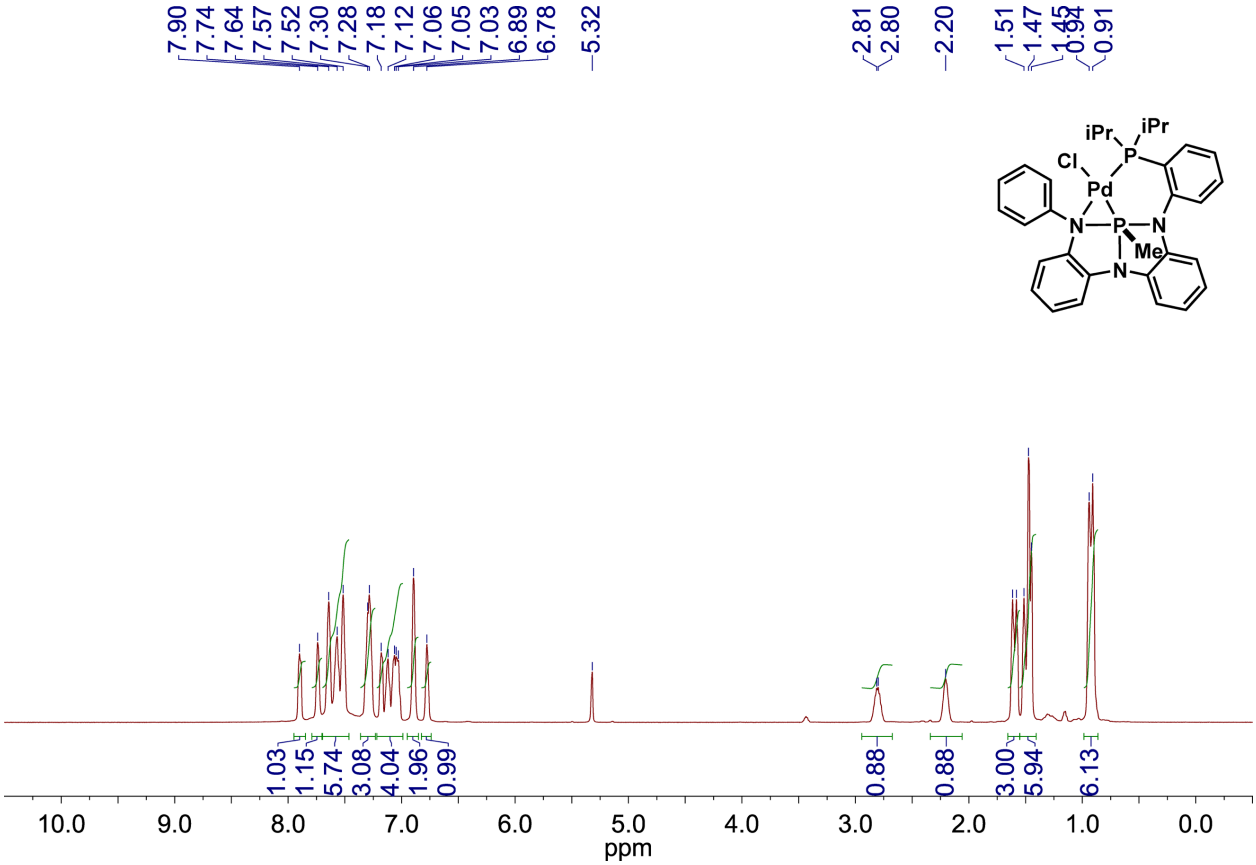


**Figure D-28.** $^{1}$H NMR spectrum of PdCliPr$_2$PNNNPMe **(5.7′)**.

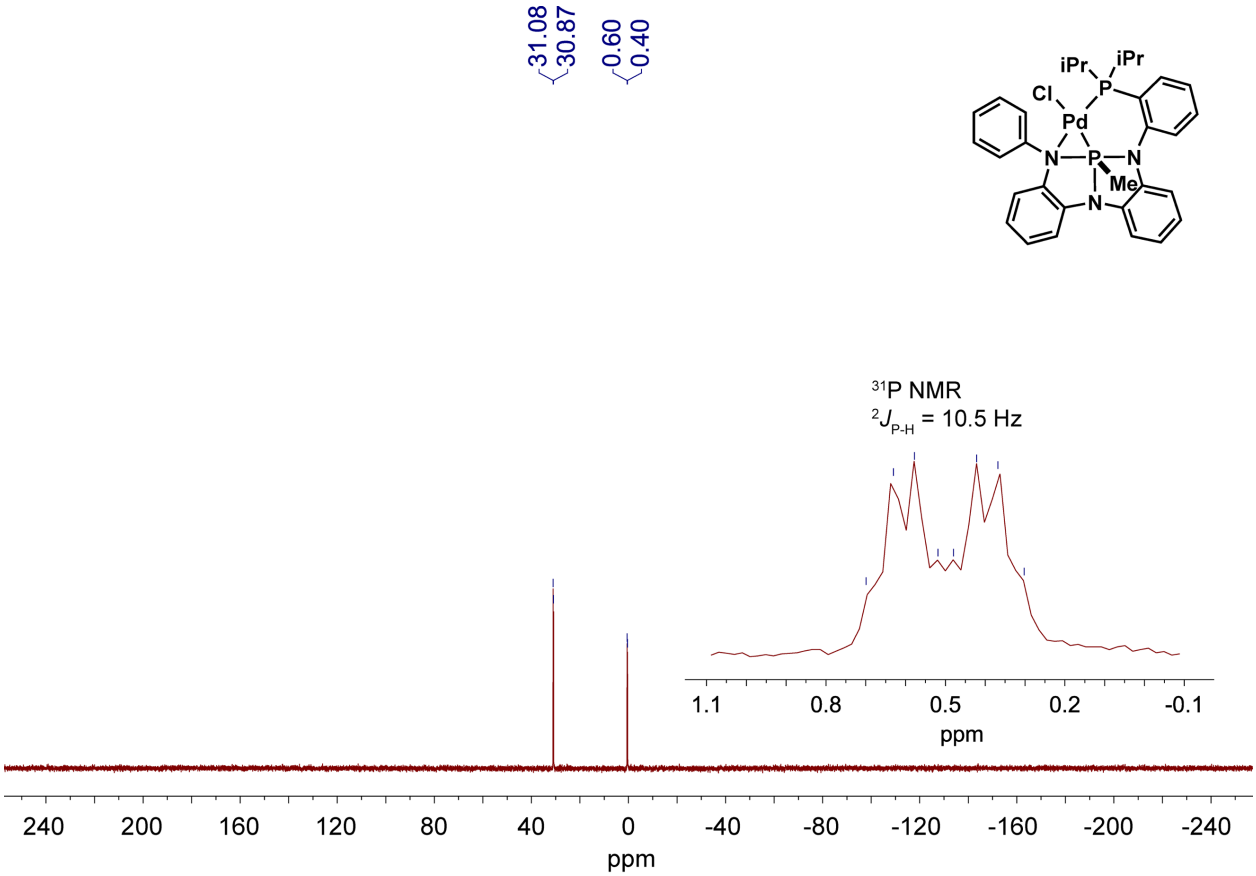


**Figure D-29.** $^{31}$P NMR spectra of PdCliPr$_2$PNNNPMe **(5.7′)**.

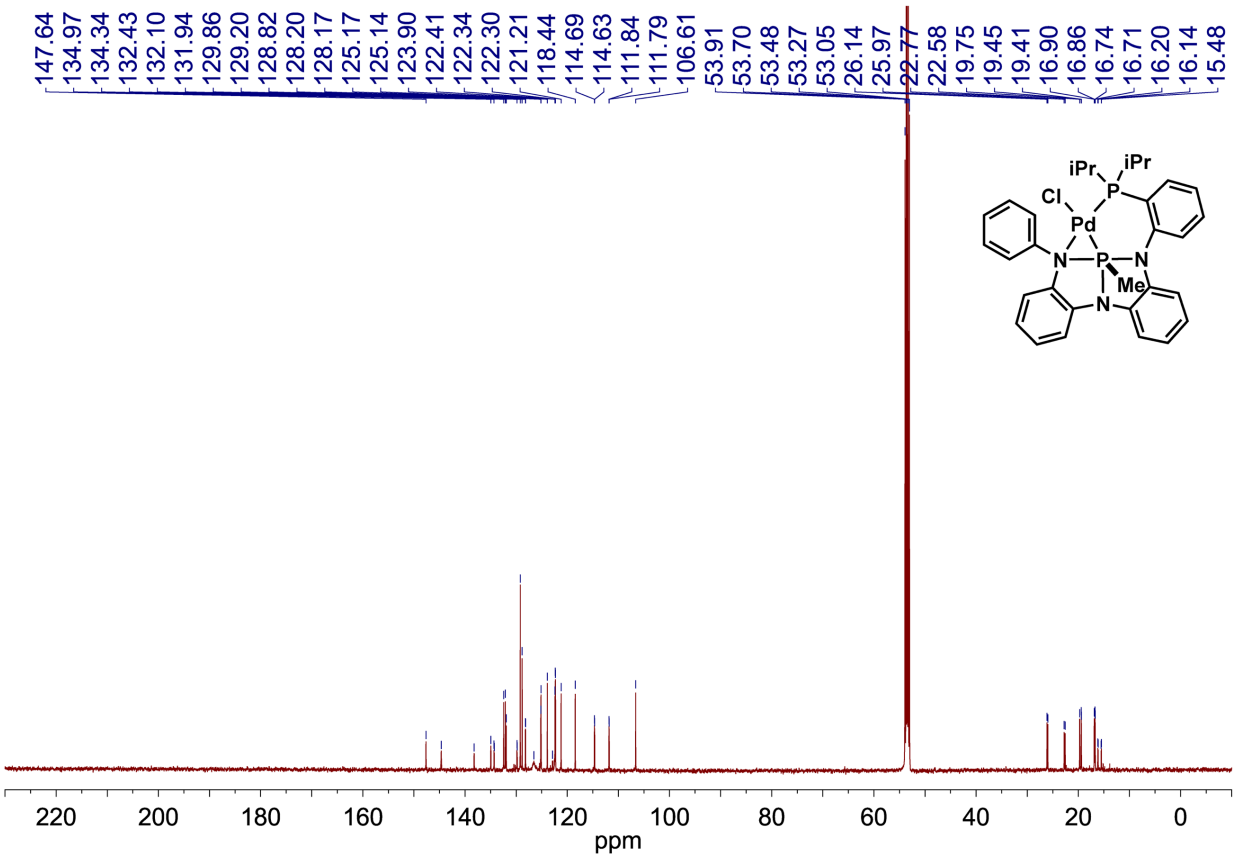


**Figure D-30.** $^{13}$C NMR spectrum of PdCliPr$_2$PNNNPMe **(5.7′)**.

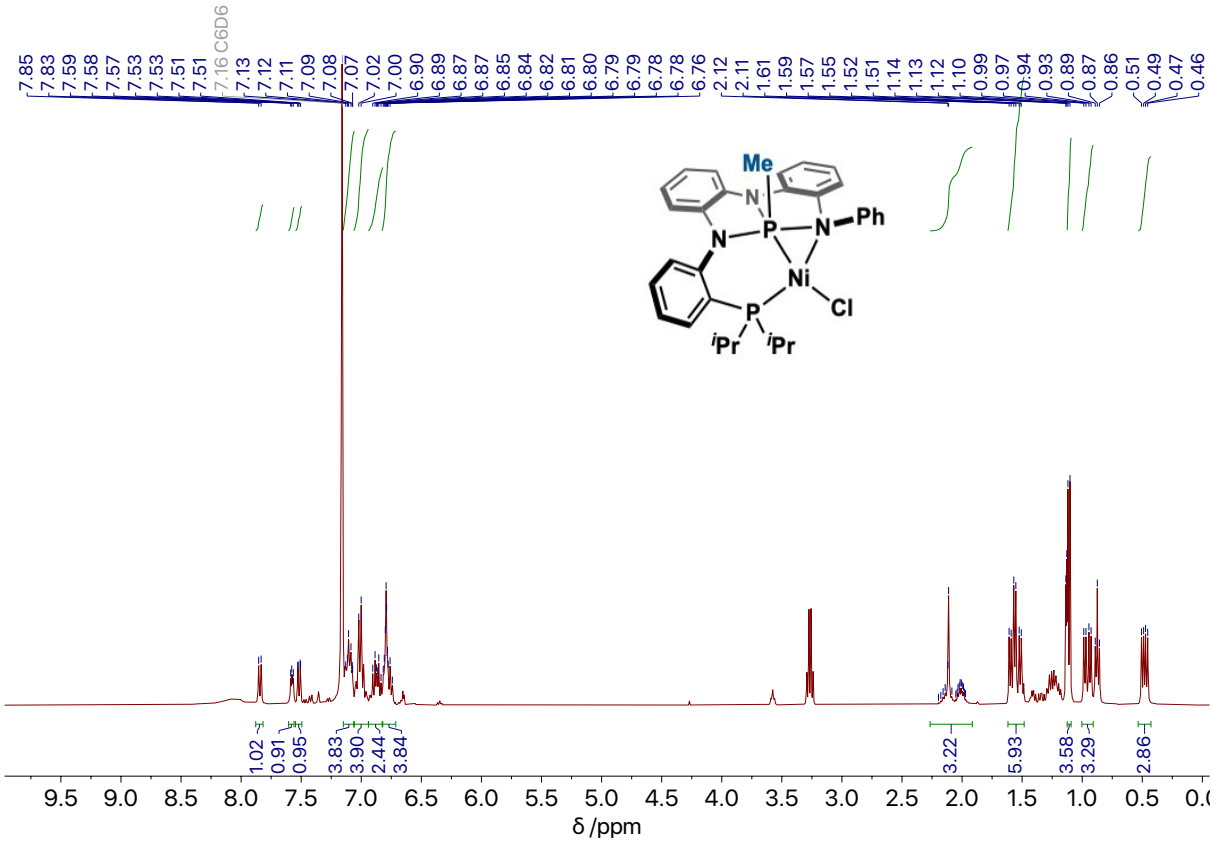


**Figure D-31**. $^{1}$H NMR spectrum of NiCliPr$_2$PNNNPMe **(5.8´)**. Residual $^{1}$H peak of small amounts of Et$_2$O from crystallization remain in the spectrum.

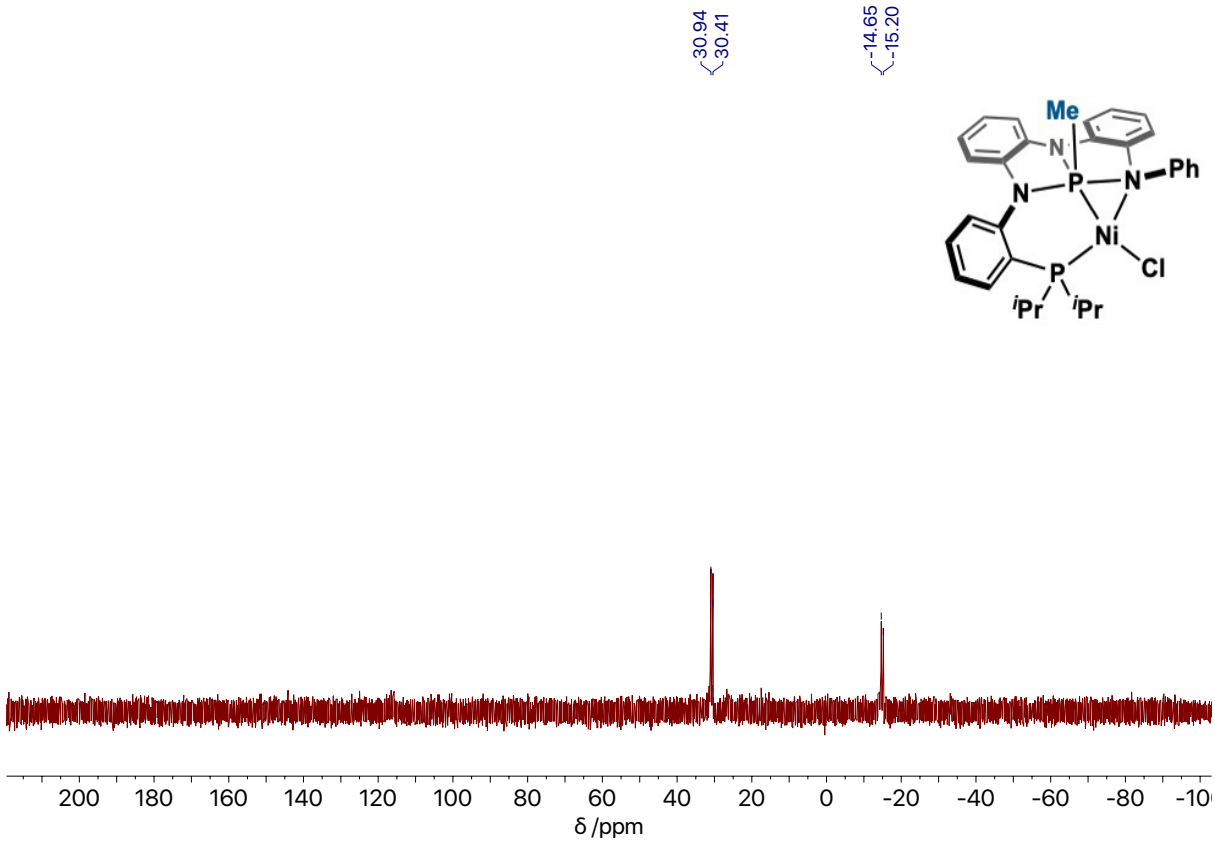


**Figure D-32.** $^{31}P\{^{1}H\}$ NMR spectrum of $NiCliPr_2PNNNPMe$ **(5.8´)**.

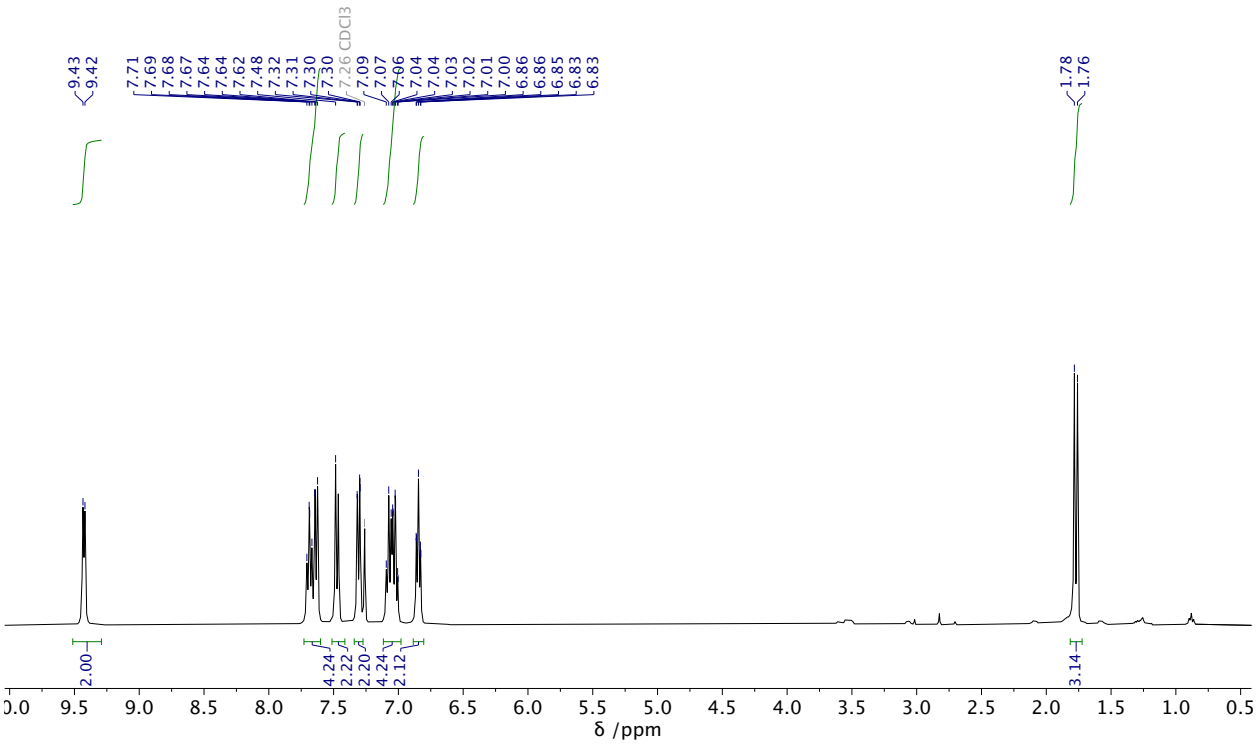


**Figure D-33.** $^{1}$H NMR spectrum ($CDCl_3$) of **5.10´**.

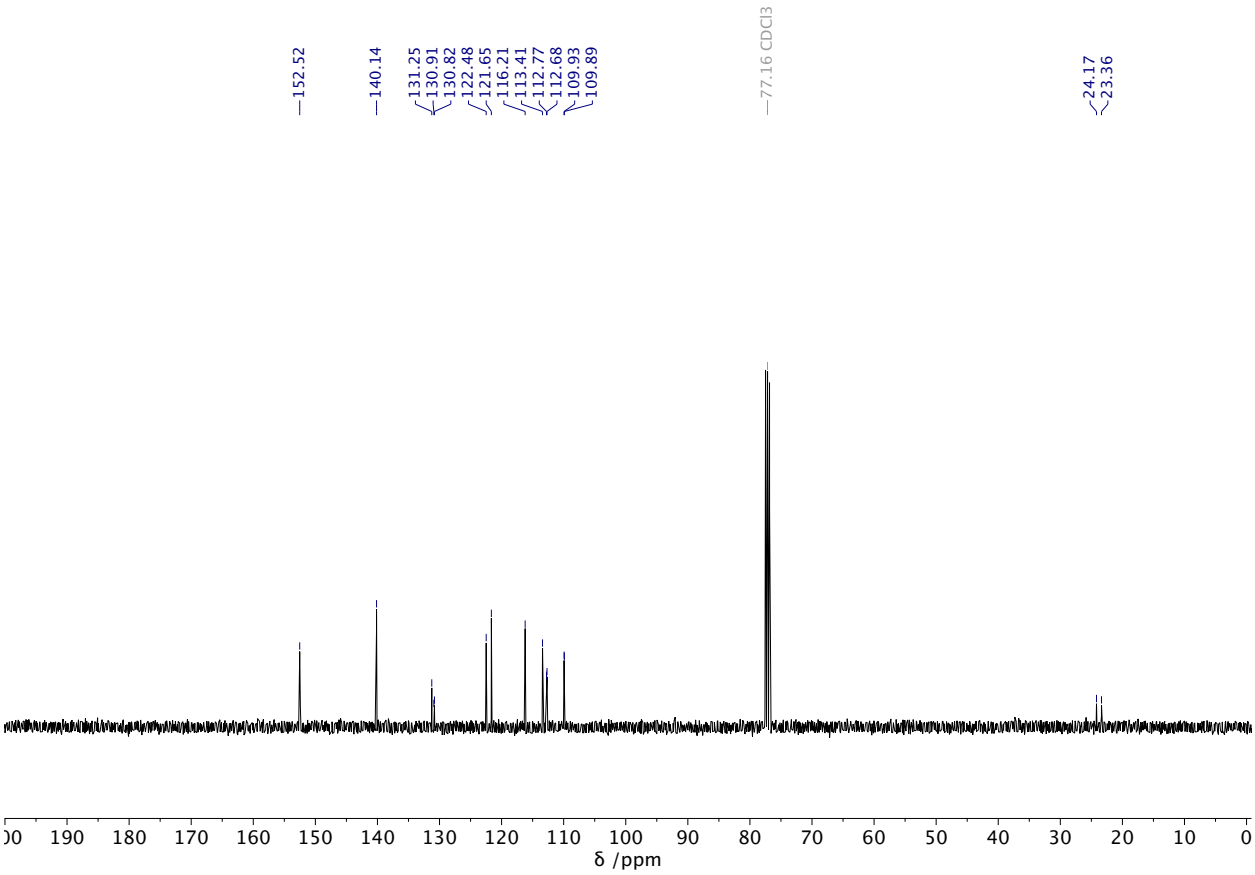


**Figure D-34.** $^{13}C$ NMR spectrum ($CDCl_3$) of **5.10′**.

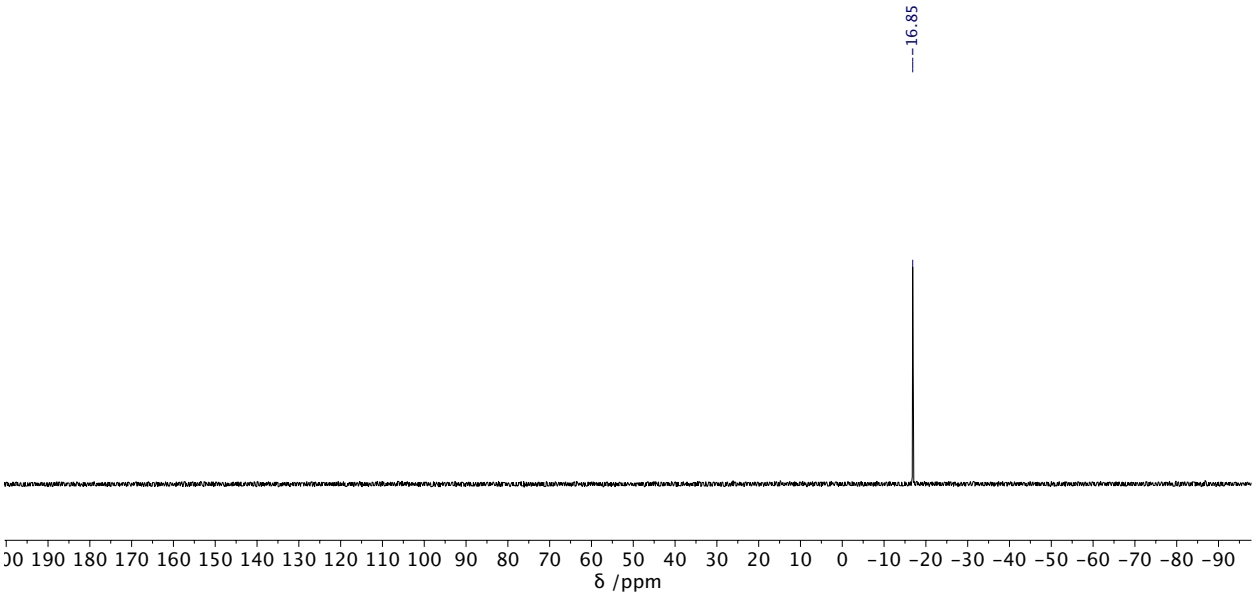


**Figure D-35.** $^{31}P\{^{1}H\}$ NMR ($CD_2Cl_2$) spectrum of **5.10′**.

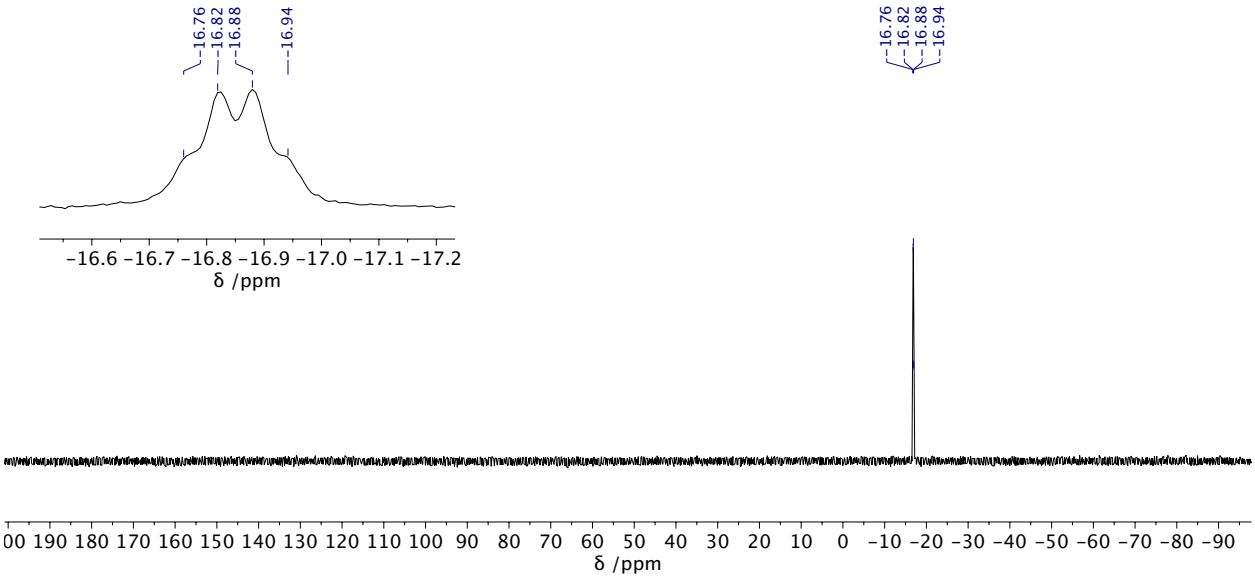


**Figure D-36.** $^{31}P$ NMR spectrum ($CD_2Cl_2$) of **5.10′**.

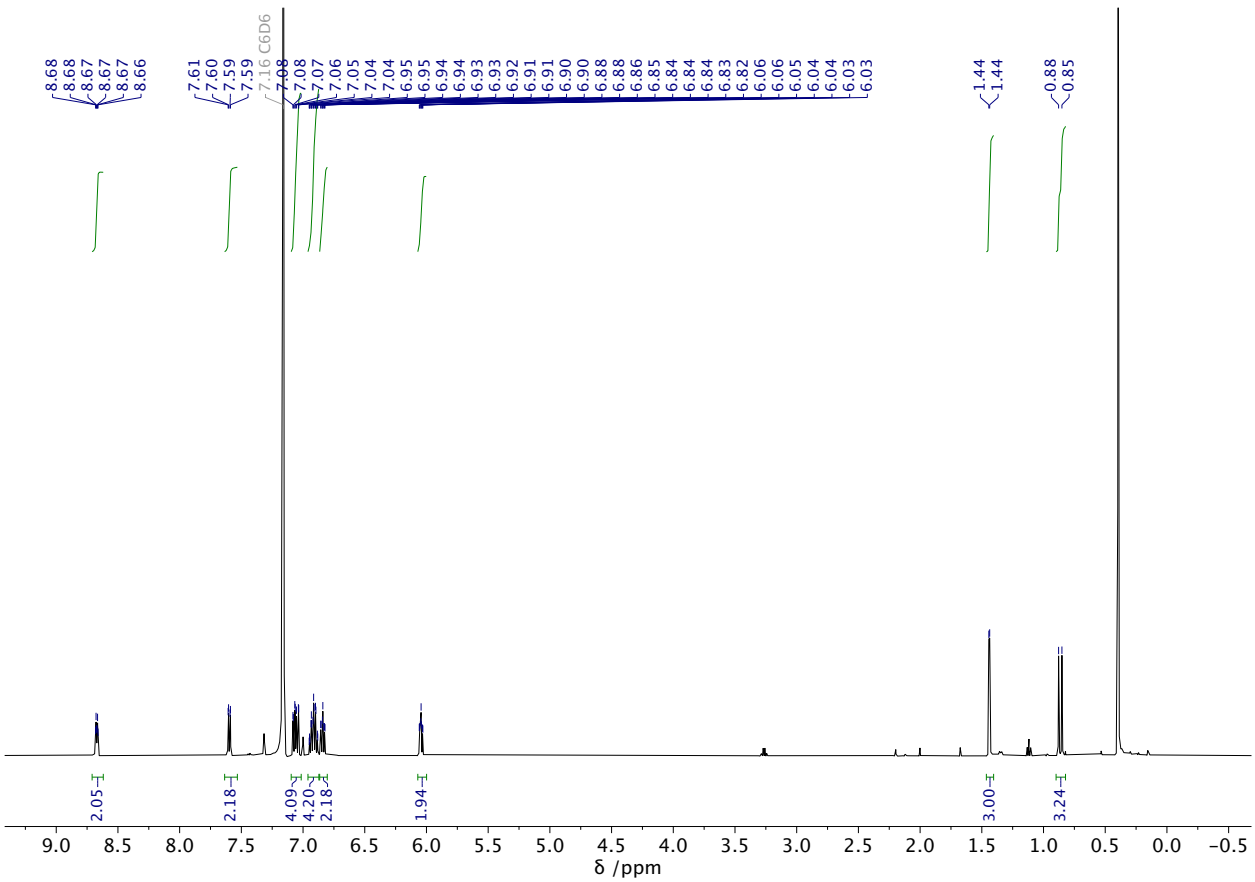


**Figure D-37.** $^{1}$H NMR spectrum ($C_6D_6$) of **5.11′**. A singlet signal at $\delta$ 0.40 ppm is residual water.

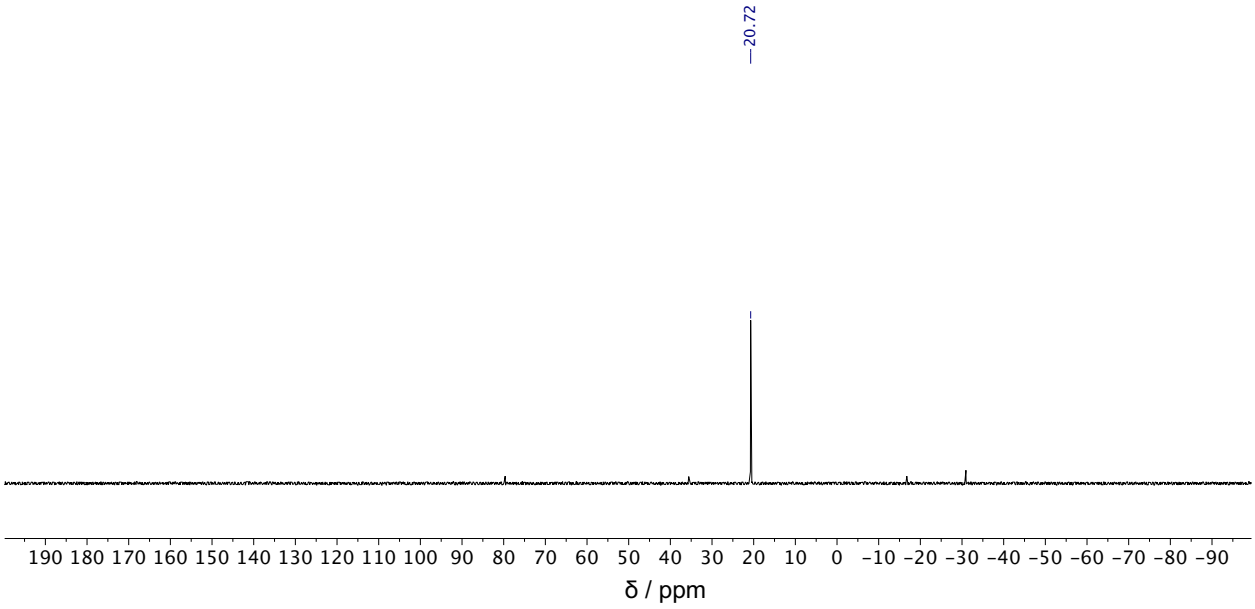


**Figure D-38.** $^{31}P\{^{1}H\}$ NMR spectrum ($C_6D_6$) of **5.11´**.

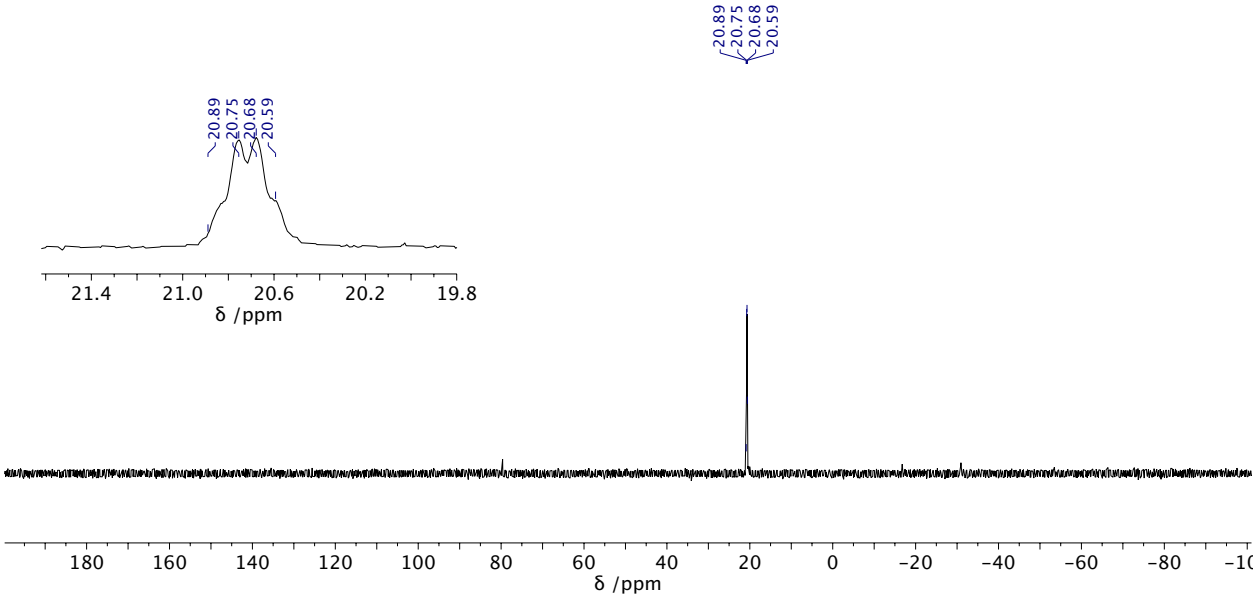


**Figure D-39.** $^{31}P$ NMR spectrum ($C_6D_6$) of **5.11´**.

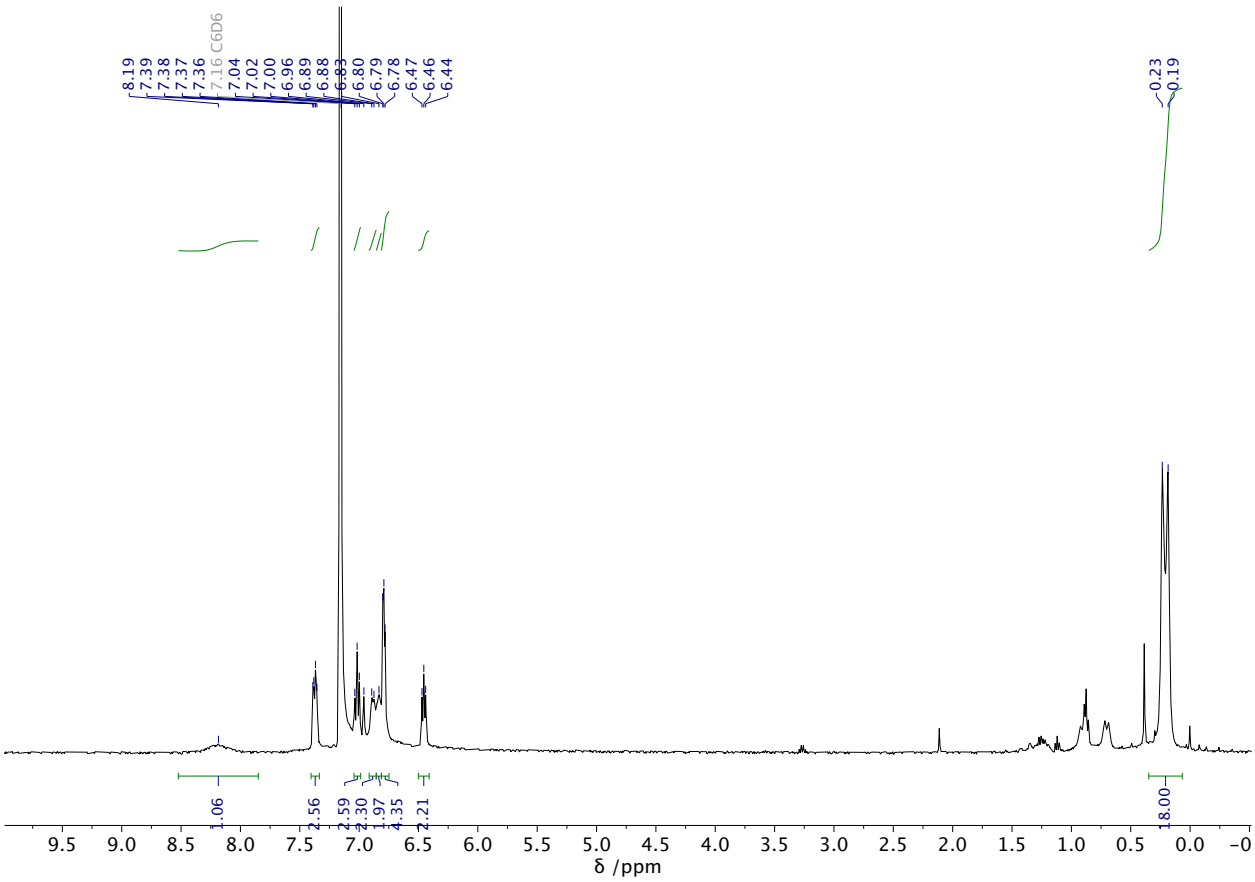


**Figure D-40.** $^{1}$H NMR spectrum ($C_6D_6$) of **5.12**.

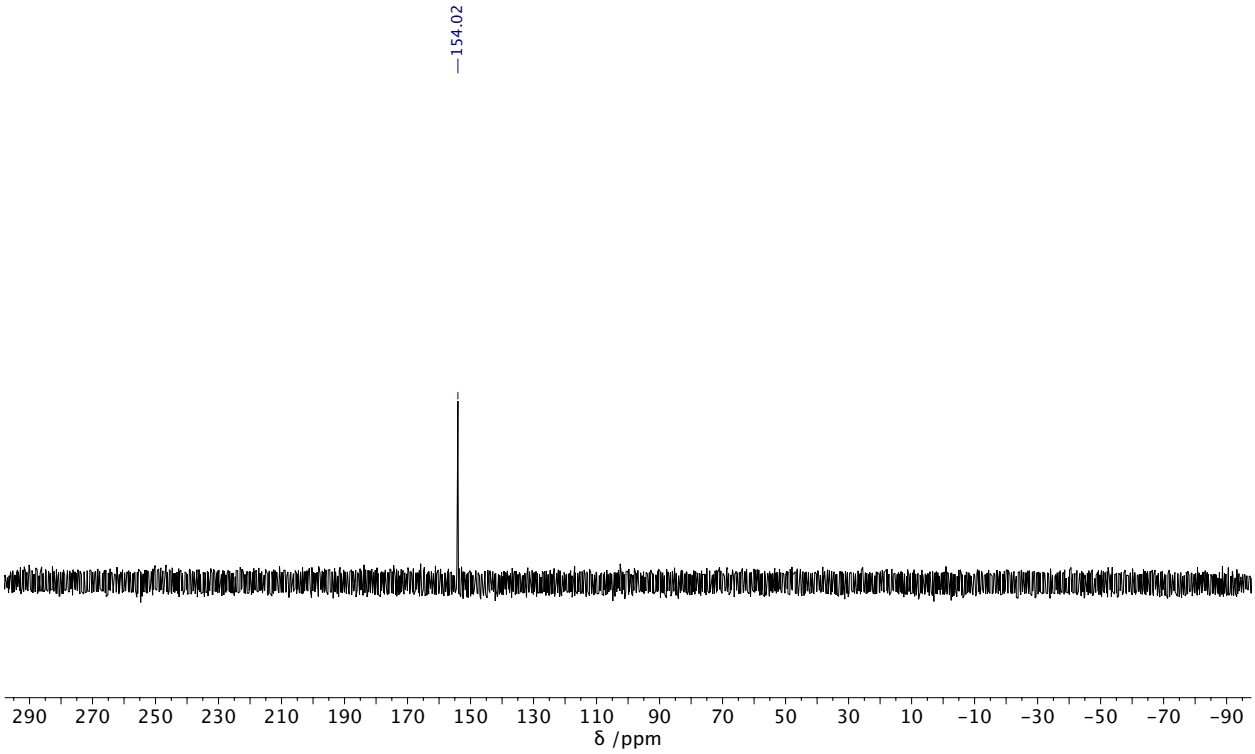


**Figure D-41.** $^{31}P\{^{1}H\}$ NMR spectrum of **5.12**.

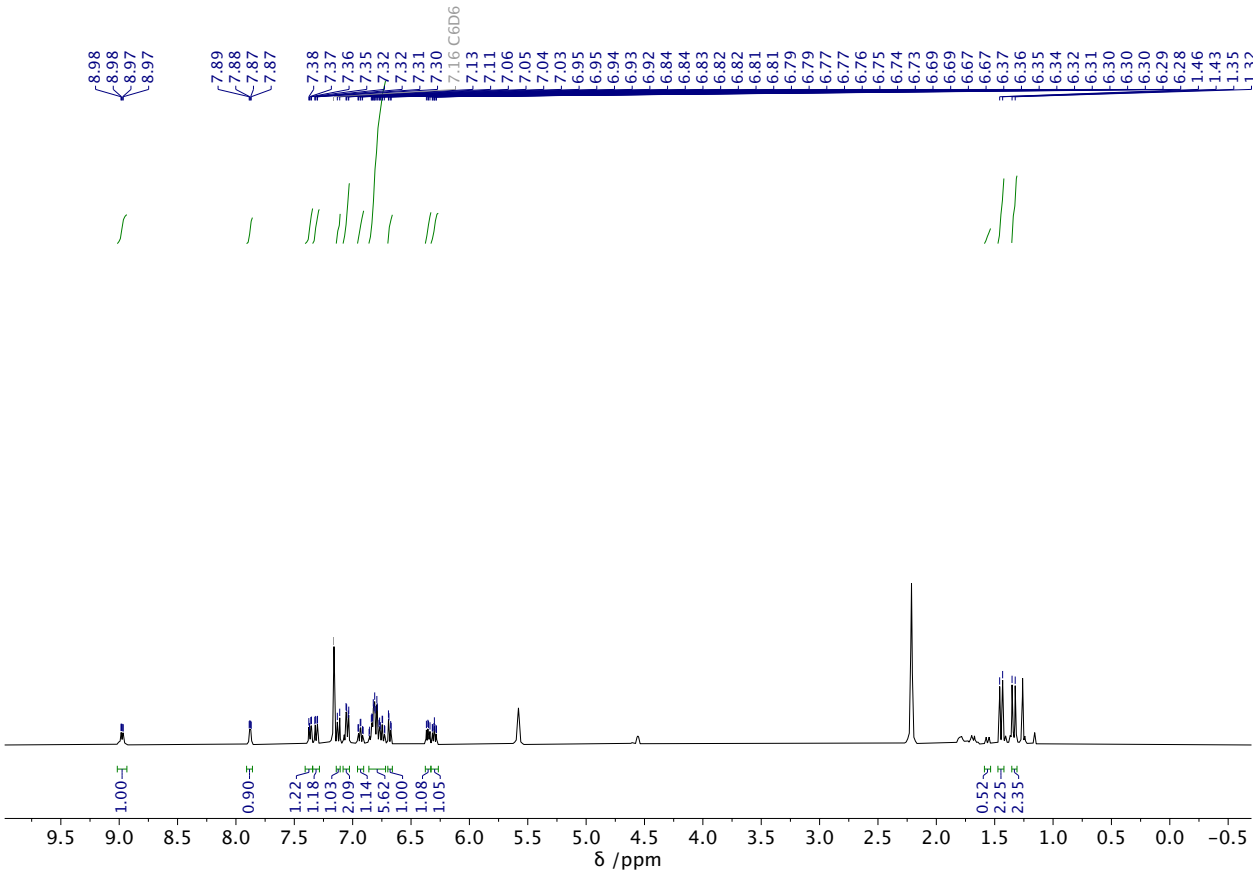


**Figure D-42.** $^{1}$H NMR spectrum ($C_6D_6$) of **5.13**. Signals of 1,5-cyclooctadiene remain in the spectrum.

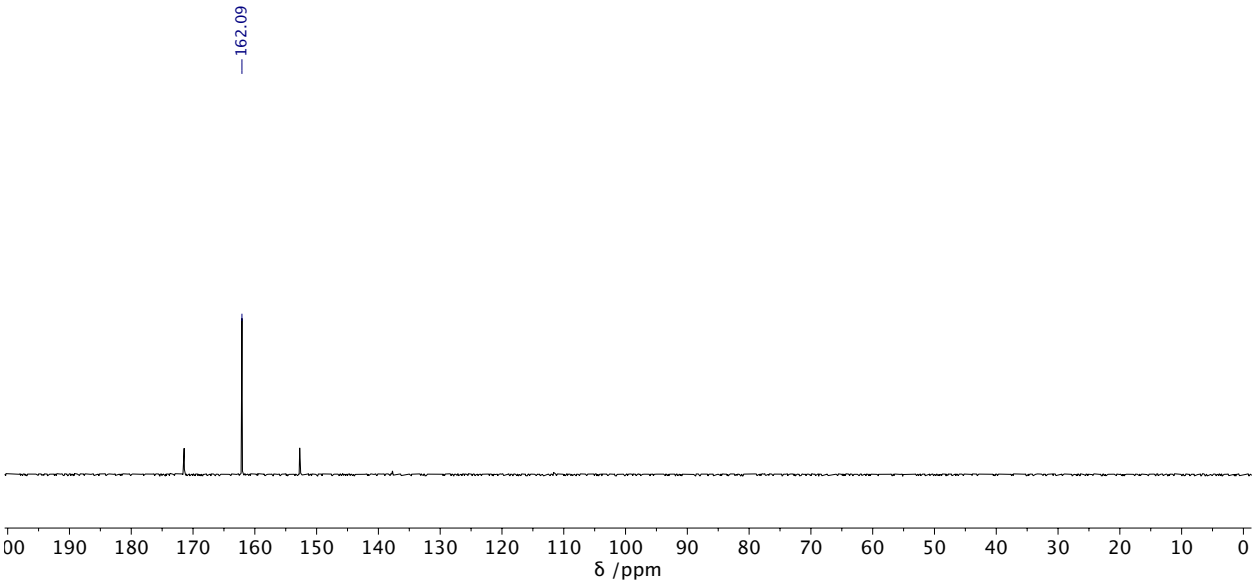


**Figure D-43.** $^{31}P\{^{1}H\}$ NMR spectrum ($C_6D_6$) of **5.13**.

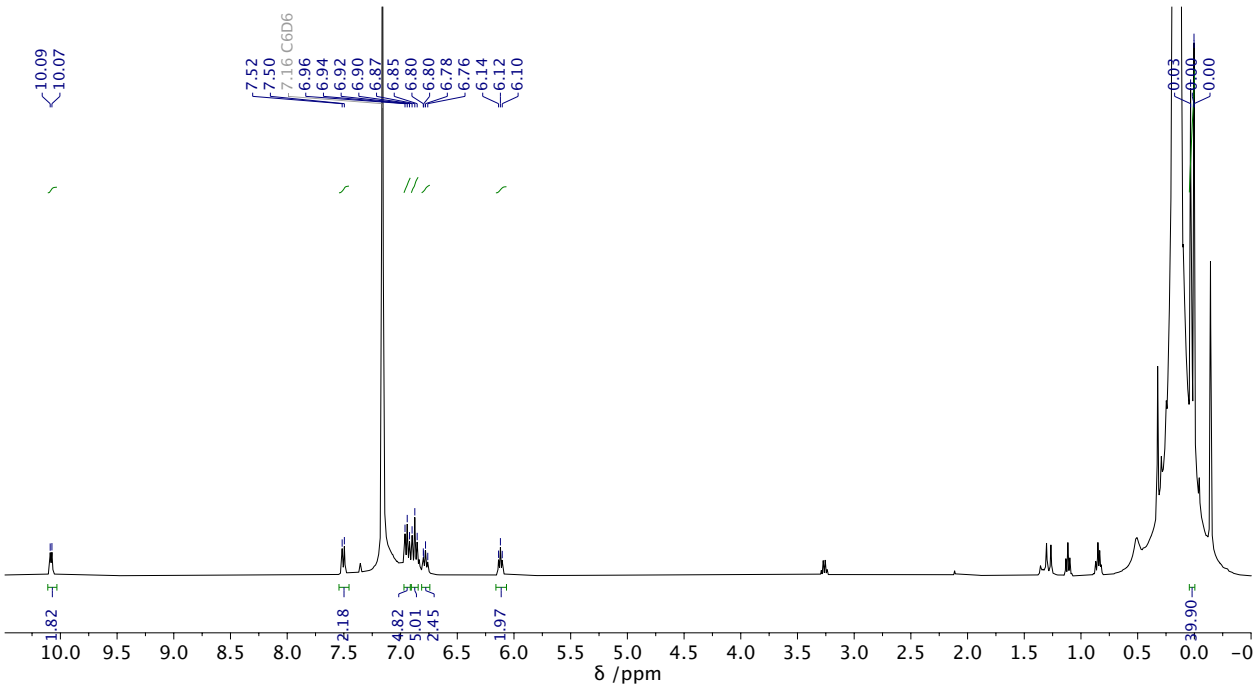


**Figure D-44.** $^{1}$H NMR spectrum ($C_6D_6$) of **5.14′**. (In-situ spectrum containing the signal of $Me_3SiCH_2Li$)

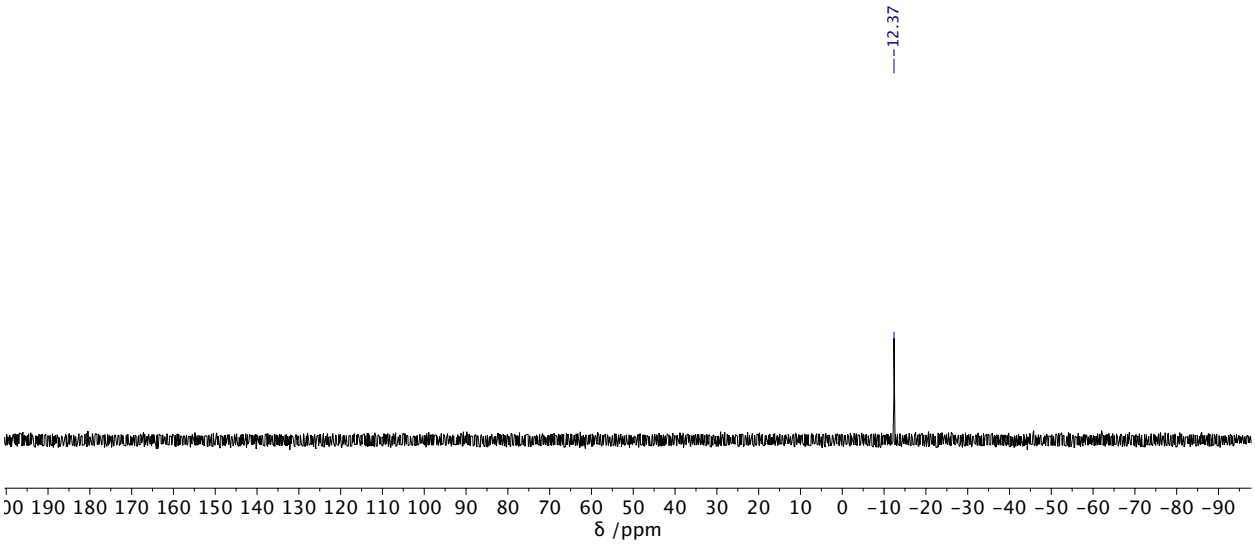


**Figure D-45.** $^{31}P\{^{1}H\}$ NMR spectrum ($C_6D_6$) of **5.14´**.

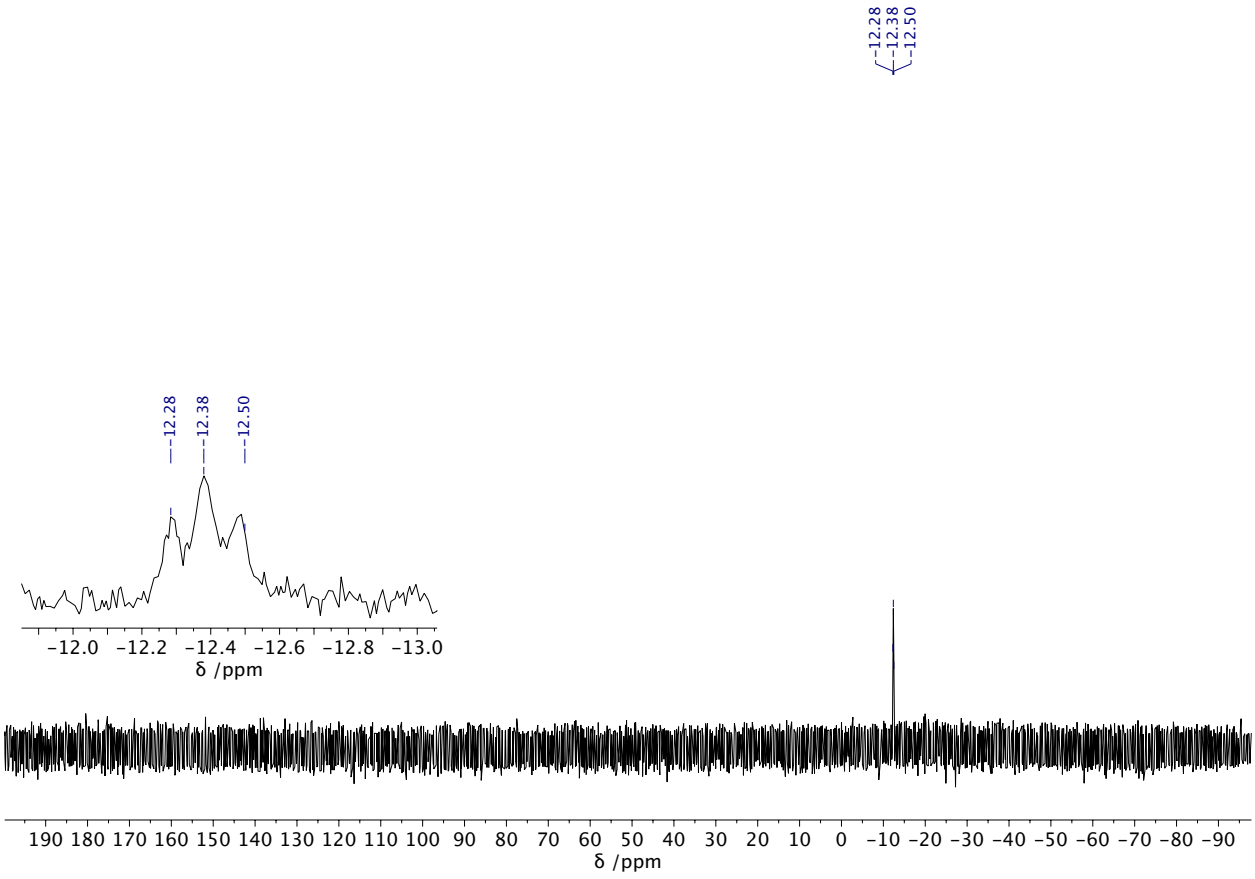


**Figure D-46.** $^{31}P$ NMR spectrum ($C_6D_6$) of **5.14´**.

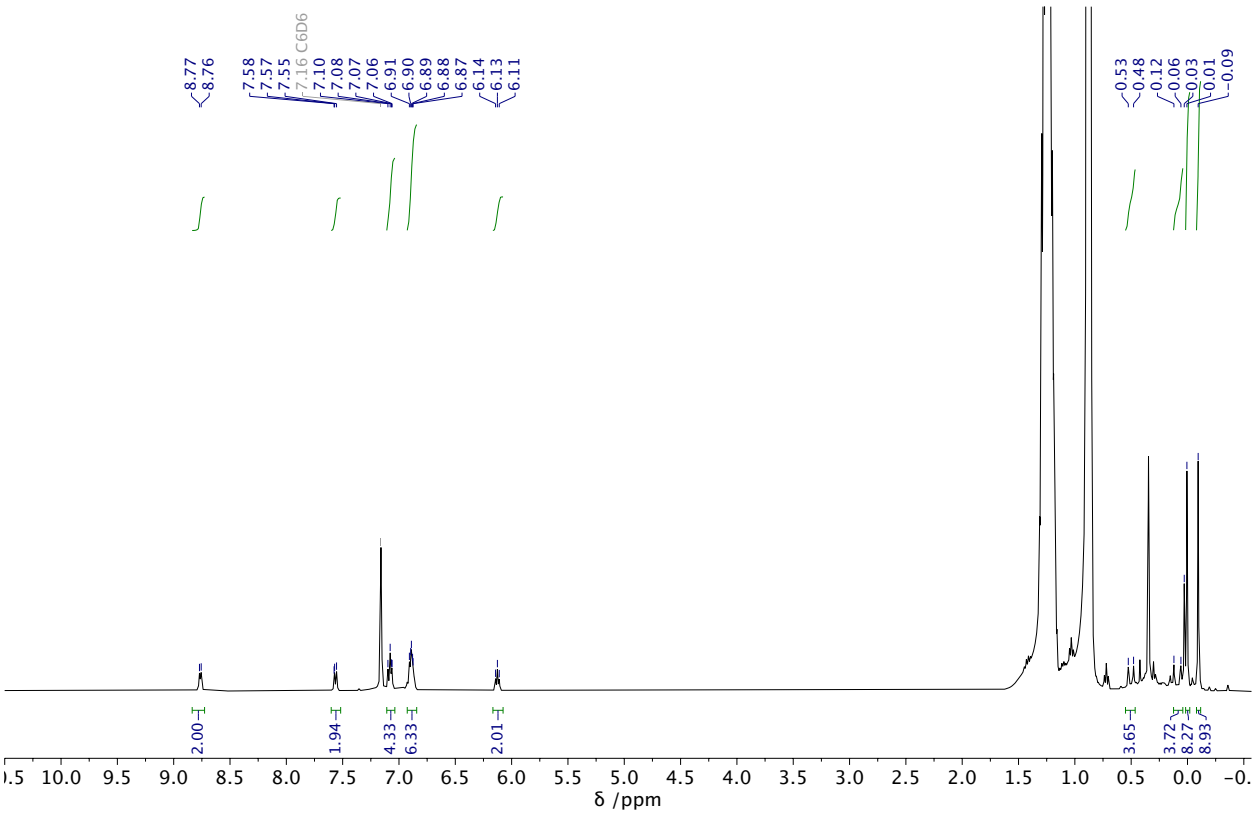


**Figure D-47.** $^{1}$H NMR spectrum ($C_6D_6$) of **5.12′**.

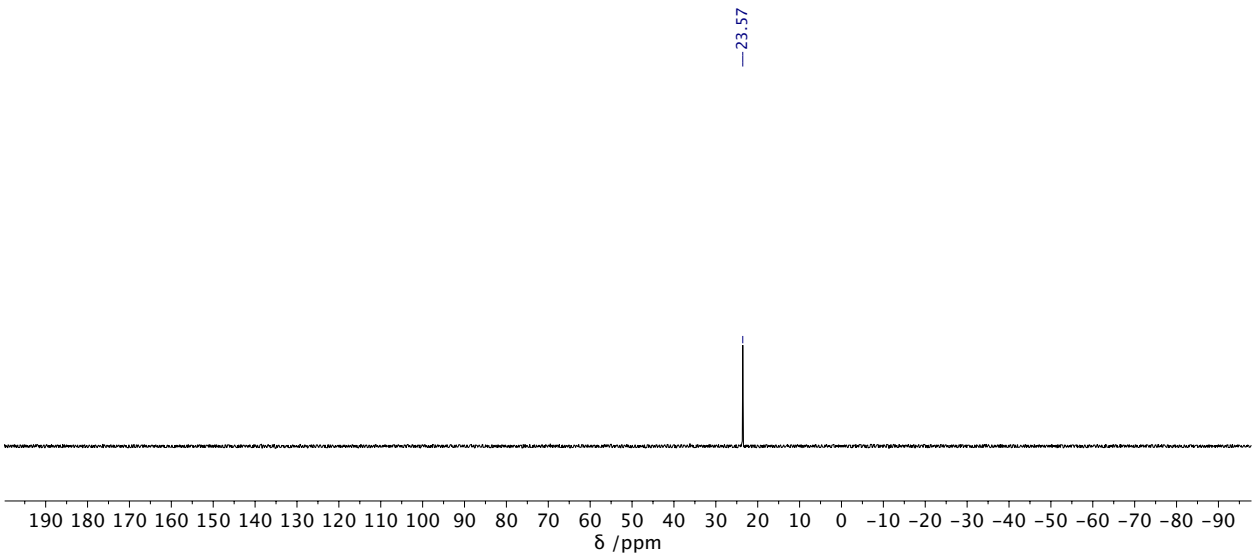


**Figure D-48.** $^{31}P\{^{1}H\}$ NMR spectrum ($C_6D_6$) of **5.12´**.

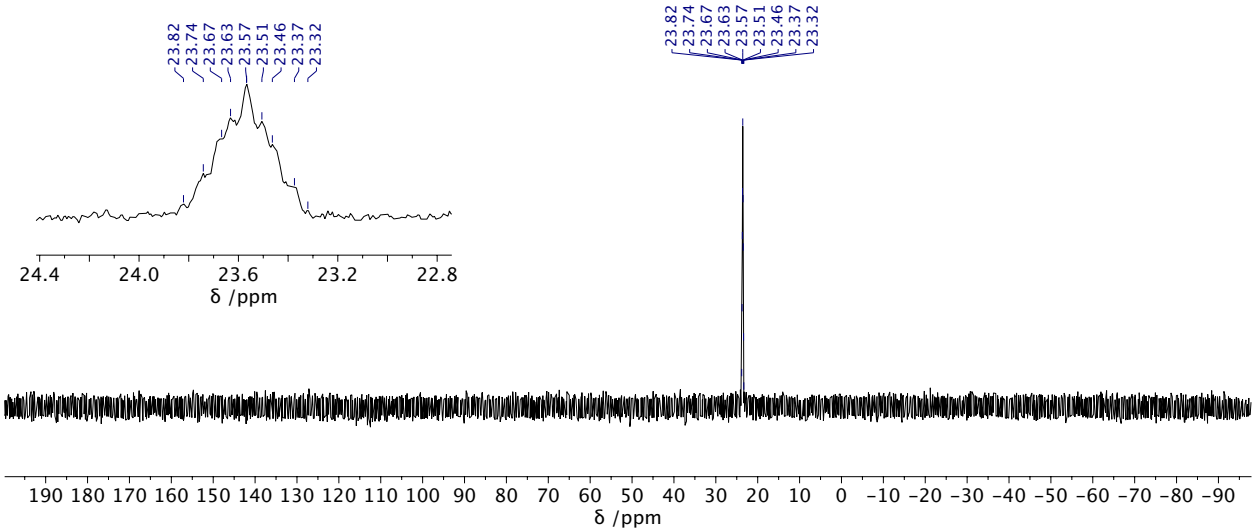


**Figure D-49.** $^{31}P$ NMR spectrum ($C_6D_6$) of **5.12´**.

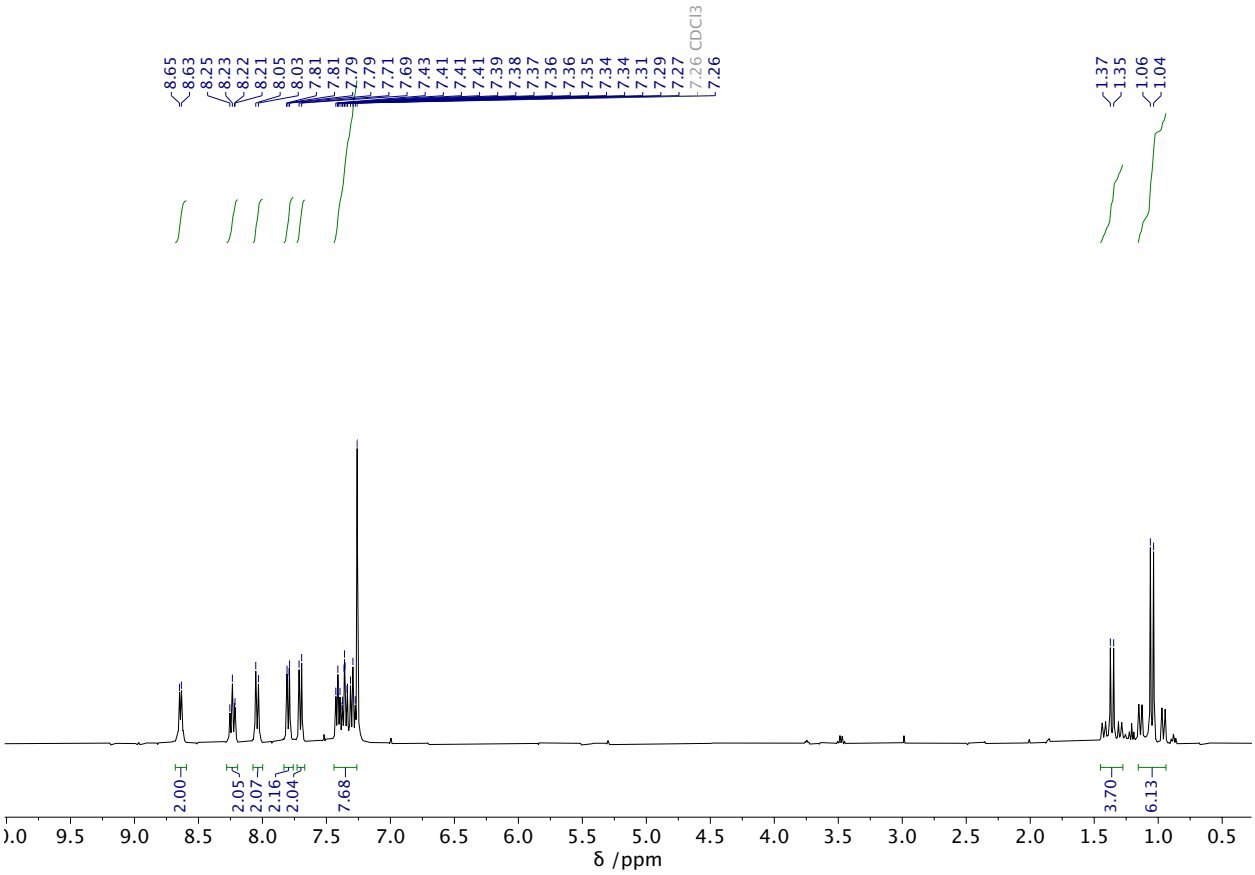


**Figure D-50.** $^{1}$H NMR spectrum of **5.15**.

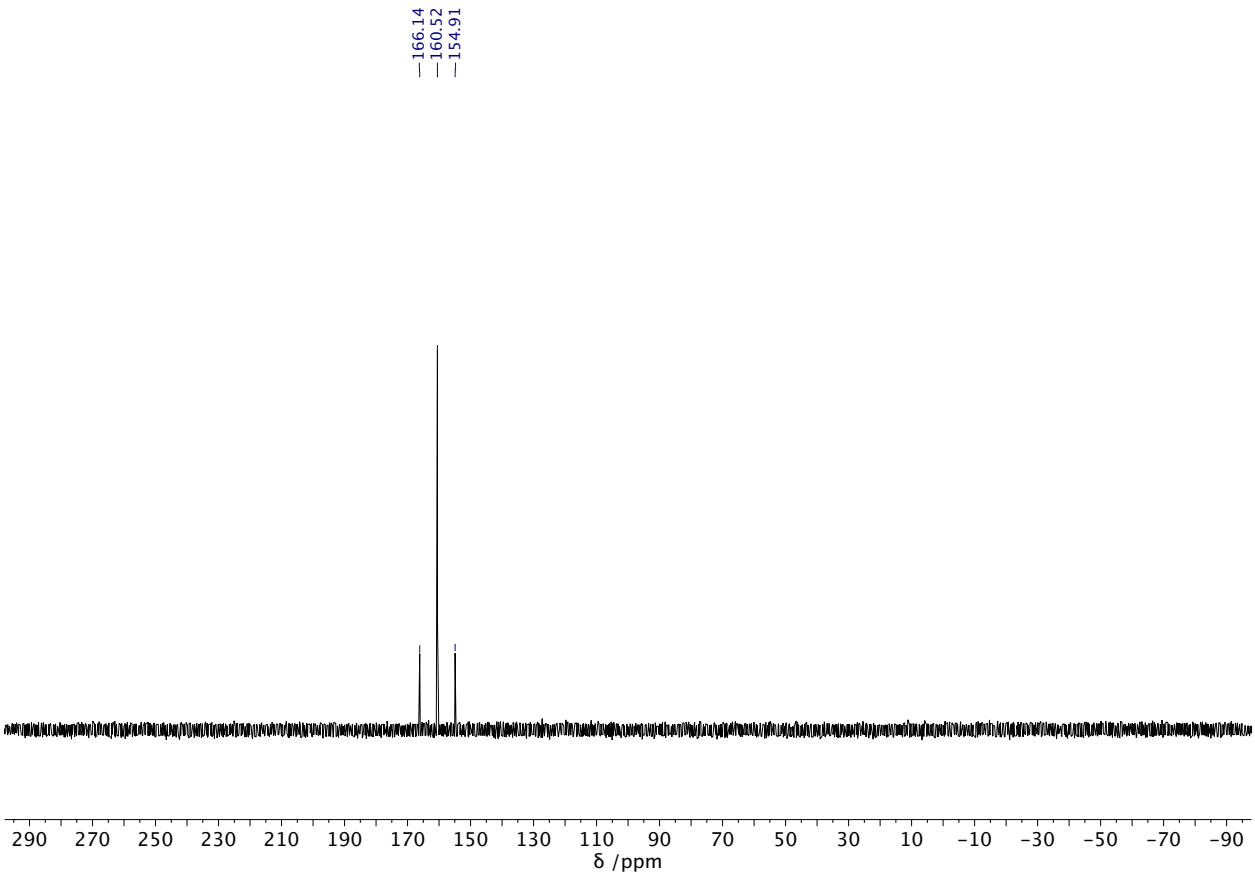


**Figure D-51.** $^{31}P\{^{1}H\}$ NMR spectrum of **5.15**.

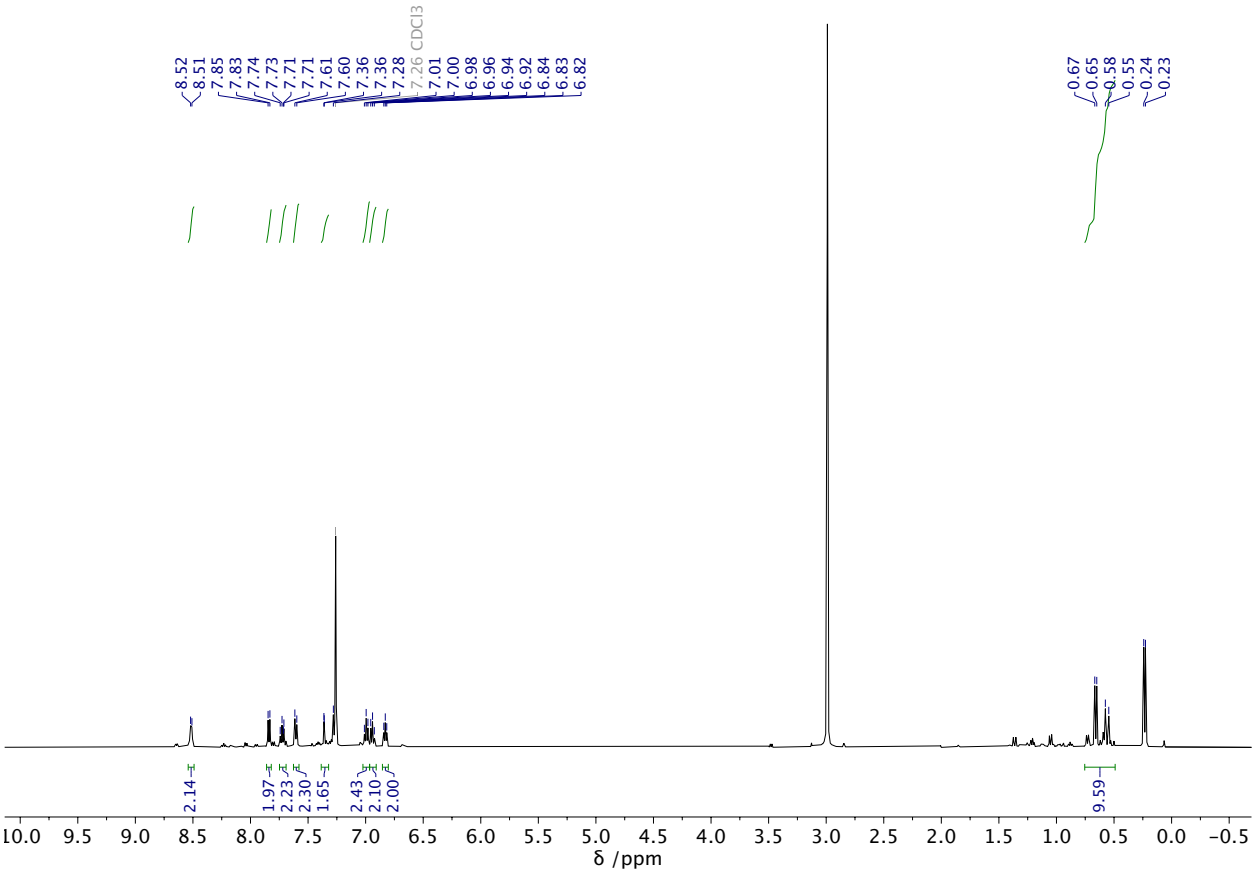


**Figure D-52.** $^{1}$H NMR spectrum of **5.16**. The signals at δ 2.99 ppm and 0.23 ppm is due to excess TASF.

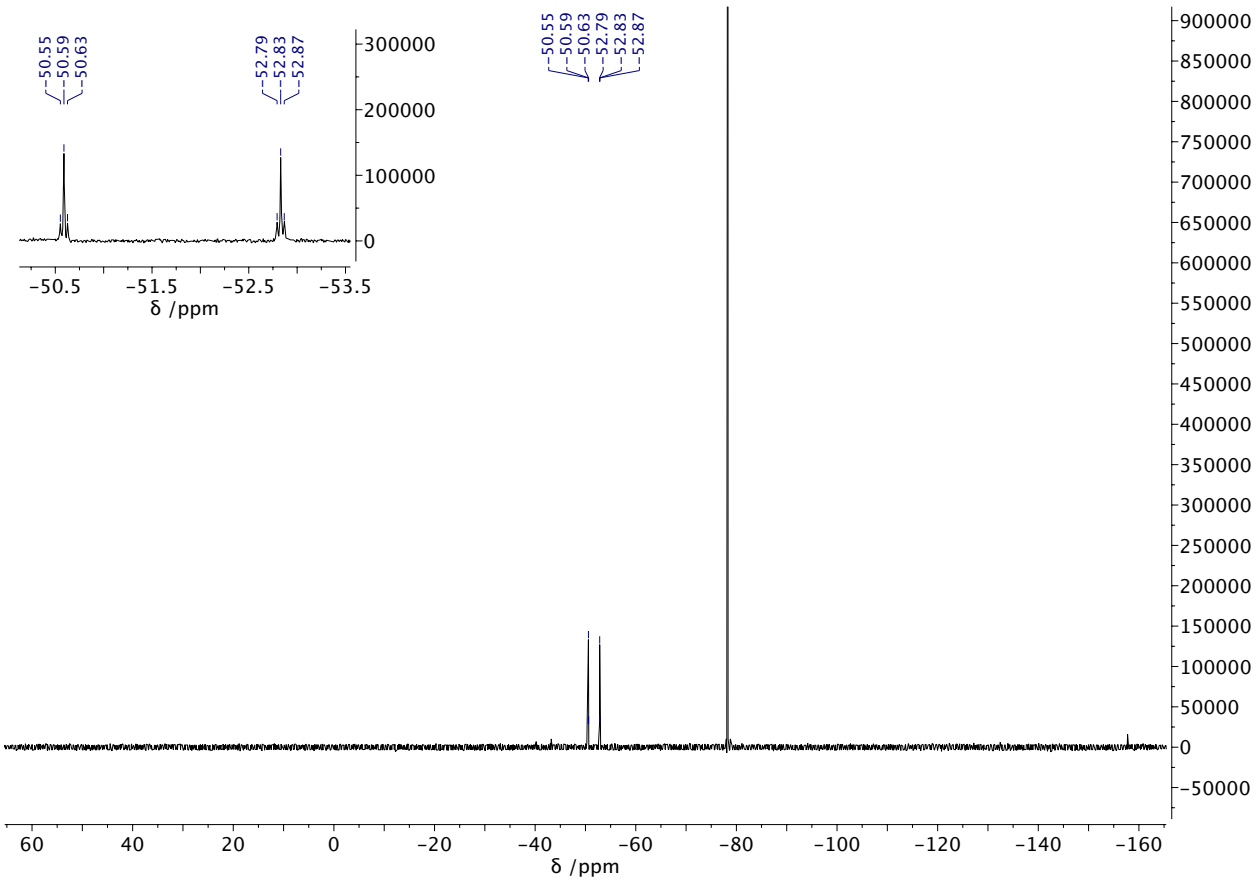


**Figure D-53**. $^{19}$F NMR spectrum of **5.16**. Note that the singlet signal at δ −78.3 ppm is due to excess TASF.

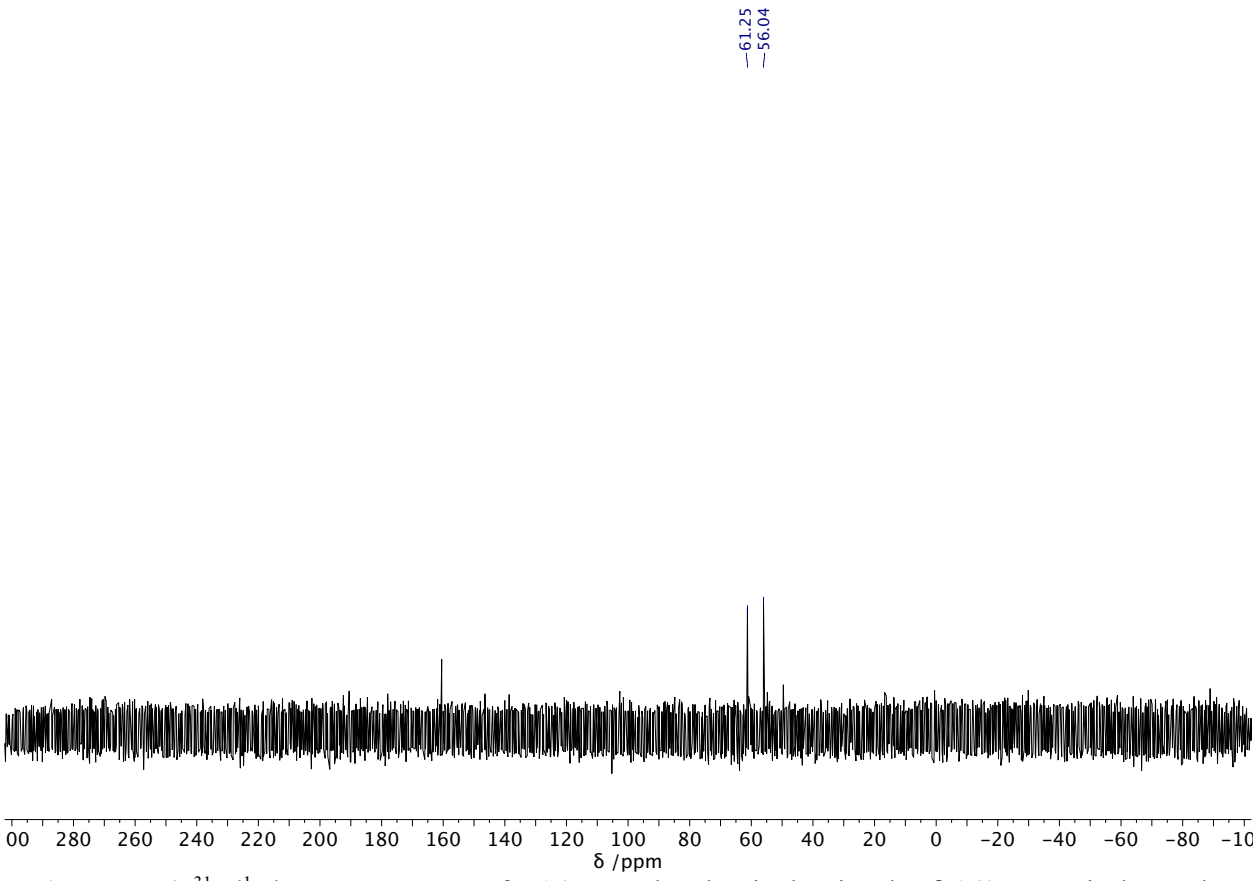


**Figure D-54.** $^{31}P\{^{1}H\}$ NMR spectrum of **5.16**. Note that the singlet signal at δ 160.5 ppm is due to the unreacted **5.15**.

## D.4. References


1. F. Neese, *WIREs Comput. Mol. Sci.*, **2012**, *2*, 73–78.
2. (a) Ramos-Cordoba, E.; Postils, V.; Salvador, P. Oxidation States from Wave Function Analysis. *J. Chem. Theory Comput.* **2015**, *11* (4), 1501–1508. (b) Postils, V.; Delgado-Alonso, C.; Luis, J. M.; Salvador, P. An Objective Alternative to IUPAC's Approach To Assign Oxidation States. *Angew. Chem. Int. Ed.* **2018**, *57* (33), 10525–10529. (c) Gimferrer, M.; Salvador, P.; Poater, A. Computational Monitoring of Oxidation States in Olefin Metathesis. *Organometallics* **2019**, *38* (24), 4585–4592.
3. (a) Knizia, G.; Klein, J. E. M. N. *Angew. Chem. Int. Ed.* **2015**, *54*, 5518-5522; (b) Knizia, G. *http://www.iboview.org/*.
4. (a) Lu, T.; Chen, F. Multiwfn: A Multifunctional Wavefunction Analyzer. *J. Comput. Chem.* **2012**, *33* (5), 580–592. (b) T. Lu, F. Chen, *Acta Chim. Sin.* **2011**, *69*, 2393 – 2406.
5. Pipek, J.; Mezey, P. G. A fast intrinsic localization procedure applicable for ab-initio and semiempirical linear combination of atomic orbital wave functions. *J. Chem. Phys.* **1989**, *90*, 4916−4926.
6. R. F. W. Bader, '*Atoms in Molecules A Quantum Theory*', Oxford University Press, Oxford, 1990.
7. (a) van Lenthe, E.; Baerends, E. J.; Snijders, J. G. *J. Chem. Phys.* **1993**, *99*, 4597−4610. (b) van Lenthe, E.; Baerends, E. J.; Snijders, J. G. *J. Chem. Phys.* **1994**, *101*, 9783−9792.